AD-A119 660 PALISADES INST FOR RESEARCH SERVICES INC NEW YORK F/G 9/5
IEEE CONFERENCE RECORD OF 1973 ELEVENTH MODULATOR SYMPOSIUM, NE--ETC(U)
1973
UNCLASSIFIED 73-CH0-773-2-ED NL

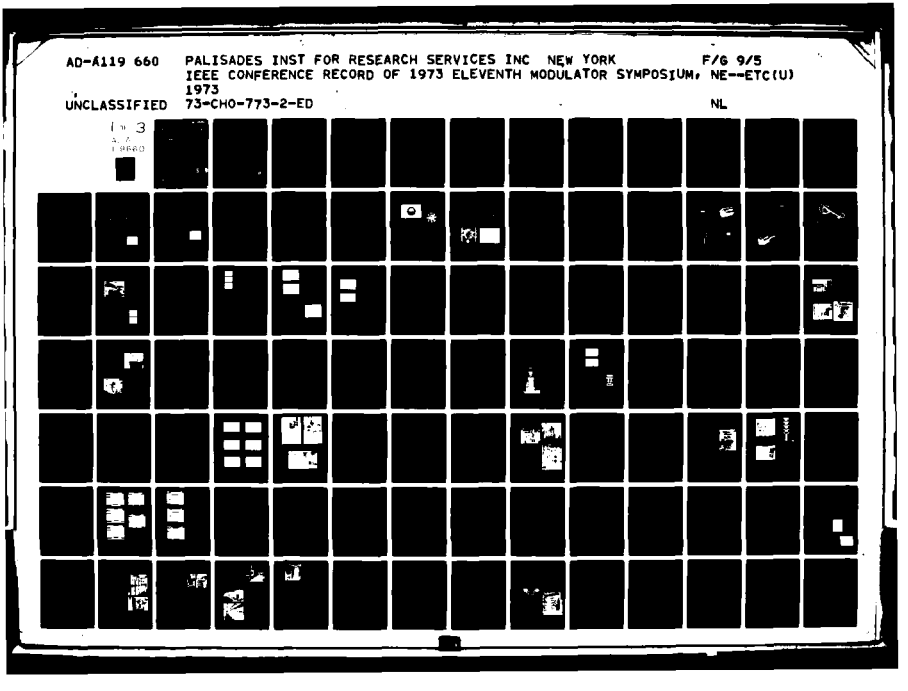

73 CHO 773-2 ED

IEEE
CONFERENCE RECORD OF
1973 ELEVENTH
MODULATOR SYMPOSIUM

September 18-19, 1973

Sponsored by the
IEEE Electron Devices Group
and
Advisory Group on Electron Devices
in conjunction with
Palisades Institute for Research Services, Inc.

73 CHO 773-2 ED

IEEE

CONFERENCE RECORD OF

1973 ELEVENTH MODULATOR SYMPOSIUM

Papers presented at the
Hotel Belmont — New York City
September 18-19, 1973

Sponsored by the
IEEE Electron Devices Group
and
Advisory Group on Electron Devices
in conjunction with
Palisades Institute for Research Services, Inc.

Printed in USA

LIST OF ATTENDEES

1973 IEEE-AGED

ELEVENTH MODULATOR SYMPOSIUM

Steven Adams	Norden Division of UAC, Connecticut
Carl D. Ahlstrom	General Electric Company, Kentucky
R. L. Alsmeyer	Raytheon Company, Massachusetts
Ernst R. Altschul	Aydin Energy Systems, California
John M. Anderson	General Electric Company, New York
Robert L. Anderson	Maxwell Labs., Inc., California
James B. Ashworth	Raytheon Company, Massachusetts
George Badger	EIMAC Division of Varian, California
Joseph Bajda	Norden Division of UAC, Connecticut
Marvin J. Barth	Albuquerque, New Mexico
Howard J. Beard	RADC, New York
Alvin D. Bedrosian	Massachusetts Institute of Technology
Leo Birenbaum	Polytechnic Institute of New York
Edward Blank	Ikor Incorporated, Massachusetts
Ronald Bowes	RCA, Pennsylvania
Robert Bradford	Stanford Linear Accelerator Center, CA
Howard M. Brady	North Arlington, New Jersey
Wolfgang G. Braun	Aerospace Research Laboratories, Ohio
Francis Bray	U. S. Naval Weapons Laboratory, Virginia
Stanley Brody	Norden Division of UAC, Connecticut
Robert E. Byram	Lancaster, Pennsylvania
Nguyen Ngoc Can	Thomson-CSF, Bagneux, France
John L. Carter	USAECOM, Fort Monmouth, New Jersey
Robert Casolaro	RCA, Cherry Hill, New Jersey
Gerald Clark	E G & G, Inc., Massachusetts
R. Cormier	Port Jefferson Station, New York
Carl R. Crager	Montoursville, Pennsylvania
John P. Craig	Texas Technical University, Texas
John E. Creedon	USAECOM, Fort Monmouth, New Jersey
T. P. Crowfoot	ASWE, Portsdown, England
Lars Dahlberg	Telefonaktiebolaget L M Ericsson, Sweden
Harvey W. Dain	Hughes Aircraft Company, California
James E. Dalmas	Bendix Communications Division, Maryland
Alain Delaye	New York City, New York
Frank DeLurgio	Emerson Electric Company, Missouri
John R. Dunstan	NELC, San Diego, California
Carl J. Eichenauer	General Electric Company, New York
Robert J. Ein	Arlington, Virginia

P. E. Faugeras ..... Cern Laboratoire II, Prévessin (France)
J. Ross Faulkner ..... Los Alamos Scientific Lab., New Mexico
Pete Fenoglio ..... New Hartford, New York
Joseph F. Ferrante ..... Maxwell Laboratories, Inc., California
Andrew F. Fikenberg ..... Baldwin, Maryland
Richard A. Fitch ..... Maxwell Laboratories, Inc., California
David Fleischer ..... E G & G, Inc., Salem, Massachusetts
Harry L. Fowler ..... Los Altos Hills, California
Lowell J. Fox ..... Litton Industries, California
Walter W. Frey ..... AIL, Deer Park, New York
E. W. Fritz ..... Kenosha, Wisconsin
Bernard Fudim ..... Calvert Electronics, Inc., New York
Robert A. Gardenghi ..... Catonsville, Maryland
F. Genis ..... Societe Omera-Segid, Argenteuil, France
Leonard Genova ..... Stanford Linear Accelerator Center, California
Robert Gibson ..... Systems, Science & Software, California
F. B. Golden ..... General Electric, Auburn, New York
Stanley Goldman ..... Granada Hills, California
Alfred E. Gordon ..... ITT, Electron Tube Division, Pennsylvania
D. M. Gossett ..... Torrance, California
R. Graham ..... Chatsworth, California
Bobby R. Gray ..... Rome, New York
G. Grotz ..... Dynell Electronics, Huntington Sta., N.Y.
J. Hartranft ..... Silver Springs, Maryland
William L. Heatherly ..... Kirtland AFB, New Mexico
W. W. Heiser ..... Raytheon Company, Massachusetts
Clarke P. Heon ..... M. I. T. Lincoln Laboratory, Massachusetts
Philip C. Herren, Jr. ..... Air Force Aeropropulsion Lab., Ohio
R. A. Hill ..... Naval Electronic System Cmd., Washington, D.C.
R. A. Hill ..... Westinghouse Corporation, Maryland
Donald F. Hodge ..... Waltham, Massachusetts
William E. Hosey ..... Westinghouse Corporation, Maryland
Joseph Howarth ..... Raytheon Company, Waltham, Massachusetts
H. M. Israel ..... Raytheon Company, Wayland, Massachusetts
Sandford Jacobson ..... Stamford, Connecticut
R. M. Johnson ..... Wantagh, New York
Shelby A. Jolly ..... General Electric Company, Kentucky
Howard L. Jones ..... La Crescenta, California
John T. Keane ..... Brookhaven National Lab., New York
W. Kestenbaum ..... Airborne Instruments Lab., New York
C. Kirka ..... Machlett Labs, Stamford, Connecticut
Leonard H. Klein ..... AGED, New York
Richard Knight ..... Sunnyvale, California
S. L. Kokoszka ..... Raytheon Company, Wayland, Massachusetts
Charles G. Kristenson ..... Hughes Aircraft Company, California

R. F. Lankshear ..... Port Jefferson, New York
Robert A. Larson ..... Brookhaven National Lab., New York
Enrico Levi ..... Polytechnic Institute, Brooklyn, N.Y.
Robert Lockey ..... Brookhaven National Lab., New York
D. L. Lockwood ..... Williamsville, New York
Colin Lucien ..... Thomson-CSF, Bagneux, France
Michael Lutz ..... Hughes Research Labs., California
John L. McAlpine ..... University of Saskatchewan, Canada
W. H. McAulay ..... San Carlos, California
Lonnie N. McClusky ..... Toney, Alabama
B. J. McGough ..... Severna Park, Maryland
Andrew J. McNerney ..... Brookhaven National Lab., New York
Lloyd Mancebo ..... Livermore, California
John T. Mark ..... Lancaster, Pennsylvania
Pierre E. Martin ..... Amherst, New Hampshire
V. Nicholas Martin ..... Raytheon Company, Waltham, Massachusetts
Rudolph Mastroianni ..... Norden Division of UAC, Connecticut
Manuel Matnick ..... Axel Electronics, Inc., Jamaica, N.Y.
David D. Meacham ..... Pearson Electronics, Inc., California
Hugh Menown ..... English Electric Valve Co.,Ltd., U. K.
Spencer Merz ..... E G & G, Inc., Massachusetts
Raffee Mgrdechian ..... Axel Electronics, Inc., Jamaica, N.Y.
Helmut Milde ..... Ion Physics Corporation, Massachusetts
Camillo Mogavero ..... U.S. Army Electronics Cmd., Pennsylvania
L. P. Motta ..... Raytheon Company, Wayland, Massachusetts
John G. Murray ..... Princeton University, New Jersey
Nigel S. Nicholls ..... Royal Radar Establishment, U. K.
William R. North ..... Framingham, Massachusetts
R. F. Nylander ..... Varian Associates, California
R. E. Nyswander ..... China Lake, California
Frank M. Oakes ..... Litton Industries, New Jersey
Joseph P. O'Donnell ..... Axel Electronics, Inc., Jamaica, N.Y.
Charles L. Page ..... General Dynamics Electronics, California
Richard J. Pankow ..... Norwalk, Connecticut
James R. Perry ..... North Syracuse, New York
Ralph M. Philip ..... General Electric Company, New York
Edward M. Piechowiak ..... Catonsville, Maryland
Cervone Piero ..... Selenia, Rome, Italy
Paul Pittman ..... Westinghouse Electric Corp., Pennsylvania
Roger Plante ..... E G & G, Inc., Massachusetts
Martin Plotkin ..... Brookhaven National Lab., New York
Ernest W. Potter, Jr. ..... Paterson, New Jersey
D. L. Pruitt ..... Cinnaminson, New Jersey

Jacob A. Randmer ..... Machlett Laboratories, Connecticut
John S. Roberts ..... Westinghouse Electric Corp., Pennsylvania
Ron Rodine ..... Ling Electronics, Anaheim, California
F. Rouffy ..... New Market, Alabama
R. M. Rowe ..... Stanford Linear Accelerator Center, California
W. J. Sarjeant ..... GEN-TEC, Inc., Canada
Sol Schneider ..... USAECOM, Fort Monmouth, New Jersey
Otto Schurek ..... Wagner Electric Corp., New Jersey
Charles L. Shackelford ..... Bethlehem, Pennsylvania
Joe Sheehan ..... Brookhaven National Lab., New York
William W. Shrader ..... Raytheon Company, Wayland, Massachusetts
Elliot Silverman ..... M. I. T. Lincoln Laboratory, Massachusetts
John Singleton ..... IEEE
David Slater ..... AGED, New York
K. M. Smalley ..... Raytheon Company, Wayland, Massachusetts
R. A. Smith ..... Baltimore, Maryland
William I. Smith ..... Palmyra, New Jersey
Howard L. Storm ..... Camillus, New York
Paul J. Tallerico ..... Los Alamos Scientific Lab., New Mexico
George W. Taylor ..... USAECOM, Fort Monmouth, New Jersey
G. F. Thomas ..... U. S. Naval Weapons Lab., Virginia
Kenneth Thompson ..... NAD, Crane, Indiana
William T. Tomlin ..... Stanford Linear Accelerator Center, California
Jerrell M. Turner ..... Air Force Aero Propulsion Lab., Ohio
David Turnquist ..... E G & G, Inc., Massachusetts
Vance I. Valencia ..... Haimson Research Corp., Massachusetts
Leonard H. Vanzant ..... Bloomington, Indiana
Ken Voak ..... Varian Associates, California
H. A. Wallace ..... Maxwell Laboratories, Inc., California
Ralph W. Waniek ..... Advanced Kinetics, Inc., California
Thomas A. Weil ..... Raytheon Company, Wayland, Massachusetts
Geoffrey W. Whalley ..... Chelmsford, England
Robert J. Wheldon ..... M. O. Valve Co. Ltd., England
Anthony B. Williams ..... Keltec Florida, Fort Walton Beach, Florida
Robert H. Wills ..... NELC, San Diego, California
P. S. Wise ..... Raytheon Company, Wayland, Massachusetts
Samuel W. Woolsey ..... Aydin Energy Systems, Palo Alto, California
D. C. Wunsch ..... Air Force Weapons Lab., New Mexico
Thomas Yingst, Jr. ..... Lancaster, Pennsylvania
B. Zarkower ..... Cober Electronics, Inc., Connecticut
Gerald Zerfas ..... RCA, Burlington, Massachusetts
Frank S. Zimmermann ..... Kirtland Air Force Base, New Mexico
Stanley Zweig ..... Axel Electronics, Inc., Jamaico, New York

FOREWORD

The 1973 Eleventh Modulator Symposium was the latest in a series beginning with the Hydrogen Thyratron Symposium in 1950. The movement of technology can be deduced readily from examination of the proceedings and records of these conferences.

There were nine sessions which covered: Solid-State Devices; Electron Beam Devices; Hard-Tube Modulators; Solid-State Modulators; Super Power Modulators; Special Techniques; Line-Type Modulators; Protective Devices and Circuitry; Thyratrons.

1973 CONFERENCE COMMITTEE

Sol Schneider, Chairman
U.S. Army Electronics Command

Howard Beard
Rome Air Development Center

John E. Creedon
U.S. Army Electronics Command

Raymond A. Hill
Naval Electronic Systems Command

Leonard H. Klein
Palisades Institute for Research Services, Inc.

V. Nicholas Martin
Lockheed Electronics Co., Inc.

Hugh Menown
The English Electric Valve Company, Ltd., U.K.

Joseph V. Stover
Hughes Aircraft Company

Thomas A. Weil
Raytheon Company

TABLE OF CONTENTS

TABLE OF CONTENTS

A NEW SOLID-STATE SWITCH FOR POWER PULSE MODULATOR APPLICATIONS, THE REVERSE SWITCHING RECTIFIER

J. B. Brewster and P. F. Pittman

Westinghouse Research Laboratories
Pittsburgh, Pennsylvania 15235

Summary

The Reverse Switching Rectifier (RSR) is a new solid-state switching device with performance optimized for short, high rate-of-rise pulse current switching. It is a two terminal device which switches from blocking to conduction upon application of a fast-rising pulse of voltage. Devices with peak pulse current ratings of 1200 A and di/dt ratings of 2000 A/μs are available with blocking voltage ratings of 1000 V at 125°C. A typical value of turn-off time is 50 μs at 25°C. Many practical pulse modulator circuits have been built using series and parallel combinations of RSR's to demonstrate the use of this device in power pulse modulator service.

1. Introduction

The generation of short, high energy pulses has for many years been accomplished by discharging an energy storage network with a vacuum or gas tube switching device. Although such devices yield reasonable performance, the life and reliability of systems using them leaves much to be desired. In addition, with the advent of transistors and associated semiconductor devices, most of the active devices in modulator systems have been converted from vacuum or gas tubes to solid-state devices, except for the power pulse switching tube for which no suitable replacement has been found.

With the advent of solid-state semiconductor switching devices in the early 1960's, the reliability and life problems which plagued modulators using vacuum and gaseous tubes for many years appeared to be solved. The thyristor, which is a three terminal gated switching device, appeared to have high potential as a replacement for the gas tube power pulse modulator switch. When attempts were made to use thyristors in modulator circuits, however, the early experience was less than satisfactory because the types of thyristors available failed at much lower power levels than anticipated, primarily because of the fact that the initial rate-of-rise of pulse current was too high to be tolerated by the device. Toward the middle of the 1960's, a generation of so-called modulator thyristors became available with improved turn-on performance resulting in an enhanced rate-of-rise of current capability. However, even these devices did not appear in suitably high ratings to be useful for the majority of power pulse modulator applications. The basic problem encountered with the thyristor is that, even though a large area of the device is available for conduction, turn-on action is initiated in a small area from which it spreads throughout the entire device. However, the time constant of the spread is sufficiently long that, in most modulator applications, only the area of the device in close proximity to the gating area conducts before the pulse is over. As a result, the percentage utilization of the total device capability is very poor.

The Reverse Switching Rectifier, abbreviated RSR, is a new two-terminal, four-layer PNPN semiconductor switching device designed especially for short, high-energy pulse generator service. The basic theory of operation of two-terminal, four-layer switching devices has been presented by several investigators whose early attempts to make a modulator switching device were unsuccessful.[1,2] A more recent effort by Westinghouse has resulted in a successful device wherein the problems encountered by earlier developers have been solved.[3] An earlier version of this device was described at the Tenth Modulator Symposium.[4] The turn-on mechanism employed is different from that of the thyristor from the standpoint that conduction is initiated throughout the area of the device, as opposed to the thyristor wherein conduction is initiated in a localized area. As a result, the RSR has superior turn-on performance and can tolerate a much higher rate-of-rise of pulse current than can the thyristor.

2. Turn-On and Conduction In The RSR

An ideal switching device turns on instantaneously and has no conducting voltage drop. The RSR, as is the case with every other switching device, is not ideal, and therefore it is of interest to discuss the ways in which RSR performance departs from the ideal switching characteristic.

The structure of the RSR is shown in Figure 1, and its VI characteristic is shown in Figure 2. Owing to the nature of the PNPN structure, the device initially blocks the flow of current in either direction. When a forward bias is applied, negligible current flows until the threshold voltage, V_T, is reached. At this point, current flows at the threshold voltage until a current sufficiently high is reached where conditions for turn-on are achieved within the device. At this point, the device goes into its conducting state wherein a large current may flow with a very low conducting voltage drop. The device remains in conduction as long as forward current exceeds the holding current, I_H. When reverse bias is applied to the device, negligible current flows until the avalanche breakdown of the reverse blocking junction is reached. At this point, current flows at the avalanche breakdown potential, and if the reverse current is made large enough, the device will fail.

The device VI characteristic shown in Figure 2 applies at dc or low frequency. However, in most modulator circuits, the RSR is connected to block the voltage of a charged pulse network until triggered on by a short, fast rising pulse. Device turn-on associated with fast pulse triggering involves a different mechanism then that already described and yields a somewhat different VI characteristic than that shown in Figure 2.

The RSR structure, shown in cross-section in Figure 1, includes a number of circular P type shorts which protrude through the upper N type emitter. The view of the upper surface of the device, also shown in Figure 1, shows the distribution and circular geometry of the P type shorts. An isometric view of a cross-sectioned device spanning the distance between two P type shorts is shown in Figure 3. When a fast-rising pulse of forward voltage is applied to the device, a capacitive current flows as the result of charge re-distribution in the vicinity of the blocking junction between the N type and P type base regions. This current, although generated uniformily throughout the device, is funneled out through the upper surface by the P type shorts as shown in Figure 3. Because the P type base regions which reach the upper surface are shorted to the N type emitter regions by the upper aluminum metalization, they prevent injection by the upper N type emitter, prohibiting turn-on. However, a lateral voltage drop is developed within the P type base region due to current crowding when a fast rising pulse causes a capacitive current to flow. This drop tends to forward bias the center portion of the N type emitter and results in injection at a point equidistance from two P type shorts designated as Point A in Figure 3. Because each set of four P type shorts constitutes a unit area with its own injection mechanism as previously discussed, turn-on proceeds at as many different points as there are unit cells on the upper surface area of the device, as opposed to the thyristor wherein turn-on occurs only in the region adjacent to the gating electrode.

The switching characteristic of the RSR departs from the ideal because a finite time is required for formation of the initial conducting area associated with each four P type shorts. However, in a practical device, the time necessary to form the initial conducting area is quite short, less than 100 ns, and in most circuits, this is negligibly small. Because the initial area of conduction is not the entire area of the device, the conducting drop realized at the instant the initial conducting area is formed is higher than the drop attained after the conducting plasma has been allowed to propagate throughout the entire active area. The propagation time is of the order of microseconds, which is far smaller than that of a thyristor, and because the initial conducting area of an RSR is a much larger percentage of the total active area than is that of a thyristor, the initial conducting drop of the RSR is less than that obtained from a comparable thyristor with conventional gate control.

An additional factor influencing the conducting drop of the RSR is heating resulting from the power dissipation when a large, fast-rising pulse current flows. Above a certain temperature, the resistivity of the semiconductor material increases with increasing temperature. The pulse current with its associated transient conducting drop, causes heating within the device during a conduction pulse, which has the effect of increasing the conducting drop.

3. Turn-Off Phenomena In The RSR

The turn-off time of an RSR is defined as the interval between the occurrence of the forward pulse current zero crossing and the instant forward voltage is re-applied. This definition of turn-off time is illustrated in Figure 4 which shows photographs of RSR current and voltage during a turn-off time measurement. The upper trace is that of RSR current including a short, high peak current pulse. The beginning of the turn-off interval is defined by the zero crossing marking the end of the conduction current pulse. The lower trace is RSR voltage which is quite low during the conduction current interval. For some time following the current zero crossing, device voltage is zero owing to the nature of the turn-off time test circuit used. After roughly 100 µs following the current zero, forward voltage with an exponential waveform is applied to the device. The peak rate-of-rise of voltage, or dv/dt, occurs at the instant forward voltage begins to rise. This value of dv/dt is the one generally specified as a condition of a turn-off time measurement.

Turn-off time depends among other things upon the shape and amplitude of the current pulse used, the rate-of-rise of the re-applied voltage, and device junction temperature. The conduction current pulse has two effects relating to turn-off time. It causes many carriers to be generated within the RSR which give rise to its highly conductive state, and owing to the high rate-of-rise of pulse current, it causes the junction temperature of the device to be elevated above that of the device heat sink. Following a forward current pulse, the carriers generated within the device must recombine before forward voltage may be re-applied to the device in its blocking state, but the process of carrier recombination is sensitive to the temperature of the silicon where recombination takes place. In addition to the temperature rise from junction to case due to pulse current dissipation, the junction temperature may be further elevated owing to an increase in case temperature.

The effect on turn-off time of elevated junction temperature is shown in Figure 5 where the variation of turn-off time with temperature is shown for four different RSR devices. The slopes of the curves for each of the devices are quite similar, and in general, turn-off time roughly doubles as junction temperature increases from 25°C to 100°C.

Turn-off time increases roughly linearly with peak pulse current and increases with increasing rate-of-rise of pulse current as well. The principal reason for this variation is that the dissipation which occurs during a pulse causes an abrupt increase in temperature which dissipates following each pulse. However, the time constant of the decay of this temperature transient is comparable to device turn-off time. As was mentioned earlier, because carrier recombination is a temperature sensitive process, turn-off time therefore increases with increasing pulse dissipation. As a result of these considerations, device turn-off time is quite intimately related to the pulse repetition frequency of the pulse modulator.

The end of the turn-off time interval is marked by the instant when forward voltage is again re-applied to the RSR. The length of this interval is dependent upon the rate-of-rise of re-applied forward voltage as shown in Figure 6. For a given value of dv/dt, turn-off time increases with increasing ambient temperature and visa versa. All of the data shown in Figure 6 was obtained using a forward current pulse of fixed amplitude and duration.

All of the turn-off time data presented in this section was obtained using circuitry which impressed upon the device under test voltages and currents of the form shown in Figure 4, where, during the turn-off interval between forward current zero and the initiation of forward dv/dt, no bias of either forward or reverse polarity was impressed. In some circuits, pulse current reverses following the forward current zero and tends to sweep out the previously conducting device. For some brief interval following the forward current zero, reverse current can flow while negligible voltage appears across the device. However, when all of the excess stored charged is removed from the device by the flow of reverse current, the reverse blocking junction recovers and attempts to stop the flow of reverse current. The reverse voltage which appears across the device at the instant the reverse blocking junction recovers can be quite high owing to the type of circuit used and the amount of distributed inductance in the discharge loop. Caution must be exercised in the application of the RSR when reverse voltage transients of this type can be generated, otherwise the device may be destroyed by an overvoltage. Typical failure levels are 200 volts V_R and 50 amperes I_R.

In general, the RSR is used in modulator circuits which employ dc resonant charging to charge a pulse forming network to a desired voltage. When command charge is used, it is desirable to delay the onset of a charge cycle following a pulse of conduction current until an interval at least equal to the device turn-off time has elapsed. In circuits where command charge is not available, a mismatch in the pulse network discharge circuitry can be arranged so that a slightly negative voltage appears on the pulse network following the end of a conduction pulse. The action of the resonant charge circuit with the residual negative voltage of the pulse network can be used to keep the RSR voltage negative for an interval equal to device turn-off time following the end of a conduction pulse.

4. Switching Performance In A Typical Pulse Modulator

A simple pulse modulator circuit illustrating the use of series connected RSR's to generate a short pulse by discharging a pulse forming network is shown in Figure 7. The pulse network is charged to a high dc voltage by the dc power supply and dc resonant charging components L1 and D6. When the pulse network becomes charged, it remains at its dc charge voltage until a pulse is applied to the primary of transformer T1. The rate-of-rise of the pulse voltage at the secondary of transformer T1 must exceed 5000 V/usec.

Prior to the introduction of a trigger pulse at T1, the charge voltage of the pulse network is impressed upon the two RSR's in series. The resistors connected in parallel with the RSR's assure equal voltage division between the two. Although only two RSR's are shown in the diagram, each one may in reality be a series connection of many devices. Diode D3 prevents shorting of the voltage of RSR1 through the pulse transformer prior to triggering.

When a rapidly rising pulse of voltage is applied to the primary of transformer T1, the voltage of the node joining the RSR's rises when the pulse voltage at the secondary of T1 exceeds the voltage applied to the common node of the RSR's by the charged pulse network. The rapidly rising forward voltage thus applied to RSR1 gives rise to a large internal capacitive current initiating turn-on as discussed in Section 2. The rapid fall of voltage which then occurs as RSR1 turns on, appears as a rapidly rising voltage across RSR2, causing it to turn on in the same manner. At this point, both RSR's are in conduction and the pulse network is discharged into transformer T2 and ultimately into the load.

The voltage and current of RSR1 are shown in Figure 8. The voltage appearing at t = 0 is the portion of the pulse forming network charge voltage appearing across RSR1, which is well below the threshold voltage of the device. At t = 0, the pulse voltage is applied and can be seen to increase the RSR voltage beyond the contribution from the charged pulse forming network. At some point slightly after t = 0, the device breaks over, and its voltage falls very rapidly. The rapid fall in voltage is terminated at a level in excess of one hundred volts at the time that pulse current begins to flow as shown also in Figure 8. The conduction voltage of the RSR then decreases with time at a much slower rate corresponding to spreading phenomena within the device. Current continues to flow until the pulse forming network has been discharged. If the reflected load impedance is less than that of the pulse forming network, a negative voltage will remain on the pulse forming network when conduction current goes to zero. The negative voltage of the network will give rise to a reverse pulse current which flows back up through the two RSR's in the reverse direction and through diode D4 as a sweepout current. When the RSR's sweepout and begin to block voltage, the flow of sweepout current is conducted by parallel diodes D1 and D2 which prevent the build-up of reverse voltage across the RSR's. Diode D4 is selected to have a sufficiently long recovery time that it recovers and blocks voltage only after RSR's 1 and 2 have recovered. When diode D4 recovers it permits the pulse forming network to remain with a slight negative voltage from which to begin the next dc resonant charging cycle. The effect of the initial negative voltage on the pulse forming network at the beginning of a charge cycle is to provide an interval equal to RSR turn-off time without forward bias so that the devices may recover and block the flow of forward current.

The circuit shown in Figure 7 and described in this section is only one of many possible modes of operation of the RSR in a modulator. Devices may be operated in series or in parallel and triggered in ways different from the one shown. The circuit described is included primarily as an illustrative example of the basic function of the RSR as a fast switching for modulator service.

5. Summary Of The T40R Ratings

Shown in Table 1 is a brief summary of some of the ratings and characteristics of the device which are especially significant for modulator service. Repetitive peak forward blocking voltage, V_{DRM}, is the maximum rated voltage the RSR can hold off without going into conduction. Devices are available with V_{DRM} ratings of 600, 800 and 1000 V. Pulse trigger voltage, V_T, is the off-state threshold voltage where turn-on begins when a 5000 V/μs trigger pulse is applied. The maximum value of V_T for all variations of the T40R is 1500 V. The maximum rate-of-rise of current, di/dt, is the maximum rated pulse current di/dt which the device will withstand subject to the other test parameters specified for the rating. Devices are available with ratings including combinations of di/dt and peak current ranging from 2000 to 4000 A/μs and 800 and 1200 A. The maximum dynamic forward voltage drop, $V_{TM(DYN)}$, is the conducting drop measured with a current of 1000 A at an interval 4 μs after the current pulse begins. Values of $V_{TM(DYN)}$ are indicative of spreading phenomena within the device and are dependent on pulse current waveshape and amplitude. Trigger response time, t_{on}, is the voltage fall time during turn-on when only trigger current is permitted to flow. By making the measurement without load current, the effects of spreading are eliminated from the measurement. Values for t_{on} of less than 100 ns are common. The definition of turn-off time, t_q, was discussed earlier. For a re-applied dv/dt of 20 V/μs, values of t_q of 50 μs are typical at a junction temperature of 25°C.

The listing of parameters in Table 1 is very brief and includes principally typical values. Furthermore, the ambient temperature at which each of these parameters is specified must be known. The characterization of the RSR and its rating for modulator service is rather complex because of the many interrelating parameters which affect device operation. The data included here simply provides a basis for a judgement as to the possible use of the RSR in modulator circuits of specific power levels or frequencies.

The RSR is available in a type DO-5 stud-mounted encapsulation employing compression bonding which eliminates one of the failure mechanisms encountered by earlier developers by permitting the silicon-molybdenum fusion to expand and contract freely as temperature changes.

Table 1. Typical Characteristics of the T40R RSR

	Symbol	Typical Value
Repetitive peak forward blocking voltage	V_{DRM}	1000 V
Pulse trigger voltage	V_T	1200 V
Rate-of-rise of current @ 1200 A peak	di/dt	2000 A/μs
Dynamic forward voltage drop @ 4 μs	$V_{TM(DYN)}$	20 V
Trigger response time	t_{on}	100 ns
Turn-off time @ 20 V/μs	t_q	50 μs

6. Conclusions

The RSR is a semiconductor switching device especially made for modulator pulse switching applications. It offers solutions to the problems which have plagued modulators for many years, namely finite life owing to the absence of a filament, and high reliability because no glass or ceramic envelope is required. Its performance is excellent because very low time jitter is found in modulator circuits using RSR's as opposed to those using thyratron tubes where jitter is a consideration. The improved life and reliability of this device, which gives rise to improved system reliability, is an advantage which will be useful for the design of future systems.

7. References

1. Walter Schroen, Kurt Hubner, Jacques Beaudouin and R. M. Scarlett, "A New High Power Four-Layer Diode As A Pulse Modulator Switch", p 1, Wescon 1964.

2. A. Loro, "A Four Layer Protective Device For Communication System Application", p. 142, International Electron Devices Meeting, December 4, 1972.

3. Technical Report AFML-TR-72-19, February, 1972, Air Force Materials Laboratory, Air Force Systems Command, Wright-Patterson Air Force Base, Ohio.

4. R. A. Hill and W. R. Olsen, "Lightweight High Power Modulator Uses RSR Switch Devices", Tenth Modulator Symposium, May, 1968, New York, New York.

Dwg. 6214A07

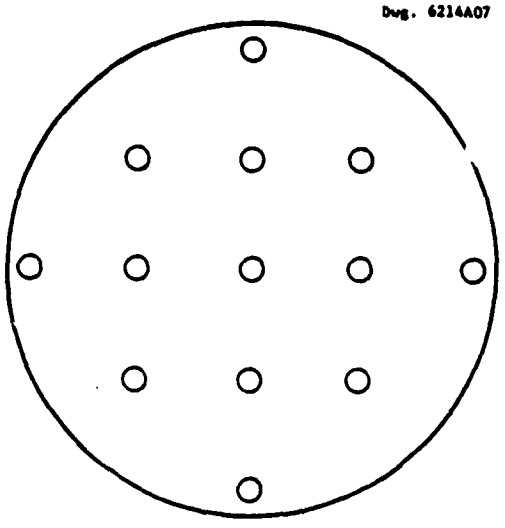

Scale, Approximately 20:1

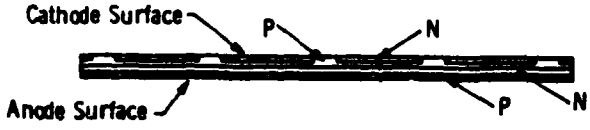

Fig. 1—RSR fusion showing location and relative size of p-type shorts

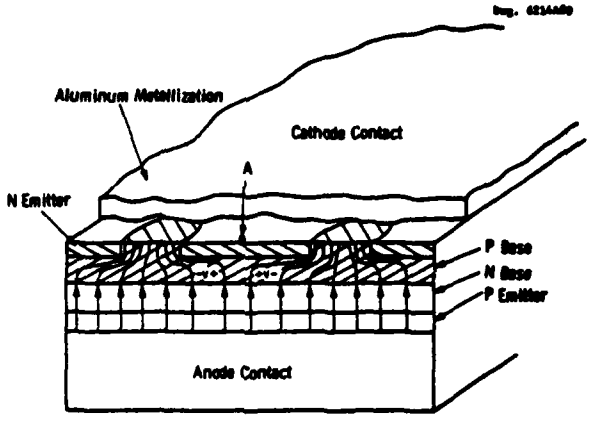

Fig. 3—Sectional view of the RSR illustrating current crowding at turn-on

Dwg. 6214A08

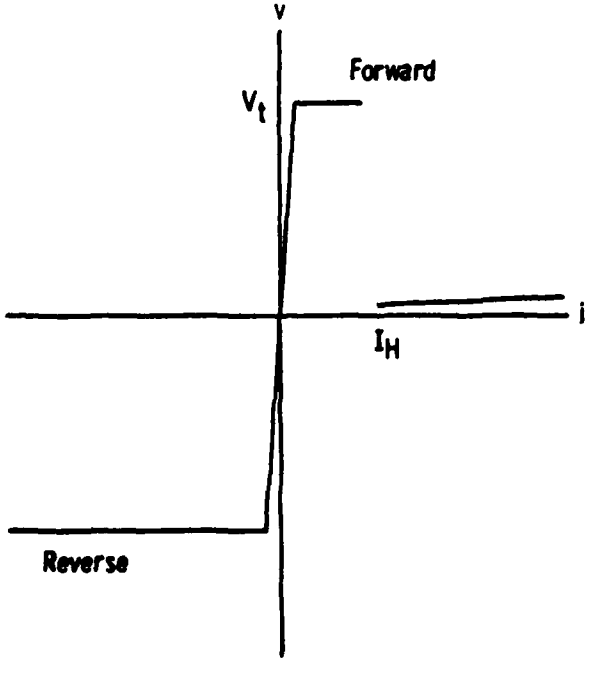

Fig. 4. RSR voltage and current display used for turn-off time measurement

Fig. 2—RSR VI characteristic

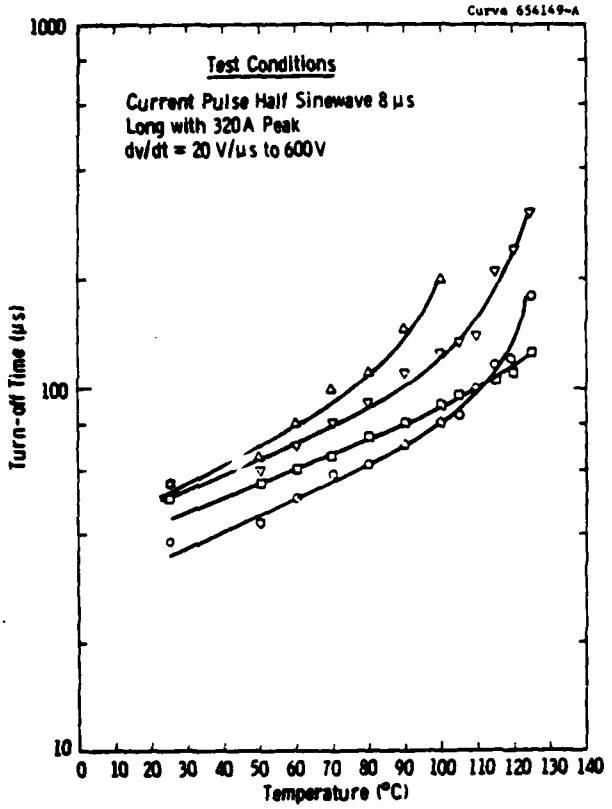

Fig. 5—Turn-off time vs. temperature for various RSR devices

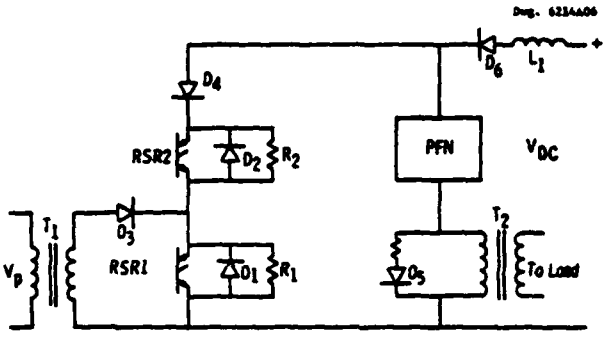

Fig. 7—Schematic diagram of typical RSR modulator circuit

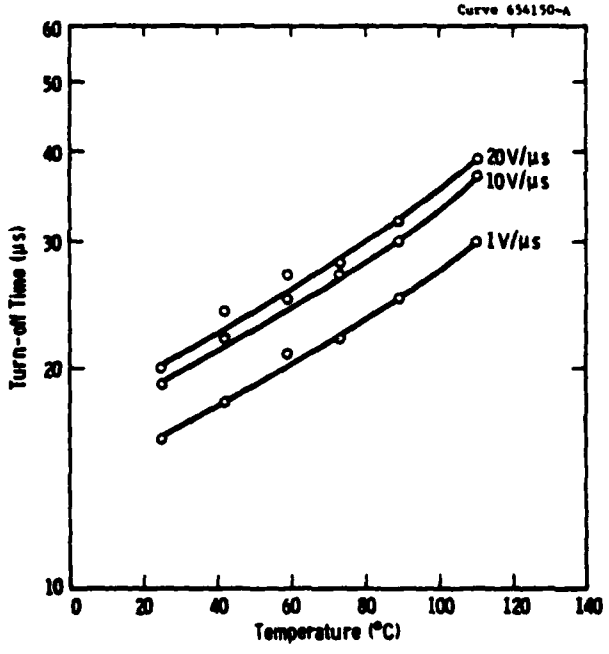

Fig. 6—RSR turn-off time vs. temperature
I_p = 100A, T_p = 11 µs, PRF = 1 Hz

Fig. 8. RSR voltage and current when functioning in a typical pulse modulator circuit

THYRISTORS FOR PULSE MODULATION AT HIGH PEAK AND AVERAGE POWERS

by

D E Crees

Hirst Research Laboratories, Wembley, England

and

N S Nicholls and F Wood

Royal Radar Establishment, Malvern, England

Summary

The design problems of a large pulse modulator thyristor for 2 KV 1 KA operation at 30 microsecond pulse length are discussed, and experimental devices are described. The performance obtained is compared with that of possible alternative devices, both solid-state and gas-discharge.

Introduction

The limited success of semi-conductor modulator devices in the medium and high power radar market seems to be the result of the high equipment cost which results from the complexities of series and parallel connection of numerous devices. This is made necessary at the present time by the limited power capability of the devices which are available.

The work to be described is an exploration of the feasibility of making a much more powerful modulator thyristor than has hitherto been achieved.

At the outset it was apparent that the current-carrying capacity of a pulse-modulator thyristor could be increased by increasing the effective area and improving the cooling Ways could be evisaged for doing this without introducing technology far outside the present state of the art, though there are a number of difficulties to be overcome. However, an increased current capability must be matched by a corresponding increase in operating voltage if an economical impedance level is to be maintained for the other components in the circuit. Because, in the conventional thyristor, there is a rapid deterioration in switching speed as the blocking voltage capability is increased, more radical innovation seemed likely to be needed to deal with this aspect.

An analysis is first given of the design problems involved in the attainment of the required characteristics. This is followed by a description of the experimental devices which have been fabricated and the results obtained. Finally, an assessment is attempted of the relative performance for a particular duty of alternative modulator switching devices, both semi-conductor and gas-discharge.

The Design of Modulator Thyristors for High Peak Currents

The basic difficulty in the design of large area devices for pulse generation is the relatively low rate of spreading of the conducting state across the cathode from its origin at the gated edge. This makes it necessary to employ an interdigitated gate and cathode structure so that a long gate-cathode edge may be accommodated without excessive device area.

The high peak anode current dictates a cathode connection of very low resistance. The best way to achieve this is by means of a pressure contact over the whole device area, so that current flow is everywhere normal to the silicon slice. The combination of this feature with an interdigitated structure presents a problem of preventing short-circuiting of the gate-cathode junction.

The overall pressure contact may be realized using the "hockey-puk" type encapsulation, which gives low stray inductance and permits double-sided cooling.

In order to ensure that the whole of a long gated cathode edge is turned on, a very large gate drive is required. In adequate gate drive could result in local overheating and even destruction of the device. By using an amplifying gate, the gate drive requirement is greatly reduced, which leads to economy in the drive circuits and allows a larger margin of safety to be provided. It would be expected that the use of an amplifying gate would restrict the range of circuit-limited rate of rise of current for which safe triggering would be obtained. Too high a value might lead to excessive dissipation in the amplifying gate region, and too low a value to only partial turn-on of the cathode edge. In fact, no difficulty has been experienced on this account in the present application with the experimental devices which have been made.

Improvement of the Speed of Turn-on of High-Voltage Thyristors

In the conventional reverse-blocking thyristor, the thickness of the N-base has to be increased disproportionately as the forward blocking voltage requirement is raised. As a consequence, the switching speed is greatly reduced, which increases power-loss in circuits giving a relatively high rate-of-rise of current.

The blocking voltage attainable with a given thickness of N-base may be substantially increased by the introduction of a heavily doped N layer between the anode P layer and the N-base. This prevents the depletion region in the forward blocking state from punching through to the anode P layer and allows a higher resistivity material to be used in the body of the N-base, in the same manner as in the PIN diode. By this means, a considerable improvement in switching speed should be obtainable, as well as reduced voltage drop in steady state conduction.

The high field strength which can be sustained with the PIN type structure gives rise to a potential problem at the edge of the device. Various approaches have been explored for dealing with this.

Another consequence of the PIN type structure is that the reverse avalanche voltage is reduced to a few tens of volts. This is considered to be not incompatible with the proposed use in a network-type pulse modulator.

Description of Experimental Devices

A large area interdigitated thyristor employing a centre amplifying gate has been designed to achieve a rating of 2 kV forward blocking voltage with a 1000 A, 30 /us trapezoidal pulse current capability at a prf of /300 pps.

Cathode area and edge length were optimised for this rating within a cathode diameter of 30 mm and the device is based on a 38 mm diameter wafer. The cathode area is 460 mm^2 and the gated cathode edge length is 320 mm with no point on the cathode more than 2 mm from the gated edge. Emitter shorts for a $\frac{dV}{dt}$ rating of 1 kV/ /us are positioned centrally in the cathode area as shown in Fig 1.

The two level gate and cathode contacts shown in Fig 2 are formed by sintered electroless nickel which is electrolitically gold plated to a thickness of approximately 4 /um to reduce the lateral resistance of the gate arms and to produce a surface suitable for a large area pressure contact to the cathode.

As an interim stage, prior to the fabrication of the N-P-NN+P structure shown in Fig 3, devices were produced by applying the interdigitated gate-cathode geometry to conventional N-P-N-P thick, high voltage vertical structure. These devices were conventionally gallium and phosphorus diffused to give N-base and P-base widths of 450-550 /um and 25-30 /um respectively, with an -base resistivity/of 150 ohm-sm/. The resulting devices clearly demonstrated the advantages of the long gated cathode edge geometry for high $\frac{dI}{dt}$, short pulse length operation.

Subsequently, 2 kV N-P-NN+P structures have been fabricated with a 120 ohm-cm -base region 220-250 /um thick and a 10 /um epitaxial N+ layer. A further,/ P-type, epitaxial layer 40 /um thick formed the anode P-emitter region.

Initially the PIN-type devices were bevelled with a 50^{o} positive bevel of the forward blocking p-n junction as shown in Fig 4, but blocking voltages were limited to 1.3-1.5 kV maximum. Later devices were negatively bevelled at $2.5\text{-}3^{o}$ as shown in Fig 5, and blocking voltages of up to 2 kV were achieved after silicone rubber passivation of the bevelled surface.

Performance of the Experimental Devices

The proper functioning of the amplifying gate system was checked by mapping thermal radiation from a device during pulse operation. Fig 6 shows the radiation pattern corresponding to a narrow (1°C) range of temperature a few degrees above ambient. It was observed on an NPNP structure of 550 /uM base thickness operating at 1.3 Kv 1 KA 1 KA/ /us 30 /usec 10 pps, and it reveals that conduction is reasonably well distributed over the whole of the cathode edge.

The anode current and voltage drop of the thyristors were measured using the arrangement shown in Fig 7. After recording the current waveform, the voltage drop was recorded in a succession of exposures taken with the oscilloscope shift voltage increased in steps. The type of result is illustrated in Fig 8. The error in voltage measurement is believed to be a fraction of a volt. Time calibration was carried out separately using calibrated delay cables. The device loss was calculated by numerical integration.

The results obtained on devices manufactured at three stages of the project are summarised in the following table. All devices had the final "horizontal" structure with the amplifying gate. They differed in the vertical direction, representing successive steps in the progression to the PIN type which was the objective.

All the devices were assessed at approximately 2 KV, 1 KA, 30 /usec pulse length, the results having been corrected/to this condition to facilitate comparison.

The rate of rise of current was mainly circuit-limited but was different in each case, being a value which roughly gives equal contributions from the loss during turn-on and during the body of the pulse. The results are shown in Table 1.

The advantage of the PIN-type from the point of view of power loss is apparent. It has the drawback of requiring protection from inverse voltage. There may be merit in integrating a diode for this purpose with the thyristor; as has been been described by Oka and Gamo[1].

Comparison of the PIN-type Thyristor with alternative Switching Devices

Comparison of the PIN thyristor with competing switching devices must take account of a wide variety of features.

The easiest aspect to quantify is power-loss, and this is attempted in the table 2.

This shows that the PIN-type thyristor is the only device offering a significant reduction in the cooling load. The higher envelope temperature permissible for a thyratron adds little convenience because other components must generally be kept much cooler.

The turn-off times have not been discussed because the value called for by the application (about 30 /usec) is not considered very difficult to meet with any/of the devices.

Perhaps more serious considerations are reliability and the cost of auxiliary circuits required, such as for triggering. Here, the thyristors seem to offer the most favourable solution. The thyratron has the advantage of not being vulnerable to trigger-circuit faults.

Conclusions

It is concluded that the well established thyratron will not be displaced from this particular field of applic-tion until the high-voltage PIN-type thyristor with amplifying gate has bee fully developed and proven reliable.

Reference 1 Electrical characteristics of High-Voltage, High-Power, Fast-Switching, Reverse-Conducting Thyristor and its Applications for Chopper Use.

Hisao Oka and Hiroshi Gamo, IEEE Transactions on Industry Applications, Vol 1A-9, No 2, March/April 1973.

TABLE 1

Experimental 2KV 1 KA 30 /usec Thyristors

Type of Device	Reverse Blocking	Reverse Blocking	PIN-type
N-base thickness /uM	550	450	240
di/dt, KA/ /usec	0.4	2.2	3.5
Total energy loss per pulse, J	0.91	0.48	0.24
Reverse blocking capability, V	2000	2000	25

TABLE 2

Approximate comparison of power losses for alternative switching devices operating at 1 MW peak, 30 /usec pulses at 330 PPS

Type of Device	Deuterium Thyratron	Reverse-Blocking Thyristor	RSR T4DR0822 (3 off)	PIN-type Thyristor
Operating voltage KV	20	2	2.2	2
Operating current KA	0.1	1	0.9	1
Anode current loss W	80	160	160	80
Heaters, etc loss W	80	-	-	-
Total power loss W	160	160	160	80

n-p-nn⁺-p STRUCTURE WITH INTERDIGITATED GATE TO CATHODE GEOMETRY.

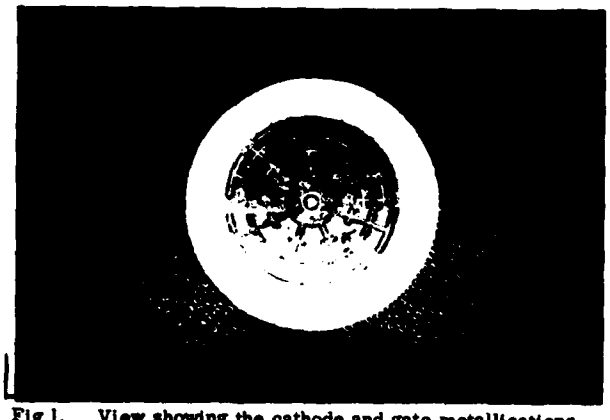

Fig 1. View showing the cathode and gate metallisations and emitter-shorts.

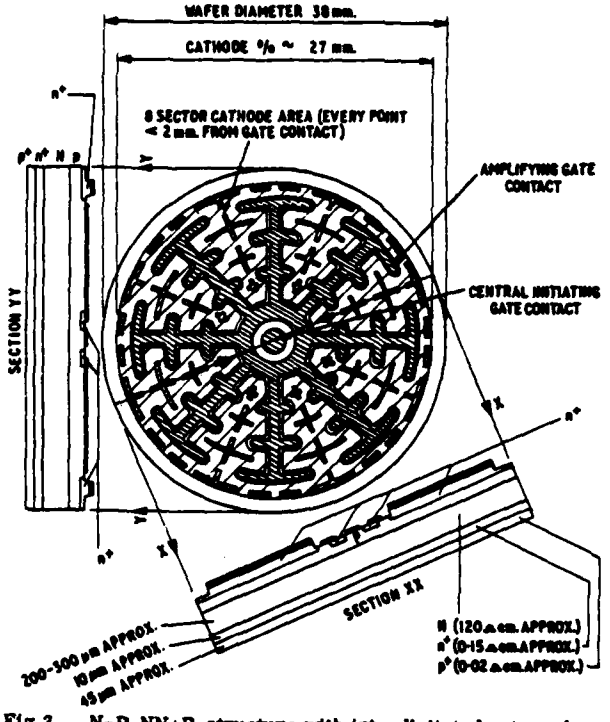

Fig 3. N-P-NN+P structure with interdigitated gate and cathode geometry.

SCHEMATIC SECTION THROUGH AMPLIFYING GATE FINGER SHOWING TWO LEVEL GATE AND CATHODE CONTACTING SYSTEM

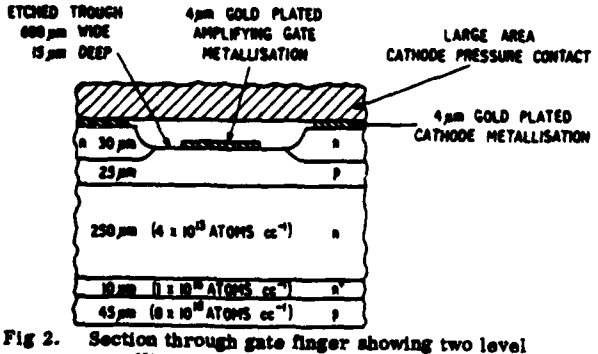

Fig 2. Section through gate finger showing two level metallisation with pressure contact to cathode.

VOLTAGE DISTRIBUTION IN A n-p-nn⁺-p THYRISTOR WITH A POSITIVE BEVEL OF THE p-n JUNCTION

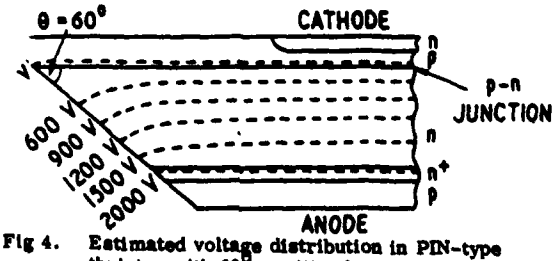

Fig 4. Estimated voltage distribution in PIN-type thristor with 60° positive bevel.

VOLTAGE DISTRIBUTION IN A n-p-nn$^+$-p THYRISTOR WITH A SHALLOW NEGATIVE BEVEL OF THE p-n JUNCTION

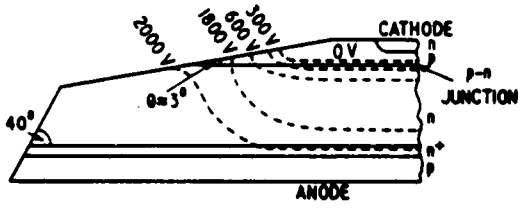

Fig 5. Estimated voltage distribution in PIN-type thyristor with 3° negative bevel of P-N junction.

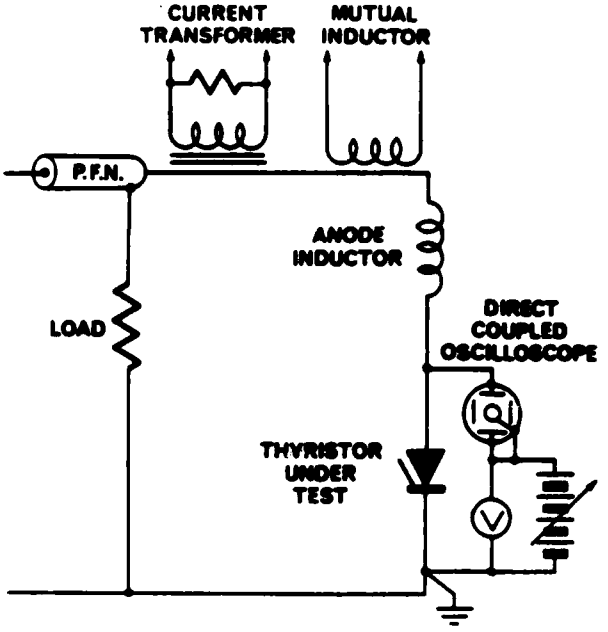

Fig 7. Circuit for measurement of voltage-drop.

Fig 6. Distribution of thermal radiation from operating thyristor.

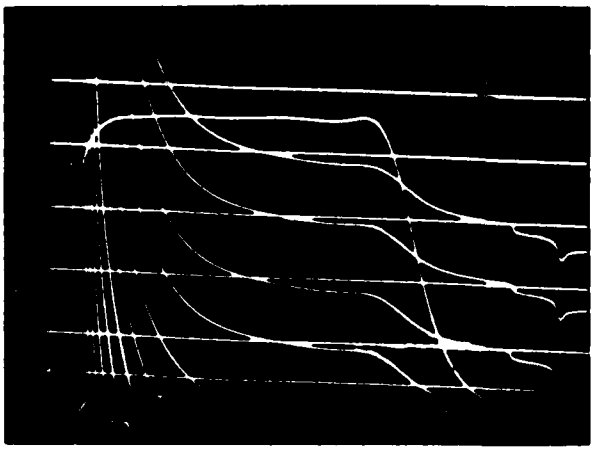

Fig 8. Typical measurement record showing voltage-drop against time with current superimposed.

CHARACTERISTICS AND CAPABILITIES OF THE MODULATOR EBS

R. I. Knight
D. J. Bates

of

Watkins-Johnson Company
3333 Hillview Avenue
Palo Alto, California

Summary

EBS (Electron Bombarded Semiconductor) devices have been designed, tested and are now available for use in a wide range of power modulation applications. Current multiplication due to electron beam illumination of a semiconductor diode results in risetimes and delay times of a few nanoseconds, on-off ratios of 10^5 or more and the ability to provide multiple or coded output pulses. EBS devices have been tested which can provide up to 400 V output pulses with less than a 3 ns risetime and an EBS device designed for high current operation has been used to produce pulses of 250 A with a 1 ns risetime. EBS devices available at the present time can be used for CRT modulation, for the modulation of injection lasers and as TWT grid modulators.

Theory of Operation

EBS devices have been developed for use in a wide range of power modulation applications. As shown in Fig. 1, an EBS device consists of an electron gun; an input structure, such as a grid or beam deflection structure; one or more reverse biased semiconductor diodes and external bias and load circuitry. The electron beam is accelerated to 10 - 20 keV in the electron gun region. When this high energy electron beam strikes the semiconductor diode, the beam current is amplified by 1500 to 4000 times due to carrier multiplication within the diode. This amplified current then flows in the external load circuit.

The amplification mechanism in the diode results from the creation of multiple electron-hole pairs by each incident high energy electron, as shown in Fig. 2. After losing approximately 4000 eV of energy in passing through the top metallization of the diode, these incident electrons interact with the semiconductor lattice to produce one electron-hole carrier pair for each 3.6 eV of residual beam energy. For a 10 keV incident electron beam this process produces a current multiplication of approximately 1600. The production of carrier pairs occurs within the first few microns of the semiconductor diode and the carriers are then separated by the high electric field in the reverse biased diode. For a diode consisting of a thin p-type top layer as shown in Fig. 2 the holes immediately return to the top contact. The electrons drift under the influence of the electric field to the back contact of the diode, and in this process current flows in the external circuit causing a voltage to be developed across the load resistance. As long as the electric field within the diode is kept above 15 kV/cm the electrons all move with essentially the same velocity and the device behaves as a linear amplifier. When a diode is properly designed, the voltage drop across the diode in the illuminated state may be only 10 to 15 percent of the bias voltage. An EBS of this type may operate at target efficiencies of 85 - 90 percent.

The output risetime for EBS devices used in modulator applications is determined by the risetime of the input signal and by the RC time constant of the diode and external load circuitry. Assuming the input risetime is negligible, the 10 to 90 percent risetime of the EBS output signal is given by:

$$t_r\,(10\% - 90\%) = 2.2\,R_L\,(C_{DIODE} + C_{EXT}) \qquad (1)$$

where R_L is the external load resistance, C_{DIODE} is the capacitance of the semiconductor diode and C_{EXT} is the capacitance of any external load.

Voltage Modulation: WJ-3653

The WJ-3653, shown in Fig. 3, is a grid controlled, convection cooled EBS which can produce output currents of 3.5 to 4.0 A into a 100 ohm load. A summary of the performance characteristics of the WJ-3653 is given in Table I.

Table I
Characteristics of the WJ-3653

Performance Characteristics	
Peak Output Voltage	350 - 400 V
Peak Output Current	3.5 - 4.0 A
Pulse Risetime (10%-90%) with 100 ohm load	3 ns
Pulse Risetime (10%-90%) with 100 ohm load shunted by 30 pF	10 ns
Duty Cycle (100 ohm load)	4 %
Delay (10%-10%, 100 ohm load)	< 2 ns
Electrical Requirements	
Cathode Voltage	-10 to -14 kV
Cathode Current	20 mA peak
Grid Bias (Ref. to cathode)	-6.5 V
Grid Pulse (Ref. to Grid Bias)	+15 V
Grid Current	5 mA peak
Target Bias	460 V
Target Current	3.5 - 4.0 peak
Heater Voltage	3.5 V
Heater Current	0.9 A

As a modulator, the unique features of the WJ-3653 are the fast output risetime, short signal delay time, 350 - 400 V output capability and the ability to provide variable pulse width and closely spaced pulses. A high degree of flexibility in multiple pulse applications is available because the WJ-3653 operates as a pulse amplifier and the pulse duration and amplitude may be controlled on a pulse by pulse basis.

A typical application for the WJ-3653 is shown in Fig. 4. In this circuit the EBS is being used to grid modulate a high

power traveling-wave tube. As a TWT modulator, particularly for ECM applications, the WJ-3653 can be used to obtain fast TWT turn-on with a signal delay, from the 10 percent point of the input applied to the EBS to the 90 percent point of the TWT grid turn-on pulse, of less than 15 ns. Fig. 4 shows the detected RF output pulse obtained from a TWT when a modulation pulse was applied to the EBS. During this test the delay through the EBS, including risetime, was approximately 14 ns.

The circuit shown in Fig. 4 provides capacitive coupling between the EBS and TWT and permits operating the TWT and EBS from a common high voltage power supply. For short pulse operation the capacitive coupling network could be replaced by transformer coupling. For long pulse operation the capacitive coupling circuit has the disadvantage of storing a large amount of energy between the EBS and the TWT. If it is desired to reduce the stored energy, the EBS may be directly coupled to the TWT by the addition of a separate high voltage supply for the EBS. An additional advantage of direct coupling between the EBS and TWT is a reduction in the circuitry connecting the EBS load and the TWT. Simplification of the coupling circuitry will typically result in improved modulator performance due to the elimination of stray capacitance and inductance associated with the high voltage coupling capacitors, and will result in improved risetime, reduced signal delay time and reduced pulse ringing.

The performance of the WJ-3653 as a TWT grid modulator has been briefly summarized. Other applications in which the WJ-3653, or higher voltage versions of this EBS, may be useful are in pulsing Pockel effect electro-optic modulators, modulating series strings of impatt diodes or for modulating a linear accelerator beam chopper.

In some of these applications it will be necessary to modulate a primarily capacitive load. The use of two WJ-3653's in the pull-up/pull-down configuration shown in Fig. 5 results in a higher duty cycle capability, higher repetition rates and improved modulator efficiency. In this circuit switching is accomplished by illuminating the diode connected to the desired output bias level. When illuminated, the diode will permit a large current to flow from the bias supply into the capacitive load until the load charges to the diode bias level. After the load has reached the charged state, the only current passing through the diode will be small leakage currents, typically 10^{-5} times the size of the peak diode currents. The switching time for a pull-up/pull-down circuit of this type is given approximately by:

$$t_r\ (10\%\text{-}90\%) = .8\ (C_{EXT} + 2C_{DIODE}) / I_o \qquad (2)$$

When operated as a pull-up/pull-down modulator either output voltage may be maintained on a continuous basis with very little modulator dissipation. The modulator dissipation limit will be determined by the size of the capacitive load and by the pulse repetition frequency.

Current Modulation: WJ-3652

EBS devices can be designed for modulation applications over a wide range of impedance and power levels. The WJ-3653, described in the previous section, is designed for operation into a 100 ohm load with a peak output power of approximately 1.6 kW. Also, two of these devices can be operated in a complementary pull-up/pull-down circuit to provide high efficiency modulation of capacitive or high impedance loads.

The WJ-3652 EBS, shown in Fig. 6, has been designed for operation into low impedance loads. This device contains a large semiconductor target which can deliver peak currents in excess of 100 A into a 1 ohm load and currents up to 250 A into a .1 ohm load. These output pulses can be produced with risetimes of 3 ns and 1 ns, respectively. The performance characteristics of the WJ-3652 are summarized in Table II.

Table II
Characteristics of the WJ-3652

Performance Characteristics	
Peak Output Current (1 ohm load)	100 A
Peak Output Voltage (1 ohm load)	100 V
Pulse Risetime (10%-90%) with 1 ohm load	3 ns
Duty Cycle	0.1 %
Electrical Requirements	
Cathode Voltage	10 - 12 kV
Cathode Current	100 mA peak
Grid bias (Ref. to cathode)	-6.5 V
Grid Pulse (Ref. to grid bias)	15 V
Target Bias	130 V
Target Current	100 A peak
Heater Voltage	10 V
Heater Current	1 A

The WJ-3652 was developed as a modulator for semiconductor injection lasers. These lasers typically require peak currents of 20 - 100 A and, for reliable operation, pulse widths must often be limited to less than 100 ns to prevent damage to the laser. In many applications these lasers can be satisfactorily modulated with SCR's. SCR modulators, however, have typical risetimes of 30 ns at the 100 A level and these modulators have limited ability to provide fast risetime, closely spaced pulses.

The fast risetime, high current capability of the WJ-3652 EBS provides the capability for modulating injection lasers in a considerably more versatile manner. In tests performed at the Army Electronics Command, Fort Monmouth, the WJ-3652 was used to modulate an injection laser with a resulting optical output risetime of less than 2 ns. The fast risetime pulse produced by the WJ-3652 also results in more efficient modulator performance since a specified amount of optical output power can be produced with reduced power dissipation in the laser diode.

A typical circuit for modulating an injection laser is shown in Fig. 7. In this circuit the output current from the EBS diode is directly coupled into the injection laser. The diode in parallel with the injection laser provides clipping for any ringing which might damage the laser diode. In this circuit the WJ-3652 acts as a pulse amplifier and can be used to provide a sequence of closely spaced pulses which can be controlled on a pulse-by-pulse basis to provide time or amplitude coding of the injection laser output.

Figure 8 shows an 80 A output pulse from a WJ-3652 into a .5 ohm load. Design improvements presently under way will result in increased output capability for the WJ-3652 and will result in an output capability of up to 350 A into an 0.5 ohm load with a risetime of less than 2 ns.

High Bit Rate Modulation: WJ-3650

Deflected beam EBS devices of the type shown in Fig. 9 can be used to provide high bit rate modulation. The deflected beam EBS consists of two reverse biased semiconductor diodes connected to a common load. When a positive input signal is applied to the beam deflection structure the beam position is shifted to illuminate the diode connected to the positive bias supply. The amplified current which results is proportional to the amount of beam deflection and this current flows through the external load producing a positive output signal. A negative input signal produces an amplified negative output signal in the same manner.

The WJ-3650 deflected beam EBS, shown in Fig. 10, can be operated at output levels up to ± 125 V with pulse rise and fall times of 1.5 ns. This EBS can be operated at up to 5 percent duty with conduction cooling and CW operation is possible if water cooling is utilized. The operating characteristics of the WJ-3650 are summarized in Table III.

Table III
Characteristics of the WJ-3650

Performance Characteristics	
Output Voltage	± 125 V
Output Current	± 2.5 A
Output Risetime	1.5 ns
Load Impedance	50 ohms
Duty Factor	5% conduction cooled, CW water cooled
Electrical Requirements	
Heater Voltage ac	5.0 V
Heater Current	0.8 A
Cathode Voltage	-15 kV
Cathode Current	3 mA
Grid Bias Voltage[1]	-150 V
Grid Pulse Voltage (peak)[2]	135 V
Grid Current	<5 μA
Anode 1 Voltage[1]	1000 V
Anode 1 Current	<5 μA
Anode 2 Voltage[1]	1500 volts
Anode 2 Current	<5 μA
Target 1 Voltage	+200 V
Target 2 Voltage	-200 V
Targets 1 and 2 Current (peak)	2.5 A

[1] Reference to cathode.

[2] Reference to grid bias.

The input pulse required for full output is only ±7 V. In the deflected beam EBS this input pulse is applied to an input structure at the same potential as the output load. This arrangement is sometimes more convenient than having the input and output voltage levels separated as required in the grid controlled devices.

Figure 11 shows an output pulse from a WJ-3650. This pulse was obtained by operating the tube at maximum positive output voltage and deflecting the beam, with an input signal, onto the negatively biased diode. The resulting output pulse has an amplitude of 200 V and a risetime of 1.5 ns. It is anticipated that the WJ-3650, as well as higher voltage and faster risetime derivatives of this device, will be used as high bit rate pulsers for electro-optic modulators and as high speed CRT modulators. The WJ-3650 has also been utilized in designs for a beam chopper for use with a linear accelerator.

Life and Reliability

While no comprehensive statistical evaluation of the life and reliability of EBS devices has been made, several life tests are being conducted at the present time. A life test under the sponsorship of the Office of Naval Research is being conducted on two WJ-3650's operating under CW conditions. Both of the devices have been operating for over 5000 hours at the present time. A high peak power life test is being conducted under the sponsorship of the Naval Electronics Systems Command. During this life test four WJ-3653's are being operated at 1.2 to 1.6 kW peak output and 4 percent duty. At the present time these devices have been operating for periods ranging from 300 to 1200 hours. These life test results, combined with the current densities and low cathode loading required in EBS devices have resulted in a projected life of well over 10,000 hours for conservatively designed EBS devices.

The three EBS devices described are the first commercially available EBS devices suitable for power modulation applications. These devices can presently provide output voltages of up to 400 V at 4 A, output currents of greater than 100 A at 100 V, and pulses of ± 100 V with a 1 ns switching time.

During the next year it is anticipated that the output capabilities of these devices will be increased. Development work presently underway will increase the output voltage available from EBS devices to 1000 V at 10 A and modifications to the WJ-3652 will increase the available output current to greater than 300 A at 150 V. It is anticipated that high bit rate modulators will become available within the next one to two years capable of up to one gigabit data rates.

Conclusions

The performance characteristics and capabilities of three EBS devices have been presented. These devices have unique capabilities for modulating voltages and currents with short signal delays and fast risetimes and they can also be used to generate output pulse trains. These pulse trains can be coded on a pulse-by-pulse basis in either time or pulse amplitude. These EBS devices are suitable for use as TWT grid pulsers, pulsers for electro-optical modulators and for pulsing injection lasers. As additional application areas are identified the voltage, current and risetime capabilities of these EBS devices will be extended to provide modulation capabilities over even wider ranges of voltage, current, power and impedance level.

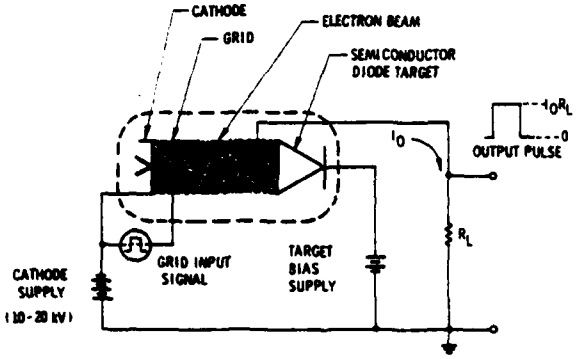

Fig. 1 - Schematic showing the elements of an EBS device. An input signal applied to the grid of the EBS controls an amplified signal in the external load circuit.

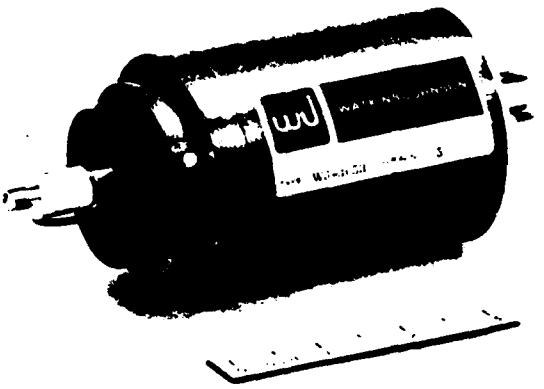

Fig. 3 - WJ-3653, Voltage Modulator EBS

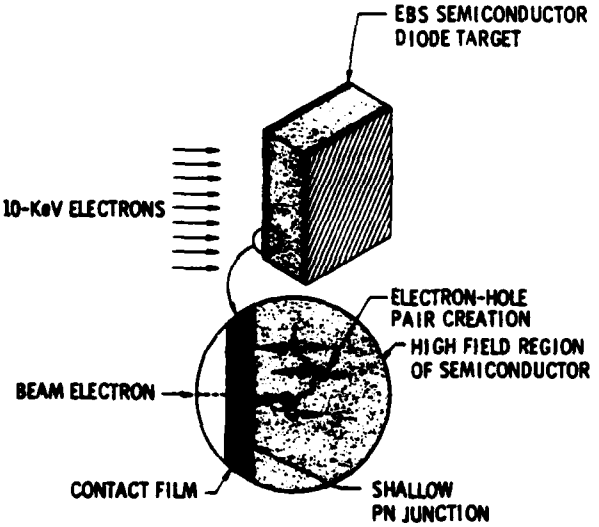

Fig. 2 - Electrons in the incident beam penetrate the diode surface contact with considerable energy. This high energy is dissipated in the formation of electron-hole pairs within the semiconductor.

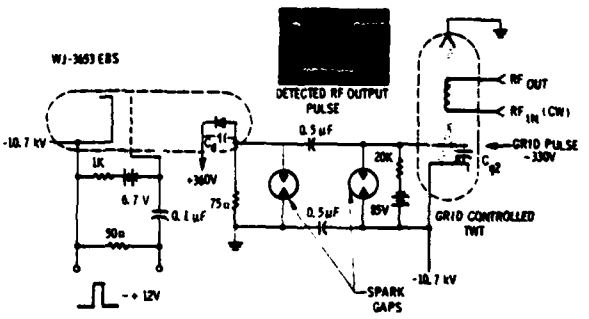

Fig. 4 - Circuit diagram illustrating capacitive coupling between the modulator EBS and grid controlled TWT.

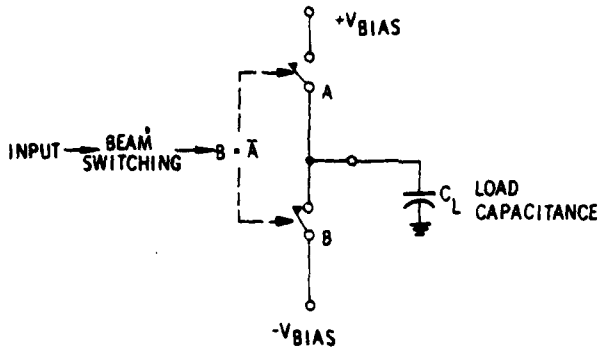

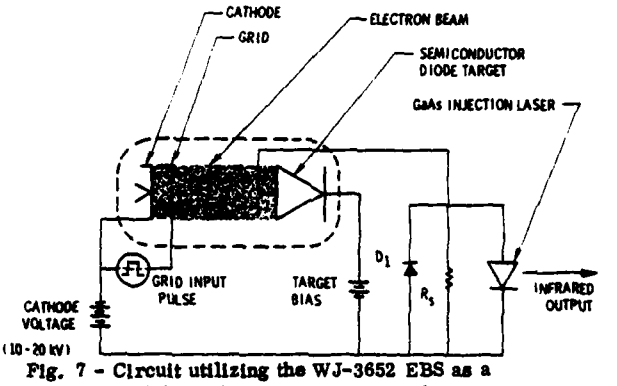

Fig. 7 - Circuit utilizing the WJ-3652 EBS as a modulator for a GaAs injection laser.

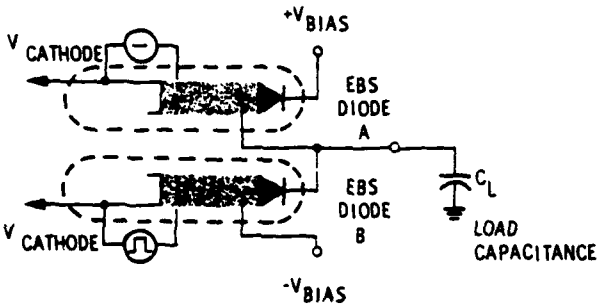

Fig. 5a- Switch representation of a pull-up/pull-down circuit. Switches A and B are used to charge the load capacitance.

Fig. 5b- Schematic showing EBS pull-up/pull-down circuit equivalent to Fig. 5a.

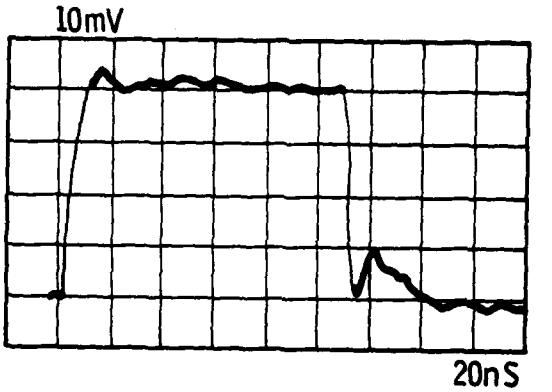

Fig. 8 - Output pulse from a WJ-3652 Current Modulator EBS. Vertical scale: 20A/div. Time base: 20ns/div.

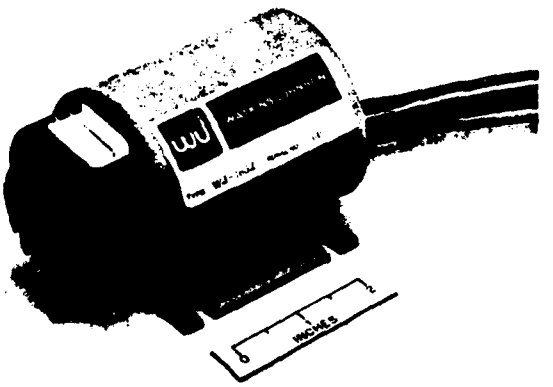

Fig. 6 - WJ-3652, Current Modulator EBS

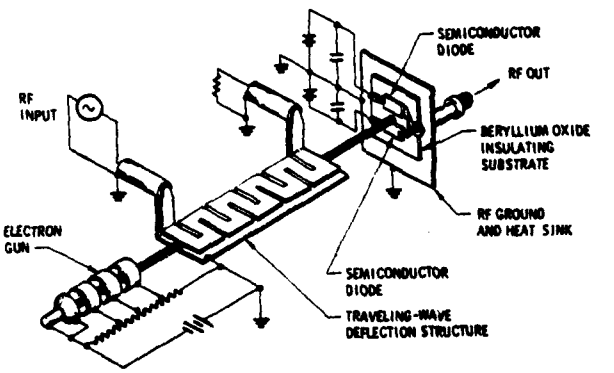

Fig. 9 - Schematic layout of a WJ-3650 deflected beam EBS.

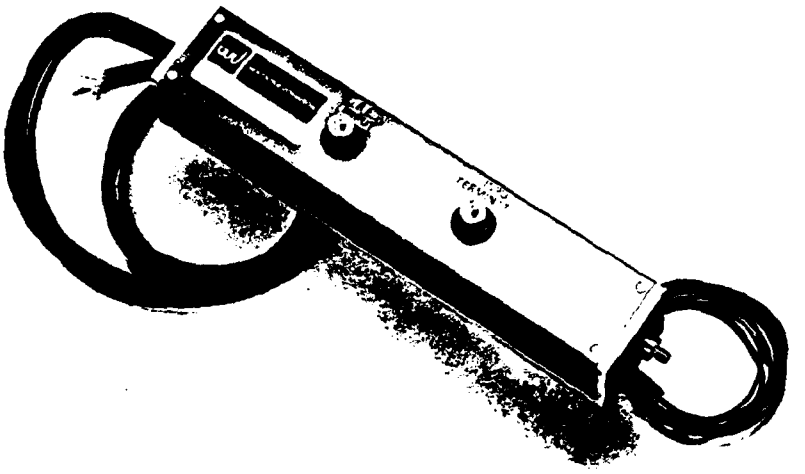

8478-2

Fig. 10- WJ-3650, Video Amplifier

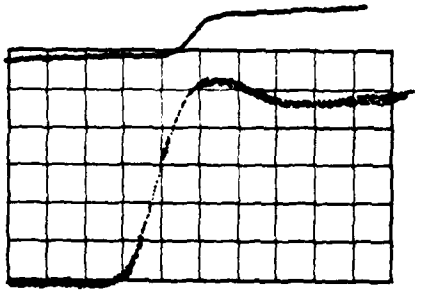

Fig. 11- The top trace is the input signal to WJ-3650. The vertical scale is 10V/div. The lower trace is the WJ-3650 output pulse. The vertical scale is -40V/div. and the time base is 1ns/div.

GENERATION OF HIGH CURRENT, LONG DURATION RECTANGULAR PULSES

P.E. Faugeras, H. Kuhn, J.P. Zanasco

CERN Laboratory II, Prévessin (FRANCE), F-016131 CERN Cedex

Summary. The excitation of the fast pulsed kicker magnets foreseen for the CERN 400 GeV proton synchrotron requires rectangular pulses with a current amplitude of 3000 A to 10 000 A, a pulse duration adjustable between 1 and 24 μsec, and short rise and fall times. These pulses are generated by a LC ladder network discharged with fast switches. Several kinds of switches have been tested : multigap thyratrons of standard design, a composite switch called "thyragnitron" and made of a normal thyratron by-passed by ignitrons, and finally special thyratrons with a second cathode assembly in place of the usual anode. Experimental pulse shapes and results of life tests for these different switches are presented and discussed.

Introduction

Several fast pulsed kicker magnet systems will be used for the injection, the fast extraction and the dumping of the proton beams of the 400 GeV proton synchrotron (SPS) which is being built by CERN [1]. In order to have a magnetic field with a sufficiently short rise and fall time each kicker system must be split into several identical magnet modules, each of them being powered by its own pulse generator. The characteristics and performances of the three systems will not be discussed in this paper, but Table I summarizes the requirements on the current pulses which are needed to excite each module of these different kicker magnet systems.

Table I

Characteristics of the different current pulses

System	Injection	Fast Extraction	Beam Dumping
Number of modules	2	4	2
Impedance	7.5 Ω	10.0 Ω	3.0 Ω
Maximum pulse current	4 000 A	3 000 A	10 000 A
Pulse duration	23.2 μs	1.0-24.0 μs	24.0 μs
Rise time	< 0.2μs	< 0.2 μs	< 0.3 μs
Fall time	< 0.3μs	< 0.3 μs	-

All the system impedances were chosen such that the maximum charging voltage of the pulse generator is limited to 60 kV, which means a pulse amplitude of 30kV max. From previous experience it is expected that these voltage values will avoid high voltage problems for the kicker magnets as well as for the pulse generators. The planned pulse repetition rate is of the order of 1 pulse per 4 seconds, except for the fast extraction which requires 3 pulses, 100 ms apart, within a period of 4 seconds.

Such high current, long duration pulses have never been obtained before hand. Therefore a pulse generator prototype has been built in order to test switches capable of passing these required amounts of charge with a reasonable lifetime.

The experimental set-up

A characteristic impedance of $Z_c = 7.5\ \Omega$ was chosen for the pulse generator prototype. This is the impedance of the inflector system, which is the first one needed for the SPS. The results described in this paper can be used directly for the fast extraction system and, to a lesser extent, for the beam dumping system. This latter system requires a higher current and a particular pulse shape, i.e. oscillations superimposed on the flat top of the pulse, while the fall time is unimportant [2].

The pulse generator

The principle of the pulse generator is shown in fig. 1. A DC power supply charges the pulse forming network (PFN) to a maximum voltage of 60 kV. Then the PFN is discharged by power switches through a transmission line into a matched terminating resistor. The transmission line is 120 m long and made of two 15Ω coaxial cables in parallel. Such a transmission line will be necessary for the final systems, as each pulse generator will be located at a distance of about 150 m from its magnet. The magnet, which is normally placed between the transmission line and the resistive load, has not been used for the tests reported here.

The pulse forming network could not be made of cables, as it was done for other kicker systems [3]. Such a PFN would need four 30 Ω cables in parallel, of a length of 2.4 km each. Even with an outer diameter of 50 mm, these cables would have an attenuation of the order of 0.5 dB/100 m, which means that the pulse would exhibit about 10% droop on its flat top, which is not acceptable. In addition this kind of PFN would be very expensive. Therefore a PFN with lumped elements has been chosen.

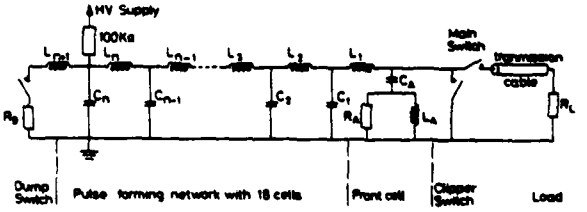

$L_1 = L_{n+1} = L_A = 6.2\ \mu H$ $\quad L_2 = 5.2\ \mu H$ $\quad L_3 = \dots = L_{n-1} = L_n = 6.63\ \mu H$

$C_1 = C_2 = \dots = C_n = 0.1\ \mu F$ $\quad C_A = 0.05\ \mu F$ $\quad R_A = R_B = R_L = 7.5\ \Omega$

FIG 1 : ELECTRICAL CIRCUIT OF THE PULSE GENERATOR

The theoretical response of a LC-ladder PFN with 18 equal cells has been published previously [4]. It has also been shown that in order to get a fast fall time and an adjustable pulse length, three switches, called main, dump and clipper switches, are necessary as indicated on fig. 1.

The 18 cells of the PFN and the front matching cell which gives the fast rise, are assembled in a large tank of 4.0 m x 1.5 m x 0.8 m, filled with mineral oil (see fig. 2). The three switches are gathered in a

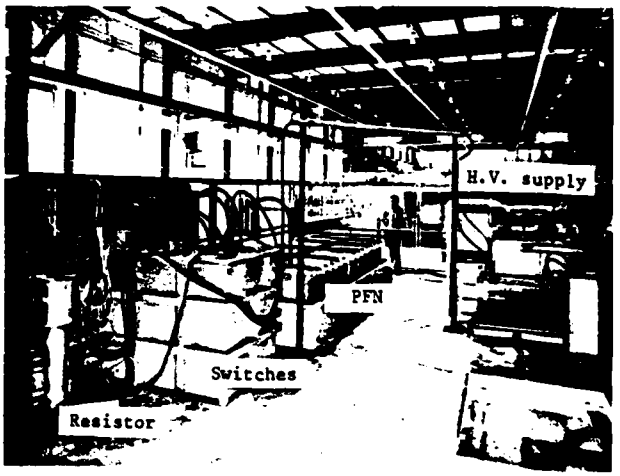

Fig. 2 Overall view of the pulse generator

separate tank, also filled with mineral oil, which is shown in front of the PFN tank on fig. 2. The two tanks are linked with two sets of two 15 Ω cables in parallel. Although this arrangement deteriorates slightly the rising edge of the pulse, it has proven to be very flexible for testing different types of switches.

The load resistor and the dump resistor are made of a stack of 10 carbon disc resistors. Each stack is immersed in mineral oil in a coaxial housing and is temperature controlled in order to adjust the value of the resistor.

Possible switches

In total 20 high power fast switches are necessary to operate all the fast pulsed magnet systems of the SPS. It is therefore very important to find switches which have a high degree of reliability and which require a minimum of maintenance.

Spark gaps have been used quite extensively in the past for similar applications [5]. They are quite simple in their principle, but have a number of disadvantages in long term operation :

- For a given gap distance and gas pressure, a spark gap allows only a small change in charging voltage. A larger change could be made by varying these two parameters, but it is doubtful if a change of a factor of 10 could be achieved during one SPS cycle, as it is required for the beam dumping system, where the voltage must track the proton energy [2].

- Triggering of a spark gap requires high voltage pulses which makes the triggering circuit complicated.

- The probability of an erratic firing of a spark gap is relatively high, generally of the order of 1°/oo.

- It is not sure that the energies to be switched can be handled by spark gaps without excessive errosion of the electrodes.

For all these reasons, spark gaps were not tried.

Although ignitrons can switch current pulses of up to hundreds of kA in the millisecond range, they are not suitable either. For 60 kV charging voltage, several ignitrons in series would be needed. Also ignitrons give fluctuations in the switching time ("jitter") of the order of 1 or 2 µs which is prohibitive for our application. Finally, their limited rate of rise of current is not compatible with our rise time requirements.

Another possible switch is the high voltage multigap thyratron which has proven to be satisfactory for pulses of up to 10 kA amplitude and 3 µs duration [6]. This kind of switch was therefore tried first.

Results with normal thyratrons

The tank for the switches shown in fig. 2 was designed firstly for the use of three English Electric CX 1171 thyratrons, which are deuterium-filled, three-gap tubes with a ceramic envelope. Each thyratron is mounted vertically in a coaxial housing, fixed on the cover of the tank. In addition, two stacks of 12 Unitrode UGE 7.5 diodes each, are placed in parallel with the dump switch. As a thyratron can pass the current only in one direction, these diodes are necessary to dump the negative current pulse which is generated when the clipper switch fires and which travels backwards into the PFN [4]. The heater power supplies and the trigger pulse transformers for the 3 thyratrons are housed in this tank which is filled under vacuum with mineral oil.

All the pulse shapes were checked at a low charging voltage of about 10 kV, which showed that the circuit of fig. 1 worked as predicted [4]. Then the voltage was progressively raised, and the main switch only was triggered, giving a pulse as shown in fig. 3a. The 5 to 95%

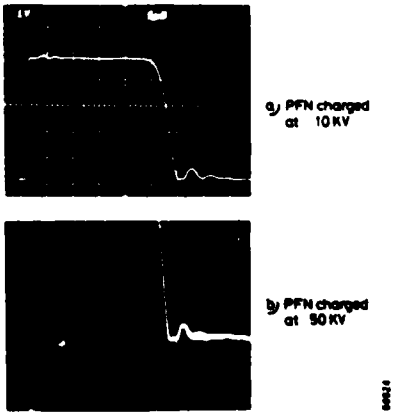

FIG.3 : PULSE SHAPE OBTAINED WITH A NORMAL THYRATRON AS MAIN SWITCH

rise time is of the order of 150 nsec, seen on the load resistor after the transmission cable. As it is unidirectional, the main thyratron passes only the positive part of the oscillations which occur normally at the fall of the PFN pulse when the clipper and dump switches are not triggered.

Above a charging voltage of 50 kV, the negative part of these oscillations started to be conducted through the main switch at a ratio of about once per 100 pulses (fig. 3 b). During the next three thousand pulses under these conditions, the number of erratic firings of the main switch increased considerably up to 10 % and consequently the DC voltage holding capability of the thyratron was strongly reduced. This effect could not be corrected by a reduction of the reservoir voltage of the thyratron.

A second thyratron tested under the same conditions gave exactly the same results. It is tentatively concluded therefore, that for high current and long duration pulses, the normal thyratron becomes very sensitive to reverse voltage, which results in back arcing and leads to the destruction of the tube. It should be noticed that because of the PFN configuration, some voltage reversal on the anode of the main switch cannot be avoided at the end of the PFN pulse, even if the clipper is fired [4].

In order to find the limits of the CX 1171, another thyratron was put in the main switch position and the clipper and dump switches were taken out of the tank. The PFN was shortened to 4 cells only, giving a nominal pulse length of 6 µs, and the charging voltage was raised progressively up to 60 kV, without any malfunctioning of the thyratron for a few thousand pulses. Two cells were then added to the PFN and the same test was repeated. The switch worked perfectly at 4 kA current amplitude and for pulse lengths of up to 12 µs. Above this limit, the same effect of back arcing as well as some indication of quenching appeared, resulting again in the destruction of the thyratron.

In conclusion, it can be said that CX 1171 thyratron can switch perfectly 4 kA rectangular pulses with a fast rise time up to a certain pulse duration. To switch longer pulses, it is necessary to have a switch which is not sensitive to voltage reversal and not subject to quenching.

The Thyragnitron

The thyragnitron principle

To overcome these difficulties, one can think of combining the advantages of both the thyratron and the ignitron. This results in the "thyragnitron" concept whose principle is shown on fig. 4. Basically, the thyragnitron is made of a normal multigap thyratron bypassed by three ignitrons in series. The thyratron provides only the steep current rise and the precise turn on, whereafter the ignitrons progressively take over the discharge current. As ignitrons can withstand large voltage reversal and inverse current, the ignitrons should be able to pass the negative overswings after the PFN fall without danger. In this way, the ignitron chain protects the thyratron from quenching and back arcing.

The thyragnitron was tested as a main switch, with neither clipper nor dump in the pulse generator. Three National Electronics NL 1039A ignitrons have been used

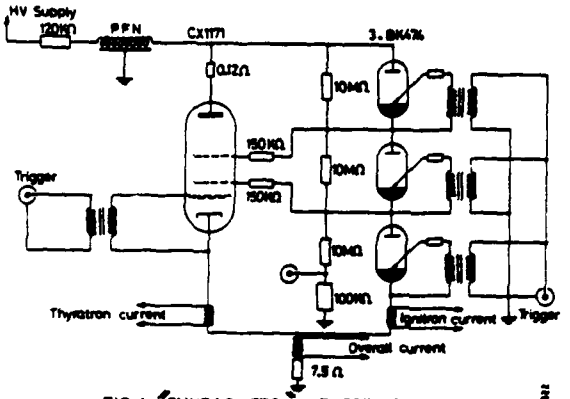

FIG. 4: THYRAGNITRON ELECTRICAL CIRCUIT

in conjunction with a CX 1171 thyratron. Three ignitrons in series are necessary to hold off the charging voltage. In a first assembly the ignitrons were mounted vertically one beside the other and with a special voltage divider different from the one used for the thyratron. This voltage divider was made of three spirals, each being built from a chain of small carbon resistors and located around the anode of each ignitron. In this way each ignitron anode is heated by the power dissipated in the divider and has always a higher temperature than the cathode, which prevents any deposit of mercury on the anode by sublimation. The CX 1171 thyratron was left in its coaxial housing, but between the PFN and the thyratron anode a small resistor R = 0.12 Ω was added. When the thyratron conducts, a voltage drop ΔV_{AC} develops between the common anode and the common cathode of the thyragnitron:

$$\Delta V_{AC} = R.I_{thy} + \Delta V_T$$

where ΔV_T is the arc voltage drop across the thyratron. R was dimensioned such that ΔV_{AC} is always higher than 3 times the minimum anode voltage which gives reliable firing of an ignitron, i.e. 3 x 100 V. The thyratron is triggered via its G2 command grid, which is biased to - 170 V, while a DC current of 25 mA is flowing through the G1 grid circuit. The same trigger pulse is used for the three ignitrons, and its relative timing with respect to the thyratron trigger pulse can be adjusted. However, in order to prevent the destruction of the thyratron in case it starts conducting spontaneously (erratic firing), the thyratron current pulse measured by a current transformer is mixed with the ignitron trigger pulse, such that the ignitron chain is always triggered when the thyratron starts to conduct. For the same reason, if the ignitron chain does not conduct when triggered, the pulse generator is stopped automatically.

Experimental results

The best results are obtained when the thyratron and the ignitron chain are triggered simultaneously. The sharing of the overall current in the two branches of the thyragnitron can be seen on fig. 5 a) and b). Both currents recombine perfectly giving the same pulse as if only one single switch were used. The thyratron current rises very rapidly as before, and then decreases continuously as the ignitrons gradually take over the current from the thyratron. One sees also

FIG.5: CURRENT SHARING IN THE THYRAGNITRON SWITCH

that the negative overswings at the PFN fall pass through the ignitron chain and that the thyratron no longer arcs back.

The ignitron current starts about 1 µs later than that of the thyratron and has a rate of rise which is given by the stray inductance L of the ignitron chain. This is demonstrated by the comparison of figures 5a) and b) with figure 5c). While figure 5c) was taken with the ignitron assembly described above for which L was measured to be 1.4 µH, the pictures 5a) and b) were taken with the ignitron chain rebuilt in a coaxial housing in order to minimize L to an estimated value of 0.4 µH. In this new arrangement which has a very low inductance, the thyratron stops to conduct just before the fall of the pulse. For charging voltages below 50 kV one can even see the thyratron extinguishing before the end of the pulse flat top.

The stray inductance L of the ignitron chain is more important at the pulse fall as it leads to a negative voltage

$$V = L \frac{dI_{ign}}{dt}$$

appearing across the thyratron. If V is higher than the arc voltage drop of the thyratron, a closed current loop can develop in the thyragnitron with some current flowing in the reverse way in the thyratron. This effect cannot be seen on the resulting pulse measured on the load, but is shown by the dotted traces of fig. 5c for which 100 pulses were superimposed. Although the power involved is relatively small, this effect can damage the thyratron, and this is why the ignitron chain was rebuilt in a coaxial housing.

With this new arrangement a life test was performed. After more than 10^6 pulses at 4 kA, 24 µs duration, at a repetition rate of 42 pulses per minute, the thyragnitron showed no sign of deterioration of performance. The rate of erratic firings of the thyratron was of the order of 2.10^{-5}, while only 3 missing ignitron current pulses were recorded.

The double cathode thyratron

Another way of overcoming the physical limitations of the normal thyratron was proposed by EEV which has manufactured a special thyratron, the CX 1171 B, which has a complete cathode assembly including a reservoir instead of the usual anode [7]. As more gas is provided to the discharge, in particular in the top gap, quenching of the discharge can be avoided for long pulses. In addition, this thyratron being completely symmetrical, it will be able to pass reverse current and be insensitive to voltage reversal.

The CX 1171 B as a main switch

This double cathode thyratron was tested first in the main switch position, with neither clipper nor dump switch in the pulse generator. The reservoir voltages of the two cathode assemblies have to be equal, as well as the two heater voltages. They were set to 5.2 V and 6.8 V respectively. To preionize the cathode assembly which plays the role of the usual anode, DC currents were maintained in the command grid circuits, i.e. 75 mA for the grid G1 and 25 mA for the grid G2. On the "Cathode" side, a DC current is also flowing through the grid G1, while G2 is biased to -170 V. The trigger pulse is applied on this latter grid, the "anode" assembly never being triggered.

No difficulty was experienced in getting the nominal 4 kA, 24 µs pulse. A preliminary life test of 150 000 pulses was carried out. At the beginning, the number of erratic firings was quite large, of the order of 1 °/oo. This was surprisingly corrected by increasing both reservoir voltages, up to 5.5 V. Indications of quenching necessitated a further increase on the reservoir voltages up to 5.8 V with again an improvement in the rate of erratics which at the end of the test was of the order of 10^{-4} or less.

Rise time and jitter are similar to those given by the thyragnitron.

Clipper after the main switch

The life test reported above was stopped to put the other two switches in the pulse generator. The dump switch was now also a double-cathode thyratron CX 1171 B. As it can pass current in both directions, the stacks of diodes are no longer necessary and were therefore removed.

To the contrary of fig. 1, the clipper, which was a double gap single cathode CX 1168 thyratron, was put after the main switch, i.e. its anode connected to the main switch cathode. In this way the fall time of the pulse should be limited only by the stray inductance of the clipper. Also the clipper has to withstand 30 kV pulses only.

Nevertheless, this arrangement has several drawbacks:

- When firing the main switch, the clipper has a strong tendency to start on its own, because of the voltage pulse appearing on its anode and which is not correctly divided across its gaps. This was corrected by adding to the usual voltage divider a 500 pF capacitor across the last clipper gap and later on by changing the CX 1168 thyratron clipper by a normal CX 1171.

- As the clipper cannot pass reverse currents, the negative overswings produced by the natural fall of the PFN pulse are transmitted through the main switch to the

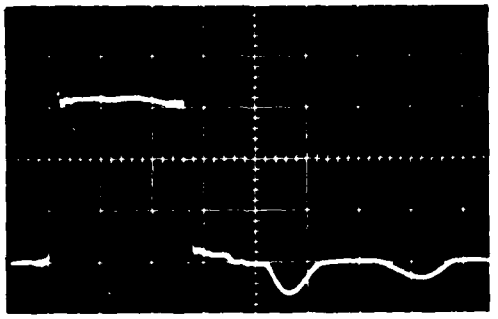

a) overall pulse on resistive load - 2 µs/div.

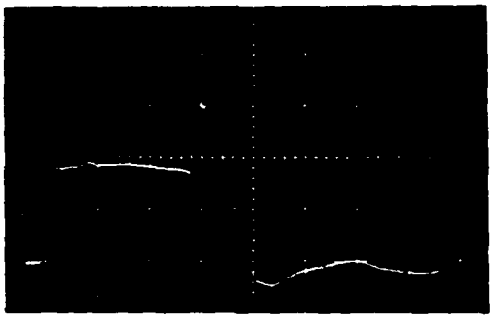

b) Main switch current - 2 µs/div.

Fig. 6 : Pulse shapes with clipper switch after the main switch
PFN charged at 60 kV

load and not short-circuited by the clipper, as expected. This is shown on the first picture of fig.6 for which the dump and clipper switches were triggered such as to reduce the pulse length down to 5 µsec.

- When the clipper conducts, the PFN is short-circuited, and the current doubles in the main thyratron reaching about 8 kA, as for the clipper (see fig. 6). This additional peak of current at the end of the pulse may reduce the life of the main thyratron and increases the probability of quenching. In case of an erratic firing of the clipper, both the main and the clipper switches have to pass 8 kA for the whole pulse length.

In spite of this, this arrangement was tested for 35000 pulses. In particular the pulse length could be varied easily between 0.5 µs and 24 µs by simply changing the relative triggering times of the three switches. This test was stopped for replacing the clipper by a double-cathode thyratron.

Clipper in front of the main switch

All three switches are now double-cathode CX 1171B thyratrons, with the clipper placed in front of the main switch as on fig. 1,i.e. the clipper and main thyratrons have a common anode connection. Several electrical circuits for exciting the thyratrons have been tried. The best results are obtained with the circuit shown on figure 7, which is the same for the

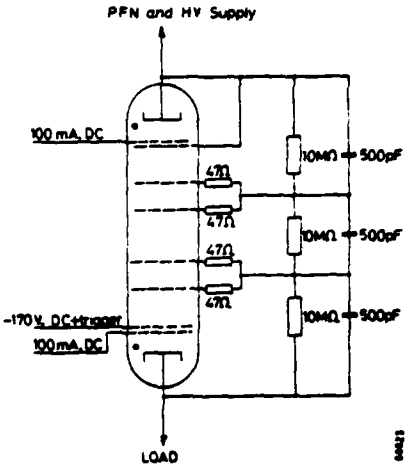

Fig. 7 Electrical circuit of the double cathode thyratron CX 1171 B

three thyratrons. Both "cathode" regions of each tube are preionized by a 100 mA DC current in the G1 circuit. The grid G2 of the "anode" side is connected directly to the high voltage, and each tube is triggered by the G2 of the "cathode" side, which is biased to -170 V.

Capacitive compensation of the resistive voltage divider is necessary for the clipper, to insure correct voltage division across this tube when the main switch is fired. Each resistive divider is made of a chain of small carbon resistors wound around the corresponding thyratron, which is then placed in a completely closed coaxial housing. In this way each thyratron is screened as far as possible against interferences from the others, which prevents that it starts spontaneously when another switch is fired. This is particularly important for the clipper.

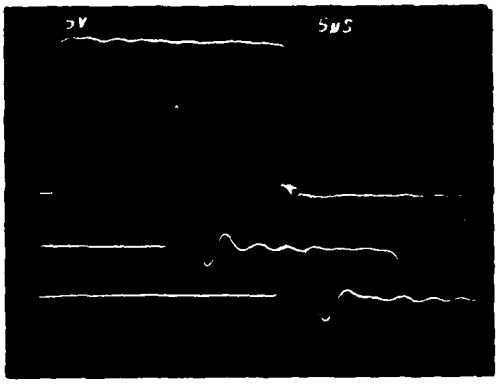

Fig. 8: Pulse shapes with clipper switch in front of main switch
PFN charged at 60 kV
a) Pulse on load resistor
b) Pulse on dump resistor
c) Clipper current

Figure 8 shows the different pulse shapes when the PFN is charged at 60 kV, and for a 24 µs pulse length. The current flowing through the main thyratron has exactly the same shape as the pulse seen on the load resistor. One clearly sees the full polarity change of the dump switch current. This switch can also work as an inverse diode, when it is not triggered and in this case, passes only the negative current pulse generated by the clipper. Here again the maximum clipper current is twice as high as the nominal pulse current.

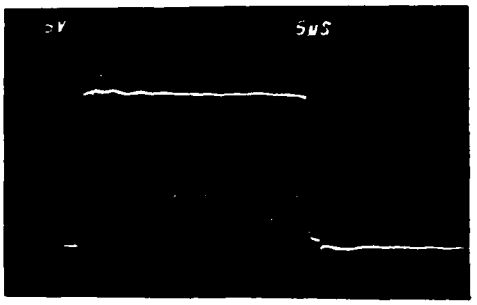

a) 5 µs/div Trigger times : main 0 µs
dump 11 µs
clipper 23 µs

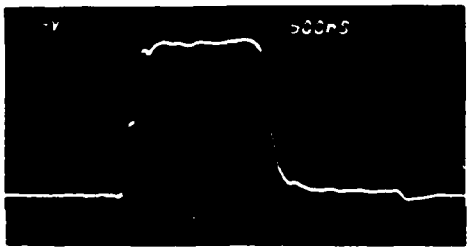

b) 500 ns/div. Trigger times: main 11 µs
dump 0 µs
clipper 12.4 µs

Fig. 9: Change of pulse duration
PFN charged at 60 kV

Figure 9 demonstrates the change in pulse lengths. Measured after the transmission cable, the rise time 10-90% is about 170 nsec and the fall time about 200 nsec. The small tail after the pulse fall is due to the current sharing between the resistive load and the clipper branch which has an impedance not infinitely small as compared to 7.5 Ω. This tail stops when the main thyratron extinguishes.

Jitters of the main and clipper tubes are slightly less than 10 nsec, but no effort was made to reduce them by optimizing the reservoir voltages.

A life test is being made and about 1 000 000 pulses at 4 kA, 24 µs have already been obtained. 40 erratic firings for the main thyratron and 35 for the clipper are recorded, which is relatively high, but some of these erratic firings were probably due to problems in the low level triggering and interlock system. Actually the rate of erratic firings is about 4.10^{-5} for the main and the clipper and 10^{-5} for the dump switch which is comparable with what has been reported for normal thyratons [8].

Conclusion

Two kinds of switches have been successfully tested, which cope with the high current long duration pulses required for the excitation of the SPS fast pulsed magnet systems.

Although simple in its principle, the "thyragnitron", made of a normal thyratron by-passed by 3 ignitrons, leads to a somewhat complicated construction. But it can be easily extended to higher currents and to pulses of longer duration. It is best suited when only a main switch is required in the pulse generator, as it is the case for the SPS beam dumping system.

With three double-cathode EEV CX1171 B thyratrons, we were able to produce 4 kA rectangular pulses, with a pulse duration adjustable between 0.5 and 24 µsec, and good performance in rise and fall times, as well as in jitter.

Both kinds of switches have been tested so far for about one million pulses, which represents about four months of full operation of the SPS accelerator.

Acknowledgements

This work was originated by W.C. Middelkoop and we have benefited from his constant support and great experience. The full comprehension and close cooperation with English Electric Valve Co. U.K., is mentionned here, in particular with H. Menown and B.P. Newton, who are gratefully acknowledged.

It is a pleasure to thank here E. Frick for his mechanical design of the pulse generator with its successive versions, and R. Barthélemy for the electronic and interlock circuitry. We also thank all of those who participated in the mechanical assembly and the tests, especially J. Hofmann and R. Tröhler.

References

1. The 300 GeV programme. CERN/1050

2. P.E. Faugeras, C.G. Harrison, G.H. Schröder, Design study of the SPS beam dumping system, CERN Lab II/BT/Int/73-5.

3. H. Kuhn, W.C. Middlekoop, H. O'Hanlon, The Design of the ISR inflector, IEEE Trans. on Nuclear Science, NS-16, 3,738, June 1969.

   D.C. Fiander, Hardware for a full aperture kicker system for the CPS, CERN/MPS/SR 71-5.

4. P.E. Faugeras, Calculations on the SPS inflector magnet and its pulse generator, CERN Lab II/BT/72-1.

5. R. Bossart et al. Multiple short and multiple channel operation of the CPS fast ejection system, CERN/PS/FES/Int.69-9.

6. A. Delizée. H. Kuhn, W.C. Middelkoop, B. de Raad J.C. Schnuriger, G. Schröder, J.P. Zanasco, The Design of the Beam Dumping System of the CERN Intersecting Storage Rings, CERN/ISR/BT/69-53.

7. H. Menown, B.P.Newton, A multigap, double-ended hydrogen thyratron, to be presented at the 11th Modulator Symposium, September 1973, New York,U.S.A.

8. D. Grier, The use of hydrogen thyratrons as high voltage switches CERN/MPS/SR/Note 69-22.

LONG PULSE SWITCH AND POWER AMPLIFIER TUBES FOR PHASED ARRAY RADAR

R. E. Byram and J. T. Mark
RCA Corporation, Electronic Components Division
Lancaster, Pennsylvania

Summary

Three new tetrode tubes are now in development in 50 kW, 100 kW, and 500 kW sizes for use as long pulse radar switch tubes, and with 10 kW, 20 kW, and 40 kW levels in long pulse UHF and L-Band rf power amplifiers. All three tubes use newly developed tungsten matrix cathodes and are currently being tested for pulse lengths from 1 to 8 milliseconds and with capability for greater pulse lengths. These new cathodes are specially developed for high current long pulses, arc resistance, and long life. Aspects of the tube design and operation in typical service life test are discussed.

Introduction

The development of long-range deep-search radar systems has created a need for long-pulse tubes capable of operation at pulse lengths up to several milliseconds. Such tubes are useful, for instance, in one approach to a phased-array system in which a multiplicity of tubes of moderate power rating is used, with the necessary phase shifting accomplished at a low power level. Long pulse tubes are needed both as switches to control the dc power applied to the systems, and as power amplifiers in the rf portions of the equipment.

New Series of Tubes

To meet this need RCA is developing a series of gridded tubes utilizing tungsten matrix, or tungsten dispenser, cathodes. A general description of this type of cathode may be found in the literature in papers by R. Levi[1], W. H. Kohl[2], and G. A. Haas and R. E. Thomas[3]. Excellent work in the study of these cathodes is being done by Dr. Haas and his associates at the U.S. Naval Research Laboratory in Washington, D.C.

The new RCA tubes using the tungsten matrix cathode are designed to have improved efficiency, reduced power requirements, and increased ruggedness over the nickel matrix oxide and thoriated tungsten types now in use. These tubes are capable of pulses from 1 to 5 milliseconds at normal duty, and 10 to 20 milliseconds at reduced duty.

Three types are presently in development. The RCA A2950 is rated for 50 kW of peak power input for pulse modulator service. The RCA A2975 is rated for 100 kW of peak power input, and the RCA A2960 for 500 kW peak power input, both for pulse modulator service.

Tungsten Matrix Cathode

Figure 1 shows a cross-section of the heater-cathode assembly used in the RCA A2960. The cathode is a cylindrical tungsten matrix which is impregnated with Barium Aluminate. The heat dam which supports the tungsten-matrix cathode is made of molybdenum. The heater spool and the heater spool lid are tantalum. These are the parts that provide mechanical support for the tungsten-rhenium heater and the associated high-alumina heater retainer ceramic. Tantalum and molybdenum parts are used rather than the more conventional nickel parts because of the operating temperature of the tungsten-matrix cathode (about 1050°C brightness temperature).

Figure 2 shows a cross-section of the RCA A2975 cathode. The RCA A2950 cathode is of similar construction. In these types, due to the sequence of manufacturing operations which require the entire heater-cathode assembly to be exposed to a hydrogen atmosphere brazing furnace, no tantalum is used, and all associated parts are of molybdenum or a molybdenum-rhenium alloy.

Advantages of Tungsten-Matrix Cathode

There are several advantages derived from the use of tungsten-matrix cathodes for military radar. The tungsten-matrix cathode has a smooth machined metallic surface. This smooth surface reduces high voltage gradients at the cathode surface and provides for excellent resistance to arcs.

The metallic emitting surface has a very low internal resistance. It is free of self-heating effects and the formation of an interface layer. As a result, internal arcing with possible gas evolution will not occur with high pulse currents. This contributes to the excellent resistance to arcs with high pulse currents, and also results in none of the pulse breakup sometimes experienced with the conventional nickel matrix oxide cathode with life. Also, unlike the oxide cathode, there is no possibility for loosely sintered particles to break off and cause interelectrode shorts.

The tungsten-matrix cathode is not damaged from bombardment by gas ions, or affected by electrons returned to the cathode through transit time effects at the higher frequencies. Provided the tungsten-matrix cathode is not operated at too low a temperature, it is less prone to poisoning by residual gas than oxide cathodes because barium and barium oxide are constantly replenished from the barium aluminate impregnate which fills the entire volume of the tungsten-matrix.

A cathode brightness temperature of 1050°C is high enough to prevent poisoning by residual gas, and yet is a moderate temperature for a tungsten matrix cathode. At this temperature cathode emission remains constant for very long life, even under conditions of high cathode loading. Using test diodes at cathode current densities as high as 10 amperes per square centimeter, constant emission for thousands of hours has been reported.

The pulse emission capability and the dc emission capability of the tungsten-matrix cathode are essentially the same. For this reason no droop in emission occurs with long pulse operation. The pulse length and emission level that can be utilized are thus not limited by the

cathode, but by the allowable dissipation of the other tube electrodes.

In the new series of RCA tubes, the dc cathode current density is held to 200-250 milliamperes per square centimeter of cathode area. This figure is double the usual rating for a nickel matrix oxide cathode, but it is moderate indeed for a tungsten-matrix cathode. At this level of dc emission, and at the cathode operating temperature being used, the life expectancy of the cathode itself is 50,000 -100,000 hours. RCA Traveling Wave Tubes using these cathodes are exhibiting 10,000-15,000 hours of life, and one European manufacturer of gridded tubes has reported CW dynamic life in excess of 13,000 hours, with the tubes still operating.

Many of the advantages that have been outlined for the tungsten-matrix cathode also apply to the thoriated tungsten filamentary cathode. The tungsten-matrix cathode is much more efficient, however, as only 1/4 to 1/2 the filament power is needed for equivalent emission levels. The tungsten-matrix cathode is also much more rugged than the thoriated tungsten filament, and not susceptible to breakage under environmental conditions or in shipment.

The advantages of the tungsten-matrix cathode in tubes for military radar systems may be summarized as follows:

1) Arc resistant operation at high pulse currents.

2) No pulse droop.

3) No pulse breakup.

4) Very long life at moderate temperatures.

Grid-Screen Construction

All three of the new RCA tetrodes are of the proven RCA cermolox construction, with the grids and screens simultaneously produced by electrical discharge cutting, resulting in perfect alignment of the grid and screen wires. The RCA A2960 uses molybdenum for the grid and screen wires, while the A2950 and A2975 have grids and screens of a copper alloy

Typical Operation as Hard Tube Modulator

In pulse modulator service the A2950, the smallest of the three tubes, is rated for 5,000 volts plate voltage and 10 amperes peak plate current at .01 duty and a one millisecond pulse width. The outline drawing of Figure 3 shows the physical size of this tube, and Figure 4 shows typical operation as a pulse modulator switching 18 kW peak power in the load.

The A2975 is rated for 5000 volts plate voltage and 20 amperes peak plate current under the same conditions. Figures 5 and 6 show the outline drawing of this tube and typical pulse modulator service switching 40 kW peak power in the load.

The largest tube, the A2960, is rated for 20,000 volts plate voltage and 25 amperes peak plate current, again at .01 duty and one millisecond pulse width. Figures 7 and 8 show the A2960 outline drawing and typical pulse modulator service. In this case 425 kW peak power is being switched in the load.

Life Results

Varied life experience has been accumulated for the A2950 in pulse modulator service and in rf service, and for the A2960 in pulse modulator service.

As a hard tube modulator the A2950 has been run for 3,000 hours at a peak plate current of 13 amperes with 1 millisecond pulses at .01 duty.

In rf service the A2950 has been operated 6,600 hours in 30 MHz CW service. DC plate current was 1 ampere and power output was 1 kW, both of which are double the values obtained from a nickel matrix oxide tube of equivalent size. The A2950 has also been operated over 5,000 hours in the visual IPA stage of a commercial TV transmitter in actual TV broadcasting use.

The A2950 heater has been cycled on and off for 20,000 cycles with no heater failure.

The A2960 has been operated in pulse modulator service for 2,700 hours with a variety of conditions to simulate random pulse width radar. Pulse width varied from 1 to 4 milliseconds and peak currents from 10 to 25 amperes.

The A2960 heater was cycled 12,000 times without failure.

Life tests of the A2950 and A2960 are continuing, and life testing of the A2975 has been started.

RF Operation

In addition to pulse modulator service which has been stressed up to this point, this new series of tubes is also useful in pulsed rf amplifier service.

Figure 9 shows a chain of two A2950 tubes giving broad band operation similar to that required in one section of a radar system that has been under consideration.

Figure 10 shows typical operation of the A2960 in pulsed rf amplifier service giving 40 kW of pulsed power output up to 400 MHz with 2 millisecond pulse width.

Many other operating conditions are possible, of course, and reference should be made to the technical bulletins [4, 5, 6], for these tube types for information on allowable inputs and plate currents at various duty factors and pulse widths. Also available is an RCA Application Note[7] describing the advantages and uses of tubes with tungsten-matrix cathodes.

Conclusion

It has been demonstrated that tungsten-matrix cathodes can be successfully utilized in gridded tubes, and that tubes with this type of cathode offer many advantages for long pulse service in military radar systems.

References

1. R. Levi, J. Appl. Phys. Vol. 24, 233 (Feb. 1952) and J. Appl. Phys. Vol. 26, 639 (May 1955).

2. W. H. Kohl, Handbook of Materials and Techniques for Vacuum Devices, Reinhold Publishing Corp. 1967.

3. G. A. Haas and R. E. Thomas, J. Appl. Phys. Vol. 38, 3969 (Sept. 1967).

4. Developmental Data Sheet - RCA Type A2950.

5. Developmental Data Sheet - RCA Type A2960.

6. Objective Developmental Data Sheet - RCA Type A2975.

7. RCA Application Note AN-4887, Tungsten Matrix Cathodes for RCA Cermolox Tubes.

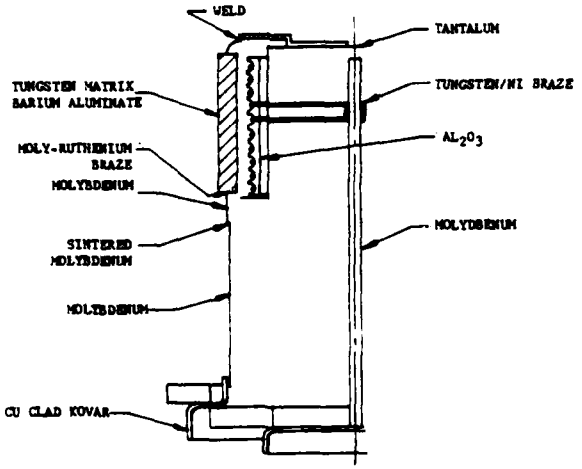

FIGURE 1 A2960 CATHODE

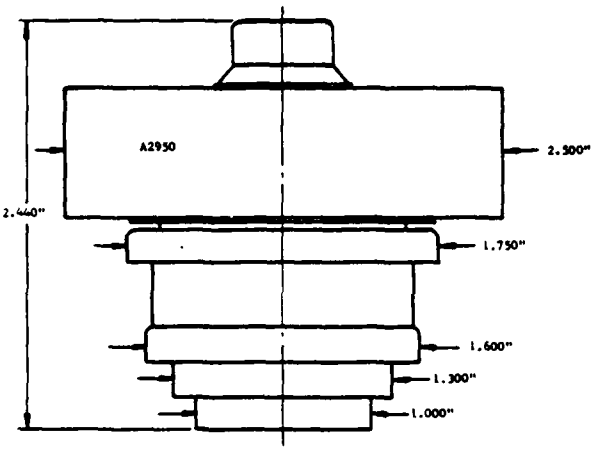

FIGURE 3 A2950 OUTLINE

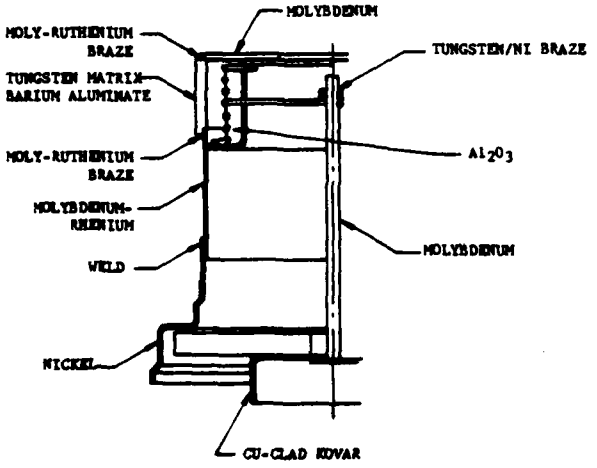

FIGURE 2 A2975 CATHODE

TYPICAL OPERATION

WITH RECTANGULAR WAVE SHAPE PULSES, DUTY FACTOR OF 0.01, AND A PULSE WIDTH OF 1000 MICROSECONDS.

DC PLATE VOLTAGE	3000	V
DC GRID-NO. 2 VOLTAGE	800	V
DC GRID - NO. 1 VOLTAGE	-120	V
PEAK POSITIVE GRID-NO. 1 VOLTAGE	25	V
PEAK PLATE CURRENT	10	A
DC PLATE CURRENT	100	mA
DC GRID-NO. 2 CURRENT	10	mA
DC GRID-NO. 1 CURRENT	50	mA
LOAD RESISTANCE	180	Ohms
USEFUL DC PEAK POWER OUTPUT AT PEAK OF PULSE	18,000	W

FIGURE 4 A2950 PULSE MODULATOR SERVICE

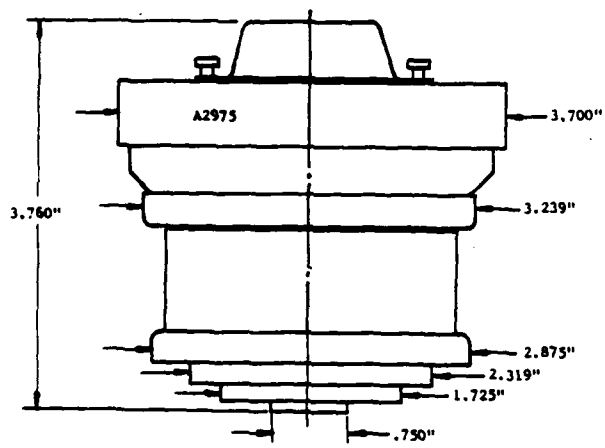

FIGURE 5 A2975 OUTLINE

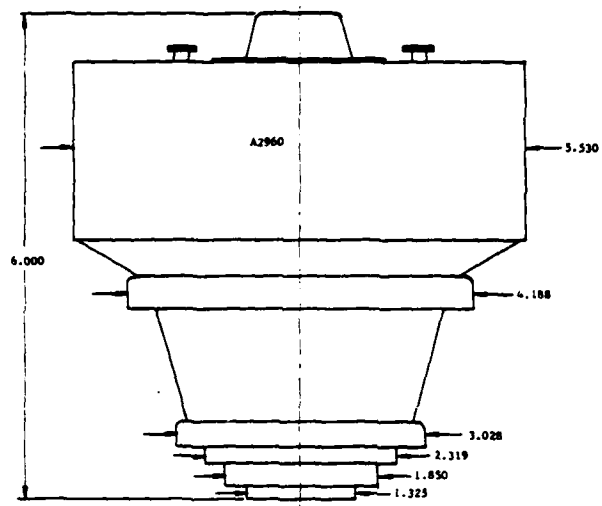

FIGURE 7 A2960 OUTLINE

OVERHEAD VIEWGRAPH LAYOUT SHEET AND WORK COPY

TYPICAL OPERATION

WITH RECTANGULAR WAVE SHAPE PULSES, DUTY FACTOR OF 1.0 PERCENT AND A PULSE WIDTH OF 1000 MICROSECONDS.

DC PLATE VOLTAGE	4,000	V
DC GRID NO. 2 VOLTAGE	1,000	V
DC GRID NO. 1 VOLTAGE	-250	V
PEAK POSITIVE GRID NO. 1 VOLTAGE	320	V
PEAK PLATE CURRENT	20	A
DC PLATE CURRENT	200	mA
DC GRID NO. 2 CURRENT	25	mA
DC GRID NO. 1 CURRENT	35	mA
LOAD RESISTANCE	100	Ohms
USEFUL DC PEAK POWER OUTPUT AT PEAK OF PULSE	40	kW

FIGURE 6 A2975 PULSE MODULATOR SERVICE

TYPICAL OPERATION

WITH RECTANGULAR WAVE SHAPE PULSES, DUTY FACTOR OF 1.0 PERCENT AND A PULSE WIDTH OF 1000 MICROSECONDS.

DC PLATE VOLTAGE	20,000	V
DC GRID No. 2 VOLTAGE	1,500	V
DC GRID No. 1 VOLTAGE	-400	V
PEAK POSITIVE GRID No. 1 VOLTAGE	50	V
PEAK PLATE CURRENT	25	A
DC PLATE CURRENT	250	mA
DC GRID No. 2 CURRENT	15	mA
DC GRID No. 1 CURRENT	20	mA
LOAD RESISTANCE	680	Ohms
USEFUL DC PEAK POWER OUTPUT AT PEAK OF PULSE	425	kW

FIGURE 8 A2960 PULSE MODULATOR SERVICE

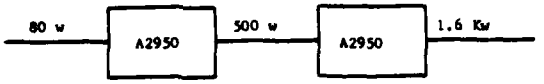

1300 MHz
50 MHz BANDWIDTH @ -1 dB DOUBLE TUNED
SCREEN PULSED CATHODE DRIVE
2000 MICROSEC. PULSE, 5% DUTY

DC PLATE VOLTAGE	1600	2200	V
PULSED GRID No. 2 VOLTAGE	800	800	V
DC GRID No. 1 VOLTAGE	-30	-26	V
DC PLATE CURRENT DURING PULSE	2.94	4.33	A
DC PLATE CURRENT	.147	.217	A
DC GRID No. 2 CURRENT	.003	.005	A
DC GRID No. 1 CURRENT	.001	.033	A

FIGURE 9 A2950 PULSED RF AMPLIFIER CHAIN

FREQUENCY	400	MHz
PULSE WIDTH	2	Millisec.
DUTY FACTOR	5	%
DC PLATE VOLTAGE	11,000	V
PULSED GRID NO. 2 VOLTAGE	1,500	V
DC GRID NO. 1 VOLTAGE	-250	V
DC PLATE CURRENT DURING PULSE	7.7	A
DC PLATE CURRENT	.39	A
DC GRID NO. 2 CURRENT	7	mA
DC GRID NO. 1 CURRENT	19	mA
OUTPUT CIRCUIT EFFICIENCY	85	%
DRIVE POWER AT PEAK OF PULSE	2.3	kW
USEFUL POWER OUTPUT AT PEAK OF PULSE	40	kW

FIGURE 10 A2960 PULSED RF AMPLIFIER

4CW 100,000 TETRODE PULSE TESTS AT RADC

By Paul Bryan and Howard Beard
Rome Air Development Center, USAF
Griffiss Air Force Base, New York

Summary

This investigation showed that this tube can provide very stable pulse performance at a wide variety of conditions well above its 4 megawatt and 40 KV ratings.

In an effort to obtain data beyond the published ratings on Tetrode Switch Tubes, the RADC High Power Laboratory conducted an investigation on three versions of the EIMAC 4CW100,000 Tetrodes. These tubes are manufactured for high power short-wave broadcast service.

SWITCHING TEST OF 4CW100,000D

Figure 1 shows the "D" Model with its socket. It had a height of about 18 inches with a fairly long stem section which supports the internal elements and results in some cathode lead inductance. The tube is shown in its test position in Figure 2. The X-Ray Shield is removed for the picture. Ten microfarads of energy storage equipped with a crowbar is in the anode supply circuit. The grid circuit was swamped with 150 ohms. The video load was a sodium-nitrite liquid resistor circulating through a heat exchanger. The test set was then limited to 20 microseconds. After cold conditioning, the tube was operated initially at low duty, low voltage and high load resistance. Several stable points at progressively higher ratings were established, as shown in Figure 3, up to 7.23 megawatts at .01 duty with a power gain of 350. Computation of power gain included the energy consumed in the 150 ohms of grid swamping. Several points of stable operation at both 1 and 1.75 KW of screen dissipation were determined.

SIX MILLISECOND ANODE DISSIPATION TEST

The next test in the series was a 500 hour anode dissipation test of an early model of the 4CW100,000E. The reason for this test was that in a previous long-pulse program extensive difficulty had been encountered with severe thermal cycling of the anode surface at low repetition rates causing fatigue failures with cracking, resulting in gas bursts and arcs. This test was conducted at a peak anode dissipation of 1.35 megawatts with 10 pulses per second of six milliseconds pulse duration. Only 8.5 ohms of current limiting was used as load resistance. The average anode dissipation throughout the test was 80,000 watts. A very noticeable red glow around the ceramic (see Figure 4) pulsed slightly with anode current. The test continued for three weeks around the clock.

The parameters of the test are listed in Figure 5. Figure 6 shows waveforms encountered. The grid operated at about 250 volts negative during the pulse. With 160 MFD of energy storage the anode voltage drop was only 2 KV. Following this test the tube was disassembled at the factory for inspection. It was found to have no damage to either the anode or other elements.

HIGH VOLTAGE SWITCHING WITH THE 4CW100,000E

The third test was an investigation of the high-voltage switching characteristics of the 'E' model of the 4CW100,000 series. Figure 7 shows the circuit employed. A 20 ampere pulser with 200 ohms of swamping was used to insure stable grid voltage. The bias supply floated in series with the grid lead on an isolation transformer. The screen was shunt-regulated to hold its voltage constant regardless of direction of current flow. The tube's initial position in the test set is shown in Figure 8. After conditioning the tube cold to 70 KV a number of points of stable operation in a switching mode were recorded, gradually working up to 70 KV. Flashover was experienced at voltages higher than 70 KV. Figure 9 shows how the test position was modified to immerse the tube in oil. This not only remedied the flashover problem, it also got rid of the X-radiation. The tube could now easily be high-potted to 90 KV and operated at 81 KV.

Figure 10 indicates much higher power gain with the 'E' model. Here you see points as high as 1500. This was with 80 KV on the tube and at a pulse width of 200 microseconds. The points at 9.68 megawatts and near there were all at a pulse width of 1 millisecond. They are also at a power gain of 30 dB. The waveforms in Figure 11 were taken at 9.68 megawatts with an anode supply voltage of 70 KV and 1660 volts on the screen.

SUMMARY

Time doesn't permit an analysis of the data however if the tube is operated with a low impedance grid circuit, a clamped screen supply and within the dissipation ratings of the grids, this tube can provide very stable pulse performance at a wide variety of conditions well above its 4 megawatt and 40 KV ratings.

We are indebted to the Eimac Division of Varian for the loan of the tubes.

This research was sponsored by the Air Force Systems Command's Rome Air Development Center

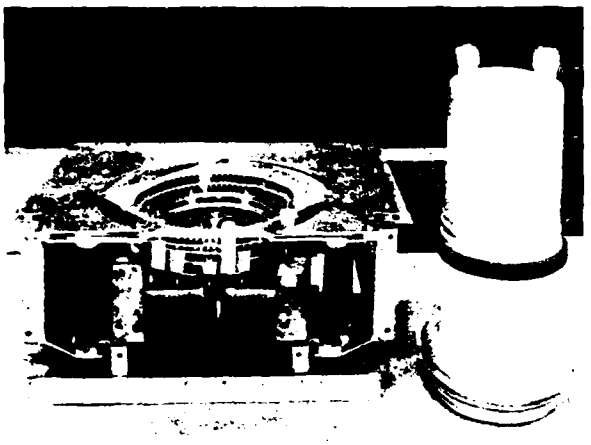

Figure 1. 4CW100,000D with socket. Large wing nut at bottom of socket engages bayonet fitting on base of tube to securely hold contact surfaces of tube against fingers in socket.

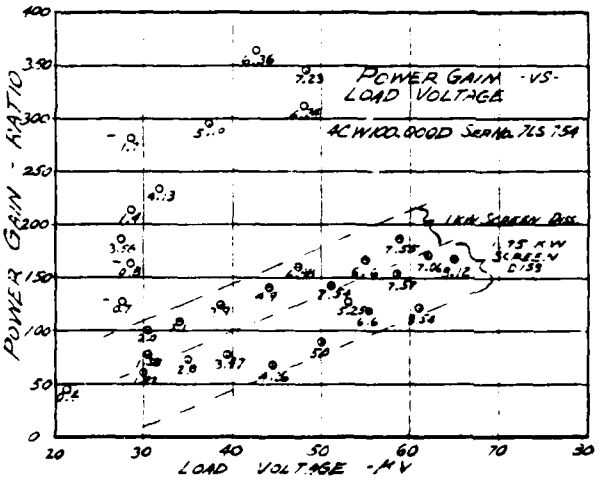

Figure 3. Figures at each data point indicate peak power in megawatts in video load. Tube rated at 40 KV and 4 megawatts.

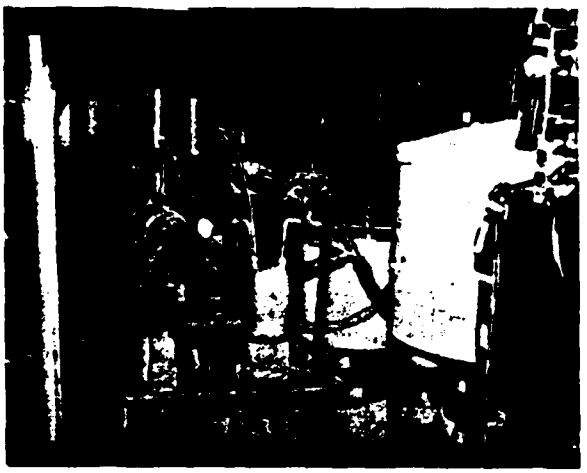

Figure 2. 40 inch glass tubes containing circulating electrolyte function as video load. 4CW100,000D operated to 65 KV in this position.

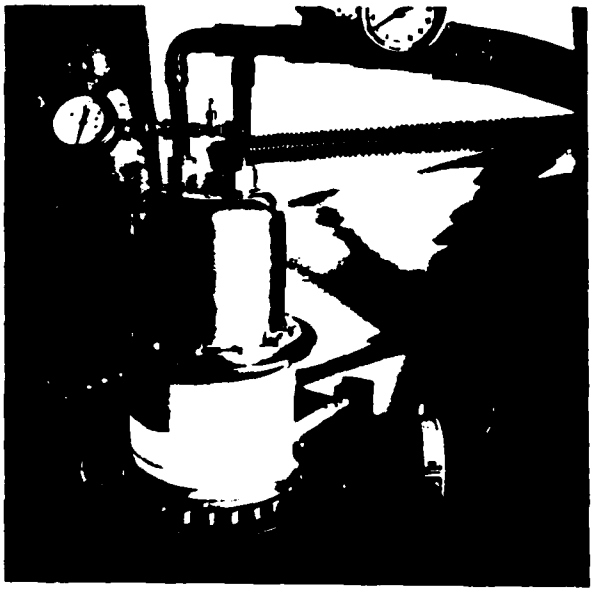

Figure 4. 4CW100,000E during 6 millisecond 1.35 megawatts dissipation test. Parasitic choke in anode circuit visible below hose.

PARAMETERS OF 500 HOUR DISSIPATION TEST

TURE: 4CW100,000E (SER. NO. 9KA1)

Anode Supply Voltage	27.5 KV
Peak Anode Current (Average during pulse)	50 Amperes
Pulse Width	6 Milliseconds
Repetition Rate	10 Pulses Per Secon
Peak Dissipation	1.35 Megawatts
Interpulse Grid Bias Voltage	-1600 Volts
Pulsed Grid Voltage	-250 Volts
Screen Voltage	2500 Volts
Average Anode Current	3.1 Amps
Anode Supply Capacitor Bank	160ufd
Anode Current Limiting Resistor	9.5 Ohms
Filament Current	220 Amps
Anode Cooling Water Flow	32.5 gals/min
Temperature Rise In Anode	10° C
Input Water Temperature	18° C
Pressure Drop In Anode Water	15 psi

Figure 5. Parameters of 500 hour dissipation test.

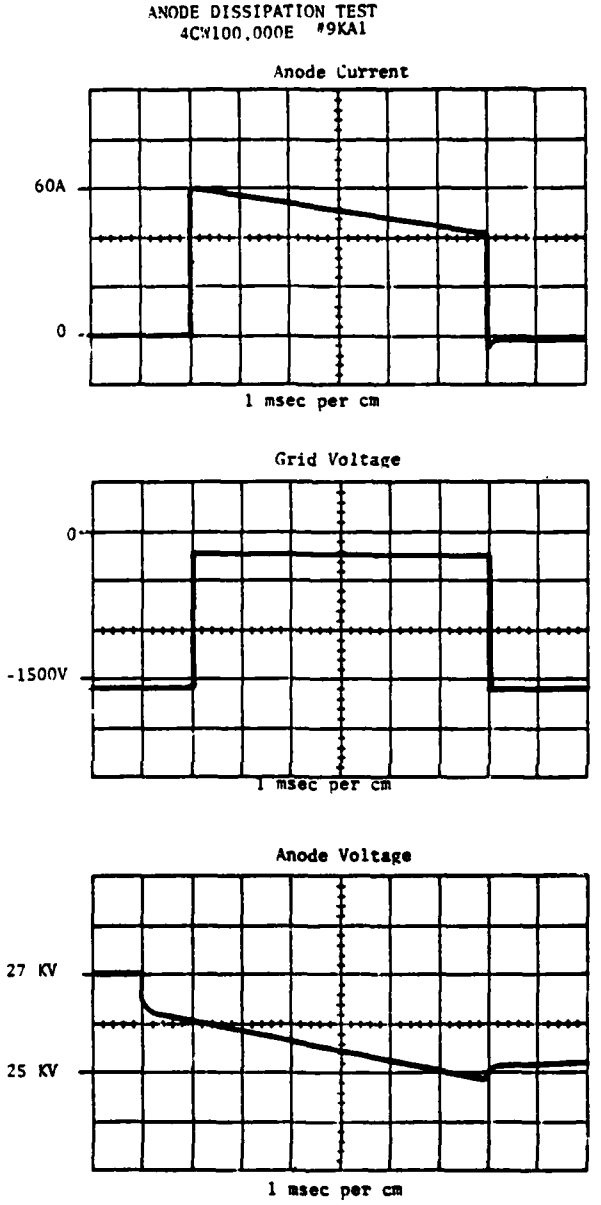

Figure 6. Average anode current during pulse was 50 amperes. Note that grid was not driven positive during dissipation test.

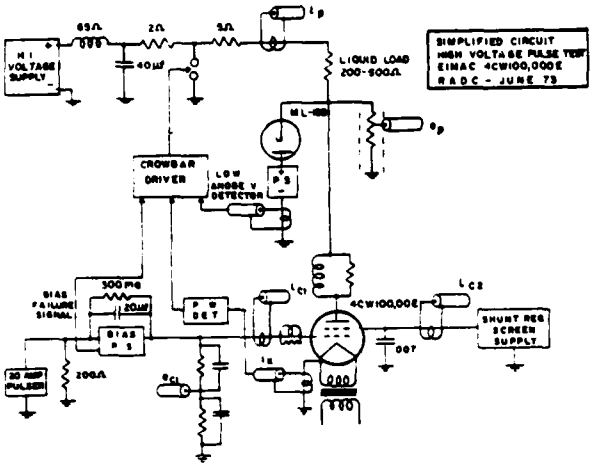

Figure 7. Simplified circuit of high voltage switching test of the 4CW100,000E. The pulse width detector actuated the crowbar if the cathode current pulse exceeded the width of the grid drive pulse.

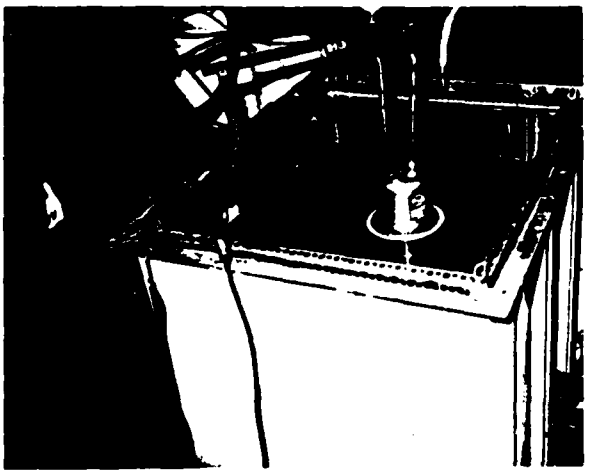

Figure 9. 4CW100,000E in modified test position immersed in 10C insulating oil. Tube was operated to 81 KV and high potted to 90 KV cold without flashover. Oil appeared to absorb X-Radiation.

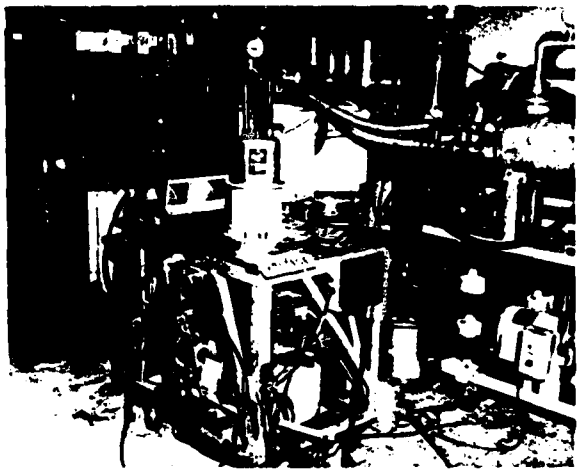

Figure 8. 4CW100,000E in test position with X-Ray shield removed. The tube was operated to 70 KV in this position.

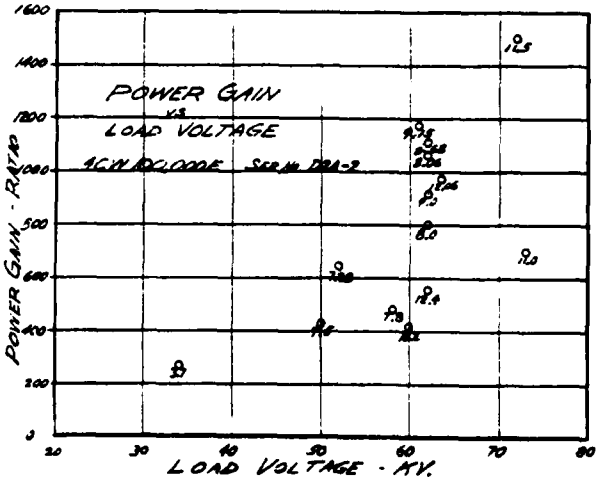

Figure 10. Figures at each data point indicate peak power in video load. Rated maximums were 40 KV and 4 megawatts peak output.

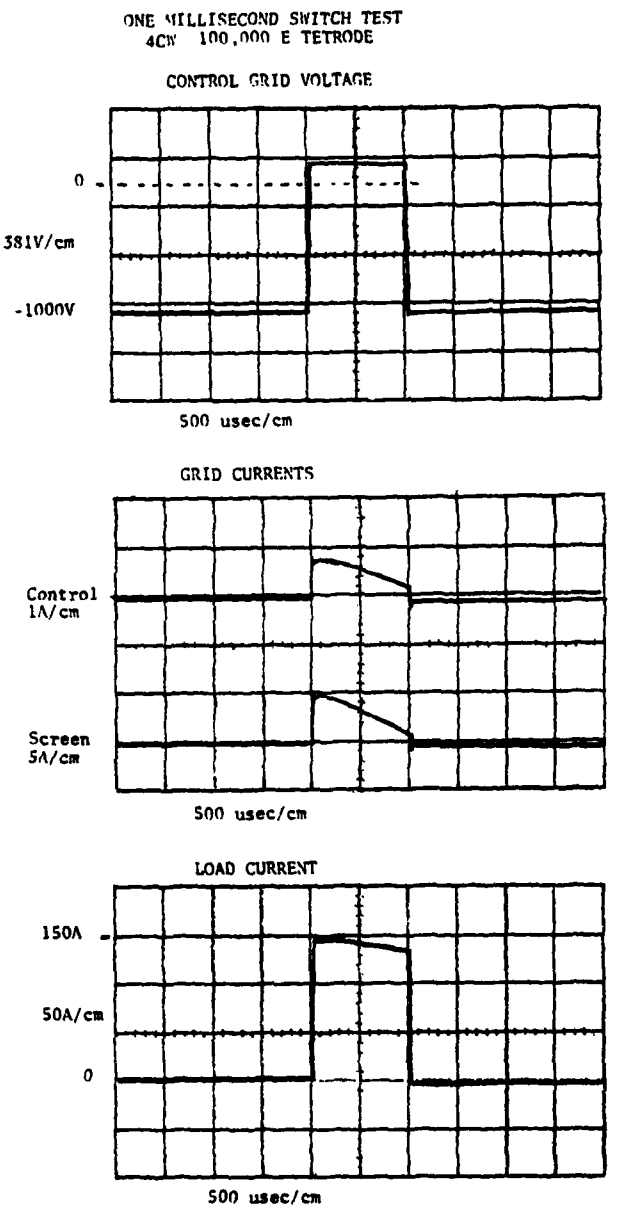

Figure 11. Waveforms of the 8.68 megawatt point shown in Figure 10.

THE CROSSED FIELD SWITCH TUBE AND ITS APPLICATION TO HIGH POWER MODULATORS

by

Michael A. Lutz
Hughes Research Laboratories
3011 Malibu Canyon Road
Malibu, California 90265

Summary

This paper describes the principles and recent development of a crossed field switch tube capable of closing and opening an HVDC circuit. The tube operates as a Penning discharge which can be controlled by an externally applied magnetic field. Several of the physical phenomena associated with this tube are described, including ignition jitter, the glow to arc transition, sputtering, gas clean-up and life. One particular tube has reliably interrupted 2.5 kA against 60 kV with a voltage recovery rate of 15 kV/μsec. Several applications for this tube are described besides those relating to power utility service. These include component protection (controlled reusable fuse), HVDC interruption for current-fed line-type modulators and substitution for hard vacuum tubes for higher power "hard tube" modulators.

Introduction

The use of a crossed field glow discharge to interrupt direct current against high forward voltage was first studied almost thirty years ago by Makinson et al.[1] in Australia. This group succeeded in interrupting 50 A against a few kV by switching off the magnetic field of a Penning discharge. They observed that such a device could be used to close a circuit as well as open it by first switching the magnetic field on and then off. It was suggested that such a device could replace hard vacuum switch tubes in some limited life, high current applications.

Since 1962, considerable research has been performed at Hughes Research Laboratories on low pressure crossed field gas discharge devices similar to those investigated by Makinson's group.[2,3,4] A major part of this program has been devoted to the design and test of high power crossed field switch tubes suitable for power utility switching applications such as HVDC circuit breakers and current limiters for AC systems. Several different tube designs have been investigated culminating in interruption voltages and currents in excess of 100 kV and several thousand amperes at recovery rates up to 15 kV/μsec. Such high recovery rates eliminate the need for shunt capacitance which is required with other HVDC interruption schemes.

This paper is divided into three basic sections. The first briefly describes the basic operating principles of crossed field switch tubes. For those readers desiring more detailed information, other, crossed field tube (XFT) literature should be consulted (Refs. 5, 6, and 7). The second section describes one tube design particularly suitable for modulator service. Test procedures and switching results are also presented. The third and final section considers three potential applications of XFT's in high power modulators. These are component protection, current-fed line-type pulser switching and hard tube substition.

Switch Tube Principles

An XFT must be capable of performing the following four functions:

1. Remain in a nonconducting state when a high forward voltage is applied (H. V. Hold-off).
2. Trigger into a conducting state upon application of the magnetic field (Ignition).
3. Conduct a high dc current in the glow discharge mode for a specified time (Conduction).
4. Interrupt this current and revert to the nonconducting state upon removal of the magnetic field (Interruption).

We shall now consider each of these functions in turn.

H. V. Hold-off

In the absence of a magnetic field, the breakdown of a gas due to an electron avalanche is governed by Paschen's law which states that V = f(pd) where V is the breakdown voltage, p is the gas pressure, and d is the interelectrode spacing. To avoid breakdown, an XFT must be designed such that the pd product is everywhere less than a critical value. Neither p nor d can be made arbitrarily small, however. Below a certain value of pressure, a high current density, low voltage glow discharge cannot be sustained. And, below a certain value of interelectrode spacing (for a given a voltage), field emission leading to breakdown will occur. Thus, the maximum operating voltage of an XFT is determined by the intersection of the field emission induced breakdown and the Paschen (gas) breakdown curves, as shown in Fig. 1. Operation in excess of 100 kV has been demonstrated using electrode spacings of 1 to 3 cm at gas pressures (hydrogen or helium) in the range 10 to 50 mTorr.

Ignition

With an operating point as shown in Fig. 1, breakdown in the absence of a magnetic field is inhibited. Ignition is then achieved by pulsing a magnetic field (oriented essentially perpendicular to the electric field) to a sufficiently high value to trap electrons in the interelectrode space so that an avalanche will occur and a plasma will form. Because of the confining effect of the magnetic field, it acts much like a local increase in pressure.[8]

The magnetic field strength B required to trigger an XFT at a given applied voltage is determined from the condition that electrons having an energy corresponding to the full applied voltage must have a

cycloidal arch less than the electrode spacing. This translates into the following equation[9]:

$$B \geq \frac{\sqrt{11.4V}}{d} \text{ gauss} \qquad \begin{matrix} d \text{ in cm} \\ V \text{ in volts} \end{matrix}$$

At 100 kV with a 2 cm electrode spacing, a magnetic field of 500 gauss or more will trigger the tube.

To achieve low (≤ 1 μsec) jitter, one cannot rely on the existence of initial electrons created by cosmic rays to start the avalanche. Experiment has shown that this results in jitter times ~msec. Instead, radioactive sources or field emitters must be employed. Jitter times <10 μsec with a 5 mCi γ emitter and < 1 μsec with a field emitting electrode have been reliably achieved. An alternate approach reported by Boucher and Doehler at the Eighth Modulator Symposium[10] is to use a low-level auxiliary discharge. This is less attractive than the two above mentioned methods, however, due to continuous electrode erosion and gas clean-up which occurs with a continuous discharge. (The tube described by Boucher and Doehler should not be confused with an XFT. While triggered into conduction in the same way, their "artatron" immediately transitions into an arc discharge which does not interrupt the circuit current when the magnetic field is removed.)

Conduction

Once ignition has occurred, the avalanche grows and a high density plasma (10^{13} -10^{14} ions/cc) is formed. Electrons are ejected from the cathode surface by secondary electron emission due to positive ion impact. Most of the current at the cathode surface is carried by positive ions because the secondary emission coefficient for light ions at low energies (< 1 kV) is much less than one. The ejected electrons fall through a thin cathode fall (~10^{-3}cm) and enter the glow column with full energy, producing enough electron-ion pairs to sustain the discharge. Because the plasma is essential equipotential, nearly all of the discharge voltage appears across the cathode fall.

The conduction voltage depends on many parameters and is typically 500 ±200 V. Relevant parameters are pressure, magnetic field shape and strength, electrode material and geometry, etc. Good confinement is best achieved using two coaxial cylindrical electrodes with an axial magnetic field. This allows the electrons (which experience a drift perpendicular to both the electric and magnetic fields) to produce ionizing collisions without suffering significant wall losses.

One major difficulty in achieving high current conduction in a modest size tube arises due to the glow to arc transition. As stated earlier, once a vapor arc is formed, suppressing the magnetic field does not interrupt the current. A major research program directed toward suppression of the glow to arc transition has been underway since 1969 and glow current densities in excess of 10 A/cm^2 can now be conducted for times ~100 μs with glow to arc transition probabilities of 10^{-3}-10^{-4} (one arc per several thousand shots).

During conduction, considerable sputtering of the cathode occurs due to the extremely high 500 V ion flux. Typical sputtering coefficients are 10^{-1} to 10^{-2} atoms sputtered/ion hitting the surface, yielding an anode directed flux of cathode metal atoms ~10^{18}/cm^2-sec at 10 A/cm^2. This has two consequences. First, gas clean-up can occur due to burial of the fill gas under the deposited metal at the anode. Second, a greatly increased glow to arc transition rate or an inability to withstand high voltage can occur if flaking of this deposited layer occurs. For these reasons, a chemically inactive gas (helium in particular) is chosen to minimize chemisorption, and heavy metals are preferred to slow the buildup of the anode layer (through decreased sputter coefficients).

Interruption

When the magnetic field is reduced below the critical value required for conduction, the electrons are no longer trapped between the electrodes and ionization ceases. Since current continues to flow momentarily, charges are swept out of the interelectrode space and the plasma density falls, resulting simultaneously in a current fall. Inductance L in the circuit will force the tube voltage V up, according to $V = L\dot{I}$ where $\dot{I}$ is the current rate of change. In the worst case limit of large inductance and negligible stray capacitance, the tube voltage rises to the maximum circuit limit while essentially the full current is still flowing. The instantaneous power dissipation in the tube at the instant the voltage hits the full value is $I_o V_o$, where I_o is the full circuit current and V_o is the peak circuit voltage. This power level can be as high as hundreds of megawatts. Under such severe electrode loading, inhibiting the glwo to arc transition and minimizing the current rise time into the load are crucial for reliable operation with minimal switching losses.

An important point which bears emphasizing is that a crossed field switch tube, by virtue of its inherent ability generate a negative $\dot{I}$, causes the circuit voltage to rise at a rate limited only by the particle loss rate within the tube and the stray capacitance. If the magnetic field within the interelectrode space could be reduced below the critical value at an extremely high rate of fall, the particle loss rate (and hence the $\dot{V}$) would indeed be limited only by the rate of collection of charged particles and the stray capacitance. In practice, however, eddy currents are induced in the electrodes which slow the fall of magnetic field. Since the critical field is not infinitely sharp but has a small, well-defined range (~5 gauss), these eddy currents slow the transition and must be minimized through judicious choice of electrode material thickness (resistivity) and field coil placement.

Experiments

Experiments have been directed towards the development of high current density, high recovery rate switch tubes suitable for modulator applications. These experiments have centered on a tube of the type shown in Fig. 2. The top funnel shaped part is the high voltage feed-through bushing. The magnetic field is applied by an external coil. A cut-away drawing of this tube without magnetic field coil is shown in Fig. 3. The interelectrode space has a 1 cm gap with 500 cm^2 of active cathode surface area. An ionizer electrode to minimize jitter is shown at the bottom of the interelectrode space.

The test circuit is shown in Fig. 4. Capacitor C is initially charged to a few kV which also appears across crossed field tube XFT. Firing the thyratron energizes the magnetic field coil which in turn ignites the XFT. Current then begins to flow in the LC circuit, storing energy in inductor L. When the magnetic field falls below the critical sustaining value, the XFT begins to dionize and L generates a voltage which rises until the spark gap fires. The current then decays with an L/R time constant.

Typical experimental waveforms are shown in Fig. 5. After reaching a peak current of 2.7 kA in 80 μsec, the field is switched off and the voltage rises to 60 kV in about 4 μsec, giving an average $\dot{V}$ = 15 kV/μsec. The break in the current trace is due to electrical noise caused by the spark gap firing.

Once this tube was conditioned to run at these levels, a reliability in excess of 99% was routinely achieved. Gas clean-up was so small that hundreds of shots could be run without a gas refill. Experiments with tubes of similar design indicate lifetimes in excess of 30,000 shots under these conditions.

Applications

Crossed field switch tubes have been developed primarily for power utility applications. Both HVDC circuit breakers and AC current limiters require the interruption of high currents against high forward voltages. It has become apparent, however, that XFT's could be useful for a variety of non power utility applications. Three such applications, protection of delicate electronic components, opening switches for high power current-fed line-type modulators and the substitution of XFT's for hard vacuum modulator tubes are discussed below.

Protection

An XFT can be placed in series with an electronic component and used as a controlled, reusable fuse. Under normal operating conditions, the XFT is closed (i.e., the magnetic field is on and current will be conducted whenever the circuit demands it). In case of a fault, the magnetic field is switched off and the XFT interrupts the current flow. Two advantages of this approach are: (1) by isolating the faulted component, the rest of the circuit can continue to function without disturbance; (2) isolating the component rather than crowbarring it provides more positive protection. Disadvantages include: (1) an insertion dissipation approximately equal to 500 V times the average circuit current; (2) limited life of approximately 10^5 Coulombs: (3) the current rise time must not exceed the formative time of the plasma (~1 μsec).

To eliminate the above three disadvantages, all of which are due to current conduction through the XFT under normal operating conditions, the XFT can be used as the switch in a forced commutation circuit with silicon controlled rectifiers (SCR's) as the bypass switch. Such a circuit interrupting module is shown in Fig. 6. The SCR's are held normally closed by a holding current from power supply PS. When a load fault occurs, the XFT is switched on and back voltages the SCR's until they have turned off. The XFT then switches off the current flow and the voltage rises across the module to the full circuit value. Because the XFT can turn off as well as on, the commutation capacitor can be rated only for low voltage. This puts a low reverse voltage on the SCR's and can provide them with a long, safe turn-off margin without the requirement for storing a large amount of energy.

The following example illustrates the advantage of low voltage forced commutation (LVFC) over full voltage forced commutation (FVFC). Assume the SCR's have a turn-off time of 25 μsec and the circuit current and voltage is 1 kA and 100 kV, respectively. To minimize the stored energy, FVFC would use a precharged 100 kV capacitor which would back voltage the SCR's to nearly 100 kV after passing through current zero at an extremely high current rate of fall. The size of the capacitor would be 25×10^{-3}C divided by 10^5 V which equals 25×10^{-8}F. The stored energy would be 1.25 kJ and a 100 kV power supply and fully charged capacitor would be on standby at all times. Of course, there are some tradeoffs which could be made such as using saturable reactors in series with the SCR's to limit the current rate of fall or storing more energy in the capacitor to limit the reverse voltage, etc. By and large, however, this type of circuit is not very attractive and has therefore seen little use in such applications.

Now consider the LVFC circuit using the on-off switching property of XFT's A precharged 25 μF, 1 kV capacitor can be used. The back voltage on the SCR's is now only 1 kV which is quite reasonable. The energy stored is only 12.5J compared to 1.25 kJ and only a 1 kV power supply is required.

Current-fed Line-type Modulators

A current-fed line-type modulator stores energy in an inductance and delivers it to a load when a switch is opened. The energy density which can be stored in magnetic fields ($B^2/2\mu_o$ = 40 MJ/m^3 at B = 10T) greatly exceeds that which can be stored electrostatically ($\epsilon E^2/2$ = 0.17 MJ/m^3 using a dielectric constant of 3.2 and E = 3.4×10^8 V/M).[11] Therefore, significant size and weight reductions can be achieved through the use of current-fed networks. For specialized applications requiring large amounts of stored energy (>100 kJ) to be delivered to a load in times < 1 msec, a current-fed network is the best way to meet the cost, size and weight requirements. The main reason why such networks have not found widespread use is due to the unavailability of a suitable HVDC opening switch.

A suitable opening switch consisting of the parallel connection of a fast acting mechanical bypass switch S and an XFT is shown in Fig. 7. Low voltage, high current supply V charges the PFN through S until the required amount of energy is stored in the PFN inductance. S then opens and generates enough arc voltage to transfer the current to the XFT (~500 V) which then continues to conduct until S has deionized and is able to withstand the full circuit voltage. The XFT then interrupts the current flow thereby energizing the load L.

One of the fast acting mechanical switches under development at Hughes is shown in Fig. 8.[12] The contacts are enclosed in sulphurhexafluoride gas at 5 atm. absolute. Current flow is from one fixed contact to one moving contact, across the contact bridge to the other moving contact and back to the fixed contact. To open the switch, the pancake coil is energized, inducing eddy currents in the metal disk which push the insulated rod upwards separating the contacts. Gas in the space above the moving contacts is compressed and directed through flow channels (puffer) at the arcs which form. This causes a rise in arc voltage sufficient to transfer the current into the shunt XFT. This switch reliably transfers currents ~2 kA in times ~2 msec and subsequently withstands voltages well in excess of 100 kV.

A first order estimate of the dissipation of the complete switch (bypass plus XFT) can now be made. During one complete cycle, dissipation occurs in four discrete steps:

1. Charging through bypass switch.
2. Arcing in bypass switch.
3. Conduction in XFT.
4. Interruption in XFT.

We define the following symbols:

I_o	Peak circuit current
R	Current path resistance of bypass switch
t(charge)	Network charging time
V (arc-max)	Maximum arc voltage of bypass switch
t (bypass opening)	Opening time of bypass switch
V (XFT)	Conduction voltage of XFT

t (bypass deionizing)	Deionization of bypass switch
V_o	Load voltage
t (XFT)	Interruption time of XFT

Assuming a linear current rise from zero to I_o, a linear arc voltage rise from zero to V (arc-max) and a linear voltage rise from (essentially) zero to the load voltage, we obtain for the one cycle switch dissipation.

$$D = \left(\frac{I_o}{2}\right)^2 R\, t(\text{charge}) + \frac{V(\text{arc-max})}{2} I_o t(\text{bypass opening}) + V(\text{XFT})\, I_o\, t(\text{bypass deionizing}) + 2\,\frac{V_o}{2}\, I_o\, t(\text{XFT})$$

The last term is multiplied by two to account approximately for XFT dissipation during the charge collection period (after current has transferred into the load). The following values are typical for the complete switch:

$R = 50\ \mu\Omega$

$V\ (\text{arc - max}) = 1\ \text{kV}$

$t\ (\text{bypass opening}) = 1\ \text{msec}$

$V\ (\text{XFT}) = 500\ \text{V}$

$t\ (\text{bypass deionizing}) = 100\ \mu\text{sec.}$

$t\ (\text{XFT}) = 4\ \mu\text{sec.}$

Assuming a modulator operating at I_o = 10 kA and V_o = 100 kV with a 1 sec. charge time, we find $D = (1.3 + 5.0 + 0.5 + 4.0) \times 10^3 = 10.8$ kJ. The greatest dissipation by far occurs during opening of the bypass switch and interruption of the XFT.

As a typical example of modulator efficiency, assume a 20 Ω load to be fed with 5 kA for 200 μsec. This requires a network inductance of 2 mH storing 100 kJ. If this inductance is charged in 1 sec. to 10 kA (by a 20 V dc supply), approximately 10 kJ are dissipated in the switch giving an efficiency of 90%.

Hard Tube Modulators

The hard tube modulator is distinguished from a line-type modulator in that only a small portion of the stored energy is delivered to the load per pulse. To achieve this, a switch tube capable of closing and opening the circuit is required. Prior to the development of the XFT, the only candidate for this function was the hard vacuum tube. The limitations of hard vacuum tubes greatly favored the development and use of line-type (voltage-fed) modulators for which closing switches were readily available. The most severe limitations of hard vacuum tubes are listed below.

1. High voltage drop (1-2 kV)
2. Low peak current (1 kA)
3. High filament power (10 kW)
4. Large size and weight
5. Fragility

In contrast, an XFT possesses the following qualities:

1. Lower conduction drop (500 V)
2. Higher peak current (> 3 kA)
3. Negligible standby power
4. Relatively compact and lightweight
5. Rugged

Limitations of the XFT must also be noted.

1. Limited life (~50,000 shots)
2. Limited pulse width range (5-100 μsec)

It thus appears that for those applications where the limited life and pulse width range are tolerable, an XFT offers significant advantages over a hard vacuum tube.

Due to the availability of a new switch tube possessing the on-off switching capabilities of a hard vacuum tube but without many of the limitations, the possibility of using a "hard tube" modulator in place of a line-type pulser should be re-examined for each particular application. Specifically, a "hard tube" modulator can offer the following advantages over a line-type pulser:

1. Easily variable pulse width
2. Simplicity
3. Flexibility--use with a variety of load impedances
4. Charge voltage much less than twice load voltage
5. Energy storage rather than pulse discharge capacitors
6. More control when used with loads with time varying impedance

Conclusions

A crossed field switch tube has been developed which is capable of closing and opening HVDC circuits. Control is exerted by a magnetic field in the range 10^{-1} - 10^{-2} T, depending on the applied voltage. Conduction voltage drops ~500 V are typical as are pulse widths in the range 5-100 μsec. One particular tube has been extensively operated as an interrupter at the 2.5 kA, 60 kV level with a voltage recovery rate of 15 kV/μsec (no shunt capacitor was required to assist interruption). Tubes of this type have demonstrated high reliability (>99%) with expected lifetimes well in excess of 10,000 shots.

The existence of an HVDC interrupter with the characteristics exhibited by XFT's makes possible many applications not heretofore possible. Two applications in the power utility area are dc circuit breakers and ac current limiters. Another application is the protection of electronic components in high power pulsers. This is accomplished by inserting an XFT in series with the component and using the XFT as a controlled, reusable fuse. SCR's can be used in series with the component instead of the XFT in order to increase life and minimize insertion loss. The XFT is then used to off commutate the SCR's in a low voltage commutation circuit which has great advantages over conventional, full voltage commutation circuits.

Current-fed line-type modulators which have not been widely used due to the unavailability of a suitable HVDC interrupter can now be considered, especially for high pulse energy applications. The XFT is used to take over current from a mechanical switch and perform the HVDC interruption Finally, used as an on-off switch, an XFT has lower voltage drop, higher peak current capability and negligible standby power when compared to any hard vacuum tube in existence today. This opens the possibility for the use of "hard tube" modulators using XFT's in a variety of applications previously requiring the use of voltage-fed, line-type modulators.

Acknowledgments

The author wishes to acknowledge that the work reported herein is the product of many individuals, including R. Harvey, G. Hofmann, R. Holly, W. Knauer and N. Reed.

REFERENCES

1. R. E. B. Makinson, J. M. Sommerville, K. R. Makinson, and P. Thoneman, "Magnetically-Controlled Gas Discharge Tubes," J. Appl. Phys., 17, 567 (July 1946).

2. W. Knauer, "Mechanism of the Penning Discharge at Low Pressures," Hughes Research Laboratories RR No. 223 (November 1961).

3. W. Knauer and R. L. Poeschel, "The Diocotron Effect in Plasmas and Gas Discharges", Proc. 7th International Conference on Phenomena in Ionized Gases, Beograd, 1966.

4. W. Knauer and M. A. Lutz, "Measurement of the Radial Field Distribution in a Penning Discharge by Means of the Stark Effect," Appl. Phys. Lett., 2, 109(15 March 1963).

5. H. Gallagher, G. Hofmann and M. Lutz, "The Crossed Field Switch Tube - A New HVDC Circuit Interrupter," IEEE Trans. on Power Apparatus and Systems, PAS-92, 702 (March/April 1973).

6. Gunter A. G. Hofmann and Michael A. Lutz, "A High Power Crossed Field Discharge for HVDC Interruption,", 2nd International Conf. on Gas Discharges, London (1972).

7. Michael A. Lutz and Gunter A. Hofmann, "The Gamitron - A High Power Crossed Field Switch Tube for HVDC Interruption," submitted to Proc. IEEE.

8. J. M. Somerville, "Sparking Potentials in a Transverse Magnetic Field," Proc. Phys. Soc., 65B, 620 (August 1952).

9. Discharge and Plasma Physics, S. C. Haydon, ed., University of New England, Armidale, N. S. W., Australia, 128 (1964).

10. G. Boucher and O. Doehler, "The Artatron, A High-Power Switch Device," Eighth Symposium on Hydrogen Thyratrons and Modulators (1964).

11. Private communication with Mr. Bruce Hayworth, Capacitor Specialists, Inc. (714) 747-4000.

12. N. E. Reed, "A Novel Switching Device for Use in an HVDC Circuit Breaker," Conference Paper (72 447-1, IEEE Power Engineering Society Meeting, San Francisco (July, 1972).

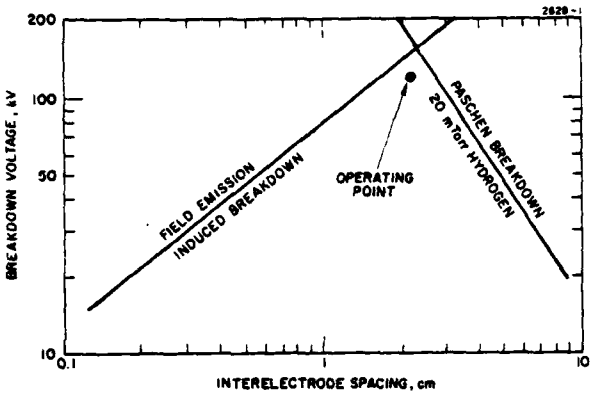

Fig. 1. Operating parameters.

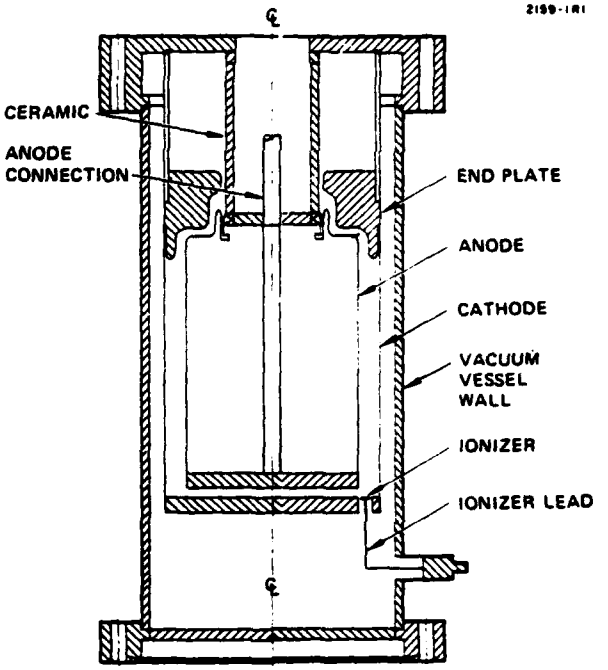

Fig. 3. Sectional view of 2.7 kA, 60 kV crossed field tube.

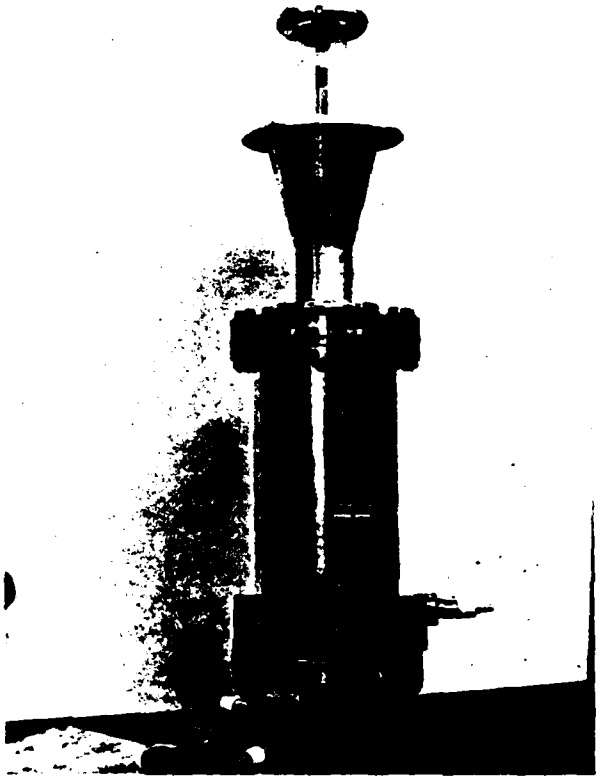

Fig. 2. 2.7 kA, 60 kV crossed field tube.

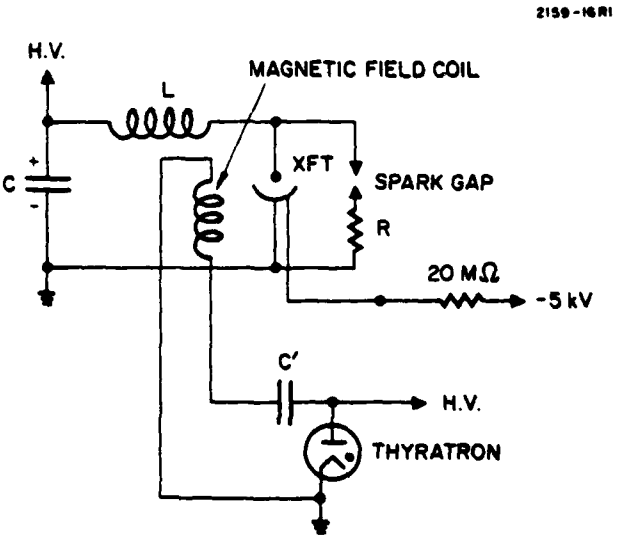

Fig. 4. Inductive energy test circuit.

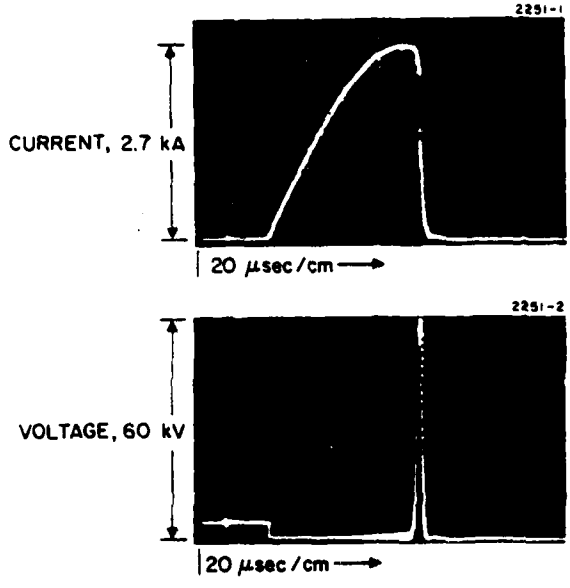

Fig. 5. Current-voltage waveforms.

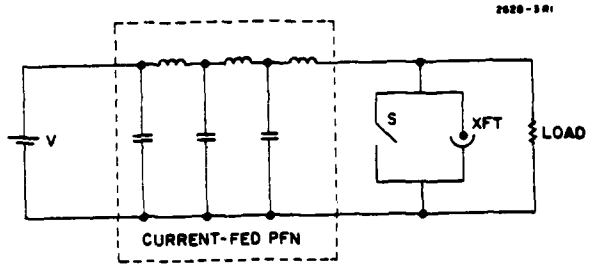

Fig. 7. Current-fed line-type modulator with mechanical bypass (inductor charging) switch S and crossed field tube XFT for HVDC switching.

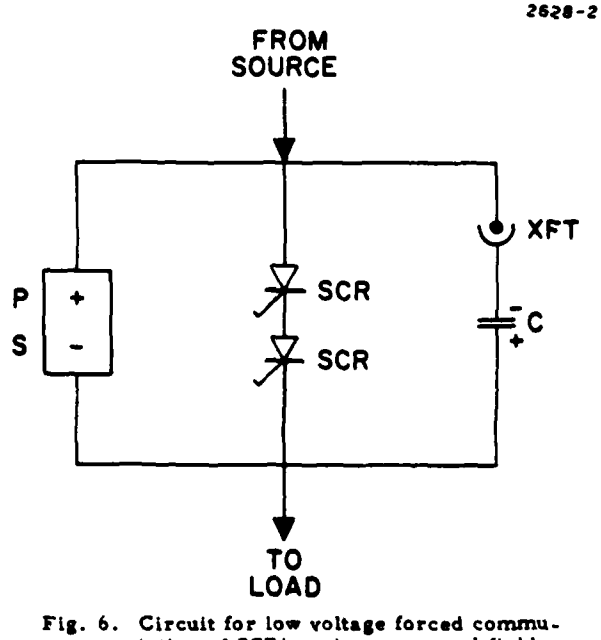

Fig. 6. Circuit for low voltage forced commutation of SCR's using a crossed field tube.

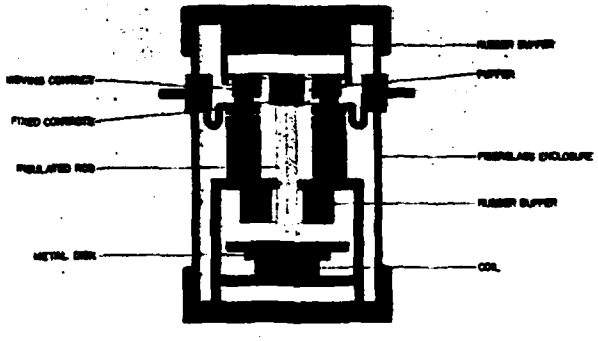

Fig. 8. Fast acting (~1 msec) mechanical bypass switch.

600 kW PEAK HIGH REPETITION RATE HARD TUBE MODULATOR*

Rudolf A. Ecken, Leonard Genova
Stanford Linear Accelerator Center
Stanford, California

Summary

This paper describes the design, fabrication and test results of a modulator for the 220 kW S-Band klystrons which are part of the proposed beam recirculating system at the Stanford Linear Accelerator Center.

The unit consists of a conventional three-phase-bridge power supply, an energy storage bank and a series modulator, with hard switch tube and associated driver circuitry.

Modulator parameters are as follows:

Pulse Voltage	32 to 37 kV Peak
Pulse Current	15 A Peak
Repetition Rate	0 to 44,000 pps
Pulse Width	2.5 μs Flat Top
Duty Cycle	13% max.

The driver circuitry floats at the switch tube cathode potential of 41 kVdc. The paper details the difficulties encountered in designing the pulse coupling, driver stages and protective circuitry. Test results are presented with pictures of pulse shapes.

Final consideration is given the latest proposal of powering 500 kW S-Band klystrons at the same repetition rate and duty cycle and adaptation of the existing modulator with minimal changes to its circuitry.

Introduction

One of the proposals for increasing the energy of the Stanford Linear Accelerator calls for recirculating the electron beam through the accelerator structure before reinjecting it for a second accelerating pass. During the storage time of 2.8 ms (which is the full interpulse period based on operation at 360 pulses per second), the beam would be completing 122 revolutions. Beam losses due to synchrotron radiation were to be compensated for by 16 klystrons operating at the accelerator frequency of 2856 MHz and pulsed at a repetition rate of 43500 pulses per second (corresponding to the recirculating period of about 23 μs).

In order to prove the feasibility of the loss compensation system we decided to build one working prototype RF amplifier. Budgetary considerations forced us to use many parts available around the SLAC site which were not optimally suited for the task at hand: for example, the cabinet was too small for the number and size of components and assemblies and the main capacitor was too low in voltage and too high in inductance necessitating series connection of two units and adding a high frequency one in parallel (which did not help the size limitation of the cabinet and was not fully effective in removing the beam voltage pulse top ringing).

*Work Supported by the U. S. Atomic Energy Commission

General Considerations

The proposed klystrons were to have the following characteristics:

Peak RF Output	220 kW
RF Pulse Width (Flat Top)	2.5 μs
Repetition Rate	43,500 pps
RF Duty Cycle	11%
Peak Beam Voltage	37 kV
Peak Beam Current	14.8 A

An existing low duty cycle klystron was redesigned and modified to take the higher average power and repetition rate. The amplifier used during system tests had its cathode structure submersed in a small oil container to minimize corona discharge around the ceramic insulator (which did not particularly help the total load capacitance).

The high repetition rate coupled with the available recovery time of less than 20 μs all but dictated the use of a hard tube switching circuit and since voltage and current requirements were moderate, we circumvented the problems associated with pulse transformers at high duty cycles by choosing a series switch arrangement. (Fig. 1)

Since the dc supply has to provide not only the klystron current but also the charging current for all the capacitances in the switch tube plate and klystron cathode circuits, the modulator pulse has to be wider than the RF pulse. A further increase seemed necessary to exclude a period of anticipated ringing at the beginning of the flat top from getting into the RF pulse. Assuming a voltage pulse flat top of 2.6 μs and a total (load and stray) capacitance of 300 pF, the average load current and modulator duty came out to be approximately 2 A and 13% respectively. Therefore the switch tube had to hold off at least the klystron voltage plus its own drop and pass 15 A of plate current with reasonable drive requirements.

We selected an Eimac Y499 tetrode which is a specially processed 4CX35000C with a voltage hold-off capability of 55 kVdc. At 2 kV drop this tube delivers more than 20 A of plate current with zero volts at the control grid and 1000 V at the screen grid. The constant current characteristics are such that any dc voltage changes, including those due to line voltage fluctuations, are attenuated by a factor of two. By setting the nominal tube drop at 4 kV it was possible to absorb $\pm$ 2 kV of dc voltage changes and still operate at full load current and within the tube dissipation rating. As a consequence we built a power supply with an output rating of 41 kV at 2 Adc.

The ac power at 530 V is stepped up to 31 kV line to line in the main power supply transformer. The input voltage was chosen to facilitate use of the unit at various locations and from different sources: during modulator tests at 530 V from a variable transformer, during production tests at 480 V using an auxiliary boost transformer, and finally in our klystron gallery at 590 V from the existing induction voltage regulators using the auxiliary transformer in a bucking arrangement. The high voltage from the

wye connected secondary is rectified in a conventional three phase bridge circuit resulting in a dc output of 41 kV at 2 A.

A single section filter composed of a 20 H choke and two 2.7 μF, 25 kVdc capacitors in series reduces the 360 Hz ripple to about 35 V peak to peak. The filter capacitor also supplies the load current of 15 A resulting in a droop of 25 V during each pulse. The stored energy is approximately 1200 joules. A 13 Ω resistor was added in series between switch tube and klystron to keep the energy dissipated in the load below a safe level of 10 joules in the event of simultaneous arcs in both tubes.

Modulator

The grid driver shown in Fig. 1 is of the floating deck type. We chose this circuit because of its inherent high speed capability and good efficiency even though it is more dangerous to service on a routine basis. The driver has to supply all the control and screen grid voltages necessary to hold the switch tube at cutoff during the interpulse period, drive it into conduction for the pulse time and return it to cutoff after the pulse. As a screen supply we used two available regulated supplies of 450 V each in series. Since the grid did not have to be driven positive, the driver could be relatively small and simple, or so we thought.

Our first driver circuit is shown in Fig. 2. It consists of bootstrap amplifier V1, cathode follower V2 and tail biter tubes V4 and V5. All tubes are normally biased at or near cutoff. A full width pulse, generated at ground level, is fed through a pulse transformer with high voltage isolation to the grid of V1. V1 conducts, thereby turning on V2 which raises its cathode and the switch tube grid potential from -700V to approximately zero volts. The pulse transformer fall time is sampled and differentiated by the tail biter circuit, and fed to V4 and V5. Both tubes conduct and discharge V2 and V3 grid circuits respectively.

In testing we found the driver to work very satisfactorily without the isolation pulse transformer. Rise and fall times of 80 ns were realized at the switch tube grid with very good flat top characteristics and little change in pulse shape between low and full repetition rates. Even with a pulse transformer the drive pulse was quite acceptable as long as primary and secondary were at the same reference level and as long as the repetition rate was below approximately 20,000 pps. At the higher rates the transformer would not reset sufficiently. Changing to a light link coupling, the necessary high level amplifier circuitry turned out to be quite bulky and the bootstrap was not capable of supplying the required charging current.

A new circuit was tried using the existing cathode follower and most of the bias and plate supplies but replacing the full width transformer coupling system with one employing separate start and stop triggers and substituting a multivibrator for the bootstrap stage. (Fig. 3)

Briefly, this circuit works as follows: a trigger is fed to the low level pulser (at ground potential). This pulser produces two output triggers, the time separation of which determines the modulator pulse width. The voltage isolating system we used to couple the triggers from ground level to the driver deck, which sits at 41 kVdc nominally, employes small low cost components and provides enough common mode rejection to eliminate feedback from "deck bounce". Start and stop channels each consist of two low voltage pulse transformers and four TV type 500 pF, 30 kV capacitors for high voltage isolation, each leg having two capacitors in series. The transformer center taps are tied to their respective reference levels, giving us a balanced system with inherent common mode rejection. The first trigger passes through the "start" channel and turns off V2-V5 which are normally conducting. The multivibrator changes state, V1 turns on, and a positive pulse is fed to cathode follower V7. The V2-V5 plate resistor was selected to be 1kΩ in order to obtain a good rise time, even though it has to dissipate nearly 1 kW. The cathode follower is used to rapidly charge the 500 pF input capacitance of the main switch tube.

The stop trigger resets the flip flop to its original condition by turning off V1, thus terminating the output pulse. The stop trigger also momentarily turns on tail biter tube V6 which rapidly discharges the main switch tube input capacitance by driving the grid more negative than its normal -700 V bias level, resulting in a measured drive pulse fall time of 80 ns. Since we utilized dc coupling throughout the driver there was no change visible in the drive pulse shape when the repetition rate was varied between 10 and 44,000 pps.

This circuit was used to check out the klystron for hundreds of hours, yet we were not completely satisfied with the output voltage waveform. At the grid of the switch tube the measured rise time was 80 ns from the 10% to 90% points, but due to the 1 kΩ driving impedance into the cathode follower grid, it took an additional 400 ns to reach the steady state value. Peaking in the plates of V2 through V5 helped, but was abandoned because it introduced some ringing on the pulse top.

The klystron beam voltage pulse (inverted) is shown in Fig. 5. Rise and fall times are about 0.5 and 1.5 μs respectively. The long fall time results from the load and stray capacitances being discharged through the klystron's rising resistance with decreasing voltage while the switch tube is cutoff. To compensate for the additional time required to reach pulse steady state voltage, the modulator pulse width was increased by approximately 500 ns and the RF pulse was delayed to fall within the flat top. As a consequence the modulator efficiency suffered. Therefore, we decided to modify the driver circuit to obtain better rise time and efficiency. Again we utilized as many of the existing power supplies and other components as possible (Fig. 4). The new circuit (Model 3) works as follows:

V1-V8 are 8 parallel tubes (6LQ6's) bootstrapped to the grid of switch tube V9. They are cutoff during the interpulse time. A low level pulse generator at ground level drives a light emitting diode (LED) for 0.3 μs. The light is transmitted through a fiber optics bundle to the deck illuminating a photo transistor. The fiber optics bundle provides the necessary high voltage isolation between ground and deck. The photo transistor triggers an IC type monostable multivibrator programmed to generate the necessary pulse width of 2.6 μs. The 5 V output pulse from the multivibrator is stepped up to a positive 100 V pulse by a low level tube type amplifier, fed into the grids of V1-V8 which in turn deliver a drive pulse to the grid of switch tube V9. Clipper tube V10 holds the V9 grid drive at approximately zero volts. At the end of the pulse V1-V8 turn off and the grid of V9 returns to cutoff bias.

To minimize klystron voltage changes caused by power supply variations, we included a regulator circuit as part of the grid driver. At our operating voltages, 600 V of bias is sufficient to cut-off the Y499 tube. The output pulse from the bootstrap stage rides on top of the bias supply. Therefore by changing the bias voltage it is possible to vary the switch tube grid voltage and thereby its drop. The regulator circuit works as follows: A decrease in the dc voltage is sampled by a voltage divider connected across the storage capacitor and is fed to the regulator circuit. Its output increases the drive to the transistor shunting a 100 V bias supply which is connected in series with the main 600 V bias supply. The total bias is reduced and the V9 grid drive increases, resulting in a decrease in switch tube drop which compensates for the lower power supply voltage.

Test Results

Figs. 6-10 show pertinent modulator waveforms. It should be noted that our viewing circuits are not perfect and introduced some ringing. These photographs were taken at the final klystron operating conditions. Because of higher RF gain, the klystron voltage was set at 33 kV rather than the design value of 37 kV. Comparing voltage (Fig. 6) and current (Fig. 8) waveforms, the effect of load capacitance charging can be clearly observed. At the present, phase measurements are being performed and therefore no attempt has yet been made to compensate for droop or otherwise shape the pulse flat top.

Conclusion

The modulator has worked satisfactorily for over 450 hours. Its reliability has been very good even though two magnetic components (filter choke and filament isolation transformer) experienced voltage breakdown and were redesigned and replaced by the vendor. There has been talk about increasing the peak klystron RF power to 500 kW, requiring 50 kV and 20 A out of the modulator. We are planning to accomplish this using a new HV transformer, a larger rectifier, a higher voltage filter network and a new switch tube (Eimac Y676 rated at 75 kV). We should be able to use the same driver with no modifications because the Y676 has higher gain and lower input capacitance.

Acknowledgements

We wish to thank Carl W. Olson for his constant guidance and William A. Johnson for his many helpful suggestions and assistance in testing.

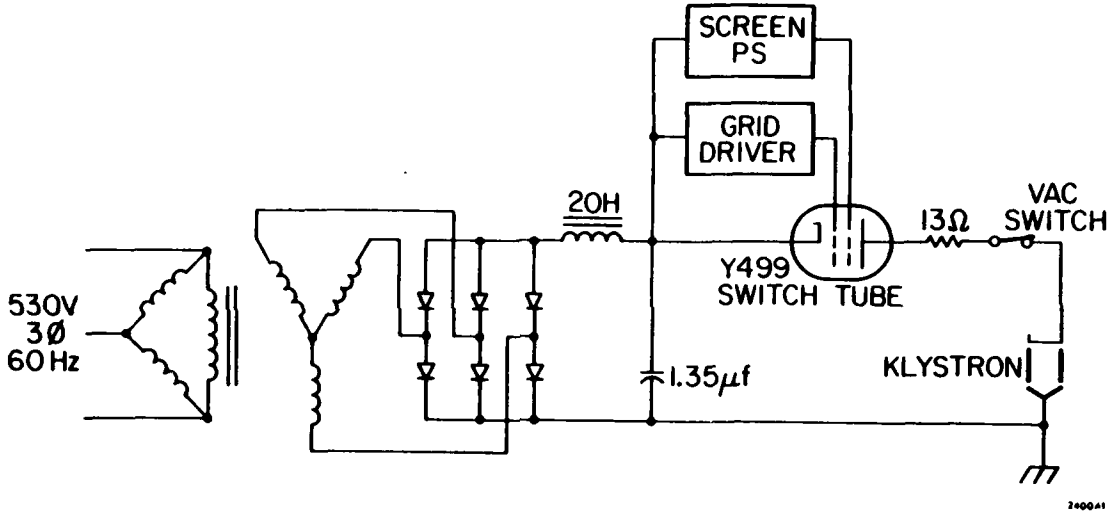

Fig. 1 RLA Modulator Simplified Diagram

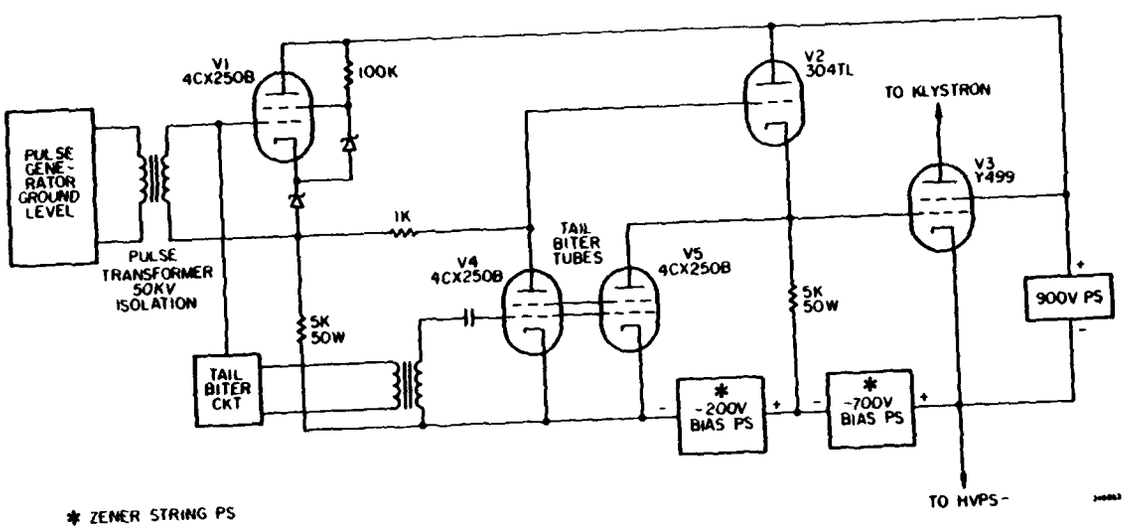

Fig. 2 RLA Modulator Switch Tube Driver Model 1

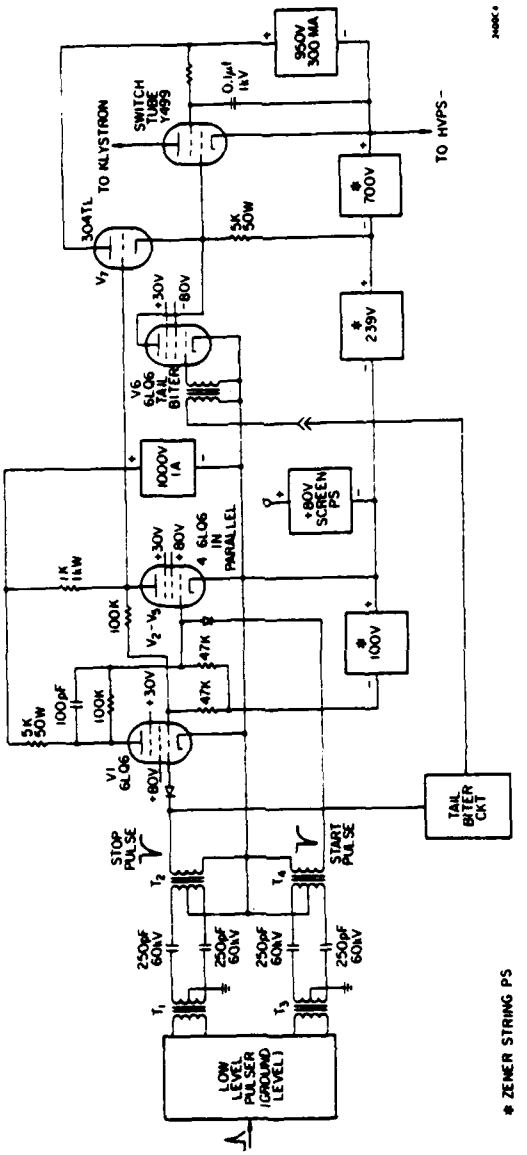

Fig. 3 RLA Modulator Switch Tube Driver Model 2

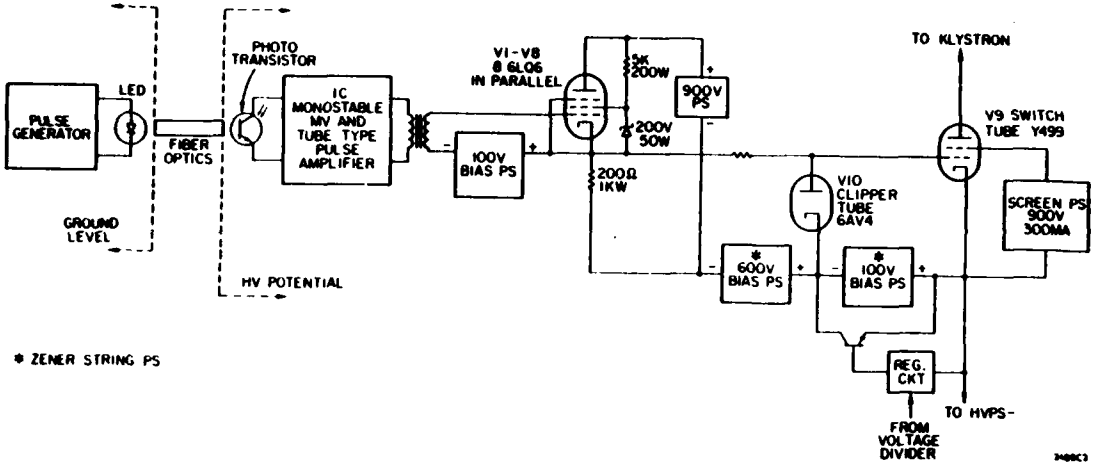

Fig. 4 RLA Modulator Switch Tube Driver Model 3

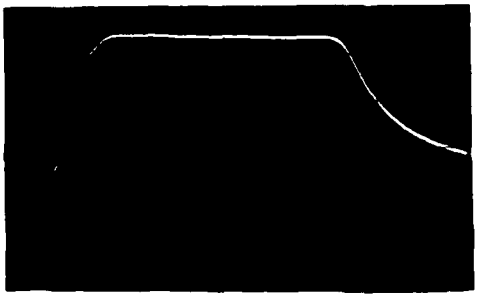

Fig. 5 Model 2 Driver. Klystron Pulse (shown inverted).
Vertical 10 kV/div
Horizontal 0.5 μs/div

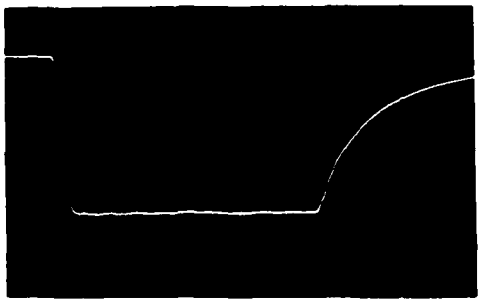

Fig. 6 Model 3 Driver. Klystron Pulse.
Vertical 10 kV/div
Horizontal 0.5 μs/div

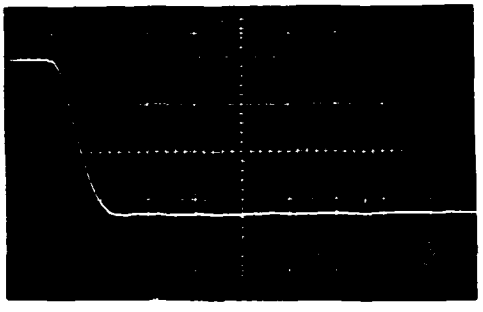

Fig. 7 Model 3 Driver. Klystron Pulse Rise Time.
Vertical 10 kV/div
Horizontal 0.2 μs/div

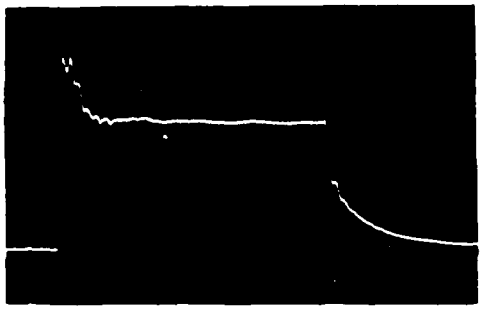

Fig. 8 Model 3 Driver. Klystron Current.
Vertical 5 A/div
Horizontal 0.5 μs/div

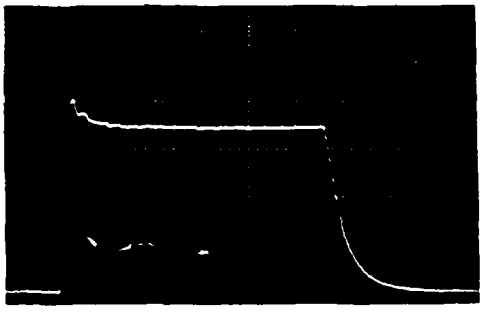

Fig. 9 Model 3 Driver. Switch Tube Grid Voltage.
Vertical 200 V/div
Horizontal 0.5 μs/div

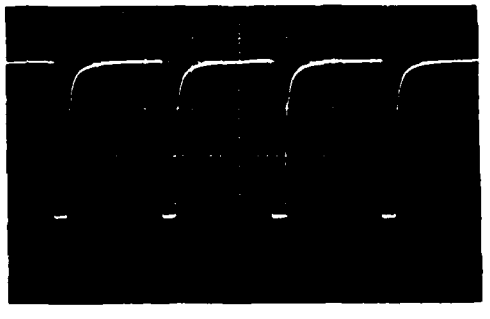

Fig. 10 Model 3 Driver. Klystron Pulse.
Vertical 10 kV/div
Horizontal 10 μs/div

NOTE: ALL PHOTOS TAKEN AT 43,500 PULSES PER SECOND.

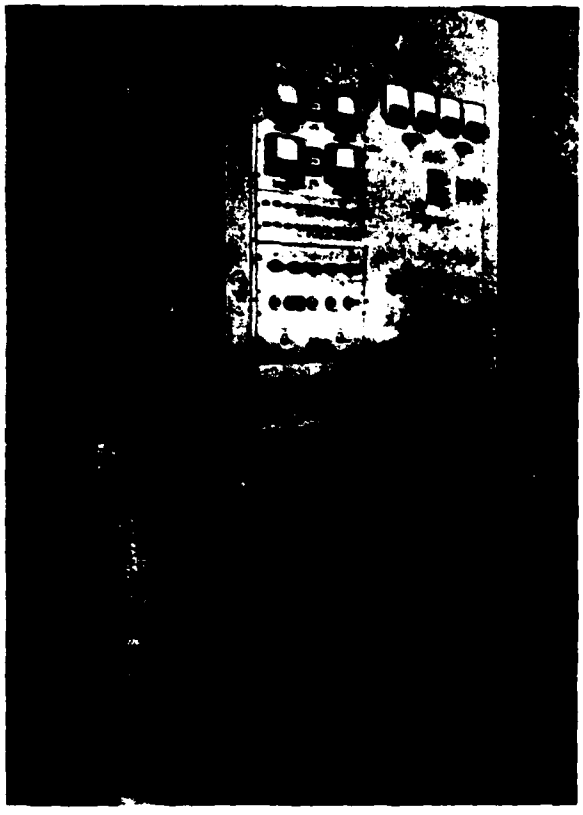

Fig. 11 Modulator Cabinet

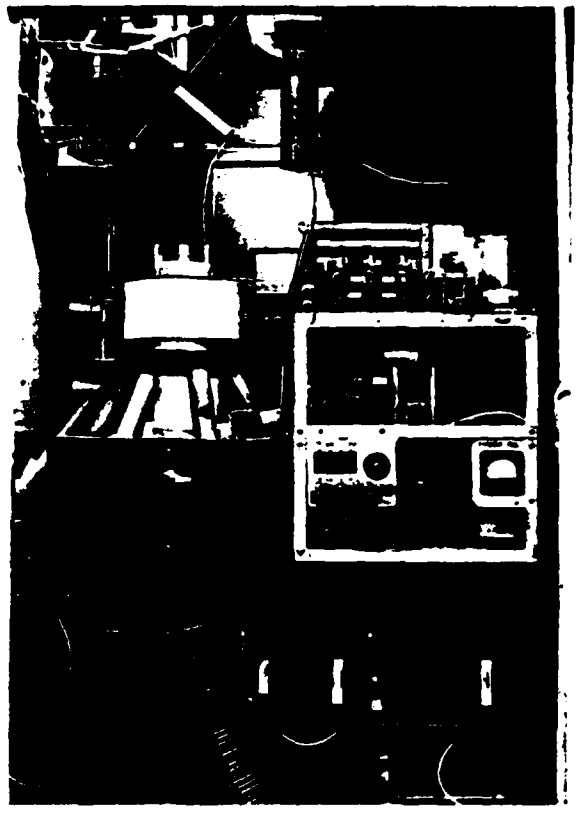

Fig. 12 Switch Tube and Driver

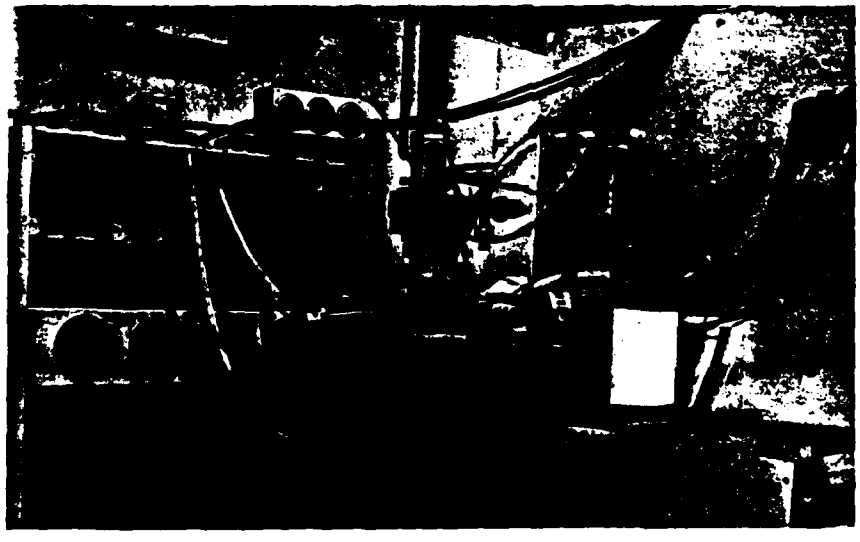

Fig. 13 Klystron Under Test

DESIGN AND PERFORMANCE OF THE LAMPF 1-1/4 MW KLYSTRON MODULATOR

Paul J. Tallerico
Robert L. Cady
James D. Doss

University of California
Los Alamos Scientific Laboratory
Los Alamos, New Mexico 87544

Summary

A design for a very reliable single-triode modulator for a 1-1/4 MW modulating-anode klystron is presented. The operating voltage is 86 kV and the variable pulse length ranges from 200 usec to 1.2 msec. The basic modulator circuit, which uses a novel Zener diode bias circuit, and several of the individual components are described in detail. Over 140,000 high-voltage hours have been accumulated on these modulators. The principal failure mechanism is grid emission from the triode. These failures can be anticipated and repaired during a normal maintenance period. The triode is then reprocessed and reused. Tube life data and a summary of the failures modes are presented.

I. Introduction

Forty-four 1-1/4 MW klystrons are used at the Los Alamos Scientific Laboratory, Clinton P. Anderson Meson Physics Facility (LAMPF), to accelerate protons from 100 to 800 MeV.

The critical requirements which influenced the modulator design are the long video pulse length of 1.2 msec and the reliability at the 86 kV operating voltage. Since the proton beam is constantly gaining velocity along the accelerator, the failure of a single modulator makes it impossible to accelerate the beam beyond that rf module.

The klystron and modulator assembly is shown in Fig. 1. The entire assembly can be moved on an airpad by two men. A complete spare klystron module is located in each of the rf cluster buildings and it takes two hours to replace a module.

II. Design Details

A. Electrical Design

A single triode is used to switch the potential of the modulating anode from the cathode potential of -86 kV to about -10 kV. The basic modulator circuit is shown in Fig. 2. The triode is biased slightly beyond cut-off and driven into saturation by the 250 V drive pulse through the 3:1 pulse transformer T2. The low end of the 100 kΩ resistor is thus grounded and the modulating anode voltage is reduced to a low value, which turns on the klystron current. The 100 kΩ resistor is made of twenty 5-kΩ wafers; thus, the "on" voltage of the modulating anode is adjustable in 5% steps. One 5-kΩ wafer may be replaced with a 2-kΩ wafer, if it is desirable to adjust the voltage in smaller steps. This feature is used to compensate for perveance variations between klystrons.

The three isolation transformers, the 100-kΩ resistor and the switch-tube enclosure are the largest components in the modulator, which is shown in Fig. 3. The transformers required special care in design. The cores are 12-mil tape-wound with 11-3/4 in. square windows. The klystron and triode filament transformers have a 2 in. x 2 in. core cross section, while the pulse transformer has a 3 in. x 3 in. core. A double Lucite shield is placed around the primaries to improve the voltage hold-off capability. The secondary windings form a 3 in. diam bundle to reduce the fields at the secondary surfaces, and copper corona shields are placed around the interior of the windows. The 3:1 pulse transformer has 125 turns on its primary and is shown in Fig. 4.

One current transformer is used to monitor the total high voltage current in the modulator. This transformer is read by the crowbar system. A second current transformer is used to monitor the cathode current in the klystron. The current transmission through the klystron can be checked by comparing the voltage developed across the 0.1 Ω collector resistor with the output of the cathode current transformer. A capacitor voltage divider is attached to the modulating anode to check the output of the modulator.

The 10 Ω resistor in the plate lead of the LPT-44 is used to monitor the triode's plate current. The duty factor of the LPT-44 and its dc plate current are monitored by a diode clipping circuit which is in parallel with a trip-off meter. The meter shuts off the high voltage supply whenever the duty factor or dc plate current exceeds a preset value.

B. The Zener-Diode Bias Circuit

The modulator was originally designed with a tetrode as the switch tube. The switch-tube power transformer had three secondaries; the filament supply, the

screen grid bias and the control grid bias.

Subsequent calculations showed that the tetrode was driven to its dissipation ratings in this circuit. In addition, the screen and control grid bias rectifiers would sometimes fail when a crowbar occurred. These problems were overcome by substituting an LPT-44 triode (a lower-voltage version of the ML-8495) for the tetrode and using a high-power Zener-diode self-bias circuit, which is now discussed in some detail.

It can be seen from Fig. 5 that:

$$e_{gk} = e_s - e_z$$

Thus, between pulses, when the input signal is zero:

$$e_{gk} = e_z$$

The next figure will show that the Zener voltage under zero-drive conditions (as well as with signal present) is actually the same value as the rated Zener breakdown potential, E_z. For proper operation it is necessary to select E_z to be the same as the rated cutoff voltage for the particular vacuum tube under consideration. A value for E_z that significantly exceeds the rated cutoff potential will increase the requirement for grid drive power. Our modulator requires nine 45 V Zeners in series to produce the proper bias.

Figure 6 illustrates the method of arriving at a graphical method for simultaneous solution of the two equations:

$I_p + I_g = I_k + f(E_{gk})$ (Plate voltage is constant)

$I_z = g(E_z)$

These curves can be plotted on the same axis, because:

$I_z + I_k$ and $E_z = -(E_{gk} + e_s)$

The Zener characteristic curve is represented by the dotted line to the left of the vertical axis for the case where $e_s = 0$. The intersection with the tube characteristic determines the vacuum tube operating point with no signal present. The level of cathode and Zener current on the graph in this area is exaggerated so that the intersection of the two curves can be clearly seen. Whenever e_s is not zero, the Zener curve must be shifted to the right by an amount equal to the level of e_s. For example, the dotted Zener curve to the right of the vertical axis represents the situation when e_s has reached a value of $E_z + E_1$ ... the case where the grid is E_1 volts positive with respect to the cathode.

It is important to realize that the voltage across the Zener diode remains essentially constant during the cutoff and the conducting modes of vacuum tube operation. While Zener dissipation during the cutoff mode can usually be ignored, the grid and anode currents flowing through the Zener in the "on" mode create a significant Zener dissipation. In the case of our modulator, these currents reach a peak of approximately 1 A, so that the peak Zener dissipation is about 400 W. Since the duty factor should rarely be higher than 14%, and since there are actually nine series-connected Zener diodes, the average dissipation per diode is limited to about 6.2 W.

For application of this method of biasing on higher power modulators, one can overcome the dissipation problem to some extent by the use of "synthetic Zener" circuitry similar to that shown in Fig. 7.

The total current carried by this circuit is $(\beta + 1)$ times that current carried by the Zener used in the circuit. This means that the transistor dissipation is β times that of the Zener, where β is the dc current gain of the transistor. Thus, with careful transistor selection, it is possible to increase the power capability by a factor of $(\beta + 1)$ over that of the original Zener. (The assumption is naturally made that the transistor has sufficient dissipation capability, i.e., $P_t + \beta P_z$, where P_t is the transistor dissipation rating and P_z is the Zener rating.)

General advantages of the Zener self-biasing method for high-voltage modulators include:

1. Increased reliability; due to the simplicity of the circuitry.

2. Economy; due to the reduced number of parts, particularly the high-voltage interface power transformer.

3. Performance; because one does not experience the pulse droop problem that is present whenever grid currents tend to charge the output capacitor in a conventional floating bias supply.

C. Mechanical Design

The complete modulator tank is 47 in. x 86 in. and contains about 400 gal of transformer oil. Several of the modulators have operated for three years with no maintenance. An oil pump is mounted on the lid of the modulator to circulate oil through the LPT-44 anode and through a heat exchanger. This heat exchanger is used to maintain a 100°F oil temperature. There is a small door on each modulator tank lid which may be opened to change either the Zener-diode bias board or the switch tube without removing oil from the modulator.

The complete modulator assembly weighs 7,000 lb. These modulators are moved over the half mile between the accelerator cluster buildings and a test building on a large forklift. The modulators are moved within a

building on airpads.

III. Performance and Reliability

The capacitance of the floating deck and transformers is 500 pF, which limits the rise time to 50 μsec. About half of this capacity is associated with the modulating anode. This rather long rise time is acceptable for our application because the fill time of the accelerator is a few microseconds. The rf is turned on during the video pulse rise to reduce arcing at the klystron and accelerator rf windows. The droop on the pulse transformer doesn't affect the output pulse because the switch tube is driven well into saturation by the drive pulse.

Over 140,000 high-voltage hours and 160,000 filament hours have been accumulated on these modulators. The maintenance required is summarized in Fig. 8 where the modulator faults which required operator action are plotted for the past eleven calendar quarters. The high-voltage hours are shown as horizontal lines and the light symbols are faults which were corrected during normal maintenance periods. The present operating cycle for LAMPF is twelve days on, followed by nine days down time. The rf systems are normally checked two days before each run period and serious faults which could shut the machine down (shown shaded in Fig. 8) are often corrected during down time. Thus, the three serious faults in 1973 were all corrected during the normal down time periods.

Excessive leakage current due to grid emission is the cause for 23 of the 24 switch tube faults, where a fault is defined as more than 3 mA leakage at 86 kV. At this level, enough x rays are produced to be a hazard at the modulator surface, although the plate dissipation rating of the LPT-44 is not approached. These tubes are reprocessed by electron-bombarding the grid with a 200 W, 200 V ac power supply. The average age of the triodes in service is 2,515 filament hours, while the average age of the triodes which need grid processing is 1,884 h. These ages indicate that the grid emission problem is only evident on a small subset of the total population. Although some reprocessed triodes are back in service, not enough time has been accumulated on them to form definite conclusions about their life.

A total of two switch-tube failures have occurred in the 140,000 h of modulator operation to date. One occurred when a filament broke after the modulator was moved and the other was a grid to filament short after an attempt at reprocessing the grid.

Of the 16 modulator faults shown in Fig. 8, 6 were faults in the oil system, 5 were shorted or open connections, 3 were Zener diode failures, and 2 were open circuits in the 100 kΩ resistor.

The survival curve for the LPT-44's is plotted in Fig. 9. From this curve, an estimate of 7,200 filament hours can be made for the tube life. Only six LPT-44's have been operated for more than 5,000 h. Thus, the life estimate may be modified as more operating hours are accumulated. The life estimate has increased by 200 h in the past year (66,500 filament hours) of operation.

IV. Summary and Conclusion

The modulator described in this paper achieves the electrical and reliability goals which are required for long-pulse accelerator applications. The size, weight, and rise time of the modulator were all increased for the sake of reliability. The most frequent failure modes can be corrected during the normal accelerator down-time periods. Thus, no accelerator shutdowns due to modulator malfunctions have occurred in the present calendar year, which includes over 33,000 high-voltage hours of modulator operation.

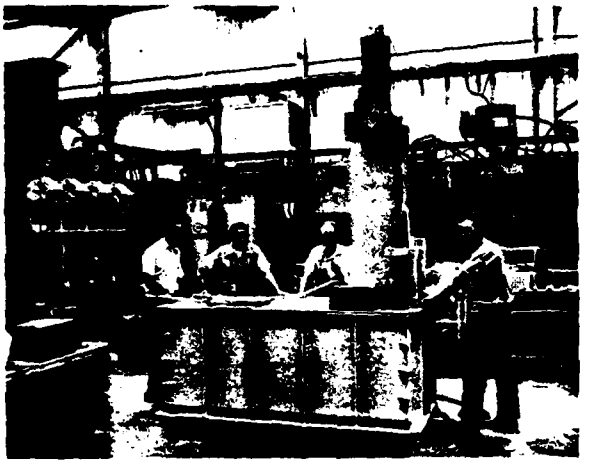

Fig. 1 Klystron and modulator assembly.

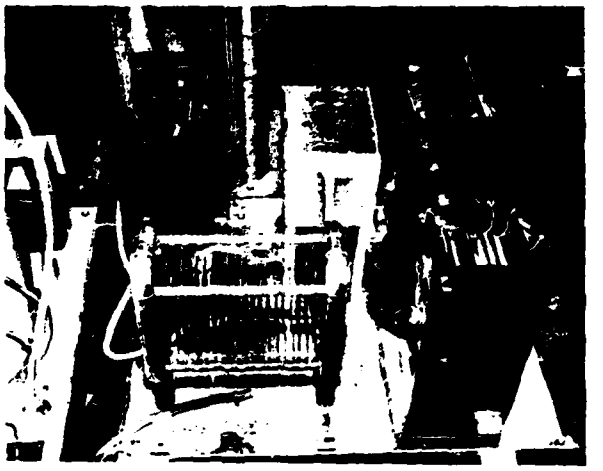

Fig. 3 Modulator components.

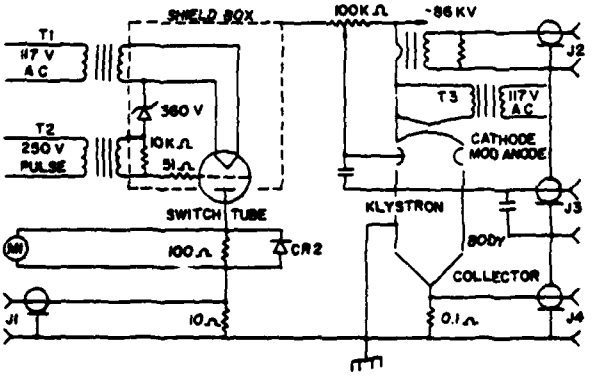

Fig. 2 Basic modulator circuit.

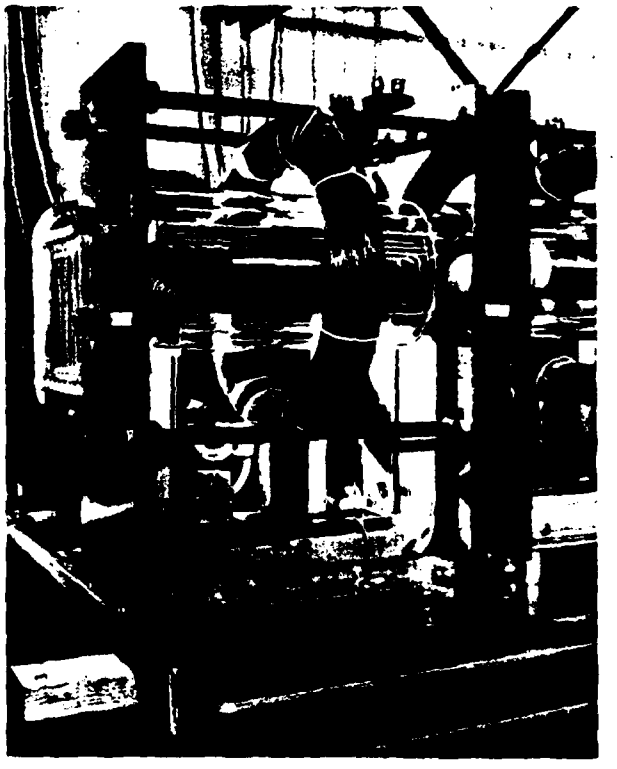

Fig. 4 Pulse transformer, 3:1.

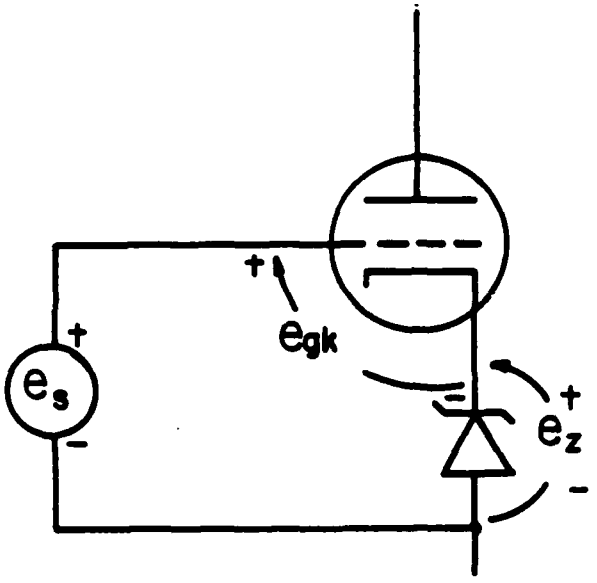

Fig. 5 Grid voltage.

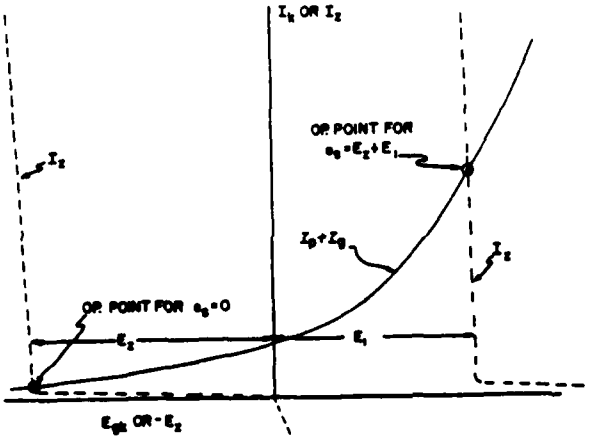

Fig. 6 Zener and switch tube characteristics.

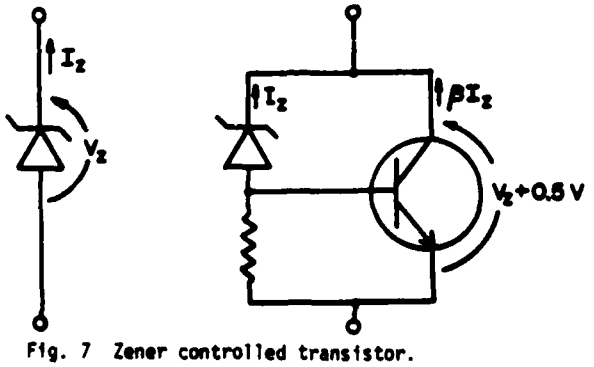

Fig. 7 Zener controlled transistor.

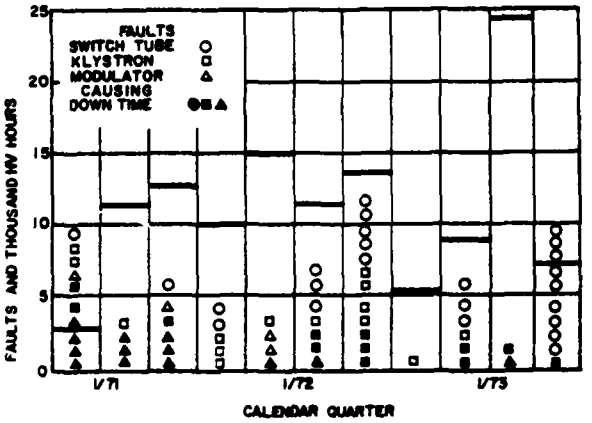

Fig. 8 Fault maintenance summary.

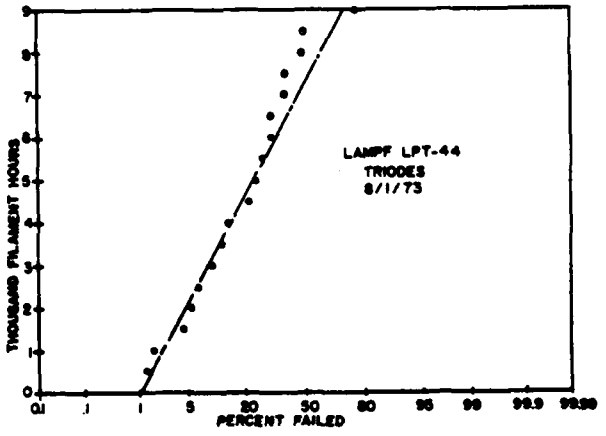

Fig. 9 Switch tube life.

TRADEX S-BAND TRANSMITTER MODULATOR

Robert N. Casolaro
RCA Corporation
Government and Commercial Systems
Missile and Surface Radar Division
Moorestown, New Jersey

Summary

The TRADEX S-Band transmitter modulator is a direct series-coupled floating-deck modulator employing three L5097 Beam Switch Tubes (BSTs) in a parallel connection as the main switch device. The modulator normally operates at a full peak-power level of 15 megawatts and a duty of 0.03 and delivers a -120 kV, 125-ampere pulse to a VKS8250 klystron load. The modulator can generate a wide range of single-pulse or burst-mode waveforms at various PRFs and allows for continuous changing of waveform during a mission without interruption of data. The constant current characteristic of the BST provides flat-top pulses, inherent regulation features and fault current limiting.

Introduction

The TRADEX S-Band radar was designed and manufactured by RCA under contract to Lincoln Laboratory. Its prime function is to track and gather data on re-entering test missiles launched from Vandenberg Air Force Base. To this end the radar, including the transmitter and its modulator, was designed to provide a high degree of flexibility in the types of waveforms that could be transmitted. The key to this flexibility is the transmitter modulator which is the subject of this paper.

The pulse output design requirements of the modulator are tabulated below:

Pulse voltage	130 kV maximum
Pulse current	140 amps maximum
Pulse duration	3 to 128 microseconds
Pulse bursts	Up to thirty-two 4-microsecond pulses spaced 7 to 28 microseconds apart (leading edge to leading edge)
Pulse pair	10-microsecond pulses spaced 13 microseconds
Rise time	1.2 microseconds (10-90% PTS)
Duty cycle	0.03 maximum
Pulse top ripple	0.1% (during RF pulse)
Pulse-to-pulse variations	0.02% (including the effects due to mode switching transients)

A hard tube modulator offered the only practical solution to the required waveform flexibility. A direct series-coupled floating-deck modulator was selected because smaller pulse top ripple was predictable. The Litton L5097 Beam Switch Tube (BST) was selected as the series switch tube because of a number of advantages gained in its use in a series modulator:

The constant current characteristics of the BST can in effect be used to achieve electronic series regulation to eliminate capacitor voltage droop during a pulse or a burst of pulses, achieve ripple reduction, and provide regulation against line voltage variations or changes in duty cycle.

The constant current characteristic of the BST also limits fault current to an arcing RF output tube to slightly more than normal. The series tube can be electronically turned off during the pulse, allowing the fault current to flow for only a few microseconds. Normal pulses can be reapplied to the RF tube as rapidly as the next pulse repetition rate.

Other modulator features include the use of fiber optics to couple command pulses to the high-voltage floating deck, a floating vac-ion system for continuous pumping and monitoring of BST gas pressure, a crowbar circuit employing a four-high stack of ignitrons, and an oil system that provides high voltage insulation as well as cooling for the BSTs and other modulator components.

This paper deals with the principal features and design considerations of the modulator. Actual waveform performance will also be presented.

General Description

The overall modulator system is depicted in the simplified block diagram of Figure 1. The High Voltage Power Supply (HVPS) is rated at -160 kV and 6 amperes DC. The 4160 VAC, 3-phase primary is protected by a high-speed two-cycle breaker which can be electronically tripped open when the crowbar is fired. The output voltage is controlled by an oil-filled tap changer with an induction regulator vernier control between steps. The output voltage is controlled over a range of -26 kV to -160 kV. The transformer dual secondary is a delta in series with a wye to provide a 12-phase output. The silicon rectifier diode stacks are employed with a 2.5:1 safety factor on PIV. A 30 H choke is used at the output of the supply for ripple reduction.

The output of the HVPS is used to charge a 5.0 microfarad energy storage bank. The bank consists of 24 individual capacitors rated at 3.3 microfarads and 42-1/2 kV, arranged in four groups of 6 each in parallel. The four groups are connected in series to obtain a 5 uF, 170 kV rating. A unique feature of the bank is that the usual fuse protection has been eliminated to obtain a bank with minimum inductance in the pulse current loop. Current limiting protection is provided by using stainless steel connecting bars between individual capacitors in the bank. In the event of a short-circuit failure of one capacitor, the dump current from the remaining

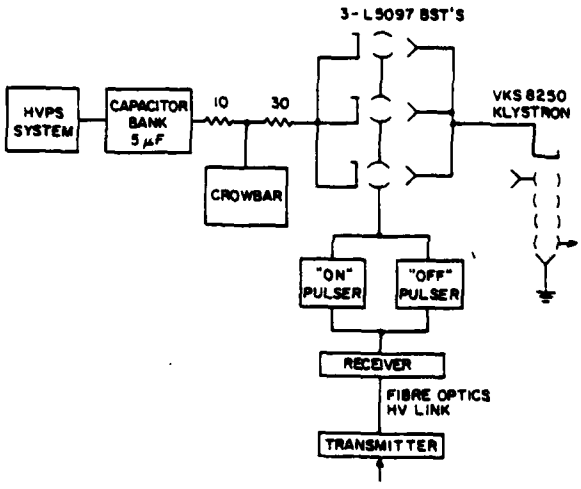

Figure 1. TRADEX Modulator Block Diagram

parallel capacitors is limited by the resistance of the stainless steel; this limitation prevents the rupture of the faulted can.

Crowbar protection is provided to protect both the BSTs and the VKS8250 klystron in the event the BSTs arc through. Four 50 kV GL37248 ignitrons are stacked in series to obtain a crowbar capable of normal operation at the 160 kV level. DC power for the floating trigger and holding anode circuits is derived from the main HVPS. The heater for all four ignitrons is at ground potential and the heat is directed at the individual anodes via a high-voltage isolating heat duct. The crowbar is kept in continuous conduction when fired by maintaining voltage on the holding anode until sufficient follow-on HVPS current flows.

The key element in the modulator system is the L5097 Beam Switch Tubes (BST). Three tubes in parallel are necessary to provide the total peak current and dissipation capability. The three tubes act as three parallel switches which, when closed, apply voltage to the cathode of the VKS8250 klystron. Each arm of the switch or L5097 BST carries approximately 1/3 of the total current. Each BST tube current is controlled by the magnitude of voltage applied between their modulating anode and cathode. The three BST mod anodes are connected in parallel (except for isolating resistors) and driven from a single "on" pulser. Approximately 12 kV is applied to the mod anode of the three BSTs to turn them "on" at full operating current level. The BSTs are turned "off" by removing voltage from their mod anode. To accomplish this rapidly the "off" pulser is pulsed into conduction to discharge the stray and mod anode capacity which was charged to the 12 kV during the "on" pulse. The "on" pulse is controlled by a gate equal in duration to the desired video pulse width to be applied to the VKS8250 klystron. The "off" pulser is activated by a shorter pulse derived from the trailing edge of the "on" gate. The duration of this shorter "off" pulse is commensurate with the discharge time of the mod anode voltage.

The "on" gate is coupled to the HV floating deck from ground-level circuitry via a length of fiber optics. All circuitry and amplifiers associated with these low-level signals are thoroughly shielded; balanced circuitry is used throughout. The rejection of extraneous and common mode signals results in an effective, trouble-free system.

A physical description of the modulator system is best facilitated with aid of several photographs of actual equipment. Figure 2 is an overall view of the modulator tank. On the left the VKS8250 klystron is seen sitting in its focus coil with its cathode extending into the oil tank below. The larger section of the oil tank on the right is where the main modulator is housed, including the BSTs. The portholes on the side make it possible to view the klystron and BST filament voltage, BST bias voltage, and mod anode power supply voltage. The tank measures 4-1/2 feet wide, 11 feet long, and 4-1/2 feet high; it holds 1100 gallons of oil.

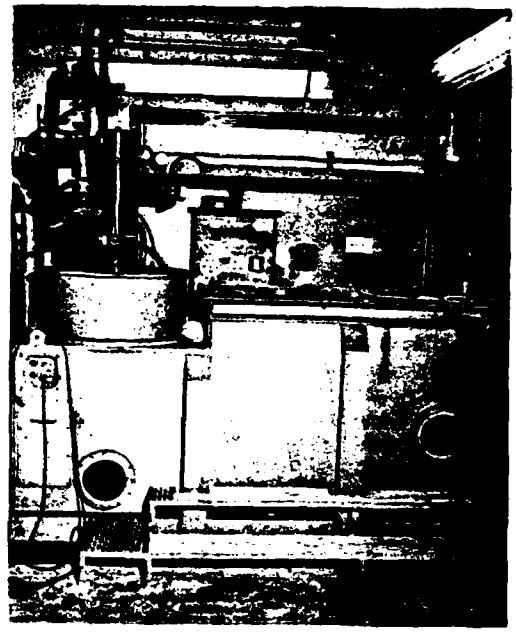

Figure 2. TRADEX Modulator Oil Tank

Figure 3 shows a top view of the high-voltage floating deck sitting in the oil tank. The three BSTs are seen with their interconnecting cooling lines. On top of each BST are corona rings protecting the floating metering circuits of the vac-ion pumps. On the right side of the photo are the "on" and "off" pulsers covered by corona-shielded enclosures. The corona cover for the "on/off" mod anode pulser power supply is seen in the lower part of the picture. Completely surrounding the HV deck is a corona shroud. At the top of the photo are the HV isolation power transformer and the isolation klystron filament transformer and its DC supply.

Figure 4 is a closeup photo of either the "on" or "off" pulser, its protective cover corona shields, and the optical transmitter and receiver with interconnecting fiber-optic link of the HV isolation pulse control system.

Figure 5 shows the overall crowbar. The lowest section is at the highest negative voltage, with the top section at ground potential. The mechanical design allows for the addition or deletion of sections to realize crowbars of different voltage ratings. Dimensionally the corona toroids are 28

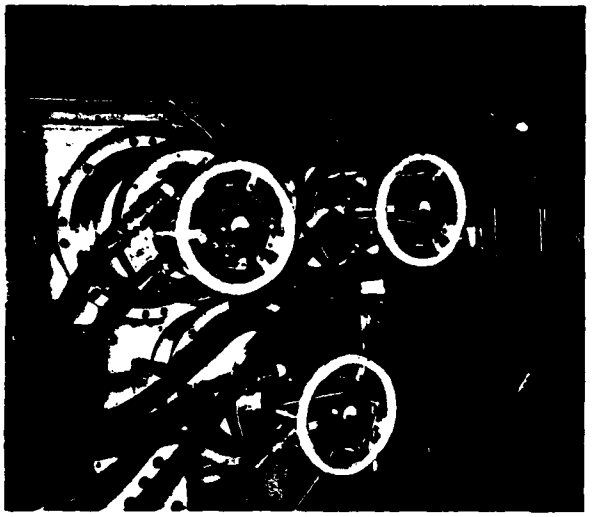

Figure 3. Modulator Deck - Top View

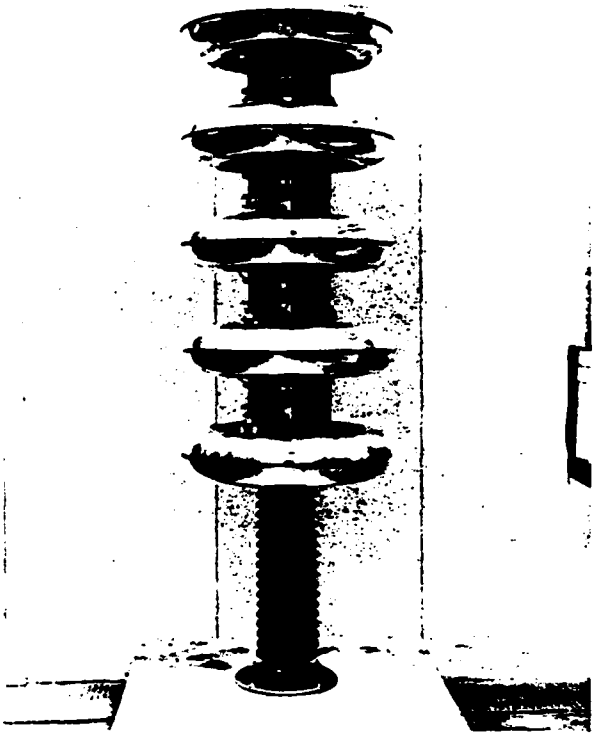

Figure 5. TRADEX Crowbar

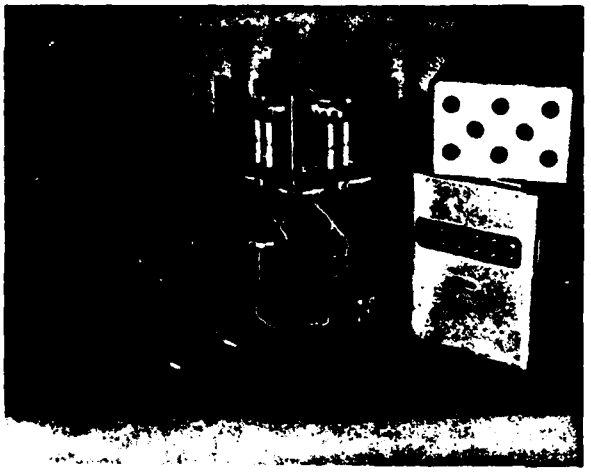

Figure 4. "On-Off" Pulser Components

inches in diameter separated by 14 inches. The overall height of the crowbar is approximately 8 feet including the bottom 3 foot insulator.

Modulator Design Considerations

Establishing the BST Operating Point

The modulator design is controlled by the characteristics of the L5097 BST which are utilized to their best advantage to achieve flat pulses and the inherent regulation features of the BST. The transfer characteristics of the L5097 BST are shown in Figure 6. The main point of interest in the BST characteristics is their good approximation to constant current curves. Once above the well-defined knee, the collector current becomes independent of the collector voltage. The BST can therefore control the current in the klystron load by operating above the BST knee and keeping the mod anode voltage constant. This technique, in effect, achieves series electronic regulation of the HVPS.

To fully realize the regulation benefits of the BST it is necessary to operate well enough above the knee of the curve to take into account:

1. capacitance droop which is approximately 3.2 kV at full peak current and the widest pulse width.
2. 4160 V AC line voltage regulation which is $\pm$1/2% or results in a DC variation of $\pm$700 V DC.
3. duty cycle regulation. By controlling the duty changes, the voltage regulation is held to less than 1 kV.

No-load to full-load regulation of the HVPS would result in 11.9 kV voltage variation. Establishing an operation point this far above the knee of the curve would present a problem of BST over-dissipation. A stringent requirement of the transmitter is to maintain coherent phase relationships while continuously switching waveforms of different duty. The effect of these step changes in duty is to put the HVPS voltage in a continuous transient state. Were these voltage

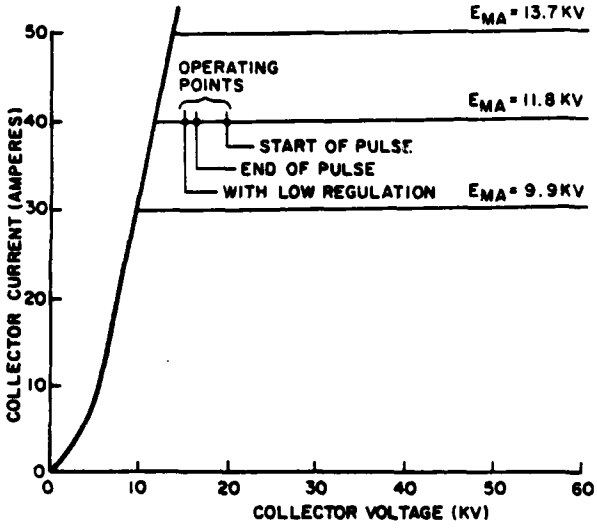

Figure 6. BST Collector Current vs Collector Voltage

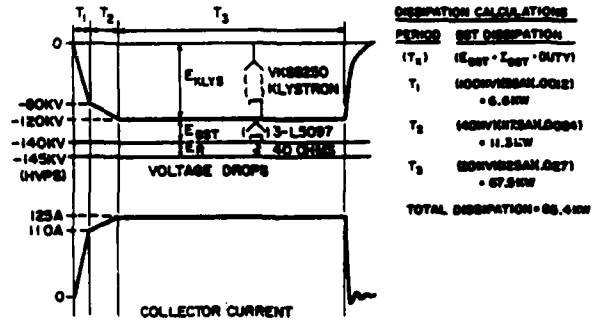

Figure 7. BST Dissipation Analysis

transients passed on to the klystron, the resultant phase pushing would be intolerable. The regulation of the series BSTs helps tremendously in reducing these HVPS transients, but it alone is insufficient for the tight phase control desired. With the aid of computer circuit performance analysis, a duty cycle balancing technique was derived to minimize these HVPS transients to within a 1 kV limit. The technique employed involves filling in additional pulses or widening the video pulses for lower duty modes.

For typical full-power operating parameters of the VKS8250 (120 kV and 125 amperes), each BST will provide 41.7 amperes. The tube drop at 41.7 amperes is just under 12 kV. Allowing another 5 kV for regulation and capacitance droop, the minimum operating tube drop of the BST is established at 17 kV. The required minimum BST collector voltage is therefore 137 kV. In practice the BST collector voltage is set at no more than 140 kV for full power operation. The HVPS voltage is set 5 kV higher (145 kV) to allow for the IR drop across the series 40 ohms. If the power supply voltage is set too low, a discontinuity will first be observed at the end of the pulse where capacitance voltage droop brings the operating point through the knee region. If the supply voltage is set high, the 90 kW (30 kW per tube) dissipation rating of the BSTs is approached.

BST Dissipation

BST dissipation can best be determined using a straight-line approximation of the actual voltage and current waveforms. These waveforms are shown in Figure 7 together with BST dissipation calculations during the rise time and flat portion of the pulse. Note that the rise time is broken into two segments to more closely approximate the actual waveforms. The dissipation is calculated as the product of the average voltage tube drop and average current, and the duty cycle of an equivalent pulse during each time segment. The result is 85.4 kW which is just below the 90 kW dissipation limit. The analysis is conservative since it does not take into account power supply capacitance voltage droop. When operating at the widest pulse width, 3.2 kV droop results in a reduction of greater than 5 kW in BST dissipation.

BST Reduction of Power Supply Variations

In the region of the normal operating point, the dynamic impedance of the L5097 is less than infinite and it is therefore not a perfect constant current source. Typical dynamic impedance of the L5097 is 75 K ohms, or for three tubes in parallel the combined dynamic impedance is 25 K ohms. To this extent the regulation of the series BST is less than perfect, as a small percentage of variations in power supply voltage will be seen at the cathode of the klystron load. The reduction factor is approximately the ratio of the klystron dynamic impedance to that of the three BSTs. The klystron dynamic impedance is dV/dI where the relationship between V and I is:

$$I = KV^{3/2}$$

and: $$\frac{dV}{dI} = \frac{2}{3} K^{-1} V^{-1/2}$$

for: $K = 3 (10^{-6})$

and: V = 120 kV operating voltage

$$\frac{dV}{dI} = \frac{2}{3} \cdot \frac{10^6}{3} \cdot \left[120 (10^3)\right]^{-1/2} = 641.5 \text{ ohms}$$

The reduction factor is therefore:

$$RF = \frac{Z_{kly}}{Z_{BST}} = \frac{641.5}{25 K} = 0.0257$$

Capacitor voltage droop of 3.2 kV is reduced to 82 (0.0257 x 3.2 kV) volts klystron cathode voltage droop, or a droop of 0.07%. The 1.7 kV line plus duty cycle HVPS voltage regulation is reduced to 44 (0.0257 x 1.7 kV) volts, or 0.04% klystron cathode voltage regulation. HVPS ripple of 0.25% is reduced to less than 0.01% (0.0257 x 0.25%) klystron cathode pulse-to-pulse voltage variation.

Contribution of Mod Anode Voltage Variation to Klystron Voltage Variations

The klystron cathode voltage variations given above are due only to HVPS voltage variations. Variations in BST mod anode voltage contribute directly to klystron voltage variations as can be seen from the following relationships:

$$I_{klys} = I_{BSTs}$$

$$I_{klys} = K_1(V_{klys})^{3/2}$$

$$I_{BST} = K_2(V_{ma})^{3/2}$$

$$V_{klys} = \frac{K_2}{K_1}^{2/3} V_{ma} = K_3 V_{ma}$$

At the operating point, K_3 is approximately 10.8.

Because of this direct relationship, a percentage change in mod anode voltage yields the same percentage change in klystron voltage. Therefore, to hold the klystron pulse-to-pulse cathode voltage variations to the specified 0.02%, the mod anode pulse-to-pulse voltage variation is held to the remaining 0.01%. This is readily accomplished with electronic regulation of the 14 kV mod anode power supply. The droop and regulation of the BST mod anode voltage must likewise be controlled because of their direct effect on klystron cathode voltage. The electronically regulated mod anode power supply is regulated to less than 0.01%. The droop in the burst mode is controlled to 2.2% by a 0.5 microfarad capacitor at the output of the supply. The addition of these variations to klystron cathode voltage brings the total cathode voltage variation to:

Percent droop (burst mode) = HVPS contribution + MA contribution

= 0.1% + 2.2% = 2.3%

Percent regulation = HVPS contributions + MA contributions

= 0.04% + 0.01% = 0.05%

Percent ripple = HVPS contribution + MA contribution

= 0.01% + 0.01% = 0.02%

BST Mod Anode "On" and "Off" Pulser Design Criteria

The mod anode voltage rise time, if not held small, could limit the rise time of the klystron cathode voltage. A mod anode voltage rise time of 0.2 μs was selected as compatible with a klystron cathode voltage rise time requirement of 1.2 μs. The "on" pulser switch tube requirement can be calculated from the input capacitance of the L5097. The input capacitance is determined from:

$$C_{in} = C_{ma\text{-}k} + C_{col\text{-}ma}(1 + g)$$

$$= 85\text{ pf} + 3.5\text{ pf}(1 + 10.8)$$

$$C_{in} = 126.3\text{ pf}$$

or for three BSTs in parallel:

C_{in} (total) = 380 pf

To charge this capacitance from a constant current source in 0.2 μs requires a charging current of:

$$I = \frac{E_{ma}(C_{in})}{\text{Rise Time}} = \frac{(12)(10^3)(380)(10^{-12})}{0.2\,(10^{-6})}$$

I = 22.8 amperes

To accomplish this, four Y543 tubes (4PR60 procured to a tighter control specification) in parallel were selected for the mod anode "on" pulser. A simplified schematic of the "on" pulser is shown in Figure 8. The Y543 tube selection was based on low cost and ease of driving from a solid-state grid pulser. The four Y543 tubes readily supply more than 20 amperes charging current during the pulse rise time with 0 grid voltage and 1250 V screen volts. During the flat portion of the pulse, the Y543s supply a mod anode intercept current of less than 0.3 ampere (0.1 per tube) and the tube drop is reduced to a few volts. To prevent over-dissipation the screen voltage is supplied from a soft line, allowing the screen voltage to drop to a safe level during the pulse. During the rise time of the pulse when there is a peak current demand, the voltage is held up by a small capacitance in the output of the screen supply.

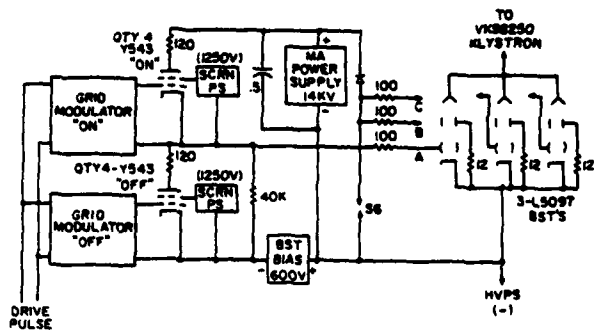

Figure 8. VST Modulating Anode "On-Off" Pulser Schematic

Each grid modulator consists of a pair of DTS804 high voltage transistors in an "on/off" circuit arrangement which swings the Y543 grids between 0 and a -600 volt bias level.

Performance Review

A series of oscilloscope photos of the different waveforms exemplify the performance of the modulator. All the pictures are taken at the same operating level, which is typical of the normal field operation. Peak current is set at approximately 105 which is 84% of normal full-power operation. Power supply voltage is 130 kV versus a normal full level of 140 kV.

Figures 9, 10, and 11 show the individual BST pulse currents. Note that the balance is good; this has been the general experience with all tubes tested. The very flat pulse is also noted.

Figure 12 is of the klystron cathode voltage and current. The voltage droop is due to the capacitor divider viewing

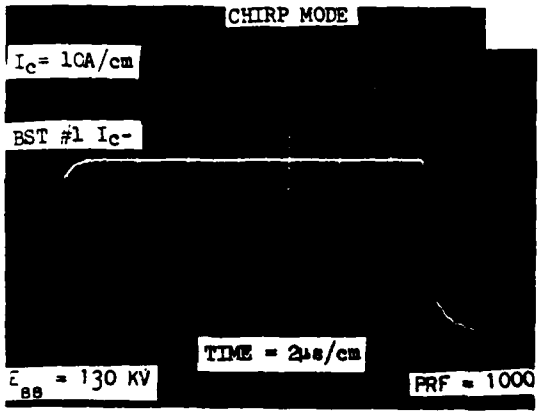

Figure 9. BST Collector Current No. 1 Waveform

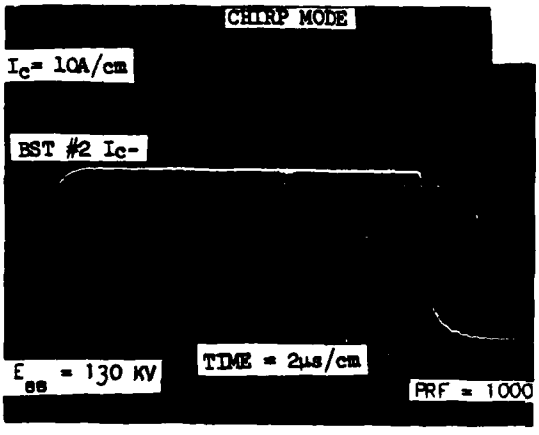

Figure 10. BST Collector Current No. 2 Waveform

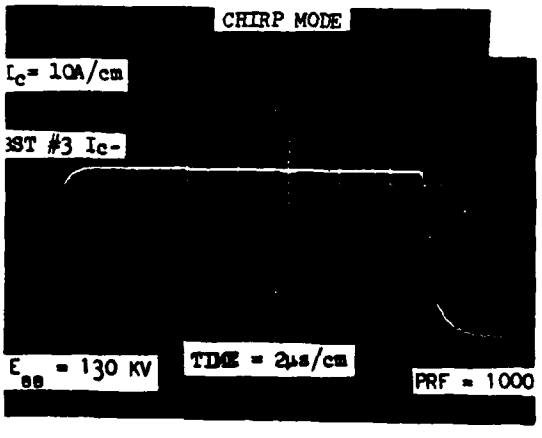

Figure 11. BST Collector Current No. 3 Waveform

circuit since the cathode voltage is as flat as the current pulse. The current front-end ripple, which was not present in the prior BST current waveforms, is caused by deck capacity current. The ringing is initiated by a 5 kV step in deck voltage due to the IR drop across the series 40 ohms in the pulse current loop. The klystron cathode viewing transformer is located on the power supply side of the BSTs and therefore includes deck capacity current.

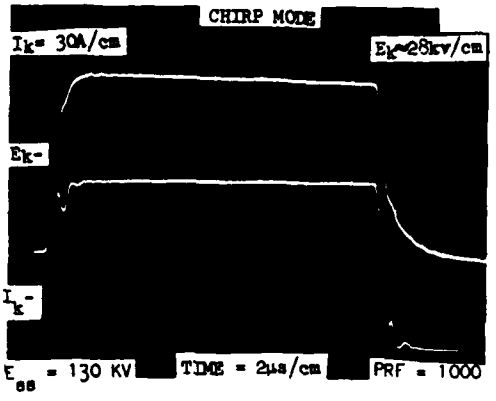

Figure 12. Klystron Cathode Voltage and Current Waveform

Figure 13 shows the klystron cathode current for a pulse pair mode. The pulses are closely spaced just about at their limit of 3μs. The second pulse in this case is wider than the first to balance duty cycle. The RF pulses used are the same width.

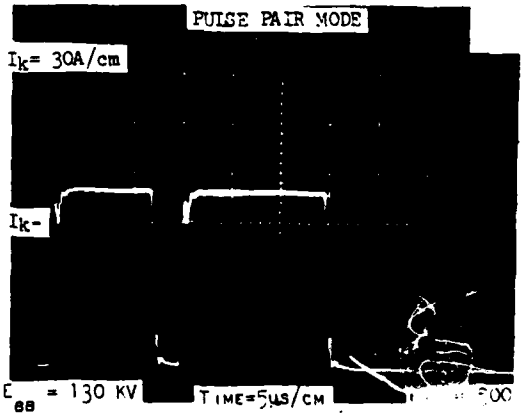

Figure 13. Klystron Cathode Current - Pulse Pair Mode Waveform

Figures 14 and 15 show an overlay of the third and thirty-second klystron current pulse of a burst mode, differing respectively in pulse spacing of 28 μs and 7 μs. For the wider spacing the overlay is nearly perfect. For the narrow spacing the thirty-second pulse shows the effect of mod anode voltage power supply droop where interspace timing is not long enough to aid in recharging the capacitor.

Figure 16 shows the negligible transient when switching between burst and chirp mode of operation. For this case, three fill-in pulses are added after each burst for duty cycle balancing.

L5097 BST Experience

During the development phase, a number of problems had to be solved to bring the tube to its present state. Two of these problems were high voltage phenomena and were referred to as "ticking" and "burning." The "ticking" was small

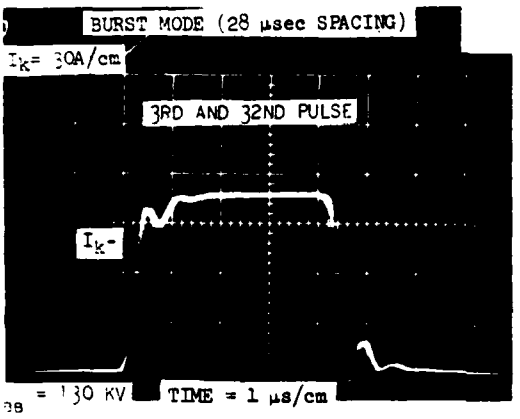

Figure 14. Klystron Cathode Current - Burst Mode Third and Thirty-Second Pulse Comparison (28 μs Spacing)

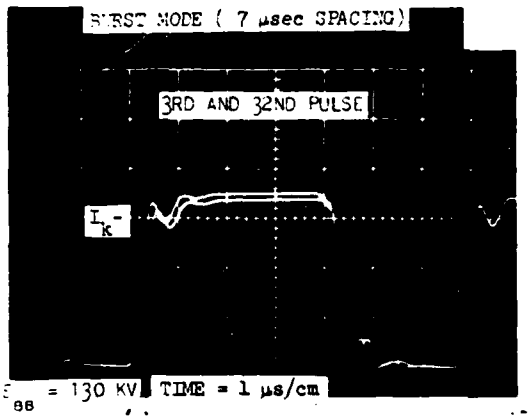

Figure 15. Klystron Cathode Current - Burst Mode Third and Thirty-Second Pulse Comparison (7 μs Spacing)

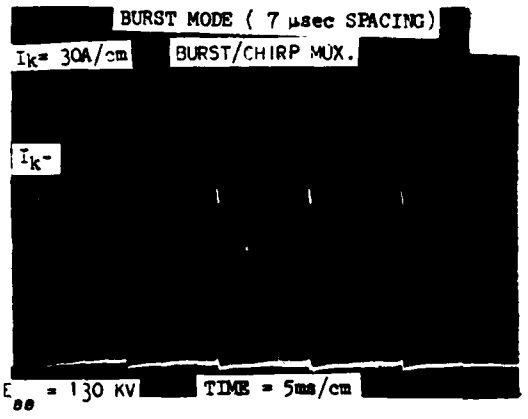

Figure 16. Klystron Cathode Current - Burst and Chirp Mode Switching Transient

sporatic impulses of tube current during the interpulse period. The "burning" phenomena appeared as an oscillation which sometimes interfered with low-level circuitry or led to a tube arc. Both of these problems have now been controlled using a high-resistance insulator coating and an asymmetric geometry between the collector and shield insulator region. Litton reports that there is still a tendency for burning to occur following a severe tube arc although this has not been a TRADEX experience. TRADEX uses resistors between shield and cathode which act to limit fault arc current and thereby suppress the tendency for burning to occur.

A third development problem was cathode stability. This was solved by replacing the passive nickel cathode with an activated nickel.

About 30 switch tubes have been delivered to a number of customers during the past year with a very high yield and no exceptions to specifications.

Of seven full power tubes delivered to TRADEX, only four have been used significantly; these have accumulated a total of 4406 hours with no failures. The maximum hours on any one tube to date is 1722 hours.

Early development tubes which were procured as half-power tubes produced three failures; it is noted that the solution to the problems previously discussed had not been incorporated into these early tubes.

Acknowledgment

This work was sponsored by the Advanced Ballistic Missile Defense Agency under a subcontract of M.I.T. Lincoln Laboratory.

AEGIS AN/SPY-1 CFA CONSTANT-CURRENT HARD-TUBE MODULATOR

K.M. Smalley

Raytheon Company, Wayland, Massachusetts

Summary

This paper describes a modulator employing four switch tubes each supplying a crossed-field amplifier tube operating at 13 KV and 22 amperes peak. Separate modified 4CX5000R tetrode switch tubes for each CFA, operating in the constant-current mode, allow a 25:1 reduction in the size of the filter capacitor bank required to limit droop and ripple. Constant-current operation also permits an individual CFA to arc without affecting operation of the other three CFA's. Continued arcing of a CFA causes a circuit to close a vacuum relay, shorting out the malfunctioning CFA until it can be replaced, still without shutting down the modulator. Only one switch tube driver employing paralleled 4CPX250K tetrodes is required, as a tapped zener string allows individual setting of switch tube grid drive voltages. No floating power supplies are required, as the zener string and the switch tube driver screen and grid-bias voltages are obtained from the bleeder for the switch tube bias supply. Other features of this compact modulator are a shunt clamp regulator with switch tube screen voltage compensation, automatic switch tube driver current reduction after pulse risetimes, pulse-width limiting, and remote location of HVPS filter banks.

AEGIS SPY-1 TRANSMITTER

Aegis is being developed by RCA for the Navy as a *sophisticated electronic response to anti-shipping* threats from manned aircraft, air-to-surface missiles, and - to a slightly lesser extent - undersea missiles during the late 1970's and 1980's. The system is designed to integrate target detection and tracking, command-decision and weapons control processes to afford fast reaction and massive, accurate firepower for fleet protection.

The AN/SPY-1 radar system, the major element of the weapon system is a computer-controlled, S-band multi-function phased-array system capable of automatically searching, detecting and tracking multiple targets at long range. The SPY-1 radar also provides automatic transition to a fire-control quality track and provides mid-course command guidance to semi-active homing interceptor missiles.

The SPY-1 radar transmitter equipment developed by Raytheon under subcontract to RCA includes eight high-voltage power supply cabinets, an input amplifier consisting of two redundant low-power TWT amplifiers, four cabinets housing driver/pre-driver units and two cabinets housing the final power amplifiers.

Redundancy and load-sharing are implemented throughout to insure system reliability. The redundant low-power TWT's are both operated continuously, one on line and the other as a standby that feeds a dummy load. The driver/pre-drivers, each containing two TWT/CFA channels, are provided with automatic switching. Three cabinets are required in operation, and the fourth is in a ready state. If any one of the three becomes inoperative, the fourth is automatically switched in via activation of video triggers.

The final amplifiers consist of two cabinets, each containing 16 Varian SFD-261 CFA's and four modulators. The tubes are arranged in groups of four and share a common modulator and high voltage power supply. Each CFA is mounted in a slide-out drawer for maintenance.

This paper describes the CFA modulators used in the driver portion of the driver/pre-driver cabinets and the final amplifiers.

Transmitter Block Diagram

Figure #1 shows a basic block diagram of all the CFA modulators in the transmitter and their high voltage connections to the high voltage power supplies. There are eight driver CFA's, and 32 final CFA's. The even-numbered power supplies on this diagram each have a single output going to a final modulator which supplies four CFA's. The odd-numbered power supplies have an additional output going to a driver modulator which supplies two CFA's. Driver No. 4 is a spare which normally is not pulsed unless there is a failure in one of the other three driver cabinets. Thus four of the power supplies have a 50% greater load than the other four. However, in order that all high voltage power supplies be interchangeable, they are identical and designed to power modulators supplying a total of six CFA's.

Modulators - Basic Elements

Figure #2 is a diagram of the basic elements of a driver and final modulator, together with the high voltage interconnections with a high voltage power supply. The 12 microfarad storage capacitor in the HVPS supplies the pulse current for all six CFA's. Separate high voltage relays are used in each output line so that maintenance operations may be performed on either a driver or a final modulator without necessitating that its associated HVPS be shut down. The high voltage relays may be opened while the HVPS is on, providing that the associated modulator is not pulsing, but may not be closed without shutting down the HVPS, as excessive surge currents would be drawn by the modulators to charge up the local 0.1 microfarad storage capacitors required at each modulator. These capacitors are used to supply current through the switch tubes to the CFA's during the rise time and initial portion of each pulse, and limit the voltage excursions on the switch tube cathodes during this time to less than 200 volts.

As can be seen in the diagram, each of the modulators contains only a single switch tube driver to drive two or four switch tubes. The modulators in driver cabinets have essentially the same circuitry as used in the final cabinets except for the number of CFA's that they can drive. In fact, the switch tube driver units and the power supplies for the same are identical, both electrically and physically. The descriptions which follow apply to a final modulator, which supplies four CFA's.

While the circuitry is the same in both modulators, the CFA's used in the driver operate at a pulse current one ampere greater than the CFA's used in the final. The currents in the switch tube are nominally one ampere greater than the specified minimum CFA pulse currents, due to the currents drawn by the modulator tailbiter resistors and to allow for tolerances in HVPS voltages.

Final Modulator Specifications and Capabilities

CFA pulse voltage	13 KV nom.
CFA pulse current	22 a nom.
CFA voltage rise time	200 nsec. max.
CFA voltage fall time	6 μsec. max.
CFA current rise time	100 nsec. max.
CFA current fall time	100 nsec. max.
CFA dynamic resistance	60 ohms nom.
CFA and stray capacitance	140 pf approx.
Switch tube current into short circuit	32 a approx.
Switch tube voltage drop	2 KV min.
Switch tube holdoff voltage	25 KV min.
Preheat time	30 sec. min.

Modulator Output Stage

Figure 3 shows a simplified schematic of the modulator output stage associated with one switch tube and one CFA. All portions of the circuit except R1 and C1 are repeated four times in each modulator.

The switch tube, V1 is a modified water-cooled version of the 4CX5000R and the modifications consisted primarily of adding a water jacket for high-pressure water cooling and increasing the grid-to-screen ceramic height from 1.0 to 1.8 inches in order to obtain increased voltage creep distance. Tests have shown this tube to have internal voltage holdoff capabilities in excess of 50 kV. It has a unipotential mesh cathode allowing use of a.c. on the filaments. It has the following maximum ratings in this application:

Anode dissipation	6 kW
Anode current	28 Amps peak
Anode voltage	+28 kVdc
Screen voltage	+1.5 kVdc
Control grid bias voltage	-1.0 kVdc
Duty cycle	0.01

At the pulsing condition of E_b = +2 kVdc, E_{c2} = +1250Vdc, and E_{c1} = -680Vdc, the limits for i_b = 24 amps peak (the driver modulator switch tube current) are as follows:

e_{gk} = +215 volts peak ± 30 volts.

i_{c1} = 0.5 amperes peak maximum

i_{c2} = 0 to 2.2 amperes peak maximum

For i_b = 23 amps (the final modulator switch tube current), e_{gk} is approximately 20 volts below that for 24 amps.

There is also a requirement that under the final pulsing condition, if the anode voltage is increased from 2kV to 8kV, the anode current shall increase from 23 amps to 27 amps ± 1 ampere. This provides a dynamic resistance of 1500 ohms ± 25%.

At the normal maximum holdoff conditions of E_b = +20 kVdc, E_{c2} = +1250 Vdc, and E_{c1} = -680 Vdc, the anode current is specified not to exceed 3 ma. This ensures minimum wasted power dissipated in the switch tube during the interpulse-period.

Since the dynamic resistance of the CFA is approximately 60 ohms, high voltage power supply variations and droop are reduced by $\frac{1500\Omega}{60\Omega}$ or 25:1, assuming constant switch tube control-grid and screen-grid voltages.

Only the secondary winding of T1 that is used to power the filament of one switch tube is shown. T1 is actually a 3Φ high voltage isolation transformer used not only to provide filament power to the four switch tubes at modulator deck level, but also to provide line power for all the power supplies used in the modulator at high voltage deck level. This transformer has eight high-current secondary terminals, two for each of the four 75 ampere filament loads. In addition, it has four other secondary terminals. It requires only four low-current primary terminals for the 3Φ leads and a cabinet ground connection. To minimize the number of high-voltage terminals required, and especially to eliminate the need for high-voltage, high-current bushings on the transformer, it was decided to mount the transformer on the high voltage deck.

C4 and C5 are pulse bypass capacitors for the filament windings of the transformer.

C1 provides pulse current for the rise-time and initial portions of each pulse for all four switch tubes. R1 is used for current-limiting and to dampen modulator deck ringing.

R2, R4, and C2 (which is actually made up of four 500 pf capacitors mounted around the periphery of the switch-tube socket) are used to prevent UHF and VHF parasitic oscillations.

E1 is a 2000 volt spark-gap used to prevent damage to the modulator driving circuits and power supplies in the event of an arc within or on the external surface of a switch tube. Should such an arc occur, and not self-extinguish, thereby loading down the screen power supply, an overload circuit is included in the supply to interrupt primary power to the screen supply power transformer for a sufficient period of time for the fault to clear. The circuit is self-resetting.

C3 is the pulse storage capacitor for the switch tube screen circuit and R3 is used to isolate it from the screen power supply.

R5 is used to limit the current through the switch tube and the CFA to less than 4000 amperes should there be an arc in both devices simultaneously.

T2 is a pulse current-viewing transformer used for the fault circuits provided to sense excessive pulse and average CFA currents.

K1 is a high-voltage vacuum relay used to short out a CFA in the event of excessive CFA arcing. When this relay is de-energized, shorting the anode of

the CFA to ground, the associated switch tube essentially runs into a short-circuit. However, because of the high dynamic resistance of the switch tube, the current into the short-circuit is limited to only about 30 amperes. There is no appreciable effect on the other switch tubes powered by the same switch tube driver and screen power supply. The switch tube anode dissipation rating is sufficient to operate into a short-circuit at full duty cycle for a sustained period of time.

This feature can also be used to replace a defective CFA without necessitating shutdown of the HVPS or the modulator. When it becomes necessary to replace a CFA, a manual control is used to de-energize K1, the door for the respective CFA is opened at the front of the cabinet causing an additional protective shorting-bar to drop on the CFA cathode line.

R6 is used as a tailbiter resistor to dissipate the energy in the stray capacitances, shown as C_s, at the end of each pulse. R7 is a sampling resistor used in the ground return of the tailbiter resistor to provide a sample of the CFA voltage pulse for the wide-pulse and CFA arc fault circuits.

Switch-Tube Driver

Figure 4 is a simplified schematic of the switch tube driver used to drive the control-grids of the four switch tubes in one modulator.

V1 and V2 are the driver and tailbiter tubes, respectively. For simplicity, these are shown as single tubes on this schematic. However, two tubes are used in each of these stages to obtain adequate drive voltage rise and fall times while charging and discharging the approximate 600 picofarad load (120 picofarads per switch tube grid-to-cathode plus 120 picofarads miscellaneous circuit capacitance). The tubes are Eimac 4CPX250K's which have the following significant features in this application:

- Air-cooled, radial beam tetrode
- Designed specifically for pulse applications
- Covered by military specification MIL-E-1/1670
- Have high use (10,000 sockets in the FPS-85 radar)
- Low heater power (15 watts)
- Low input capacitance (14 pf)
- Small size
- Light weight
- High anode voltage ratings (7000 volts)
- Fast cathode warm-up time (30 sec)
- Low drive voltage requirements (200 volts)
- Low drive current requirements (zero)
- Moderate cost
- Long-life (4000 hr. service-life guarantee in FPS-85 radar).

Power for the anode of V1 is provided by the +1250 Vdc power supply. All other necessary voltages, with the exception of the clamp supply, are provided by the -1000 Vdc power supply, either directly or by means of bleeders and zener diodes.

During the interpulse periods, current flows from ground through CR1, R2, VR1 through VR10, VR11, and R1. The current amplitude is:

$$\frac{1000V - (10)\ 5.6V - 180V}{36K + 2K} = 20ma.$$

The current through R2 and C13 in parallel charges C13 to the +760 volt screen voltage required by V1.

The current through VR1 through VR10 in parallel with C1 through C10 charges each of the capacitors up to 5.6 volts.

The current through VR11 provides -180 V grid bias for V1.

R1 is used to complete the current path and also as a grid-bias return resistor for the grids of the four switch tubes connected to the outputs of the driver. It has a 40 volt drop during interpulse periods.

C11 is the storage capacitor used to supply current to R1 during pulse-time. C12 supplies pulse current to V1 during pulse-time.

R5 in parallel with C15 reduce the control-grid and screen-grid voltages of V1 after the rise-time of each pulse. This results in a considerable reduction of anode power dissipated in V1.

CR1 becomes reverse-biased during pulse-time so that there is no leakage to ground of the voltage on C13 during pulse-time.

T1 and T2 are the pulse transformers for the grids of the driver and tailbiter tubes, respectively. An essential requirement for T1 was low primary to secondary capacitance, as the secondary winding takes an excursion of close to 1000 volts between interpulse-time and pulse-time. Excessive capacitance requires extra driving current from the transistor supplying T1.

CR2 is the clamp diode to hold the bottom of the string of zener diodes to the regulated clamp voltage.

C14 is the clamp storage capacitor. Its value was selected large enough to limit the increase in voltage during the longest pulse to an acceptable value, as the clamp regulator current capability and response time were not designed for intrapulse regulation.

R3 is a sampling resistor for clamp current to provide a voltage to the modulator fault circuit. VR12 limits the amplitude of this voltage to 6.8 volts.

VR13 is used to provide grid bias voltage for the tailbiter tube, V2. Note that 740 volts screen voltage for V2 is provided by connecting the screen to deck ground.

C15 is a pulse storage capacitor to supply current for the tailbiter tube at the end of each pulse.

R4 is used as a bleeder for C15 and also to complete the current path for VR13.

Connecting the anode of the tailbiter, V2 to the screen of the driver tube, V1 results in a faster fall time for the driver over that obtained with it connected to the cathode, due to the additional 720 volts applied to the anode of V2.

The filaments of both V1 and V2 are supplied by a dual winding transformer, with the winding for V1 having low capacitance to the core and the other winding.

A detailed discussion of the low-level circuits between the "start" and "stop" trigger signals supplied to the modulator deck by transformers from ground level and the driving signals supplied to T1 and T2 will not be included. The solid-state circuits are conventional and include pulse-width limiting to prevent excessive modulator pulse width in the event of a missing "stop" pulse.

Clamp Regulator

The clamp regulator is used to discharge the excess energy stored in the clamp capacitor during each pulse. Since it is used as a current sink, a shunt regulator is used to minimize power requirements. It has a programming feature that allows the clamp voltage to vary in a selected proportionality to a change in switch tube screen voltage. It requires only a +15 volt power supply and a small amount of current from the +1250 volt screen supply as a "keep-alive" for the regulator during non-pulsing conditions. It consists essentially of a compensated voltage-divider, reference, differential-amplifier, level-translator, driver stage, and the shunt power transistor.

Figure 5 is a complete schematic of the regulator. The compensated voltage-divider consists of R1, C1, R2, C2, R3, C3, and R4 and has a nominal ratio of approximately 1:37 for input to the differential-amplifier versus regulated output voltage. R16 is used to couple in a variable amount of feedback into R3 from the +1250 volt power supply. With the potentiometer set fully counterclockwise, variations in the +1250 volt power supply will not affect the output voltage of the clamp regulator.

VR1 is the precision voltage-reference for the regulator. R4 and R8 are used to make the impedances of the reference and the output of the voltage-divider approximately equal for temperature stability of the regulator.

The reference and divider output signals are compared in the differential-amplifier Q1, the output of which is applied to the level translator Q2, which drives the emitter-follower stage Q3.

The shunt dissipating elements consist of Q4 in a series with VR2. VR3 is used to prevent excessive voltage from appearing across Q4 in the event of malfunctions in other portions of the circuit.

Fault Circuits

The modulators contain the following video and dc fault circuits for protection and malfunction indication:

A peak current fault circuit senses excessive pulse current which might occur should there be simultaneous arcs in both the switch tube and the CFA. The threshold of this circuit is a pulse current of greater than 50 amperes occurring for greater than 1 μsec.

An average current fault circuit senses excessive average current which might occur due to a malfunction in the modulator drive circuits causing operation at an excessive duty cycle. The threshold of this circuit is 200 ma.

A wide-pulse fault circuit senses excessive pulse width of the CFA voltage pulse which might occur due to a malfunction in the modulator drive circuits, switch tube bias failure, or a shorted switch tube. Since this circuit senses voltage, not current, it can be used to detect these types of faults even prior to pulsing operation. A current sensing circuit would require that rf drive pulses be applied to the input to the CFA in order that the CFA draw current. The threshold of this circuit is a CFA pulse voltage of greater than 10 KV occurring for 20 μsec longer than the longest normal pulse.

A CFA arc fault circuit senses that the pulse impedance of the load on the switch-tube is below a normal level, which would occur when a CFA arcs. The threshold of this circuit is the condition when the sum of the $\frac{\text{CFA pulse current}}{23}$ and the $\frac{\text{CFA pulse voltage}}{13\text{KV}}$ is greater than 0.5. Note here that the polarity of CFA pulse current is positive and the polarity of CFA pulse current is negative.

A modulator power supply fault circuit senses failure of the +15V, +200V, +1250V, or clamp regulator power supply voltages. A sample of each of these supply voltages is applied to a summing circuit which senses failure of any one or more of these voltages.

A modulator fault circuit senses the absence of clamp current into the clamp capacitor during any modulator pulse. This fault circuit employs a bistable multivibrator which is triggered by the "on" trigger to the modulator low level circuits at the high voltage deck level. A signal generated by the clamp current resets this bistable within a fraction of a microsecond later, with a properly functioning modulator.

A peak current fault or a wide pulse fault requires immediate removal of energy from the circuit and thus when either of these faults is detected, a trigger signal is sent to the crowbar to divert energy from the fault within 5 microseconds. A recycle circuit is included in the high voltage power supply to turn high voltage back on again within 0.5 seconds after one of these faults. Should three of these faults occur within a 60 second period, recycling will not take place, and the high voltage power supply must be reset manually.

An average current fault causes modulator trigger signals to be inhibited and the high voltage power supply prime power contactor to be opened, but the crowbar is not fired. Reset after a fault must be done manually.

Sensing of a single CFA arc fault simply causes a lamp indicator on the front panel of the cabinet to come on for a period of approximately 10 seconds. Should 3 or more CFA arcs be sensed within a period of 60 seconds, the fault circuit causes the high voltage vacuum relay to be de-energized, thus shorting out the defective CFA. However, this vacuum relay is not capable of interrupting pulse currents without damage to the relay. Thus simultaneous with de-energizing the coil circuit of the relay, the fault circuit causes interruption of triggers to the modulator for a period of 50 msec. in order for the relay contacts to make the transition to closed condition (CFA shorted) before triggers are re-established. Therefore, if CFA arcing results in any particular CFA being shorted out, there is a 50 msec. period of time when pulsing of all CFA's in that modulator is interrupted.

A modulator fault or a modulator power supply fault does not result in any protective action taking place, as any of these faults either result in no pulsing of the switch tube, or that the switch tube grid will be turned on continuously, which fault will be sensed by the wide pulse fault circuit. Indicator lamps are located on the modulator deck to show if either one or both of these faults exist. In addition this information is fed to ground level to an indicator lamp on the front panel of the cabinet.

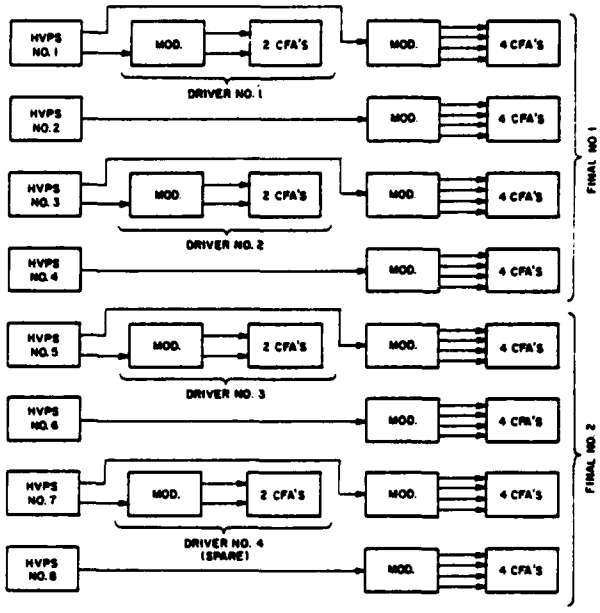

Figure 1. Transmitter block diagram

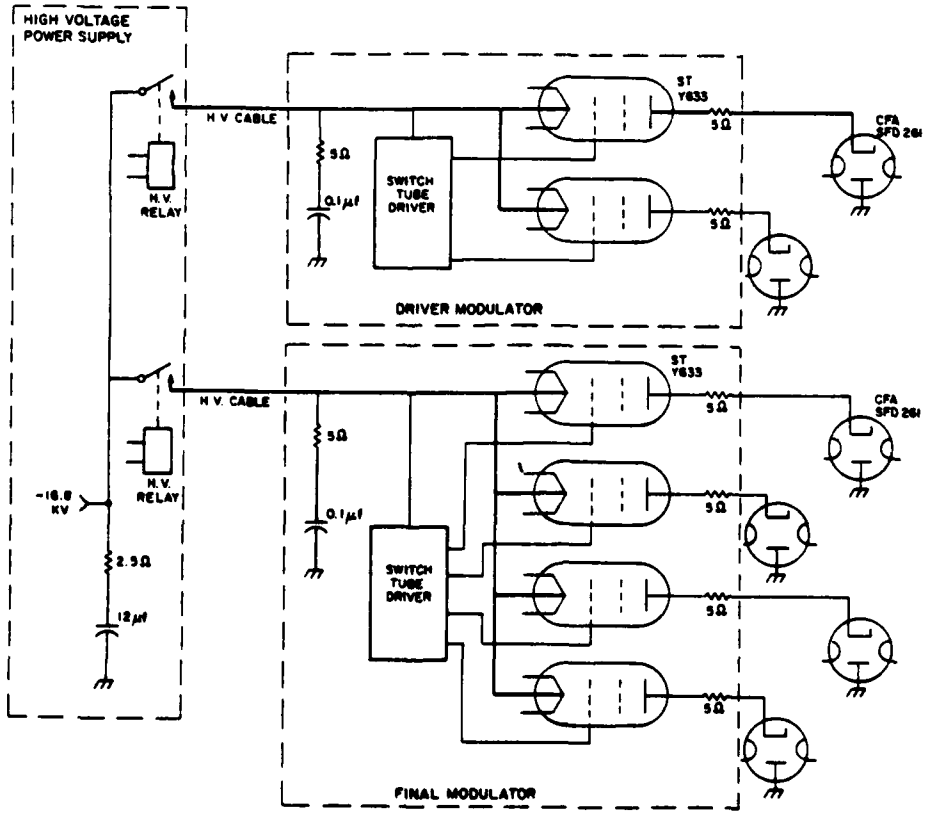

Figure 2. Driver & final modulators Basic elements

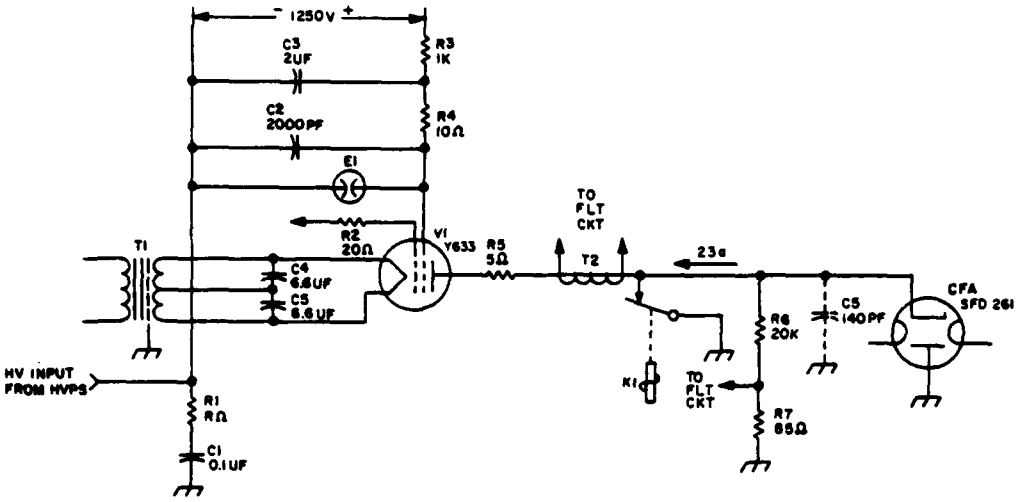

Figure 3. Modulator output stage

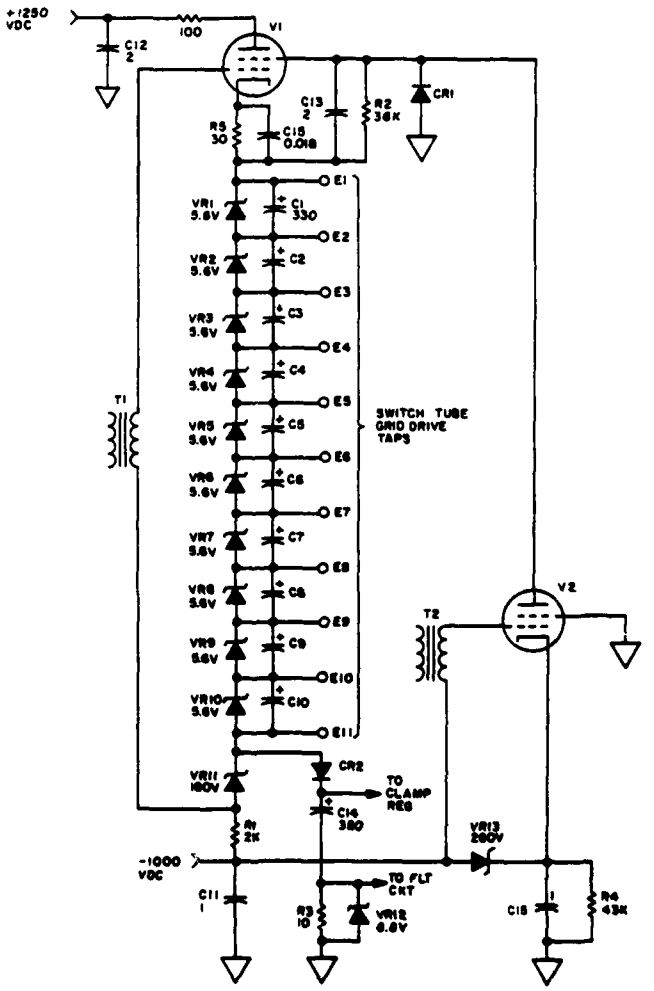

Figure 4. Switch tube driver

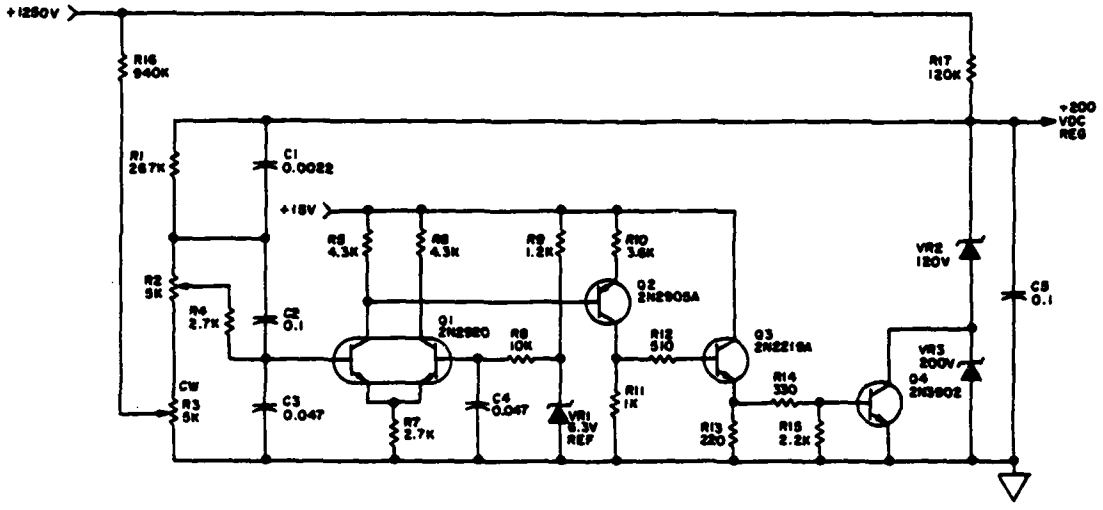

Figure 5. Clamp regulator

A CONSTANT CURRENT HARD TUBE MODULATOR

by

Ralph Alsmeyer

Raytheon Company

Wayland, Massachusetts

1. Introduction

Modern air defense radars require reliable stable high-power transmitters. This paper describes the modulator for the final amplifier stage for such a transmitter. It is completely solid state except for the high-power switch tube and the crowbar spark gap. The modulator drives a crossed-field amplifier tube (CFA).

The electrical specifications are as follows:

1. Prime power: 10 KHz, 1 phase, sine wave
2. Pulse output:
   - 2.1 Voltage: 28 to 31 Kv peak
   - 2.2 Current: 34 to 41.5 amperes
   - 2.3 Duty cycle 0 to several percent
   - 2.4 Duration: variable over a 50/1 range
   - 2.5 Rise time (V): less than 80 nsec (50 to 90%)
   - 2.6 Fall time (V): less than 2 μsec (90 to 50%)
   - 2.7 Droop (I): to produce less than 0.2°/μsec phase shift in the CFA output

The mechanical characteristics are as follows:

1. Environment: military field operation
2. Packaging: housed in an oil filled cast aluminum tank
3. Cooling: by ethylene-glycol/water solution from an external cooling unit.

2. General

The modulator block diagram is given in Figure I. It is of the floating-deck configuration.[1] The switch tube is specially tested version of the 4CW-50000 tetrode operating in the constant current mode. This mode of operation offers several advantages:

a. The storage capacitor size is minimized, as ripple and droop are greatly attenuated by the high plate resistance of the switch tube rather than being accented as they would be if the CFA were directly connected to the HVPS through a "bottomed" switch tube.

b. The Δe_b which occurs across the CFA load when frequency is changed is absorbed automatically by the switch tube thus allowing the wide-band capabilities of the CFA to be fully utilized.

c. The output current during CFA arcing or short circuit is maintained below the crowbar trip level thus minimizing transmitter "kick outs". This current level is sufficiently low enough to permit full peak power testing of the modulator without the need for a high-power dummy load if the output is short circuited.

The modulator block diagram is presented in Figure I which is described below:

The switch tube grid bias, screen, and filament power supplies, along with the grid pulse drive assembly (PDA) and its power supply, are located on the floating deck. Prime power (10 KHz) is fed to the deck through a high voltage isolation transformer.

Fault-sensing circuits in the power supplies feed fault signals to the PDA where they are sensed by an "OR" circuit which drives a light-emitting diode. The optical fault signal is transferred across the HV interface via a glass-fiber light pipe to a light receiver which supplies the signal for external fault indication.

The output pulse is initiated and terminated by externally supplied 0.3 μsec. "ON" and "OFF" trigger pulses which are fed to the floating deck by pulse isolation transformers. The PDA contains a latch circuit to maintain it on for the pulse duration.

The high-voltage power supply (HVPS) is a simple single-phase full-wave-bridge capacitor-input (2 μF) circuit. The high voltage is regulated at -33 to -36 kV ±1% by controlling the input 10 kHz voltage. The regulator loop error signal is derived from a precision voltage divider located in the HVPS.

The crowbar is a high vacuum triggered spark gap (EG & G Type GP15B-50) which discharges the filter capacitor through 5 ohms.[2] The gap is triggered by solid state circuitry, SCR capacitor discharge.

The voltage fall time specified for the CFA is not very stringent and so a resistive tail biter is adequate.

3. Design Details

Switch Tube

The switch tube is specified to deliver 40 amperes of anode current at:

- e_{g1} = 75 v peak
- e_b = 2.2 kv
- E_{G2} = 1.1 kV
- i_{G1} = 2 a maximum
- r_p = 1000 ohm minimum over the operating range of e_b

The filament is supplied from a center-tapped DC source in order to minimize heater hum modulation of the output current pulse.

HVPS - The power supply pulse droop.

$$\Delta E_{bb} = \frac{i\Delta t}{c} = \frac{41.5}{2 \times 10^{-6}} = 20.75 \text{ V/}\mu\text{sec}$$

Where i is the pulse current and c is the storage capacitance. This yields the maximum output current droop,

$$\Delta i_b = \frac{\Delta E_b}{r_p} = \frac{20.75}{1000} = 20.75 \text{ ma/}\mu\text{s}$$

The low dynamic impedance of the CFA is neglected here because it is small compared to r_p.

Phase modulation of the CFA output,

$$\Delta\phi = \frac{\Delta ib}{ib} \times 100 \times K = \frac{20.75 \times 10^{-3}}{40} \times 10^2 \times 2 = 0.104^\circ/\mu\text{sec}$$

Where K is the phase pushing figure for the CFA, $2^\circ/\%\ \Delta ib$ maximum

Tail Biter

The tail biter has a resistance of 17 K ohms.

The load capacitance was estimated to be:

Switch tube anode	:	55 pf max
CFA cathode	:	58
Strays	:	70
		183 pF maximum

The discharge time constant $RC = 1.83 \times 10^{-10} \times 1.7 \times 10^4 = 3.12\ \mu s$.

From $V = e^{\frac{-t}{RC}}$

$t = RC \ln 1/V_1 - RC \ln 1/V_2$

and

$t_f = 3.12 \ln (1/.5 - 1/.9) = 1.83\ \mu\text{sec}$

The CFA specification for fall time (t_f) is 2 μsec maximum, 90 to 50%.

Pulse Drive Amplifier

As indicated above, the PDA delivers grid drive pulses to the switch tube which are of constant amplitude and having their duration determined by the "ON" and "OFF" trigger pulse spacing. The schematic of this circuitry is given in Figure II. In this diagram Q3, 4, 7 and 8 form a "totem pole" switch for the output pulse which is clamped in amplitude by the zener diode VR4. CR22-25 provide isolation for the grid bias. Q2 is a latch circuit which maintains Q3 and 7 turned on for the pulse duration. Q5 is a trigger amplifier and Q6 and 9 form a complementary one-shot multivibrator. The biased diodes CR15 and 18 were included to improve the trigger noise immunity for the input circuits.

During the interpulse interval, all transistors are in the off state and the output is held at approximately -500 volts by R30 and 31. C4 is charged to 15 volts through CR5 and R6, 34 and 39.

When an "ON" pulse is applied to J1A1, it is amplified by Q5 and transformer coupled to the bases of Q3 and 4 which then supply current to charge the load capacitance. As the output level goes positive, Q2 is turned on through CR7 and 8 and R7 to maintain Q3 and 4 in the on state. With the base voltage clamped by VR3 and negative feedback developed across the emitter resistors, Q3 and 4 become parallel constant current generators to feed the switch tube grid with the clamp circuit absorbing the excess current. With 150 volt collector supply and the emitters clamped at approximately 80 V, the switch transistors do not saturate and thus their storage time is minimized. Speed up capacitors bypass the emitter resistors in order to generate a fast output rise.

An "OFF" pulse applied to J1A2 turns on the monostable, which generates a 1.5 μsec drive pulse for the off transistors Q7 and 8. We found it necessary to stretch the system "OFF" trigger (0.3 μsec) in order to maintain the off transistors in conduction long enough for the on transistors to recover. When the output voltage goes negative, the latch circuit turns off. If an "OFF" trigger fails to appear, the latch will turn itself off when C4 becomes discharged. This limits the pulse duration to slightly longer than the longest required pulse duration.

The switching transistors are DELCO DTS-804 units which are tested for turn-on time to meet our requirements, as this is not a part of the commercial specification. They are operated at V_{CR} = 650 volts which is well below the 1000 volt rating. Texas Instruments TIP 553 transistors were found to work equally well.

The overall PDA delay for turn-on is 180 nsec and the turn-off delay is 280 nsec.

For the pulse duration, the "ON" transistors supply an emitter current I_E.

$I_E = \frac{6.8V - 0.7V - 0.8V}{3.82 \text{ ohms}} = 1.39$ amperes per transistor

At V_{CE} = 70 volts, this is well within the transistor safe operating area for normal or shorted load conditions.

With two transistors 2.78 amperes is produced. If the switch tube grid draws its maximum rated grid current (2 amperes) then 0.78 amperes is absorbed by the clamp circuit. This provides adequate margin for temperature and tolerance variations.

Figure IV shows the rise and fall time of the PDA output pulse into its rated load of 390 pF while immersed in oil. The rise time in air was found to approximate by 1.5 times faster.

The circuit was proven to operate stably and without damage into an arcing or shorted load.

Switch Tube Filament

Providing a center tap for the DC filament supply turned out to be somewhat tricky in that the voltage divider must pass the total switch tube cathode

current. The voltage drop across the divider is degenerative with respect to the grid drive. With the values used (See Figure III) the worst case drop across the divider at one time constant (82 μs) would be

$$V = .63 \times (41.5 + 2 + 2) \times 2.05 = 58 \text{ volts}$$

which is large compared to the grid and screen supply voltages. To ease this problem, the circuit shown in Figure III was devised. In this circuit the grid return and HV returns are provided by separate dividers. In this configuration, the HV return may be an RC circuit as the voltage drop is small with respect to the plate voltage, and the r_p of the switch tube greatly limits the effect of the exponential response of this circuit to the current pulses. The grid return circuit is resistive and thus does not distort the grid drive shape.

4. Mechanical

As mentioned above, the modulator is housed in a dielectric-oil-filled tank. Its dimensions are approximately 23" high X 27.5" wide X 38" deep. It weighs 1143 pounds, including the CFA tube.

A liquid-to-liquid heat exchanger facilitates cooling the oil by the externally supplied coolant (glycol/water solution).

The switch tube cathode seal is cooled by oil circulated in the tank by an internal pump. The anode is cooled by the glycol/water system.

The modulator is "hard mounted" into the transmitter cabinet.

5. Performance

A typical CFA current waveform as viewed through a current transformer having a rated droop of 0.15%/μsec is given in Figure V.

The modulator was found to be capable of producing pulse groups with a minimum spacing between pulses of 20 μsec.

The modulator "breadboard" model has been successfully operated for many hours. It has survived simulated and actual CFA and switch-tube arcs.

With a shorted load, the switch tube current is approximately 20% greater than normal.

References

1. H. Nettsheim and F. Lewis, "Some Techniques for the Design of High-Power Vacuum Tube Pulse Modulators", Proceedings of the Sixth Symposium on Hydrogen Thyratrons and Modulators.

2. L. B. Woolhaver, "The Use of Triggered Spark Gaps as Crowbars", Proceedings of the Seventh Symposium on Hydrogen Thyratrons and Modulators.

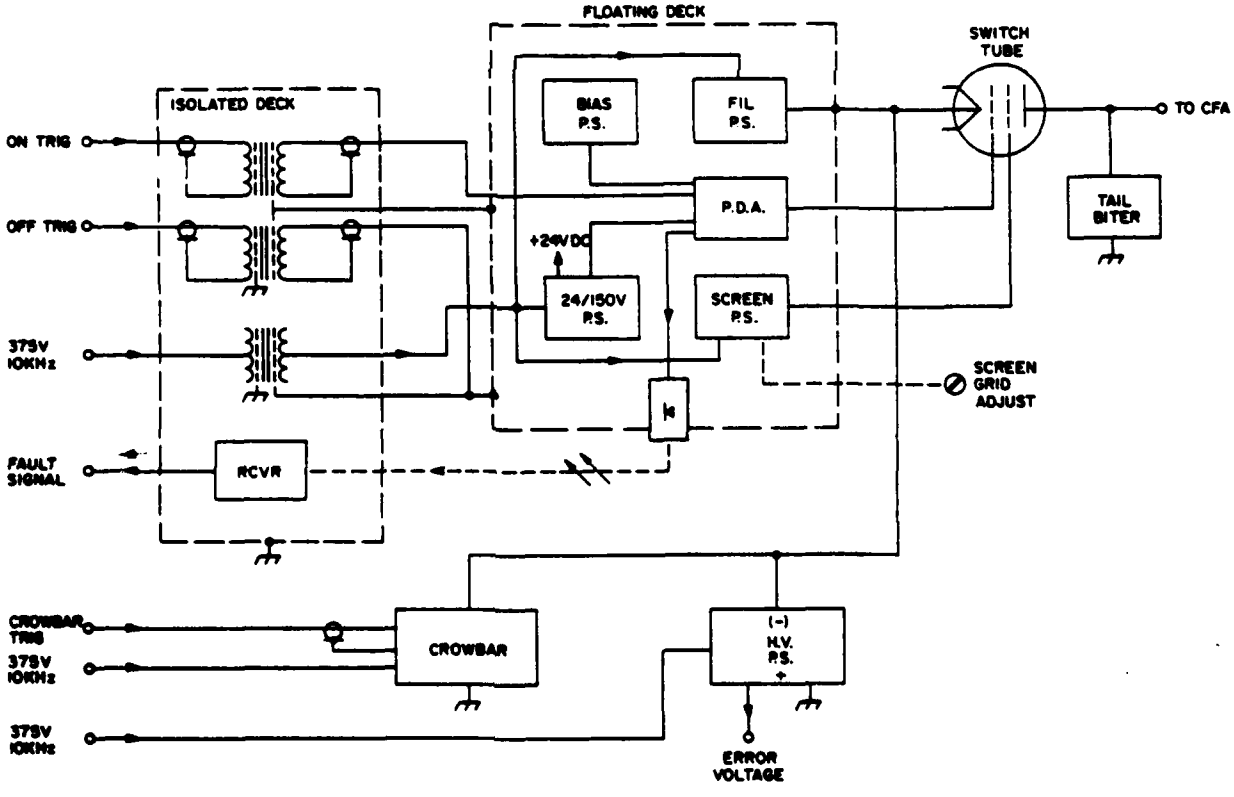

Fig. I

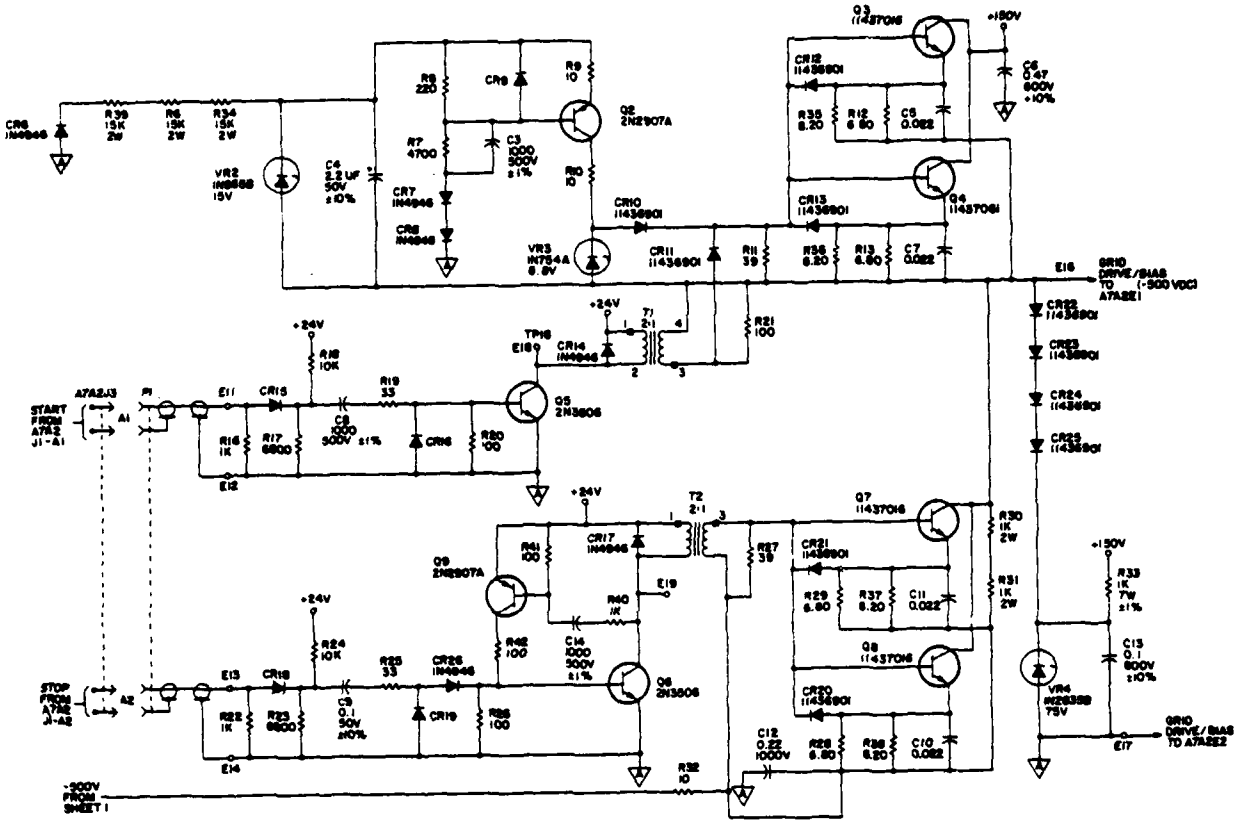

Fig. II

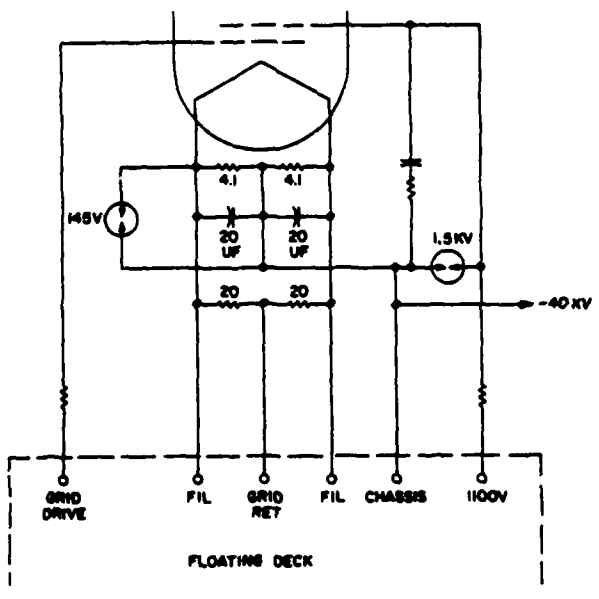

Fig. III

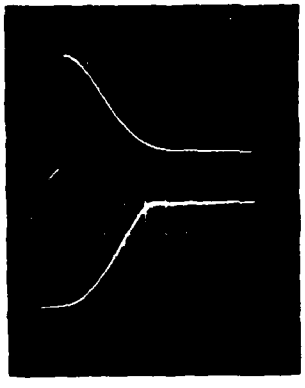

Figure IV
Fall Time
Rise Time
Horizontal = 50 μs/cm
Vertical = V Uncalibrated

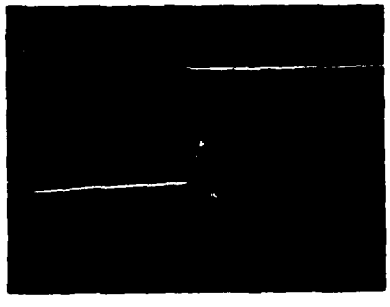

Figure V
CFA Current
Horizontal = 20 μs/cm
Vertical = 10 amp/cm

HIGH POWER LONG PULSE DISTRIBUTED AMPLIFIER TRANSMITTER

Duard L. Pruitt
RCA Corporation
Government and Commercial Systems
Missile and Surface Radar Division
Moorestown, New Jersey

Summary

A multi-megawatt distributed-amplifier transmitting system for use in a VHF radar system was designed and constructed by RCA's Missile and Surface Radar Division in the late 1960's. The transmitter employs 72 power tetrode tubes, in six power amplifiers of 12 tubes each. The pulse width varies from a few hundred microseconds up to several milliseconds, determined by screen grid pulsing of the power tetrodes. Thus the high power RF amplifier tubes serve as their own pulse modulators. The duty cycle may vary from very low up to 11% maximum.

The instantaneous RF bandwidth is almost three octaves. The entire transmitter system occupies more than 18,000 square feet of floor space, and is believed to be the world's highest power distributed amplifier.

Introduction

Distributed-amplifier techniques have been used for years. At first, in 1936,[1] they were used in "low-power video" amplifiers.[2,3] Distributed amplifiers were developed in later years for high-power applications, such as ionospheric sounding and ECM in the VHF and low-UHF ranges.[4]

Since the mid-50's, the prospect of VHF radar systems has been an intriguing one, but one that required new approaches to power amplification. Broadband transmitter systems were most desirable, with goals of 2-1/2-to-3-octave instantaneous bandwidths, set for operation in the low-VHF range. In the late-60's, the Missile and Surface Radar Division undertook the development of a very-high-power broadband VHF transmitter system; distributed-amplifier techniques were successfully applied to solve the technical problems involved.

The transmitter system described in this paper was developed for broadband operation, and achieved a bandwidth of almost three octaves with multimegawatt peak-power output and duty cycles up to 11%. The development and subsequent analysis of this transmitter system included extensive analytical computer studies of high-power distributed-amplifier operation.[5,6,7,8,9,10]

Configuration and Performance

Figure 1 is a block diagram of the transmitter system. Six high-power amplifier (HPA) chains are used to generate the total output power. Each HPA has a separate distilled-water cooling system; one "raw water" cooling system is used for the entire transmitter. A single high-voltage DC power supply and capacitor storage bank system supplies DC power to all six amplifier chains. Four levels of high-voltage DC are fed to each amplifier: 4, 11, 13, and 15 kVDC. As indicated in Figure 1, each HPA feeds a separate antenna, with the total output power combined in space.

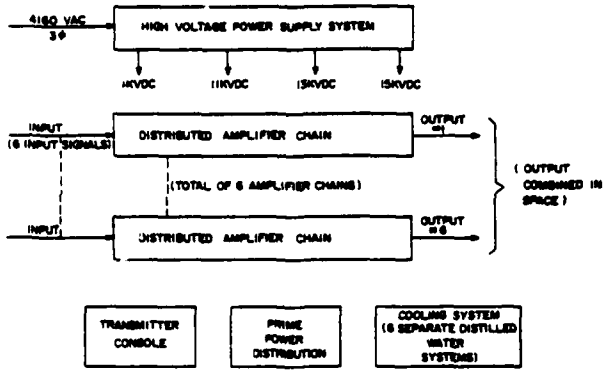

Figure 1. Transmitter System Block Diagram

The transmitter system, exclusive of the high-voltage power supply (HVPS) and cooling equipment, occupies 90x100 ft (9,000 square feet) of high-overhead floor space. The HVPS capacitor bank occupies an additional 20x120 ft of floor space. The HVPS units are located outdoors. The distilled-water cooling system occupies 60x120 ft of floor space. Total floor space required by the transmitter system is then 18,600 square feet.

High-Power Amplifiers

Figure 2 is a simplified schematic of a single high-power amplifier (HPA). Each of the six HPAs uses 12 RCA 4641 power tetrodes in a distributed-amplifier circuit.

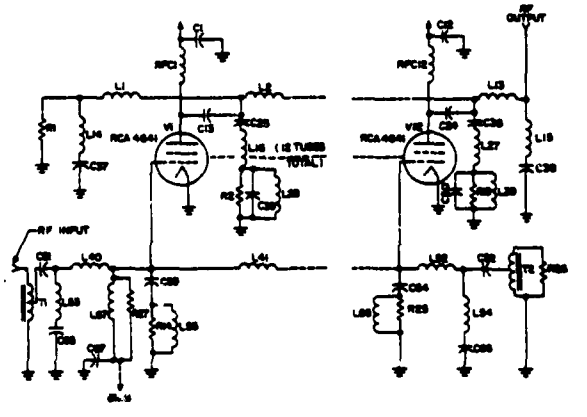

Figure 2. Simplified Schematic of a Single High-Power Amplifier; Six HPAs are used in the Transmitter System

Grid-line impedance is 5-1/2 ohms. Broadband ferrite core transformers are used to match the grid line to a 50-ohm source at the input end and to a 50-ohm termination at the output end. Operation is essentially Class A, with all 12 HPA tubes operated at the same grid-bias voltage.

The screen grid of each power tetrode is individually pulsed, and the peak-pulse voltages are adjusted to obtain the desired "video" plate currents. These video plate currents are set with zero RF input drive. When RF drive is applied, the peak-pulse plate currents increase due to nonlinearity in the 4641 tube characteristics.

As shown in Figure 2, the low-pass grid line is made up of inductors L40, L41,..., L52 in conjunction with the tube-input capacitances plus the circuit capacitance. As mentioned previously, impedance is 5-1/2 ohms. Networks (C53, L55, R14) introduce high frequency loading to help suppress parasitic oscillation. The input drive power is transformed from 50 to 5-1/2 ohms by RF transformer T1. The drive power is terminated in R26 (50 ohms).

The plate line consists of inductors L1,..., L13 in conjunction with tube-output capacitances plus circuit capacitances. The plate-line cutoff frequency is the same as that of the grid line, so that plate-line phase shifts match the grid-line phase shifts. Plate-line impedance is tapered from a high impedance (at reverse termination R1) to a lower impedance at the RF output. The output line is a 6-1/8-in.-diameter 50-ohm coax.

Harmonic content in the plate-current waveform is high because of characteristic tube nonlinearity - as high as -12 dB for the second harmonic and -15 dB for the third harmonic. These harmonics are removed in a high-power harmonic filter, located between the transmitter and the antenna.

Since the plate and grid line mid shunt impedances theoretically go to infinity at the cutoff frequency, the amplifier will tend to oscillate at or near cutoff. This tendency is prevented by plate-line networks (C25, L16, L28, C39, R2) and eleven other identical networks. These "oscillation suppressors" are double-tuned circuits, tuned slightly below the cutoff frequency, which couple 50-ohm loads tightly to each plate at the tuned frequency.

The DC plate voltage is fed to the HPA tube plates via RF choke coils RFC1, RFC2,..., RFC12. The RF voltage present on the plate line builds up gradually from input end to output end, i.e., the maximum RF voltage appears at the plate of tube V12, and minimum RF voltage appears at tube V1, as a general rule. Reflected power from the load (VSWR) and plate-line imperfections may partially upset this simple picture, without changing the general pattern. Since the RF voltage varies from tube to tube, efficiency can be maximized by "grading" or "tapering" the DC plate voltage. In the HPAs of this equipment, the DC plate voltage is graded as follows: tubes V1 to V4, 11 kVDC; tubes V5 to V8, 13 kVDC; and tubes V9 to V12, 15 kVDC.

The 15-kVDC level used on V9 through V12 provides a generous minimum plate voltage for ideal conditions. High VSWR loads, coupled with the rise in circuit mid-shunt impedance at the top of the band, cause a reduction in the minimum plate voltage for some tubes. For example, a VSWR of 2:1 coupled with maximum frequency operation could cause inadequate minimum plate voltage at tube No. 12. Excessive screen current is prevented by use of a "soft" screen supply (using a series resistor). This also causes a small drop in total power output, which is tolerated for these extreme conditions.

The HPA tubes are screen pulsed, from individual screen pulse "regulators." Peak screen voltages are adjusted at the HPA local control panel, which also displays the resulting peak plate currents.

Figure 3 shows a finished HPA unit. Several of the RCA 4641 tetrode tubes may be seen in this photograph. Figure 4 is a photograph of the HPA control panel (local control console) outside the HPA room. HPA tube filament and screen voltages are individually controlled, and peak plate currents, peak screen currents, and peak screen voltages are monitored on peak reading meters at this console.

Figure 3. High-Power Amplifier

Figure 4. HPA Control Panel

Each HPA assembly is 5 ft wide, 20 ft long, and about 8 ft high; it is housed in a shielded HPA Room measuring 30 ft square and 12 ft high. The 12 HPA screen voltage pulsers and 3 crowbar units are also housed in the HPA Room.

Screen Grid Modulator

Figure 5 is a simplified schematic of one of the 72 screen grid modulators. These units were named "screen grid regulators" since the output pulse at the switch tube cathodes is electronically regulated. Amplitude of the output

pulse is controlled by an external potentiometer. Four kilovolts DC (from the HVPS system) is supplied to the modulator via DC fuse F1 and crowbar E1. E1 is a triggered spark gap.

The series switch tube/regulator function is supplied by tetrode V1 (Eimac Y517). A monostable multivibrator, controlled by external start and stop triggers, controls the output pulse duration. Pulse amplitude regulation is achieved by comparing the pulse amplitude at V1 cathode with the DC voltage on 1000 μF capacitor C1. Diode stack D1 conducts when the cathode pulse voltage exceeds the DC voltage on C1, causing a voltage drop across the 0.23 ohm resistor. The feedback amplifier operates on V1 grid voltage to maintain a constant voltage drop across the 0.23 ohm resistor (approximately 0.5 volt).

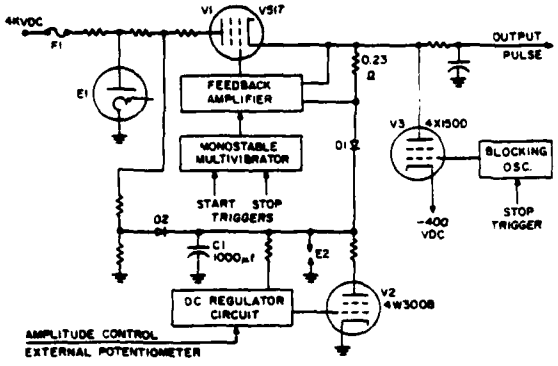

Figure 5. Screen Regulator, Simplified Schematic

The DC voltage on C1 is regulated by shunt regulator V2, a 4W300B tetrode. The shunt regulator circuit is controlled by a remote external potentiometer, which thus also controls the peak pulse voltage amplitude.

Tetrode V3 (4X150D) serves as a "tailbiter" to reduce pulse fall time. V3 is driven by a blocking oscillator which is in turn triggered from the "stop" trigger.

The screen grid modulators were designed and constructed by Energy Systems, Inc., Palo Alto, California.

HPA Tube Arc Protection

It is well known that high-power tubes are subject to internal flash arcs during operation - the "Rocky Point effect."[11] If not interrupted, the arc will damage, or destroy, the tube.

In the design, a conventional ignitron crowbar[11] is used to interrupt the power-tube arc. Plate arcs are sensed by thresholding the signal from a plate-pulse current transformer, feeding logic circuitry which fires the appropriate crowbar for the tube concerned. A memory circuit lights a lamp to show which tube arced. There is one crowbar for each voltage level on each HPA - i.e., three crowbars per HPA and 18 crowbars per transmitter system.

Each HPA crowbar chassis receives plate voltage from the high-voltage power supply system via a high-voltage silver/sand fuse. When the crowbar fires, the associated fuse opens up, thus isolating the faulted unit from the HVPS. The remaining five HPAs continue to operate as if nothing had happened. A remotely operated fuse changer is used to switch to a new fuse, thus returning the HPA involved to operational status. Each fuse changer contains five fuses. After five operations of a given crowbar chassis, the HPA room is opened up to replace the blown fuses. The fuse is designed to allow for easy field replacement of the fuse wire.

Figure 6 shows a view inside the HPA room, with the fuse changer in the foreground. The row of 12 screen-pulse regulators is in the middle of the room, with the high-power amplifier in the background.

Figure 6. HPA Room

High-Voltage Power Supply System

Figure 7 is a block diagram/simplified schematic of the HVPS and capacitor bank system.

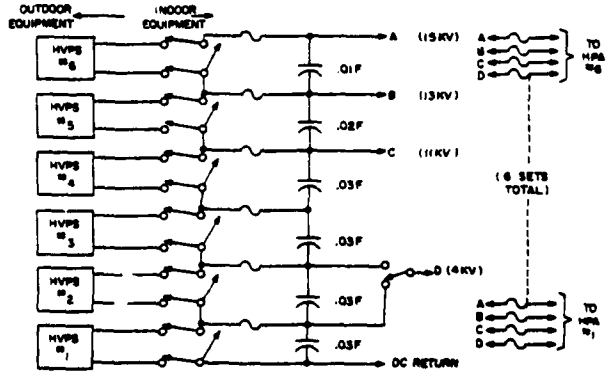

Figure 7. High-Voltage Power Supply (HVPS) System

Six identical high-voltage DC power supplies are used, with the outputs connected in series. Each supply is fed from a 4160 VAC, three-phase source, and each supply contains its own 4160 VAC three-phase circuit breaker. Each supply is 12-1/2x14x9 ft high. The output rating per supply is 2 to 5 kVDC (variable by remotely-controlled load-tap changer). Thus, the HVPS system is capable of a maximum output voltage of 30 kVDC, although the typical operating value is 15 kVDC maximum.

An indoor switch matrix permits isolation of any of the six supplies for repair or maintenance as required. The

system can supply full required voltage with any one supply down, though the tapered-plate-voltage feature is partially lost if either supply No. 5 or No. 6 is down.

The pulse currents are drawn from the series-connected capacitor banks. As shown in Figure 7, the six capacitor banks vary in size from 0.01 to 0.03 F. Maximum rated energy storage capacity is 1.875 megajoules; normal storage is 0.55 megajoules.

Twenty-four large coaxial cables (similar to RG-17) feed the four high-voltage levels (4, 11, 13, and 15 kVDC) to the six HPAs. Each line has a protective input fuse, or back-up fuse, for the crowbar fuse.

The six high-voltage power supplies are individually controlled from a remote, centrally located console. ON/OFF and RAISE/LOWER controls are provided, with complete voltage and current metering.

Figure 8 shows the six outdoor-mounted HVPS units. Figure 9 is a view of the capacitor room, with the switching matrix on the wall to the left and the capacitor banks to the right in the photograph. Figure 10 is a view of the central transmitter control console (TCC). The HVPS controls and various monitoring functions are located at the TCC.

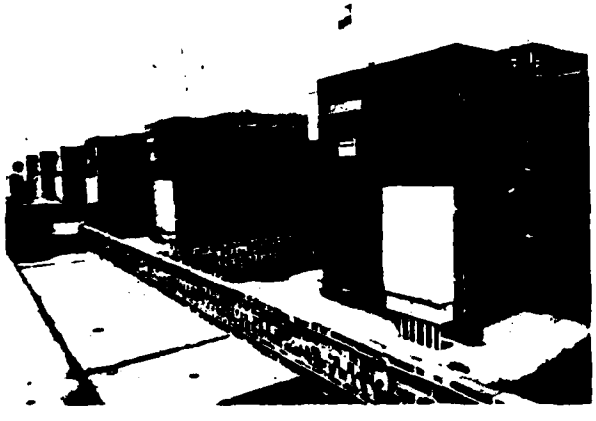

Figure 8. High-Voltage DC Power Supplies

Figure 9. Capacitor-Bank Room

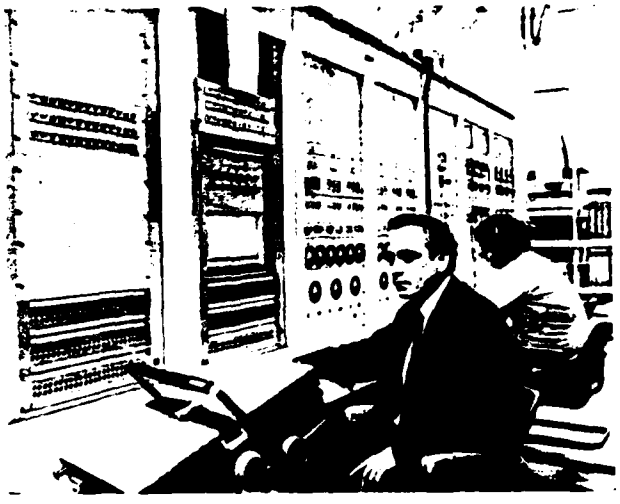

Figure 10. Transmitter Control Console

Driver Amplifiers

The intermediate-power amplifier/driver must supply a minimum of 800 W peak RF drive power to each HPA input. Six driver units are used, one for each HPA.

The input from the system exciter is 60 milliwatts peak to each of the six IPA/driver cabinets. The intermediate-power amplifier (IPA) is a small distributed amplifier containing six type-8233 tetrodes. IPA grid-line impedance is 50 ohms, thus matching the 50-ohm exciter cable with no requirement for impedance transformation. IPA plate-line impedance is 300 ohms, and typical power output is 3 W peak. A 2:1-voltage-ratio RF transformer matches the 300-ohm IPA plate line to a 75-ohm coaxial line which carries the 3 W IPA output to the driver input.

The driver grid-line impedance is 75 ohms, and the driver plate-line output impedance is 200 ohms. The driver is another small distributed amplifier, using 10 type 8122 tetrodes. The driver output power (800 to 1000 W peak) is transformed to the 50-ohm level by a 2:1 (voltage ratio) ferrite transformer, and fed to the HPA via 7/8-inch 50-ohm coaxial line.

Figure 11 shows the IPA-Driver, fault-sensing logic, and "local-load-center" cabinets. The IPA-driver circuitry occupies a 2/1 cabinet at the left, while the fault-sensing logic occupies a single cabinet in the center.

Cooling System

The six outdoor units of the HVPS are self-cooled, with oil-to-air radiators to transfer the waste heat to the atmosphere. All indoor units are in an air conditioned environment, with forced, cooled air circulated continuously.

Waste heat from the HPA tubes, HPA filament power supplies, and HPA screen pulsers, is removed by a distilled-water system. Each HPA tube plate is cooled by a 60 gal/min flow of high purity water (720 gal/min for all 12 tubes in an HPA). Typical flow for the remaining water courses is 1 to 2 gal/min/water course.

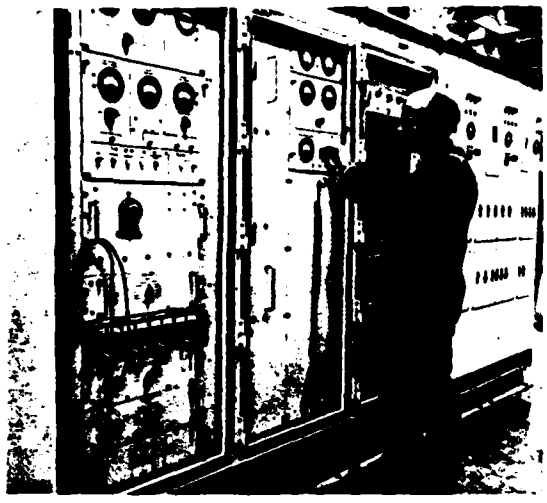

Figure 11. IPA-Driver, Fault Logic, and Load Center

The water system (for each HPA) consists of a 2000-gal stainless-steel storage tank, demineralizing equipment, a 1000-gal/min, 100 psig pump, and copper distribution piping with flow interlock switches. Secondary (raw water) cooling is provided by outdoor cooling towers.

Acknowledgements

The author wishes to acknowledge the many contributions of Dr. William G. Hoover, Granger Associates, to the design of this transmitter system. Dr. Hoover was retained as a technical consultant throughout the program.

Dr. Leon S. Nergaard of RCA's David Sarnoff Research Laboratories (since retired) contributed theoretical analyses and many consultation sessions; T. Douma, RCA Missile and Surface Radar Division (retired 1970), supported the design effort with theoretical analyses and calculations. Many others at RCA's Missile and Surface Radar Division, Electronic Tube Division, and David Sarnoff Research Laboratories also made important contributions to the program.

This work was sponsored by the U.S. Air Force under Contract No. F 19628-67-C-0209.

References

1. Percival, W. S., British Patent Specification No. 460,562, applied for 24 July 1936.
2. Ginzton, Hewlett, Jasberg, and Noe, "Distributed Amplification," Proceedings of the IRE (Aug. 1948).
3. Horton, Jasberg, and Noe, "Distributed Amplifiers: Practical Considerations and Experimental Results," Proceedings of the IRE (July 1950).
4. Rodgers, P. H., "Large Signal Analysis of Distributed Amplifiers," Engineering Research Institute, University of Michigan. Technical Report No. 52, Contract No. DA-36-039 s c 63203, July 1955.
5. Douma, T., Private Communication.
6. Douma, T., Private Communication.
7. Douma, T., Private Communication.
8. Douma, T., Private Communication.
9. Douma, T., Private Communication.
10. Hoover, W., and Pruitt, D., Private Communication.
11. Parker, W. N., and Hoover, M. V., "Gas Tubes Protect High Power Transmitters," Electronics (Jan. 1956).

HIGH POWER SOLID STATE MODULATOR FOR COHERENT AGILE MICROWAVE AMPLIFIER

By Giovanni Scerch
Selenia S.p.A. - Rome - Italy

SUMMARY

The present paper describes an high power broadband microwave amplifier realized for a pulse compression, M. T. I. or frequency agile radar system.
After a short description of the amplifier global network, the most important solutions are pointed out, i. e. H. V. microsecond protections, grid modulator circuit, H. V. -ground levels interfaces, amplifier processor.
The overall performances obtained are also given.

1. OUTLINE

The amplifier hereafter described is a part of a radar system using pulse compression combined with M. T. I or frequency agility.

As we know, a pulse compression implies the transmission of long pulses, with a relatively low peak power at low repetition rate. These pulses will be modulated in frequency, amplitude, phase, single or combination of, in order to allow their compression into the receiver and to obtain therefore the required level of resolution capability, detection sensibility and maximum unambiguous range. (1)
Frequency agility means for the transmitter unit the use of large band tube having special characteristics and of a suitable RF driver in order to obtain a sufficiently constant power over the total band range. (2)
The M. T. I. system requires high phase and amplitude stability. (3)

2. AMPLIFIER CHARACTERISTICS

Taking into account the above mentioned system requirements, the power amplifier characteristics are set up, i. e. peak power above 100 KW, transmitted by pulses ranging within 100 μs, amplitude and phase codified, having some hundreds of pulses per second of repetition rate and average transmitted power ranging up to several KW.

The instantaneous bandwidth wherein the frequency agility takes place is approximately 10%.
The tube used is a gridded electron gun T. W. T. (4) and may be driven directly from a solid state amplifier due to its high gain (50 db approx).
The electronic circuitry designed for this tube allows:

a) High phase stability, both into the transmitted pulse train (a few r. m. s. degrees) and from train to train (some tenths of degrees r. m. s.), with a cathode phase sensitivity of 100 deg/KV and a grid phase sensitivity of 1 deg/V.

b) High amplitude stability (many tens of dB below pulse amplitude) with a cathode amplitude sensitivity of mdB/V and a grid amplitude sensitivity of about 10 mdB/V.

It has been possible to reach such values designing the cathode H. V. P. S. and grid modulator circuits (where voltages ripple are the main causes of unwanted phase and amplitude modulations), extremely stable in voltage.

Hereafter, after a short glance to the amplifier global network, the most important production highlights of the amplifier will be pointed out.

It must be said that this amplifier is definitely a general purpose model which is able, besides its present use, to amplify radio frequency power with any type of phase and frequency modulation within the bandwidth of microwave tube with high level of phase and amplitude stability and to pulse modulate such R. F. through the TWT grid modulator.

3. AMPLIFIER SCHEMATIC DIAGRAM

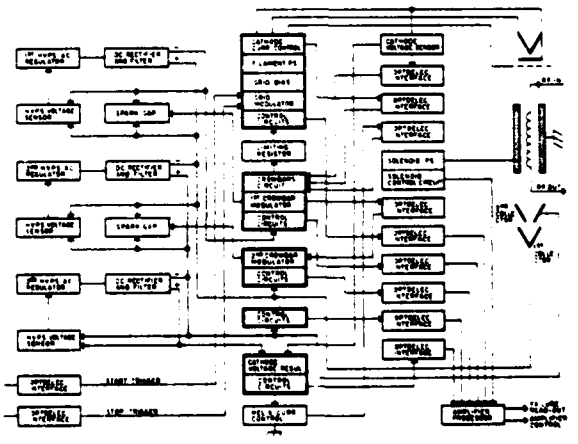

Figure 1. Amplifier schematic diagram

On fig. 1 we illustrate the schematic diagram of the implemented amplifier. As we said before, a TWT has been used as microwave amplifier. It has two depressed collectors to increase its efficiency. Among different possible solutions to realize H.V. cathode and collectors path, the one with three series power supplies has been chosen, because it presents some advantages. The TWT has a shadow gridded electron gun, with grid mu approximately 20.
It is focused by an electro-solenoid, supplied with a very stable power supply. Also microwave tube filament is fed with a D.C. stabilized power supply.
As it can be seen from fig. 1, the amplifier circuits are referred to five different voltage levels.
All triggers and logic signals are transferred among different voltage levels and between these and ground through optoelectric transducers coupled by fiber optics.

4. H.V. CIRCUITS AND PROTECTIONS

The H.V. section, which supplies the cathode voltage while adequately depresses the two collectors, has been obtained including three series power supplies. Each one of these is a.c. regulated following the power supply D.C. voltage variations by using triacs. This allows to buffer automatically, within the percentage limits, the slow variations of the power supply D.C. voltage (main line variation and static load variation, switching R.F. on-off with electron beam on). The triac use permits, moreover, if appropriately driven, to have high voltage step up gradually and aperiodically even during "switching on", avoiding transient oscillating phenomena and their related overloads on circuitry.
This philosophy also allows, as we will see later, to stop immediately (ms) the triacs conduction, in case of H.V. circuits failure.

The phase stability required by the amplifier involves cathode voltage stabilization within 10^{-4}. Such stability has been reached by D.C. electronic voltage regulator, which controls the cathode voltage within 1 μs, by changing the voltage of the third power supply of the series pertaining to the second collector. In this way, we obtain cathode specified stability by varying voltage of the second and subsequentially of the first collector.

We will make hereafter some considerations on protections designed for the power supplies in order to avoid damage to microwave tube.

a) As we know, only a very small amount of the total energy contained into the H.V. capacitors (in our case about 1000 Joule) is normally delivered to the tube for each pulse. This would also entail that, in case of arcing inside the tube, the total energy could be discharged into the tube, thereby destroying it. It will be necessary in such case to cut power coming to the tube. Some tens of Joules for a few microseconds duration seem to be reasonable max amount for safety protection of the tube under consideration.

b) Since the tube is focalized by an electro-solenoid, some reduced or interrupted power to it would bring a loss of focus and subsequent helix current increase, which cannot be tolerated by the same for more than a few microseconds.

c) We must also consider some possible loss of control of grid modulator. Therefore the amount of the tube conductivity time must be kept within safe limits.

Regarding para a), the quantity of energy which is fed back to the tube in case of arcing is strictly correlated to actual arc impedance. It is clear that, being possible to maintain a low impedance arc, the problem could be solved by accepting a reasonable amount of adequate cathode series resistor. Therefore such arc impedance must be different in value depending on arcs frequency, time elapsed between arcings and phenomenon characteristics.

Regarding para b), some solution to the problem could be to procure some microseconds tube grid interdiction as soon as the above mentioned failure arises.

The analogous could be employed in order to solve the problem explained in para c).

However, solutions of this kind appear not properly fit to fully solve the problems, keeping in mind the tube price and the safety factors required by the tube manufacturer to approve the modulator and the protections philosophy. Therefore, the proposed solutions, although actually delivered, appear only as redondant ones. On the other hand, some completed crowbar system (5) realized with two hydrogen vacuum spark gaps set in parallel to higher rating H.V. (6) capacitors, allow to deviate in some known, safe and adequately designed way the correlated energy, as soon as cathode or helix current, or transmitted pulse duration override safety levels.

Contemporarily to the crowbar action, the TWT grid will be interdicted within microseconds and the conduction of triacs stopped into H.V. power supplies.

By using CAD (ECAP method) the H.V. circuit correct function has been checked during the crowbar intervention for dissipated energy as well for transients on cathode and collectors voltages.

5. GRID MODULATOR CIRCUIT

The TWT grid modulator has been completely implemented using solid state techniques.

It presents a large flexibility by being able to form single pulses whose length varies from 1 microsecond to several hundreds of microseconds, or pulse trains of any position and duration.
The rise and fall time of grid pulse, on a capacity equivalent to the TWT grid capacity, is less than 1 microsecond. The minimum distance between two pulses may approximately be 2 microseconds (modulator recovery time). Within a single pulse (up to hundreds of μs), with or without amplitude modulation, the am-

plitude variation is less than 10^{-3}, while from pulse to pulse it is about 10^{-4}. It is to be pointed out that in radar systems under consideration, the RF input power is supplied to the microwave tube when the electron beam is on, in order to reduce the jitter on the RF pulses.
The receiver being open between a pulse and the following on the train, this requires very low rise and fall time for beam pulse in order to reduce the time during which the noise is emitted by the tube in "beam on, RF off" conditions.

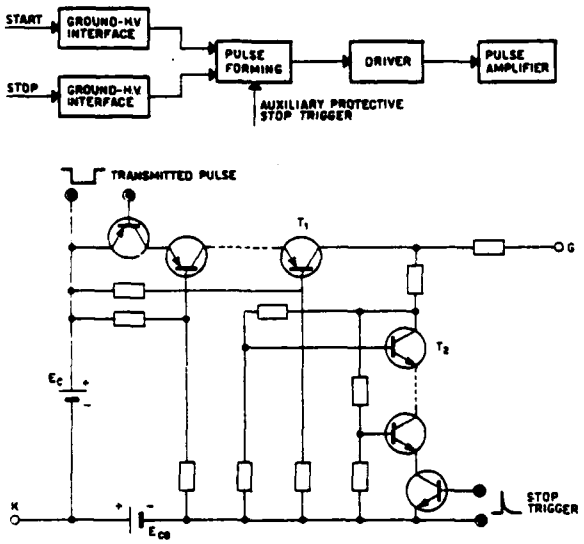

Figure 2. Grid modulator schematic

The low level circuit and the power stage realized for the grid modulator to be able to supply a swing voltage of about 2.5 KV are shown in fig. 2.
The amplification stage is realized by two transistor chains suitably polarized.
In off condition the power supply E_{CO} polarizes the grid to cut-off value.
The pulse to be amplified, switching in ON condition the T_1 chain, makes the TWT tube amplify through the E_C power supply. At the end of the pulse an auxiliary stop trigger makes the T_2 chain conductive causing a fast pulse fall time and modulator recovery.

6. GROUND-H.V. LEVEL INTERFACES

One of the most important problems which comes out in a power amplifier as the one described, which presents circuits referred to different H.V. levels (tube filaments and grid modulator referred to cathode voltage, crowbar circuits for H.V. referred to cathode level but insulated from the previous ones for the whole cathode voltage, first and second collector circuits referred to their respective voltages) is to transfer information and signals through different voltage levels. This information may be of two types:

a) Trigger for the control of start and stop of each transmitted train pulse or for the crowbar operation.

b) Logic levels which allow to define correct behaviour of different circuits referred to the H.V. levels. These logic levels are to be transferred to transmitter logic unit referred to ground level to guarantee a safe automatic and faultless functioning.

In the amplifier considered, the problem has been solved by the use of transmitting and receiving electro-optics transducer coupled by fiber optics.

This system has been studied in order to have a good flexibility, to perform variable connections up to a few meter length with any kind of track, and to obtain maximum system efficiency and safety.

A PN gallium arsenide infrared emitting diode, with maximum spectral output at 9000 A, has been chosen, as electro-optic transducer. (7) for its high internal and external efficiency.

A PIN silicon photodiode with max spectral response near 9000 Å with high radiation sensitivity and with very fast response time has been chosen as opto-electric transducer.

The optic transmission line and its matching to the two transducers has been studied in order to strongly reduce the losses. (see fig. 3) (8).

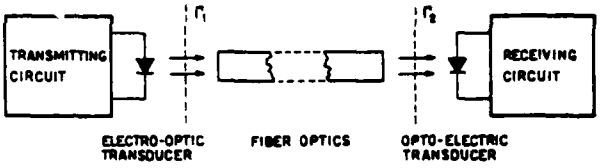

Figure 3. Ground - H.V. levels interface

The transmitting line chosen is built-up by many parallel core fibers covered with a thin glassy coat, (cladding) which has a refraction index suitably more than the core refraction index. The propagating light direction in the core is chosen in order to determine total reflection on the coat. Therefore, the light propagates through each optic fiber with many reflections, without leaving the fiber itself. (9) The fibers, in being arranged into parallel layers, give a transmission duct of about .5 cm of diameter of max mechanical flexibility. Of course, these parallel layers determine some non-conductive zones towards the inside of the whole fiber, giving rise to packaging losses p_1 (within 10%, with the chosen fiber).

As far as concern transmission attenuation losses p_2 due to the fiber attenuations and to total reflection on single walls, they are evaluated to approx 10% for 1 meter.

Special care has been given to obtain maximum trans-

mission coefficients Γ_1, Γ_2 (10) between fibers and transducers considering the transmitting coefficient as a ratio between the average energy flux per time unit and exposed areas within the two materials on their respectively exposed surfaces.
As a matter of fact, light coming from the photoemitter hits the frontal flat and optically polished surface of the fiber nucleus; part will be reflected and part will propagate inside the fiber itself.

It has been found that this transmitting coefficient is practically constant for the incidence angles between 0° and 20° and almost equal to 0,9.
This result has permitted no critical coupling between transducers and fibers.

The realized system shows optics efficiency of approximately 60%.

Due to remarkable receiver sensitivity, it is possible to get a current of some /uA in reception while transmitting an optic power of about 1 mW.
The obtained system which is extremely compact, is shown in fig. 4.

Figure 4. Ground-H.V. levels interface pictorial

The total delay between the electric transmitted and received signals is of about 0.1 /us and the system bandwidth is within some Mc/s.

7. TRANSMITTING PROCESSOR

The various parameters to be checked to ensure a correct operation of this equipment are measured by solid state circuits giving an output to HLL logic levels of the ON/OFF type. These outputs are processed through a series of HLL logic circuits which elaborate them and determine the position of the transmitter-controlled parameters (radiation, ready, failure).

Besides evaluating the transmitter condition, these logic signals are also sent, through some interfaces to a failure indicator. Through a demultiplexer series which are explored sequentially by a internally generated clock, the failure logic signal is decodified and provides failure signalling through lighted numerical indicators. Therefore a number of two figures, which gives in code the eventual failure indication, is obtained.

Furthermore, all transmitter operative controls are made by HLL logic circuits.

8. CONCLUSIONS

The amplifier described herein has been completely manufactured and the complete radar system has been checked.

The results obtained are corresponding to the required specifications and the behaviour is very reliable. From the M.T.L. point of view, the improvement factor is about 40 dB. The phase and amplitude stability are within the requested values.

The total amplifier efficiency is about 20%.

The unit production, the first of which is now under test, presents 0,8 x 2,4 x 1,7 m. height dimension and its weight is approximately 1.300 Kg.

A pictorial of the amplifier breadboard is shown in fig. 5.

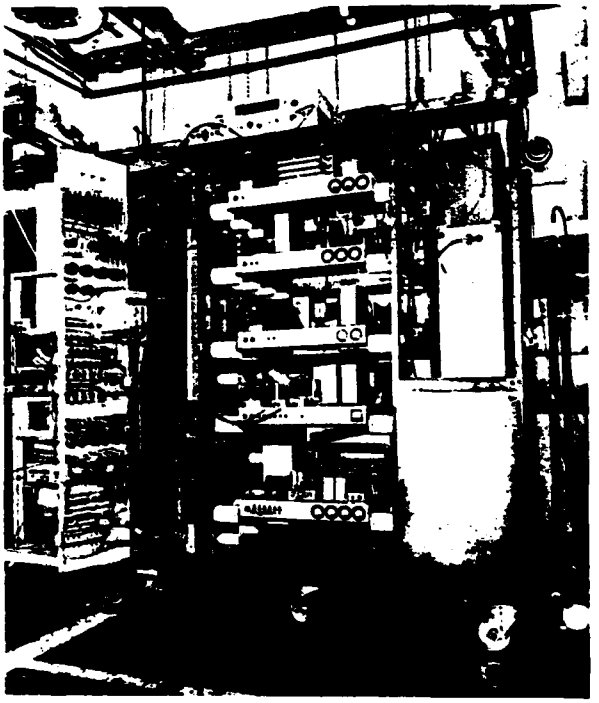

Figure 5. Amplifier breadboard pictorial

REFERENCES

(1) MERRIL J. SKOLNIK:
Introduction to radar systems - para 10.9
McGraw-Hill Book Company

(2) As ref. (1) - para 12.10

(3) As ref. (2) - chapt. 4.

(4) MERRIL J. SKOLNIK:
Radar Handbook - page 7.34
McGraw-Hill Book Company

(5) G. SCERCH:
Protezioni elettroniche con rapidità del microsecondo per trasmettitori radar (microseconds electronic protections for radar transmitters)
Alta Frequenza - Vol. XXXIX N. 7 - 1970

(6) J.M. LAFFERTY:
Triggered Vacuum Gaps.
Proceedings of I.E.E.E - January 1966

(7) D. HILL:
Internal quantum efficiency of GaAs electroluminesciency diodes.
J. App. Phys. 36, 1965

S.V. GALGINAITIS:
Improving the external efficiency of electroluminescent diodes.
J. App. Phys. 36, 1965

(8) N.S. KAPANY:
Fiber Optics.
Accademic Press - 1967 N.Y.

(9) Guidelines to line guides.
Electronics - August 31, 1970 - page 64

(10) BORN - WOLF:
Principles of Optics Electromagnetic Theory
Pergamon Press - London - N.Y. - 1959

SOLID-STATE MODULATOR TECHNIQUES TO PROMOTE FAST PULSE FALL TIMES

V. Nicholas Martin

RAYTHEON COMPANY *
Microwave and Power Tube Division
Equipment Engineering Group
Waltham, Massachusetts

SUMMARY

This paper describes solid-state tail-biter switching circuitry for grid drive tail-biters in hard-tube modulators and tail-biters employed in high pulse repetition rate line-type modulators used in short range search and mapping radars.

Tail-biter circuits are most advantageous in producing fast fall times in the video pulses used to drive high power rf amplifiers. Fast fall times are required to minimize rf transmission of coherent signals or noise in the period of time immediately following that of peak pulsed radar power transmission to enhance the detection of closein targets and to conserve power dissipation in hard-tube modulator switches.

This paper describes the use of SCRs in tail-biter circuits that overcome dv/dt limitations which formerly precluded their use in such applications. Results of laboratory experimentation and actual circuit implementation in production systems are described.

INTRODUCTION

Past studies and solutions to pulse modulator problems have, for the most part, centered about means for obtaining optimum flatness at the top of the pulses used to drive rf power amplifiers.[1] This is of special concern in sophisticated pulse doppler radar systems, where pulse voltage droop in amplitude variations produce rf phase shifts in the output signals that degrade system performance.

In other instances where pulse voltage fall time is important, as in the application of shuttering laser beams, vacuum tube tail-biter circuits have been developed[2].

The need for fast video pulse fall times may be grouped in two categories: a) to minimize rf transmission, coherent or noise, immediately following the pulse time duration of maximum power to permit optimum detection of closein radar targets and b) to provide power conservation in the modulator switch-tubes in hard-tube modulators.

Prior art precluded the use of thyristors or SCRs because of their inherent dv/dt limitations manifested during the rising portion of the video pulses. Thus, if fast rising voltage pulses were to be applied across a load shunted by a tail-biter circuit comprising one or more series-connected SCRs, the SCRs would self-fire and prevent the main (flat) portion of the pulse power from passing into the load.

Circuits employing transistors and SCRs are reported herein that have been developed to replace vacuum tubes that were sometimes used in the past, resulting in substantial savings in size, weight, and power, as well as enhancing reliability.

THEORY

The pulse modulator problem can best be illustrated by considering the fundamental circuit shown in Figure 1a. Here, a modulator switch is keyed at a specified pulse repetition rate to transfer power from a high voltage source to a load. The high voltage source is represented by a battery or energy storage capacitor and the load is shown as a resistor shunted by distributed capacitance, C_d.

Figure 1b shows the voltage-time relationship across the load. The ideal waveform desired across the load would be a curve following points A-C-B-D-E-F. The reactive impedance of the distributed capacitance, however, causes the load voltage to follow the curve inscribed by points A-B-D-F. The area of interest in this discussion is the falling portion of the waveform, D-F, and how to bring it close to D-E. No attempts will be made on improving the rise-time, A-B, to liken it to C-B, since peaking circuits and other techniques have been reported elsewhere in the past.

Figure 1c shows the basic modulator driving a klystron or traveling wave tube, which can be represented as a diode, if their rf structures are neglected. Their load characteristics follow $i = ke^{3/2}$, as opposed to $i = \frac{e}{R}$, as in the case of a purely resistive load. Here it should be realized that in the post-pulse period, after point D in Figure 1b, the capacitor discharges no longer into a resistance load, but into a varying impedance that increases with time, thereby stretching out the fall time to D-G. This distributed capacitance, it must be noted, comprises the capacitance between the secondary windings of the power amplifier filament transformer and ground, the internal interelectrode capacitance of the rf amplifier to ground, the high voltage cathode lead connections to ground, and portions of the modulator switching elements (depending upon the type of circuit and parts placement) and ground.

In the past, banks of resistors have been placed in shunt with the high power amplifier tubes, to present a lower impedance to the distributed capacitance in the post-pulse period, thereby discharging this capacitance faster. The waste of power is usually prohibitive, since these resistors dissipate energy also during the main flat portion of the pulses.

Another approach was to shunt the rf amplifier with an active element, such as a vacuum tube that would be keyed only during the post-pulse period.

* This work done while in the employ of the Lockheed Electronics Company.

Figure 2a shows the vacuum tail-biter in shunt with an rf power amplifier load. Here it can be seen that the vacuum tube, with its associated circuitry, inserts the additional capacitance C_{d2} of its filament transformer, tube elements, and trigger circuitry. This additional shunt capacitance makes the vacuum tube tail-biter somewhat self-defeating by requiring it to discharge the total shunt capacitance of both tubes.

Figure 2b shows the idealized tail-biter represented as a switch that would be closed periodically at the end of each pulse duration. To accomplish this, based upon hold-off or forward breakover voltage ratings, one or more series-connected solid-state switching elements would be ideal switches. For example, transistors for relatively low capacitor discharge currents and SCRs for peak currents in excess of 20 amperes at switching speeds in approximately 100 ns.

SCR LIMITATIONS AND CIRCUIT COMPENSATION

One of the parameters of an SCR is its dv/dt rating. Currently available SCRs have rate of voltage rise ratings of from 100 to 1000 volts per microsecond. When considering that the absolute rise time requirements of magnetron tubes and other high power rf tubes are in the order of 50 - 100 ns, or as expressed by the magnetron manufacturers as rate of rise of voltage of 100 to 140 kV per microsecond, it is obvious that the SCRs cannot meet the ratings when series-connected in shunt across the tubes.

Self-triggering of SCRs due to excessive dv/dt is caused by a capacitive current equal to the product of the anode-gate capacitance of the SCR and the rate of rise, dv/dt of applied anode voltage. Forward blocking voltage cannot be reapplied until after the minority carrier charge stored in the device as a result of previous forward conduction has been dissipated to a level that can be controlled by the gate bias.

The author's approach was to prevent sudden application of voltage as represented by the rising portion of a rectangular waveform by forward biasing the SCR. Figure 3 shows the basic circuit approach. Here a dc bias voltage V_{AB} is connected permanently to the anode of the SCR. A blocking diode D1 is connected to isolate the anode of the SCR from the pulsed terminal A.

When the indicated pulse waveform, having an amplitude V_{AB}, is applied across terminals A and B, current only flows through the load resistor and the distributed capacitance C_d. At time t_1, SCR1 is gated, causing it to break down and the distributed capacitance discharges through the SCR. In addition, a much smaller current is passed through the bias supply isolating resistor R, whose value is so large as to starve the SCR by limiting the bias supply current below the minimum rated holding current. This latter action enables the SCR to recover and await another pulse operation. Thus, instead of a fall time extending from t_1 to t_2, with the rapid firing of the SCR, the fall time occurs at very close to t_1, depending upon SCR turnon time and inherent delay.

Figure 4 shows an embodiment of this circuit approach used with variations in actual circuit applications to follow.

GRID DRIVE CIRCUIT WITH SCR TAIL-BITER

Figure 5 shows a tail-biter incorporated in the grid circuit of a hard-tube modulator developed at LEC in 1964, whose positive output pulses were used to drive groups of cascaded rf amplifiers. The input capacitance of the 4PR60B pulse tetrodes is 50 pf each, that would result in the fall-time recorded as shown in Figure 6a. A 2N2619 SCR was employed in the tail-biter, resulting in the fall-time shown in Figure 6b. More recently, a much faster turnon SCR 2N4204 was substituted showing the results in Figure 6c.

In this particular application, a delay multivibrator tracks the trailing edge of the main pulse, whose width is varied by the main multivibrator pulse generator. In all cases from 200 ns to 200 μs of main output pulse width, the fall time remains constant at 100 ns between 10-90% points when using the 2N4204.

It must be noted that there is no separate forward bias supply feeding the anode of the SCR. Instead, the anode is connected through a 100 K resistor to the HV floating deck, while its cathode is tied to the -300-volt bias supply used to cut off the 4PR60B switch-tubes during the interpulse period.

GRID DRIVE CIRCUIT WITH TRANSISTOR TAIL-BITER

In a more recent development of a tracking radar system, it was required to provide variable output pulses from 1 to 8 μs at 35 to 25 kHz pulse repetition rates, respectively. A transformer-coupled hard-tube modulator was selected to drive the cathode-pulsed klystron power amplifier. The high pulse repetition rate precluded the use of SCRs, since reliable recovery could not always be achieved by starving the SCR of holding current at elevated ambient temperatures during the short interpulse periods associated with these high pulse repetition rates. For this application, high voltage transistors were used in the tail-biter. Overshoot on the leading edge was provided to ensure fast rise-time, but the peaking circuitry has been omitted from Figure 7a, which shows this circuit, to better illustrate the circuit components of the tail-biter.

Referring to Figure 7a, the main pulses having a time duration t_0 to t_7 are fed through pulse transformer T1 to the driver transistor Q1, which is connected in a boot-strap amplifier circuit, patterned after conventional vacuum tube boot-strap drivers.

The turnon of Q1 causes the grid of 4CX5000R (8170W) switch-tube to swing from -300 volts to approximately +40 volts, resulting in grid current flow and the grid capacitance to charge to the grid potential and remaining at this positive potential during the main portion of the grid pulses.

When the driver pulses are terminated after 7 μs of time duration, tail-biter pulses, t_b coincident in time with t_7 are fed to T2, which in turn, drives Q2 into conduction. The low impedance path of the saturated transistor Q2 and its 22-ohm collector current limiting resistance discharge the distributed capacitance, resulting in approximately 150 ns fall-time. Figure 7b shows the voltage pulse taken at the grid of the 8170W hard-tube switch. Here it can be seen that voltage shaping is introduced during the

rising portion of the waveform and the tail-biting action, described above, produces the fast fall-time.

If a tail-biter were not used, the fall time would be much greater than 1 μs, resulting in the conduction of the switch-tube for this extended period of time. This would result in added plate dissipation and increased power supply requirements. For example, at 35 kHz switching rates, when the main portion of the transmitter pulses is 1 μs, without the tail-biter the switch-tube dissipation would be substantially greater, resulting in much longer fall-times in the klystron driven by this modulator.

LINE TYPE MODULATOR WITH SCR TAIL-BITER

Success was reported on the first generation Lockheed rotor blade antenna helicopter radar in which high power 80-ns pulses were switched at 30 kHz by means of SCRs. [3] In the higher powered 160 kW pulsed modulator, used to provide 100 and 500 ns pulses to a 30 kW magnetron, a conventional ceramic thyratron was used as a switch-tube in the modulator.

Magnetron emission during the fall-time portion of the 100-ns drive pulses dictated the requirement for a tail-biter circuit. Without an rf suppression circuit immediately following pulse transmission, magnetron noise would obliterate the display of echo returns of closein targets.

In view of the need for compactness and lightweightedness of the helicopter radar transmitter, cumbersome vacuum tube tail-biters could not be used. The 15 kV potential across the magnetron precluded the use of a series string of SCRs. It was decided to place the SCRs across the primary of the pulse transformer.

Figure 8 shows the finalized circuit. The -2 kV bias can be obtained from the same plate transformer providing the power to the modulator if a center-tapped transformer were available. In this case reverse-connected high voltage rectifiers can be used to get both polarities of voltage.

Fast switching MCR-1336-9 thyristors are used to switch up to 40 amperes of peak current in the tail-biter during the fall-time portion of the modulator pulses. The saturable reactor L1 delays the turnon of the SCR junctions to ensure low voltage drop and uniform current density through the junctions.

The tail-biter action is initiated by a 2N3507 emitter-follower, which drives the SCR gates. Because of inherent time delays in the turnon of the SCRs and a phase shift between primary and secondary voltages of the pulse transformers, resulting in time delay in the time domain, the initiating tail-biter pulse timing must be adjustable from the start of the main pulse to a later instant as evidenced by tail-biter action on the magnetron voltage fall-time. Final optimization is made by observing either a radar "A" scope or PPI display.

VARIABLE PULSE-WIDTH BLOCKING OSCILLATOR WITH SCR TAIL-BITER

In radar systems featuring long and short range modes of operation, a single blocking oscillator is sometimes used to generate the required long and short time-duration grid-drive pulses used to gate a TWT RF amplifier. Long duration pulses are generated by means of a conventional transistor blocking oscillator.

Short duration pulses have been produced by the same blocking oscillator by changing the DC bias through an auxiliary winding on the transformer, as shown in Figure 9a. Actual operation has shown, however, that the short term pulses vary in time duration considerably between transformer lots and with temperature. Moreover, when TWT's are replaced to suit the different manufacturers' clamped grid voltage specifications, a commensurate change in loading of the blocking oscillator occurs. This results, in turn, in a variation in pulse-width of the output pulses.

In radar timing systems having a fixed receiver on-time referenced to a master clock zero-time, variations in transmitter turn-off time could produce a spill-over of Radiate energy during the receiver on-time. This would block the receiver and blank out the display of signal returns from close-in targets, as shown in Figure 9b.

A system improvement may be achieved by restoring the same DC bias to the blocking oscillator for both long and short range operation. The addition of a time delay flat-pack and SCR tail-biter, curtails both long and short pulse operation at the same points in time, regardless of loading of the blocking oscillator, as shown in Figures 10a and b.

Initially, turn-off of the B.O. was attempted by turning off gate-drive to its base. Variations in storage time effects, however, ruled out this approach. An embodiment of the tail-biter circuit is shown in Figure 11. Here, it can be seen that a turn-off pulse fires the SCR at an established constant time delay from the system zero time.

A variation of this technique may be employed to generate variable pulse-width coded pulse trains from a fixed-width blocking oscillator by varying the turn-off time of the blocking oscillator pulse duration through the application of a tail-biter circuit.

CONCLUSIONS

The experimental results presented in this paper, based upon circuitry in use in military radar systems, shows that thyristors or SCRs can be used successfully as tail-biter switches to provide fall-times of 100-200 ns. Extension of circuit techniques, including voltage equalizing elements and corona shielding, would enable SCRs to be used in super-power modulators in future radar transmitters.

REFERENCES

1. "Hard-Tube Modulator Techniques That Permit Utilization of Minimum-Size Capacitor Banks" - V.N. Martin, LEC; Proceedings of the 7th Symposium on Hydrogen Thyratrons and Modulators, Fort Monmouth, New Jersey, 1962.

2. "High-Efficiency Solid-State Line-Type Modulator and Active Tail-Biter Adaptable to Pulsing Capacitive Loads" - V.N. Martin, LEC; Proceedings of 8th Symposium on Hydrogen Thyratrons and Modulators, Fort Monmouth, New Jersey, 1964.

3. "Switching of 80-Nanosecond High Power Pulses at 30 kHz Rates by Means of SCR's" - V.N. Martin, LEC; Proceedings of 10th Modulator Symposium, USECOM New York, N.Y., May 1968.

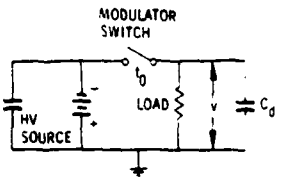

Figure 1a. Basic Pulse Modulator

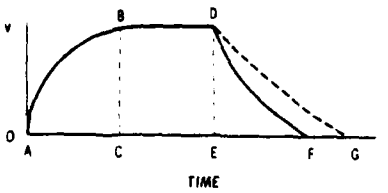

Figure 1b. Voltage-Time Relationship Across the Load

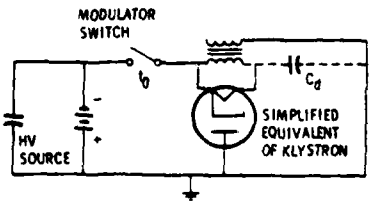

Figure 1c. Basic Modulator Driving Diode Type of Load

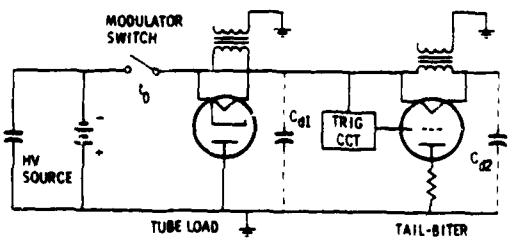

Figure 2a. Basic Hard-Tube Modulator with Tube Load and Vacuum Tail-Biter

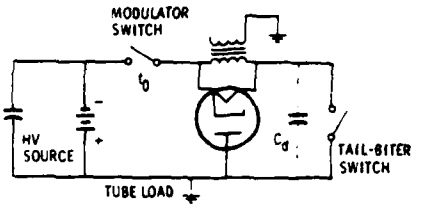

Figure 2b. Basic Hard-Tube Modulator with Ideal Tail-Biter Switch

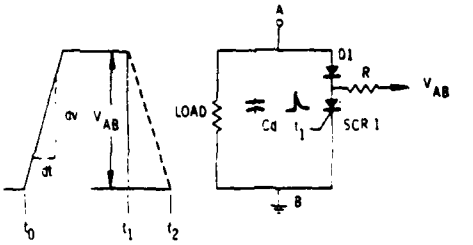

Figure 3. Basic Circuit Used to Compensate for SCR $\frac{dv}{dt}$ Limitations

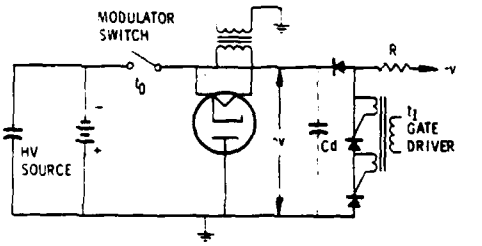

Figure 4. Embodiment of SCR Tail-Biter in Basic Pulse Modulator

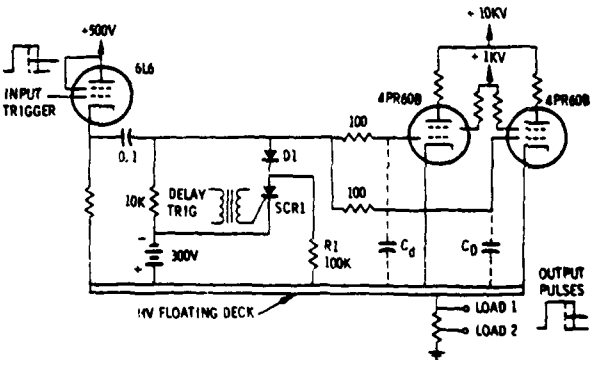

Figure 5. Grid Drive Circuit with SCR Tail-Biter

AD-A119 660 PALISADES INST FOR RESEARCH SERVICES INC NEW YORK F/G 9/5
IEEE CONFERENCE RECORD OF 1973 ELEVENTH MODULATOR SYMPOSIUM, NE--ETC(U)
1973
UNCLASSIFIED 73-CH0-773-2-ED NL

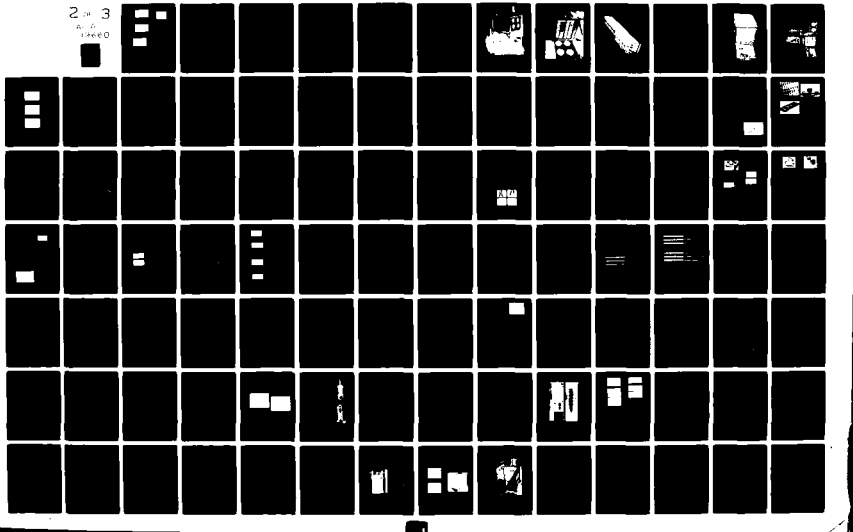

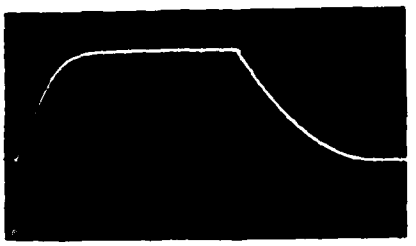

Figure 6a. Fall-time without Tail-Biter

Figure 6b. Fall-time with 2N2619 Tail-Biter

Figure 6c. Fall-time with 2N4204 Tail-Biter

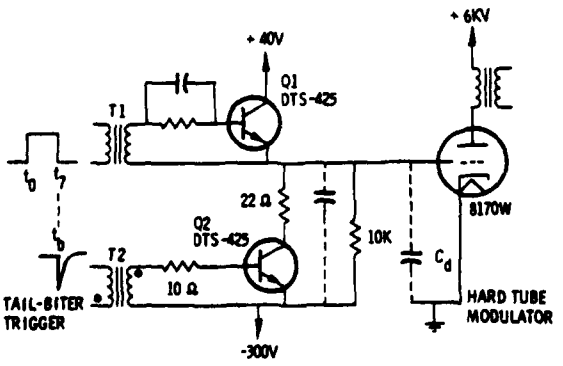

Figure 7a. Transistor Tail-Biter in Grid Drive Circuit

0.5 μsec/cm
100 v/cm

Figure 7b. Grid Voltage Waveform with Peaking and Tail-Biting

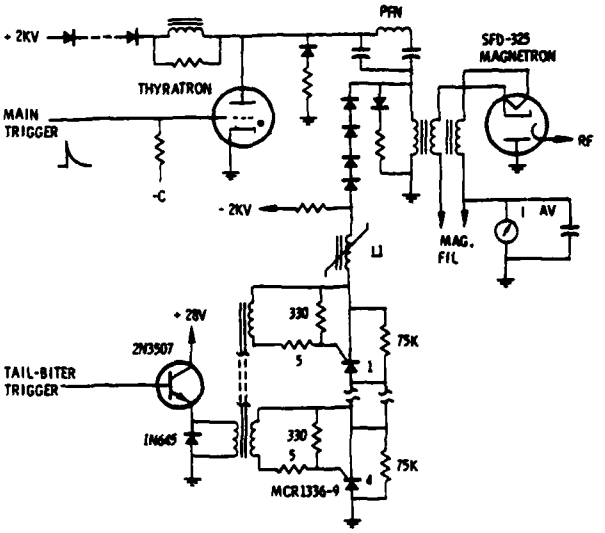

Figure 8. Line-Type Modulator with SCR Tail-Biter

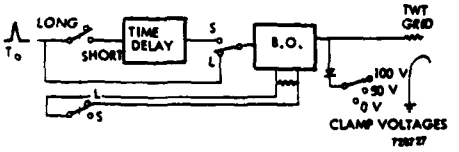

Figure 9a. Blocking Oscillator Providing Dual Time Duration Pulses by Varying Bias on DC Core.

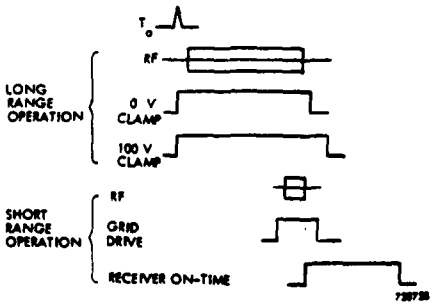

Figure 9b. Timing Chart Showing Variations in Termination of Transmitter Pulses.

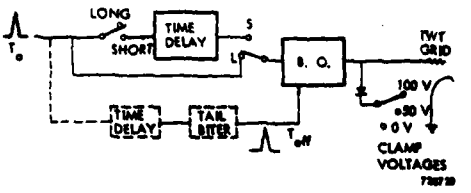

Figure 10a. Blocking Oscillator with Tail-Biter to Precisely Terminate End of Pulses.

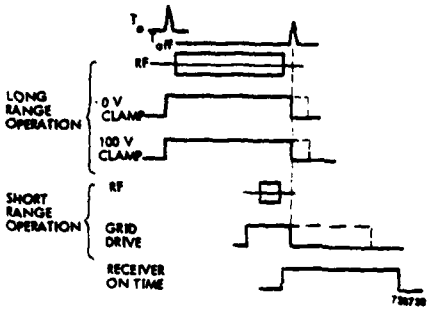

Figure 10b. Timing Chart Showing Tail-Biter Action in Turning Off Pulses Precisely

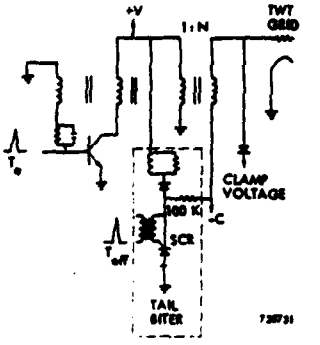

Figure 11. Tail-Biter Circuit Addition to Blocking Oscillator to Produce Variable Time Duration Output Pulses.

APPLICATION OF THE RSR SWITCH

R. A. Hill and R. A. Smith

Westinghouse Electric Corporation
Baltimore, Maryland

Summary

The Reverse Switching Rectifier (RSR), a four layer - two terminal solid state switch, has been successfully applied in several pulse modulator designs. The modulators have demonstrated high reliability and have achieved a substantial reduction in size and weight compared to conventional designs. Thorough testing has been performed including extensive operation under load fault conditions. The RSR modulator design techniques are now being applied in a number of new programs.

1. Introduction

Application of the Reverse Switching Rectifier (RSR) as a discharge switch in line type modulators has been successfully established. Two high power, solid state modulators using RSR devices were built and tested to demonstrate the feasibility of low voltage, modular design. The primary goal of these programs was to improve reliability and reduce size over that of existing systems. In both cases, a 50% reduction in size and weight was realized with reliability greatly increased. Additional laboratory tests have proven the RSR capability for high current, high di/dt, and high voltage stack operation.

Figure 1 shows a block diagram of the modulators. It is a basic line type modulator circuit with the addition of command charge, over/under voltage protection, and system trigger timing. The module PFN's are DC resonantly charged from the power supply when the charging SCRs are switched on. The trigger timing circuit provides sufficient time delay for RSR recovery following each pulse. Protective circuits inhibit the command charge trigger in the event of a fault or improper circuit condition.

2. Navy Solid State Modulator

The "Navy Solid State Modulator" was developed under contract for the Navy Department Bureau of Ships Electronics Divisions. Table I shows the specifications of the modulator. Figures 2 and 3 show views of the overall modulator and the module cabinet respectively.

Eight pulse modules, producing a total output power of 3.27 MW peak and 22.6 KW average, are located in the cabinet with all electrical connections made by quick disconnect plugs. The pulse transformer tank is attached to the rear of the cabinet and shares a common oil bath with the load resistor tank. A cooling system for the load resistor consists of an oil pump and liquid to liquid heat exchanger located beneath the cabinet. The power supply, controls, and command charging circuits are located in an adjacent cabinet. Module detail is shown in Figure 4. The pulse forming network is sandwiched between two fiberglass channels which also provide insulated mounting for the RSR heat sinks, trigger capacitor, and module fuse. Connectors are at the far end. The pulse network coils may be manually jumpered to provide pulse widths of 16, 32, or 55 microseconds. Each network has a 3.5 ohm impedance and is rated for 2,600 volts. There are 28 sections per network and the capacitors utilize dry type insulation. Construction of the modules allows easy replacement of individual section capacitors in the event of failure. The design of the modulator includes provisions for additional modulator techniques such as De-Q-ing regulation, Syntap (Synchronous Tap Changing), pulse leveling, and pulse width agility.

Tests to characterize performance of the modulator began with the 32 microsecond pulse width mode of operation since this provided the highest duty. The initial tests showed excessive recovery time was required by the RSR devices. This was caused by high open circuit inductance (L_{OC}) of the pulse transformer. After reducing the L_{OC} to obtain increased backswing, the recovery time limitation was eliminated. Performance specifications were then met at all desired PRF's. All subsequent tests were made with no operational problems encountered.

3. RADC Lightweight Pulser

The "Lightweight Pulser" was developed under Air Force Contract for the Rome Air Development Center. Table 2 lists the operating parameters of the pulser. Figure 5 shows the module cabinet and the pulse transformer oil tank.

Twenty plug-in modules are used to obtain 10 MW peak power output. Each module has a 1.6 ohm pulse network which produces a 900 volt pulse at 560 amps. The total power is combined in a single pulse transformer having a turns ratio of 130:1. The pulse transformer oil tank adjoins the module cabinet. Individual module fuses, their indicators, and the trigger amplifier are located on the door. Figure 6 shows the entire modulator and VA-145 Twystron load. The power supply and charging circuit are contained in the smaller cabinet.

Although each module was thoroughly tested before assembly into the modulator, a switching difficulty in the 20 module assembly was encountered. The cause of this problem was traced to excessive and unequal inductance in the trigger buss wire. Coaxial cable was used to replace the wire buss and satisfactory trigger operation was obtained. After this connection was made, measurement showed the overall modulator to have less than 1 nanosecond of time jitter.

4. Load Arc Considerations

Tests were conducted to determine the effect of load arcs on the RSR switch. During a load arc the peak current in a line type modulator switch nearly doubles and is followed by ringing. Although several hundred load arcs occurred while testing the Lightweight Pulser at full power, there were no RSR failures. In another test with a single module load, arcs were simulated by connecting a thyratron across the secondary of the output pulse transformer and switching it during the pulse. Figure 7 shows peak current conducted by an RSR switch while operating in this circuit. Figure 7a shows a normal pulse with an amplitude of 1,100 amperes. In Figure 7b the thyratron is triggered on at mid-pulse and in Figure 7c the load arc is simulated on the pulse leading edge. This produced a peak current of 1,900 amperes. These tests were performed at a PRF of 400 PPS.

5. Device Protection

Practical RSR switch assemblies use two or more devices in a series string. Switching is initiated by applying a voltage pulse to a portion of the string and depending on circuit energy to overvoltage the remaining portion in an avalanche manner. Thus, the circuit being switched must have sufficient energy and voltage to trigger some portion of the string. Without sufficient trigger energy, the device junction area will not completely turn on and failure may result. On the other hand, if the voltage across the string is too high, it will switch without an applied trigger. Therefore, a voltage "window" detector is used in conjunction with the command charge circuit to provide undervoltage/overvoltage protection when charging the PFN module.

Device recovery time is somewhat circuit dependent. This is particularly true in the event of a load arc. When large ringing currents are present in the post pulse period this tends to increase the conduction time. In order to prevent reapplication of voltage before the device has recovered, a delayed command charge circuit is employed. In some circuits which have a natural commutating characteristic with enough delay, the command charge is not necessary.

In conventional line type modulators, a damping resistor is used in series with the inverse diode to dissipate network energy following a load short. However, high voltage develops across the resistor causing high inverse voltage on the switch. Care must be exercised in the design of an inverse clamping circuit to prevent harmful inverse voltage on the switch following a high current conducting period.

Other protective methods are general in nature and require only good design practice. Some of these include proper heat sink cooling, equalized load sharing, device rating limitations, and proper mechanical installation.

6. New Applications

The development of a solid state modulator was recently started for an airborne radar. This design uses a single series string of 14 RSR's and requires a minimum hold-off voltage of 10 KV, and a peak current capability of 100 amperes. The peak power is 500 KW. The modulator pulse widths are 0.5 microseconds, and 2.5 microseconds with repetition rates of 300 PPS, 500 PPS, and 1,100 PPS. The goal of this program is to increase the overall reliability of the modulator.

A major program currently in the design and prototype development stage utilizes the modulator RSR technique for the Air Route Surveillance Radar, ARSR-3, for the FAA. This radar modulator design incorporates 20 RSR modules, each with four RSR's in series. Each module is resonantly charged to 2,600 volts. The 20 RSR module outputs are combined in a high turns ratio pulse transformer similar to those used in the modulators previously described. The transformer primary current is 11,000 amperes. The basic operating parameters are:

Peak Power	12 MW
Average Power	14 KW
Pulse Width	3 Microseconds
Repetition Rate	360 Average (staggered)
Output Voltage	122 KV
Output Current	93 Amperes

The developments and programs described above all have utilized the RSR in the standard DO5 rectifier package. There is interest in both repackaging the RSR and increasing its power handling capabilities. The flat package or hockey-puck design is an obvious choice for a new package design which lends itself readily to more efficient series stacking and cooling of the devices. Device voltage ratings of 1,200 volts and peak current ratings of 5,000 amperes are anticipated for future RSR's.

7. Conclusion

This paper has very briefly high-lighted some of the modulator applications and developments utilizing the RSR which have been accomplished since the 10th Modulator Symposium in 1968. In 1973, we find the RSR in new designs and its use expanding to new programs. Both the multi-module design and the series string techniques are being applied where one or the other offers particular advantages. Both claim improved reliability, smaller size, and lighter weight than corresponding thyratron designs in many applications. The modular design offers the additional advantages of low voltage circuitry and continued modulator operation even with some module failures. We now look forward to new applications, taking advantage of the RSR's high power capabilities, and look further ahead to even higher power devices.

8. Acknowledgements

The "Lightweight Pulser" was developed under Air Force Contract F30602-68-C-0094 for the Rome Air Development Center. The "Modular Solid State Modulator" was developed under Navy contract N0039-70-C-1506 for the Navy Department Bureau of Ships Electronics Divisions.

The authors would also like to acknowledge the substantial contributions of Edward H. Hooper and Howard S. Feldmesser on several of the programs described.

9. References

1. R.A. Hill and W.R. Olson, "Lightweight, High Power Modulator Uses RSR Switch Device", pp. 155-163, Proceedings 10th Modulator Symposium May 21-22, 1968.

2. Final Technical Report, RADC-TR-69-33, March,1969, Rome Air Development Center, Air Force Systems Command, Griffiss Air Force Base, New York.

3. Final Development Report, Contract N00039-70-C-1506, 13 November 1970, Navy Department Bureau of Ships Electronics Divisions.

4. Technical Report, AFML-TR-72-19, February, 1972, Air Force Materials Laboratory, Air Force Systems Command, Wright-Patterson Air Force Base, Ohio.

5. P.F. Pittman and J.B. Brewster, "A New Solid State Switch for Power Pulse Modulator Applications: The Reverse Switching Rectifier", 11th Modulator Symposium, September 18-19, 1973.

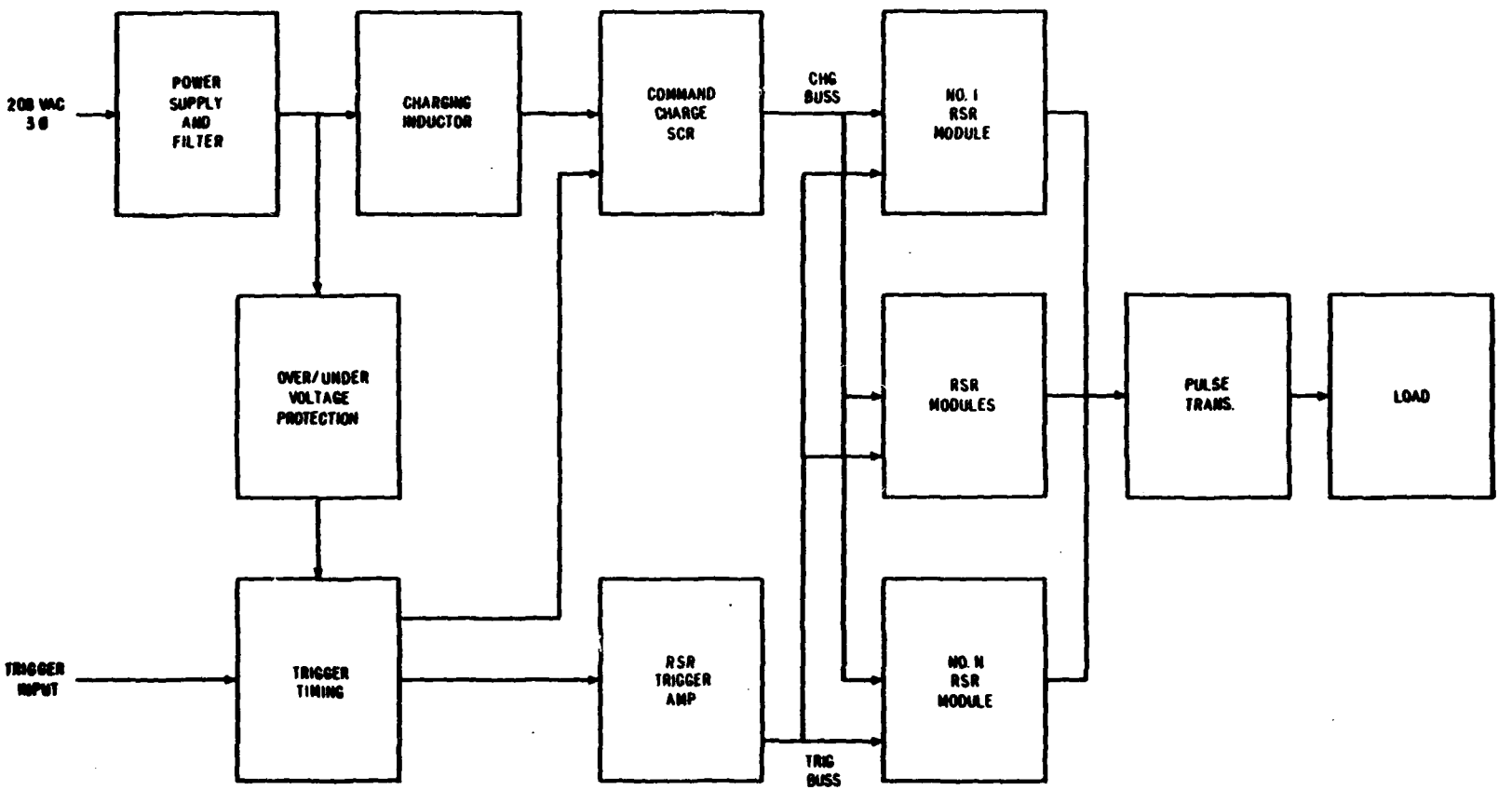

FIGURE 1. RSR MODULATOR BLOCK DIAGRAM

TABLE I

NAVY SOLID STATE MODULATOR

PEAK POWER	3.27 MW
AVERAGE POWER	22.6 KW
OUTPUT VOLTAGE	78 KV
POWER SUPPLY VOLTAGE	1,250 V
PRF	300, 210, 75 PPS
PULSE WIDTH	16, 32, 55 μSEC
PULSE RISE TIME	1.8 μSEC
PULSE TRANS. RATIO	68:1
NUMBER OF MODULES	8
WEIGHT	1,000 LBS.

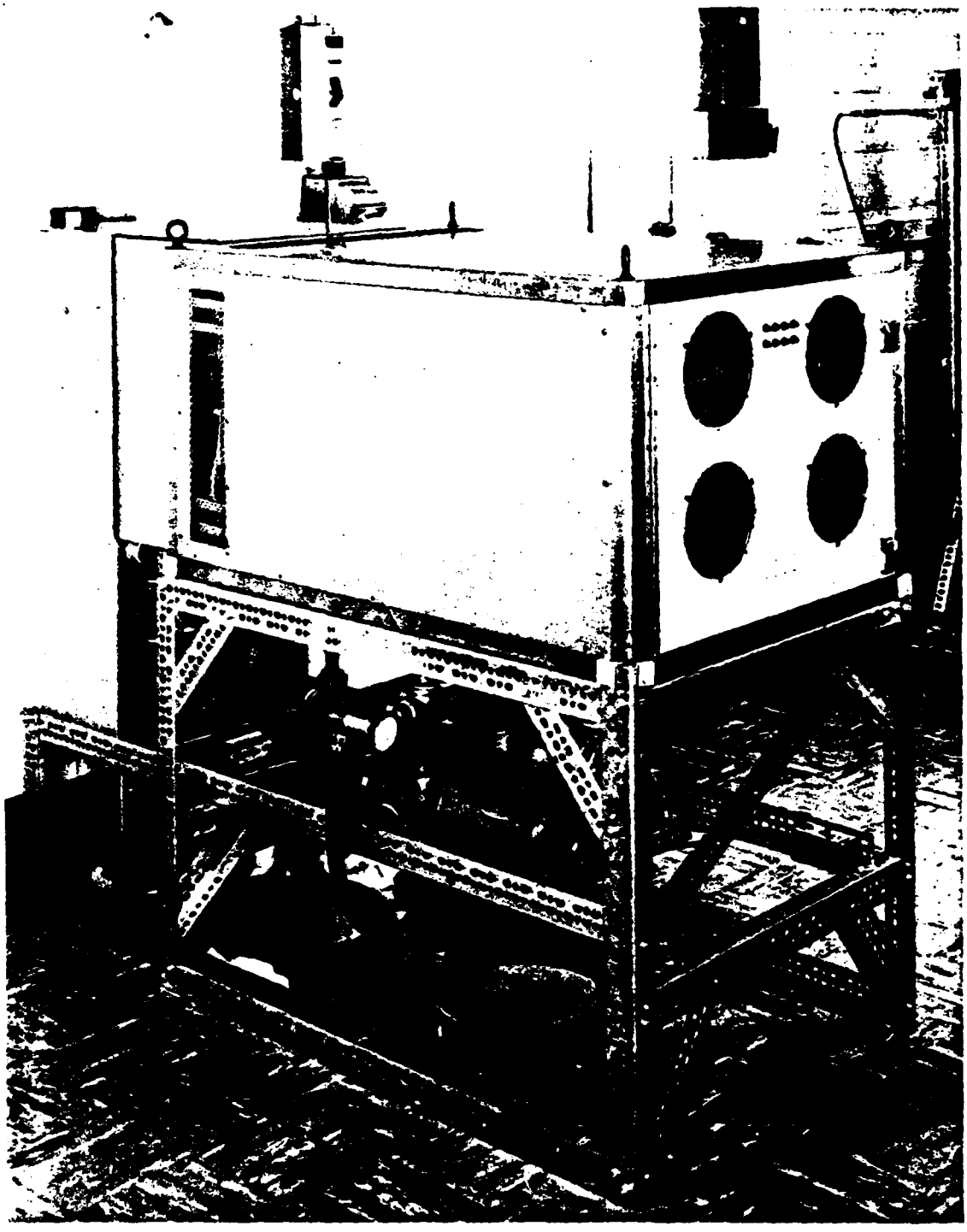

FIGURE 2. NAVY SOLID STATE MODULATOR

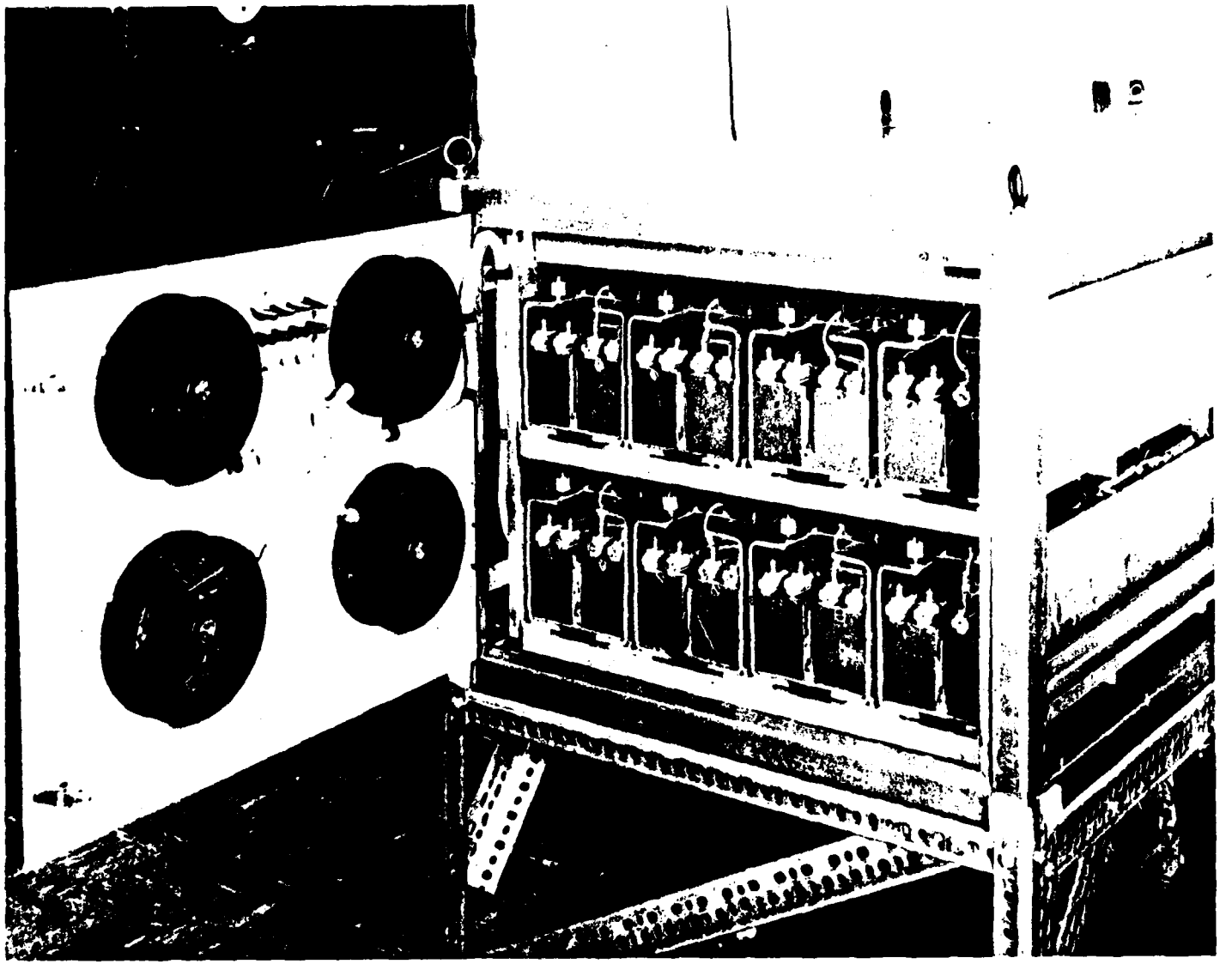

FIGURE 3. NAVY SOLID STATE MODULATOR WITH PLUG-IN MODULES

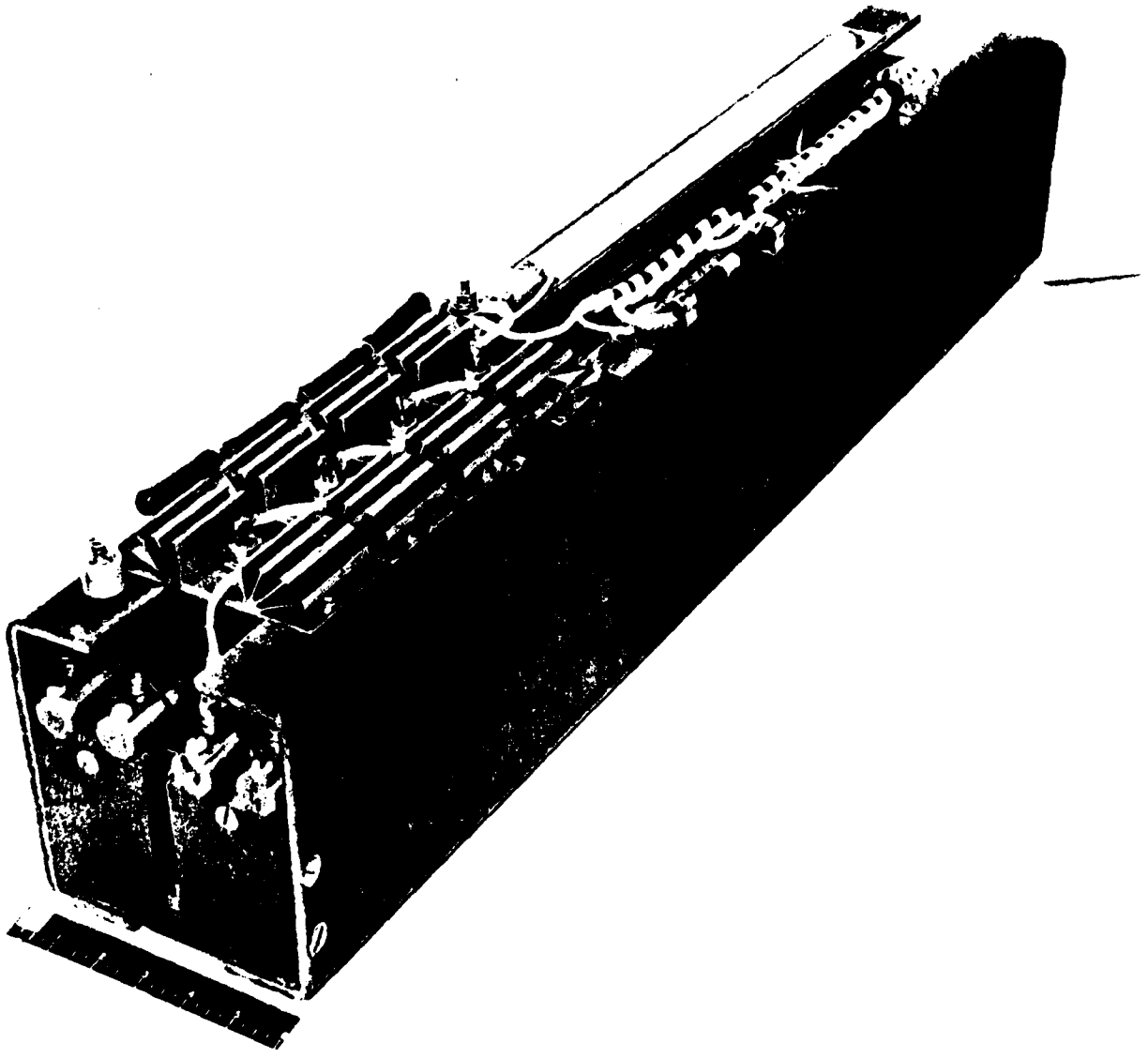

FIGURE 4. MULTIPLE PULSEWIDTH MODULE

TABLE II

RADC LIGHTWEIGHT PULSER

PEAK POWER	10 MW
AVERAGE POWER	20 KW
OUTPUT VOLTAGE	120 KV
POWER SUPPLY VOLTAGE	1000 V
PRF	300 PPS
PULSE WIDTH	7.5 μSEC
PULSE RISE TIME	0.6 μSEC
PULSE TRANS. RATIO	130:1
NUMBER OF MODULES	20
WEIGHT	600 LBS.

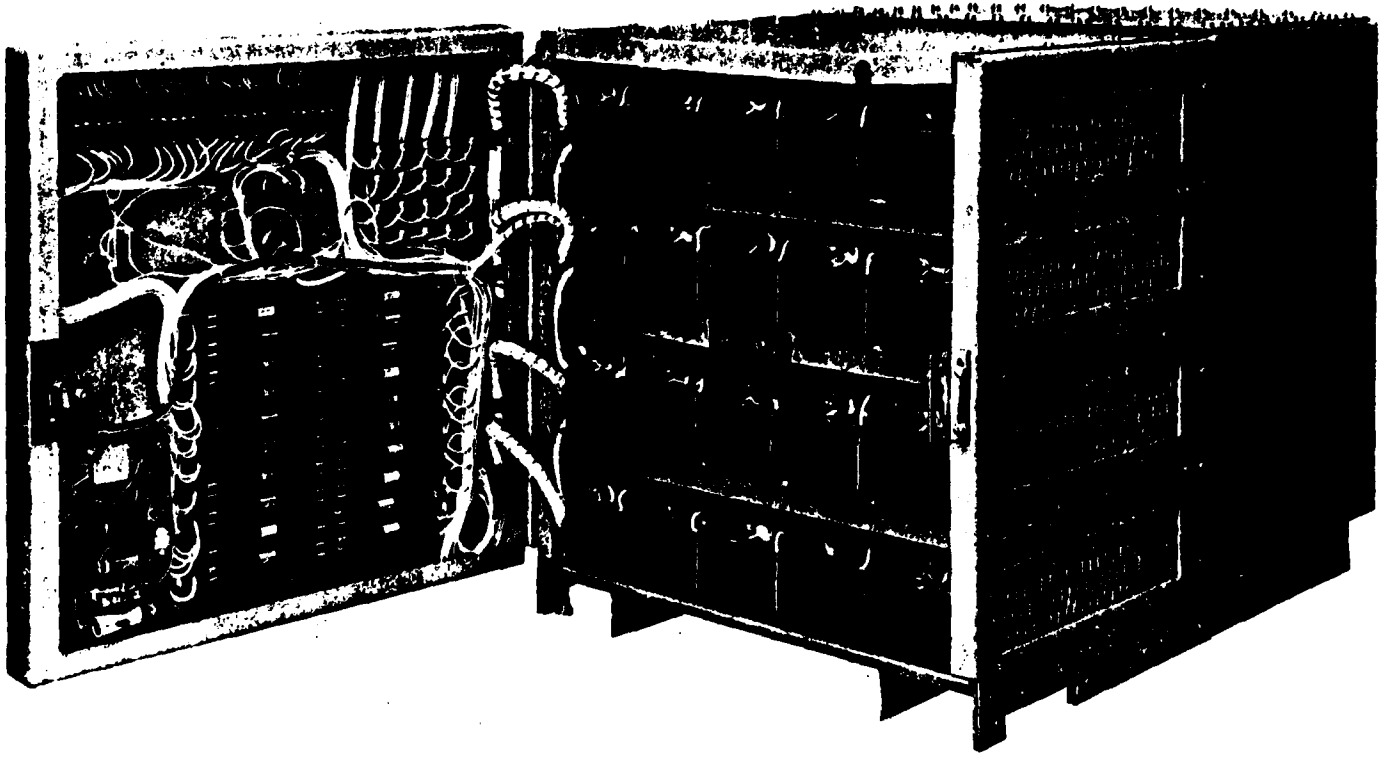

FIGURE 5. RADC LIGHTWEIGHT HIGH RELIABILITY PULSER

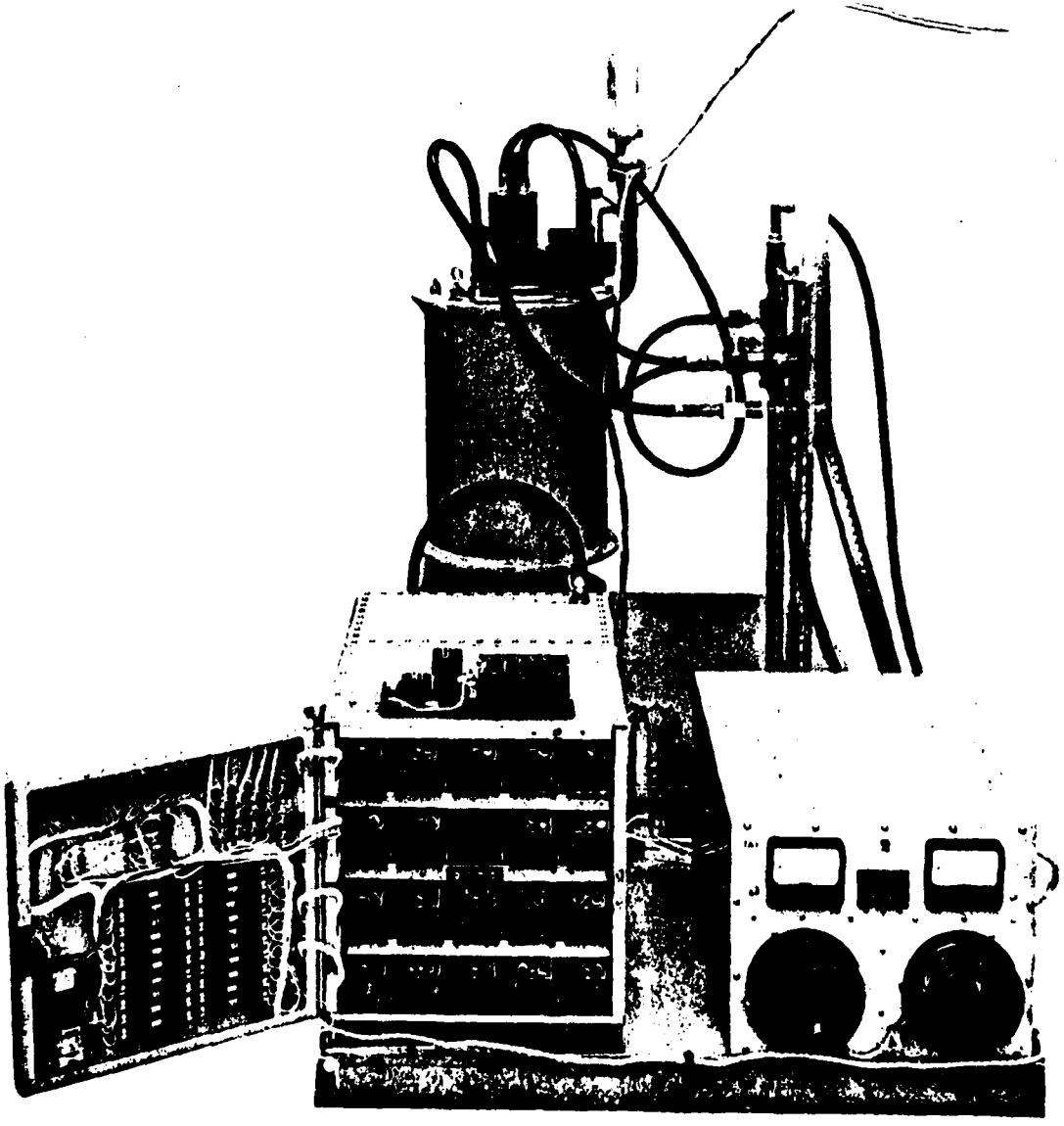

FIGURE 6. PULSER WITH TWYSTRON LOAD

LOAD ARC TESTS

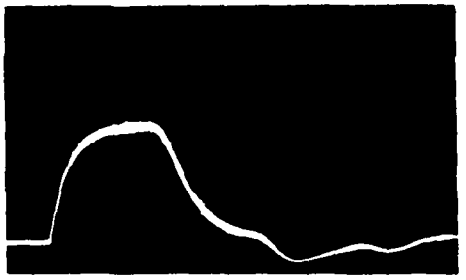

NORMAL PULSE

500 AMP/CM

1 μSEC/CM

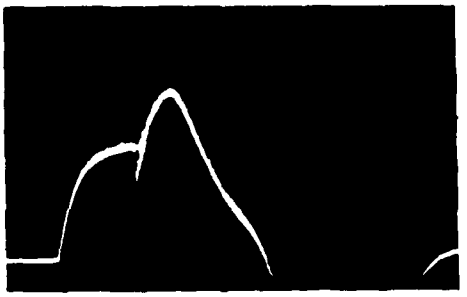

SHORT AT MID-PULSE

500 AMP/CM

1 μSEC/CM

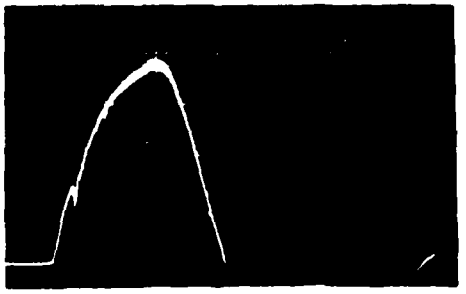

SHORT AT
LEADING EDGE

500 AMP/CM

1 μSEC/CM

FIGURE 7. LOAD ARC SURVIVAL TEST

DESIGN CONSIDERATIONS FOR SUPER POWER PULSE MODULATORS

Duard L. Pruitt
RCA Corporation
Government and Commercial Systems
Missile and Surface Radar Division
Moorestown, New Jersey

Summary

Design criteria are discussed which are particularly pertinent to super power (gigawatts peak, megawatts average) artificial line-type modulators. A sample design is illustrated which uses 60 hydrogen thyratron switch tubes in 30 unit modulators to supply 2.5 gigawatts peak power and 10 megawatts average power. A concept physical layout is shown for the sample design.

Introduction

The requirement for power pulse modulators with outputs of several gigawatts peak and several megawatts average has created a new generation of design problems. Multiple numbers of the largest available switching devices, in parallel and/or series arrangements, are required to generate the specified power levels. Technical and/or economic reasons may indicate use of even larger numbers of smaller switching devices. Interaction among individual "modules" of a multi-module modulator can cause serious problems, especially under fault conditions.

"Exotic" methods of pulse power generation, such as explosions, cryogenics, mechanical motion, etc., do not appear to be practical at this time. "Hard tube" modulators, using gridded vacuum tubes, are technically feasible and have certain advantages such as timing versatility and ability to interrupt fault currents during the pulse. Disadvantages include a requirement for a large capacitor storage bank and a comparatively large cathode heater power requirement. In addition, economic problems arise when applying presently available tubes to the gigawatt peak power requirement.

Thus the artificial line type modulator appears to be the best choice for satisfying the gigawatt requirement with presently available technology. The remainder of this paper will be concentrated on design aspects of line-type modulators as related to the gigawatt peak power requirement.

Artificial Line Modulator Features

Delayed (or command) Charging

Referring to the block diagram of a line type modulator as presented in Figure 1, the second block (item 2) represents a circuit for delaying the charging of the main PFN following each pulse.

The delayed charging switch function has been occasionally employed in the past in multi-PRF type modulator systems. It can contribute significantly to the operating stability of such a system by performing the following functions:

1. By delaying recharging of the PFN following a pulse, it avoids stressing the main switches until necessary to do so at PRFs less than maximum. This reduces spurious arcing of the main switches by making it unnecessary for the switches to hold off twice the power supply voltage for long periods of time.
2. If separate hard-tube delayed charging circuits are employed associated with each main switch, the hard tube may be cut off when the associated thyratron arcs, thus isolating the HVPS and preventing a system shutdown. This is an alternative to having a separate HVPS for each thyratron channel.
3. It provides stable deionization of and minimizes anode bombardment of the main switch by isolating it from the power supply immediately following the pulse. This is an important consideration when the main switch is pushed to maximum operating limits as required by very high peak and average power specifications.
4. It makes PFN/load match uncritical to main switch deionization, since residual PFN energy can dissipate in the load or inverse clipper, allowing switch shutoff prior to recharging. This allows flexibility of load circuit behavior.
5. It stabilizes the charging level of the PFN by allowing a period for removal of residual (post-pulse) energy on the PFN prior to recharging, regardless of PFN/load match relationships.
6. In a multi-channel pulser, delayed charging permits the option of staggering of the charging cycles of several PFNs. This reduces the level of harmonics of the PRF in the prime power system for a given size main filter bank, or conversely, allows use of a smaller main filter capacitor bank for a given harmonic level requirement. The main switches must be able to withstand more lengthy periods of interpulse voltage holdoff for this advantage to be realized: i.e., the advantage of (1) above is compromised. However, when a large number of channels is employed, a separate delayed charging switch for each channel still promotes stability of operation, for once charging is completed for the given channel, it isolates the HVPS from a main switch that does prefire, thus avoiding system shutdown otherwise caused by overloading the power supply. The circuitry can be arranged so that the faulted circuit recovers prior to the next charging cycle.

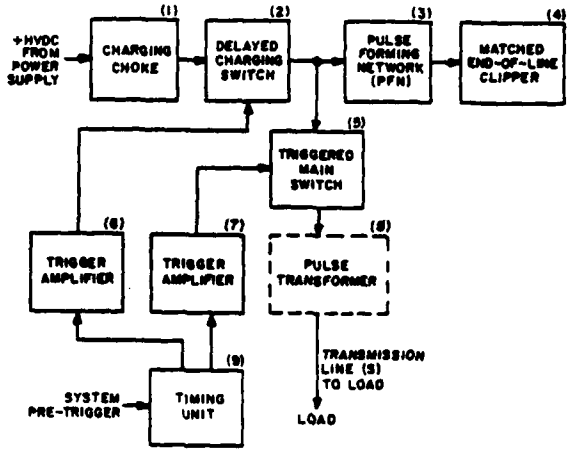

Figure 1. Block Diagram of Line Type Modulator for High Peak and High Average Power Service

Charging Diode

A silicon charging diode (not shown) may be required for one of several reasons, depending on the nature of surrounding circuitry. For example, it has historically been employed to prevent back discharge of the PFN at repetition rates below the resonant value. For very-high-energy pulsers it can also serve to isolate the main switches in multichannel systems; i.e., when several PFNs are charged from a common source, separate charging diode assemblies for each PFN will prevent other than the associated PFN from discharging into the load via a given switch. Finally, in modulators employing bidirectional spark gaps as delayed charging switches, it assures deionization of the delayed charging switch when charging of the PFNs is completed by effectively opening the charging circuit after the charging current has stopped and the PFN voltage exceeds the source voltage. When a triode, tetrode, or thyristor delayed charging switch is used, a charging diode is not normally required.

The Matched End-of-Line Clipper (EOLC)

The matched end-of-line clipper (4) includes a series arrangement of a matched load resistor and an inverse diode assembly placed at the end of the PFN remote from the main switch. It prevents voltage reversal on the PFN under conditions of load arcing by draining the energy of the PFN in a single pulse when the main switch end of the PFN is short circuited. Significant inverse voltage does not appear at the switch end of the PFN following the arc. This avoids stressing the charging inductor (or delayed charging switch) to three times normal voltage. It also tends to prevent arc-back of the thyratron switch following a load arc. Without the EOLC, thyratron arc-back is normally caused following a load arc by sudden complete reversal of PFN and switch voltage, immediately following conduction of twice normal current by the switch.

The end-of-line clipper may also contribute to a deionization process for the thyratron which avoids destructive anode bombardment and prolongs thyratron life in a modulator system which does not employ delayed charging.

Coaxial Load Cables

The use of relatively large numbers of paralleled high-voltage coax cables to connect the pulse from the discharge circuit to the load permits placing the load device distances in the order of one hundred feet from the pulser without significant deterioration of pulse rise time or shape due to cable mismatch for pulse durations in the order of 20 microseconds.

Charging Choke

The charging choke (Item 1) performs the usual function of resonant-charging the pulse network to twice the supply voltage. It will not be discussed further except to point out that, in a large system employing a multiplicity of "unit modulators," the charging choke is one of the components which could be common to a number of unit modulators. In the limit, a single charging choke can be used to supply charging current to all of the unit modulators. Use of a single charging choke in a multiple modulator system may negate some of the advantages of delayed charging cited earlier.

Pulse Transformer

For most practical modulator configurations, a pulse transformer is required to match the modulator output impedance to a load impedance which is usually higher. For switches operating up to approximately 50 kV, the primary impedance will normally be less than 1 ohm, necessitating careful and clever design in the primary circuit to limit stray inductance to a value low enough so that required rise times are achieved. A primary connection consisting of a multiplicity of flat-plate, parallel-plate transmission lines may be required.

For super-voltage thyratrons, high-voltage spark gaps, or heroic solid-state stacks for switches, it may be possible to eliminate the pulse transformer.

Switching Devices for Line-Type Modulators

Hydrogen Thyratrons

Since the early days of World War II, hydrogen thyratrons have been the almost unanimous choice for line-type modulator switches. Today, thyratron designs exist for anode voltages up to 160 kV and anode currents up to 10,000 amperes peak and 15 amperes average. See Table I for a representative sampling.

Table I. Hydrogen Thyratron Ratings

Type and Manufacturer	Maximum Ratings epy kV	ib kA	Ib A	Pb (10^9)
HY-5 EG&G	40	4	7	160
CH-1191 Tung-Sol	50	4	8	72
KU-275 ITT	50	5	8	400
CH-1222 Tung-Sol	50	10	15	180
GHT-9 M-O Valve	35	5	15	100
CX-1175 English Electric	80	6	6	140
CX-1192 English Electric	120	6	6	140
CX-1193 English Electric	160	6	6	140
ZT-7004 General Electric	50	4	7	55
Experimental (Signal Corps)	250		4	
Proposed (Signal Corps)	70		30	

For high duty-cycle service, the anode voltage (epy) and average anode current (Ib) are the limiting ratings. Applying a suitable derating factor, the average power capability per thyratron ranges from 125 kW (HY-5) to 420 kW (CX-1193). Other factors enter into tube selection, of course, such as price, proven performance, and cost of the auxiliary circuitry.

Thyratrons have a long history of reliable and satisfactory performance in radar systems. With suitable derating, life of many thousands of hours has been obtained.

However, in systems using a combination of many hydrogen thyratron switches, serious problems have been encountered. For example:

1. An apparent need for a "warm up" period of many seconds before stable operation is achieved.

2. An occasional "pre-fire" or "hang up" may shut down the entire system.

In continuous duty systems, the "warm up" requirement (1) is hardly noticeable, while the "hang up" problem (2) can be handled by the techniques discussed in the section on delayed charging. For intermittent duty applications, the "warm up" problem is more serious, though its effects can be minimized by use of a triode or tetrode charging switch as discussed in the same section.

Spark-Gap Switches

The use of a spark-gap switch or switches in a suitable line-type modulator configuration offers as major potential advantages system economy and simplicity as compared with the use of a large number of thyratrons. The economy and simplicity result from the following spark-gap characteristics:

1. High power capability per switch. Fewer switches and fewer modulator channels.

2. High operating voltage levels, pulse transformers not necessarily required.

3. Simplicity of switch construction as compared with thyratrons.

4. Ready repairability of switches (in-field) including cleaning, electrode adjustment, and electrode replacement when necessary.

5. Relative immunity to spurious triggering due to relatively high trigger energy levels required.

These advantages can be realized however, only when development of high-energy, high-PRF spark-gap switches is *successfully* demonstrated. Until then, important risk factors include:

1. Spurious arc rate

2. Electrode erosion

3. Rate of contamination of insulators by arc residues

4. Stability of deionization characteristics at high PRFs

5. Potential cooling problems

The Blumlein circuit may contribute to easing the spark gap design problem. Using a conventional circuit, the switch holds off 2 V and passes I to deliver pulse power to V x I; i.e., the product 2 VI is switched to deliver power equal to the product VI. Using the Blumlein circuit, the switch holds off V and passes 2 x I so a switch product of 2 VI also delivers pulse power equal to VI. It may be seen that although the *same switching* product is required using the Blumlein circuit, the maximum circuit voltage encountered is equal to the load voltage; i.e., in a transformerless conventional configuration, a PFN charge at 400 kV is necessary to deliver pulses at 200 kV. However, the PFN charge level is only 200 kV using the Blumlein circuit. The spark gap designer must therefore decide whether his switch design is optimized switching twice the load voltage or twice the load current. Clearly, corona problems are the lesser using a pair of equal electrode area 200 kV switches as compared with a single 400 kV switch.

Perhaps the largest road block to use of spark gaps is the lack of life data in continuous duty systems at relatively high pulse repetition rates. For intermittent duty systems, especially at low repetition rates, spark gaps are more easily applied.

Solid State Switches

Two varieties of solid state switching devices appear to be serious switch candidates:

1. The RSR (reverse-switching rectifier).

2. High-speed gate-controlled thyristors.

The RSR was described in an earlier paper in this symposium.

High-speed gate-controlled thyristors (SCRs) have been developed, or are being developed, by a number of semiconductor manufacturers. The features which tend to be common to these developments are:

1. An auxiliary, built-in trigger SCR.

2. Interdigitation applied to the interface between the "trigger" SCR and the main SCR GATE.

Using these techniques, di/dt of 1000 amperes per microsecond or more appears feasible in relatively large SCRs. Alternatively, small SCRs can be made to provide high di/dt rates without necessarily resorting to interdigitation or auxiliary amplifying SCRs.

Since solid-state devices are, by their nature, relatively small and thus limited in power handling per device, thousands of devices are required for the total switching function of a super-power modulator. Thus the solid-state switch designer's problem is how to combine many devices *in series* and/or parallel combinations to obtain an effective, reliable switch. Assuming he (the designer) can solve this problem, the solid-state switch will have impressive advantages:

- Solid-state reliability
- No warm up; no overhead heater power
- Ultimately, small and compact

Crossed-Field Interrupter as a Modulator Switch

The crossed-field interrupter switch tube, discussed in a previous paper in this symposium, has been proposed as a very-high-power closing switch. Life considerations would appear to limit consideration of this device to intermittent duty systems.

HVPS System Features

Typically for very-high-power line-type modulators the HVPS system includes stacked equal-voltage rectifier circuits driven by dual delta and wye secondary windings in the main rectifier transformer to provide 12-phase rectification. A

high-speed protective circuit breaker at the transformer input protects the silicon from fault overloads. An induction regulator with one second speed and one per cent automatic regulation based on sensing dc load voltage provides for voltage control and stabilization. Automatic tap changers or systems such as the Glenn Pacific Variable Transformer Voltage Control System serve as alternative choices to the induction regulator.

Rectifier system load regulation is typically 5 - 10 per cent and for continuous duty systems, transient changes in voltage level during turnon and turnoff are acceptable.

A filter capacitor bank bypasses the ac components of the resonant charging periodic sinusoidal current waveform, reducing harmonic currents of the PRF in the prime power line current.

The capacitor bank size is generally not critical to PFN voltage charging level. With no capacitor bank, the regulation impedance of the HVPS systems acts as an essentially non-dissipative damping element in series with the charging inductor and PFN capacitance. The circuit driving voltage is the full open-circuit EMF of the source; i.e., there is no dc voltage regulation component since the power supply current is a semi-sinusoid rising to its peak and returning to zero each cycle of charging. The power lines conduct all the ac components of the charging current waveform.

The addition of a filter capacitor bank results in sustaining the dc rectifier current from cycle to cycle, but the ac components of charging current are bypassed around the power line source to a degree dependent on the filter size, PRF, and system regulation impedance.

Harmonic currents in the power line may disturb telephone service in the vicinity of the prime power lines, or cause interference with other electrical equipment served by the prime power source or adjacent to the power lines. In cases where a dedicated but marginally-sized prime power generator is available to the modulator, the harmonic currents may affect the system KVA requirement adversely or distort the generator waveform significantly.

For typical applications where harmonic line currents may be troublesome, the filter bank may be made from 3 to 10 times the value of PFN capacitance, depending on harmonic requirements.

Critically Damped Charging Using the HVPS Impedance

RCA has successfully breadboarded a system in which no filter bank is employed, and the regulation impedance of the rectifier transformer is large enough (20%) to nearly critically damp the PFN charging rather than permit resonant charging. Figure 2 displays this approach, employing conventional notation for LTM circuits where appropriate.

In this approach to PFN charging, the rectifier diodes act also as holdoff diodes, permitting variable PRF operation (including single shot) without the requirement for extra components. By allowing 10% PFN voltage overshoot, the charging period is shortened as compared with full critical damping. Charging efficiency approaches that of resonant charging, since the circuit damping impedance is primarily due to commutation in the rectifier/transformer circuits and is largely non-dissipative in nature. The PFN charging level does not tend to "run away" even under conditions of repeated load arcing. With no main filter bank, crowbarring as a protection measure is not required.

This is an economical versatile approach to PFN charging, attractive when the harmonics of the charging current waveform can be tolerated in the prime power source.

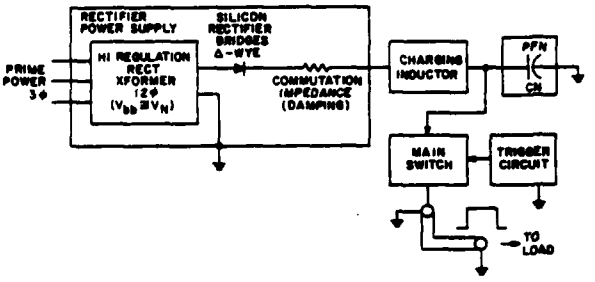

Figure 2. Economical Variable PRF, Lightweight, LTM with Low Loss Critically Damped PFN Charging

Power Supply Crowbarring and Fusing as an Alternative

A crowbar circuit is desirable or necessary in systems employing large energy storage banks to protect circuit components from the stored energy when faults occur. This is particularly true in cases where a multichannel system is operated from a single dc supply source, since the power handling capability per channel is much less than the system power available to cause damage under fault conditions.

Typically, a multiple-triggered ignitron is used to protect very-high-power systems. Multiple triggering avoids recharging of the filter bank following recovery of the crowbar prior to the main circuit breaker interrupting the fault.

High voltage fuses may provide an economical alternative to crowbarring as a protective measure, particularly for laboratory type experimental equipment, or for equipment in which numerous full fault conditions are not anticipated. For example, if vacuum tubes are employed to interrupt faults in a multi-channel modulator system, fuses may be employed as backup devices for occasional instances in which the hard tube also arcs. Sometimes fuse blowing is deliberately accelerated by triggering a small crowbar type ignitron which also shunts the fault current from the defective channel until the fuses blow.

Common Components in Multiple Channel Modulators

The minimum number of required PFNs and line switches is determined by available switch ratings. The total filter capacitor bank size is not significantly affected by modularization of the channels. However, the number of HVPS units, voltage controls, circuit breakers, charging inductors, pulse transformers and other auxiliary circuit items is optional between one common unit and N units (one per thyratron channel).

A sound design supported by a backlog of experience, but perhaps more costly than necessary, could include one component of each type per channel. The system would employ N separate modulator systems integrated by an intelligent control system.

By judicious choice of circuit technique, it may be feasible and economical to employ a single fully-rated common unit or at least less than N units for some or all of the major components mentioned.

Sample Design

Electrical Design

Table II gives the specification requirements for a super power pulse modulator. Additional constraints include use of state-of-the-art components wherever possible. A detailed tradeoff analysis was made to arrive at a suitable choice for a near-future, continuous-operation modulator.

Table II. Modulator Specifications

Peak Power:	2.5 Gigawatts
Average Power:	10 Megawatts
Peak Load Voltage:	200 Kilovolts
Peak Load Current:	12.5 KiloAmperes
Pulse Width:	20 Microseconds
Pulse Rise Time:	5 Microseconds Maximum
Repetition Rate:	200 Pulses per second
Duty:	Continuous Operation

Table III is a repeat of the thyratron types shown in Table I, with added data pertinent to the design under consideration. The required number of thyratron channels varies from a low of 26 (CX-1193) to a high of 85 (HY-5).

After further tradeoff studies, including thyratron tube cost and auxiliary equipment cost, the KU-275 type was chosen for the sample design. Figure 3 is a simplified schematic of the modulator designed to meet the requirements of Table II.

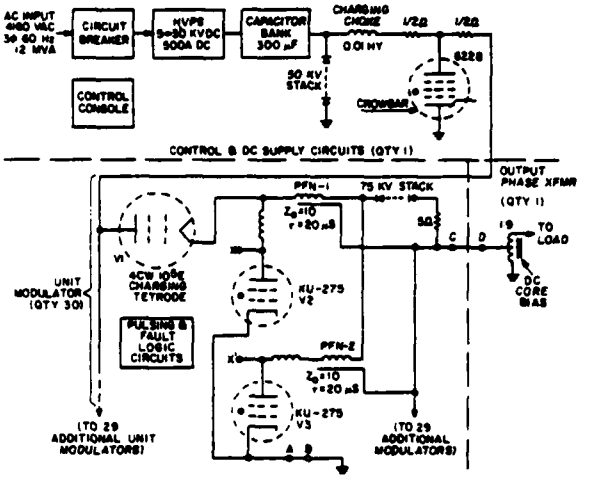

Figure 3. 2.5 Gigawatt Modulator

To minimize size, weight, and cost, common components are utilized to the maximum extent possible. Thus a single large power-supply/capacitor-bank/charging-choke/crowbar complex is used. Thirty "unit modulators" are employed with two thyratron/pulse network combinations per unit modulator, and one charging tetrode per modulator. As discussed earlier, individual control of the delayed charging tetrodes allows isolation of a faulty unit modulator without necessitating total modulator shutdown. A single matched end-of-line clipper is used for each unit modulator to prevent inverse voltage at the thyratron anodes or charging tetrode cathodes. An overmatched load is utilized to minimize thyratron anode dissipation.

Provision for reversing the output polarity is included; also, provision for using thyratrons other than the KU-275. Specifically, a "twice-average-current" thyratron can be substituted for the pair of KU-275's by connecting a link from X to X'. The KU-275 thyratrons are not directly in parallel, but are isolated by the pulse network impedance.

Table III. Hydrogen Thyratron Comparisons

	Maximum Ratings				Proposed Operation						
Type and Manufacturer	epy kV	ib kA	Ib A	Pb (10^9)	epy kV	ib kA	Ib A	Pb (10^9)	P/Tube MW	N min	N Prop
HY-5 EG&G	40	4	7	160	36	1.75	7	12.6	0.126	80	85
CH-1191 Tung-Sol	50	4	8	72	44	2.0	8	17.6	0.176	57	60
KU-275 ITT	50	5	8	400	44	2.0	8	17.6	0.176	57	60
CH-1222 Tung-Sol	50	10	15	180	44	3.75	15	33	0.33	31	33
GHT-9 M-O Valve	35	5	15	100	30	3.75	15	22.5	0.225	45	48
CX-1175 English Electric	80	6	6	140	65	1.5	6	19.5	0.195	52	55
CX-1192 English Electric	120	6	6	140	100	1.5	6	30	0.300	34	36
CX-1193 English Electric	160	6	6	140	140	1.5	6	42	0.420	24	26
ZT-7004 General Electric	50	4	7	55	44	1.75	7	15.4	0.154	65	70
Experimental (Signal Corps)	250		4		220	1.0	4	44	0.440	23	25
Proposed (Signal Corps)	70		30		62	7.5	30	93	0.93	11	12

A single output pulse transformer accepts pulse power from the 30 unit modulators in parallel. An autotransformer configuration with DC core bias is used to obtain an optimum pulse transformer design.

Figure 4 shows an alternative DC supply and charging circuit for lightweight systems. A relatively high frequency alternator supplies three-phase AC power to a step-up plate transformer and rectifier. (If desired, a dual system could be used with Δ and Y secondary rectifier circuits connected in series to obtain a 12 phase ripple.) Air core reactors in the AC line limit charging currents. No capacitor bank or charging choke is used; the charging waveform is that of an overdamped resistive charging system. However, since the damping impedance is inductance in the AC line, there are no resistive losses. Staggered charging intervals can be used to reduce peak loads on the AC source.

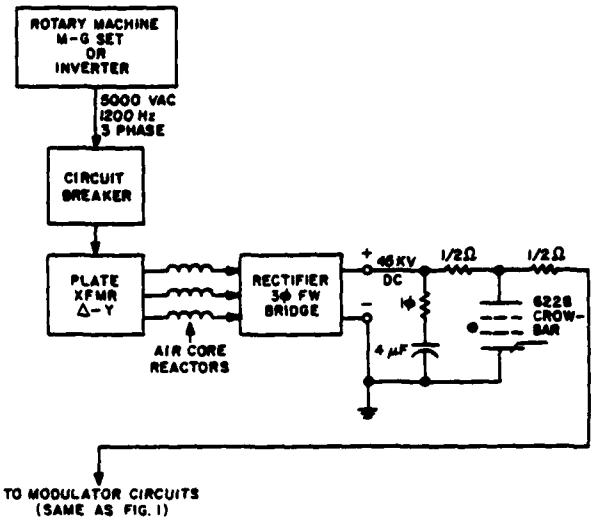

Figure 4. Alternate Charging Configuration

Physical Layout

Figure 5 presents a concept of one of several physical layouts considered. The unit modulators are arranged two high, and two wide in a mirror image relationship on either side of a ground wall. Eight of these foursomes are arranged in a straight line, with the output pulse transformer located in the middle. A ground shield surrounds the entire modulator complex, making intimate contact with both vertical and horizontal internal walls.

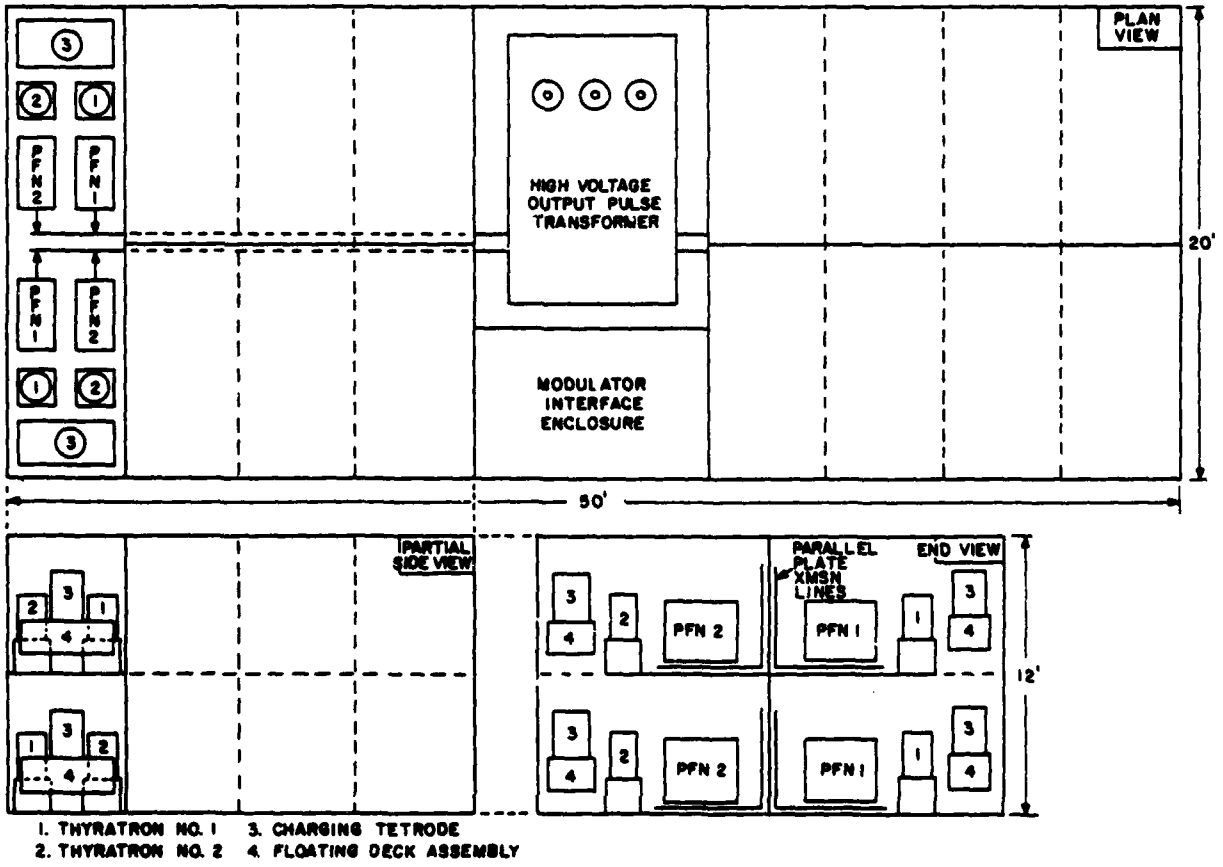

Figure 5. Layout Concept

This configuration contains spaces for 32 unit modulators, two of which could be standby or operating spares. The modulator outputs are connected to parallel plate transmission lines as shown in the figure. Thus eight primary pulse transmission lines lead up to the pulse transformer (four from either side). The pulse transformer output is conducted to the load via three parallel 50 ohm coaxial cables. The entire 10-megawatt average-power modulator complex (less HVPS and charging choke) is housed in a space 12 feet high, 20 feet wide, and 50 feet long.

Acknowledgments

The author wishes to acknowledge the extensive use of material originally generated by W. I. Smith, RCA MSRD. Also, use was made of ideas contributed by W. R. Mayhew, RCA MSRD.

This paper is based on studies performed for the U.S. Air Force under contract No. F30602-73-C-0151, Rome Air Development Center, Griffiss Air Force Base, New York.

COMPACT, ULTRA-HIGH DENSITY MARX GENERATOR

Capt Daniel M. Strickland
Capt William L. Heatherly

Air Force Weapons Laboratory
Kirtland AFB, N.M.

Introduction

This report presents the results of an Air Force Weapons Laboratory (AFWL) program to develop a compact, high-density energy storage system to satisfy various electromagnetic pulse (EMP) simulation requirements. Such requirements range from small, 1-MV ground-based simulators to elevated or air-supported simulators producing tens of megavolts. Based on studies performed during the High Altitude Simulation (HAS) program and reported in the EMP-HAS report series, it was concluded that the most versatile and promising pulse generator system for matching this broad range of requirements would utilize a Marx generator and "distributed" peaking capacitor circuit.[1]

The two main constituents of such a system are a Marx generator and a peaking capacitor.

1) A Marx generator is necessary to initially generate the very high voltage required and to provide a store of energy that will produce the low-frequency components of the final output wave. The Marx generator is a method of storing energy at a relatively low initial voltage and, by very fast gas switching, to connect many parallel capacitors in series to generate a short impulse of extremely high voltage. The advantages of an impulse generating system such as the Marx generator are that flashover or voltage breakdown within a system is absolutely voltage and time dependent. Therefore, it is possible for some applications to impulsively generate very high voltages and remove the voltage from the load or test object prior to the occurrence of a flashover. This phenomenon is principally due to the finite transit time of the streamers that initiate the conducting currents which result in system flashover. See references 2 and 3 for a more detailed discussion of Marx generator theory.

2) A peaking capacitor, which is a small but very fast energy store, provides the high-frequency content of the wave and enables one to achieve the required very fast rise time. The distributed peaking capacitor is unique in that it is matched to the general shape of the system into which the pulse is to be launched and, in effect, becomes a part of the wave guide.[4] Therefore, if the impedance of the distributed peaking capacitor is sufficiently low to pass the wave front, then transit time effects within the peaking capacitor itself will not affect the basic rise time observed on the generated wave shape. A smooth transition between the fast or high-frequency components of the wave and the tail or low-frequency components is accomplished by initially charging the peaking capacitor with the Marx generator. During the course of the charging of the peaking capacitor, the inductance of the loop formed by the Marx generator and the peaking capacitor is charged to the desired output peak current level at the time the maximum output voltage of the system appears on the peaking capacitor. When this condition is achieved, that is, the voltage on the peaking capacitor is equal to the desired output and the desired output current is flowing in the loop inductance, the main output switch is closed and the wave is launched into the system.

This circuit is shown in a pseudo-electrical/physical schematic in figure 1. This configuration shows a single pulser module driving a parallel plate transmission line simulator. Figure 2 shows how this module might look physically. If one needed more voltage and/or energy, the modules could then be configured into a distributed source array of n series and m parallel elements. Figure 3 shows a 2 X 2 array of modules producing twice the voltage and four times the energy of a single module.

The key element in such a distributed source module is the Marx generator which not only must be of ultra-high time precision to allow the modules to be properly time phased, but which also must be compact, lightweight, and low inductance, especially for the large elevated systems. The other elements of the system are certainly important but the technology for such items as the output switches and peaking capacitors has been fairly well advanced by other programs. The module structure which must also be lightweight is unique to the particular system and cannot be designed universally. Consequently, the bulk of our development effort was directed towards the Marx generator for a compact, high-density, distributed source module.

The result has been named the Molecule Marx to indicate that it is a building block for assembly of larger systems. Although the system described here was designed for 2 MV, the modular nature of the Marx itself allows for variation of design output and energy storage. The 2 MV, 18-kJ Marx weighs 460 lbs for a density of 39 joules per pound, the highest ever achieved. The Marx operates at a stress of 1 MV/m in ambient atmospheric pressure SF_6, has an inductance of 800 nh/MV, and can be erected with a jitter (1σ) of less than 10 nsec over a 7:1 voltage range.

The design details presented here are intended to enable one to fully understand the philosophy and practice of building compact, high-density Marx generators. The "Molecule" design is extremely flexible allowing for many different choices of stage voltage and energy, number of stages, types of capacitors and resistors, and construction materials. Since individual requirements differ it is most likely that the reader will adapt the Molecule design to his particular needs rather than produce a carbon copy. Indeed, the Marx described here is only a prototype; it is not a polished, production engineered unit. Consequently, a detailed drawing package does not exist which could be used to exactly reproduce this Marx with no other information. However, if any group wishes to obtain details of the Molecule Marx design which could not be included in this report, additional drawings are available for reference at the Air Force Weapons Laboratory.

Design

Circuit

The 2 MV Molecule Marx is shown schematically in figure 4. Table I gives the component parameters with

respect to the schematic. The Marx consists of 20 stages, of 100 kV each, which are balance charged; i.e., the two capacitor terminals are charged to plus and minus 50 kV, respectively. The balance charging required that the first and last capacitors be isolated from ground during charging. One technique for doing so is to use untriggered half-gaps or switches which operate at half the voltage on the full, triggered switches. In figure 4 the half-gaps are those marked S_1 and S_{21}. The triggered switches operate with a total gap spacing of 0.243 inch and a trigger electrode is positioned one third of the total gap distance from one electrode. Thus there are effectively two gaps formed by the three electrodes and the long gap is twice the length of the short gap.

The trigger pins are connected in an M=3 configuration, i.e., the pins of each switch are resistively connected to the pins of switches three stages away. This technique has been called a "Martin" Marx after J. C. Martin, who developed the technique, of the Atomic Weapons Research Establishment, Aldermaston, England.[3] The Martin technique has been adopted in all the passively coupled, ultra-high precision Marx generators known to the authors.

Structure

The Molecule Marx is assembled on a rigid skeleton. All components can be installed or removed without disassembly of the skeletal structure which consists of four basic units: stage trays, stage spacers, tie rods, and end plates. A bottom view and side view are shown in figures 5 and 6.

Capacitors

The basic capacitor used in the Molecule Marx is shown in figure 7. It is a 100 kV, 0.18-μfd unit with a density of 100 joules per pound. The internal construction of a generalized capacitor of this type is shown in figure 8.

Because the head of the capacitor was not designed to hold off 100 kV externally it was necessary to make the following modifications. First a Celcon or Delrin barrier was hot-air welded to the existing head. This barrier in theory provided all the insulation needed to operate at 100 kV in SF_6. However, to ensure against a bad weld joint, which would produce a flashover and damage the capacitor, sheet insulation was added to each side of the head. One sheet is a piece of 10-mil Mylar, and the other is a commercial dielectric sandwich of 3-mil of polypropylene between 2 sheets of 1-mil Kraft paper. The dielectric sandwich sheet is placed in contact with the capacitor terminal to allow the paper to grade the static charge distribution near the terminal. Connections to the capacitors were made with receptacles which attach with screws to the existing capacitor rail terminals.

To prevent the compression of the Marx column from damaging the capacitor bodies, a thin strip of 1/4-inch sponge rubber was glued to the cases. The rubber not only cushions the capacitors but also provides enough friction to hold them in place with no other supports.

Switches

Housing. The original prototype switches utilized an acrylic tube housing with end caps held on by nylon screws. After some use at high pressure these screws would shear and have to be replaced. Additionally the electrodes were held in position by threaded rods which screwed into matching holes in the housing. These threads were sealed with epoxy and tended to develop leaks. These mechanical problems were compounded by an electrical problem. To prevent external flashover from the main electrode connections to the trigger connection, it was necessary to cement acrylic barriers to the outside of the housing. These joints were troublesome and had a propensity to arch through tiny bubbles in the cement. Consequently, a new set of switches was fabricated with an injection molded Lexan housing (figure 9). In this new design the external insulation is part of the housing, thus eliminating glue joint problems; the end caps are simple plugs which are glued in with PS-30 acrylic cement; and the housing is molded with internal flats for O-rings of gasket sealing of the electrode connections. In addition the capacitor connections are insulated from adjacent ones by an overlapping portion of the housing. The switch tongue is cemented into a socket on the back of the housing. It is this tongue which fits into the slot in each stage tray, providing mechanical support as well as insulation for the stage switches.

Electrodes. The main switch electrodes are Mallory 1000 rods with hemispherical ends. They are mounted in the housing with a flat head screw which seats in a countersunk hole in the capacitor connector and threads into the electrode. A small flat is ground on each side of the electrode for holding with a wrench while tightening. The gas seal is presently provided by a thredseal O-ring located between the flat end of the electrode and the molded flat on the inside of the switch housing. This causes two problems, however. First, the O-ring will not fully compress to make a metal-to-metal contact between the electrode and the metal part of the thredseal. This results in an error in gap setting unless the electrodes are ground off slightly. Second, the metal part of the thredseal is electrically floating with a gap between it and the electrode. Consequently, during Marx charging this gap arcs and reduces the stability of the switches with a reduction in self-breakdown voltage. In addition the lifetime of the switch housing is degraded by the arcing and failure occurs from an internal track around the wall of the switch. The operating data presented in a later section were all taken with switches which had this problem, and the results are discussed relative to this problem. However, a design modification is being implemented to correct this problem. The thredseal will be removed completely and an O-ring grove cut in the flat end of the electrode to provide a direct seal with the switch body. The edge of the flat end will also be rounded slightly to reduce field enhancement. This geometry will then be nearly identical to the original prototype geometry which used epoxy to seal the screw threads directly. Internal switch dimensions were the same as in the molded housing, and no internal tracks were observed after many thousands of shots.

The trigger electrode is a tungsten carbide scriber point mounted in a threaded brass rod. Since it is expected to erode more rapidly than the main electrode, it was designed to be quickly removed externally and replaced with a new one as necessary.

Connections. The electrical connection between switch and capacitor is made with the connector shown in figure 9. This piece is permanently attached to the switch during assembly and mates with the capacitor by being plugged into the capacitor receptacle. In other words, during the Marx assembly the switches are connected electrically and mechanically by simply being plugged in. Connection to the charging chain is made through a pin which is pressed into the connector. A flexible resistor plugs into this pin and another pin located on the grading rings. Connections to the trigger pin are made via the buss bar at the

bottom of the switch. The trigger pin is threaded into the buss bar which is mounted to the switch with nylon screws. Banana or pin plugs are screwed into the buss bar for resistor connections.

Grading Rings

A novel split-ring technique is used for grading the "Molecule" Marx generator. While conventional rings are electrically continuous and operate at a single potential on each ring, the split rings are divided into two sections separated by insulating spacers (figure 10). One section is electrically connected to the top of its associated stage switch, and the other section is connected to the bottom of that switch. Thus, one full-stage voltage appears between the sections during charging, but after switch closure (during erection) the sections equalize in voltage.

The ring sections (figure 10, Piece No. 1) can be fabricated from any material suitable for conventional rings, e.g., electrical conduit, aluminum tubing, or copper pipe. The shape can either be rectangular, as shown, or circular depending upon the particular Marx design. The cross-sectional dimensions are chosen to provide adequate spacing between the rings and the Marx core.

The section spacers (figure 10, Piece No. 2) can be fabricated from any high-dielectric strength material and can either be molded as one piece or formed by gluing several pieces together, taking necessary care in the positioning of glue seams. In the prototype Molecule Marx, for example, the spacers are made by gluing two rubber cane tips to a polyethylene disc. The spacers must provide a snug, friction-fit around the grading ring. A metal plug is inserted to terminate the tubing in a round end to shield the sharp edges which could cause an arc through the spacer. The rings are supported on the Marx structure in any desired position by dielectric rods. Electrical connections to the rings are made by appropriate techniques such as soldering, clamping, or with threaded inserts such as Molynuts or Rivnuts.

Resistors

Two types of resistors are presently used in the Molecule Marx: wirewounds and a conductive silicone elastomer tubing. The wirewounds are used as primary charging resistors. Five, 2000-ohm Dale RS-10 wirewounds are soldered into a string, fitted with brass end terminals, and slipped inside a plastic tube. A panduit strap is clamped around each end of the tube to hold the string of resistors in place. The brass resistor terminals have holes drilled in them which mate onto banana plugs attached to the grading rings. Since the rings are split they provide convenient attachment points for both the positive and negative charging chains. The stage capacitors are then either hardwired to the grading rings or connected through another resistor string. This sideways resistor connection is preferable because it damps erection transients which might otherwise overvoltage the inter-ring capacitance and produce an arc between grading rings. However, the sideways resistance must be small compared to the main stage charging resistance so that proper grading of the Marx is maintained after erection.

In the Molecule Marx the sideways resistance connection is made through a short piece of the conductive elastomer tubing with 1/4-inch ID, 3/8-inch OD, and a nominal resistance of 1000-ohms. Each end of the tubing is fitted with a female receptacle electrode held in place with a Panduit strap, one electrode of which mates to a grading ring plug and the other which mates to the pin on the capacitor connector.

The trigger resistors are also constructed of the silicone elastomer tubing and utilize similar electrodes which mate with banana plugs on the switch buss bars. The manufacturer can produce the elastomer in almost any shape desired with resistivities from 10-ohm-cm up to 100,000-ohm-cm. Both the sideways resistors and trigger resistors in the Molecule Marx utilize a 10-ohm-cm material, but a higher resistivity is required for the main charging resistors. Although the wirewounds are satisfactory for the main charging resistors, it is intended that they too be replaced by the resistive tubing as soon as suitable material is received.

Operating Data

Ambient Insulation

The Molecule Marx operates in an ambient environment of atmospheric pressure gas. Up to 50 kV per stage, or 1 MV output, the ambient gas can be air, but above this level a hard gas such as SF_6 is recommended, however, because some evidence exists which indicates that Freon 12 forms conductive decomposition products in a high corona environment. After sustained operation in Freon 12, a thin layer of a soot-like material (probably a carbon product) builds up on insulator surfaces and can produce a flashover. No such effect is noticed in SF_6.

Inductance

Inductance was determined by measuring the ring frequency of the Marx firing into a short circuit. After subtracting the contribution from circuit loop inductance (calculated by a technique in ref. 5) the effective inductance of the Marx was found to be approximately 1.6 microhenries, or 80 nanohenries per stage. This value is consistent with that obtained by calculating the inductance contributions of an individual stage (Table II).

Jitter

The jitter of Marx erection is basically a measure of the variation in erection time of the Marx. Although absolute erection time is difficult to measure it can be relatively defined as the time between application of a firing signal and voltage first appearing across a load on the Marx. The technique used to measure Molecule Marx erection jitter is a standard one which involves displaying the trigger signal and the output waveform on the same oscilloscope trace (figure 11). The trigger signal is used to trigger the oscilliscope. If the signal is identical from shot-to-shot and the oscilloscope properly adjusted, repetitive displays of the trigger signal should result in perfectly overlapping trigger signal traces. Any non-overlapping of the Marx output signal then represents jitter.

During jitter measurements the net effective delay in the trigger signal circuit was about 5 nanoseconds. That is, if 5 nsec are added to the time between the trigger signal and Marx output as measured on the oscilloscope, a measure of the erection delay can be obtained. Figures 12 through 19 show five shot overlays of the trigger signal and the Marx output for various charging voltages and switch pressures. The first short, triangular signal is the trigger signal to the Marx differentiated by the trigger probe.

The second slowly rising signal is the Marx output measured by the voltage probe. In all cases the Marx output was negative and the trigger signal was positive (trigger cable charged negative). The trigger signal is displayed negative because it was inverted by the B input of the 1831A direct access plug-in.

Using figure 12 as an example, the delay on the scope trace is approximately 70 nsec, and adding the 5 nsec trigger input delay yields an erection delay of 75 nsec. In figure 13 the total erection delay is only about 35 nsec because the switches are being operated at a higher voltage and they fire more quickly than at the lower voltage. This relationship, however, does not necessarily hold if a different gas is used at the higher voltage.

The series of eight traces show representative performance of the Marx between 14 kV and 100 kV per stage, or in total voltage between 280 kV and 2 MV. (In reality the Marx will erect reliably as low as 4 kV per stage, or 80 kV total, with 0 psig air in the switches, but the erection jitter is quite high.) The worst jitter is indicated in figures 18 and 19, which show a ± 10-nsec spread about the mean value of delay. The jitter in figures 13, 14, 15, and 16 is unmeasurable, and even in figure 12 is quite low (about ± 5 nsec).

As mentioned previously, these data were taken with the switches which used a "thredseal" to seal the main electrode connections. Because of the instability produced by arcing between the electrode and the metal part of the "thredseal" it was necessary to heavily pressurize the switches and use a high percentage of SF_6 to achieve voltages above 70 kV. Consequently, the jitter increased. It is felt that once this problem is rectified, the low jitter performance can be maintained over the full operating range. Even so, the Marx presently operates with better than 10-nsec jitter over a 7:1 voltage range (14 kV to 100 kV) which is adequate for many requirements. A new set of switches which will correct the top end instability is presently being fabricated, and new data will be published when they are available.

References

1. EMP-HAS Technology Reports, Air Force Weapons Laboratory, Kirtland AFB, NM, September 1970

2. AFWL EMP-HAS 3-6, Technology Report 2, High Altitude Generator Study, Appendix: Fundamentals of Marx Generator Theory and Practice, Kirtland AFB, NM, September 1970

3. Fitch, R.A., Marx and Marx-Like High-Voltage Generators, Maxwell Laboratories, Inc., San Diego, CA

4. AFWL EMP-HAS 3-7, Report 4, Ground Based EMP Pulser System, Appendix A: Conventional and Distributed Peaking Capacitor Generators, Kirtland AFB, NM, September 1970

5. Grover, F. W., Inductance Calculations: Working Formulas and Tables, Dover Publications, New York, 1946

Bibliography

Advanced Distributed Source Generator Test and Development Plan, Air Force Weapons Laboratory, Kirtland AFB, NM, August 1971

Advanced EMP Pulse Generator Test and Development Plan, Air Force Weapons Laboratory, Kirtland AFB, NM, March 1971

Baum, C.E., Editor, Pulsed Electrical Power Note Series, Air Force Weapons Laboratory, Kirtland AFB, NM

The RES-N Pulser - An Electrical Analysis, PAR 70-12, Pulsar Associates, Inc., La Jolla, CA, December 1970

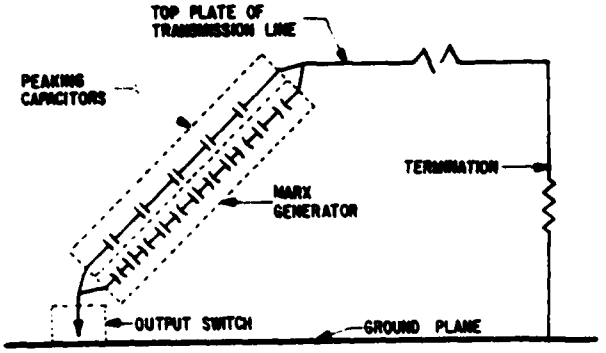

Figure 1. Schematic of Distributed Peaking Generator Configured to Drive a Parallel Plate Simulator

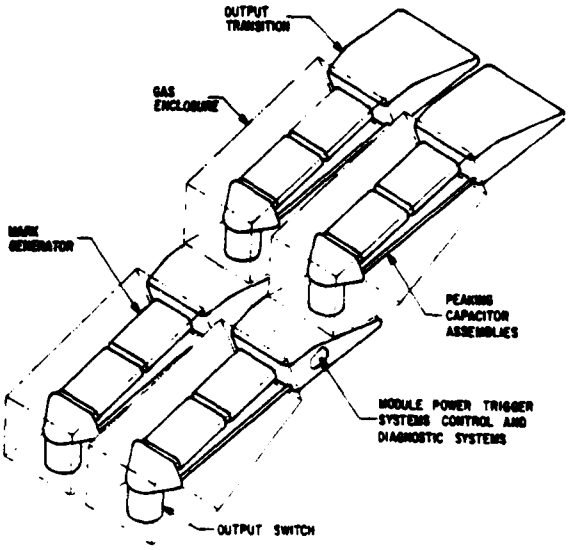

Figure 3. 2 X 2 Array of Distributed Peaking Generator Modules for Driving a Parallel Plate Simulator

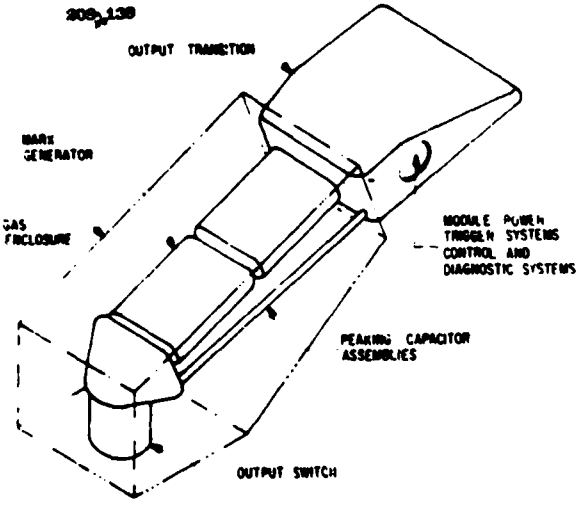

Figure 2. Generalized Physical Layout of a Distributed Peaking Generator for Parallel Plate Simulators

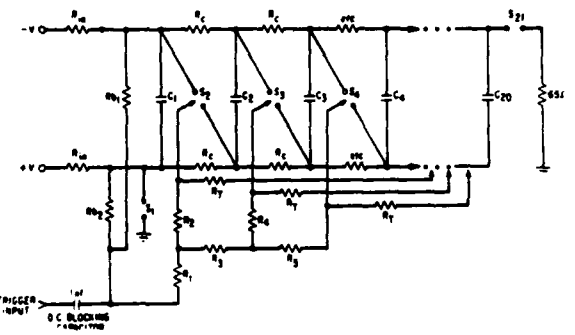

Figure 4. Schematic of the 2-MV Molecule Marx Generator

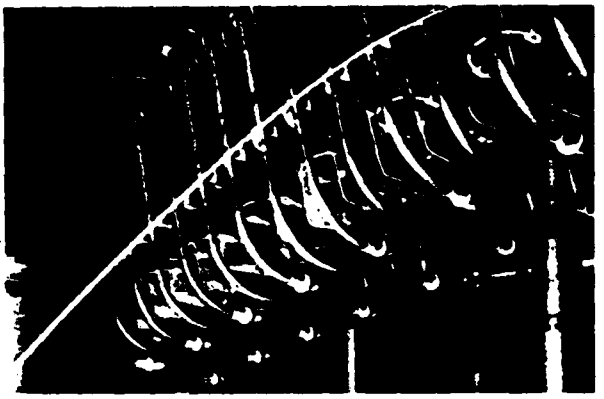

Figure 5. Bottom View of Marx Generator

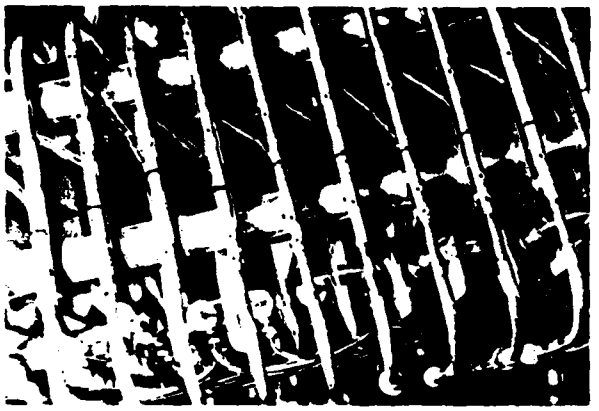

Figure 6. Side View of Marx Generator

Figure 9. Assembled Marx Switch

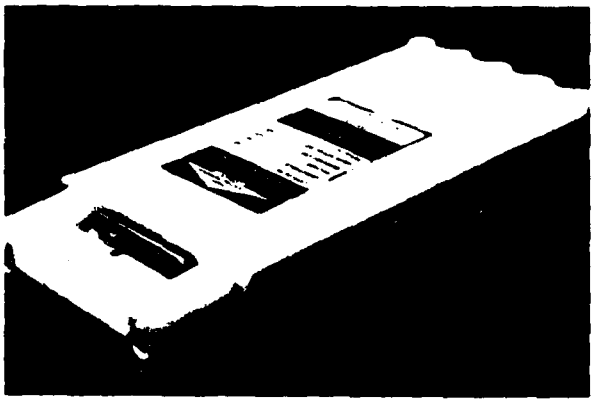

Figure 7. 100 kV Stage Capacitor

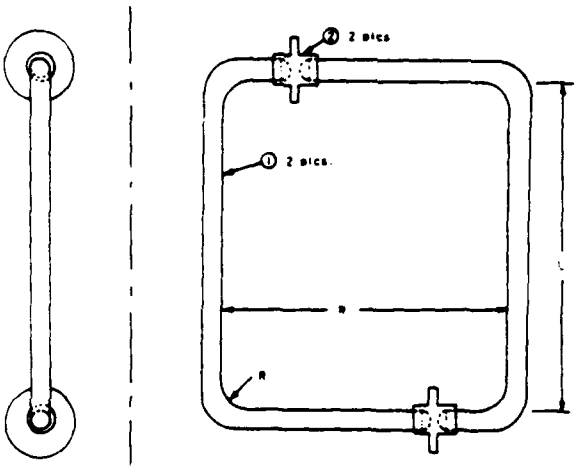

Figure 10. Grading Ring Profile

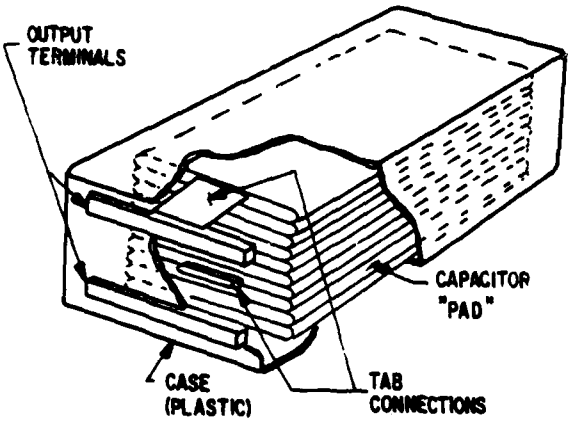

Figure 8. Construction of Generalized Plastic Cased Capacitor

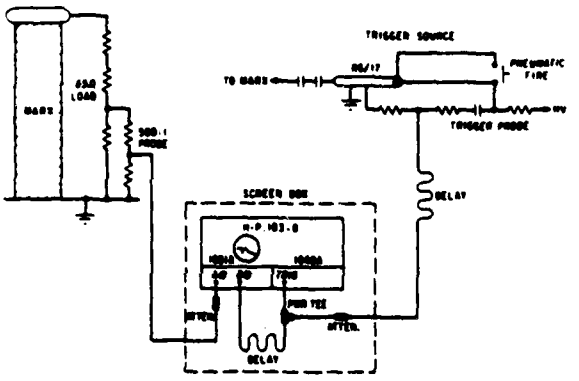

Figure 11. Diagnostic Circuit for Marx Jitter

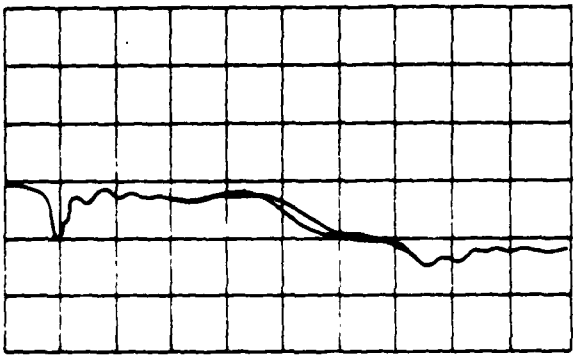

Marx Stage Voltage: 14 KV @
Trigger Charge Voltage: 60 KV
Switch Gas Type: Air
Switch PRESSURE (psig): 0
Pressure V_{SB}: 18 KV
Sweep Speed: 20 nsec cm
5 Shots Superimposed

Figure 12. Jitter Measurements (14 kV)

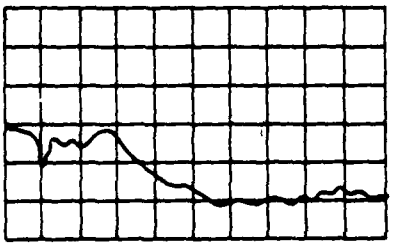

Figure 13. Jitter Measurements (40 kV)

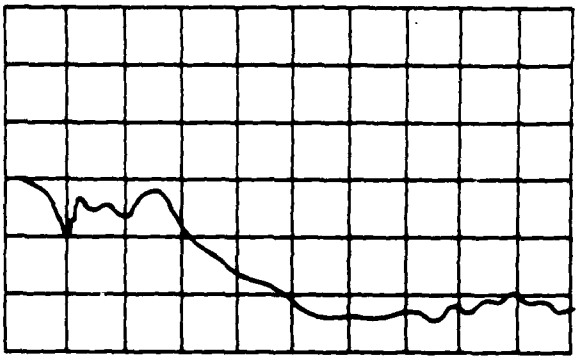

Marx Stage Voltage : 46 KV @
Trigger Charge Voltage: 60 KV
Switch Gas Type: Air
Switch Pressure (psig): 40
V_{SB}: 50 KV
Sweep Speed: 20 nsec/cm
5 Shots Superimposed

Figure 14. Jitter Measurements (46 kV)

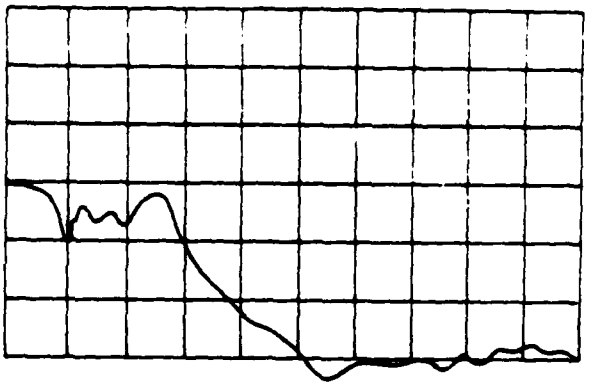

Marx Stage Voltage: 60 KV @
Trigger Charge Voltage: 60 KV
Switch Gas Type: Air
Switch Pressure (psig): 60
V_{SB}: 72 KV
Sweep Speed: 20 nsec cm
5 Shots Superimposed

Figure 15. Jitter Measurements (60 kV)

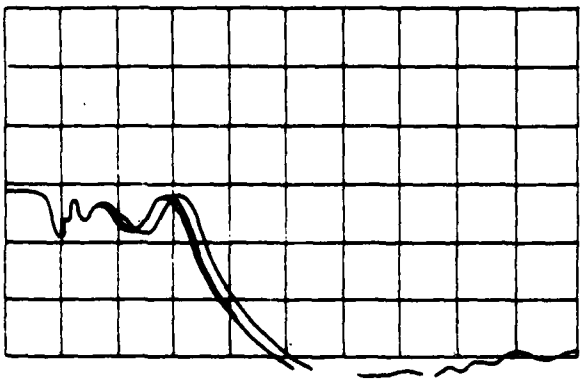

Marx Stage Voltage: 70 KV
Trigger Charge Voltage: 80 KV
Switch Gas Type: Air
Switch Pressure (psig): 80
V_{SB}: 80 KV
Sweep Speed: 20 nsec cm
5 Shots Superimposed

Figure 16. Jitter Measurements (70 kV)

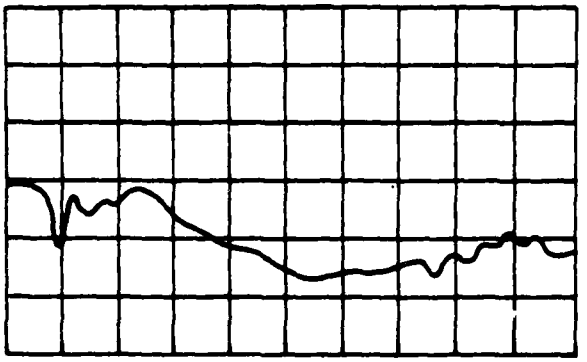

Marx Stage Voltage: 70 KV
Trigger Charge Voltage: 80 KV
Switch Gas Type: 90 N_2 10 SF_6
Switch Pressure (psig): 82
V_{SB}: 75 KV
Sweep Speed: 20 nsec/cm
5 Shots Superimposed

Figure 17. Jitter Measurements (70 kV)

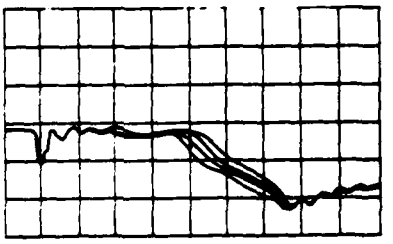

Figure 18. Jitter Measurements (90 kV)

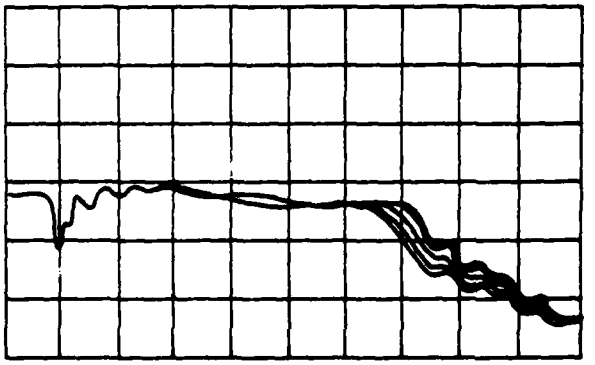

Marx Stage Voltage: 100 KV
Trigger Charge Voltage: 80 KV
Switch Gas Type: 10% N_2 90% SF_6
Switch Pressure (psig): 70
V_{SB}: ?
Sweep Seed: 20 nsec/cm
5 Shots Superimposed

Figure 19. Jitter Measurements (100 kV)

PULSE GENERATORS AND MODULATORS FOR LASER APPLICATIONS

L. N. McClusky, E. L. Roy, W. H. Gurley, C. M. Bowden,
A. H. Werkheiser and Charles Cason

US Army Missile Command
Redstone Arsenal, Alabama 35809

Summary

A high voltage pulse generator has been constructed for laboratory use in powering a high average power pulse laser. The pulse generator has three 500 kVA power transformers, a 3-Φ rectifier and four mechanically synchronized 5-stage Marx generators. At 70 kV charge voltage 7350 J are stored. Instabilities in the laser load are observed at approximately 70 kV charge. Very satisfactory 4 second operations of the pulse generator have been achieved at a PRF of 50 pps which corresponds to an average output power of 280 kW at 300 kV peak.

Modulator requirements applicable to pulsed electron beam augmented gas laser are described. A range of parametric examples are given for three groups of lasers typified by three electron beam options - cold cathode, plasma cathode and hot cathode. Requirements are set in relation to 100 kW average laser output power delivered from the various example laser systems. Pulse repetition frequencies are in the range 10 to 2500 pps. Three example pulse widths, 2, 20, and 100 microseconds, are specified. Average pulse powers delivered to loads range from 165 to 670 kW. The difficulties to be met in achieving certain pulse drive conditions are illustrated by a simple R, L, and C circuit analysis where inductance as low as 0.27 microhenry will be required in a modulator circuit delivering 500 kW to the load. In specific examples, pulse voltage requirements are as high as 250 kV. Pulse currents run as high as 50,000 amperes.

I. Laboratory Pulse Generator for an Axial Pulsed Gas Laser

A. Design Objectives

There is an increasing need in the pulsed gas discharge laser field for high performance pulse generators capable of driving large laser devices under a variety of conditions and configurations.

Recently the need arose for a generator to drive four axially pulsed CO_2 laser tubes which were optically coupled in series. Performance objectives of the pulse generator were as follows:

a) Output sections - 4 independent, synchronized operation

b) Discharge voltage - 300 kV/section

c) Output energy - 1400 joules/section

d) PRF - 1 to 50 pps

e) Run duration - 20 seconds maximum

f) Maximum average power to load - 280 kW.

The performance objectives were based on discharge of a 0.03 microfarad capacitor into a single laser tube. Design objectives called for rapid construction of the pulse generator, using standard, readily available components wherever possible to eliminate a development lag.

B. Design Details

The circuit shown in Figure 1 was used. It contains four idential Marx generator sections of five stages each. Synchronization is obtained by coupling the lower stages through a single switch. There are separate switches for all other stages. Charging of the Marx stages is through parallel resistor networks from a 70 kVdc source. Values of components selected for the design are as follows:

a) $R_1 - R_{40}$ = 16 kohm (eight 2 kohm, 200 W in series)

b) $R_{41} - R_{44}$ = 3.2 kohm (five R_1 in parallel)

c) $C_1 - C_{20}$ = 0.15 μfd, 100 kVdc (0.1 μfd and 0.05 μfd parallel)

d) $S_1 - S_{19}$ = specially constructed switch.

The resistor networks were selected to achieve capacitor charging in three time constants at 45 pps. Resistors used in the upper and lower capacitor legs are standard 200-watt wirewound units which are on the electronic supply market. Each charge leg contained eight resistors in series to withstand maximum output voltage from the Marx circuits. The design subjects charge resistors to 10 times their normal rated dissipation for the 20-second run durations at maximum charge voltage and PRF. Tests on these resistors showed that there is sufficient heat capacity and convective cooling during the 20-second overload periods to withstand this service.

Three-foot diameter rotating discs having commutating bars mounted on each disc gave an equivalent air blast to avoid the "arc-hang" problem. The physical arrangement is shown in Figure 2. Each disc serves two switch sections except for the center disc which serves the synchronizing function. Four 1-foot long commutating bars were mounted on each disc so that the ganged switch assembly could provide a 50 pps switch rate at 750 rpm. The ganged switch discs are rotated by a variable speed dc motor capable of delivering up to 30 horsepower for short run durations. At the 50 pps output rate, which is equivalent to 750 rpm, windage and friction loads are about 20 horsepower.

The power supply arrangement is shown in Figure 3. Three 500 kVA substation transformers were used in reverse to step up from 4160 volts. The three-output phases were wired delta to furnish 70 kVdc from the three-phase full-wave rectifier. Since large size reactors were not available, voltage variation over a continuous range could not be obtained. Ballast resistors were used between the transformer output connections and the rectifier input as added protection against catastropic breakdown.

C. Pulse Generator Performance

The pulse generator was tested using laser tubes as loads. Additional charging resistance was used to soften the circuit in terms of power supply loading. The power supply transformers were wired for delta output giving about 70 kV charge voltage. Figures 4

and 5 show charging voltage and current traces at 11.5, 18, and 25 pps. The relatively slow responses shown on these curves are due to heavy filtering in instrumentation circuits required by the Marx circuit generated electrical disturbance. At 11.5 pps, there is a noticeable lag in buildup of charge voltage. Referring to the current trace, it can also be seen that there is abnormal persistence in charge current. This is evidence of "arc-hang" at the lower switching speed. With switch speed increased to yield 18 pps output, there is only a slight tendency toward "arc-hang". With further switch speed increase to 25 pps output, there is good clearing of arcs. For the preceding tests, charge resistance remained fixed.

Remedial measures for "arc-hang" conditions are further demonstrated by the results shown in Figure 6. This illustration is a composite photograph of switch performance under different charge resistance and switch velocity conditions. Approximately eight switch pulses are recorded in each photograph. The pulse rate was held at 20 pps in each case. Figure 6(a) shows a severe "arc-hang" condition on every pulse. The switch disc rotated at 5 rps for this case. In Figure 6(b), charge resistance was approximately doubled and "arc-hang" occurred about every other pulse. In Figure 6(c), two commutating bars had been removed from the switch disc and switch speed was doubled to 10 rps. Charge resistance was the same value as used for Figure 6(a). Switching action is acceptable. In Figure 6(d), charge resistance was approximately doubled. Here, ideal switching action is evident. By judicious selection of charge resistance and switch velocity, all pulse rates up to 50 pps were accommodated in this laboratory pulse generator.

Figure 7 shows typical output voltage and current delivered to the laser loads under normal laser discharge conditions. The current trace represents total current delivered to four laser tubes which would be about 55 amperes per tube. When discharged into a low resistance load or a severe laser arc, a generator section rings at about 150 kilohertz. This represents a total circuit inductance of about 38 microhenries.

The original four-section pulse generator has recently been modified to provide two-output sections. Each section has eight stages and is charged to 70 kV maximum. Due to recall of the borrowed 500 kVA power transformers, the pulse generator is now powered from two small laboratory power supplies. These power supplies will support only a 4-pps output capability from the pulse generator. Operation of this modified version has been on a very dependable daily basis.

Experiences with the Marx-based pulse generator indicated reliable and satisfactory operation up to 50 pps using a relatively simple rotating switch. Performance of the generator did not falter even under near short circuit output conditions caused by arc discharges in the laser loads. This pulse generator design represents a quick, relatively inexpensive and reliable solution to some experimental requirements existing at the time. Although this particular generator design did not lend itself to compact packaging, two major size reduction measures can be undertaken. The switch can very likely be miniaturized through use of an SF_6 gas environment. Insulating oil can be used to reduce space requirements for resistors and capacitors. In the future, performance more refined than that offered by the basic Marx circuit will be expected of pulse generators to meet requirements of the newer generation of electron beam controlled gas lasers. These requirements are discussed in the following sections of this paper.

II. Projected Pulse Generator and Modulator Requirements for E-Beam Lasers

One objective of this paper is to identify characteristic E-beam laser electrical requirements. While this cannot be done for the general case, specific examples may be cited which are useful to illustrate the range of parameters anticipated. Chosen laser examples are based on currently planned CO_2 laser requirements. Details of the laser kinetics used to establish the present example requirements are described elsewhere.

A. E-Beam Laser Description

Pulsed electron beam lasers can be placed in three groups for purposes of identifying pulse drive requirements. These groups are characterized by the type of electron beam gun being used - cold cathode, plasma cathode, or hot cathode. Past experience has been almost entirely restricted to use of hot cathode guns in pulsed gas lasers. Use of cold cathode guns is recent and then only in a single shot mode. Although no large plasma cathode guns have been tested, they potentially have desirable characteristics for laser applications and undoubtedly they will receive increased attention in the future.

Figure 8 is a sketch of a typical cold cathode E-gun and laser cavity structure. A plasma cathode E-gun is very similar to the cold cathode type. The hot cathode electron gun is physically larger than the other types and can be thought of as an electrical equivalent to a grounded anode, high voltage triode, or tetrode. The laser cavities can be thought of as identical for the three types of electron guns and electrically independent of these guns except for a special case that will be explained later. The lasing process is controlled by the electron beam. The primary electron beam passes through a foil window separating the gun vacuum chamber from the gas in the laser cavity. Some of the laser gas molecules are ionized as the high energy electrons move through the laser gas. The secondary electrons become a conducting plasma between the drift field electrodes. As electrical energy from the applied field is dissipated in the laser gas, a very large fraction of this energy excites laser levels by secondary electron-molecule collisions. The gas releases laser radiation and is also heated, thereby generating the weak shock waves shown in the figure. This type of process has been used in CO_2, CO, DF, and other electric lasers.

B. Conceptual Modulator Systems

Figure 9 is a simplified block diagram of the modulator arrangement for a hot cathode electron beam laser. The electron gun is essentially a final stage modulator device requiring grid drive. Since the gun cathode is held at a high negative dc voltage, the grid modulator must float at this potential. The drift field or laser cavity must be pulsed synchronously and probably with a small time delay from the electron gun. For drift field dimensions greater than about 5 centimeters, the required pulse polarity is positive. For dimensions less than about 5 centimeters, the preferred pulse polarity is negative.

Figure 10 is a simplified block diagram of the modulator arrangement for cold and plasma cathode electron beam lasers. The electron guns are essentially passive loads which must be driven with negative polarity pulses. The drift field is normally driven with positive polarity pulses for large laser cavity dimensions and with negative polarity pulses for small cavity dimensions, as in the previous case. There is

a distinct possibility that the drift field of cold and plasma E-guns lasers may be made to self-switch merely by pulsing the electron gun. This technique has not yet been adequately investigated. Should the technique be feasible only through reduction of drift field potential to a point that laser performance is severely degraded, then the pulsed drift field will be preferred.

C. Laser Examples and Assumptions

Three model laser types were chosen based on E-beam gun capability. The cold cathode gun can supply a peak current density in excess of 1 amp/cm^2. There are difficulties in operating this gun for pulse periods exceeding 2 microseconds. The hot cathode gun is limited to peak current densities of about 20 mA/cm^2 and therefore does not produce a sufficient current density to operate a laser for pulse periods less than about 30 microseconds. Although the plasma cathode gun works well and supplies the required beam current density to operate from 2 to and beyond 100 microseconds, large guns have not been built and tested. The pulse time widths chosen typify a special capability of a gun type and cover the main time widths which may be of interest. Pulse periods of 2, 20, and 100 microseconds were chosen as examples which are proven to be useful for the cold-, plasma-, and hot-cathode gun, respectively.

The example laser size is determined by the output optical energy and electrical conversion efficiency. An assumed 100 kW average optical beam power was required at pulse rate of 10, 50, 1000, and 2500 pps, depending upon the type of gun example chosen. Pulse widths of 2 and 20 microseconds can support a 20-percent conversion efficiency and 100 microseconds a 15-percent conversion efficiency, all at 6 kV/cm at 1 atm. Output energy densities of 50 joules/liter of active laser volume are assumed as a high practical value based on experimental data. The resulting assumed systems are: (1) cold cathode, 50-PRF 40-liter volume having a drift field electrode and matching electron beam area of 2.66×10^3 cm^2 and a 2500-PRF 0.8-liter volume with a corresponding area of 283 cm^2; (2) hot cathode, 10-PRF 200-liter volume with an area of 8.9×10^3 cm^2 and a 1000-PRF 0.2-liter volume with an area of 200 cm^2. The cold cathode gun current efficiency is assumed to be 20 percent with a 0.5 A/cm transmitted current density while the hot cathode gun efficiency is assumed to be 25 percent with a 0.001 A/cm^2 transmitted current density. A large plasma cathode gun example is not given because detailed information on its operational characteristics does not exist.

The input electric pulse energy required by the gun is controlled by pulse width and beam voltage. Gun yield is a desired current density in a specified beam area. A square wave I - V characteristic is assumed for the energy required because it closely approximates the expected pulse shape, having a 95-percent voltage rise over 10 percent of the pulse width followed by a 10-percent drop in voltage and then an unspecified tail. The input electric energy and corresponding voltage and current into the laser volume are based again on the volume, area pulse width, and conversion efficiency. The same idealized square wave assumption, pulse shape, etc., made for the gun electric requirements are also used for the laser pumping electric requirements.

The simplest circuit which one could assume was used to determine the general range of capacitance and inductance which one could expect. The assumptions for the circuit assume an idealized series switch that interrupts the circuit at the end of the pulse, which is described above. The cold cathode gun would be controlled by a switch or more likely by a PFN. The drift field is assumed to switch off when gun current turns off. Although in practice there will be a fairly long tail in the drift current, it quickly drops below a significant level as the electrons recombine, and therefore it does not carry a significant quantity of energy.

Table I summarizes the results of the example lasers assumed.

III. Analysis of a Simple Laser Modulator Circuit

The first step in designing a CO_2 laser modulator system is to choose a specific circuit. The simplified circuit as shown in Figure 11 was assumed as an example case. The basic switching system is not specified.

Referring to the figure, R_L is the resistance of the ionized gas which is time dependent and controlled by highly nonlinear processes. Assume that it is a constant during the discharge time to illustrate the current-voltage domain of interest. The gas is assumed ionizied by hot or cold cathode E-beam guns for comparison for modulation requirements. Let R_s be the source resistance. From elementary circuit analysis the capacitor voltage, V, as a function of time, during discharge, is

$$V = \begin{cases} V_o e^{-\tau} \left[\dfrac{\sinh\left(\sqrt{1 - r^2}\ \tau\right)}{\sqrt{1 - r^2}} + \cosh\left(\sqrt{1 - r^2}\ \tau\right) \right] & \text{for } r < 1 \\ V_o e^{-\tau} (1 + \tau) & r = 1 \\ V_o e^{-\tau} \left[\dfrac{\sin\left(\sqrt{r^2 - 1}\ \tau\right)}{\sqrt{r^2 - 1}} + \cos\left(\sqrt{r^2 - 1}\ \tau\right) \right] & r > 1 \end{cases} \quad (1)$$

where

$$\tau = (R_s + R_L)t/2L \quad (2)$$

and

$$r^2 = 4L/(R_s + R_L)^2 C \quad . \quad (3)$$

The voltage across the load resistance is

$$V_L = \begin{cases} \dfrac{2V_o R_L e^{-\tau} \sinh\left(\sqrt{1 - r^2}\ \tau\right)}{(R_s + R_L)\sqrt{1 - r^2}} & \text{for } r < 1 \\ \dfrac{2V_o R_L \tau e^{-\tau}}{(R_s + R_L)} & r = 1 \\ \dfrac{2V_o R_L e^{-\tau} \sin\left(\sqrt{r^2 - 1}\ \tau\right)}{(R_s + R_L)\sqrt{r^2 - 1}} & r > 1 \quad . \end{cases} \quad (4)$$

A family of curves is plotted in Figure 12. This figure is a graphical representation of Equation (3) with some modifications. The term "normalized voltage" which appears in this figure represents V/V_o, and "reduced time" represents τ of Equation (2). In this manner, Equation (3) can be plotted as dimensionless quantities.

Similarly, Equation (4) is plotted in Figure 13. The only difference here is that the "normalized voltage" refers to

$$\frac{V_L}{V_o}\,\frac{(R_s + R_L)}{R_L}$$

The load current and voltage are required to meet certain pulse shape characteristics. The required rise time is such that the load current or voltage reaches 95 percent of its maximum value in 0.1 t_p (t_p = pulse length). The allowed voltage droop on the capacitor is 10 percent. There is only one value of r which meets this requirement (Figures 12 and 13):

$$r = 0.12 \quad . \tag{5}$$

For this value of r, a 10-percent capacitor voltage droop occurs at

$$\tau = \tau_p = 15 \quad . \tag{6}$$

To uniquely define the four parameters R_s, R_L, L, and C, two more relations are needed.

The maximum power transfer condition

$$R_s = R_L \tag{7}$$

is assumed. The last relationship required can arise from a commonly stipulated parameter. Let E_D equal the amount of energy deposited in the laser cavity per pulse:

$$E_D = \frac{\langle V_L \rangle_{avg}^2\, t_p}{R_L} \quad . \tag{8}$$

This simple relationship is possible because the load resistance is assumed constant. V_L is a time varying quantity and must be averaged over one pulse length.

$$\langle V_L \rangle_{avg} = \frac{V_o}{t_p} \int_o^{t_p} \frac{2R_L\, e^{-\tau} \sinh\left(\sqrt{1 - r^2}\,\tau\right)}{(R_s + R_L)\sqrt{1 - r^2}}\, dt$$

$$= \frac{2\, V_o\, R_L}{\tau_p (R_s + R_L) r^2} \left\{ 1 - e^{-\tau_p} \left[\frac{\sinh\left(\sqrt{1 - r^2}\,\tau_p\right)}{\sqrt{1 - r^2}} + \cosh\left(\sqrt{1 - r^2}\,\tau\right) \right] \right\} \tag{9}$$

$$\langle V_L \rangle_{avg} = \frac{0.2\, V_o\, R_L}{\tau_p\, (R_s + R_L) r^2} \quad . \tag{10}$$

For the particular choice of r and τ_p,

$$\langle V_L \rangle_{avg} = \frac{0.926\, R_L\, V_o}{R_s + R_L} \tag{11}$$

and

$$E_D = \frac{0.857\, R_L\, V_o^2\, t_p}{(R_s + R_L)^2} \quad . \tag{12}$$

Equations (5), (6), (7), and (12) are all that are required to define R_L, R_s, L, and C for given t_p and V_o. V_o is the maximum voltage on the capacitor and is usually a derived quantity rather than a stipulated one. The laser system usually defines the drift field voltage, but, from the above, the voltage is just $\langle V_L \rangle_{avg}$. Therefore, from Equation (11), V_o can be derived from the drift field voltage.

There are other quantities of interest once the values of R_L, R_s, L, and C have been determined: $\langle I \rangle_{avg}$, ΔW, and P, where $\langle I \rangle_{avg}$ is the average current flowing through the laser gas during a pulse, ΔW is the energy supplied by the capacitor for each pulse, and P is the average power supplied by the capacitor. In each case, the equations which will be derived would have to be modified if crowbaring techniques were used:

$$\langle I \rangle_{avg} = \frac{\langle V_L \rangle_{avg}}{R_L} \quad . \tag{13}$$

W_o is the initial energy on the capacitor

$$W_o = \frac{1}{2}\, C\, V_o^2 \quad . \tag{14}$$

If D is the decimal equivalent of the specified droop (0.1),

$$\Delta W = W_o[1 - (1 - D)^2]$$

$$\Delta W = 0.19\, W_o \qquad (\text{for } D = 0.1) \quad . \tag{15}$$

If f_p is the pulse rate of the modulator system

$$P = \Delta W\, f_p \quad . \tag{16}$$

Example 1

Drift field voltage = 100 kV = $\langle V_L \rangle_{avg}$

Energy deposited in laser cavity per pulse = 10^4 J = E_D

Pulse length = t_p = 2 microseconds

Pulse rate = f_p = 50 pulses/second.

Employing the above equations:

$$V_o = 216 \text{ kV}$$

$$R_L = 2\Omega = R_s$$

$$L = 0.267 \text{ } \mu\text{henry}$$

$$C = 4.64 \text{ } \mu\text{fd}$$

$$\langle I \rangle_{avg} = 5 \times 10^4 \text{ amp}$$

$$W_o = 1.08 \times 10^5 \text{ J}$$

$$\Delta W = 2.06 \times 10^4 \text{ J/pulse}$$

$$P = 1.03 \text{ MW}$$

It must be realized that the calculated values merely represent the maximum inductance and minimum capacitance allowed. For larger inductances, smaller capacitances and changes in the values of R_L and R_s will result in a less than an optimum situation with less energy being deposited in the laser cavity.

Example 2

Drift field voltage = 12.5 kV = $\langle V_L \rangle_{avg}$

Energy deposited per pulse = 200 J = E_D

Pulse length = 2 μsec = t_p

Pulse rate = f_p = 50 pulses/sec

$$V_o = 27 \text{ kV}$$

$$R_L = 0.641 \text{ ohm} = R_s$$

$$L = 0.0855 \text{ } \mu\text{henry}$$

$$C = 14.46 \text{ } \mu\text{fd}$$

$$\langle I \rangle_{avg} = 2 \times 10^4$$

$$W_o = 5270 \text{ J}$$

$$\Delta W = 1000 \text{ J/pulse}$$

$$P = 50 \text{ kW}$$

TABLE I. REQUIREMENTS FOR IDEALIZED LASER MODULATOR DESIGNS

	Gun Modulator	Drift Field Modulator		
Gun Type	Cold	Cold	Plasma	Hot
PRF (Hz)	50/2500	50/2500	50/2500	10/1000
Voltage (kV)	-250/-140	+100/-17	+100/-17	+135/-12
Current (kA)	6.7/0.7	50/5.9	5/0.59	0.75/0.083
Energy to Load, R_L (kJ)	3.3/0.2	10/0.2	10/0.2	67/0.67
Pulse Width (μsec)	2	2	20	100
Pulse Risetime*				
Pulse Droop**				
Power to Load (kW)†	165/500	500	500	670
Duty Cycle	0.0001/0.005	0.0001/0.005	0.001/0.05	0.001/0.1
Run Duration††				
Maximum L (μH)	5/26	0.27/0.38	38.5/26.6	180/140
Minimum C (μfd)	0.2/0.05	4.6/3.2	3.2/4.6	17/22

*95% voltage at 10% of width.

**10% of voltage.

†Average

††20 seconds.

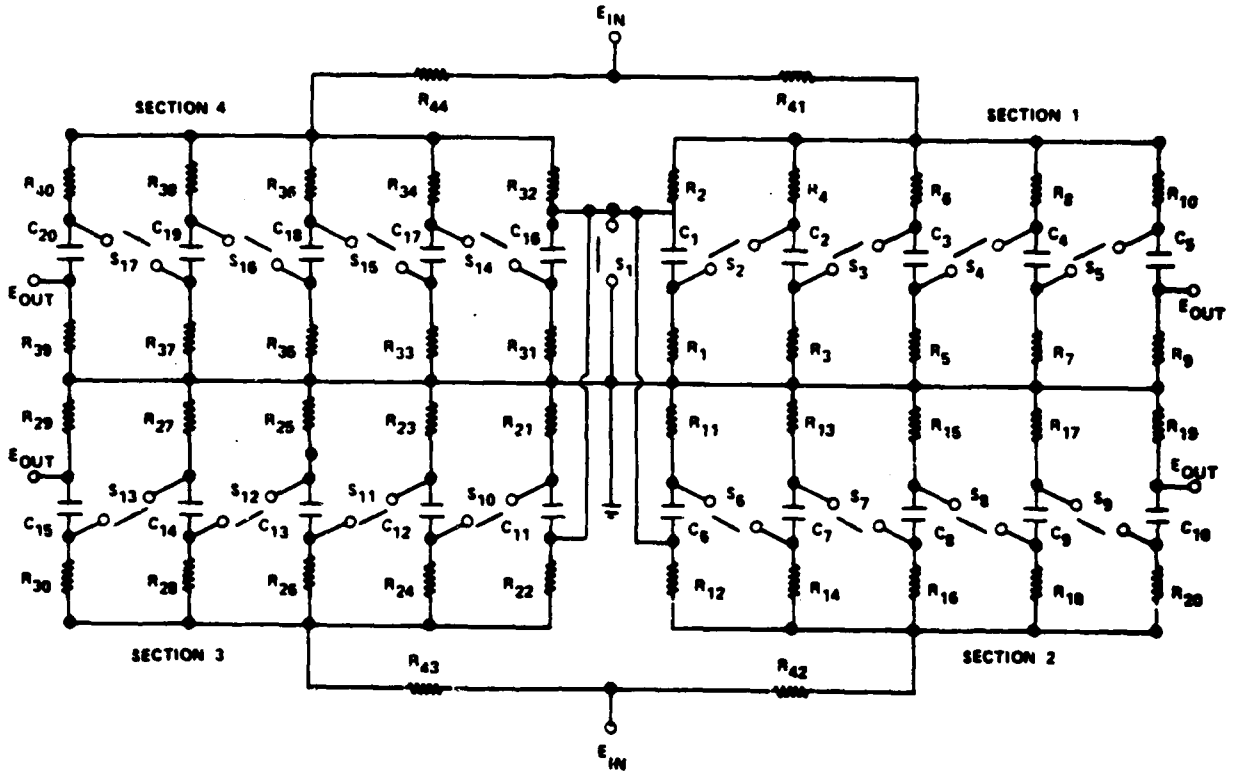

Figure 1. Schematic diagram of quad section pulse generator.

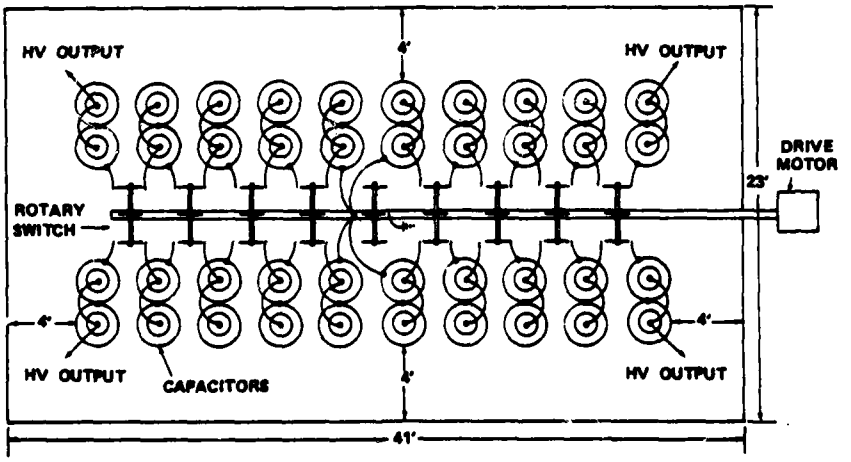

Figure 2. Layout of capacitors and rotary switch in quad section pulse generator.

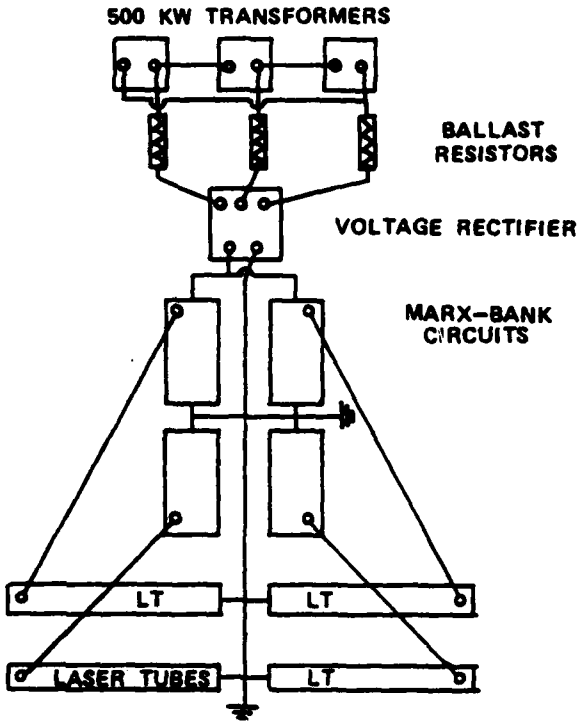

Figure 3. Laser power supply arrangement.

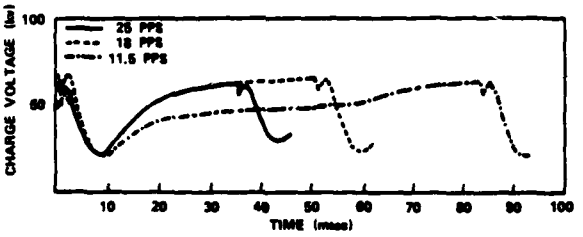

Figure 4. Marx circuit charging characteristics.

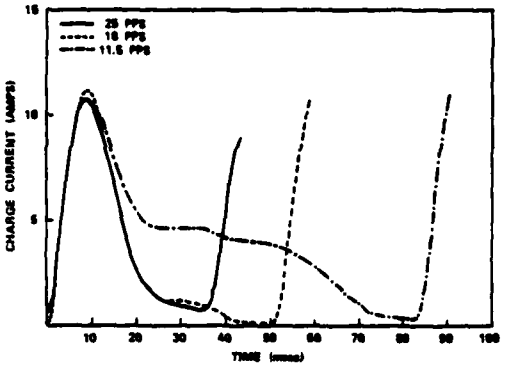

Figure 5. Marx circuit charging characteristics.

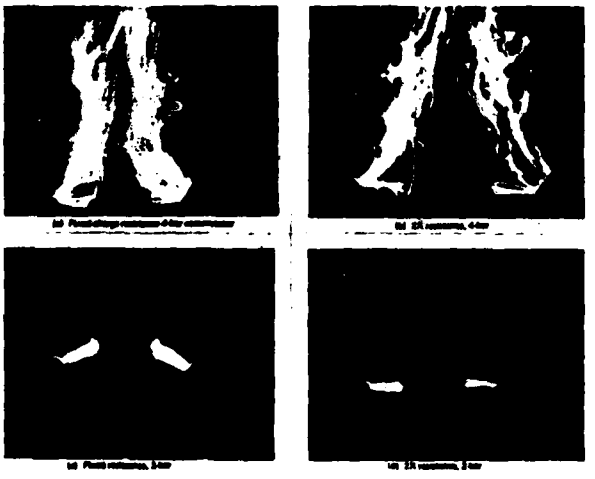

Figure 6. Switch performance at 20 pps.

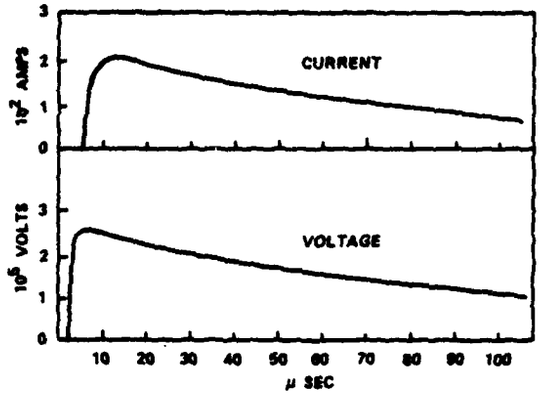

Figure 7. Typical laser tube current and voltage.

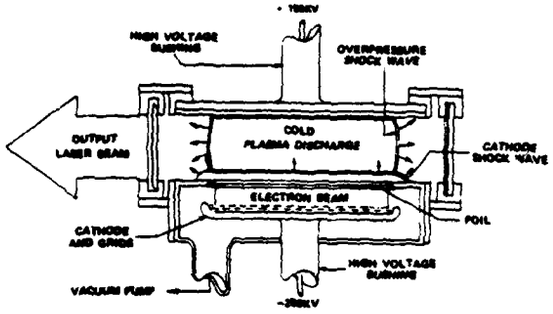

Figure 8. Electron beam controlled laser structure.

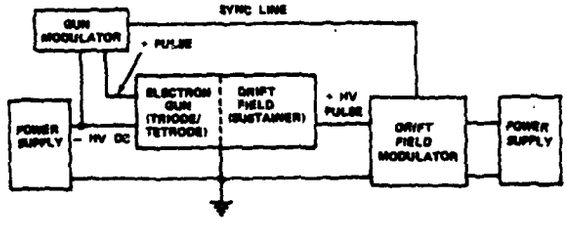

Figure 9. Pulsed laser with hot cathode electron beam augmentation.

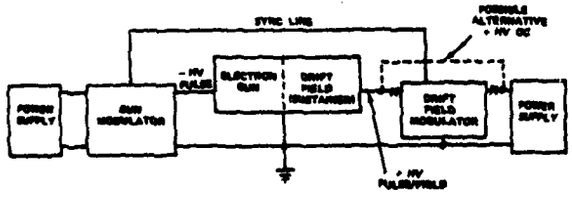

Figure 10. Pulsed laser with cold cathode or plasma cathode electron beam augmentation.

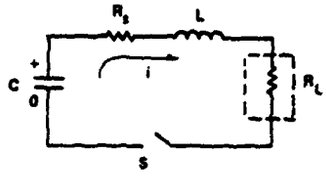

Figure 11. Simplified RLC modulator circuit.

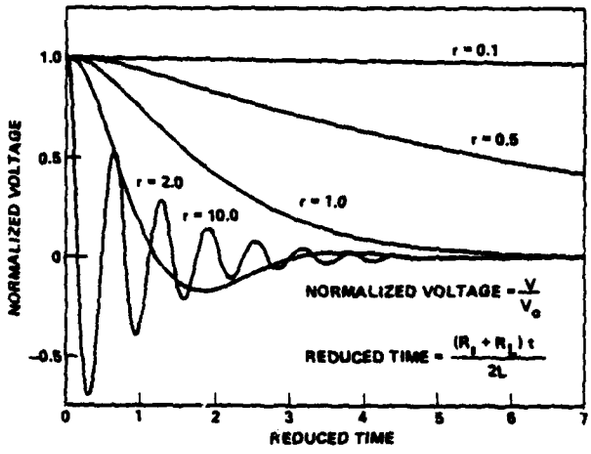

Figure 12. Normalized capacitor discharge voltage.

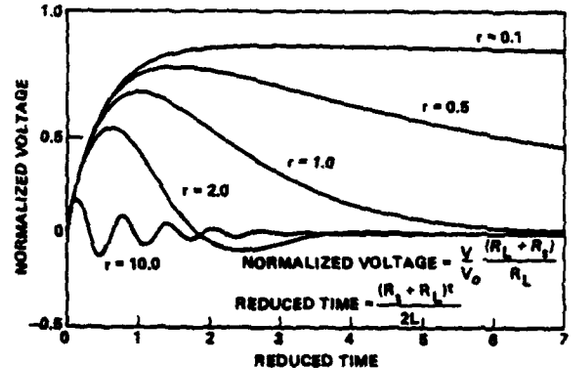

Figure 13. Normalized load voltage.

HIGH VOLTAGE PULSE GENERATORS FOR KICKER MAGNET EXCITATION

D.C. Fiander, D. Grier, K.D. Metzmacher, P. Pearce
CERN, Geneva, Switzerland

1. Summary

The fast ejection facilities at the CERN 28 GeV proton synchrotron (CPS) are being continually expanded to meet the increasing demand for fast ejected beams. The paper describes three new pulse generator systems for the excitation of the kicker magnets of these facilities. Firstly a pulse generator for the fast ejection from the CPS of any desired number of the twenty circulating proton bunches is treated. This equipment can perform up to six ejections per machine cycle with a minimum interval of 25 milliseconds. Extensive life testing of the principal elements such as thyratron switches, cable pulse forming networks and pulsed resonant power supplies is reported on.

Secondly the paper describes the development of a pulse generator for the transfer at 50 usec intervals of single bunches of the proton beam from the CPS to the new 300 GeV machine (SPS) in construction at CERN.

Finally the development of a programmable eleven step pulse generator for the CPS/SPS transfer is described. This generator allows the shaving of the CPS beam during eleven turns, and because of the CPS/SPS diameter ratio, allows the SPS to be uniformly filled. Cable pulse forming networks and thyratrons in a series chain are used to produce the programmable "staircase" waveform which is required. Its satisfactory operation during beam ejection trials is discussed.

2. Introduction

Fast extraction of the accelerated proton beam of the CERN 28 GeV proton synchrotron (CPS) has been a routine operation for the last ten years. The extraction is performed, in the main, by the combined effects of two elements, a relatively fast but low powered magnet known as a "kicker", and a relatively slow but high powered magnet known as a "septum". The kicker magnet induces a betatronic oscillation in the circulating beam; with correct phasing of kicker and septum, the beam which has been kicked passes inside the aperture of the septum magnet and is extracted from the CPS. The beam which has not been kicked continues to circulate outside the septum magnet aperture and is unperturbed.

The original kicker magnets of the CPS were of the reduced aperture, plunging type, i.e. of an aperture smaller than the minimum necessary at injection. In consequence, these could be plunged forward into their working position only after the accelerated beam had shrunk in size. This undoubted complication from the mechanical standpoint had the important advantage of requiring a lower pulse voltage for magnet excitation.

The continued expansion of the fast ejection requirements and the increase in the accelerated beam intensity and emittance highlighted the shortcomings of this plunging magnet system in terms of field rise time, flexibility and useful aperture . In consequence, the decision was taken in 1971 to include in the CPS improvement programme a new static full aperture kicker magnet system which would efficiently undertake the future fast ejection programme. It is the pulse generators of this new kicker system which are described in section 3.

The decision to construct the 300 GeV accelerator (SPS) on the CERN site at Geneva permits the CPS to fulfil a further role as its injector at an energy level of about 12 GeV/c. Two possible transfer schemes were proposed[1]. The first was a bunch by bunch transfer in which the 20 circulating bunches of the CPS would be fast ejected one by one, in a total time of 1-2 milliseconds. For such a scheme, it was proposed to employ the full aperture kicker magnets already mentioned but excited from pulse generators of much higher repetition rate. Laboratory tests were made on prototypes and are reported in section 4. The second transfer scheme was a "continuous" extraction of the beam during 10 or 11 CPS revolutions. This transfer is achieved by a programmable fast orbit bump in conjunction with electrostatic and electromagnetic septum magnets. As such an extraction system was untried on any of the world's large accelerators, it was decided to mount a full scale trial on the CPS. This proved successful and the decision was taken to employ "continuous"extraction for the CPS/SPS transfer. The pulse generators for the excitation of the programmable fast orbit bump magnets used in these trials are described in section 5, together with the proposals for the final equipment which must be installed in 1975.

3. Pulse generators for routine fast ejection from the CPS

3.1 Operational requirements

The Full Aperture Kicker (FAK) system is the fast element of the fast ejection process. If this process is to have high efficiency, the field rise time of the kicker magnets must not exceed the proton-free interval between bunches of the circulating beam. Furthermore if partial ejection of the beam is required, then the field fall time must satisfy the same condition. In the CPS the bunch interval is 105 nsecs and the bunch length foreseen for high intensity operation (10^{13} protons per pulse) is 30 ns. Theoretically, the FAK field rise and fall times must not be greater than 75 ns; in practice, the design has been based on 5-95 % times of 70 ns.

Up to six ejections are required per CPS cycle, with a minimum interval of 25-50 ms. The pulse length must be adjustable so as to eject from 1 to 20 bunches per ejection. The kick strength of the system has to be adjustable such that constant beam displacement is obtained at the septum magnet over the full energy range of fast ejection (typically 10-28 GeV/c).

3.2 Choice of system

The choice of system to meet these operational requirements is further influenced by the available space for magnets on the CPS beam line, by arbitrary high voltage limits and by the performance and reliability of the high voltage switching.

In order to obtain the required kick strength in the specified rise time, at reasonable levels of pulse generator voltage, it is necessary to employ a modular magnet system. In this way, the total kick is the sum of the individual magnet kicks whereas the excitation voltage is limited to that which is necessary to establish the field in a single magnet. An arbitrary pulse forming network (PFN) charging voltage of 80 kV was set, resulting in a 9 magnet system.

The best field rise time is obtained from a delay line single turn magnet. The performance of such a magnet is however significantly influenced by the choice of characteristic impedance due to parasitic inductance in the capacitor branches. Best performance is obtained from

magnets of high Z_o. Unfortunately, the machine space occupied by the system increases linearly with Z_o. This conflict between machine space and performance was resolved by the compromise choice of Z_o = 15 ohms.

The FAK system therefore required 9 identical pulse generators of Z_o =15 Ω, PFN charging voltage 80 kV, pulse length variable over the range 105-2100 ns and minimum pulse/pulse interval of 25 ms. The current rise time into an ideal load had to be sufficiently fast so as to meet the specified field rise time, taking into account the propagation delay of the magnets, chosen as 55 ns. Measurements showed that the field rise specification could be met provided the pulse current rise time (10-90 %) into an ideal load did not exceed 33 ns.

Spark gap switching would have ensured a fast current rise time but was rejected in favour of thyratron switching on account of jitter and voltage hold off problems which were anticipated with a 25 ms pulse interval. The required rate of rise of current, about 90 Amperes per ns, was considerably in excess of the tube maker's published rating but was felt to be attainable with careful thyratron housing design.

Two options were available for pulse length variation. The first, as used for the existing CPS fast ejection[2] and also that of Serpukhov[3], employs an artificial PFN with three switches - a main switch for the pulse front, a short-circuiting switch or "clipper" for the pulse tail and a dump switch for discharging any residual line energy into a terminator. The second option is to use a very good quality cable PFN switched by a main switch at one end for the pulse front and a dump switch at the remote end for the pulse tail. It was this second option which was chosen as it was felt to give greater simplicity and hence greater reliability. It also reduced the number of expensive thyratron switches in the system.

Fig. 1 shows the schematic diagram of the pulse generator for one magnet of the multi-magnet FAK system.

3.3 PFN Design and Performance

Low attenuation gas impregnated polythene tape cable is used for the PFN. Its tubular inner and outer conductors are respectively of copper and aluminium. The dielectric consists of 60 lapped polythene tapes, pressurised to 9 atmospheres with SF_6. Semi-conductors are avoided at the dielectric/conductor boundaries in the interests of low attenuation.

The chosen cable impedance of 15.0 Ohms is not ideal from either voltage stress or attenuation standpoints but a single cable is preferred to a parallel system of higher impedance cables on account of mechanical simplicity. The cable outer diameter is 54 mm, this being judged the upper limit from the point of view of bending radius and installation. The resulting attenuation is 0,44 dB/100 metres at 10 MHz and the maximum electric stress 13 kV/mm.

The cable attenuation distorts the pulse derived from the PFN causing droop of the flat top and a "tail" after the pulse fall. The flat top droop is proportional to the per unit cable attenuation and $\sqrt{\text{pulse length}}$. For the chosen cable, the droop is 1.4 % for the longest required pulse of 2100 ns.

The "tail" of a pulse derived from a PFN is normally due to the deformation of the "off" step function by two traversals of the cable. In the case of double ended switching, the tail is due to the deformation of the dump switch step function after single traversal of the cable. The double switched PFN therefore has less "tail" than a single switched PFN. The "tail" is sensibly constant irrespective of the pulse length - this is not a disadvantage in a kicker magnet system where the field must fall between proton bunches irrespective of the number

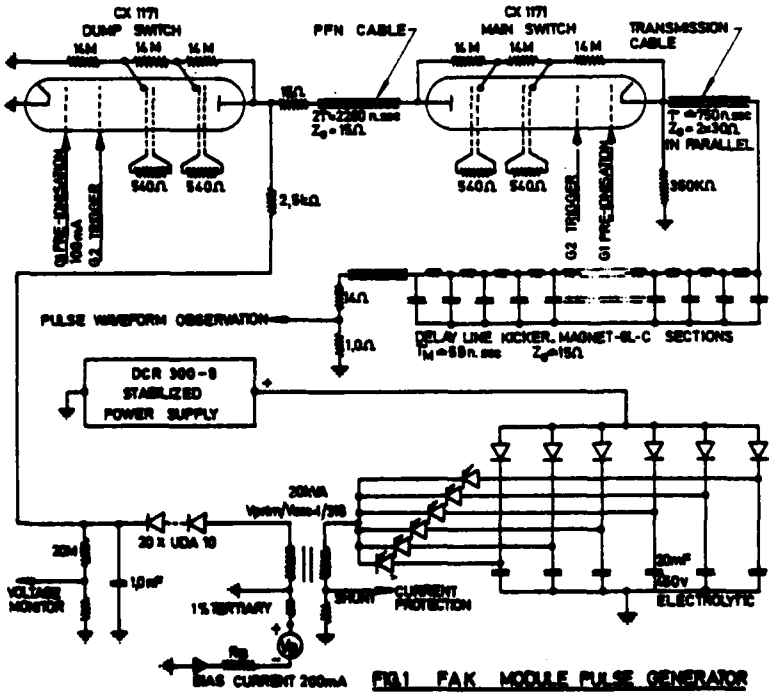

FIG 1 FAK MODULE PULSE GENERATOR

previously ejected. Typical "tail" amplitudes for the system are 2.5 % at 100 ns and 1.5 % at 200 ns.

The pressurised cable is ionisation free at 70 kV RMS 50 Hz. The gas pressurisation also allows compact terminations to be used, minimizing the mismatch in impedance. The PFN cable termination is shown in Fig. 2.

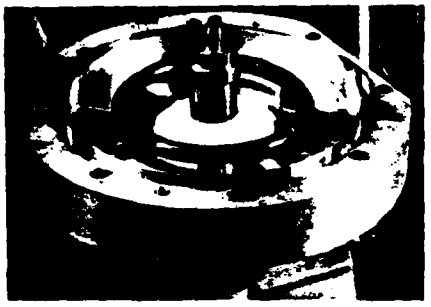

Fig. 2 - PFN Cable Termination

3.4 Power Supply

The power supply for recharging the PFN is shown in Fig. 1. It is basically a pulsed resonant system using a step up transformer to couple a primary electrolytic capacitor to the PFN via a HV diode. The PFN charging time is 3.7 ms. Typical recharging current and voltage waveforms are given in Fig. 3.

Fig.3 Power supply waveforms

In order to make full use of the transformer core a tertiary winding with d.c. bias is provided. This tertiary circuit also controls the transformer backswing and determines the minimum permissible pulse to pulse interval if core saturation is to be avoided.

"Doorbell" module diodes rated for 200 kV are used to isolate the PFN from the power supply. This has the advantage of avoiding transformer saturation should the PFN fail to be discharged. The operational flexibility between power supply trigger and PFN discharge is thus much greater than in a directly coupled system. An R-C filter is necessary to protect the diode stack from the fast dump switch pulse.

Multiple shot operation is achieved by using multiple primary electrolytic capacitor banks with individual thyristors. These banks are recharged during the CPS cycle which has a minimum duration of 1 second.

The short term stability of a given shot from cycle to cycle is better than 2 per mil. However, thermal drift from a cold start over the first few hours of operation can cause a 2-3 % variation in output voltage for fixed primary capacitor voltage. This problem is overcome by a step by step servo which compares the PFN voltage measured by high voltage divider against the preset reference. The charging voltage of the primary electrolytics is then adjusted step by step to maintain the PFN voltage within a dead-band of 0.2 kV.

3.5 H.V. Switching

Both the main and dump switches are triple gap ceramic envelope thyratrons, type CX1171. The switching performance of the CX1171 meets the requirements for the project provided that the PFN is recharged from a pulsed resonant supply. Under these conditions, the 10-90 % rise time for the required current of 2.7 kA is between 28 and 30 ns. Jitter, including low and intermediate voltage electronics, is generally less than 6 ns. Certain tubes exhibit approximately twice this jitter when new, there being a distinct jump in anode delay time for certain pulses. The result is that the pulse rise on multi-exposure photographs is presented as two separate bands. This effect usually disappears after the tubes have pulsed a few million times (Fig. 4).

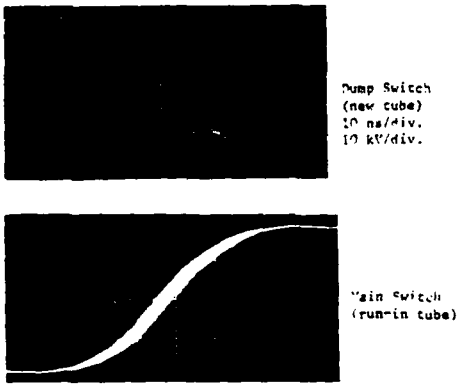

Fig. 4 : Pulse rise time and jitter

The use of slow recharging power supplies is not recommended because the tubes break down spontaneously during the recharging period. This can be prevented by lowering the reservoir voltage but then the fast pulse rise time is lost. Fig. 5 demonstrates this effect; anode voltage is plotted against recharging time for a constant reservoir voltage and spontaneous breakdown rate.

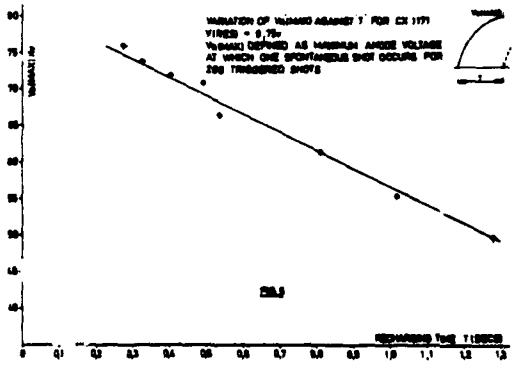

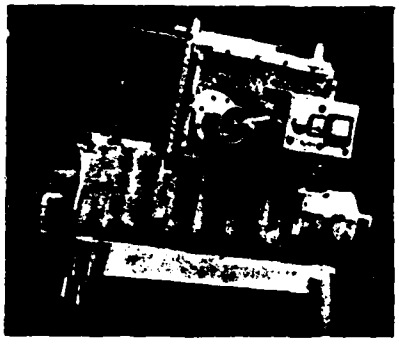

Fig. 6: CX1171 Main Switch

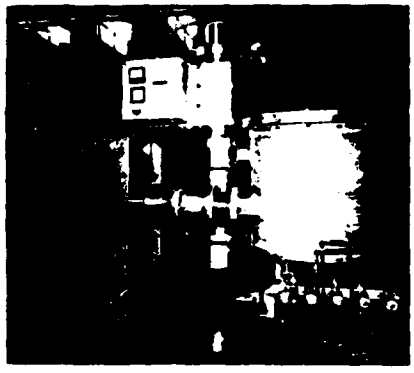

Fig. 7 - CX1171 Dump Switch

The main switch assembly is shown in Fig. 6 with one of its protective covers removed. The gas filled PFN cable is connected on the right and the transmission cables leading to the magnet are in the bottom left hand corner. The CX1171 of the main switch operates with floating cathode. The heater, reservoir and grid 1 supplies are derived from an insulated Faraday cage (visible on the face of the equipment). This cage is supplied with stabilised 220 Volts via an oil insulated isolating transformer. Adjustment of reservoir voltage and hence rise time is possible with the equipment pulsing.

The CX1171 is lodged in a coaxial housing of 162 mm diameter. The dielectric between tube and housing is a mixture of oil and epoxy resin cylinders. Forced oil circulation is used to maintain the dielectric strength and remove heat. The initial oil filling is made under vacuum.

Grid 1 is d.c. primed at 100 mA. A photoelectric device enables the grid 1 current to be used as an interlock in the PFN charging circuit. Grid 2 is pulsed via a 1:1 inverting and isolating transformer. Typical grid 2 rise time is 50 ns to 1000 Volts unloaded.

Voltage division across the series gaps of the CX1171 is effected by chains of 2W carbon mass resistors, the total resistance per gap being 14 M. Capacitive compensation of this voltage divider is not necessary for the PFN recharging time of 3.7 ms.

The dump switch assembly is shown in Fig. 7. This assembly embraces not only the CX1171 tube but also the 15 Ω dump resistor and the high voltage components of the pulsed resonant power supply. The dump switch and dump resistor are so arranged that the tube operates with grounded cathode. This simplifies the supply arrangements for the tube heater, reservoir and grid 1. In other respects, the dump switch design follows closely that of the main switch with the same choice of dielectric and forced oil circulation.

The 15 Ohm dump resistor is a large carbon mass assembly which uses 1 Ω Morganite discs. Fourteen discs are stacked with interleaved porous metal washers, the assembly being kept under 400 kg load by a compression spring. Cooling oil is delivered to a central oil gallery passing axially through the stack. The oil is forced through the porous metal washers, effectively cooling the discs on all faces. The resistance has a negative coefficent of 0.3 % per °C. Minor alteration of the resistance value is made by adjustment of the cooling oil temperature. Resistance stability both during the pulse and from pulse to pulse is excellent.

A very similar type of terminator is used for absorption of the pulse transmitted to the magnet.

3.6 Proving Tests

For the purposes of verifying the pulse generator performance and for life testing its components, the circuit of Fig. 8 was constructed. This allowed the

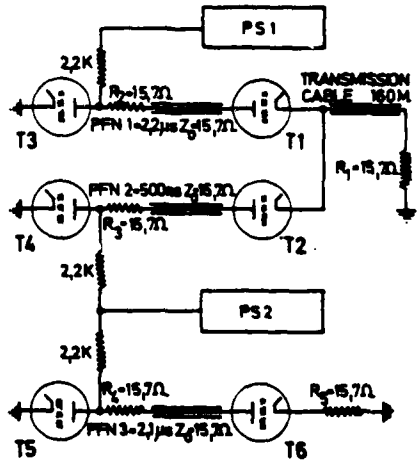

FIG 8. PULSE GENERATOR TEST CIRCUIT

simultaneous testing of six CX1171 tubes (T1-T6), two pulsed resonant power supplies (PS1 - 3 shots/cycle; PS2 - 6 shots/cycle), three cable PFN's, five terminating resistors and a transmission cable. Three of the thyratrons operated as main switches and three as dump switches. Further two main switch thyratrons T1, T2 had

their cathodes coupled, this in order to prove the arrangement which would be necessary if bunch by bunch transfer were chosen for the CPS/SPS ejection system. It was found that tubes T1 and T2 were able to withstand the pulse inverse voltage provided that their respective PFN's were not charged. The system was operated on a one second cycle, PS1 furnishing 3 pulses at 50 ms intervals followed by 6 pulses from PS2, again at 50 ms intervals.

The tests were carried through to the stage shown in Table 1. Tube failures were limited to two, T3 and T4 both due to filament failure. High voltage failures were limited to two breakdowns in solid polythene flexible cable used for coupling terminator R1 to the gas filled cable transmission line. As will be seen from Table 1, most major components survived more than 8'000 hours of operation and 10^8 pulses. Further there was virtually no fall off in switching performance of the tubes either in respect of rise time or jitter.

Table 1

Position	Tube Type	Filament Hours	Pulses x 10^6	Remarks
T1	CX1171	7176	70,3	
T2	CX1171	6530	113.2	
T3	CX1171	9421	109.3	failed-heater O/C
T4	CX1171	6833	124,3	failed-heater O/C
T5	CX1171	8006	144.0	
T6	CX1171	12220	203.5	

3.7 Present State of Project

The project is in the state of final assembly with a view to its operation for beam extraction in early 1974. The kicker magnets have been built and tested in their vacuum tank and will be installed on the beam line in September 1973. Performance meets the design specification except in respect of the remanent field. This will be corrected at a later date by replacing certain of the magnet ferrite C-cores with better material.

The pulse generator construction is well advanced. (Fig. 9).

Fig. 9 Final assembly of FAK pulse generators

Commissioning tests will start in September. As the pulse generator design follows very closely the successful equipment used for the proving tests, it is not anticipated that major problems should occur. One spare pulse generator has been built and commissioned. It has served for kicker magnet testing. The pulse output into a matched load is shown in Fig. 10.

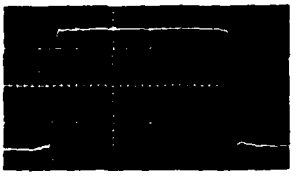

Fig. 10 : FAK Pulse Generator into matched load

4. CPS/SPS Bunch by Bunch Transfer Pulse Generator

The bunch by bunch transfer method between the two synchrotrons in only an extension of the well tried single bunch fast ejection process. The proposal was therefore to use the FAK magnets reported on in the previous section but excited by fixed length pulses derived from separate short PFN cables charged to 40 kV. The major difficulty anticipated for the process lay in the switching performance at high repetition rates, bearing in mind the specified interval of 50 μs between ejections. Further problems were anticipated in developing power supplies capable of rapidly recharging the PFN's. Laboratory models were constructed to verify that the difficulties could be overcome.

4.1 General description of Pulse Generator

The complete scheme foreseen for this form of CPS/SPS transfer is shown in Fig. 11.The short cable PFN's

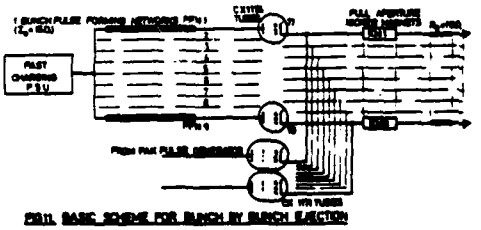

Fig. BASIC SCHEME FOR BUNCH BY BUNCH EJECTION

(2τ = 105 ns; Z_o = 15 Ω) are switched by CX1154 tubes into their respective FAK magnets. Further the CX1154 cathode is coupled to that of the CX1171 of the slower repetition rate pulse generator reported in section 3. All 9 short PFN's are recharged from a single fast cycling power supply.

For the purpose of laboratory tests only one short PFN and CX1154 switch were built. However in order to provide a representative load for the fast cycling

power supply, an additional PFN cable and switch were added so as to bring-up the total PFN cable capacitance to that of 9 short PFN's (Fig.12). The CX1154 was mounted in a low inductance coaxial housing similar in design to that of the CX1171 already described.

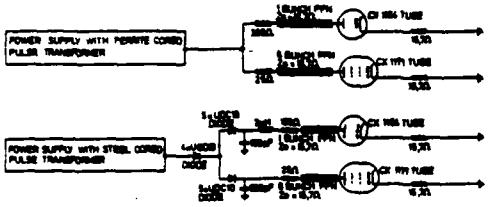

FIG 12 TEST SCHEME TO SIMULATE THE PFN LOADING

Initially two solutions were retained for the fast cycling power supply, although both involved the principle of resonant charge. The first was resonant charging from a storage line of wave propagation time exceeding the whole ejection process (i.e. > 1 ms) using a CX1154 tube as the switching device for controlling the instant of recharge. The second was by resonant charging via a step up pulse transformer, the energy being stored in 20 primary capacitors having individual thyratron switches. After preliminary laboratory trials, the long storage line solution was abandoned in favour of the pulse transformer because the latter was more reliably controlled and switched.

In fact, two variants of the pulse transformer were constructed for the laboratory tests. The first[4] is shown in Fig. 13. It uses a ferrite cored pulse transformer, the secondary being directly coupled to the PFN load. Pulsed premagnetisation is employed to obtain a core flux swing from - 2 kG to + 3 kG. The transformer core recovery system involves a quarter turn tertiary winding with diode and damping resistor together with an inverse diode and R, C elements across the secondary winding. 1 uF primary capacitors are used, switched by

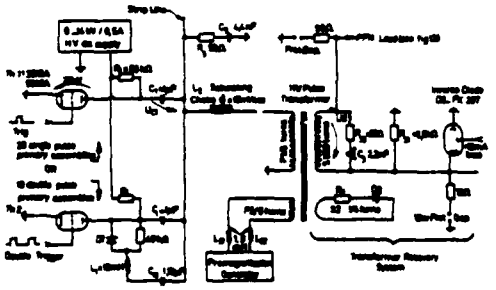

FIG 13 FERRITE CORED TRANSFORMER POWER SUPPLY

5949A thyratrons. The supply is able to charge a 40 nF load to 40 kV in 7 us at intervals of 50 us. For economy reasons only 10 primary capacitors and switches were provided for the laboratory tests. The second supply [5] is shown in Fig. 14. It is a speeded-up version of the type of supply previously described in 3.4,

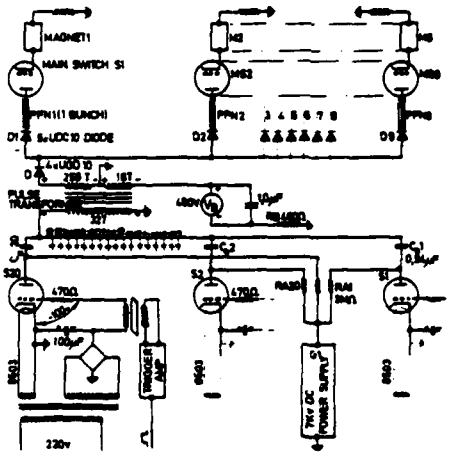

FIG 14 STEEL CORED TRANSFORMER POWER SUPPLY

using a 4 mil strip wound silicon steel core transformer of low leakage inductance. It is able to charge 40 nF to 40 kV in 14 us and the transformer backwing is sufficiently fast for the supply to be used at 50 us intervals without causing core saturation. The primary capacitors are 1 uF, switched by 8503 thyratrons. Again for economy reasons, only 4 primary circuits were provided for tests.

4.2 Results of Laboratory Tests

It was possible to produce a train of up to ten pulses into a matched load at 50 us intervals using the ferrite cored pulse transformer power supply. Similarly a train of up to four pulses could be obtained from the steel strip cored transformer power supply. With suitable adjustment of reservoir voltage, the CX1154 switched reliably at 50 us intervals. However certain interesting effects were observed which may be summarised as follows :

a) the rise time of the first pulse of the train was significantly (20-30 %) slower than the rise time of all subsequent pulses in the train (Fig. 15).

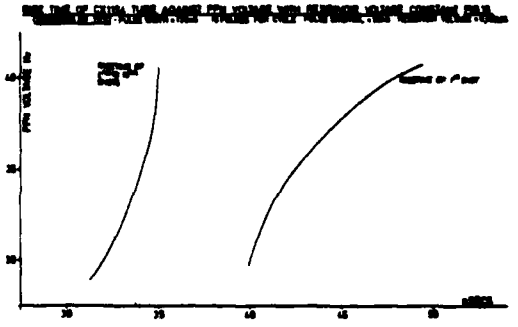

b) raising the reservoir voltage to improve the first pulse rise time would result in spontaneous breakdown of the CX1154, initially on recharging for the last pulse of the train. Further increase of reservoir voltage would cause CX1154 breakdown progressively earlier in the train.

c) the pulse rise and flat top were independent of the type of resonant power supply used. The pulse fall was not, due to the fact that both power supplies released a certain energy into the pulse fall, degrading the fall with respect to the rise. In the case of the ferrite-cored device, the tail energy depended on the design of the transformer core recovery system. In the case of the steel cored device, the energy depended on the filter necessary to protect the semi-conductor diodes from the CX1154 switching surge.

d) switching performance of the CX1154 was less consistent when generating an irregularly spaced pulse train of minimum interval of 50 μs. In these circumstances, the pulse rise time could lie between the extremes noted in a), and the onset of spontaneous breakdown occurred at lower PFN voltages.

e) the slower recharging of the PFN by the steel cored transformer system appeared to lessen the risk of CX1154 spontaneous breakdown.

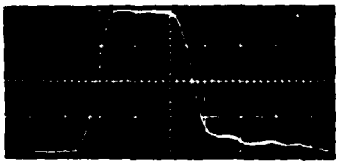

50 nsecs/div.
5 kV/div
V_{PFN} = 40 kV
V_{RES} = 6.1 Volt

10 superimposed pulses showing the 1st slow pulse and long tail

20 nsecs/div
10 kV/div.

Fig.16 PFN charging using the steel cored transformer

Oscillograms of the performance of the pulse generator are shown in Fig. 16. The upper photograph shows ten superimposed pulses of the train; the first pulse rise is clearly slower than the rest. The lower photograph shows the PFN voltage for four pulses of the steel cored pulse transformer supply. Fig. 17 gives the results of the best possible pulse rise times for a ten pulse train as functions of PFN and reservoir voltages.

In conclusion, it can be said that this fast cycling pulse generator worked well but was subject to certain limitations, which would in all probability have been even more serious for a 20 pulse train. Whether or not the quality of the pulse train would have been acceptable for excitation of the FAK magnets for the CPS/SPS transfer is questionable. For this reason, coupled with the advantage of inherently smaller emittance of continuous transfer, the bunch by bunch system was abandoned.

V_{RES}	t_r 1st Pulse	t_r 2nd-10th Pulse	PFN Test (kV)
5.92	50 nsecs	36 nsecs	
6.02	48 "	34 "	
6.07	45 "	33 "	
6.11	40 "	32 "	
6.15	37 "	30 "	30
6.2	37 "	30 "	
6.25	35 "	28 "	
6.4	33 "	27 "	
6.55	30 "	25 "	
5.97	50 "	36 "	
6.06	42½ "	35 "	
6.15	40 "	32½ "	35
6.2	37½ "	30 "	
6.25	35 "	30 "	
6.1	48 "	35 "	
6.15	48 "	34 "	40
6.2	48 "	34 "	
6.04	50 "	37 "	
6.07	50 "	35 "	45

Fig. 17 - Table of Results

5. CPS/SPS Continuous Transfer Pulse Generator

The continuous extraction method[6] of transferring the CPS beam to the SPS consists of locally bumping the beam turn by turn onto an electrostatic "shaving" septum. The length of the beam shaved off by the septum over 11 turns corresponds to the circumference of the larger SPS ring to which it is transferred before being further accelerated. Further the shaved beam has a smaller emittance than that of the circulating CPS beam. The lateral bumping of the CPS beam is done by two lumped inductance, two turn ferrite cored dipole magnets. The first magnet kicks the beam and the second identical magnet, located downstream of the electrostatic septum, cancels the kick, leaving the beam undisturbed in the rest of the ring.

5.1 General description of Pulse Generators

The magnets are powered by two identical pulse generators[7] delivering a "staircase" current pulse with 11 steps (Fig. 18). Each step in the pulse deals with one turn of the CPS beam and therefore lasts one CPS proton rotation time (2.1 μs). The magnitude of each step is set to give a constant ejected beam current of the shaved beam.

Fig. 19 is a simplified schematic of the dual "staircase" pulse generator which was built for feasibility studies. The design is based on standard RG220U coaxial cable pulse forming networks (PFN's), switched by high voltage thyratrons.

About 10 ms before the magnet pulses are required, the PFN's are charged simultaneously by pulsed resonant power supplies, pairing the PFN's in pairs. For a "climbing staircase" pulse (the normal case) PFN 1A and 1B are charged to the lowest voltage, about 25 kV, and PFN 11A and 11B to the highest voltage, about 50 kV.

Each pulse forming network (of travelling time τ) and associated thyratron, when triggered, contributes a square current pulse of width 2τ which arrives in the magnet after having traversed the intervening PFN's and

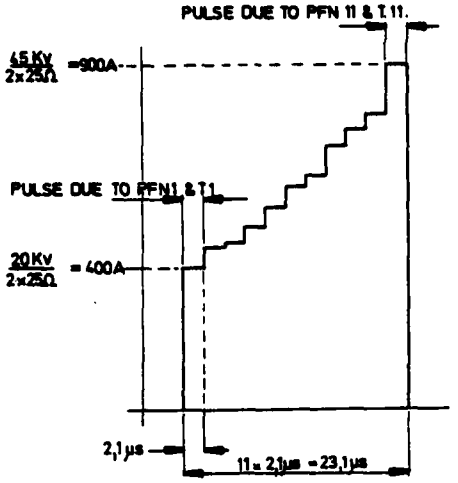

FIG 18. 11 STEP STAIRCASE PULSE

thyratrons. If the thyratrons T1 to T11 are sequentially triggered with a delay of τ between each trigger pulse, the PFN discharge pulses arrive as a pulse burst in the magnet with the tail of one pulse coinciding with the start of the next, thus producing a theoretically perfect "staircase" output pulse of total length 11 x 2 τ = 22τ. In practice, the pulses suffer from the usual transmission attenuation causing rise time and flat top distortion which affects the pulse from T11 much more than from T1. The switching delay of the thyratrons, which, if uncorrected, would produce gaps between the fall of one pulse and the rise of the next, is compensated by adding approximately 200 ns to the PFN length and triggering the thyratrons slightly early. The energy in the added length of PFN is found in the tail of the total output pulse which does not reach the magnet before the CPS is emptied of protons.

Figs. 20 and 21 show two typical output pulses of the pulse generators. It can be seen that the rise time to flat top of the first step, determined mainly by magnet inductance and system impedance, is less than that of the last step which has traversed all eleven PFN's and the transmission cable before reaching the magnet. Fig. 21 illustrates that the pulse generator is capable of delivering negative steps, and in fact, can produce almost any pulse shape built up step by step provided the reverse voltage across a thyratron is within acceptable limits. This flexibility has been of great use in trimming the staircase pulse to compensate for coherent beam oscillations resulting from minor imperfections in certain machine elements.

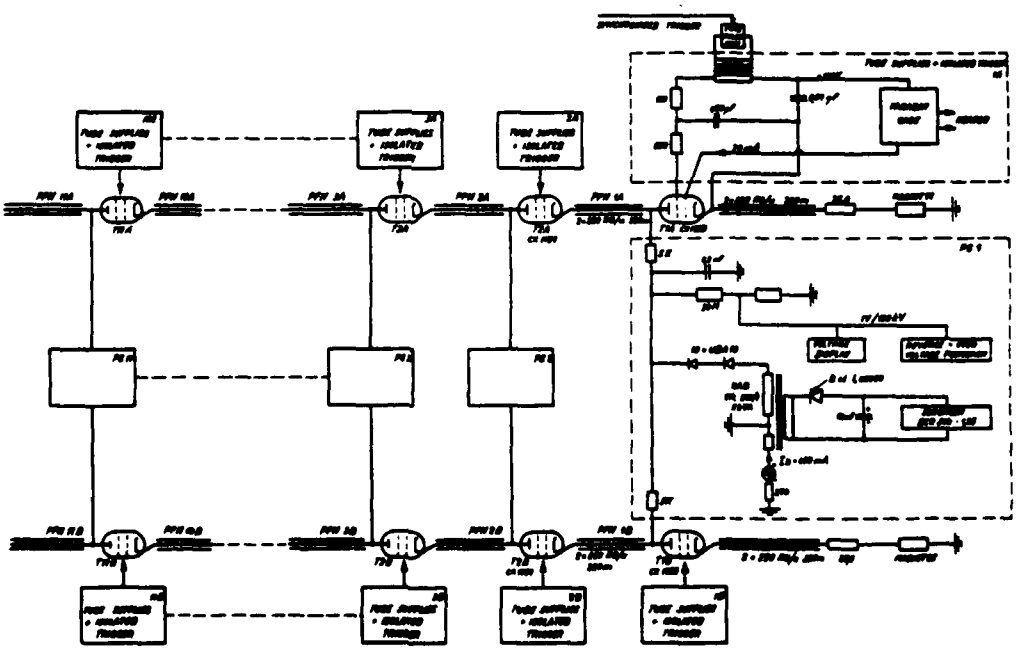

Fig. 19 - Schematic diagram of "staircase" pulse generator

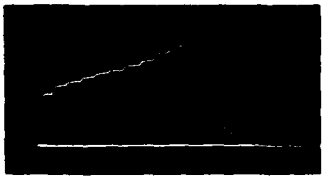

5us/div.
300 A/div.
(= 48 kV PFN 11)

Fig. 20 : Typical staircase output pulse showing steps and pulse tail

Fig. 21: Ascending and descending staircase pulse used in CPS trials

5.2 Results of Trials on the CPS

5 μsec/cm

Fig. 22 External beam current with bumpers excited with waveform of Fig. 21

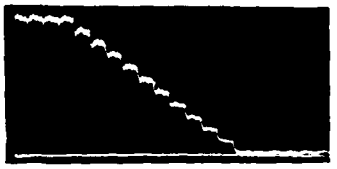

5 μsec/cm

Fig. 23. Falling intensity of PS circulating beam over 11 turns corresponding to ejected beam intensity of Fig. 22

Ejection trials started in early May 1972 since when a number of successful ejections have been made under various controlled conditions. Figs. 22 and 23 show respectively the ejected beam current in the transfer channel from CPS to SPS and the falling intensity of the CPS circulating during 11 turns.

5.3 Proposed final equipment for CPS/SPS transfer

The specification for the transfer hardware to be installed in the CPS in 1975 is somewhat stiffer than it was for the experimental apparatus; the intensity of the CPS beam will be increased and the kick required from the bumper magnets is considerably greater. For this reason, it is proposed to split each magnet and its associated staircase pulse generator into two components. The base of the pulse will be furnished by a lumped element storage line of 23 μs pulse length, switched by a thyratron into its own magnet. The remainder of the staircase waveform will be produced by a pulse generator similar to the prototype described above, pulsing into a second magnet. This approach has a number of advantages.

Firstly, since the individual magnets are shorter, the magnet inductance is lower and the pulse rise time is reduced. The voltage on the PFN's of the staircase part of the system is lower than it would be otherwise and enables the continued use of RG220U cable as storage lines. Lastly, the reflections at the magnet, due mainly to the large fast front step, are confined to the base pulse generator where they are much more easily absorbed than in the multi-thyratron staircase generator.

6. References

1. Design of the European 300 GeV Research Facilities, Vol. II, Chapter 3.
2. Design Study, Fast Ejection Channel A, Serpukhov 70 GeV Proton Synchrotron - CERN/PS/FES/TN-49.
3. Operation Straight Flush - H. van Breugel at al - CERN/NPS/Int. 67-11.
4. Experimental Results on a Fast Cycling Pulsed H.V. Power Supply - A. Brückner, A. Plunser - CERN/72-5.
5. A Proposal for a Pulse Generator for Bunch by Bunch Transfer CPS/SPS - D. Fiander, P. Pearce - CERN/MPS/SR Note 71-37.
6. Continuous Transfer from CPS to SPS - C. Bovet - 300/DI/PA/INS 2.
7. Fast bumper magnets and associated Pulse Generators for 11 turn Extraction - D. Fiander - CERN/MPS/SR 72-2.

ANALYSIS OF PHASED ARRAY RADAR POWER SUPPLY SYSTEMS OPERATING UNDER VARIABLE PULSE LOADING CONDITIONS

C. J. EICHENAUER, JR.
General Electric Company - HMES
Syracuse, New York

Detailed quantitative analyses of phased array power systems are often required as a result of the radar system's variable pulse templet operating conditions. A matrix format, with system capability factors forming columns and system operating modes forming rows, is presented as a useful type of display for the quantitative results of a power supply system analysis. Four alternate forms of system analysis are then examined, use of steady state techniques, use of analog computer techniques, development and use of special purpose digital computer programs, and use of one of the general purpose user oriented circuit analysis programs. Examples of a power supply system analog computer analysis and a CIRCUS 2 digital analysis are presented. Advantages and disadvantages of each method of analysis are discussed.

INTRODUCTION

A number of complex operating requirements, inherent in current phased array radars, often necessitate a detailed analysis of the radar transmitter's power supply system. Evaluation of a candidate power supply system design typically involves consideration of three interrelated areas, first , the prime power generating equipment's output capabilities, second, the a-c to d-c conversion equipment's output capabilities, and third, the system's component parts capabilities. These three capability areas should in turn be evaluated in terms of the radar system's operating requirements which typically include a power supply energization or snap-on mode, a constant duty factor pulse templet loading mode, a variable duty factor pulse templet loading mode, and a transmitting tube fault diversion mode. Figure 1a illustrates in simplified block diagram form the capability areas by means of number designators and the operating modes by means of letter designators. Figure 1b illustrates a simplified matrix format which is useful for displaying the quantitative results of an analysis. In a typical analysis, the required information is most effectively obtained by means of computer aided design techniques. Before examining several alternate approaches for obtaining such quantitative results, the three capability areas of the matrix will be expanded for purposes of clarification.

EVALUATION CRITERIA

Turning first to the prime power source capability related areas, figure 2a tabulates a number of factors which are frequently of significance. It should be noted that in the illustration shown below the tabulation, some of the elements indicated may not be of a controllable nature or otherwise defined in a full quantitative sense. However, as a minimum the distribution system impedance and the nature of all major attached circuit loads must be defined if the system's prime power/a-c to d-c converter interface voltage regulation and voltage unbalance are to be established. The voltage and/or current distortion present at the interface is a complex function involving the impedances and commutating effects associated with the a-c to d-c converter and the impedances (sometimes of a variable nature) associated with the generator. During the snap-on and fault diversion modes, quite high inrush currents and rates of change of current frequently occur. In addition to the factors just noted, saturation of iron core components may further accenuate these high current effects. Finally, line thump, which has been defined as the peak instantaneous power deviation about the maximum average power load, may be a factor of particular significance where certain classes of variable duty factor pulse templets are encountered.

Expansion of the a-c to d-c conversion area capabilities is shown in figure 2b. In this case, in contrast to the prime power source area, the characteristics of the major blocks indicated below the tabulation are basically under the control of the equipment designer. For example, in the snap-on operating mode, some over-shoot in the d-c output voltage would typically be expected due to the unloaded nature of the converter. However, by performing appropriate design tradeoffs with the circuit components involved, it is frequently possible to limit this over-shoot to a relatively low figure percentagewise. No load to full load regulation of the supply is likewise an area where improved performance can be affected by design tradeoffs. With regard to the two pulse stability areas noted, the first, intrapulse voltage variations, is easily predicted for simple constant pulse duration and constant repetition frequency pulse templets. For representative pulse burst groupings associated with phased array applications the problem is considerably more difficult. Finally, if pulse-to-pulse (or burst-to-burst) voltage variations are to be determined, the problem can become quite complex if a fairly high degree of accuracy in the results is to be obtained.

Turning now to the system components capability areas, figure 2c tabulates several component degrading factors of significance. Transmitting tube arcs with subsequent fault diverter action can result in high rates of change and high absolute values of current throughout the system. Where iron core components are involved, these fault currents may lead to saturation which in turn will accelerate the deterioration of inadequately rated components. Damaging mechanical stresses may occur in components utilizing windings with inadequate bracing for the forces involved. Additionally, damage can result from excessive I^2t products in semiconductor devices. Finally, the high rates of change of current in conjunction with circuit inductances are often responsible for transient voltage spikes capable of deteriorating all classes of components.

CIRCUIT ANALYSIS TECHNIQUES

If the elementary matrix described previously is now reconstructed utilizing the expanded capability definitions, a display similar to figure 3 will result. Typical areas of interest have been indicated by X symbols for each of the four indicated equipment operating modes. The question now arises as to the most effective method of obtaining quantitative solutions for the 31 separate and distinct areas of potential interest indicated by the matrix. At least four methods are applicable, the choice depending on the nature of the problem and the degree of

accuracy required of the solutions. These are indicated in figure 4.

Manual Approach

The term manual solution is intended to depict use of the techniques available prior to the introduction of the computer to aid in engineering designs. Manual solutions can provide quite adequate results for analysis of traditional constant pulse duration and constant pulse repetition frequency radar systems where regulation effects are of little consequence. An electronics text of 20 years ago summarized this approach quite well when it stated the following with regard to power supply regulation. "All that will be done is to warn the student who encounters a regulation problem that the physical concepts must be reduced to the simplest and most concise forms. All mathematical shortcuts must be used or else the student will find himself hopelessly submerged under a complex mass of calculations."

Analog Approach

The second approach, use of analog computer techniques, overcomes many of the shortcomings of the manual method of solution. An example of a representative phased array power supply system analyzed by means of analog computer techniques is shown in figure 5. The particular system required the capability of operating from either a public utility prime power source or a local motor generator set prime power source. The character of each of the 6 serial areas involved will be described briefly.

The generator power source of area A was supplied from five 1250 KVA, 13.8 KV, three phase diesel generators connected in parallel. For purposes of analysis, the transient reactance of these machines was utilized and its value was taken as 18%. This figure, when referenced to the 480 volt bus level used for equipment operation, had the value of 0 + .00663 ohms indicated on the block diagram. When a public utility power source as indicated in area A' was used in the analysis, a 2% reactance was selected, and when referenced to the 480 volt bus level, the ohmic values indicated resulted.

A bank of three 2000 KVA distribution transformers was provided in area B to affect the 13.8 KV to 480 volt step down function. At this juncture, the power system fanned out to supply energy to the N transmitter groups which comprised the total R-F generation system. These transformers had a representative reactance of 6% which when translated to the 480 volt level resulted in an overall value of 0 + .0023 ohms.

The remaining four areas will be noted as per group items. The first, an induction voltage regulator of area C performed the functions of lowering the line voltage applied to the rectifier during snap-on and correcting for loading variations during operation. It introduced the resistance and reactance values noted when in its boost position. The line reactors of area D provided current limiting to reduce stresses of both an electrical and mechanical nature during the snap-on and crowbar modes of operation. Finally, the last three phase component, the rectifier transformer of area E, was a dual secondary unit having the resistive and reactive values indicated.

Block F depicts the dual three phase rectifier stacks, dual filter reactors, dual energy storage capacitor banks, and pulsed loads. The actual loads involved in this application were dual depressed collector traveling wave tubes having the two operating levels with respect to cathode noted on the diagram. Body voltage for the tubes was obtained from a separate regulated source and was not a part of this analysis.

Two solutions obtained from this circuit configuration will be shown to illustrate the capabilities of the analog computer for a constant duty factor pulse templet operating condition and for a variable duty factor operating condition. The first solution, shown in figure 6, is for the circuit described when the motor generator set is providing the prime power to the system.

Traces 12 and 13 depict the output d-c voltage from prime collector to cathode. The expected charge and discharge cycles of the storage capacitors, consistant with the constant duty loading, can be seen to prevail.

Traces 10 and 11 depict the a-c input aspects of the power system. Trace 10, a representative line current delivered by one phase of the generator, can be seen to demonstrate the traditional stair step waveshape associated with a delta-wye transformer connection. Trace 11 depicts a representative line to neutral terminal voltage of the generator. If the phase voltage and line current products for each phase are plotted, the instantaneous phase power products of traces 1, 2, and 3 will result. Then, if these three waveform are added together the waveform or trace 4, shown inverted, will result. This is the peak instantaneous power referred to in the thump definition described previously. It will be noted that this wave has a six times line frequency component and a lower frequency prf related component. It is the latter component whose deviation from the average power level determines the thump level which in this simulation is only a few percent.

The impact of a variable duty factor pulse templet is indicated by reference to figure 7. The pulse repetition frequency was retained at the same value as in the previous run, however, variable pulse durations were introduced. In addition, the line reactors were removed and prime power was obtained from the public utility source.

The d-c output voltage of traces 12 and 13 can be seen to wander quite radically from their steady state values shown in figure 6. In addition, the excursion of peak instantaneous power in trace 4 indicate that if this pulse templet were to be used with a system having low thump specifications, considerably more design optimization would be necessary.

From these two solutions some basic advantages and shortcomings of the analog computer approach can be observed. On the positive side, first, quite complex circuits can be solved relative to those possible with the manual approach, second, optimization solutions may be readily obtained once the basic circuit configuration has been programmed and debugged, and third, excellent correspondence between the simulation data and actual hardware can be realized. On the negative side, first, the absolute accuracy obtainable from the solutions is limited by the allowable vertical excursions of the tracing pens and by the width and consistency of the line traced, second, high speed transients are generally not accurately displayed due to insufficient speed of response of the pens, and third, while not apparent from the solutions, highly skilled programmers and experienced equipment operating personnel are necessary if reliable information is to be obtained.

Special Purpose Digital Approach

Turning now to digital computer techniques useful for power supply system analysis, two approaches were noted in figure 4, special purpose and general purpose circuit simulations. The term special purpose simulations is intended to encompass those programs prepared for analysis of specific circuits or types of circuits. When available for solution of the type problem at hand, such programs represent probably the fastest and most economical form of solution available. However, modifications to such programs to adapt them to the solution of modified or revised types of circuts may present a formidable programming task.

General Purpose Digital Approach

The general purpose simulations, or as they are frequently called, the user oriented circuit analysis programs, include such widely available types as those shown in figure 8. The abbreviated names ECAP, CORNAP, SCEPTRE and CIRCUS are expanded for purposes of definition. It is possible for an individual who is almost totally unfamiliar with computer techniques to prepare complex circuit analysis programs, debug them, and obtain accurate quantitative results within a relatively short period of time. An example of a second phased array power supply system using the CIRCUS 2 analysis program will be briefly described.

Figure 9 illustrates the diagram of a circuit similar to the one described using the analog simulation techniques. In this system, individual group generators were utilized rather than the common generator bus system noted previously. At the left of the figure, SV1, SV2 and SV3 represent the three generator phases while L1L, L2L, and L3L represent phase inductances equivalent to the 10% reactance of the generator.

A solid state contactor has been simulated by resistors SS1, SS2, and SS3. Practical implementation of this circuit would be by means of back-to-back SCR's whose triggers are interrupted when three phase interruption is to occur. The SCR pairs would then interrupt as their respective line currents passed through zero. Such a simulation may be readily accomplished by preparing a CIRCUS model capable of providing very low resistance in the normal mode of operation of SS1, SS2, or SS3 while transferring this resistance to the megohm level when the current passes through zero.

The triple triangle to the right of the contactors represents the delta primary windings of two three phase rectifier transformers. The windings, their copper losses, and the core losses are represented by the L_, RL_, and RS_ quantities respectively. Any desired turns ratio may be established between the primaries and the wye connected secondary windings. Secondary winding resistances and leakage inductances are depicted in series with each transformer leg. In this case these values coincide with 1.5% resistance and 7.6% reactance.

Rectification is accomplished by diodes DI1 through DI12. A wide variety of semiconductor models may be programmed if desired. A commutation transient suppressor consisting of the R8-C1 series circuit was found to be a necessity for limiting diode inverse voltage transients.

Inductors LF1 and LF2 were filter reactor models programmed to simulate the saturation of the reactors under high current fault operation. Pulsed current sources PJ1 and PJ2 simulate the traveling wave tube body and collector load currents discharging the two energy storage capacitor banks. These pulsed current sources may be programmed to simulate any desired form of pulse train. Finally, R9 and R9A represent very high or very low resistor values programmed to simulate crowbar fault diverter action.

It will be noted that number designations have been assigned to each discrete junction (or node) involving two or more circuit components. The components connected between nodes are referred to as elements (in the case of resistors, capacitors or inductors) and as devices for all other components. Since the voltage across any component, current through any component, and/or voltage between any two circuit nodes may be obtained in either tabular or plotted form as a function of time, one of the problems of a CIRCUS analysis lies in limiting output to a level which will not submerge the analyst under a mass of detailed (but unnecessary) circuit information. Examples of snap-on, constant duty factor pulsing, variable duty factor pulsing, and crowbar output displays will be presented.

While all of the snap-on areas of interest denoted in figure 3 are readily available from a CIRCUS analysis of the circuit of figure 9, only the key input/output areas will be described. Figure 10 illustrates the three phase line inrush currents associated with the first 50 milliseconds of snap-on (i.e. the 3 phase line contactor is assumed to close at time zero). This inrush is characterized by peak inrush currents of approximately 7 times normal full load values, distorted and unsymmetrical waveforms, and a decay of current to essentially zero within three cycles of the line waveform. With regard to output voltages, figure 11 illustrates that the outputs of the two d-c supplies reach their steady state values within about 50 milliseconds, and that they overshoot their full load values by approximately 12 and 15% respectively.

Fifty milliseconds after snap-on initiation, pulsing at full duty factor operation is programmed and 40 milliseconds later the pulse duty factor is reduced to one quarter this value. As before, all matrix values are readily available, however, only two key areas will be described, pulse-to-pulse voltage stability and d-c output voltage regulation. This information is more readily obtainable from a tabulation rather than a plot. Figure 12 illustrates a portion of a multi-page tabulation from which such information may be obtained. It should be noted that the time increments may be established for any desired degree of printout precision, hence, intrapulse values may also be obtained if desired. A summary of the desired information is shown in condensed form in figure 13.

For the crowbar diverter simulation three key areas were of interest - the peak a-c line currents involved, the length of time required for the solid state contactor to clear the fault, and the nature of any line voltage transients introduced as a result of the line interruptions. Figure 14 displays the nature of the three line currents wherein line 2 interrupts 2.8 milliseconds after the crowbar was initiated. At this time the power supply operates single phase and it may be noted that lines 1 and 3 simultaneously interrupt 9.4 milliseconds following crowbar initiation. Figure 15 illustrates the line-to-line a-c voltages at the primary of the rectifier transformer. It should be noted that severe transients occurred at this interface prior to the optimization of appropriate R-C circuits at the input and output of the solid state contactors.

These examples illustrate only the fundamental capabilities of a program such as CIRCUS in aiding in the solution of phased array power supply problems. By simple extensions of the program, areas ranging from line type pulsers to regulated d-c power supplies may readily be simulated. One precaution should be noted. When analyzing circuits involving widely different time constants, the shorter time constant will establish the time step size used by the program to obtain its solutions. Hence, if excessively large computer charges are to be avoided, carefully considered circuit modeling should be incorporated.

From the preceeding discussion it may be seen that appropriate analytical tools are available to cope with most present generation phased array power supply system problems. The flexibility of these analytical tools recommend their use for a wide variety of problem solutions in the power supply and modulator areas.

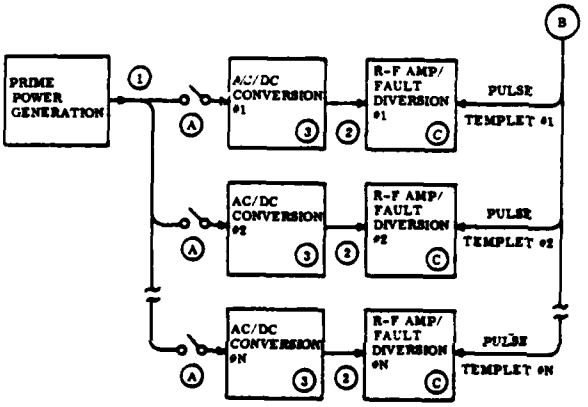

FIGURE 1A POWER SYSTEM BLOCK DIAGRAM

OPERATING MODES / CAPABILITY	(1) PRIME POWER GENERATION OUTPUT	(2) AC/DC CONVERSION OUTPUT	(3) SYSTEM COMPONENTS
(A) SNAP-ON			
(B) CONSTANT PULSE TEMPLET			
(B) VARIABLE PULSE TEMPLET			
(C) FAULT DIVERSION			

FIGURE 1B BASIC EVALUATION MATRIX FORMAT

RELEVANT FACTORS IN PRIME POWER SOURCE AREA

- LINE VOLTAGE REGULATION
- LINE VOLTAGE UNBALANCE
- LINE VOLTAGE AND/OR CURRENT DISTORTION
- LINE INRUSH CURRENTS AND/OR RATES OF CHANGE
- LINE THUMP

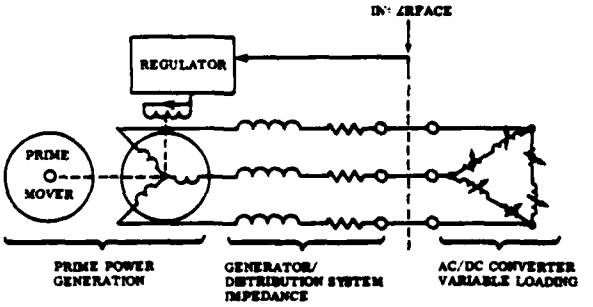

FIGURE 2A

RELEVANT FACTORS IN AC-DC CONVERTER OUTPUT CAPABILITIES

- DC VOLTAGE OVERSHOOT
- DC VOLTAGE REGULATION
- INTRAPULSE VOLTAGE VARIATION
- PULSE-TO-PULSE VOLTAGE VARIATION

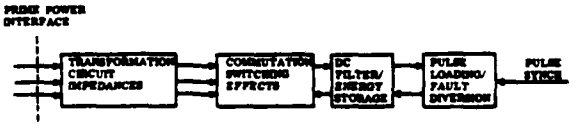

FIGURE 2B

RELEVANT FACTORS IN COMPONENT CAPABILITIES

- DC FAULT CURRENTS/RATES OF CHANGE
- CURRENT INDUCED COMPONENT STRESSES
- VOLTAGE INDUCED COMPONENT STRESSES

AFFECTED COMPONENTS

- TRANSFORMERS
- REACTORS
- CAPACITORS
- RESISTORS
- DIODES
- SWITCHING/DISCHARGE DEVICES

QUANTITATIVE ANALYSIS METHODS

- MANUAL CALCULATIONS
- ANALOG SIMULATION
- SPECIAL PURPOSE DIGITAL SIMULATIONS
- GENERAL PURPOSE DIGITAL SIMULATIONS

FIGURE 4

FIGURE 2C

CAPABILITY FACTORS / OPERATING CONDITIONS	① LINE VOLTAGE REGULATION	② LINE VOLTAGE UNBALANCE	③ LINE VOLTAGE/ CURRENT DISTORTION	④ LINE INRUSH CURRENTS/ RATES OF CHANGE	⑤ LINE THUMP	⑥ DC VOLTAGE OVERSHOOT	⑦ DC VOLTAGE REGULATION	⑧ INTRAPULSE VOLTAGE VARIATION	⑨ INTERPULSE VOLTAGE VARIATION	⑩ DC FAULT CURRENTS/ RATES OF CHANGE	⑪ CURRENT INDUCED COMPONENT STRESSES	⑫ VOLTAGE INDUCED COMPONENT STRESSES
	SOURCE RELATED					OUTPUT RELATED				COMPONENT RELATED		
SNAP-ON	X		X	X	X	X				X	X	X
CONST. PULSE/ DUTY LOADING		X			X		X	X	X			X
VARIABLE PULSE/ DU. LOAD	X	X	X		X		X	X	X			X
CROWBAR	X		X	X	X					X	X	X

FIGURE 3 EXPANDED ANALYSIS MATRIX

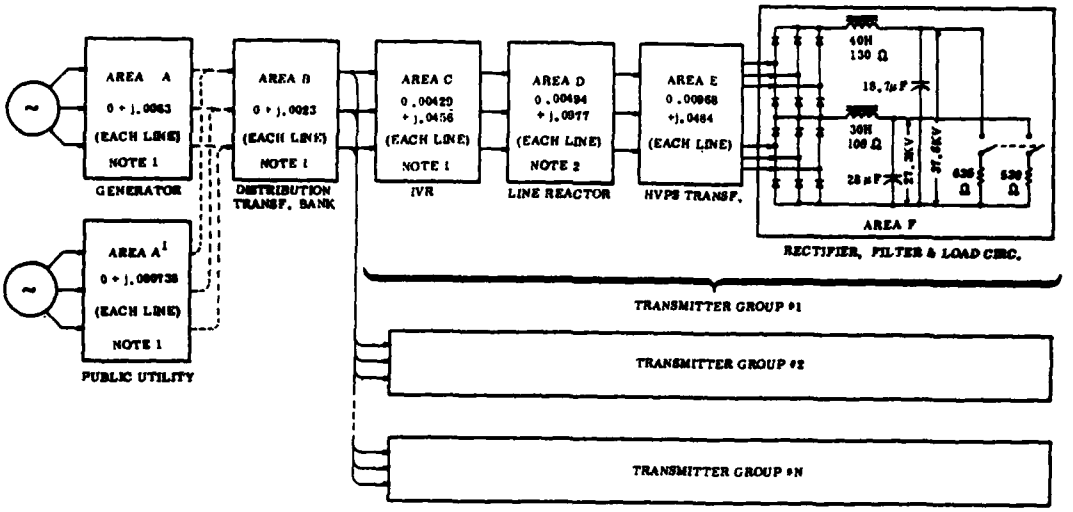

NOTE 1 - THE VALUES SHOWN IN AREAS A, A', AND B WERE MULTIPLIED BY N TO PROVIDE A SINGLE THREE PHASE PATH FOR COMPUTER SIMULATION (EXCEPT FOR "CROWBAR" ANALYSIS).

NOTE 2 - 0+ j 0 ALSO USED IN SOME TESTS

Figure 5 Overall Equivalent Circuit Constants Used For Simulation

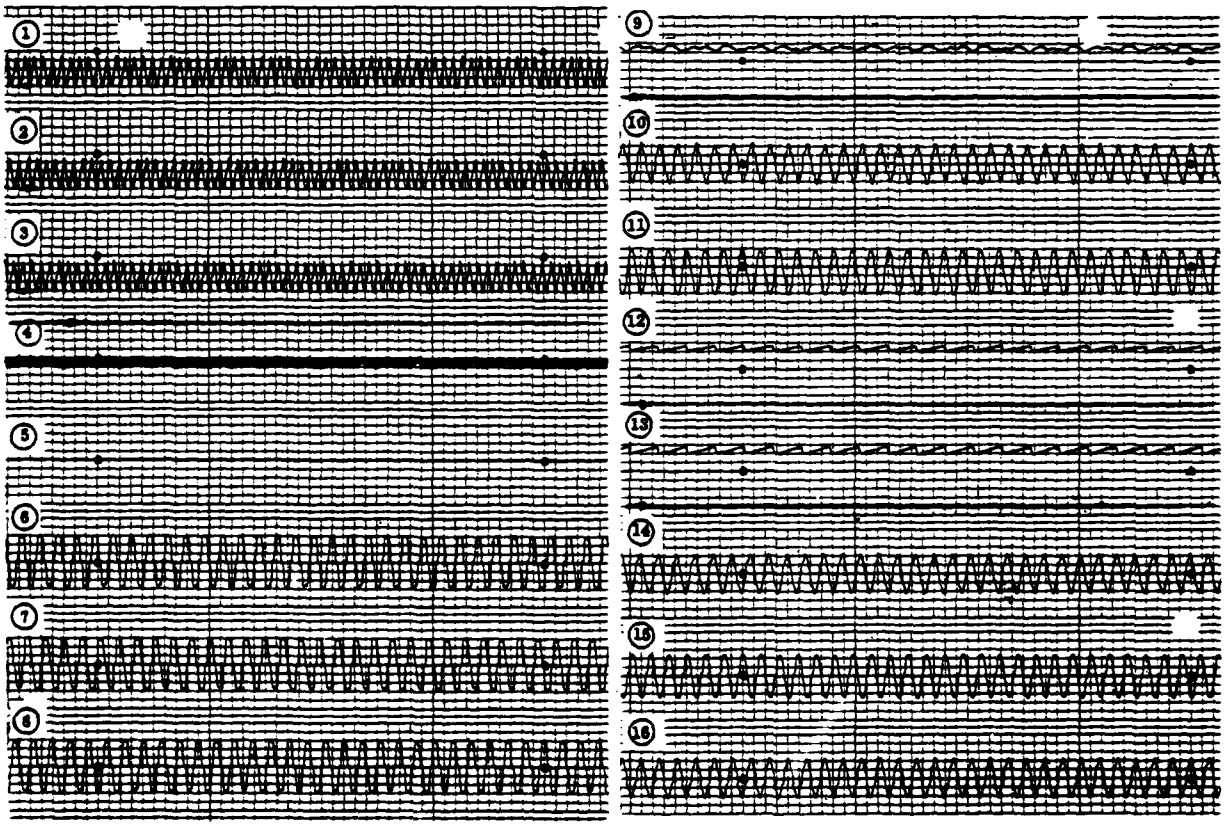

Figure 6 Power Circuit Waveforms For Generator Source, Line Reactor Limiting, and Constant Pulse Templet

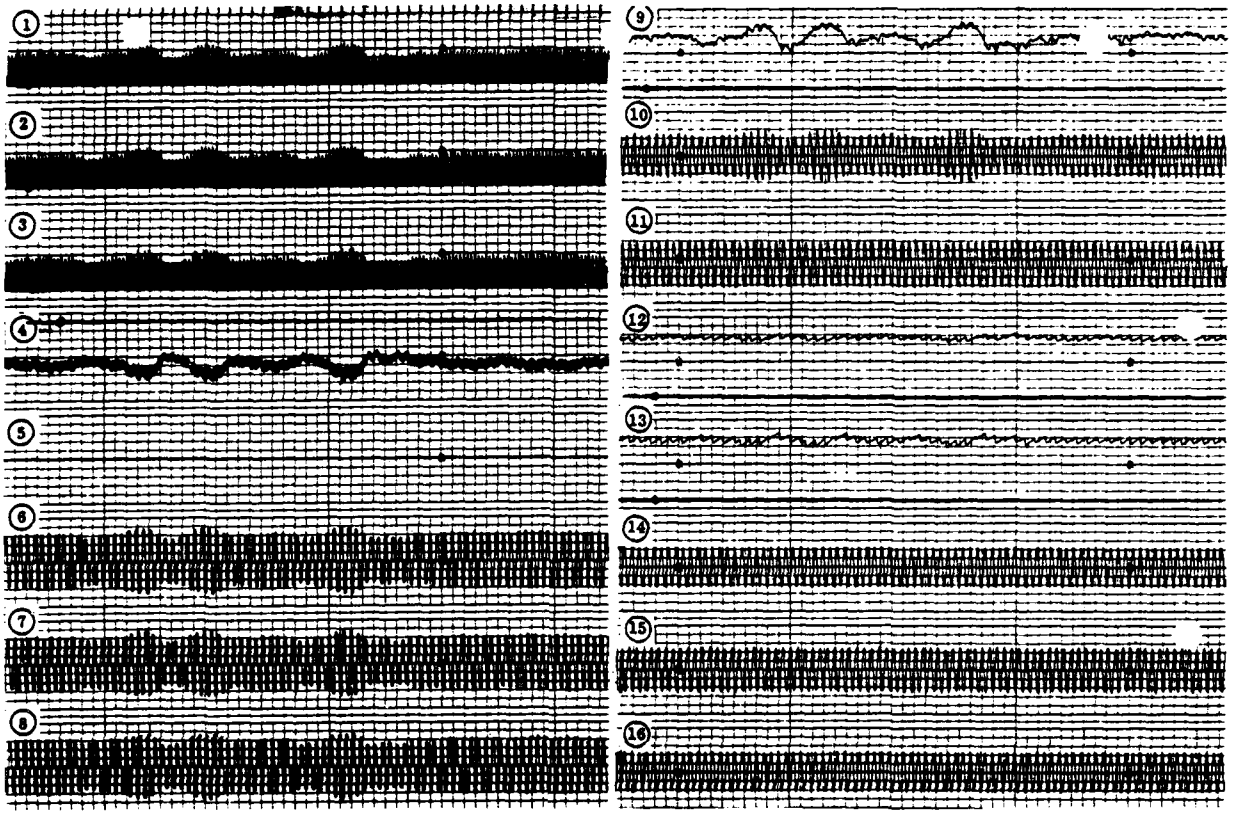

Figure 7 Power Circuit Waveforms For Generator Source, Line Reactors Removed, and Variable Pulse Templet

USER ORIENTED CIRCUIT ANALYSIS REGULATOR

ECAP - A Program for linear d-c or a-c analysis of circuits.

CORNAP - A linear circuit analysis program which provides solutions in the S-plane as well as frequency and time response information.

SCEPTRE - A non-linear circuit and system analysis program for d-c and transient solutions.

CIRCUS - A program for d-c and non-linear transient analysis of both linear and non-linear circuits.

FIGURE 8

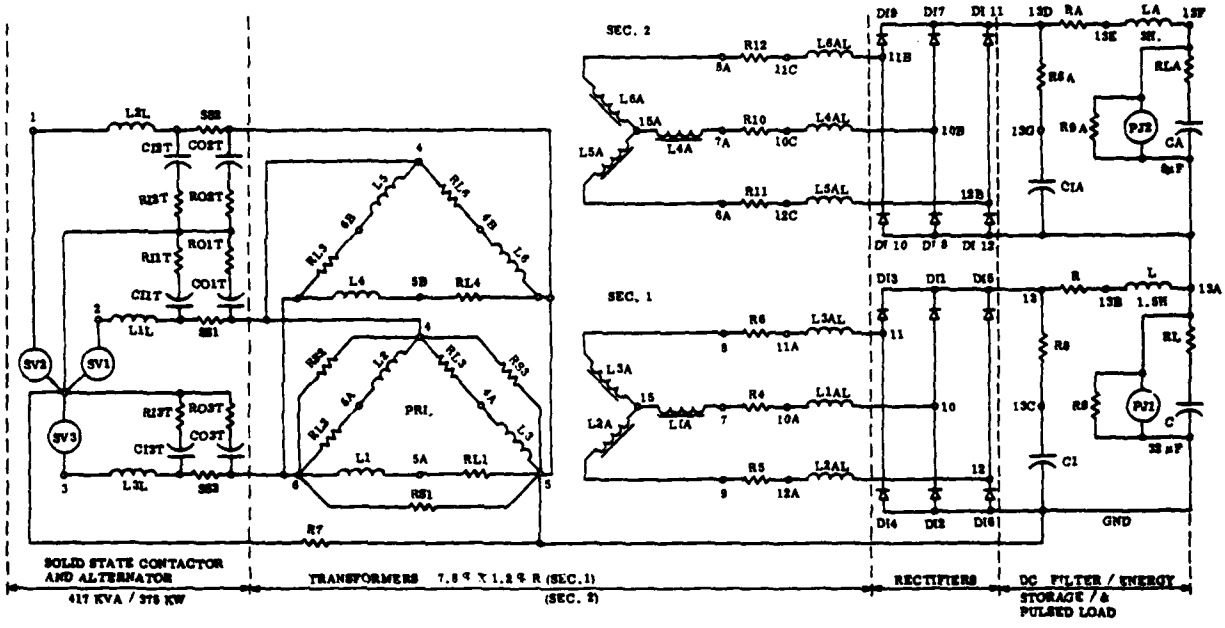

LEGEND:

1. SV1, SV2, AND SV3: THREE GENERATING PHASES OF A Y CONNECTED 60-HERTZ ALTERNATOR.
2. SS1, SS2, AND SS3: SOLID STATE CONTACTORS
3. L1L, L2L, AND L3L: TRANSIENT/SUBTRANSIENT INDUCTANCE OF EACH ALTERNATOR PHASE.
4. L1, L2, AND L3/L1A, L2A, AND L3A: PRIMARY/SECONDARY EXCITING INDUCTANCE OF TRANSFORMER 1.
5. L4, L5, AND L6/L4A, L5A, AND L6A: PRIMARY/SECONDARY EXCITING INDUCTANCE OF TRANSFORMER 2.
6. L1AL, L2AL, AND L3AL: LEAKAGE/INDUCTANCE PER PHASE OF TRANSFORMER 1.
7. L4AL, L5AL, AND L6AL: LEAKAGE/INDUCTANCE PER PHASE OF TRANSFORMER 2.
8. RL1, RL2, AND RL3/R4, R5, AND R6: PRIMARY/SECONDARY WINDING RESISTANCE OF TRANSFORMER 1.
9. RL4, RL5, AND RL6/R10, R11, AND R12: PRIMARY/SECONDARY WINDING RESISTANCE OF TRANSFORMER 2.
10. RS1, RS2, AND RS3: COMBINED CORE LOSSES OF TRANSFORMERS 1 AND 2.
11. DI1 THROUGH DI12: ZERO CAPACITANCE DIODE MODELS
12. R AND RA: DC FILTER REACTOR RESISTANCES FOR PS1 AND PS2, RESPECTIVELY.
13. L AND LA: DC FILTER REACTOR INDUCTANCES FOR PS1 AND PS2, RESPECTIVELY.
14. R8 AND R8A: TRANSIENT DESPIKING RESISTORS FOR PS1 AND PS2, RESPECTIVELY..
15. C1 AND C1A: TRANSIENT DESPIKING CAPACITORS FOR PS1 AND PS2, RESPECTIVELY.
16. C AND CA: DC FILTER/ENERGY STORAGE CAPACITORS FOR PS1 AND PS2, RESPECTIVELY.
17. R9 AND R9A: TWT FAULT DIVERTER RESISTANCE FOR PS1 AND PS2, RESPECTIVELY.
18. PJ1 AND PJ2: TWT COLLECTOR/BODY CURRENT PULSE SIMULATORS.
19. NOMINAL DC OUTPUT OF POWER SUPPLY 1: 25 KILOVOLTS AT 9.6 AMPERES AVERAGE (13A, GND).
20. NOMINAL DC OUTPUT OF POWER SUPPLY 2: 16 KILOVOLTS AT 1.5 AMPERES AVERAGE (13F, 13A).

Figure 9 Circuit Diagram of Circus 2 Simulation

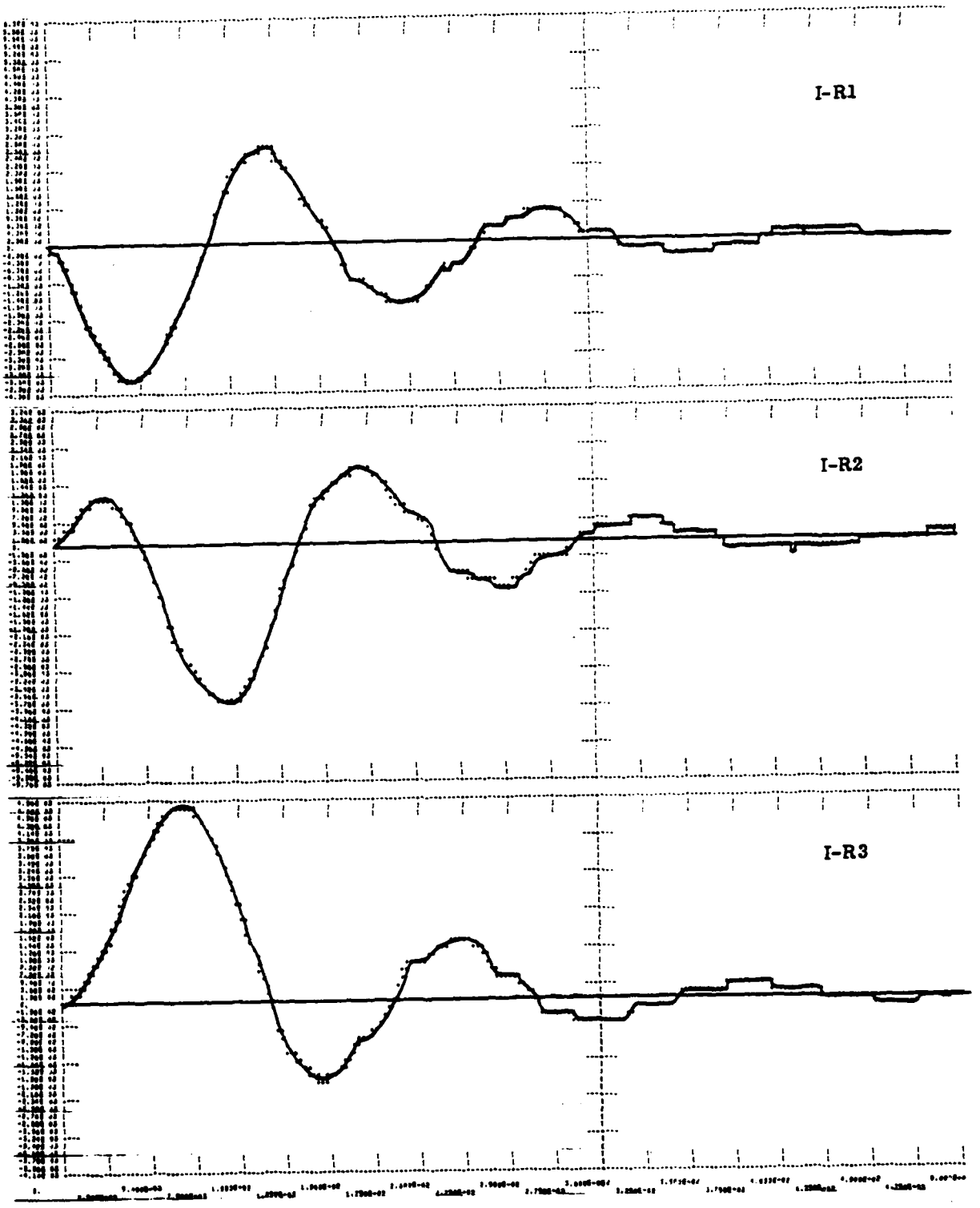

FIGURE 10 SNAP-ON INRUSH 3ϕ LINE CURRENTS

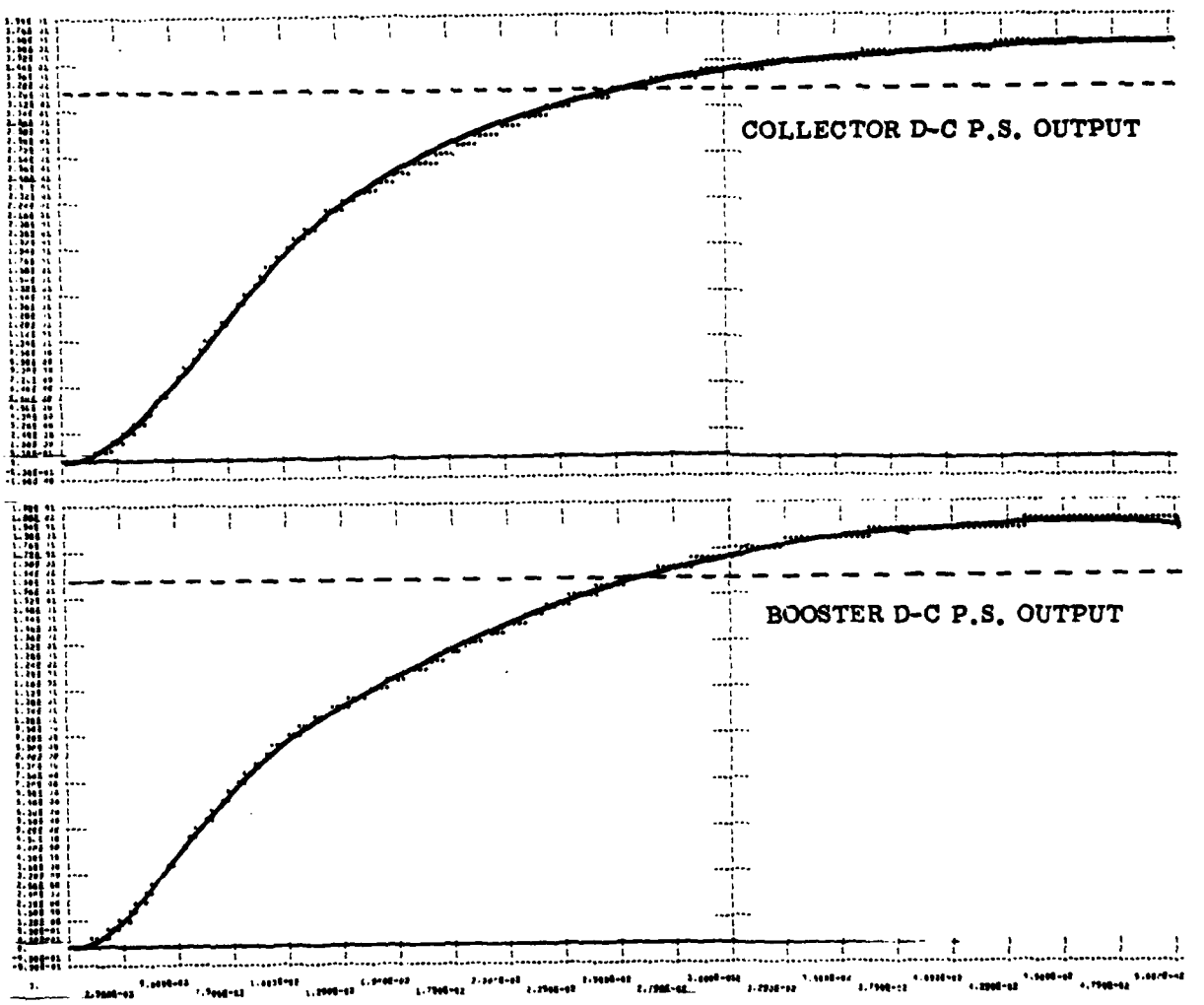

FIGURE 11 SNAP-ON D-C OUTPUT VOLTAGES

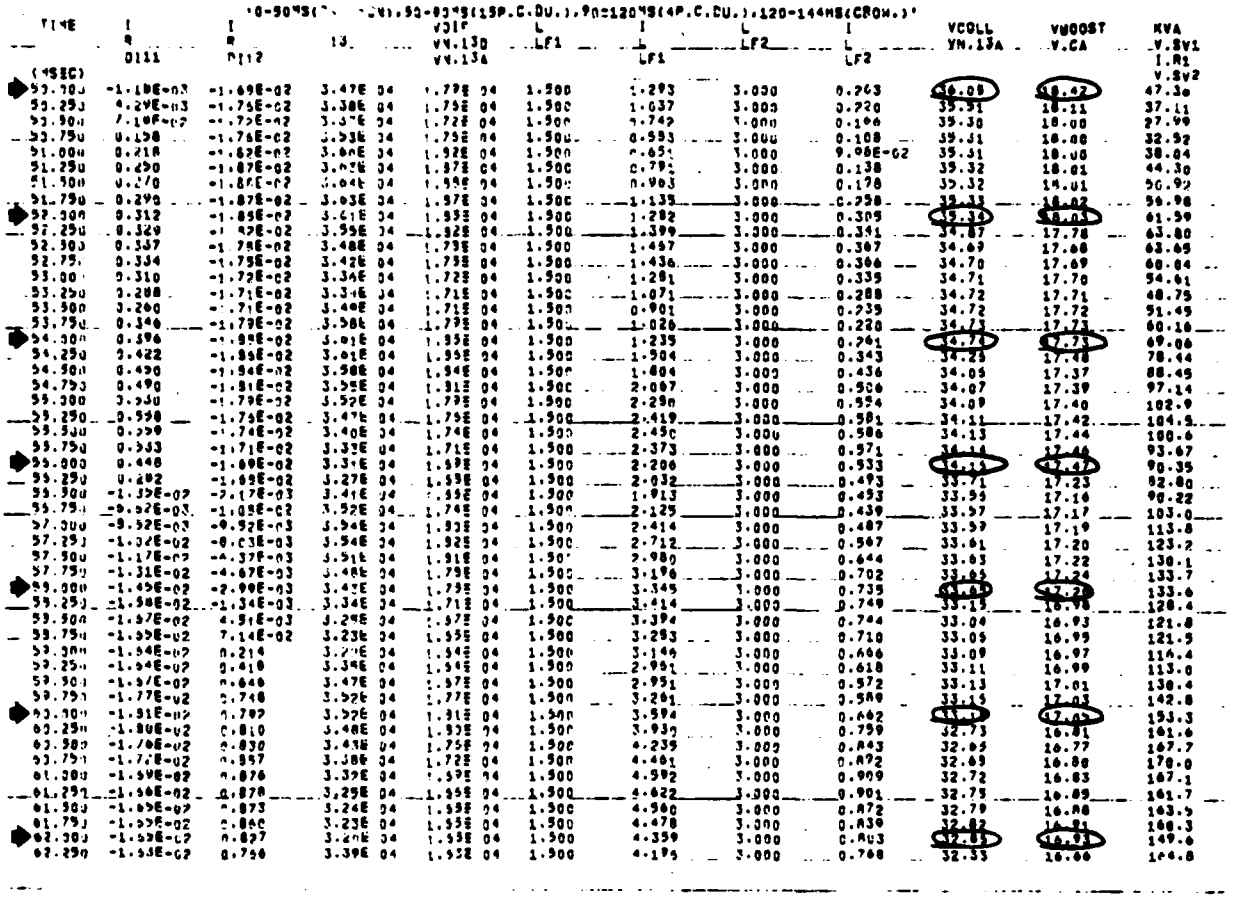

TIME (MSEC)	I 8 0111	I 8 0112	13.	VDIF VN.13D VN.13A	L LF1	I LF1	L LF2	I LF2	VCOLL VN.13A	VWOOST V.CA	KVA V.SV1 I.R1 V.SV2
53.000	-1.18E-03	-1.69E-02	3.47E 04	1.79E 04	1.500	1.293	3.000	0.263	36.08	18.42	47.36
53.250	4.29E-03	-1.76E-02	3.38E 04	1.75E 04	1.500	1.037	3.000	0.220	35.91	18.11	37.11
53.500	7.19E-03	-1.72E-02	3.37E 04	1.72E 04	1.500	0.749	3.000	0.156	35.38	18.00	27.99
53.750	0.138	-1.76E-02	3.53E 04	1.75E 04	1.500	0.593	3.000	0.108	35.41	18.08	32.52
54.000	0.218	-1.82E-02	3.64E 04	1.82E 04	1.500	0.651	3.000	9.98E-02	35.31	18.08	38.04
54.250	0.290	-1.87E-02	3.75E 04	1.87E 04	1.500	0.791	3.000	0.138	35.32	18.01	44.36
54.500	0.270	-1.87E-02	3.64E 04	1.88E 04	1.500	0.903	3.000	0.178	35.32	18.01	50.92
54.750	0.290	-1.87E-02	3.63E 04	1.87E 04	1.500	1.135	3.000	0.258	35.33	18.02	56.98
55.000	0.312	-1.85E-02	3.61E 04	1.85E 04	1.500	1.282	3.000	0.309	35.34	18.03	61.59
55.250	0.329	-1.82E-02	3.55E 04	1.82E 04	1.500	1.399	3.000	0.341	34.87	17.78	63.80
55.500	0.367	-1.78E-02	3.48E 04	1.79E 04	1.500	1.497	3.000	0.367	34.69	17.68	63.65
55.750	0.334	-1.79E-02	3.42E 04	1.79E 04	1.500	1.436	3.000	0.366	34.70	17.69	60.84
56.000	0.310	-1.79E-02	3.34E 04	1.72E 04	1.500	1.281	3.000	0.335	34.71	17.70	54.61
56.250	0.288	-1.71E-02	3.34E 04	1.71E 04	1.500	1.071	3.000	0.288	34.72	17.71	48.75
56.500	0.260	-1.71E-02	3.44E 04	1.71E 04	1.500	0.901	3.000	0.235	34.72	17.72	51.45
56.750	0.346	-1.79E-02	3.58E 04	1.79E 04	1.500	1.026	3.000	0.220	34.73	17.73	60.16
57.000	0.396	-1.85E-02	3.61E 04	1.85E 04	1.500	1.235	3.000	0.261	34.74	17.74	69.06
57.250	0.422	-1.85E-02	3.61E 04	1.85E 04	1.500	1.504	3.000	0.343	34.25	17.48	78.44
57.500	0.490	-1.84E-02	3.58E 04	1.84E 04	1.500	1.804	3.000	0.436	34.05	17.37	88.45
57.750	0.490	-1.81E-02	3.55E 04	1.81E 04	1.500	2.007	3.000	0.506	34.07	17.39	97.14
58.000	0.530	-1.79E-02	3.52E 04	1.79E 04	1.500	2.298	3.000	0.554	34.09	17.40	102.9
58.250	0.558	-1.76E-02	3.47E 04	1.79E 04	1.500	2.419	3.000	0.581	34.11	17.42	104.5
58.500	0.239	-1.74E-02	3.40E 04	1.74E 04	1.500	2.450	3.000	0.586	34.13	17.44	100.6
58.750	0.563	-1.71E-02	3.32E 04	1.71E 04	1.500	2.373	3.000	0.571	34.14	17.44	93.67
59.000	0.448	-1.69E-02	3.31E 04	1.69E 04	1.500	2.206	3.000	0.533	34.11	17.43	90.35
59.250	0.282	-1.69E-02	3.27E 04	1.69E 04	1.500	2.032	3.000	0.493	33.71	17.23	92.80
59.500	-1.33E-03	-2.17E-03	3.41E 04	1.69E 04	1.500	1.913	3.000	0.453	33.93	17.16	98.22
59.750	-9.92E-03	-1.08E-02	3.52E 04	1.74E 04	1.500	2.125	3.000	0.439	33.97	17.17	103.0
57.000	-8.52E-03	-8.92E-03	3.54E 04	1.83E 04	1.500	2.414	3.000	0.487	33.99	17.19	113.8
57.250	-1.02E-02	-8.63E-03	3.54E 04	1.82E 04	1.500	2.712	3.000	0.567	33.61	17.20	123.2
57.500	-1.17E-02	-4.37E-03	3.51E 04	1.81E 04	1.500	2.980	3.000	0.644	33.83	17.22	130.1
57.750	-1.31E-02	-4.67E-03	3.48E 04	1.79E 04	1.500	3.196	3.000	0.702	33.84	17.24	133.7
58.000	-1.45E-02	-2.99E-03	3.45E 04	1.79E 04	1.500	3.345	3.000	0.735	33.85	17.25	133.6
58.250	-1.58E-02	-1.34E-03	3.34E 04	1.71E 04	1.500	3.414	3.000	0.749	33.15	16.91	128.4
58.500	-1.67E-02	4.91E-03	3.29E 04	1.67E 04	1.500	3.394	3.000	0.744	33.04	16.93	121.8
58.750	-1.69E-02	7.14E-02	3.23E 04	1.65E 04	1.500	3.293	3.000	0.710	33.05	16.95	121.5
59.000	-1.64E-02	0.214	3.22E 04	1.64E 04	1.500	3.146	3.000	0.666	33.09	16.97	116.4
59.250	-1.54E-02	0.410	3.34E 04	1.64E 04	1.500	2.991	3.000	0.618	33.11	16.99	113.0
59.500	-1.47E-02	0.648	3.47E 04	1.67E 04	1.500	2.951	3.000	0.572	33.13	17.01	130.4
59.750	-1.77E-02	0.748	3.52E 04	1.77E 04	1.500	3.281	3.000	0.589	33.15	17.03	142.8
60.000	-1.91E-02	0.792	3.52E 04	1.91E 04	1.500	3.594	3.000	0.662	32.73	16.81	153.3
60.250	-1.80E-02	0.810	3.48E 04	1.93E 04	1.500	3.936	3.000	0.759	32.73	16.81	161.6
60.500	-1.70E-02	0.830	3.41E 04	1.75E 04	1.500	4.239	3.000	0.843	32.65	16.77	167.7
60.750	-1.72E-02	0.857	3.38E 04	1.72E 04	1.500	4.461	3.000	0.892	32.69	16.86	170.0
61.000	-1.69E-02	0.876	3.39E 04	1.69E 04	1.500	4.592	3.000	0.909	32.72	16.83	167.1
61.250	-1.68E-02	0.878	3.25E 04	1.65E 04	1.500	4.622	3.000	0.901	32.75	16.85	161.7
61.500	-1.65E-02	0.873	3.24E 04	1.65E 04	1.500	4.580	3.000	0.872	32.79	16.88	153.5
61.750	-1.65E-02	0.860	3.23E 04	1.65E 04	1.500	4.478	3.000	0.838	32.82	16.91	144.3
62.000	-1.65E-02	0.827	3.40E 04	1.65E 04	1.500	4.359	3.000	0.803	32.83	16.91	149.6
62.250	-1.65E-02	0.750	3.39E 04	1.65E 04	1.500	4.195	3.000	0.768	32.53	16.66	144.8

FIGURE 12 REPRESENTATIVE TABULAR PRINTOUT FROM CIRCUS ANALYSIS

Millisec.	Coll. P.S. KV At Start Of Pulse	Booster P.S. KV At Start Of Pulse	P. P. S.	Coll. ΔV Pulse To Pulse	Booster ΔV Pulse To Pulse
50.0	36.08	18.42	800.0	-	-
52.0	35.34	18.03	800.0	-740.0	-390.0
54.0	34.74	17.73	800.0	-600.0	-300.0
56.0	34.15	17.47	800.0	-590.0	-260.0
58.0	33.68	17.26	800.0	-470.0	-210.0
60.0	33.18	17.05	800.0	-500.0	-210.0
62.0	32.86	16.92	800.0	-320.0	-120.0
64.0	32.50	16.79	800.0	-360.0	-140.0
66.0	32.20	16.67	800.0	-300.0	-120.0
68.0	31.93	16.56	800.0	-270.0	-110.0
70.0	31.70	16.45	800.0	-230.0	-110.0
72.0	31.53	16.36	800.0	-180.0	- 90.0
74.0	31.40	16.29	800.0	-130.0	- 70.0
76.0	31.39	16.20	800.0	- 10.0	- 90.0
78.0	31.37	16.07	800.0	- 20.0	-130.0
80.0	31.44	16.00	800.0	+ 70.0	- 70.0
82.0	31.51	15.97	800.0	+ 70.0	- 30.0
84.0	31.47	15.96	800.0	- 40.0	- 20.0
86.0	31.51	16.03	800.0	+ 40.0	+ 80.0
88.0	31.55	16.10	800.0	+ 40.0	+ 70.0
90.0	31.54	16.11	800.0	- 10.0	+ 10.0
97.5	33.08	17.08	133.3	+1560.0	+110.0
105.0	34.18	17.51	133.3	+1050.0	+490.0
112.5	34.77	17.79	133.3	+440.0	+240.0
120.0	36.06	17.99	133.3	+290.0	+140.0

Coll. Reg. = (36.06 - 31.54)/31.54 = 0.112 } For max.
Boost. Reg. = (17.99 - 16.11)/16.11 = 0.111 } to min. Dz.

FIGURE 13 PULSE-TO-PULSE ΔV AND P.S. REGULATION

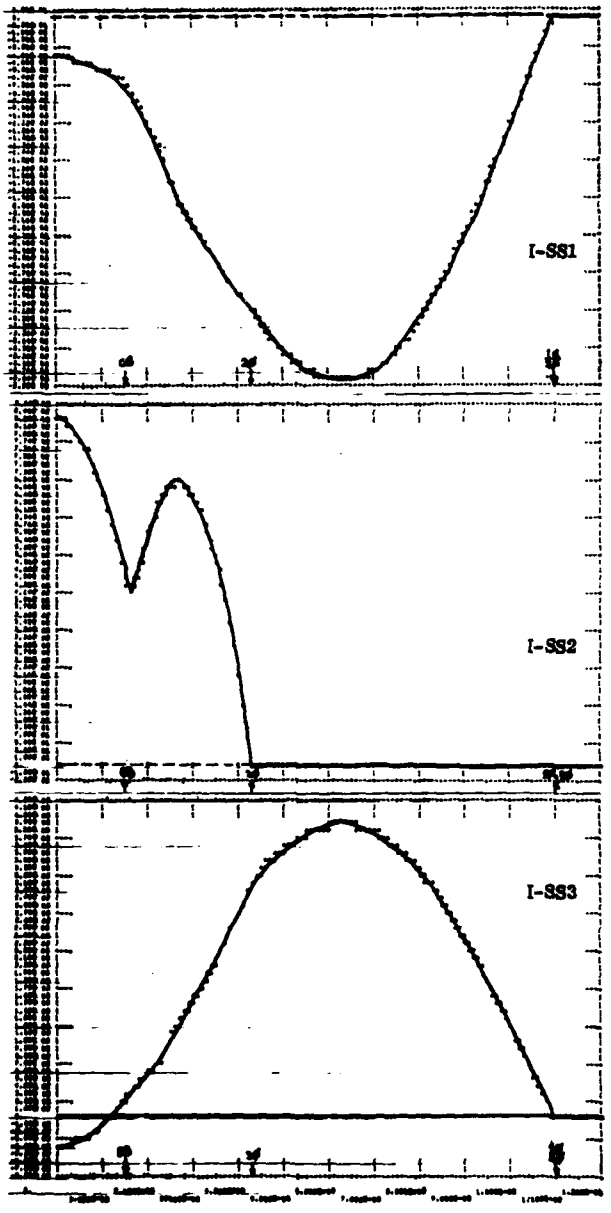

FIGURE 14 CROWBAR INRUSH CURRENTS ON 3ϕ LINE

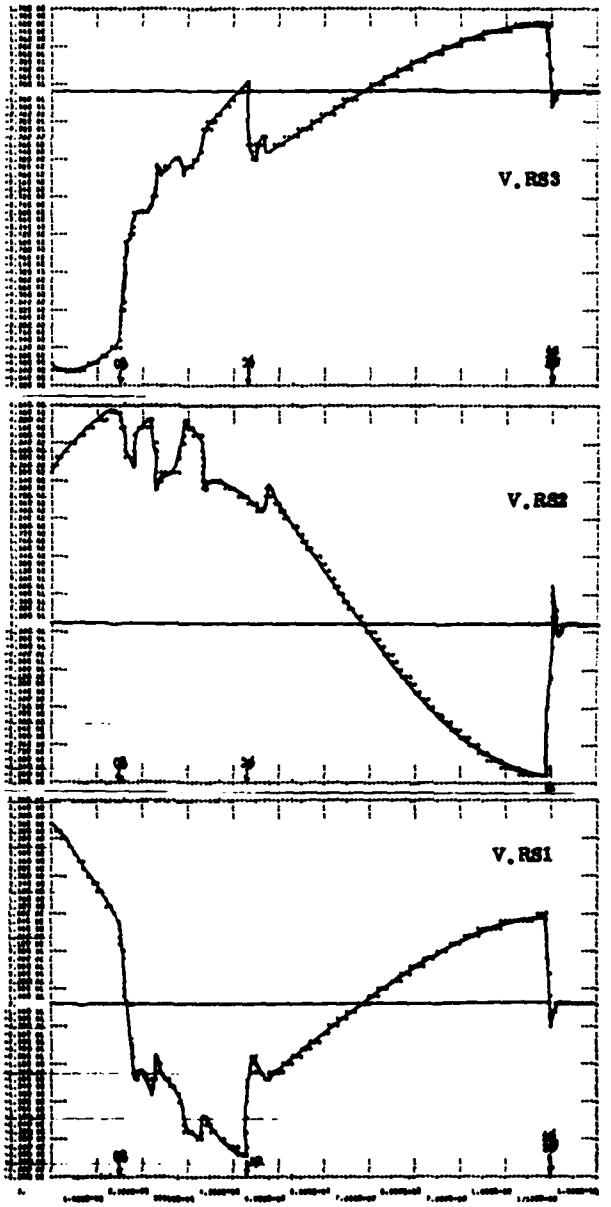

FIGURE 15 CROWBAR 3ϕ LINE-LINE VOLTAGES

THE GENERATION OF HIGH FREQUENCY SINUSOIDAL AND PULSE WAVEFORMS USING HYDROGEN THYRATRONS

L. J. Kettle B. P. Newton
English Electric Valve Co. Ltd.
Chelmsford, Essex, U.K.

Summary

The circuit of a high efficiency, high frequency sinewave generator using a hydrogen thyratron switch is described and some of its uses are mentioned. Further, a combination of this circuit with a standard pulse modulator circuit enables a high frequency pulse generator to be built which allows a longer than normal recovery period for the thyratron.

Although the techniques for generating high power sinusoidal waveforms at high frequencies are well-established, extension of these techniques to frequencies of the order of 20 kHz is less satisfactory in many respects. This is partly because of the need to use iron-cored inductors for the various tuning and feedback windings and partly because of the relatively low efficiency inherent with high vacuum thermionic devices. This is acceptable with R.F. transmitters but in the 20 kHz regime the power is normally required for operating electric furnaces or similar equipment and high efficiency is an economic necessity.

Inverter circuits using thyristors provide a solution at low power levels whilst hydrogen thyratrons enable the power output to be increased considerably. Inverter circuits, however, tend to be relatively complicated and also involve the use of specially designed iron-cored inductive elements. Thus any method of generating considerable amounts of power in a simpler manner and at high efficiency is of great advantage to users of high frequency induction furnaces and similar equipment.

One such method has been used for several years as a source of low frequency power and the technique has recently been extended to the higher frequencies by replacing ignitrons with hydrogen thyratrons. Fig. 1 shows a circuit of this type, the principle of operation being as follows.

Assuming that energy is circulating in the oscillatory circuit L_1C_1 and that the latter is supplying energy to the load, the thyratron V is recurrently triggered at an instant when its anode voltage is falling towards zero but is positive in polarity. C_1 and C_2 in series then cause a half-sinusoidal current to flow through L_2 and V, thereby reversing the voltage across V and also increasing the energy stored in C_1 in readiness for the next cycle of the oscillation. This reversal of voltage is apparent from Fig. 2 and for so long as this reversal persists, conduction through V is not possible. The trigger circuit should be such that the control grid becomes negative within this period of negative anode voltage, thereby gaining control in readiness for the next cycle of oscillation. There is clearly an optimum phase relationship between the waveform of the oscillatory voltage and the instant of triggering and, similarly, a maximum frequency at which a particular type of thyratron can be operated. However, using a small glass thyratron, type 8503 for example, satisfactory operation at 40 kHz has been obtained with power outputs of up to 4 kW.

With a pulse generator circuit of the conventional type shown in Fig. 3, the time available for recovery of the switching thyratron is ultimately dependent upon the resonant frequency of the charging circuit and also upon whether or not the pulse forming network is matched to the load. In practice such circuits can operate satisfactorily up to several kilohertz, above which the time available becomes comparable with the recovery time of the thyratron and reliable operation is then difficult to achieve.

By combining an oscillator (Fig. 1 type) with a variant of the conventional pulse generator (Fig. 3) the resulting hybrid circuit becomes one which not only generates the charging waveform required for the pulse generator but also allows considerably more time for thyratron recovery than would otherwise be possible. With such arrangements it has been found possible to operate at frequencies up to at least 20 kHz when using either a CX1157 ceramic or 8503 glass thyratron as the switching device. If suitably triggered, the circuit first converts the d.c. supply to a.c. at the triggering frequency and then uses this

waveform to charge the pulse forming network. The triggering of the thyratron generates the pulse and simultaneously returns just enough energy to the oscillatory circuit to ensure that the correct voltages are available in readiness for the next cycle of operation. Fig. 4 shows one such circuit whose principle of operation is as follows:-

Assuming that the resonant circuit L_1 C_1 has an oscillatory current circulating within it, thyratron V is triggered when the voltage at the point A is approaching zero but is still positive. This discharges the pulse forming network N, thereby generating a pulse in the load R. Simultaneously C_1 and C_2 in series cause a current to flow through D, L_2 and V. This current is half-sinusoidal in waveform and results in reversal of the voltage across V and in the restoration to the tuned circuit L_1C_1 of the energy lost in the previous cycle of oscillation. The reversal of voltage persists until the point A again swings positive, thereby allowing time for recovery of the thyratron. In practice this reversal time can be further increased by the expedient of triggering V at a frequency higher than the natural frequency of oscillation of the tuned circuit. This has the effect of advancing the phase of the instant of triggering relative to the sinusoidal waveform, thereby increasing the amplitude of the oscillation and hence the duration of the inverse voltage applied to the thyratron.

Once the voltage at A again passes zero and becomes positive, diode D conducts so that N effectively becomes part of the resonant circuit for this portion of the cycle. N thus charges to the peak positive voltage excursion of the resonant circuit, after which diode D ceases to conduct and leaves N charged in readiness for the next cycle (Fig. 5).

Variants of this circuit are possible, for example the triggering of V may take place at a sub-multiple of the resonant frequency of the tuned circuit. This is advantageous with regard to the design of the resonant circuit but it is limited in application because it reduces the time available for recovery of the thyratron.

Mention has been made of the technique of triggering at a p.r.f. higher than the natural frequency of the circuit L_1C_1. This can be done to increase the duration of the negative excursion of the thyratron anode and so to permit operation at higher frequencies but of necessity it does this by increasing the amplitude of the oscillation relative to the H.T. available. In practice this permits a considerable voltage step-up to be obtained, a magnification of four times, for example, being readily achieved. Such a step-up in voltage causes the circuit to draw more current from its power supply, thus making it possible to trade high current at low voltage for low current at high voltage.

The circuit of Fig. 1 is a high-power source of approximately sinusoidal waveform whose amplitude is readily adjustable. It is very suitable for applications such as electric furnaces, pre-heating of plastics and the like. Its advantage lies not so much in particular applications as in the simple and efficient manner by which it generates a.c. power whilst using a minimum of components.

If the output voltage across the tuned circuit of Fig. 1 is rectified, then by tuning the circuit L_1C_1 or by varying the triggering frequency, a variable supply of d.c. voltage is obtained from a fixed d.c. source. Similarly, in the case of the pulse generating circuit of Fig. 4, this enables the pulse amplitude to be varied even though the H.T. supply may be incapable of adjustment. In either case this amplitude may be easily stabilised by sampling or feedback techniques.

The uses of the pulse generator are those normal with such apparatus, but this arrangement has the advantage of being able to generate pulses at variable voltages and at frequencies which by normal techniques are quite unattainable.

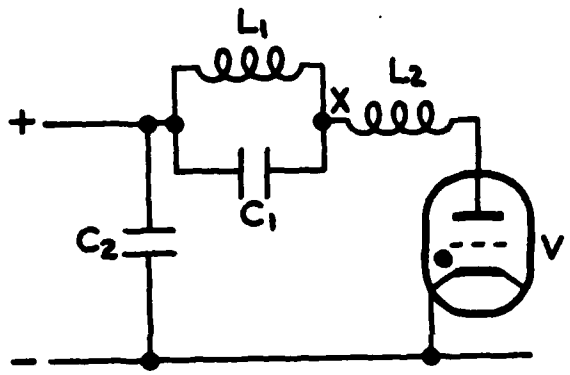

Figure 1

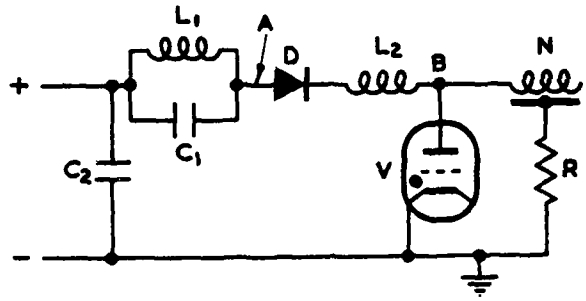

Figure 4

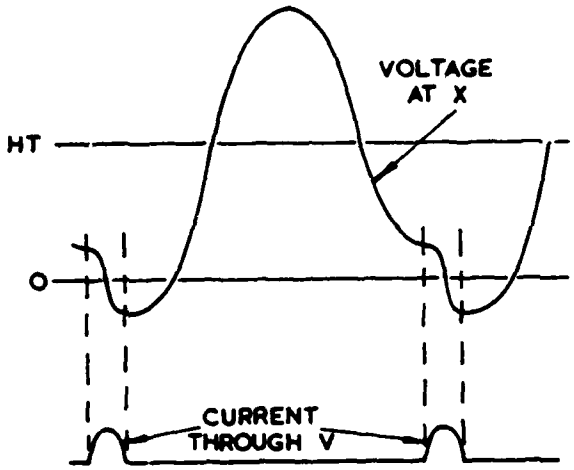

Figure 2

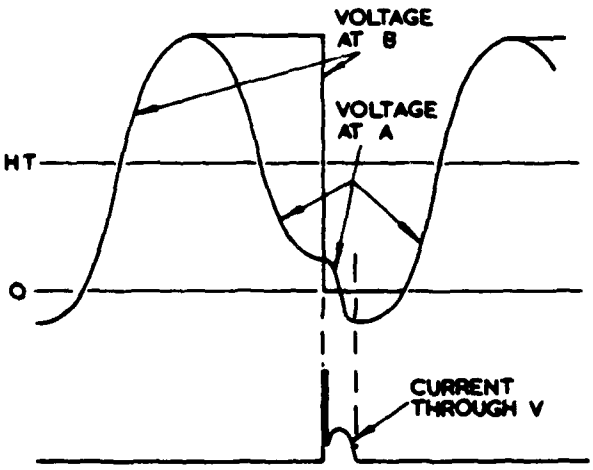

Figure 5

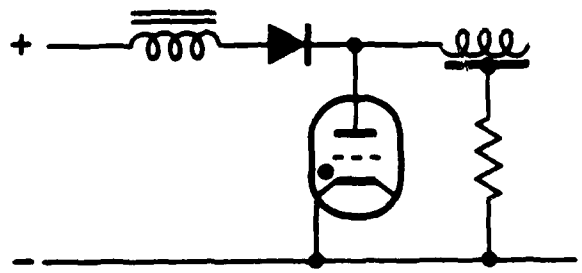

Figure 3

QUENCH MODULATOR FOR COLD-CATHODE CROSSED-FIELD AMPLIFIER

William I. Smith
RCA Corporation
Government and Commercial Systems
Missile and Surface Radar Division
Moorestown, New Jersey

Summary

A radar transmitter designed by the Missile and Surface Radar Division of RCA has achieved versatile performance through use of a type SFD-257 crossed-field amplifier. This CFA features a cold cathode whose emission is initiated by RF drive and terminated (quenched) by a hard-tube modulator-driven electrode. The performance and design features of the tranamitter are described, with emphasis on the specialized pulse shaping and hard-tube modulator required by the quench electrode.

Introduction

The AN/MPS-36 radar, RCA's most advanced type instrumentation radar in production, employs a Varian type SFD-257 crossed-field amplifier tube in a versatile, coherent, one megawatt transmitter. System performance requirements including target velocity measurement and coded pulse operation demand the following transmitter pe :formance features:

- Coherency, incidental phase and amplitude modulations more than 30 dB down
- Variable peak power, 1 kW to 1 Megawatt
- Variable duty cycle up to 0.1%
- Variable PRF up to 640 pps
- Selectable pulse widths, 0.25, 0.5 or 1.0 microsecond
- Variable spacing of coded pulses, with as many as five quarter microsecond pulses in a burst
- Instantaneous bandwidth 500 MHz (5400 to 5900 MHz)

Advantages of the SFD-257 are listed below:

- The intrinsic efficiency of the tube exceeds 50%.
- The tube is essentially a passive device, consuming no power until it is called upon to amplify the input signal.
- It requires only a low energy modulator in contrast to a full cathode pulser. In essence, the amplifier acts as its own switch tube.
- The "cold cathode" feature makes the amplifier *insensitive to duty cycle*, up to the maximum specifications. The pulse widths, groupings, and/or repetition rate may be changed instantly without the need of heater programming.

The tube does not need an elaborate crowbar; in fact, the only fault sensing and protection in the system are accomplished with meter relays on an average current basis.

Transmitter Features

The transmitter receives 50 milliwatts CW and timing command triggers. In response it delivers one megawatt RF pulses to a high-power variable attenuator and in turn to the system antenna, as in Figure 1.

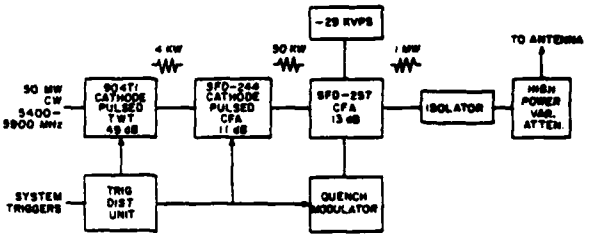

Figure 1. AN/MPS-36 Transmitter Amplifier Chain

Because of the nature of the SFD-257 CFA, the high-power (final) stage does not require a cathode voltage pulse modulator. DC voltage is continuously applied to the cathode. Input RF excitation starts cathode emission via secondary emission effect. At the end of the pulse as excitation is removed, free electrons are extracted from the tube by application of a carefully shaped and timed video pulse to a special electrode in a process called "quenching." Quenching is necessary to prevent the tube from oscillating in a self-excited mode at a frequency near the lower band edge after RF excitation is removed. The absence of high level modulation and the relatively high efficiency of both the semi-final and final stage crossed-field contribute to the relatively high efficiency and compactness of the moderately high power sophisticated transmitter.

In particular, the coded group (burst) of five quarter-microsecond pulses is handled efficiently by shaping the pulses in the lower level amplifiers. This avoids relatively high losses due to the charging and discharging of the stray capacitances associated with pulsing the final amplifier cathode circuitry. Such losses typically are a significant fraction of the power of a quarter-microsecond video pulse, and substantially lower transmitter efficiency.

For operation with quarter-microsecond pulses, the quench modulator losses are not negligible (560 watts in the burst mode at full duty out of a corresponding total input power

of 2160 watts). However, the losses are significantly less than RCA has experienced pulsing a magnetron with operating point characteristics similar to those of the SFD-257, operating in the burst mode at the same power output level.

The high-voltage power supply for the final stage CFA is specially designed to provide stable system operation notwithstanding an occasional tube arc. Any high voltage electron tube has a sporadic arc rate when high voltage is continuously applied. Transmitter tripout may result in loss of very expensive data in the missile range instrumentation application. Consequently the cathode power supply (-29 kVDC) first current-limits, then terminates the arc current electronically, and finally, automatically restores the CFA cathode voltage so operation may continue. Transmitter downtime due to an arc is less than one second.

Emission Quenching

Figure 2 represents the final CFA and its associated circuitry.

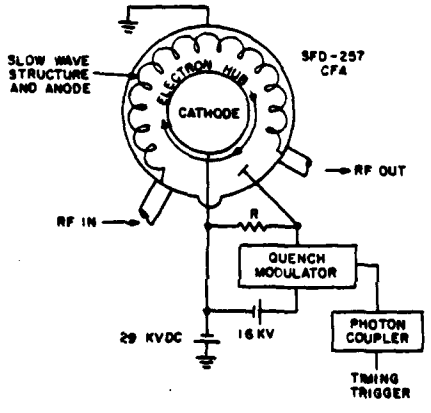

Figure 2. Simplified Schematic of Final Amplifier Stage

During the pulse a re-entrant "hub" of electrons orbits the cathode surface. RF excitation causes secondary emission from the cathode surface to initiate, then continuously replenish the hub. Removal of RF drive and simultaneous extraction of the free electrons in the hub by applying a positive voltage to an electrode exposed to the orbiting electrons, causes electron activity in the tube to cease.

An interesting phenomenon has been observed related to the quenching process. If the amplitude and timing of the quench signal are not appropriate, the tube oscillates in the noisy lower band edge mode following the pulse. Spurious energy generated apparently leaks from the region of the cathode stem and causes multiple triggering of low-level solid-state video drive circuits. The combination of operation in the wrong mode and abnormally high duty cycle due to the extra pulses degrades the performance of the CFA in subsequent operation, even though proper quenching is restored. Higher than normal CFA interpulse leakage current flows and the tube spectrum is noisy. Normal performance can be restored by a seasoning process in which the tube operating voltage level is gradually increased. Interpulse leakage current returns to its normal level and the spectrum noise disappears.

Figure 3 displays timing and amplitude relationships between the envelope of RF drive, quench voltage pulse, and quench current pulse. Several requirements on these relationships must be met if stable tube operation is to be realized. First, the quench voltage must reach a level of at least 12.5 kV before the RF drive level falls below 12.5 kW or 25 per cent of normal drive power. Second, the quench voltage must be sustained between 15 and 17 kV until the RF drive level has decreased to 10 watts or below. If either requirement is violated, the tube will break into the undesired noisy self-excited oscillation at a frequency near the lower band edge as mentioned earlier. Note that the peak current of the quench electrode occurs at the 12.5 kV voltage point when the relationships are as stated above.

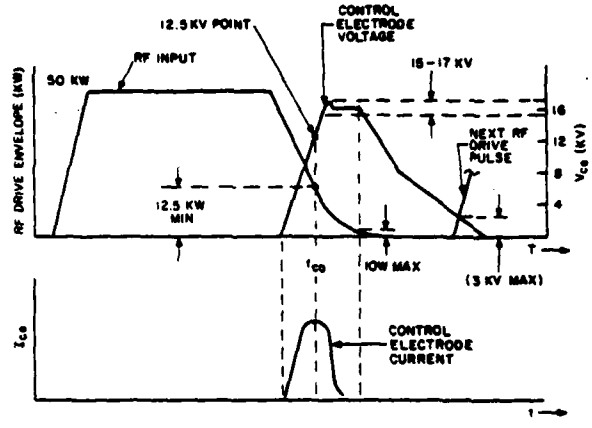

Figure 3. Timing and Amplitude Relationship RF Drive and Quench Voltage

The quench pulse may be started earlier (higher up on the tail of the RF drive envelope) without instability. In this case the RF output pulse is foreshortened as compared with the drive pulse, and the quench current modulator will draw a longer and higher amplitude current pulse.

In the case of burst mode operation, the quench voltage from the previous pulse must be caused to fall below 3 kV before the ensuing pulse appears. Otherwise, the front edge of the ensuing RF pulse will be distorted by quenching effect. The latter requirement necessitated the use of a "tail biting" resistor (R in Figure 2), shunting the quench electrode circuit to discharge stray capacitance promptly after the quench modulator keying is terminated. This resistor loads the quench modulator and lowers system efficiency as an effect of burst mode operation.

The rise time of the 16 kV voltage pulse is approximately 0.1 microsecond (10 - 90%). The peak quench current is 16 amperes as compared with normal peak tube current of approximately 60 amperes.

Referring to Figure 4, the quench modulator in the subject transmitter employs three paralleled Y-543 tetrodes switching a 16 kVDC power supply floating at CFA cathode potential.

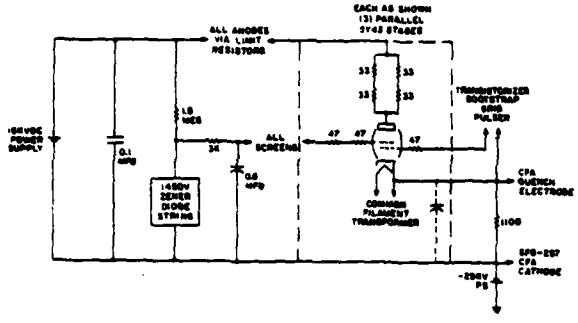

Figure 4. Quench Pulser for SFD-257 Crossed Field Amplifier

The switch tube grids are transistor-driven. Response time of 0.1 microsecond was achieved in the solid-state grid pulser by shaped turn-on and turn-off base drive pulses for the transistors. This relatively high speed performance using a parallel pair of DTS-804 transistors was necessary to effective quenching for burst mode operation. Figure 5 indicates the grid pulser circuit. The SY43 tetrodes are biased off to -650 V via an L/R high frequency compensator network between pulses. The DTS-804 transistors connect a 100 V power supply to the grid-cathode circuit of the switch tubes while the quench electrode is conducting.

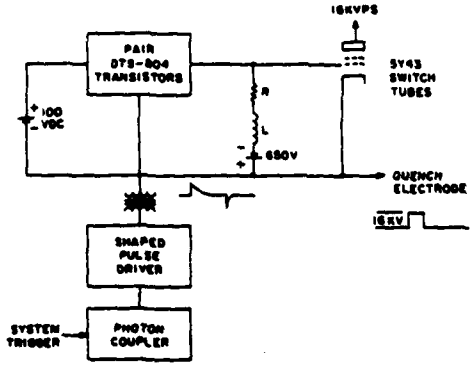

Figure 5. Transistorized Bootstrap Grid Pulser for Switch Tubes

Similar circuitry is employed in the modulators for the first and second amplifier stages of the transmitter. A transistor-drive Y-543 tube switches a 16 kV power supply for the 8041T TWT cathode, and a similar combination switches a 9 kV power supply for the SFD-244 conventional forward-wave type crossed-field amplifier.

Shaping and timing requirements for the relatively critical burst mode pulse waveforms discourage sharing a common modulator circuit between the first and second stages.

Figure 6 displays the quench voltage pulses and RF output envelopes for burst mode operation, superimposed on a 0.5 microsecond per centimeter time base.

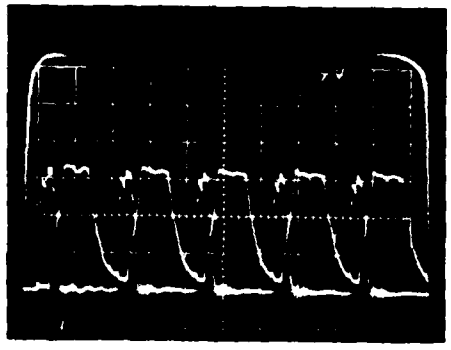

Figure 6. Display of Quench Voltage Pulser and RF Output Envelopes in Burst Mode Operation

Conclusion

The modulator described delivers emission-quenching pulses for the CFA in accordance with empirically derived requirements for the burst-mode operation as well as all other required modes of operation. The result has been stable and reliable operation from the final amplifier tube and transmitter.

Acknowledgement

Material contained in this paper is excerpted from a recent article by the author and A. Wilczek of Varian Associates. The article "CFA Tube Enables New-Generation Coherent Radar" was published in the August 1973 issue of Microwave Journal.

DESIGN CHARTS FOR DROOP-COMPENSATION NETWORKS

Thomas A. Weil
Raytheon Company
Wayland, Mass.

Summary

The principles of pulse droop compensation with passive RLC networks are well known, but the practical application of these principles has been hindered by the complexity of analyzing even the simplest cases quantitatively. This paper presents the results of a computer analysis of droop-compensation methods. The tradeoffs are described, and the results are presented in charts that show directly the loss in efficiency versus the amount of droop before and after compensation. The charts also provide the data necessary to determine the component values to provide the selected droop-compensation performance.

Droop Compensation

Introduction

The size and weight of the energy-storage capacitor bank required for an active-switch modulator is strongly affected by the amount of droop permissible[1]. Therefore, in applications where size and weight are critical and where a slight reduction in efficiency is tolerable, passive droop-reduction techniques may be advantageous. A simple droop-compensation circuit is shown in Fig. 1, with L and RS serving to reduce the droop seen by the load. The waveforms for this circuit are shown in Fig. 2; the droop before compensation, V_B, is reduced to the smaller variation, V_A, after compensation. At the start of the pulse, the load voltage is reduced by the drop across the resistor RS; during the pulse, the inductor L gradually shorts out RS, which tends to compensate for the reduction in voltage available from the capacitor bank C as its voltage droops during the pulse, as shown. The reduced voltage variation at the load during the pulse is achieved at the expense of some power absorbed by the series compensating network during the pulse, and, as might be expected, the better the compensation, the higher the loss. A suitable choice of compensation network thus requires a quantitative evaluation; this paper presents data to facilitate this tradeoff.

The simple compensation network shown in Fig. 1 is applicable to most active-switch modulators[1] as well as to DC-operated devices such as gridded or mod-anode-pulsed linear-beam tubes, control-electrode CFA's, RF-keyed CFA's, and Class-C RF amplifiers such as solid-state modules. The results of the analysis also apply to certain other cases, as will be mentioned later.

Networks Considered

The network shown in Fig. 1 may be called a "first-order" droop compensation network, because it contains only a single reactance. Although higher-order networks can be considered, they are beyond the scope of this paper. Furthermore, higher-order networks have difficulty ensuring that residual stored energy left from one pulse does not affect performance on the next pulse; the first-order network shown in Fig. 1 has negligible carry-over from one pulse to another, because of its inherent damping, unless the system duty cycle is extremely high. The analysis that follows assumes that currents in the compensation network die out fully during the interpulse period, which is valid as long as the interpulse period is many times longer than the time constant of the compensation network, as will normally be true.

Analysis

Even the "simple" first-order droop-compensation network shown in Fig. 1 is surprisingly complicated to analyze, a fact that may have contributed to the relatively limited usage of such networks in the past. Although such an analysis is nearly prohibitive by hand calculation, it is a very simple problem for modern computers, the real challenge being to organize the voluminous results into convenient form for routine use.

In the network of Fig. 1, L and RS may be chosen independently; these values determine the initial drop across the network and the time constant of the network, which, compared to the pulse duration, determines how nearly the drop across the network goes to zero during the pulse. These choices, in turn, determine the net peak-to-peak variation in the pulse delivered to the load and the loss in efficiency that results. The choices available also permit overcompensating or undercompensating the load voltage at the end of the pulse compared with the load voltage at the start of the pulse, as shown in Fig. 3. The analyses made showed that, if the objective is to minimize the peak-to-peak voltage variation over the pulse duration, the best improvement for a given loss is obtained when the network values are chosen to make the load voltage end at the same value it started at, shown as ΔV_2 in Fig. 3. Therefore, the results that follow are all given on that basis, which, incidentally, simplifies the eventual calculation of component values for any particular circuit.

From the computer viewpoint, this problem is a simple linear transient analysis with a narrow range of circuit time constants, so that accurate integration is readily achieved with a moderate time-step size. The computer program calculates how the voltages and currents vary during the pulse and keeps track of power drawn, power lost, and power output. Maximum and minimum values of load voltage are also noted. The resulting voltage variation and power loss can be tabulated for various cases of interest, and waveforms can be plotted for inspection. Fig. 4 shows

typical load voltage waveforms for a circuit with 10% droop before compensation (DBC) and with various values of time constant in the droop-compensation network. The data from these runs can then be used to generate a graph showing efficiency loss for various values of droop or voltage variation before and after compensation, as shown in Fig. 5.

Results

As shown in Fig. 5, the curve that starts (for example) at 10% voltage variation with no loss applies to cases of 10% droop before compensation, etc. It can be seen that, as with many things in life, "the rich get richer and the poor get poorer"; i.e., if the circuit has little droop before compensation, it can be improved a lot with little loss, while a circuit that has a lot of droop incurs a lot of loss even if the droop is reduced by a small factor. It appears that very large improvement factors (greater than, say, ten) are not likely to be used, because a circuit with little droop to begin with doesn't need it, while a circuit with a lot of droop can't afford it (from an efficiency standpoint).

Tolerance effects also argue against attempting to reduce droop by a large factor by this technique. Since the correction is "open loop", component tolerances will cause the amount of compensation to vary; the widest variations probably will occur if electrolytic capacitors are used (e.g., for solid-state transmitters), since these have both wide initial tolerances and wide changes in value with temperature and with life. Variations in load current also have an effect on the droop compensation, although this effect is less significant. Changes in transmitter pulse duration also change the droop compensation, but as long as the pulse is no longer than the value for which the compensation was designed, the resulting load voltage variations will not be greater than for the long pulse, but the pulse may no longer end at the same value of voltage it started at.

Using the Charts

Fig. 5 thus provides the data needed for droop compensation tradeoffs. For example, if a system requires the load voltage to vary no more than 2.5% over the pulse duration, a certain capacitor bank size would be required without compensation. The capacitor bank can be cut in half and the droop corrected to 2.5% at the expense of 1.2% loss, as shown by point A, or the bank can be reduced by a factor of 4 (resulting in 10% droop before compensation) and corrected to 2.5% at the cost of 4% loss in efficiency, as shown by point B.

Once the desired point is selected, the droop compensation network component values may also be obtained from the data in Fig. 5, using the time-constant data shown; the required T/TC value (pulse duration divided by time constant) obtained from the curves is then used in the formulas below. For example, to correct 5% droop to 1% requires a T/TC of about 1.8, as shown by point C in Fig. 5.

First, the value of RS (see Fig. 1) is obtained from:

Let X = T/TC, as obtained from Fig. 5.

Let DBC = Droop before compensation.

The "Initial Drop" (at the start of the pulse) across RS is independent of the value of L, and should be made equal to

$$\text{Initial Drop} = \text{DBC}\left(\frac{1}{1-e^{-x}}\right)$$

For convenience, values of $\left(\frac{1}{1-e^{-x}}\right)$ are given in Fig. 6.

For example, if T/TC = 2 and the DBC is 10%, the initial drop is 11.7%, and RS should be made equal to 11.7% of the load impedance, RL.

The value of L is then obtained simply from

$L = RS\,\frac{T}{X}$, where T is the pulse duration.

The required initial voltage on the capacitor bank is the sum of the desired load voltage at the start of the pulse plus the initial drop across the droop-compensation network.

Side Effects

It should be noted that the use of a droop compensation network results in a slightly increased voltage appearing across the load (or series switch device) during the interpulse period, because the capacitor bank voltage must be set higher to begin with to allow for the drop across the network, and because there will be a slight backswing across the droop-compensation network immediately after the pulse. The backswing is never greater than the initial drop and occurs at the end of the pulse when the capacitor bank has drooped, so this effect should be small; only the increased capacitor bank voltage itself should be significant, depending on how much droop-before-compensation is chosen. The load simply sees the full capacitor-bank voltage before the pulse begins, as indicated in Fig. 2.

Alternative Circuit

As indicated earlier, the data of Fig. 5 can also be applied to certain other cases, as shown in Fig. 7. For example, the source in Fig. 7 could be a line-type modulator, with L_M representing the pulse-transformer magnetizing inductance, which may draw a linearly-rising magnetizing current that subtracts from the load current, tending to cause a drooping load-current waveform. R2 and C2 have been added to this circuit to cancel this droop; this may be preferable in some cases instead of the series network of Fig. 1, as would be the case if the source in Fig. 7 were a current source. On the other hand, the alternative circuit of Fig. 7 is not usable with DC-operated loads, because C2 would charge up before the pulse begins.

For the compensation network in Fig. 7, the same calculations are made as before, except that if the "initial drop" required is 8%, then R2 is chosen to draw 8% as much current as the load, assuming C2 is initially not charged at the start of the pulse; i.e., R2 would be 12.5 times the load resistance. C2 is then chosen to provide the required time constant; i.e.,

$$C2 = \frac{T}{(R2)(X)}$$

where T is the pulse duration, as before.

Conclusion

First-order droop compensation networks can provide significant reduction in energy-storage capacitor bank size and weight at a small-to-moderate cost in efficiency. The charts presented should allow the best choice to be made for any particular application.

References

1. Radar Handbook, McGraw-Hill, 1970, pp. 7-78 and 7-83.

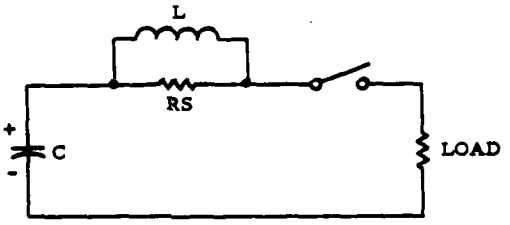

FIG. 1. FIRST-ORDER DROOP COMPENSATION NETWORK

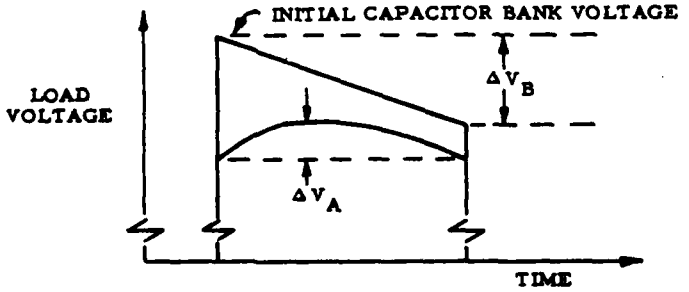

FIG. 2. LOAD VOLTAGE WAVEFORMS BEFORE AND AFTER DROOP COMPENSATION

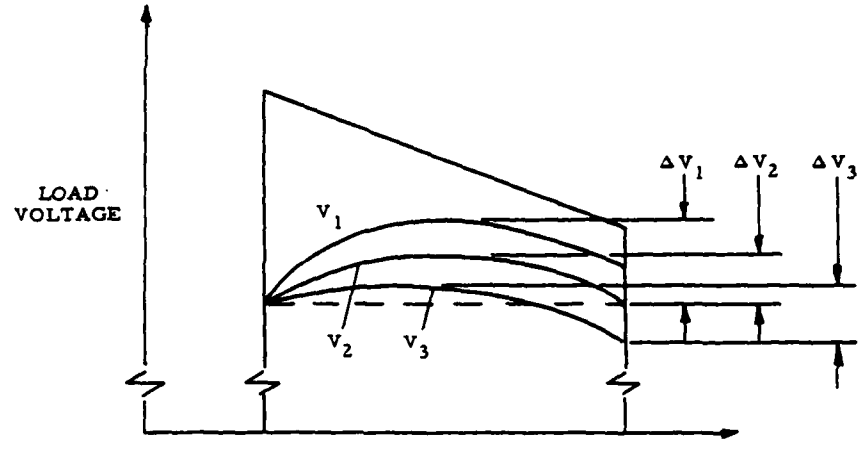

FIG. 3. DROOP COMPENSATION WAVEFORMS FOR THREE NETWORK VALUES

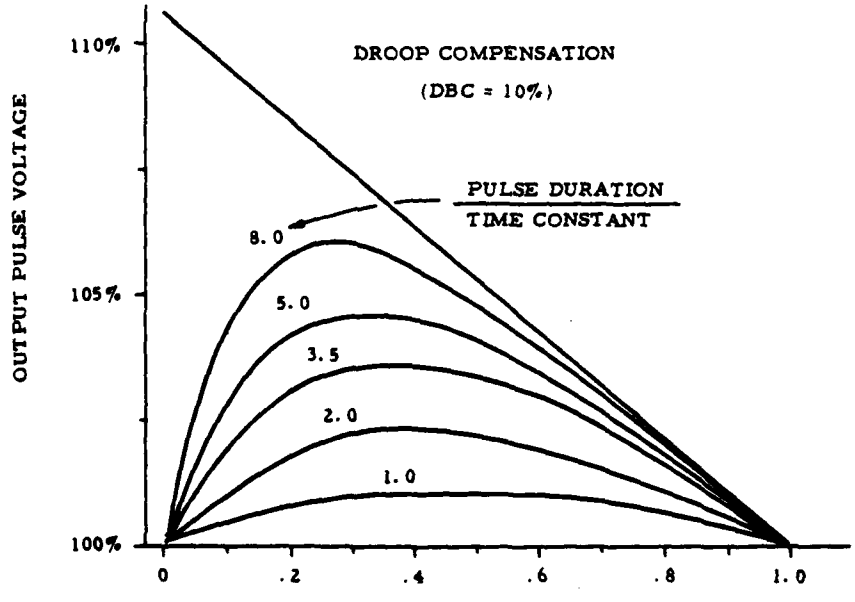

FIG. 4. DROOP COMPENSATED LOAD VOLTAGE WAVEFORMS

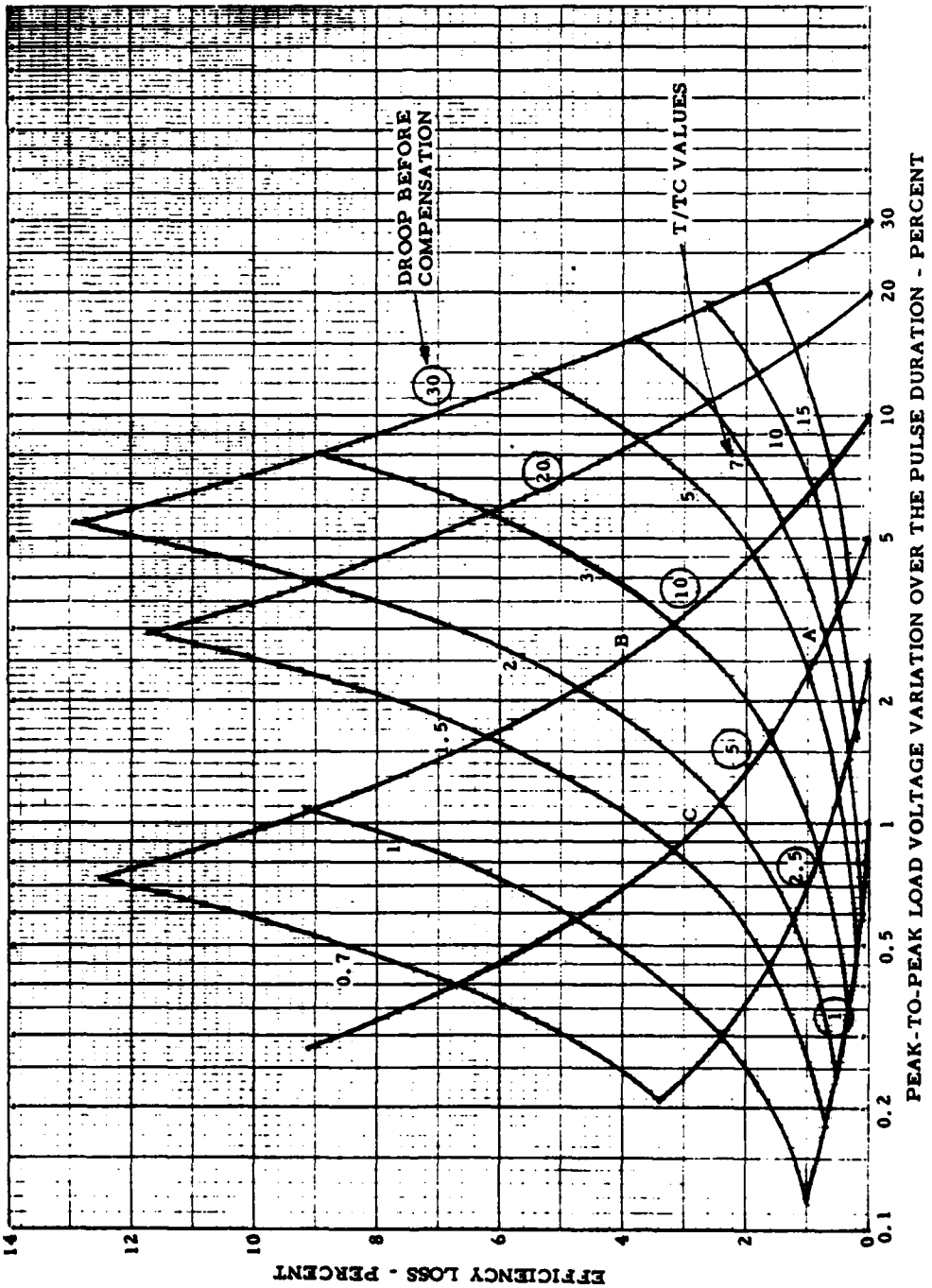

FIG. 5. DROOP COMPENSATION DESIGN CHART

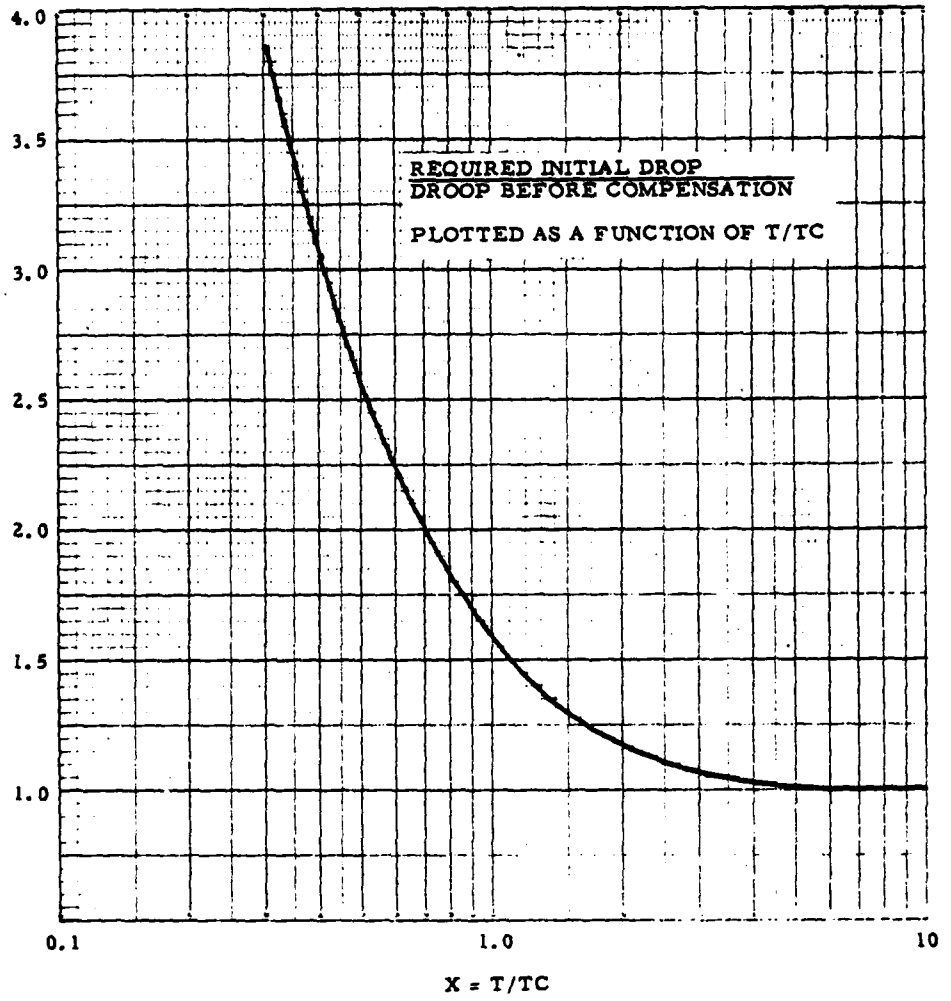

FIG. 6. REQUIRED INITIAL DROP

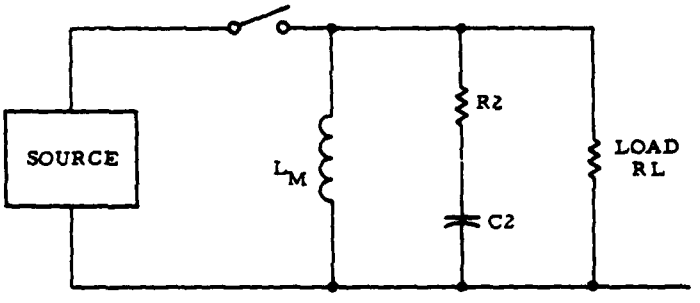

FIG. 7. ALTERNATIVE DROOP COMPENSATION METHOD

VERY HIGH FREQUENCY PULSE GENERATORS USING HYDROGEN THYRATRONS

B. P. Newton G. J. Scoles
English Electric Valve Co. Ltd.
Chelmsford, Essex, U.K.

Summary

Two circuits are described which have been developed to provide high voltage pulses at repetition rates up to 200 kHz. Mention is made of fast recovery hydrogen thyratrons capable of operating in these circuits.

A requirement arose for a pulse generator able to generate bursts of 16,000 volt pulses at a recurrence frequency of 200 kHz. The load (a Pockel cell) was basically capacitive and it was apparent that a pulse current of several amperes was necessary if a rise time of 20 nanoseconds were to be achieved. A hydrogen thyratron was chosen as the switching element not only because it can pass high peak currents but also because it is easily triggered by a low power grid pulse and the rate of rise of current in its anode circuit is not limited by the rate of rise of grid voltage.

The factor which limits the maximum working frequency of a thyratron is its recovery time and as the pulse recurrence frequency of 200 kHz allowed less than 5 microseconds both for recovery of the thyratron and the subsequent recharging of the pulse forming network or capacitor, it was likely that conventional techniques would be inadequate to solve this problem. The solution involved the development of a fast-recovery hydrogen thyratron, as well as the use of special techniques for triggering its control grid and re-applying anode voltage. Two pulse generators were designed, one being suitable for use where all the equipment could be grouped together, the other being more complex but able to drive a load at a point remote from the actual pulse generator.

The CX1198 thyratron as finally developed had three grid-electrodes, the first serving to pre-ionise the gas in the vicinity of the cathode, the second being used as the triggering grid, whilst the third functioned as an earthed screen. The control electrode was enclosed within an earthed box which constituted the third grid, the assembly being arranged so that the discharge was constrained to pass through a series of narrow, staggered slots. This type of thyratron when correctly driven has an effective recovery time of the order of 2 microseconds.

In order to assist the control grid to effect recovery it was necessary to apply a signal of negative polarity immediately following conduction and its effective impedance had to be substantially zero until recovery had occurred. This was achieved by a variant of the "break modulator" technique wherein a current continuously flowing in the primary circuit of a double-wound transformer is momentarily interrupted to generate a trigger pulse. This causes a current to flow in the secondary winding, thereby overcoming the initial bias to drive the grid of the thyratron positive and so initiating conduction. During conduction the bias voltage appears across the secondary winding; this has the effect of increasing the current flowing and so increasing the energy stored in the self-inductance of the transformer. Restoring the primary current then causes a reversed voltage to appear across both windings of the transformer, the practical effect of which is to drive the grid sharply negative (relative to the bias) and to make available a relatively large current which then assists in clearing up the plasma from the vicinity of the grid. This mechanism (Fig. 2) results in extremely rapid recovery of control by the grid, times of the order of 2 microseconds being typical for the CX1198 with this grid circuit, which is shown in Fig. 1 in skeleton form.

The charging circuit should be one in which positive voltage is kept from the thyratron anode for as long as possible after conduction. Fig. 3 shows a previously devised circuit which meets this requirement and is of particular interest in that a small negative voltage is applied to the thyratron anode immediately following conduction and that, due to the absence of any positive d.c. supply, it is impossible for the thyratron to go into continuous conduction.

The circuit operates as follows:-

Assuming that C is initially uncharged, V is rendered conductive by applying a positive-going pulse to its grid. Current builds up linearly in the inductor L during this period and when V again becomes non-conductive the energy stored in L is transferred to C by charging it sinusoidally to a high voltage. A diode can be introduced at X in order to prevent reversal of current but in this application it is better to optimise the various parameters and to trigger the thyratron at the instant of maximum voltage on C. T discharges C via the load R after which V is again made to conduct and the cycle repeated. Fig. 4 shows the anode waveform obtained at a recurrence frequency of 250 kHz.

The fast-fronted output pulse so generated is of negative polarity and has an exponential decay determined by the time constant CR. Its amplitude is slightly less than the voltage V to which C is charged, the corresponding current maximum being determined by V/R at about 15 A. By replacing the single capacitor of Fig. 3 by two and altering the circuit to the form shown in Fig. 3 (a), a pulse can be generated which has an initially flat top which merges smoothly into an exponential tail as before.

As the circuit of Fig. 3 necessitates the cathodes of T and V being at different potentials, an alternative arrangement has been devised in which the circuit operates in a substantially identical manner but with both cathodes arranged to be at the same potential. This involves replacing L by two separate inductors L_1 and L_2 and coupling their ends together by means of capacitance as shown in Fig. 5. L_1 and L_2 are then effectively in parallel, the storage and subsequent transfer of energy to C taking place almost exactly as in the original arrangement. Provided that C_1 and C_2 are appreciably larger than C, the voltage and current waveforms of the two versions are very similar and the output pulses indistinguishable. With the modified circuit it will be apparent that a power supply of positive polarity is required, whereas the original circuit operates from a negative supply. L_1 and L_2 of Fig. 5 can be separate as shown but in high power applications it is advantageous if they are magnetically coupled together. This results in a more economical design without in any way affecting the performance of the circuit.

Tubes of the CX1198 type were operated in both these circuits for long periods under burst mode conditions and so long as C was of the order of 100 pF and stray capacitances were minimised both circuits could be made to operate at the required rate of 200,000 pulses per second satisfactorily.

The second type of circuit was developed for situations where the load was located some distance away from the pulse generator, and this of necessity increased the stray capacitance considerably. This meant that as C had to be several times this capacitance the whole equipment had to be scaled up to suit. The limiting factor was the rating of the C1149/1 tetrode and the choice then lay between using several in parallel or of finding an alternative circuit which could generate more power in a relatively simple manner.

If an inductively charged pulse generating circuit is operated without a charging diode it can work satisfactorily in three different ways, according to whether it is driven at resonance or above or below the resonant frequency. Of these, the below resonant mode results in current reversal in the charging inductor occurring immediately before conduction of the switching device, the reverse current continuing after conduction and causing the anode to be driven negative for a period which depends upon the degree of departure from resonance. As this is a desired characteristic, the system (Fig. 6) was investigated and was found to work in the manner described although it could not be made to withstand the full 16 kV at 200 kHz. A compromise was devised in which two circuits of this type were arranged to work alternately into a common load, each circuit therefore only having to run at 100 kHz. The circuit was optimised with the capacitor of Fig. 6 being replaced by a cable-type pulse forming network. A pulse transformer was introduced in order to reduce the peak voltages occurring on the thyratron anode and coaxial cables. The corresponding increased peak current (230 amperes) was within the thyratron capability. The pulse length of 100 nanoseconds was determined by the cable length.

The output rise-time specification of 20 nanoseconds necessitated the development of a special type of transformer which used cables effectively in series at one end and in parallel at the other. This provided a perfect match between the network and transformer and introduced no distortion of the waveform. In the U.K. this type of transformer was first devised by S. W. Redfearn for the Harwell linac circa 1950 and the 1:4 ratio version used is shown in Fig. 7. This gives an impedance ratio of 1:16, in

the same way as with a normal transformer of 1:4 turns ratio and causes voltages to appear from end to end of the four cables in the ratio of 0, 1, 2, 3 respectively. Hence by winding three of the four cables on an iron core with relative turn ratios of 1, 2 and 3, the effect is similar to a perfect transformer shunted by inducatance. Since the pulse currents flow only along the cables and actual transformer action is not involved, no deterioration of waveform is introduced other than that normal with cables of the length used.

The transformer used four cables identical to the four which formed each of the pulse forming networks so that perfect matching between them was automatically achieved. The 1:4 ratio meant that it was only necessary to charge the networks to 8 kV to get a 4 kV pulse at the transformer input and hence one of 16 kV at its output. Similarly the voltage at the thyratron anode rose to a maximum of about 10 kV (at the instant of current zero in the charging inductors) and was 8 kV at the instant of triggering.

This charging circuit (Fig. 8) is less suitable for high frequency working because it does not hold the thyratron anode negative for such a large fraction of the cycle. However, the combined effect of halving the recurrence frequency and of reducing the anode voltage of the thyratron resulted in an arrangement which functioned satisfactorily. The alternate firing of the two thyratrons enabled an effective frequency of 200 kHz to be achieved without difficulty and no interaction between the two half-circuits was experienced.

The two types of pulse generator described were devised with emphasis on different factors. The first circuit was designed to run at as high a frequency as possible with a fast recovery thyratron and is reliable because the only result of the thyratron self-triggering is a low amplitude or missing pulse. It can only be used for light loads because of the limitations imposed by the current-carrying capacity of the pulse tetrode through which energy is stored in the inductor L (Fig. 3). The second circuit is based on the conventional pulse modulator used in many radar sets and can be operated with much heavier loads. The use of the special pulse transformer allows some freedom of choice of load impedance for a given pulse power. However, this circuit is more complex and for a given pulse recurrence frequency the component values are more critical.

The CX1198 thyratron which has been operated in these circuits is of glass envelope construction as shown in Fig. 9. Since the requirement was for bursts of pulses at 200 kHz this design was capable of withstanding the dissipation involved. For continuous operation a ceramic thyratron of the GHT14 shield grid type could be used so that the higher electrode dissipations may be more adequately dealt with. (Fig. 10)

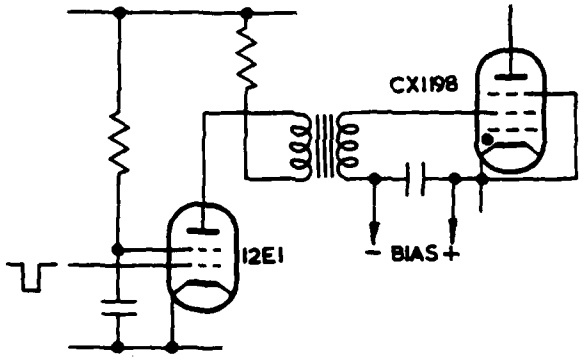

Figure 1

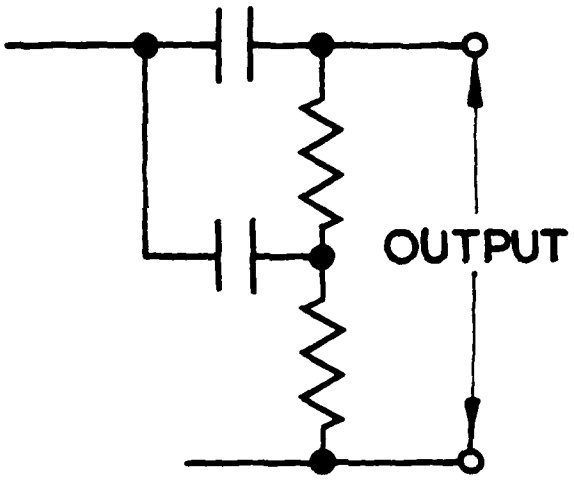

Figure 3A

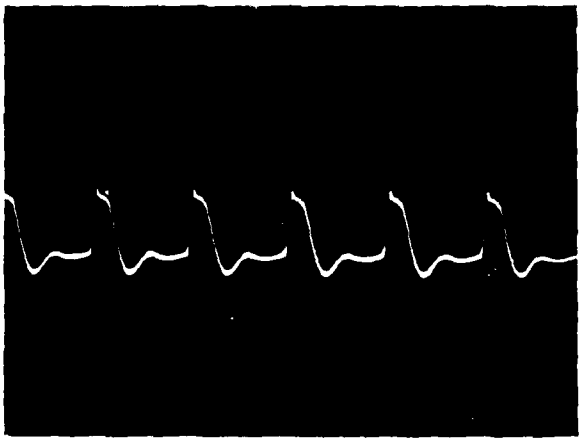

Figure 2

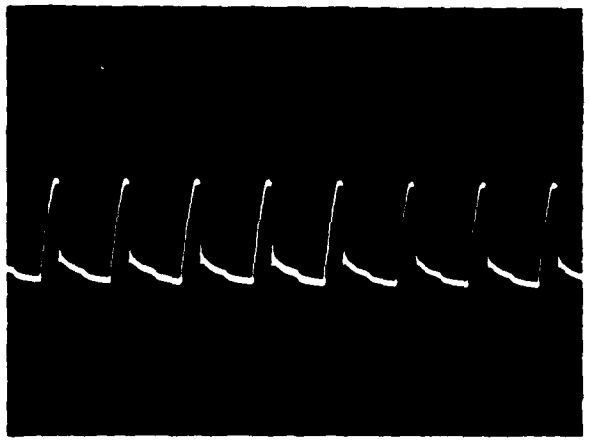

Figure 4

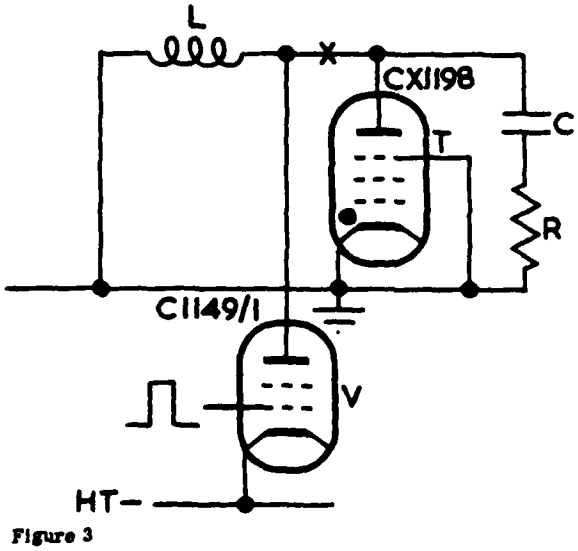

Figure 3

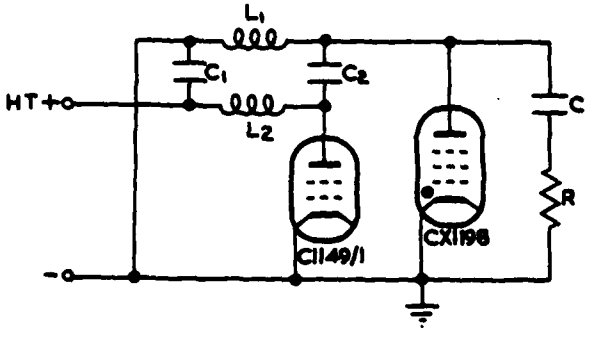

Figure 5

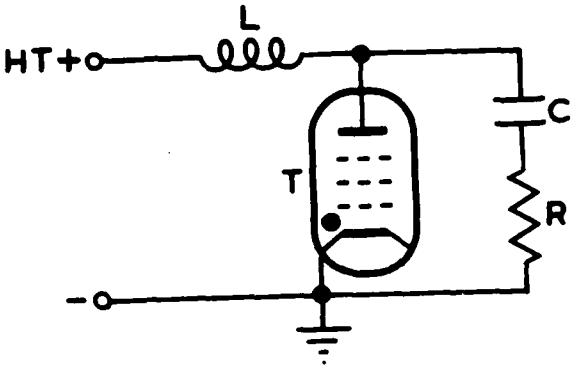

Figure 6

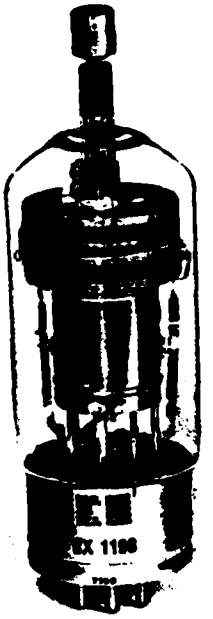

Figure 9

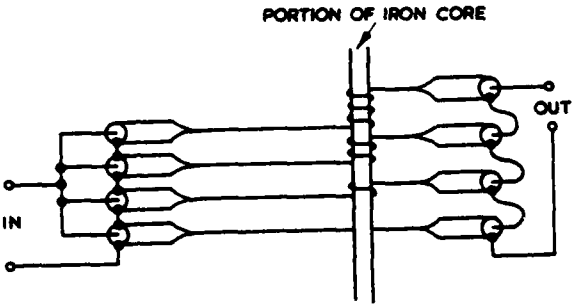

Figure 7

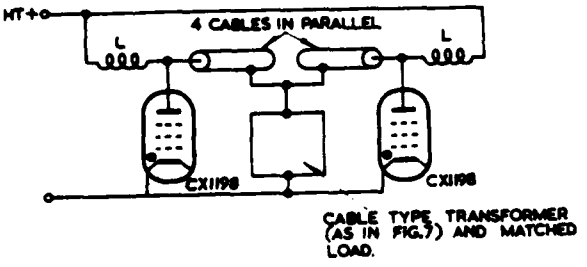

Figure 8

Figure 10

PULSE GROUP OPERATION OF HIGH POWER LINE TYPE MODULATORS*

Robert M. Rowe

Stanford Linear Accelerator Center
Stanford University, Stanford, California 94305

Summary

The development of a high power double pulse line type modulator is described. The design goal output of this modulator was two 185 kilovolt 2.5 microsecond pulses with an interpulse separation of 23 microseconds.

In order to produce two closely spaced pulses the network of a SLAC standard 65 megawatt single pulse modulator was split electrically, but not physically. An additional hold off diode, thyratron and end of line clipper were installed thus enabling the two networks to function independently while sharing a common charging inductor and power supply.

The interaction problems, i.e., sympathetic firing, etc., encountered and the methods used to solve them are discussed.

Introduction

One of the proposals for increasing the beam energy of the Stanford Linear Accelerator requires that the electron beam be recirculated through the accelerator before being delivered to the experimental area. This will result in a doubling of the energy of the delivered beam, but also requires that the 245 high power line type modulators and klystrons deliver two accelerate pulses separated in time by approximately 23 microseconds (the transit time of the 10,000 meter accelerator structure and return drift tube).

General Description

In order to determine the feasibility of obtaining this type of performance from a conventional line type modulator as quickly and inexpensively as possible it was decided to use one of our standard modulators as the development vehicle. Also, to further reduce costs, as much of the existing circuitry and hardware as feasible was to be used. With those constraints in mind the following overall design objectives (including the output pulse transformer) were drawn up:

Peak power output (each pulse)	30 MW
Average power output	65 kW
Output voltage	185 kV max
Output current	160 A
Load impedance	1160 ohms
Pulse length, flat top (each pulse)	2.5 μs
Risetime (each pulse)	0.7 μs
Falltime (each pulse)	1.2 μs
Pulse top ripple (each pulse)	$\pm$ 0.5%
Pulse separation (nominal)	23 μs
Pulse group repetition rate	360 per second

If one looks at the schematic diagram (Fig. 1) of the standard SLAC single pulse modulator, an approach to the problem immediately suggests itself. Since the network is already split into two parallel 10 section networks, which are discharged simultaneously into a common load, it would also appear to be possible to discharge them individually into the common load. In order to accomplish this a second switch tube and driver are needed as well as duplicate charging diodes. The latter are required to properly isolate network number 2 after network number 1 has been discharged. The single charging transformer is retained and the networks are charged in parallel, as usual. In order to protect the second network from over voltages due to load arcs, an additional end of line clipper circuit is also required. (These modifications are shown schematically in Fig. 2.)

Changing from a 20 section series parallel network to two ten section series networks without changing the values of the individual pulse capacitors necessitated a change in value of the network inductance and turns ratio of the pulse transformer. Assuming an equivalent rectangular output pulse width of 3.4 microseconds and a total network capacity, C_n, of 0.14 μF, the new network inductance, L_n, was determined from the familiar expression,

$$L_n = \frac{\tau^2}{4C_n} \quad .$$

This yielded a network inductance of 20.6 μH, or about 2 μH per coil. Each coil can be roughly tuned by changing tap points and finely tuned by means of an aluminum slug. The P.F.N. and switch tube compartment of the standard single pulse modulator is shown in Fig. 3. The double pulse modulator is the same except the single switch tube is replaced by two GE 7890's which are placed side by side on the mounting plate. The driver chassis for the second thyratron was outboarded for this experiment.

The pulse transformer was the last major item required for the system. The transformer that is used on the Stanford Linear Accelerator to match the high power RF drive klystron amplifiers to the main modulators is rated 75 kW average power at 250 kV peak pulse voltage and thus appeared suitable for the job. This transformer has a 72 turn secondary and a 6 turn primary. The turns ratio required to match the new 12.3 ohm networks of the double pulse modulator to the 1160 ohm klystron load is 9.7 to 1. However, it has been our experience that a 5 - 10% positive mismatch between P.F.N. and load results in improved switch tube operation and increased modulator efficiency. A turns ratio of 9:1 will prodice the desired mismatch and was easily obtained by increasing the primary turns from 6 to 8. No other modifications were made to the output pulse transformer.

The peak flux density in the pulse transformer core must also be investigated. This is not easy to do with great precision in the case of closely spaced pulses and nonlinear loads. However, some rough approximations can be made. The pulse transformer operates with a biased core. As the result of a 15 A direct reset current the core remanent flux is nominally negative 9 kG. The flux swing per pulse is 13 kG and the recovery between pulses (neglecting any contribution from the reset current since the time constant of this circuit is approximately 1 ms) is approximately 7 kG. Thus, the estimated peak flux density in the core at the end of the second pulse is plus 10 kG. This is approximately the same post pulse core condition that exists under normal single pulse operation of this transformer.

Operating Experience

With all modifications complete, the modulator was ready to try out. In order to facilitate the inevitable debugging procedure, a high power salt water resistor was used to load the pulse transformer for the initial trials. On the first runup all was well until the power supply voltage reached 6 kV (approximately 60 kV peak pulse output per pulse). At that point switch tube number 2 starting firing simultaneously with tube number 1. It was obvious that stray coupling of pulse number 1 into the grid circuit of tube

*Work supported by the U. S. Atomic Energy Commission.

number 2 was causing the problem. Two solutions suggested themselves: shield the grid circuit of the second tube or lower its grid circuit impedance. Because of the layout of the swtich tube compartment and the high voltages involved, effective shielding posed some rather formidable mechanical and electrical problems. Therefore, the latter solution was tried first. Stable operation was achieved when the number 2 tube grid shunt capacitance was increased to 500 pF and shunt resistance lowered to 5 ohms (Fig. 2). The resulting output pulses are shown in Figs. 4a,b,c. On the resistance load pulse spacings as close as 10 μs (leading edge to leading edge) were obtained. Maximum pulse output voltage was limited, as predicted, by the onset of pulse transformer core saturation which occurred at approximately 190 kV.

At this point the modulator was turned over to the klystron group for their tests. The beam voltage waveforms obtained on a standard SLAC klystron of microperveance 2 are shown in Figs. 5a,b,c. From the waveforms of Figs. 5b and 5c it can be seen that the pulse top ripple obtained was more like $\pm 1.7\%$ than the design goal of $\pm 0.5\%$. The additional pulse top ripple is principally attributable to the mismatch that exists between the pulse transformer characteristic impedance and the dynamic impedance of the klystron load. (The transformer was designed to drive a 1000 ohm load.)

In summary it appears that pulse group operation of high power line type modulators is entirely feasible and does not require elaborate shielding or other exotic techniques. Required, however, are much lower grid circuit impedances with an attendant substantial increase in grid driving power.

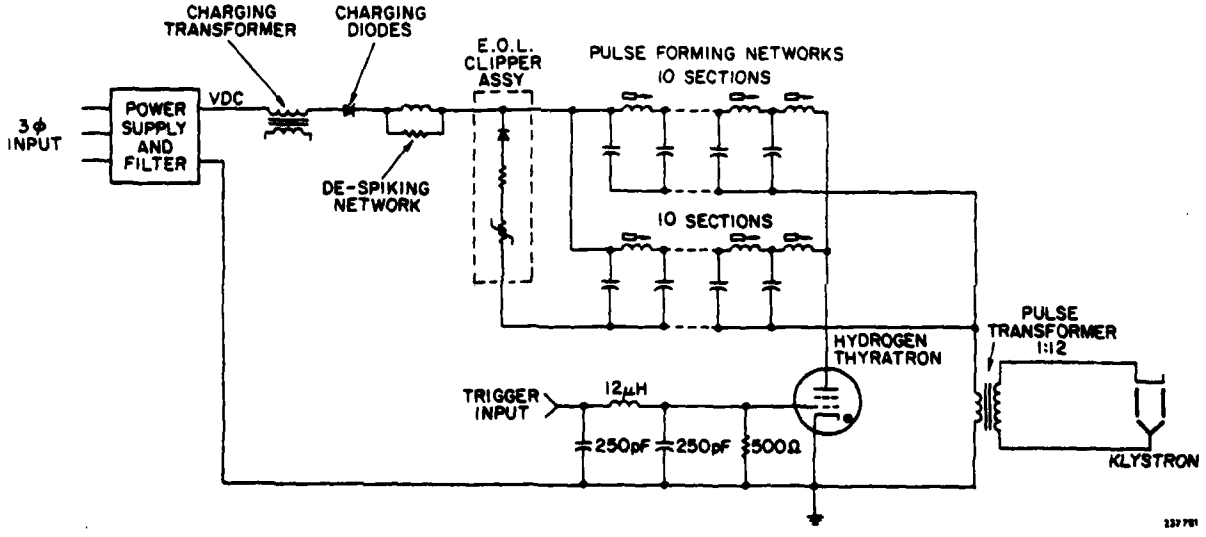

FIG. 1--Schematic diagram of simplified single pulse modulator.

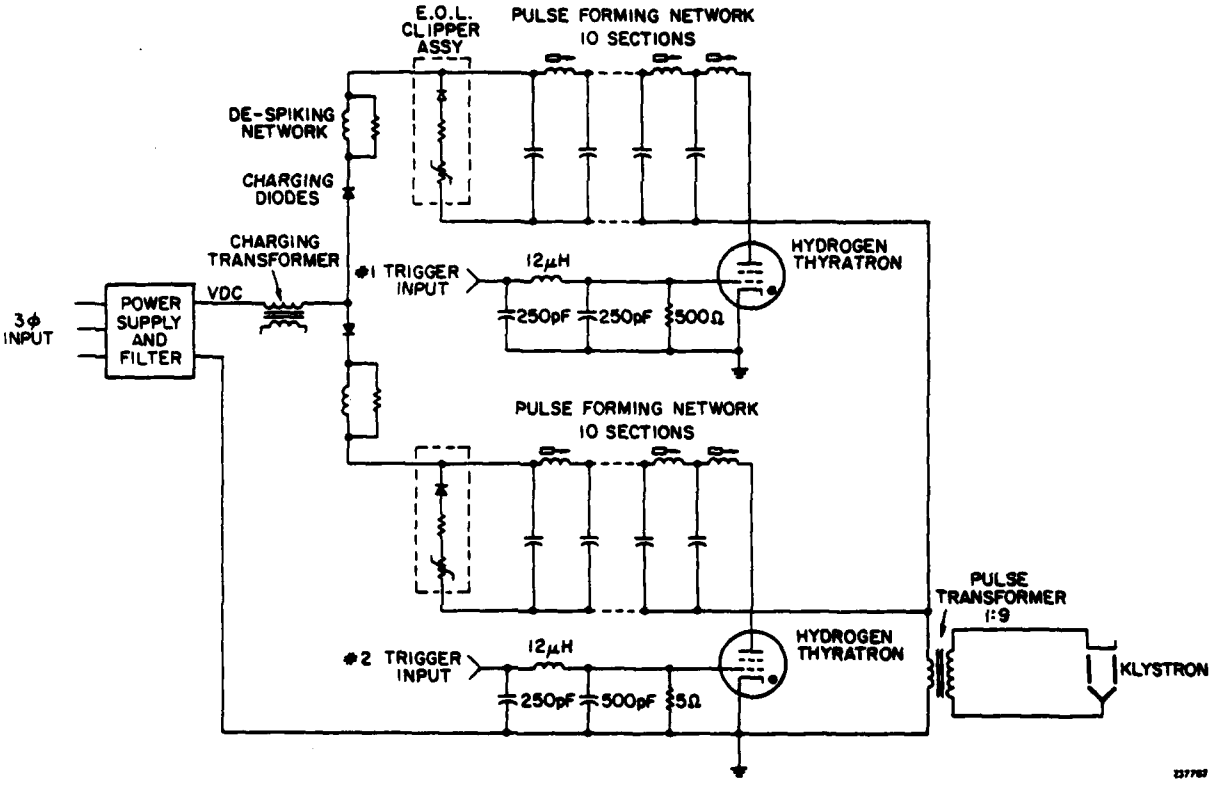

FIG. 2--Schematic diagram of simplified double pulse modulator.

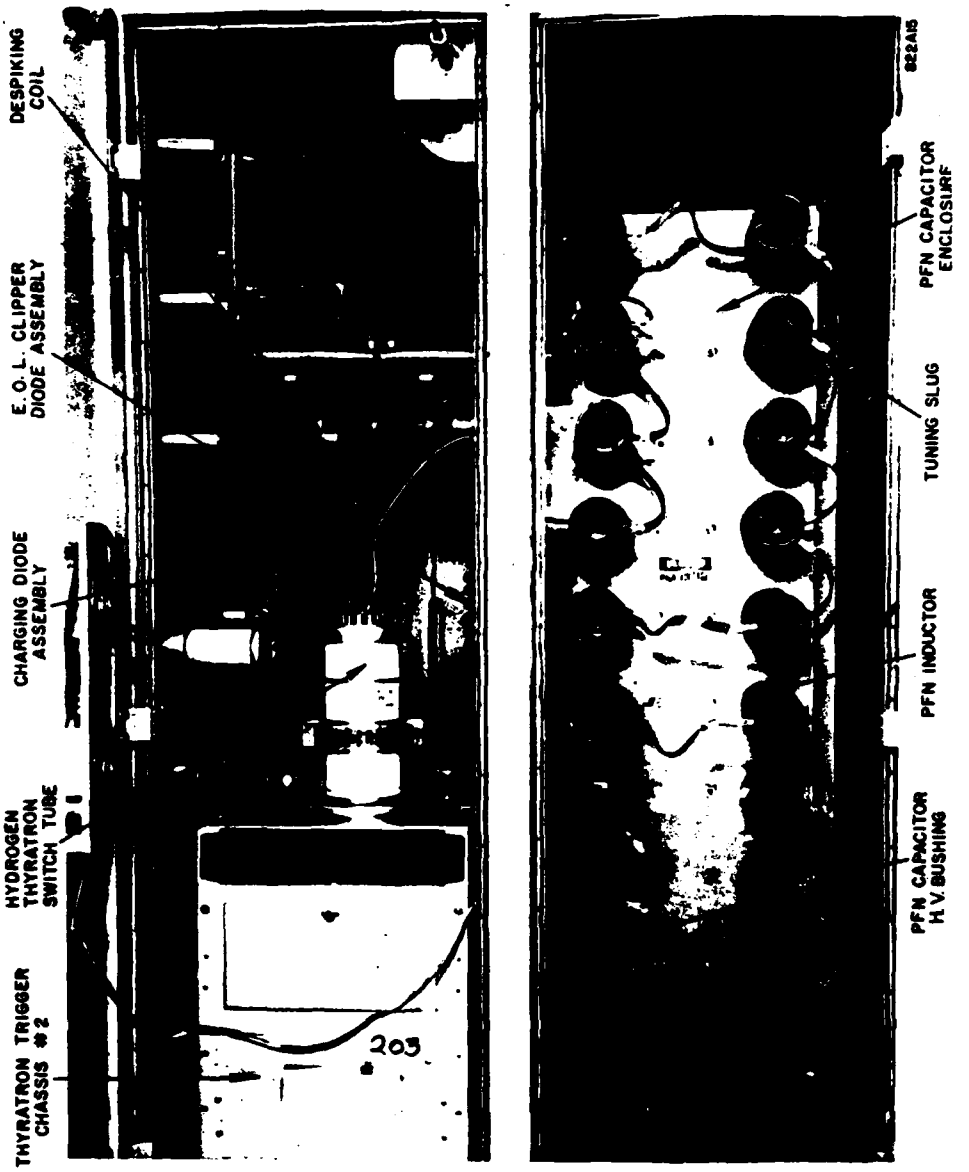

FIG. 3--P. F. N. and switch tube compartment.

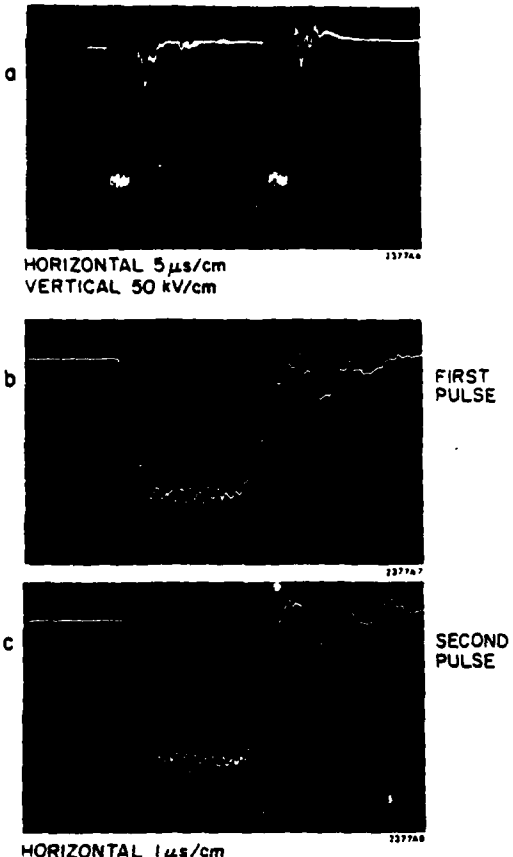

FIG. 4--Modulator output to resistive load.

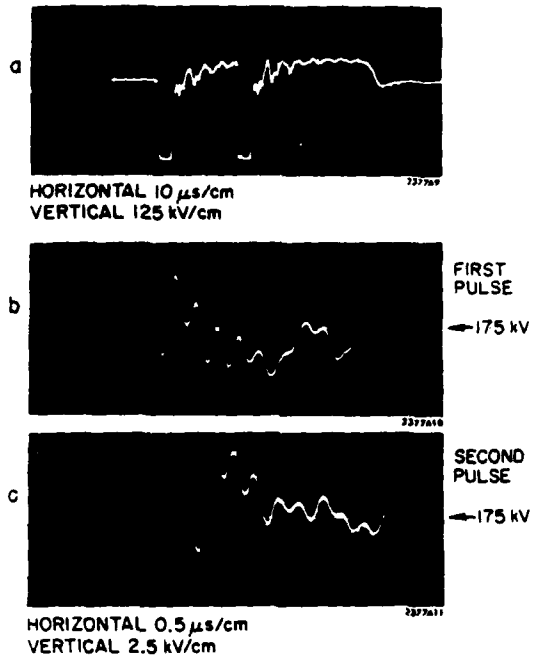

FIG. 5--Modulator output to klystron load.

TRIGGERED CHARGING TECHNIQUES FOR PULSE GENERATING CIRCUITS

G. J. Scoles
English Electric Valve Co. Ltd.
Chelmsford, Essex, U.K.

Summary

This paper describes several different circuits which can be used to obtain reliable triggered charging. For hydrogen thyratron modulators with duty cycles in excess of 0.001 it is usually necessary to delay the recharging of the pulse forming network to allow time for switch tube recovery.

Pulse generators using pulse forming networks are well known and in the majority of applications a circuit such as that shown in Fig. 1 operates in an entirely satisfactory manner. Because the charging diode D conducts immediately its cathode becomes more negative than its anode, it follows that in some cases the time available for the switching thyratron V to recover after conduction may be insufficient for reliable operation. Some improvement may be achieved by mismatching the load or by using the maximum possible inductance for the charging inductor but such techniques cannot always be used or they may not be adequate in all cases.

By replacing D by some device which can be triggered, it then becomes possible to delay the recharging of the pulse forming network until such time as recovery of the thyratron is complete, thereby ensuring reliable operation of the equipment. One obvious way of doing this is simply to replace D by a second thyratron and to trigger the latter once recovery of the switching thyratron is complete. In practice this method does not always work, although once the reason for its failure is understood it then becomes possible to devise variants which do. The problem arises because of the grid-anode capacitance of the triggered charging diode: when the main switch tube fires it causes the cathode of the charging thyratron to go suddenly negative and because this leaves the grid more positive the charging tube conducts at the wrong time.

Fortunately a simple but satisfactory solution to the problem exists, as illustrated in Fig. 2. Here a small capacitor C is connected in parallel with the charging thyratron V_2 and the grid circuit is carefully screened from everything except the cathode. This has the effect of coupling the anode and cathode together and consequently "sandwiches" the grid between them. The parallel-connected inductor L_2 and resistor R_2 act to delay the change of potential occurring across C and V_2 and in this way to render any grid-cathode signal generated within V_2 too small for triggering to occur.

This arrangement works well in practice, especially when V_2 is a glass-envelope thyratron such as the CX1159, where the grid anode capacitance is relatively small. Resistor R_1 is added merely to limit any current which might flow from C through V_2 when the latter first conducts and its actual resistance is normally so small that it does not appreciably affect the above explanation. It will be seen that C behaves to some extent as if it were in parallel with L_1 and this has the effect of decreasing the frequency of the "ringing" which can occur immediately V_2 ceases to conduct. L_1 can be critically damped by means of resistance and capacitance in series and so a technique exists which can be used successfully to control the instant of initiation of charging of the pulse forming network in a pulse generating circuit.

A simple and obvious variant of the standard modulator circuit which first comes to mind when engineers require to use triggered charging techniques is to interchange the position of the diode device with the charging inductor. L_1 then acts to isolate V_2 from the transients caused by V_1 and in most cases this makes C unnecessary. The disadvantage of such an arrangement, however, is that any ringing of L_1 following the cessation of conduction of V_2 has the effect of making its cathode potential go positive and in the absence of damping this voltage may approach three times that of the power supply. The excessive transient inverse voltages produced can destroy the thyratron and quite a few heater transformers have been lost in this position. This system, though simple and effective, is thus only suitable for relatively low voltage applications, typically 10 kV power supplies. Two further circuits exist, however, which

are in some ways preferable to those already described.

The first of these can take several forms, that of Fig. 3 being easier to explain though less likely to be used in practice. Here L_1 is the normal charging inductor (as in Fig. 1) whilst L_2 and V_2 replace the diode D. The inductance of L_2 is much greater than that of L_1 and its function is to allow a small current to flow in and out of the pulse forming network N, thereby causing inverse voltage to appear across V_1 immediately following its conduction.

Assuming that N has charged cosinusoidally through V_2 and L_1 to slightly more than twice the supply voltage, an inverse voltage at once develops across V_2 and L_2 in parallel. Thereupon V_2 ceases to conduct and a current commences to build up in L_2. This has the effect of slightly discharging N, the lost energy being stored in the inductance of L_2. After V_1 has been triggered to generate an output pulse, this energy becomes available to charge N to a slightly negative potential and so apply an inverse voltage to V_1. This in turn makes more time available for recovery of V_1, after which the current flowing through L_2 has fallen substantially to zero. V_2 is now triggered to recharge N via L_1 and the cycle repeats itself.

The circuit of Fig. 3 is liable to the same capacitive effects as that of Fig. 2 and, of course, the same techniques could be used to minimise them. However, it is relatively simple to rearrange the circuit in such a way that (a) the effect cannot occur, (b) the cathode of V_2 can be directly earthed and (c) inductor L_1 can in certain cases be eliminated. Fig. 4 shows this version and it will be seen that L_2 has been provided with a voltage-reversing secondary winding, across which thyratron V_2 is connected. For lower power applications a thyristor can replace V_2 satisfactorily.

V_2 can be triggered to initiate the charging of N exactly as in Fig. 3 circuit but here the cathode of V_2 is earthed and the anode positive prior to triggering. L_1 determines the charging cycle whilst the self-inductance of L_2 is effectively in parallel with V_2 and so controls the current which provides voltage reversal for N. Varying the ratio of the two windings of L_2 enables the performance of V_2 to be optimised. If L_2 is designed to have sufficient leakage-inductance, then this can be made equivalent to L_1 and the latter entirely eliminated as a physical entity. The presence of leakage inductance (or of L_1) decreases the rate of application of voltage to V_2 when V_1 triggers and so makes premature triggering of V_2 extremely unlikely.

The arrangement of Fig. 4 is clearly preferable to that of Fig. 3, its only practical disadvantage being the need to design a double-wound inductor for L_2.

The second of the preferred arrangements is shown in Fig. 5. Here L_1 and D_1 are as in Fig. 1, the thyratron V_2 and rectifier D_2 being additional. L_1 isolates V_2 from sudden transients whilst D_1 behaves very nearly as in the conventional circuit (Fig. 1). Because the stray capacitance to earth at A will normally considerably exceed that at B, it follows that when conduction through V_2, L_1 and D_1 ceases most of any ringing voltage will occur at B whilst the voltage at A will not depart appreciably from that of the supply. Triggering V_2 controls the charging of N as in all these arrangements but with this particular circuit a minor peculiarity occurs following the triggering of V_1. This is because a charge is left on the stray capacitance associated with L_1, V_2, etc., and when V_1 conducts this capacitance will discharge through L_1, D_1 and V_1. A small half-sinusoidal current will flow and in the absence of D_2 this would result in charging the strays to a negative potential. Although not deleterious in itself, this voltage reversal increases the forward voltage across V_2 and the inverse voltage across D_1 so it is preferable for the reversal to be eliminated. Rectifier D_2 conducts immediately such reversal commences to occur, thereby converting the second half of the current waveform from sinusoidal to exponential. Resistance R can be included in series with D_2, its value being chosen to provide a suitable compromise between the duration of this exponential current decay and the appearance of a short-duration reversal of voltage at the cathode of V_2.

In theory such a reversal might assist slightly in the recovery of V_1, but as the flow of current through D_2 only occurs at a time when V_2 is non-conductive, there is no possibility of V_1 and V_2 conducting simultaneously and so short-circuiting the power supply. D_2, of course, must be rated to withstand the supply voltage in reverse, but the mean and peak currents flowing through it are very small.

A further method of triggered charging using grounded grid techniques was suggested by N. S. Nicholls in a paper read at the Seventh Symposium. This system has

now operated satisfactorily for several years. One possible limitation, however, is the obvious risk to the thyratron grid circuit if the silicon diode does not turn on quickly enough.

From these descriptions of several methods suitable for initiating the charging of pulse generating circuits it is clear that quite a number of solutions exist. The choice between them will depend upon the circuit parameters and upon the ratings and availability of the various components. However the circuit of Fig. 5 is probably the easiest in practice to engineer for reliable operation.

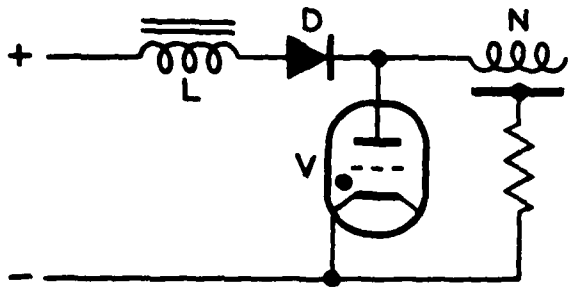

Figure 1

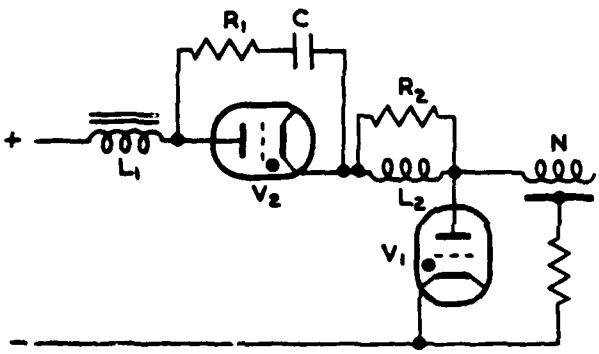

Figure 2

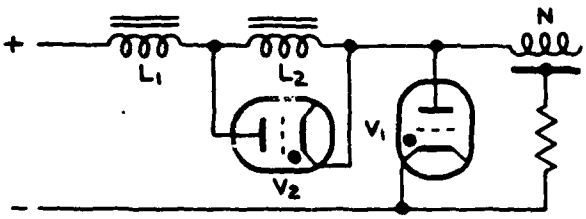

Figure 3

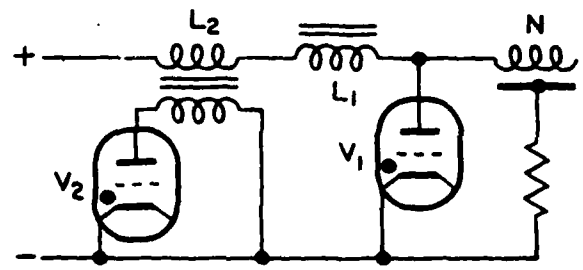

Figure 4

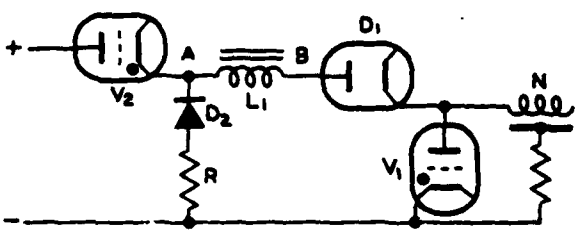

Figure 5

CHARGING AND STABILISING SYSTEM FOR A PULSED CROSSED-FIELD AMPLIFIER USING AN SCR-SWITCHED ULTRASONIC INVERTER

by

T P CROMPCOT

Admiralty Surface Weapons Establishment

Portsmouth, Hampshire, UK

and

G W WHALLEY

GEC MARCONI Research Division

Great Baddow, Essex, UK

Summary

The system described is used to provide a very stable 10 kV d.c. power supply for an RF switched CFA. The stability is provided by a novel quantum stabilisation method using a controllable high frequency inverter to charge an EHT reservoir capacitor to an accurately determined level. The use of a high inverter frequency greatly reduces the bulk of the power supply by eliminating all mains frequency transformers and filters. Similar techniques have also been successfully used for high stability pulse forming network charging systems.

Introduction

The system described in this paper was devised to transmit a stable radar pulse. For shipborne use a compact, lightweight high efficiency equipment was essential. Also a wide range of variation and transients on the ship's mains electrical supply had to be catered for to avoid the need for a separate generator.

The cold-cathode, RF switched crossed-field amplifier (CFA) offers a high conversion efficiency and small size compared with other classes of RF amplifier. This type of CFA is almost self modulating which avoids the necessity for a high power pulse modulator. The tube requires a high stability EHT supply and a small modulator for beam quenching.

A high frequency power inverter can enable a compact power system to be made and it can be controlled to achieve the high EHT stability required. A system using a high frequency inverter can also be made tolerant to a wide range of variation in supply voltage.

The CFA Transmitter

This transmitter is used as the power output stage for a versatile experimental radar. The CFA used generates 100 kW peak power RF pulses at a mean power of up to 3 kW. The radar system requires a stability of $\pm$ 1° in phase from pulse-to-pulse which must be maintained over a range of P.R.F.s extending from a few hundred hertz to many kilohertz. The pulse length and mean power are variable and the P.R.F. is also subject to variation of up to $\pm$ 10% from pulse-to-pulse. The stability must be maintained under all these operating conditions.

The CFA used is a re-entrant beam, cold-cathode RF-switched device. The electron beam is switched on by the RF drive of 5 kW peak power generated by a small grid-pulsed TWT. At the end of the RF drive pulse the electron beam is shut-off by applying a pulse to a turn-off electrode which forms part of the cathode. Because of the CFA's self modulation capability only a stable 10 kV d.c. power supply is required to provide the 22A current pulses necessary. The general arrangement of the transmitter is shown in Figure 1.

The phase pushing characteristic of the CFA requires a stability of $\pm$ 5 parts in 10^4 from the d.c. power supply to maintain the $\pm$ 1° phase change from pulse-to-pulse. Using a conventional power supply would require bulky smoothing components as well as a hard valve series stabiliser. The combination would be prohibitively large and heavy and would not make the best advantage of the CFA's small size and its high efficiency of about 50%. The size of a conventional power supply of this nature is determined by the mains frequency and if a much higher frequency could be used then the size of the step-up transformer and the ripple smoothing components would be greatly reduced. The system described here utilises a high frequency inverter for this purpose. The general arrangement of the power supply is shown in Figure 2. The 400 Hz a.c. mains supply is rectified and the resulting d.c. is then chopped by a high frequency SCR inverter, transformed to 10 kV, rectified and used to supply the reservoir capacitor from which the CFA draws its current pulses. The inverter is also used to stabilise the EHT voltage by a "quantum" charging technique described below.

Stabilisation

Voltage droop requirements dictate an EHT reservoir capacitor of about 3 nF. This capacitor must be recharged during each interpulse period, with a voltage stability of $\pm$ 0.05%.

A stabilising and charging method has been developed[1] which employs a high-frequency, high-power inverter to generate pulses, or "quanta" of charge, Figure 3. The EHT reservoir is recharged during the interpulse period to the required voltage level and then the inverter is gated-off. Providing the inverter frequency is sufficiently high, the increment in EHT voltage for each charging pulse can be made small. The size of each increment defines the possible variation in the final voltage and hence, the stability.

Variations in supply voltage, ripple and transients will influence the amplitude of each charging pulse. However, the stability is defined only by the magnitude of the final pulse. Therefore, for a high inverter frequency, the total EHT voltage is changed by only a very small proportion for relatively large variations in supply voltage.

For the 7 kW system reported here, an inverter frequency of 21 kHz was necessary to give a stability better than ± 0.05% against a d.c. input voltage variation of 250 V to 310 V and against a R.F. variation of ± 10%, pulse-to-pulse.

RF Power Inverter

The 21 kHz 7 kW inverter was required to operate directly from a 3-phase 400 Hz supply, to avoid the bulk of a 400 Hz isolating transformer and that of a mains ripple filter. Apart from the stabilisation technique, the use of a high inverter frequency also enabled a compact power conversion system.

"On-line" starting was desirable to eliminate the need for a 400 Hz variable auto-transformer. Since the RFT reservoir is initially discharged, the inverter must be able to accept a load varying from a short-circuit to the normal impedance after starting. In addition, once the inverter is running, a varying load match must be accommodated due to input voltage variations whilst the output voltage (RFT voltage) is stabilised to a constant value.

A series-commutated circuit was considered most suitable for a high-frequency, thyristor-switched inverter. This was principally because the thyristor current and voltage waveforms are approximately defined by sinusoids, giving good conditions for high frequency switching.

The basic series-inverter, Figure 4, requires a closely defined load impedance. Variations in impedance are reflected in large changes in critical parameters such as peak re-applied thyristor voltage and load current. Low load impedances would lead to intolerable voltage and current levels.

To overcome the problem of sensitivity to load impedance, a modified circuit was employed, Figure 5. With the modified system, stored energy in the commutating inductors is returned to the mains supply if the inductor voltage swing exceeds a defined level. When designed correctly, this inductor-voltage-limiting, or "IVL" system enables operation into a load varying from short-circuit to normal impedance. IVL is also compatible with the "gated" operation by interruption of thyristor triggers, required for the quantum stabilisation method.

Each thyristor switch comprises two series devices. Each device is a Westinghouse[3] (UK) Type D1170A thyristor with a peak repetitive voltage rating of approximately 550 V and a recovery time of about 5 μs. The switches are fired alternatively and pass half-sinusoidal current pulses of up to 200A peak. The switching-loss for each device is approximately 105 W for an inverter input power of 8.25 kW, ie giving a total thyristor loss of about 5%.

Mica-dielectric commutating capacitors are used. The commutating inductor/IVL transformer units are wound on a ferrite air-gapped core and immersed in transformer oil for insulation and cooling purposes. The effectiveness of an IVL system is impaired by the leakage inductance of the IVL transformers and of the current-return loop. For the developed inverter, careful attention was paid to minimising these parameters.

The RFT step-up transformer (108:1) is wound on a "Rumetal"[2] toroidal core and immersed in transformer oil. A view of the 7 kW transformer withdrawn from its container is shown in Figure 6. The miniaturisation gained through a high inverter frequency is clearly demonstrated. The RFT rectifier bridge is also contained in the transformer can and is mounted above the transformer. An earthed screen is provided between primary and RFT secondary.

Operational System

The complete stabilised power supply system is outlined by the block diagram shown in Figure 7.

The three-phase supply (208 V line) is bridge-rectified to provide a d.c. input to the inverter of approximately 300 V. No mains ripple smoothing is incorporated, but high-frequency inverter current components are supported by a reservoir capacitor, to compensate for the series inductance of the supply.

The inverter is protected by a fast-acting thyristor switch and crowbar system, interposed between the supply and the reservoir. In the event of an arc in the CPA, and subsequent RFT crowbar operation, the inverter triggers are gated and the 300 V series-switch opened. Because of the short-circuit capability of the inverter, the inverter will commutate correctly with the RFT crowbarred.

In the event of failure of an inverter component during normal operation, the 300 V crowbar is also fired to protect the inverter thyristors.

The 21 kHz inverter output is stepped-up to approximately 10 kV, bridge-rectified and applied to the RFT reservoir-capacitor. The RFT voltage is sampled during the charge cycle and the inverter gated-off when the stabilised reference level is reached. Because of the load-match tolerance for the inverter, it is possible to pre-set this level to any value in the equivalent range 2.5 kV-12.5 kV. Apart from setting the final operating point, this facility is particularly useful for tube-conditioning exercises. Independent protection against the RFT voltage rising above a safe level is provided by sensing the RFT transformer primary voltage.

Typical waveforms illustrating the stabilisation sequence are shown in Figure 8. In this case, the inverter R.F. had been reduced because the system power requirement was reduced to about 2 kW. The design stability of ± 0.05% was achieved with the final system for a total input voltage perturbation of 60 V (ie 20%).

A further advantage of the system is that an "open-circuit" capability exists. Once the RFT reference level is reached with the load disconnected, the inverter is switched off. Occasional bursts of operation are then required to make-up leakages in the RFT circuit. For the radar system, sector-blanking (an interruption in transmission over a defined arc of aerial revolution) is therefore possible.

The peak re-applied thyristor voltage increases by only 10% when the load varies from normal impedance to short circuit, demonstrating the effectiveness of the IVL system.

The measured efficiency for the complete system is approximately 90%. The principal losses are dissipated in the switching thyristors, RFT transformer and commutating inductors/clamping transformers.

A photograph of the complete experimental inverter power supply is shown in Figure 9 and a view of the equipment installed in the transmitter cabinet, in Figure 10. The inverter power supply, including the stabilisation control and trigger generation systems occupied a frame approximately 60 cm x 50 cm x 50 cm

and weighed about 70 kg. For a fully-engineered model, size and weight would be significantly reduced.

PFN Charging

Since the system described above will charge and voltage-stabilise a capacitor, the same technique is applicable to the line-type modulator. In this case, the PFN capacitors are completely discharged during each load pulse. Since the equivalent change in capacitor voltage per inverter pulse is much larger, a second low-power inverter may have to be used during the final stage of the charge to achieve the desired stability. This is because the stability is defined by the amplitude of the last charging pulse.

Such a system replaces the charging choke, LF input filter and LF step-up transformer in a conventional system. Stabilisation against ripple and mains transients is achieved together with the possibility of a wide range of control of PFN voltage. A further advantage lies in the fast switch-off by interruption of inverter triggers and the short-circuit capability, which give a built-in fast fault protection for the modulator.

Acknowledgements

The authors wish to thank The Ministry of Defence (Procurement Executive) and The Technical Director, GEC-Marconi Electronics Limited for permission to publish this paper. The authors would like to emphasise that the following team were also responsible for the success of the work reported: D J C Lewis (ASWE); M F Cryer, M J Gamage, P J Fitz and C G Collar (Marconi).

References

1. British Patent Application No 41056/72.

2. Telcon Metals Ltd, Crawley, UK.

3. Westinghouse Brake & Signal Co Ltd, Chippenham, Wiltshire, UK.

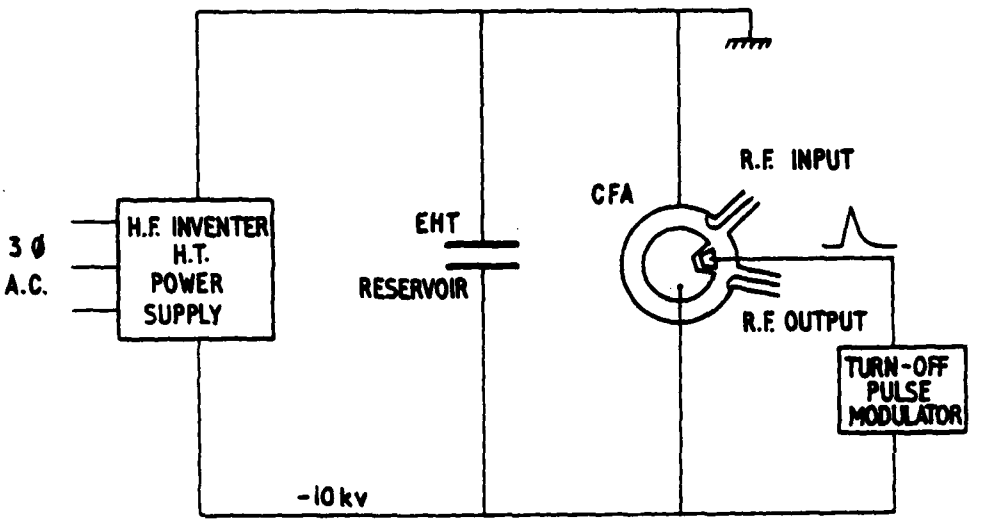

Figure 1

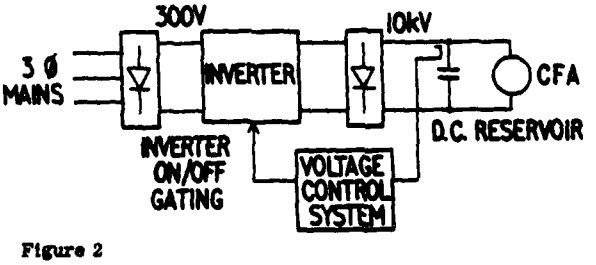

Figure 2

FIG. 3. QUANTUM CHARGING PRINCIPLE

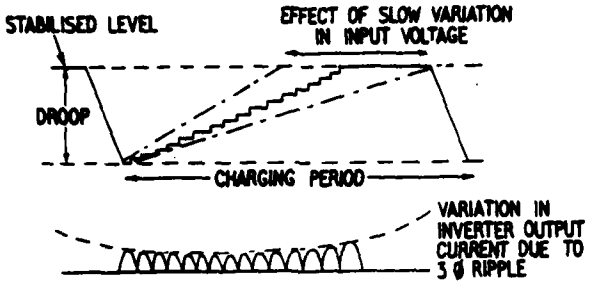

Figure 3

FIG. 4 BASIC SERIES INVERTER CIRCUIT

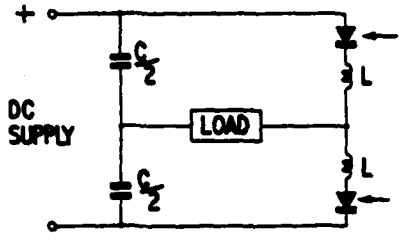

Figure 4

FIG. 5 MODIFIED SERIES INVERTER WITH IVL

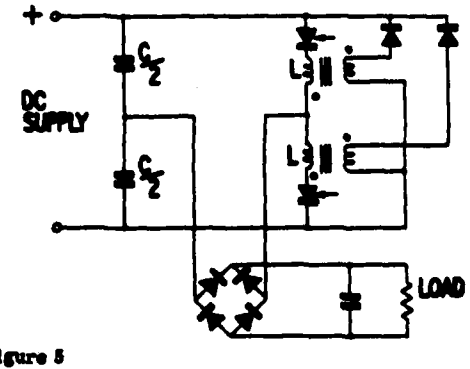

Figure 5

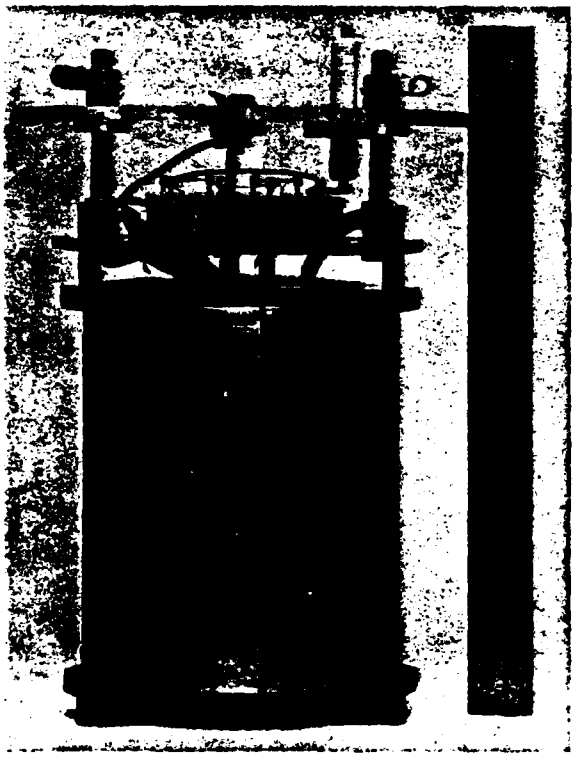

Figure 6

FIG 7 SYSTEM BLOCK DIAGRAM

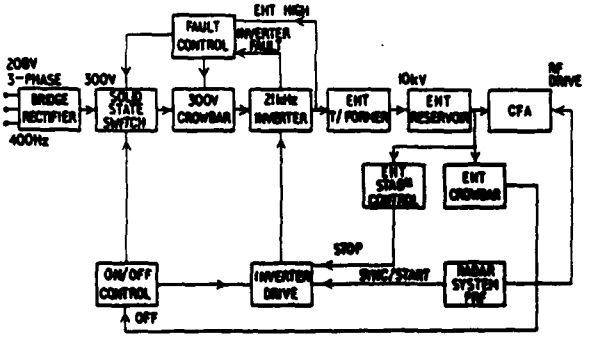

Figure 7

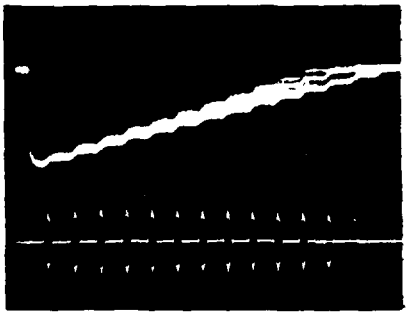

EHT
50V/cm

INVERTER
CURRENT
250 A/cm

100 μs/cm

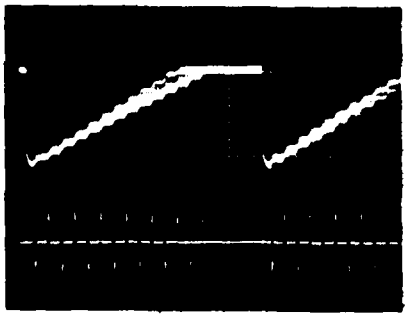

EHT
50V/cm

INVERTER
CURRENT
250 A/cm

200 μs/cm

Figure 8

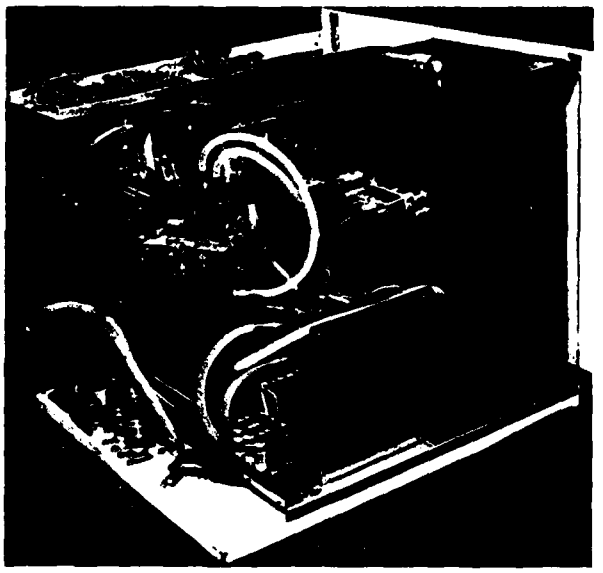

Figure 9

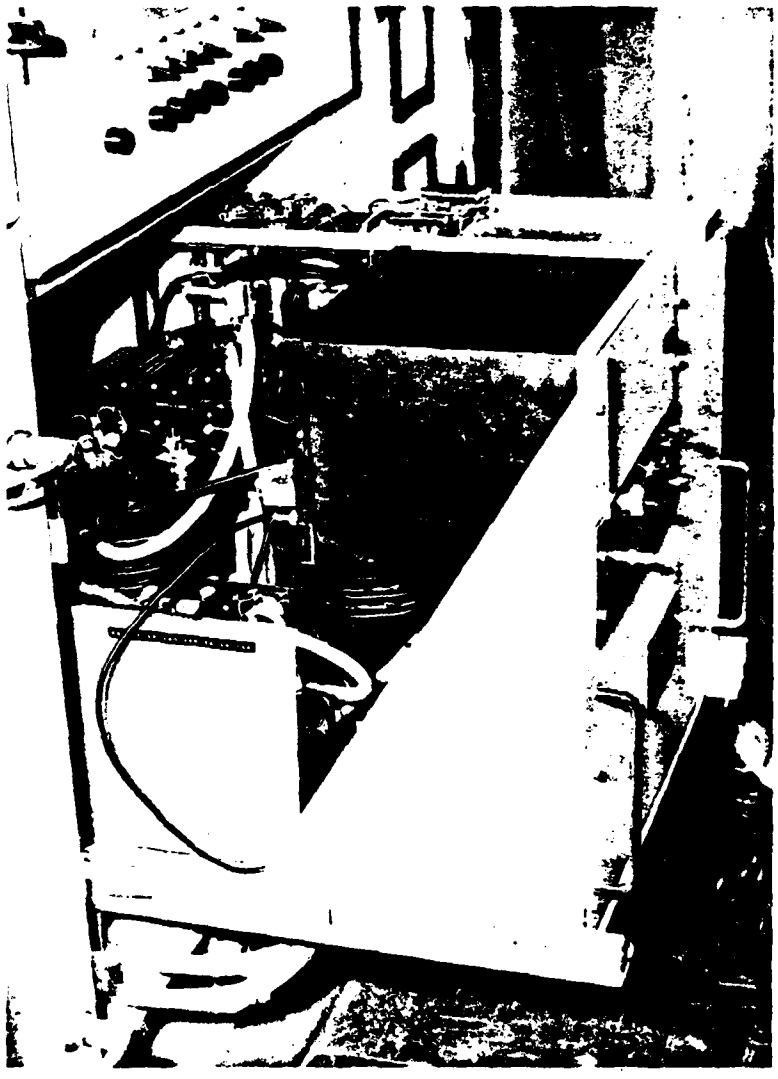

Figure 10

A POST-CHARGE REGULATOR

K. M. Smalley

Raytheon Company, Wayland, Massachusetts

Summary

This paper describes a novel regulator for a line-type modulator to reduce pulse-to-pulse load voltage ripple due to variations in PFN charging voltage. Control of the PFN voltage is accomplished by dividing the conventional PFN into two series-connected networks, and dissipating the excess charge on one of the networks. In many cases, the extra network can be a simple capacitor. Regulation is accomplished by use of a closed-loop regulator which senses the interpulse voltage of the series connection of PFN's and controls a solid-state dissipative element to reduce the total voltage to the desired value. The dissipating element need only have a voltage-rating somewhat greater than the peak-to-peak ripple variations in charge voltage existing without the regulator. The regular is all solid-state, and circuitry is all ground-based. There is no necessity for a fault-current diverter across the dissipative element, as a short to ground at any point in the circuit (such as thyratron "hangfire") will not damage the regulator. In applications involving staggered repetition rates, closer regulation of pulse-to-pulse resonant charge voltage can be obtained than with regulators that maintain the D.C. HVPS voltage constant. This is possible because the regulator will compensate for variations due to leakages in the charging diode and switch, and for dielectric absorption in the PFN, as well as for changes in the D.C. HVPS voltage.

Block Diagram

Figure 1 shows a block diagram of the regulator as connected to a line-type modulator. The regulator is shown within the area enclosed by dashed lines. The remainder of the circuitry is conventional for a line-type modulator. As can be seen, the regulator consists of the pulse-forming network B, the voltage-divider used to sense the sum of the voltages on PFN's A and B, the voltage-reference, the differential-amplifier to compare these two inputs, and the voltage-controlled dissipative element to discharge the excess voltage on PFN B.

Operation of the circuit is as follows: During the resonant-charge period, the capacitors in PFN's A and B are charged in series by the power supply and charging reactor through the charging diode.

During the remainder of the interpulse period, some of the charge in PFN B is removed by the dissipative element. The voltage-divider, voltage-reference, and differential-amplifier in conjunction with the voltage-controlled dissipative element, form a closed-loop regulator to remove the appropriate amount of charge on the capacitors in PFN B so that the voltage from point X to point Y is constant at the end of each interpulse period.

After the regulator has reduced the voltage on PFN B to the correct value so that the sum of the voltages on the two PFN's is the desired resonant-charge voltage, any further decrease in voltage on either of the PFN's due to leakage current in the charging-diode, switch, or the networks themselves, or current drawn by the voltage-divider requires that the regulator be capable of putting a ramp characteristic on PFN B to remain within regulation until the end of the longest interpulse period. For this reason, a small current source as shown on the diagram is required.

The principal advantage of the use of two networks is that the maximum voltage appearing on the dissipative element is only a small fraction of the total peak resonant-charge voltage. For instance, if the peak-to-peak value of variation in resonant-charge peak voltage is somewhat less than 10 percent of the nominal value, PFN B may be selected to have an impedance of one tenth of the impedance of PFN A. The maximum voltage appearing on PFN B (and on the dissipative element) will then be only one tenth of the resonant-charge peak voltage.

An additional advantage of the two-network arrangement is that, due to the fact that regulation is accomplished at a much lower voltage level, the current source used to compensate for interpulse droop on PFN A can be obtained from a proportionately lower supply voltage.

During the pulse discharge cycle of the modulator, the circuit behaves in the same manner as one containing a single PFN of impedance equal to the sum of PFN's A and B charged to a voltage equal to the sum of the voltages across the two networks.

The dissipative element may be either vacuum tube(s) or semiconductor(s).

Simplified Circuit

A simplified circuit of a transistorized regulator is shown in Figure 2.

In the voltage reference portion of the circuit, R1 supplies current to the reference diode VR1. R3 and potentiometer R2 are used to adjust the reference voltage input to the differential amplifier to accommodate tolerances in the reference diode and to allow adjustment of the regulated voltage.

Should the regulator requirements be such that only short-term regulation be required to minimize pulse-to-pulse variations in PFN voltage, the d.c. - stable reference circuit may be replaced by a voltage-divider on the high-voltage power supply. The output of the voltage-divider should have a capacitor of sufficient size that its time-constant is large compared to interpulse periods or pulse train intervals.

The compensated voltage-divider is comprised of capacitors C2 and C3, resistors R7 and R8, and compensation-trimming potentiometer R9. C2 and R7 usually are made up of many resistor-capacitor sections connected in series so that precision components, more easily obtainable in low-voltage units, may be used. The total resistance of the divider should be as high a practicable value as possible to minimize discharge of PFN A between the end of the resonant charge period and the following pulse. Other factors influencing value selection include variable

leakages of the compensating capacitors, resistor value stability under humidity and condensation conditions, and maximum permissible output resistance of the divider.

Q1 is the differential amplifier transistor. Depending upon regulator stability requirements, it may be necessary to use a Darlington or other compound transistor configuration here to obtain a sufficiently high input impedance such that variations of same will not result in excessive variations in divider ratio. R6 is used to supply a constant current to the emitters of the differential amplifier from the negative supply voltage, E2. If necessary, R6 may be replaced by a transistor-supplied constant-current source.

The buffer and level-translator stage is comprised of transistor Q2, and emitter and collector resistors R10 and R11. VR2 is used to limit the maximum positive and negative voltage levels supplied to Q3. In many cases, the capacitance and storage-times of a zener in this location are unacceptable. If such is the case, a resistor is used to supply current to the zener, and it is decoupled from the base of Q3 by a fast recovery diode. Then an additional diode is required between the base of Q3 and ground to limit its reverse base voltage.

Q3 is the power transistor used to dissipate the excess charge in PFN B during the regulation period. R12 in conjunction with VR2 is used to limit the peak current for second-breakdown and recovery considerations. For optimum design, the current is usually limited to the minimum value that will allow regulation to be obtained by the end of the minimum interpulse period.

CR2 is used to isolate Q3 from PFN B at the end of the pulse, when the PFN's become negatively charged due to the load mismatch provided to ensure recovery of the switching element.

Voltage E3 supplies current through R13 to recharge the capacitors in PFN B during the interpulse period to allow the regulator to maintain a constant voltage from the top of PFN A to ground when the voltage on PFN A droops due to leakage currents and loading of the voltage-dividers. E3 should preferably be a large voltage compared to the maximum voltage appearing on PFN B to minimize current-supply variations over the operating range of voltages across PFN B. It may be desirable to put an inductor in series with R13 of such value that the $\frac{L}{R}$ time-constant be long compared to the interpulse period. To conserve dissipation in the circuit, it may even be desirable to replace R13 with a transistor-supplied constant-current source.

PFN B is designed such that the resonant-charge voltage appearing on it at the end of the charge cycle is equal to the peak-to-peak voltage variations appearing on PFN A plus an allowance for minimum voltage-drop on Q3, ramp voltages required on PFN B, tolerances in values of capacitance of PFN's A and B, and regulator drift.

In many cases, PFN B need only be a capacitor, rather than a network. This is especially true for short pulses, on the order of a few microseconds or less. If PFN B is merely a capacitor, it will contribute droop to the pulse waveform. The percentage droop contributed by use of a capacitor is approximately equal to the percentage ratio of the capacitance of PFN A over the value of capacitance replacing PFN B. If necessary, PFN A may be designed with a rising characteristic during the pulse to nearly eliminate this droop.

The discharge network comprised of R14 and CR3 is used to remove any voltage remaining on PFN B at the end of each pulse. If this network were not included, the voltage remaining on PFN B at the end of the first pulse would be negative, which would not allow PFN B to charge up sufficiently during successive resonant charge times to allow the regulator to have its full dynamic range. The time-constant of the circuit formed by this resistor and the total capacitance of PFN B should be small compared to the resonant-charge period, although the smaller the resistor value, the larger the peak current that the diode must accommodate.

Output Stage Using Series-Connected Transistors

Should the voltage requirements of the output stage exceed that obtainable with a single high-voltage transistor, several transistors may be used in series. Figure 3 shows an arrangement using three series-connected transistors.

Transistors Q4, Q5, and Q6 are the output power transistors and they are driven by Darlington-connected transistors Q1, Q2, and Q3. Resistors R1, R2, and R3 are used to apportion the voltage stresses on the driver and output transistors. Resistors R4, R5, and R6 are used to prevent leakage current in the driver transistor from turning on the output transistors. R7, in conjunction with the voltage-limited input provided by the buffer stage, limits the peak current in the output stage. VR1, VR2, and VR3 are protective zener diodes used to prevent excessive voltage from appearing across any of the driver or output transistors.

The combined gains of the Darlington-connected transistors should be high so that equalizing resistors R1, R2, and R3 may have large values. This resistive divider must be supported by the current-source used to provide the ramp characteristic on PFN B.

For an optimum design, the equalizing resistors will not have equal values. The values should be selected so that at minimum voltage and maximum current in this stage, the voltages are approximately equal, taking into account the fact that the driver transistor base currents make the current increase in progressively higher resistor sections.

Timing Diagrams

Figures 4a, b, and c show the interpulse voltage waveforms appearing on PFN A, PFN B, and the sum of both PFN's, respectively. The waveform amplitudes on all three figures are to the same scale. For clarity, the waveforms represent rather extreme conditions of a regulator correcting for ± 10 percent changes in power supply voltage, 4 percent droop on the PFN during the interpulse period, and a resonant-charge period consuming only one-third of the interpulse period.

Curves A, B, and C are for conditions of low, nominal, and high power supply voltage, respectively.

The resonant-charge period is from t_0 to t_1. The regulation period is shown as occurring between t_1 and t_7. In actuality, the regulator becomes active prior to the end of the interpulse-period, somewhat flattening the top of the resonant-charge waveforms on PFN B.

Figure 4a shows the top of the resonant-charge voltage waveforms on PFN A, and the droop appearing on the network for the remainder of the interpulse period.

Figure 4b shows the entire interpulse voltage waveforms on PFN B during the interpulse period. Curve A shows that for the low power supply voltage condition, the voltage decreases exponentially until time t_2, at which time the slope changes from negative to an essentially constant positive slope to make up for droop in PFN A. Curve B shows that for the nominal power supply voltage condition, the slope is constant until time t_3, due to the current-limited operation explained previously. Then the voltage decreases exponentially until time t_4. Curve C shows that for the high power supply voltage condition, the current-limited operation occurs for the longest period of time, from t_1 to t_5, and the slope does not turn positive until time t_6.

Figure 4c shows the top of the resonant-charge and regulation period waveforms for the sum of the two networks. It is obvious in this diagram that regulation is obtained after times t_2, t_4, and t_6 for the three power supply voltage conditions, respectively. Therefore, as long as the thyratron is not fired until after t_6, the voltage will be within regulation, regardless of the variations in peak resonant-charge voltage.

Conclusion

By inserting a small PFN in series with the ground return of the primary of the pulse transformer in a line-type modulator, we are able to effectively regulate the resonant-charge voltage by means of a closed-loop solid-state regulator. Since the voltage on the added PFN need only be slightly greater than the total variations in peak resonant-charge voltage occurring without a regulator, it is feasible to use transistors to dissipate the required amount of charge on this PFN during interpulse periods. The regulator's capability of compensating for leakage discharge of the main PFN throughout the interpulse period is of particular advantage for applications involving staggered repetition rates.

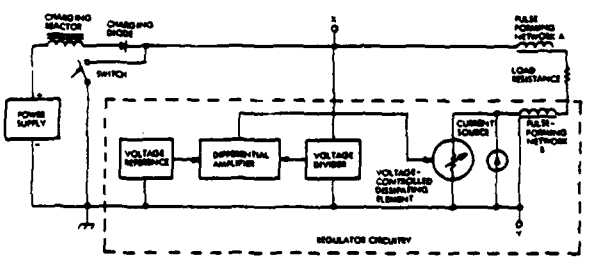

Figure 1. Block diagram

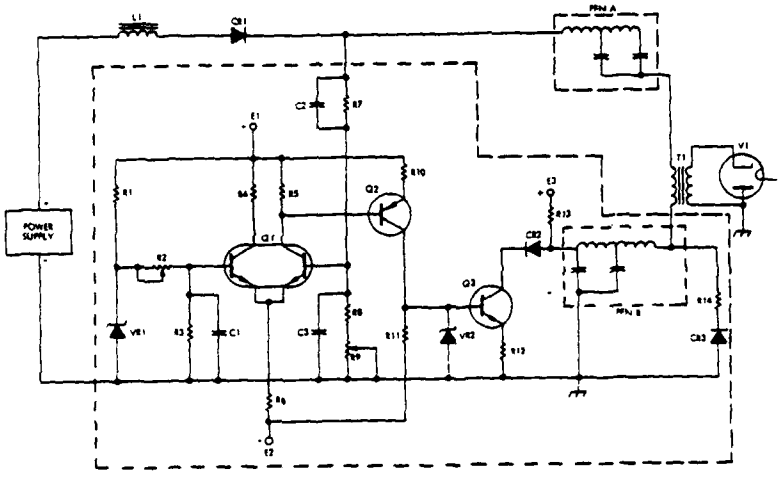

Figure 2. Simplified Circuit

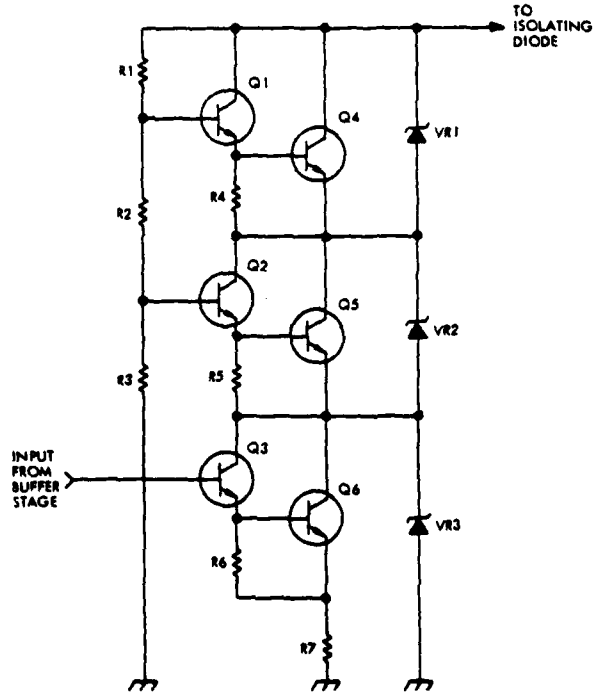

Figure 3. Output stage using series transistors

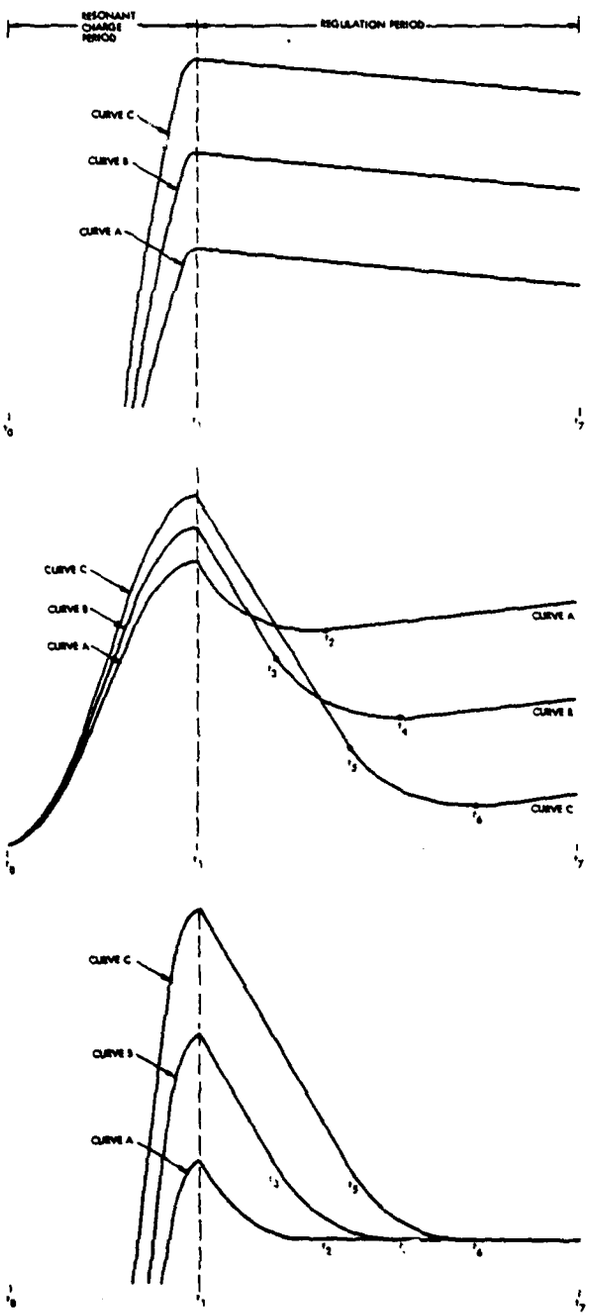

Figure 4. Timing diagrams

a. Interpulse voltage on PFN A
b. Interpulse voltage on PFN B
c. Sum of interpulse voltages on PFN's A & B

AD-A119 660 PALISADES INST FOR RESEARCH SERVICES INC NEW YORK F/G 9/5
IEEE CONFERENCE RECORD OF 1973 ELEVENTH MODULATOR SYMPOSIUM, NE--ETC(U)
1973
UNCLASSIFIED 73-CH0-773-2-ED NL

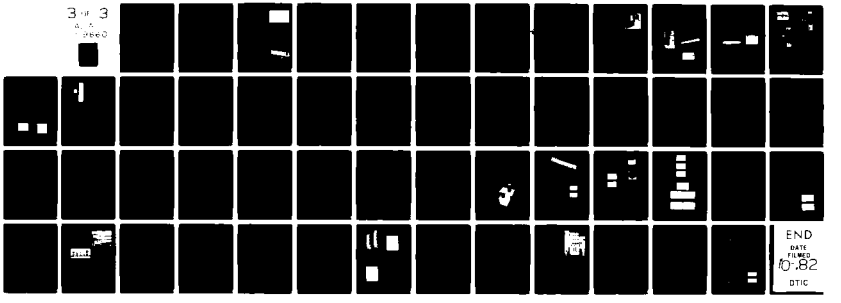

HIGH VOLTAGE FUSES FOR PHASED ARRAY RADAR TRANSMITTERS

S. Schneider, A. Buffa, and J. Carter

US Army Electronics Command
US Army Electronics Technology and Devices Laboratory
Fort Monmouth, New Jersey 07753

SUMMARY

In large phased array radar systems utilizing microwave amplifier arrays connected to a common power supply, it is necessary to provide isolation between a faulted amplifier and the other amplifiers in the array. A series interrupter in the form of a high voltage fuse has been evaluated for this application. The high voltage fuse is attractive due to its low voltage drop, low cost, size and weight. A 50 kV fuse with a current rating of 4 A RMS and a current interruption time of less than 20 μs has been developed. This type of fuse has been found satisfactory for the majority of phased array transmitter applications.

INTRODUCTION

In large phased array radar systems utilizing microwave amplifier arrays, the size, weight and cost of an individual energy source for each amplifier requires consideration of the use of a common energy source for a number of amplifiers, it is necessary to provide isolation between a faulted amplifier and the other amplifiers of the array. The conventional crowbar or energy diverter is unsatisfactory since they dump all the energy in the source, thus shutting down all the other microwave amplifiers connected to the common source. A series interrupter which will only disconnect the faulted amplifier is required. A review of the various types of series interrupter showed that a high voltage fuse was desirable for the following reasons.

a. The voltage drop of the fuse is lower than any other device. Therefore, the reduction of microwave amplifier efficiency is less.

b. The cost, size and weight of the fuse is lower.

c. The device is simple and can be made highly reliable.

The major disadvantage of the fuse is that it is a one-shot device and must be changed after each fault. The decision was made to develop a high voltage fuse for use in phased array radar transmitters. A program was initiated to develop a fuse to meet the following requirements.

Operating Conditions

Peak Current	- 16 A
Average Current	- 1 A
RMS Current	- 4 A
Ambient Temperature	- 40° F to +125°F
Voltage	- 50 kV dc
Fault Current	- 160 A
Clearing Time *	- 10 μs

* Clearing Time is defined as the time for current conduction to cease.

The clearing time and peak current were arbitrarily chosen as an objective. The stringency of this requirement was because of the non-availability of hard information on the fault dissipation capabilities of microwave amplifiers. The operating conditions are compatible with the amplifiers being developed for use in ballistic missile defense radar systems.

DEVELOPMENT PROGRAM

A fuse rated at 5 kV and 1 A RMS was developed and built in large numbers for use in the FPS-85 radar system several years ago. This fuse formed the basis of two approaches to the problem. The first approach was an ECOM internal program to develop techniques to use the existing 5 kV, 1 A fuse in series-parallel combinations to obtain the required 50 kV, 4 A rating. The second approach was an external program to develop a single fuse to operate at 50 kV and 4 A RMS.

The high voltage DC fuse consists of an exothermically burning wire embedded in an air-excluding encapsulating compound. The wire consists of palladium over an aluminum core, with about equal cross sectional area of each. In the design of a sensitive fuse, there is a conflict between the RMS current carrying requirements and the interrupt time requirements. High RMS current carrying capacity requires that a large cross-section be used while a very sensitive fuse must be built with a small wire cross-section. The solution of the problem is to surround the wire with some substance which transfers a large amount of heat away from the wire. The encapsulating material used is filled epoxy with the filling agent being fine grain sand. This material has many desirable features but is not a very good thermal conductor. It also begins to vaporize at a temperature less than the ignition point of the fuse wire.

SERIES OPERATION OF 5 kV FUSES

The 5 kV, 1 A fuse has been produced in large numbers for several years. This fuse has performed satisfactorily in the FPS-85 radar system. Therefore, an internal investigation was carried out to determine if the fuses could be operated in series to satisfy the 50 kV voltage requirement. The major problem with series operation of fuses is to insure that when a fault occurs that all fuses blow at the same time, so that the voltage rating of the individual fuses is not exceeded causing external arc-over or restrike. Tests were conducted with a number of fuses in series with a capacitor shunting each fuse to insure that the fault current would flow long enough to blow all of the fuses in the chain. This technique was found satisfactory. Later tests showed that the fuse characteristics were uniform enough to insure complete blowing of each individual fuse without the by-pass capacitor.

The measured clearing time of the 5 kV fuses as a function of peak current is shown in Figure 1. A number of these fuses were tested and found to be very uniform with respect to clearing time. A 20 kV,

2 A RMS series parallel combination of the 5 kV fuses is shown in Figure 2. A 50 kV, 4 A RMS chain was also constructed. The voltage and current of this combination as a function of time after initiation of the fault is shown in Figure 3. The clearing time at peak current of 900 A is about 11 μs. These chains were tested at USAECOM and Hughes Aircraft Co. Similar results were obtained at both locations.

DEVELOPMENT OF 50 kV, 4 A RMS FUSE

A nine-month development program was placed with the Bendix Corporation, Contract No. DAABO7-72-C-0039, to develop a single fuse to satisfy the technical requirements. A number of approaches were investigated, however, the final design closely resembles the 5 kV, 1 A fuses described in the previous section. The fuse used five 1.5 mil Pyrofuse wires encapsulated in sand-filled epoxy. A photograph of the fuse is shown in Figure 4. The fuse is 12 inches in length, has a core 2 inches in diameter, with caps 2.12 inches in diameter. The cover is Lexan with a wall thickness of 0.12 inches.

TEST CONDITIONS

High voltage testing was accomplished with a DC power supply, an energy storage capacitor, and a high voltage switch. The capacitor was charged by the power supply and discharged through the fuse. Current limiting resistors were used to control the peak current through the fuse. The circuit of the test set up is shown in Figure 5. The current through the fuse was monitored with a current transformer while the voltage across the fuse and on the energy storage capacitor was measured by a special high voltage probe. The one-shot voltage and current waveforms are recorded by a camera synchronized with the high voltage switch.

TEST RESULTS

The voltage and current characteristics of the fuse, when subjected to fault conditions, were recorded on a photograph.

The information contained in the photograph was plotted on graph paper using a larger scale for detail analysis. A plot of the data for a 50 kV single fuse is shown in Figure 6. Peak current, voltage across the fuse, and dissipation are plotted as functions of time. A limiting resistor was used to control the peak current through the fuse. Plots for peak currents of 160 A, 290 A, 500 A and 600 A are shown in Figures 6, 7, 8 and 9. It is seen that the clearing time, or time required for zero current, through the fuse varies inversely with the peak current. The clearing time for 160 A peak current is 140 μs, and for a peak current of 600 A, the clearing time is 20 μs.

The plotted data is used to compute the energy and charge dissipated in the fuse and limiting resistor. The charge in coulombs is found by integration of the current waveform. The energy in joules dissipated in the fuse is found by integration of the dissipation waveform. The energy in joules dissipated in the resistor is found by integration of the square of the current multiplied by the resistance of the limiting resistor. The computations are checked by comparing the sum of the energy dissipated in the fuse and resistor with the energy lost from the energy storage bank during the fault.

In Case I, shown in Figure 6, the energy dissipated in the fuse is 60 joules and in the resistor is 386 joules, for a total of 446 joules. The total energy lost from the energy storage bank is 438 joules.

In Figure 7, Case II, for 290 A peak, the energy required to blow the fuse is 106 joules. The total energy dissipated is 382 joules while the energy lost from the energy storage bank is 303 joules. The difference can be explained by the lack of precision in measuring the voltage. A 4 percent error in voltage on the capacitor could account for the difference. In Case III, Figure 8, for 500 A peak current, the energy required to blow the fuse is 51.1 joules and the energy lost in the resistor is 186.4 joules for a total of 237.5 joules. The energy lost from the energy storage bank is 230 joules. The data for Case IV, 630 A peak is shown in Figure 9. The energy required to blow the fuse is 68.12 joules while 151.28 is lost in the resistor for a total of 219 joules. The energy lost from the energy storage bank is 216 joules, which compares favorably with the total energy dissipated in the fuse and resistor. The clearing time in microseconds is plotted as a function of peak current in Figure 10, using the data presented above. The straight line fits the emperical equation.

$$t = 0.26\, i_b^{-\frac{3}{2}} \qquad (1)$$

where t is in sec and A in amps

The total charge passed by the tube as a function of peak current is also shown on the same graph. The curve is also a straight line and has the equation.

$$q = 8 \times 10^{-5}\, i_b^{-\frac{2}{3}} \qquad (2)$$

where q is in coulombs and A in amps

These two equations show the desirability of operating with the highest peak current that the construction of the microwave amplifier will permit.

The resistance of the faulted fuses as a function of time for Case I, II and III is plotted in Figure 11. The initial slow increase in resistance is due to the heating of the fuse wire by the fault current. The fuse wire then vaporizes and forms a plasma. The resistance remains nearly constant until the plasma starts to deionize. As the plasma deionizes, the resistance rapidly increases towards infinity to interrupt current flow. It should be noted that the ionization and deionization time for the three fault current levels varies over a narrow range, while the time required to heat the wire to the ionization temperature varies over a much wider range.

The curves for all cases show the same characteristics. The current decreases slowly due to increased resistance of the fuse wire. There is an abrupt increase in the slope of the curve when the plasma formed by the melted fuse wire deionizes.

AMPLIFIER PROTECTION

The test results presented above can be used to determine the amount of energy dissipated in the structure of the microwave amplifier. The energy dissipated in the microwave amplifier is the product of the charge through the circuit and the voltage drop across the microwave amplifier.

The data presented above can be used to compute the total charge. Unfortunately, very little information is available on the voltage drop across the arc of a faulted amplifier. The best information indicates that the voltage drop is a nominal 100 volts.

Using this value, the energy dissipated in the microwave amplifier is plotted in Figure 12. The values range from 0.15 to 0.80 for the cases considered here. There is also very little information available on the amount of energy required to damage a microwave amplifier during an arc. The most fragile type of amplifier in common use is the gridded gun traveling wave tube amplifier. A survey of all manufacturers of this type of amplifier indicates that 10 joules is a conservative value. The fuses tested during this investigation limit the energy to a value well below the potential damage range.

CONCLUSIONS

The high voltage DC fuse is a practical answer to the problem of fault protection for the microwave amplifier array. In order to dissipate the lowest amount of energy in the microwave amplifier, the smallest current limiting resistor possible should be used. The maximum peak current that can be passed by an amplifier without damage is a function of tube construction. Reliable data on the impedance of the amplifier during a fault and the maximum peak current than can be passed by the amplifier is required in order to design reliable protective circuits using series interrupters.

The fuse does not significantly degrade amplifier performance since it has a low voltage drop. The device is cost effective in comparison with competitive devices and also has a high degree of reliability. The major disadvantage is the fact that a blown fuse must be replaced before the faulted tube can be recycled.

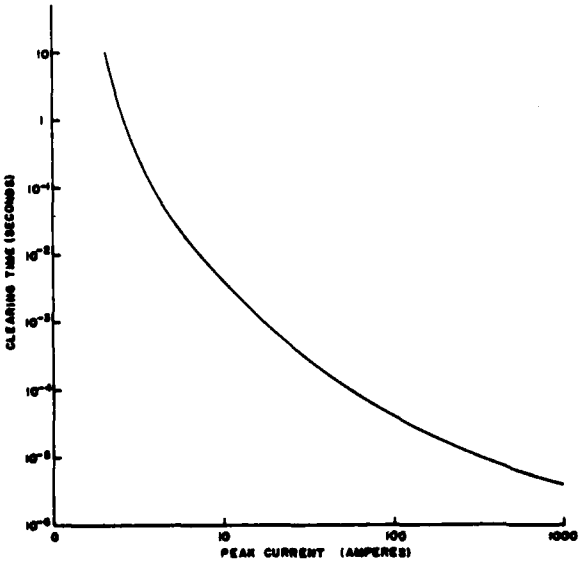

FIG. 1 PLOT OF CLEARING TIME AS A FUNCTION OF PEAK CURRENT
BENDIX 5 K.V. 1 AMP FUSES

Figure 2

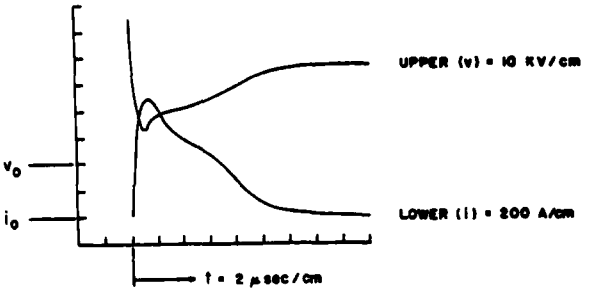

FIG. 3 40 EA BENDIX 5 KV-1 A FUSES IN SERIES-PARALLEL

$C = 2\ \mu FD$

$E_C = 50\ KV$

$R_l = 39.2\ \Omega$

$R_{FUSE} = 5.4\ \Omega$

$R_{TOTAL} = 44.6\ \Omega$

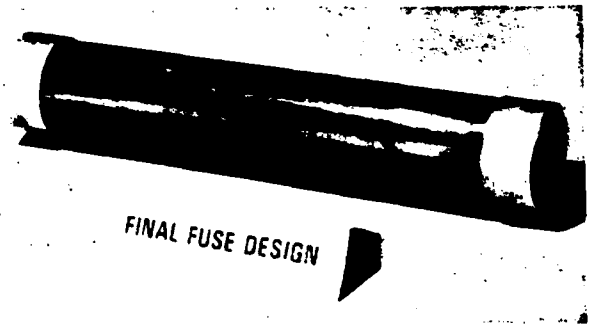

Figure 4

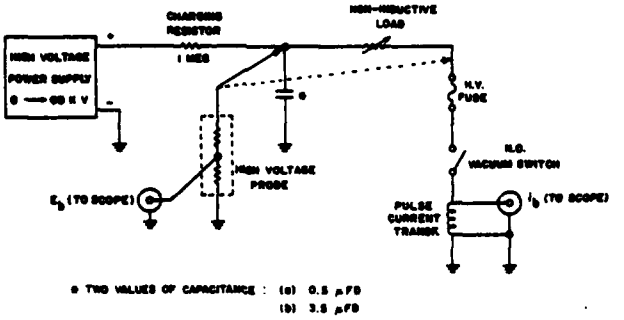

FIG. 5 TEST EQUIPMENT

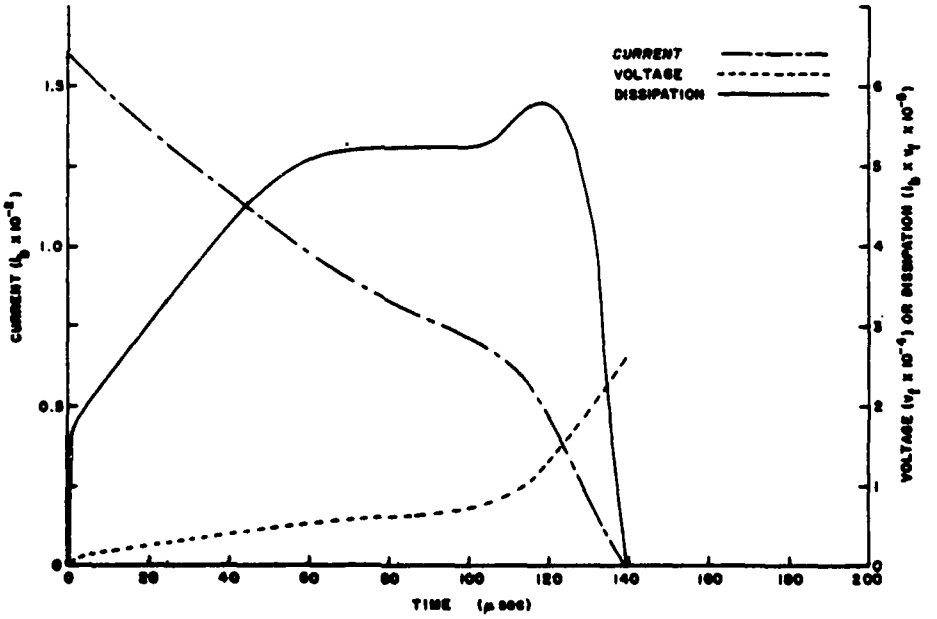

FIG. 6 PLOT OF CURRENT, VOLTAGE & DISSIPATION AS A FUNCTION OF TIME
50 K.V. 4 AMP FUSE (150 AMPS PEAK)

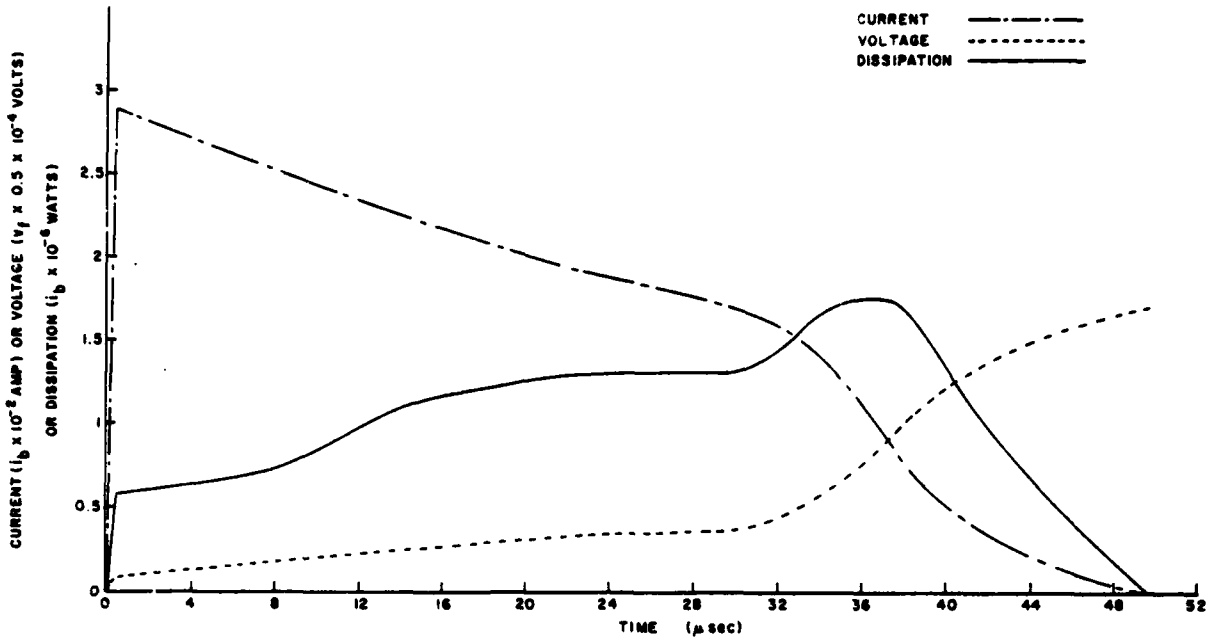

FIG. 7 PLOT OF CURRENT, VOLTAGE & DISSIPATION AS A FUNCTION OF TIME
50 K.V. 4 AMP FUSE (290 AMPS PEAK)

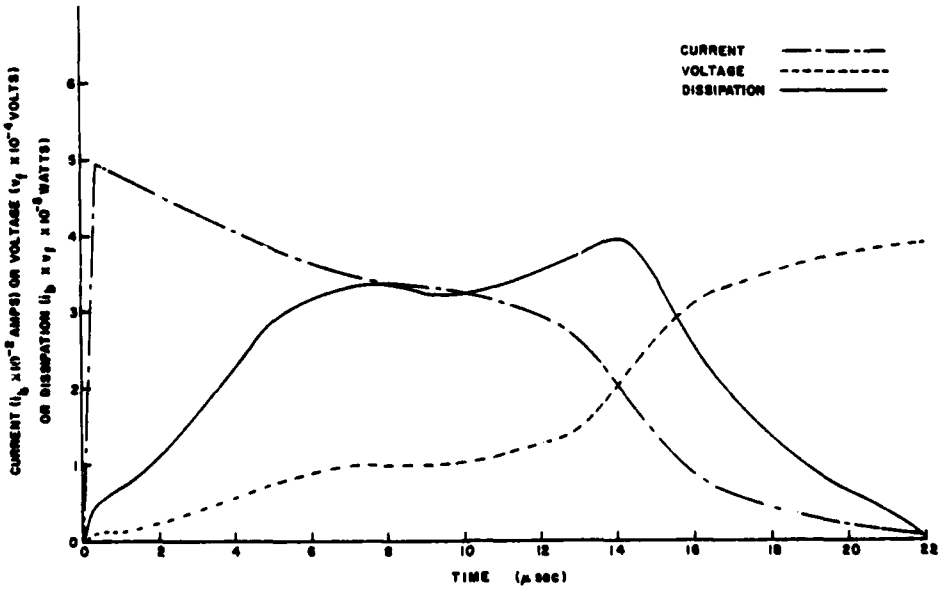

FIG. 8 PLOT OF CURRENT, VOLTAGE & DISSIPATION AS A FUNCTION OF TIME
50 K.V. 4 AMP FUSE (490 AMPS PEAK)

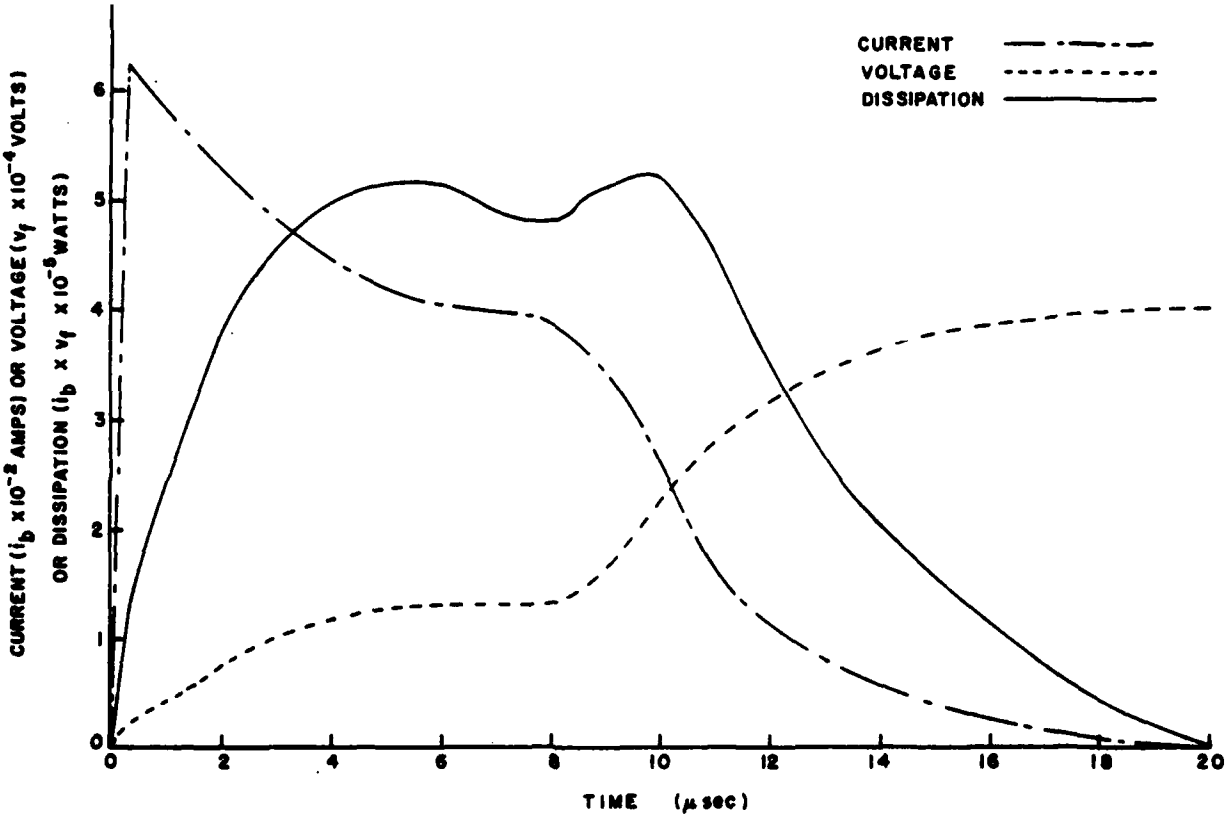

FIG. 9 PLOT OF CURRENT, VOLTAGE & DISSIPATION AS A FUNCTION OF TIME
50 K.V. 4 AMP FUSE (620 AMPS PEAK)

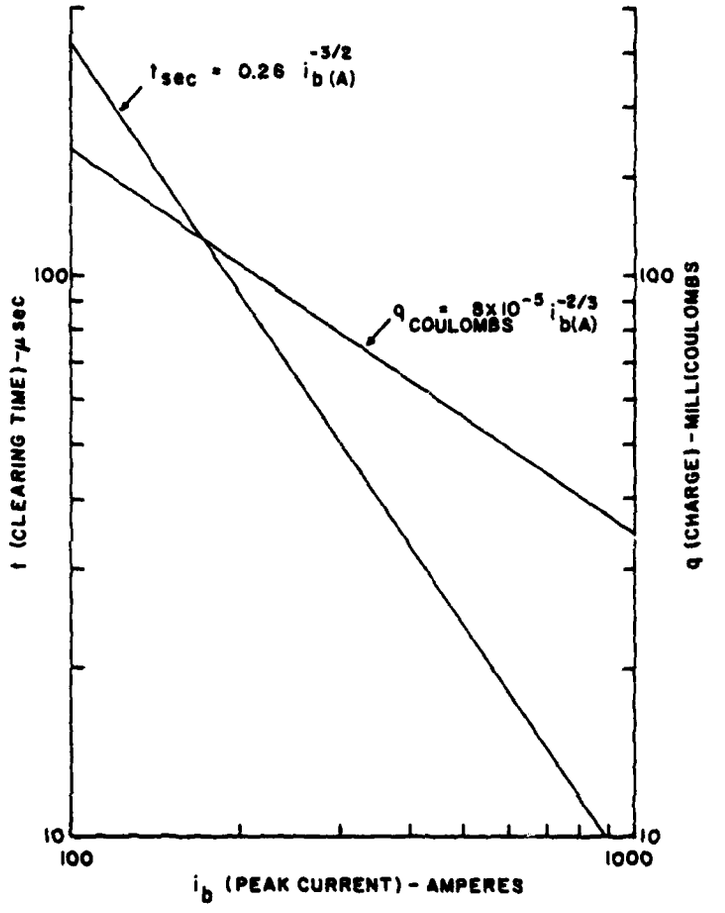

FIG. 10 CLEARING TIME & CHARGE AS A FUNCTION OF PEAK CURRENT

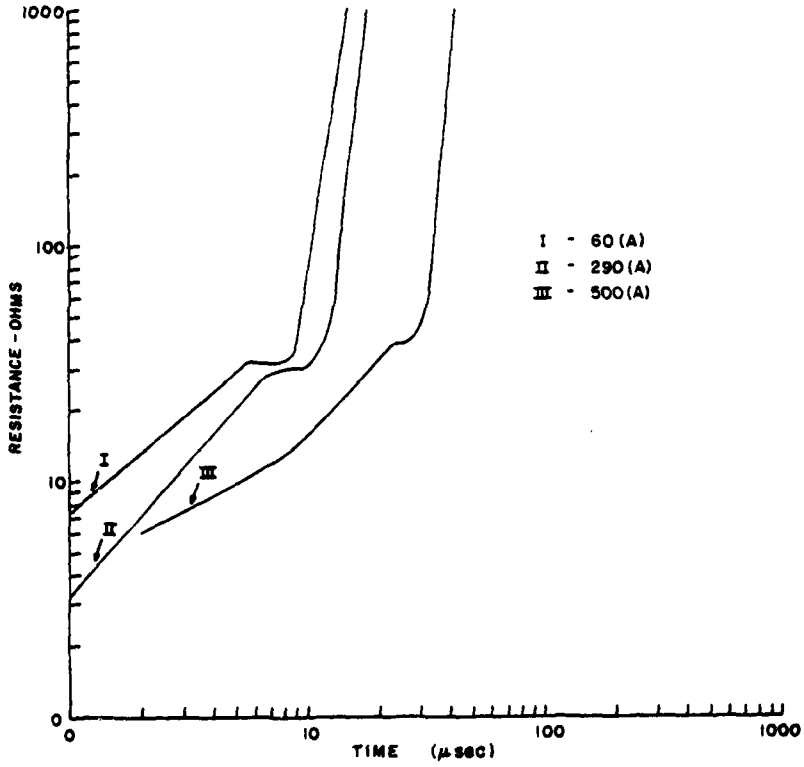

FIG. 11 RESISTANCE AS A FUNCTION OF TIME
50 K.V. 1 AMP FUSES

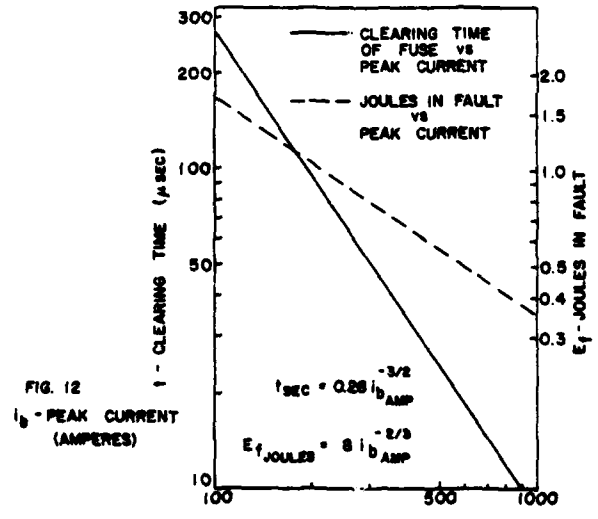

FIG. 12
i_b - PEAK CURRENT (AMPERES)

FIG 12 i_b - PEAK CURRENT (AMPERES)

EVALUATION OF HVDC FUSES AS TWT PROTECTIVE DEVICES

by J. V. Stover
HUGHES AIRCRAFT COMPANY
Fullerton, California

Introduction

This paper concerns itself with the evaluation of series-parallel assemblies of Bendix 5 kV, 1A rms fuses to obtain 50 kV, 4A rms operation; the evaluation of Bendix 50 kV, 4A rms fuses; and the evaluation of Hughes 50 kV, 4A rms experimental fuses. The purpose of this evaluation was to determine the adequacy of the protection provided to a high power, grid pulse modulated traveling wave tube (TWT) in an unattended, multiple transmitter system. Such a system may have several TWTs operating from a single power supply, and it becomes highly undesirable to shut down or crowbar the entire supply should only one tube experience a fault.

Portions of this work were sponsored by Rome Air Development Center, U.S. Air Force, in cooperation with the U.S. Army Electronics Command.

Fuse Evaluation Circuitry

A TWT amplifier, its associated HVPS, and integral energy storage bank shown in Figure 1 was utilized in the evaluation of the fuses. The operating ratings of the TWT utilized is shown in Table I. A simplified schematic of the circuitry used to evaluate the fuses is shown in Figure 2. In this circuitry the fuses were tested under representative pulsed conditions until, in most cases, thermal equilibrium was achieved by the flow of rated rms pulse current before interruption. The values of series current limiting resistance used was as required by the TWT manufacturer. A regulated inverter type TWT beam power supply was used. The triggers to the inverter power supply were inhibited within approximately 1 millisecond after the fuse under test had blown. This limited the follow-through current in the event that neither the fuse nor the TWT are cleared. A crowbar type energy diverter normally shunting the energy storage bank, ESB, was delayed by approximately 100 microseconds and used as backup TWT fault protection in the event the fuse restruck. With the exception of meters V1 and V2, the fuse, the two voltage dividers, and the additional crowbar delay; the circuitry and its operation were identical with that used normally for the operation of the TWT.

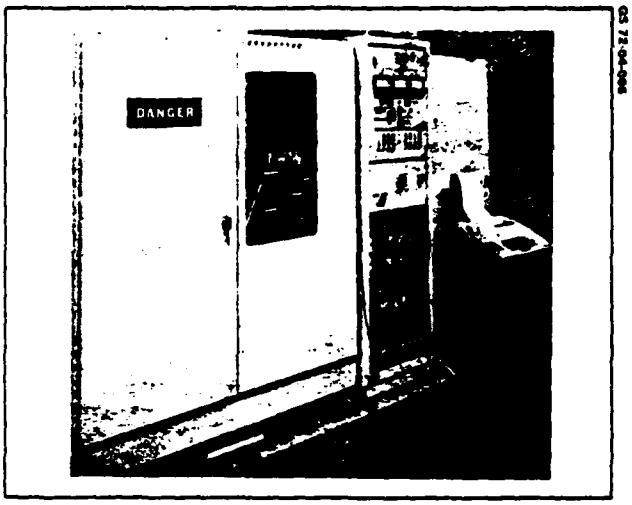

Figure 1. The TWT Amplifier Used to Evaluate HVDC Fuses

TABLE I. TYPICAL OPERATING RATINGS OF THE TWT USED TO EVALUATE HVDC FUSES

Body to Cathode Voltage	-42.0 kV
Collector to Cathode Voltage	-42.0 kV
Cathode Current, Peak	17.0 Amperes
Duty Cycle	0.06
Modulation	Shadow Grid
TWT Type	Coupled Cavity
Focussing	PPM
Frequency	S-band

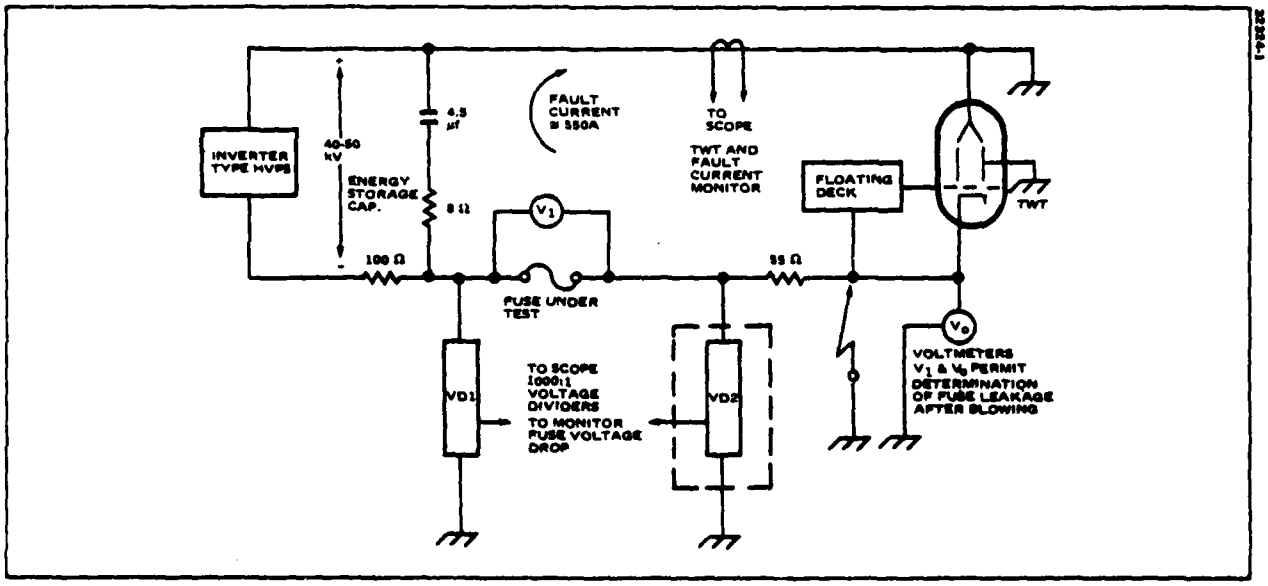

Figure 2. Fuse Test Circuit Using a TWT

The fuse test fixture was installed in an available space between the TWT and the ESB cabinets and is as shown in Figure 3. Instrumentation to record the voltage drop across the fuse during test was provided by two 1000:1 Ross Engineering Company compensated voltage dividers while the current through the fuse was sensed using a Pearson Model 301 pulse current transformer. The data was recorded using a Tektronix Model 555 dual beam oscilloscope and a Polaroid camera. An additional test circuit was devised to monitor leakage current through the fuse after fuse interruption. This circuitry is shown schematically in Figure 4. After each fuse was blown, high voltage was re-applied to the ESB and leakage current through the fuse was indicated by meters M1 and M2.

The characteristics of the TWT were monitored before and after fuse testing. The TWT positive grid voltage required to obtain a given cathode current was noted before and after each test as a decrease in cathode emission would strongly indicate that cathode poisoning was occurring due to metal ions from arc erosion depositing on the cathode surface. Also, the ion pump current and the elapsed time required for the TWT to achieve a normal ion pump current level were monitored and any variations from normal arcing with crowbar fault protection were noted. TWT body current was also monitored to determine if the body interception had increased due to reduced beam transmission caused by either gun defocussing or damage to the slow wave structure. Next, the grid bias voltage required to obtain beam current cut-off was monitored to determine if any damage had been done to the control grid.

Lastly, the TWT was RF tested to note any changes in its RF characteristics. For all fuse testing performed, there was no evidence to indicate that any damage occurred to the TWT as a result of testing the Bendix 5 kV, 1A fuse assembly, the Bendix 50 kV, 4A fuses, or the Hughes 50 kV, 4A fuse.

Evaluation of Fuse Assembly using Bendix 5 kV, 1A Fuses

To achieve the rating of 50 kV, 4A rms using the 5 kV, 1A rated fuses, 10 each of the 5 kV fuses were assembled in a series string to obtain a rating of 50 kV, 1A rms. A parallel arrangement of 4 series strings was used to raise the rating to 4A rms. The fuse assembly with fuses installed is shown in Figure 5.

Each 5 kV, 1A fuse has a typical resistance of 3.5 ohms, resulting in each series connected string of 10 fuses measuring typically 35 ohms. The overall resistance of the 50 kV, 4A series-parallel assembly typically measures 8.75 ohms. These fuse assemblies were tested with the fuse installed in the circuit in Figure 2 with voltage divider, VD2, disconnected. Fuse interruption was accomplished by shorting the high voltage TWT floating deck to ground by use of a standard grounding stick. Other tests were performed by allowing the TWT to arc.

An oscilloscope photograph of a typical test result is shown in Figure 6. In each case the fuse assembly was carrying 4.0 rms amperes of pulse current just prior to shorting the TWT cathode to ground or just prior to a TWT gun arc. An attempt was made, as shown by the data

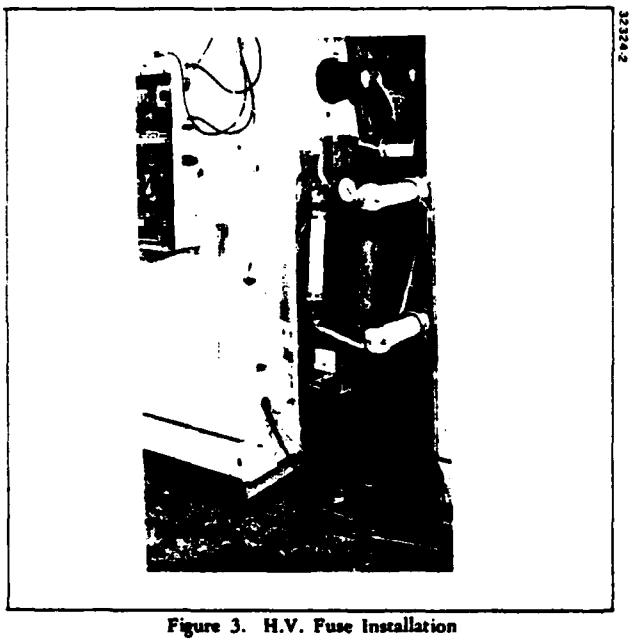

Figure 3. H.V. Fuse Installation

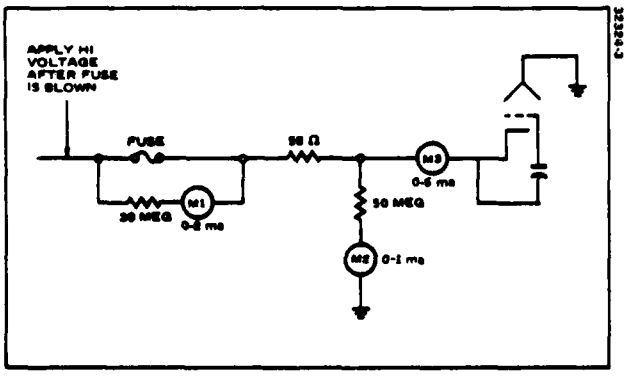

Figure 4. Fuse Leakage Test Circuit

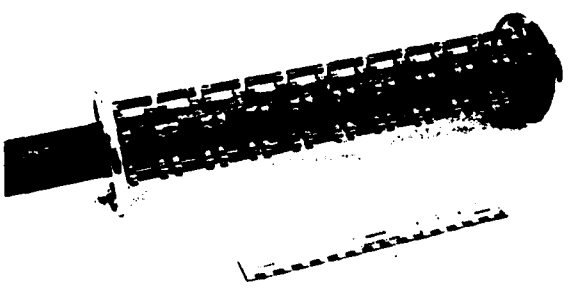

Figure 5. The Hughes Fuse Assembly of Bendix 5 kV, 1A Fuses to Form a 50 kV, 4A Rating

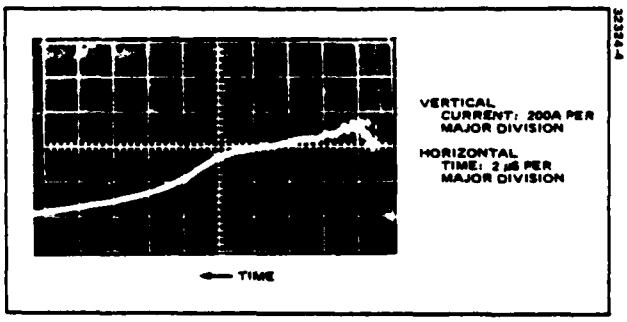

Figure 6. S/N1 Fuse Assembly Fault Current for a TWT Cathode to Ground Short Circuit with ESB Charged to -42.5 kV and Fuse Assembly in Series with 55.0 ohms. Fuse assembly carrying 4A rms of pulsed current prior to short circuit.

in Table II, on S/N 1 through 4 fuses, to allow the fuse assembly to reach thermal equilibrium before inducing a fuse interruption; however, considerable thermal heating of the fuse clips was experienced which would have caused sufficient temperature rise to initiate fuse interruption. As a result thermal equilibrium was not achieved in the tests at Hughes. The 50 kV, 4A fuse assemblies were inspected after a successful interruption, and it was found that approximately 10 percent of the 5 kV, 1A fuses had not interrupted. The non-interruption was found to occur randomly and probably is associated with non-uniformity of fuse characteristics. In all cases, the fuse assembly successfully protected the TWT.

The fuse assembly tests at Hughes achieved the successful interruption of 500 peak amperes at -42.5 kV in 20 to 27 μs. This would correspond to 125 peak amperes per single fuse. This fuse interruption time corresponds quite well with ECOM data.

Evaluation of Bendix 50 kV, 4A Fuse

Fifteen Bendix 50 kV, 4A fuses were supplied by ECOM for evaluation by Hughes to determine if the fuses can adequately protect a high power TWT. Figure 7 is a photograph of one of the fuses. The fuses were serialized by Hughes. Serial Numbers 1-6 were tested in the circuit of Figure 2 using the TWT as the load with voltage divider, VD2, disconnected. These fuses were not allowed to reach thermal equilibrium carrying rated rms pulse current, but were caused to interrupt by a manual TWT cathode to ground short circuit or a TWT gun arc shortly after reaching rated current.

Fuse Serial Numbers 8-15 were tested in the circuit of Figure 2 using the TWT as the load with voltage divider, VD2, connected. These fuses were allowed to reach equilibrium carrying rated rms pulse current before fuse interruption was initiated.

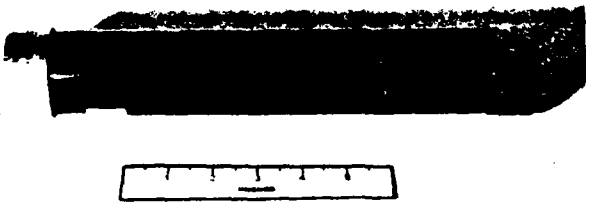

72-11-181

Figure 7. The Bendix 50 kV, 4A Fuse

The data on Serial Number 7 was inadvertently lost.

In addition, fuses Serial Numbers 12-15 were instrumented with adhesively mounted temperature indicators which discolored when that temperature was attained.

After fuse interruption, the fuses were high potential tested using the circuit in Figure 4. Lastly, several fuses which were to be tested by manually shorting the TWT cathode to ground, were short circuited through a piece of aluminum foil. By measuring the hole diameter left in the foil, the quantity of energy allowed by the fuse into the short circuit was determined.[1] Based upon the data presented in the paper referenced, less than 1 joule of energy was transferred by the fuse into the foil. Small indentations in the foil at the point of the arc were observed, but no puncture.

Typical fuse voltage and current waveshapes obtained upon fuse interruption of Serial Number 13 are shown in Figure 8. Figure 10 is a photographic enlargement of the 0.001 inch thick aluminum foil through which Serial Number 13 fuse was short circuited. Figure 9 illustrates the fuse voltage and current waveshapes obtained upon restrike of the Serial Number 15 fuse. Figure 11 is a photographic enlargement of the 0.001 inch thick aluminum foil through which the fuse was short circuited.

Typical fuse voltage and current waveshapes such as shown in Figure 8 were graphically ed to determine the fuse resistance as a function me, the charge transferred through the fuse to the arc the energy required to cause fuse interruption. T dix 50 kV,

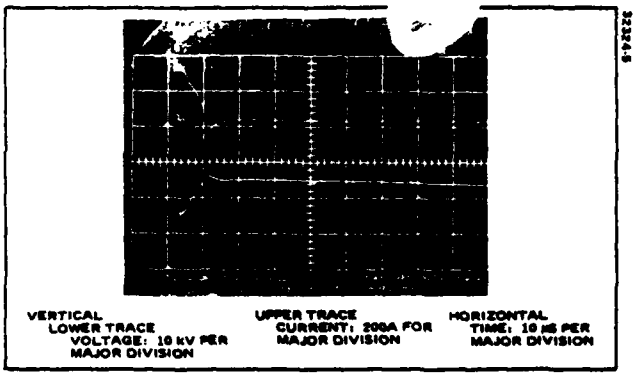

32324-5

Figure 8. Voltage Across and Current Through Serial Number 13 Bendix 50 kV, 4A Fuse on a Manual TWT Cathode to Ground Short Circuit

TABLE II. TEST RESULTS OF THE 50 kV, 4A, RMS FUSE ASSEMBLY USING BENDIX 5 kV, 1A RMS, FUSES

Fuse S/N	Test Conditions	Remarks
1	S/N 5 TWT at 42 kV, 17A peak, tp = 200 μs. 30 Min. @ 2.9A rms, 15 min. @ 3.18 A rms.	Fuse interruption due to self heating, no data.
2	S/N 5 TWT at 42 kV, 17A peak, tp = 200 μs. 2 min. @ 2.9A rms	Fuse interruption due to self heating, no data.
3	S/N 5 TWT at 42 kV, 17A peak, tp = 200 μs. 29 min. @ 2.94A rms, 25 min. @ 3.18A rms, 3 min. @ 3.4A rms.	Fuse interruption due to self heating, no data.
4	S/N 5 TWT at 42 kV, 17A peak, tp = 200 μs. Gun arc.	No data, fuse protected TWT.

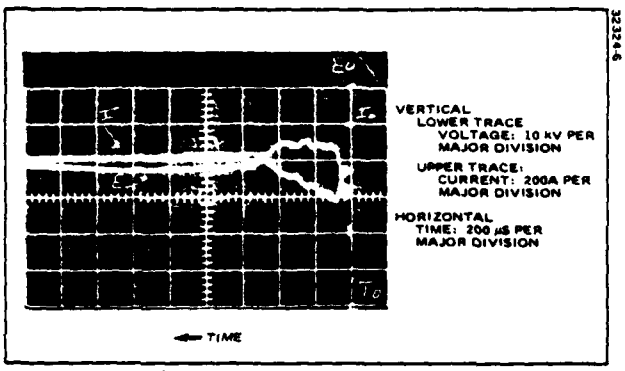

Figure 9. Serial Number 15 Bendix 50 kV, 4A Fuse with Restrike Manual TWT Cathode to Ground Short Circuit

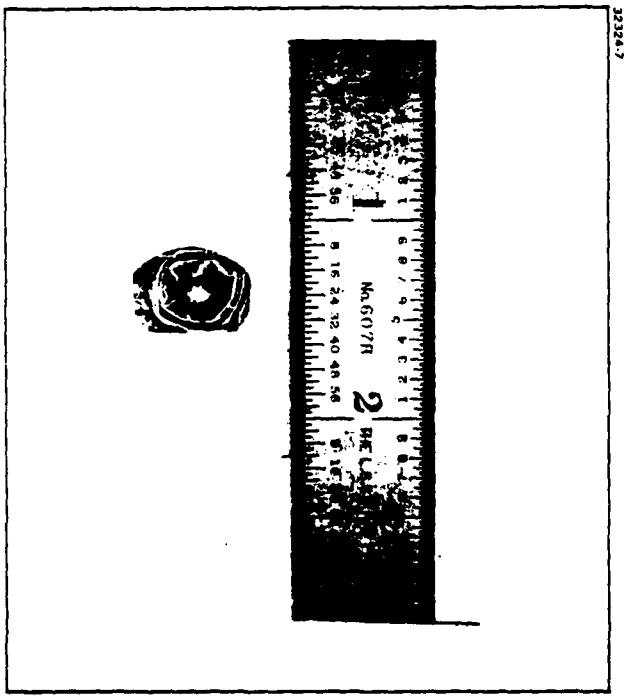

Figure 10. Arc Track on Surface of 0.001 Inch Aluminum Foil Left by Short Circuiting the Serial Number 13 Bendix 50 kV, 4A Fuse Through to Foil to Ground. No visible hole was made in the foil.

4A fuses required approximately 70 joules of energy during the interruption process and transferred approximately 2.6×10^{-3} coulombs of charge.

The Bendix 50 kV, 4A fuses tested have measured current interruption times varying from 10 to 18 μs with an average current interruption time of 14.5 μs. Table III is a tabulation of fuse test results.

All of the fuses that were tested and were not allowed to reach or even approach thermal equilibrium, were found to be free of restrike and to recover to an open circuit based upon a 50 kV, 1 hour hold dc dielectric strength test. Seven fuses were tested allowing them to reach or attempt to reach thermal equilibrium before initiating fuse interruption. Of these seven fuses, three

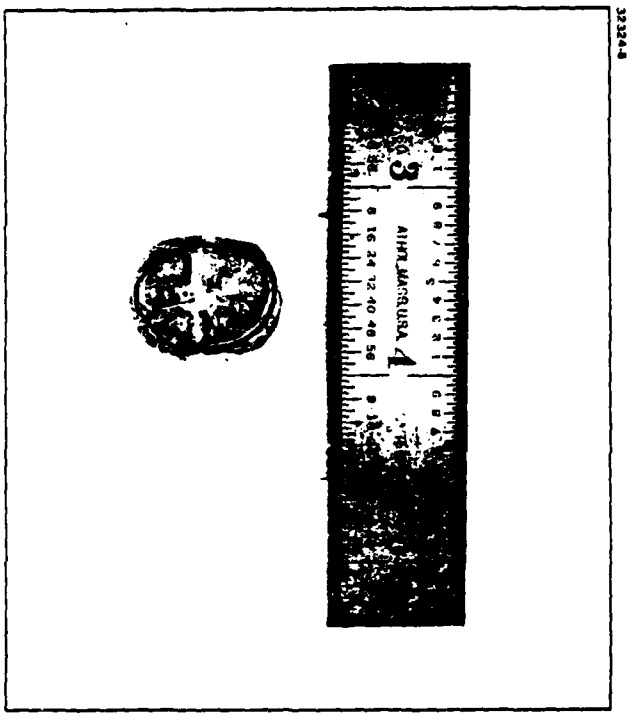

Figure 11. Hole in 0.001 Inch Thick Aluminum Foil by Short Circuiting Serial Number 15 Bendix 50 kV, 4A Fuse Caused by Fuse Restrike

fuses interrupted due to self heating. Of the four remaining fuses, one re-struck upon short circuiting; two cleared properly, but had excessive leakage upon the reapplication of voltage; and one fuse interrupted on a gun arc during the application of high voltage, and held off 50 kV for 1 hour after the interruption.

All the data taken was in an air conditioned laboratory environment at an approximate temperature of 24°C.

All of the fuses which attained near thermal equilibrium before interruption evidenced severe physical damage, such as cracked and blown out pieces of epoxy and blown out carbon deposits from the ends. In addition, the heating prior to fuse interruption caused the epoxy to bubble and melt, and the fuse to blow.

Hughes 50 kV, 4A Fuse Evaluation

The Hughes 50 kV, 4A fuse did not exist as a product, but as experimental models which were built on Hughes funding. Initial testing was performed using capacitor discharge tests at high voltage. With the permission of the government, these models were evaluated carrying pulsed currents using the test circuitry of Figure 2 in conjunction with the TWT. No evidence of damage to the TWT occurred as a result of a gun arc, when protected by the Hughes fuse. A photograph of one of these experimental models is shown in Figure 3.

Typical fuse voltage and current waveshapes obtained upon fuse interruption for Serial Number A4 are shown in Figure 12. Figure 14 is a photographic enlargement of the 0.001 inch thick aluminum foil through which the fuse was shorted. Figure 13 illustrates the fuse voltage and current waveshapes obtained upon restrike of a Hughes fuse. This restrike was purposely made to occur by physically shortening the fuse restrike distance.

TABLE III. BENDIX 50 kV, 4A FUSE TEST RESULTS

Fuse S/N	Test Conditions	High Potential Test After Fuse Interruption	Remarks
1	S/N 2 TWT ran up to -42 kV, shorted TWT to Ground	No	Interruption time: 15.6 μs
2	S/N 2 TWT ran up to -42 kV, shorted TWT Cathode to Ground	50 kV, 1 hr	Interruption time: $\approx$20 μs
3	S/N 2 TWT ran up to -42 kV, shorted TWT Cathode to Ground	50 kV, 1 hr	Interruption time: 14.0 μs
4	S/N 2 TWT ran up to -42 kV, had TWT gun arc	50 kV, 1 hr	No data. Fuse protected the TWT
5	S/N 2 TWT ran up to -42 kV, shorted TWT Cathode to Ground	50 kV, 1 hr	Scope reticule setting caused photo washout
6	S/N 2 TWT ran up to -42 kV, had TWT gun arc	50 kV, 1 hr	Interruption time: 15.5 μs Fuse protected the TWT
7	Data Lost	Data Lost	Data Lost
8	S/N 5 TWT ran up to -42 kV, accidentally blew fuse	50 kV, fuse OK	No Data
9	S/N 5 TWT at -42 kV, t_p = 200 μs. 30 min @ 4.16A rms, 10 min @ 4.34A rms	20 kV, 400 K ohms with Ohmmeter. Fuse makes sizzling sound under HV	Fuse interrupted due to self heating. No data.
10	S/N 5 TWT at -42 kV, t_p = 200 μs. 1 hr @ 4.0 A rms. Shorted TWT Cathode to Ground	<50 kV, 2 Megohm on Ohmmeter	Interruption time: 10 μs
11	S/N 5 TWT at -42 kV, t_p = 200 μs, 4A rms. gun arc	50 kV, 1 hr	No data, fuse protected TWT.
12	S/N 5 TWT at -42 kV, t_p = 100 μs. 2.25 hrs @ 3.98 A rms. Possible gun arc	30 kV, 9 mA, then 10 kV, 14 mA	No data, fuse protected TWT. Fuse Body Temp: >190°F
13	S/N 5 TWT at -42 kV, t_p = 100 μs. 0.38 hrs @ 3.72 A rms. Shorted TWT Cathode to Ground	47 kV, 5.2 mA and increasing	Interruption time: 18.0 μs Fuse Body Temp: 170°F
14	S/N 5 TWT of -42 kV, t_p =100 μs. 2.5 hrs @ 3.96 A rms	1 kV, 70 K Ohms with Ohmmeter	Fuse interruption due to self heating, no data. Fuse Body Tem: > 220°F after 1 hour.
15	S/N 5 TWT at -42 kV, t_p =100 μs. 1.25 hrs @ 4.0 A rms Shorted TWT Cathode to Ground	12 kV, 10 mA	Interruption Time: 14.0 μs with restrike. Fuse Body Temp: 190°F

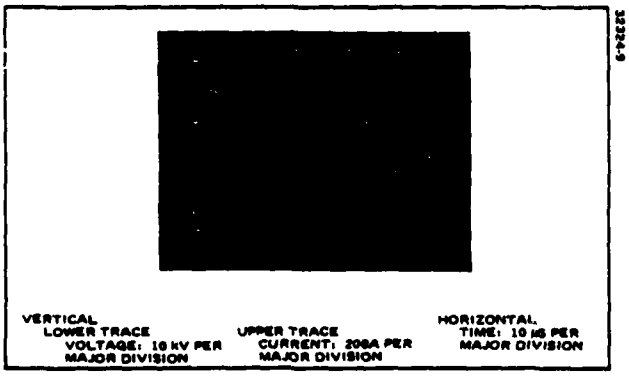

Figure 12. Voltage Across and Current Through Serial Number A4 Hughes 50 kV, 4A Fuse on a Manual TWT to Ground Short Circuit

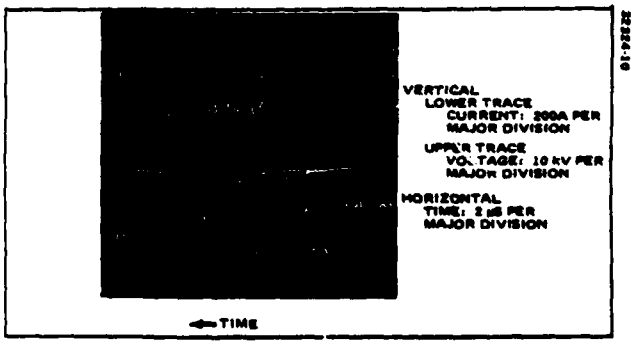

Figure 13. Specially Configured Hughes Fuse Illustrating Restrike After Manual TWT Cathode to Ground Short Circuit

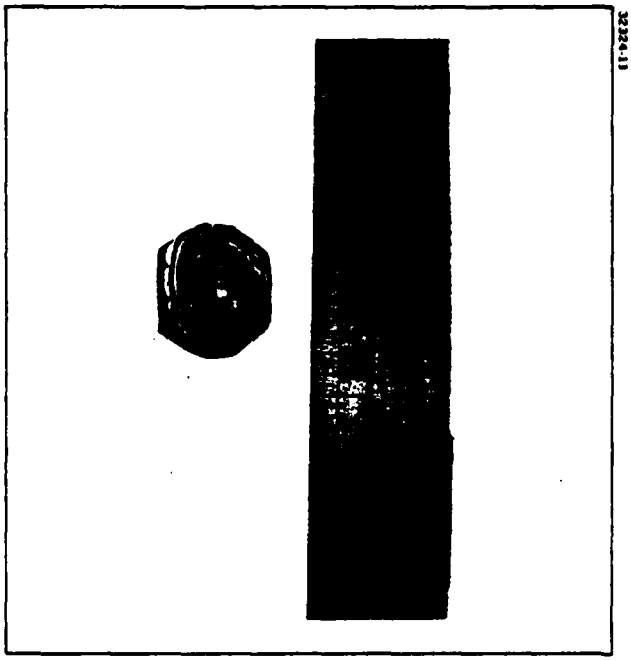

Figure 14. Arc Track on Surface of 0.001 mil Aluminum Foil After Short Circuiting Serial Number A4 Hughes 50 kV, 4A Fuse to Ground Through Foil. No visible hole was left in the foil.

Typical fuse voltage and current waveshapes such as shown in Figure 12 were graphically analyzed to determine the fuse resistance as a function of time, the charge transferred through the fuse to the arc, and the energy required to cause fuse interruption. The Hughes 50 kV, 4A fuses required approximately 40 joules of energy during the interruption process and transferred approximately 4×10^{-3} coulombs of charge.

The fuses tested have measured current interruption times varying from 15 to 18 μs with an average current interruption time of 15.6 μs. Table IV is a tabulation of the fuse test results.

Approximately one hour was required for the Hughes fuse to reach thermal equilibrium. Of all the fuses evaluated, there was no evidence of restrike nor were there any cases of fuse interruption due to self heating. Upon interruption the fuse becomes and remains an open circuit as can be ascertained from Table IV.

Similar to the other fuse testing, all data was taken in an air conditioned laboratory environment at an approximate temperature of 24°C.

Conclusions and Recommendations

The primary objective of this fuse investigation was to evaluate an assembly of Bendix 5 kV, 1A rms fuses connected in series-parallel to obtain a 50 kV, 4A rms rating; a Bendix 50 kV, 4A rms fuse; and a Hughes 50 kV, 4A rms experimental fuse to determine if a high voltage dc fuse could protect a high powered traveling wave tube. In this respect the program was a success, in that all of the fuse types did successfully protect a high power coupled cavity TWT using a high amplification factor, non-intercepting gridded (shadow gridded) gun.

However, several problems were encountered which indicated that further development was required as discussed under each fuse type.

TABLE IV. HUGHES 50 kV, 4A FUSE TEST RESULTS

Fuse S/N	Test Conditions	High Potential Test After Fuse Interruption	Remarks
A1	S/N 5 TWT at -42 kV, tp = 100 μs for 1.13 hrs. @ 4A rms. Shorted TWT cathode to ground through foil.	55 kV, 0.02 mA	Interruption time, 15 μs
A2	S/N 5 TWT at -42 kV, tp = 100 μs for 0.42 hours @ 4A rms.	No data	No data. Fuse interrupted while connecting scope due to accidental short circuit.
A3	S/N 5 TWT at -42 kV, tp = 100 μs for 0.32 hours @ 4A rms. gun arc.	No data	No data. Fuse protected TWT.
A4	S/N 5 TWT at -42 kV, tp = 100 μs for 0.083 hours @ 4A rms. Shorted TWT cathode to ground through foil.	50 kV, 0.08 mA 60 kV, 0.20 mA	Interruption time, 18 μs.
A5	S/N 5 TWT at -42 kV, tp = 100 μs for 0.83 hours @ 4A rms. Shorted TWT cathode to ground through foil.	50 kV, 0.02 mA 60 kV, 0.04 mA	Interruption time, 15 μs
A6	S/N 5 TWT at -42 kV, tp = 100 μs for 1 hour @ 4A rms. Shorted TWT cathode to ground through foil.	-42 kV, no current indication.	Interruption time, 15 μs.
A7	S/N 5 TWT ran up to -42 kV, 100 μs; shorted TWT to ground.	50 kV for 7 hours with no current indication.	Interruption time, 15 μs.

The Bendix 50 kV, 4A Fuse Assembly (5 kV, 1A fuses in series-parallel)

First, difficulty was experienced in achieving full rated rms operating current levels with the fuse carrying pulsed current at room ambient temperature. Further investigation is required into the relationships between duty, pulse width, peak pulse current and ambient temperature to obtain proper operating current derating factors. Further investigation is also required to determine the optimum method to be used in making the fuse connection. Under pulsed current operation, severe heating was observed at the fuse attachment points using fuse clips. This heating is either associated with contact interface resistance or high thermal resistance.

Secondly, approximately 10 percent of the 5 kV, 1A fuses in a fuse assembly failed to interrupt upon a load short circuit. This appeared to be due to fuse non-uniformity, but requires further investigation. In all tests, however, a sufficient number of fuses interrupted to protect the TWT.

Thirdly, the recovery characteristics in terms of hold-off voltage and leakage current for the fuse, after fuse interruption, require further investigation. This investigation should evaluate fuses operating at maximum rms ratings at maximum ambient temperature with the fuse interruption occurring after thermal equilibrium has been achieved. Data concerning these characteristics was not taken.

The Bendix 50 kV, 4A Fuse

As with the Bendix 5 kV, 1A fuses, difficulty was experienced in achieving full rated rms operating current levels with the fuse carrying pulsed current at room ambient temperature. Further investigation is required into the relationships between duty, pulse width, peak pulse current, ambient temperature, and cooling methods to obtain proper operating current derating factors. Structural damage, premature interruption, restrike, and high leakage after interruption were experienced when operating the fuses at 4A rms. Whether all undesirable characteristics can be fully eliminated by establishing proper derating factors could not be pursued under the scope of this program. It is evident, however, that the proper free-air rating for the fuse type tested is considerably less than 4A rms.

Fuses which had not been subjected to heating by long-term application of full current operated satisfactorily in terms of TWT protection, maintaining physical integrity, and lack of restrike.

The Hughes 50 kV, 4A Fuse

First, a production Hughes fuse must be designed, fabricated in quantity, and evaluated as was done in the case of the Bendix 50 kV, 4A fuse. It is encouraging that the experimental models tested experienced no restrike or long-term heating problems. Also, further investigation is required into the relationships between duty, pulse width, peak current and ambient temperature to determine the proper fuse utilization.

Postscript

The secondary objective of the fuse investigation was to determine more closely some of the more pertinent parameters associated with the optimum selection of a fuse, such as total charge transferred by the fuse, total energy required to be expended by the fuse in the interruption process, etc.

This objective was accomplished with only limited success as insufficient high quality data was taken, limited by the number of fuses evaluated and program economics. The test program resulted in the following observations:

- Interruption times for the fuses varied between 10 and 20 microseconds after the initiation of a fault. The speed is adequate to protect the TWT, if sufficient peak current limiting impedance is provided in the circuit.
- The Bendix 4A fuse expended approximately 70 joules in interruption, and the Hughes 4A fuse expended approximately 40 joules.
- The Bendix fuse transferred approximately 2.6×10^{-3} coulombs of charge during fuse interruption, and the Hughes fuse transferred approximately 4×10^{-3} coulombs.
- Based upon the aluminum foil tests, all fuses tested, with the exception of those that restruck, delivered less than one joule of energy into the fault.
- All of the fuses that were free of restrike adequately protected the TWT operated in the circuitry of the TWT test facility. Those fuses with restrike would have probably damaged the TWT if a backup crowbar circuit had not been provided.

Subsequent to this testing program, Hughes has continued to refine fuse measurement and evaluation techniques. A full discussion of this new work is beyond the scope of this paper, but a few salient points should be mentioned. Along with measurements of voltage, current, and time, techniques have been developed to determine the existence and duration of ionization within the fuse. Knowledge of ionization characteristics has proved invaluable in determining the margin of safety with respect to restrike of various fuse designs.

A much better understanding of the relationship between fuse characteristics and external circuit parameters has also been gained. For example, doubling of the circuit surge impedance can make the difference between consistent interruption and consistent restriking. It is imperative that the fuse characteristics be properly matched to the circuit voltage and impedance. Application data now exists which enables the design of a high voltage fuse protection circuit with a reliable, repeatable interruption time in the range of 3 to 25 microseconds.

Based upon the test program reported here, and upon the more recent work which now enables accurate prediction of the performance of a given fuse in a given circuit, the use of high voltage fuses to protect high power traveling wave tubes has been established as safe and acceptable circuit technique.

[1]See "Evaluation of Arc Damage to Power Triode Grid Wires", by G. Bronner, J. G. Murray, and J. P. Sorrentino, pages 970-976 IEEE Transactions on Electron Devices, December 1966, Vol. ED-13 Number 12.

IMPROVED MULTIGAP ELECTRONIC CROWBAR

William W. Shrader
Raytheon Company
Wayland, Mass. 01778

Summary

The open-air multigap crowbar has the following characteristics: (a) rapid firing after application of the trigger pulse, (b) low voltage drop after firing, (c) low energy triggering capability, (d) large range of operating voltage. Under transient conditions immediately following a load arc, however, there is a "danger zone" of operating voltages in which the crowbar partially self-fires, thus loading the trigger voltage so that reliable triggering does not occur. This paper describes a simple modification to the multigap crowbar that, under transient conditions: (1) makes it reliably self-firing at all voltages above 20 percent of its voltage rating, (2) increases the speed of self-firing at voltages near the rated voltage, and (3) ensures that the device can be triggered when the operating voltage is too low to provide self-firing.

Introduction

The open-air multigap crowbar[1] was developed at USAECOM in 1960, based on high power multigap switch studies at the University of California.[5] The need for developing this type of crowbar was based on the high operating voltages of modern transmitters, greater than 100 KV. Other available crowbar devices, such as gas filled gaps, thyratrons, or ignitrons, were not available that could operate at these voltages.

For a crowbar to be a successful protection device, it should have the following characteristics:[2] (a) rapid firing after application of the trigger pulse, (b) low voltage drop after firing, (c) low energy triggering capability, (d) large range of operating voltage, that is, it should be possible to trigger the crowbar when the applied voltage has any value from zero to full rated voltage. In addition to the above characteristics, self-firing of the crowbar when the load arcs is a desirable feature.[3]

The multigap crowbar[1,2] provides features (a) through (d) above, under static conditions. However, under the transient conditions immediately following a load arc, there is a "danger zone" of operating voltages in which the crowbar partially self-fires, and thus loads down the trigger voltage so that reliable triggering does not occur.[3]

This paper describes a simple modification[4] to the multigap crowbar that, under transient conditions: (1) makes it reliably self-firing at all voltages above 20 percent of its rating, (2) increases the speed of self-firing at voltages near the rated voltage, and (3) ensures that the device can be triggered when the operating voltage is too low to provide self-firing. This modification in no way affects characteristics (a) through (d) above under static conditions.

Discussion

Figure 1 is a simplified drawing of a multigap crowbar used to protect a klystron.

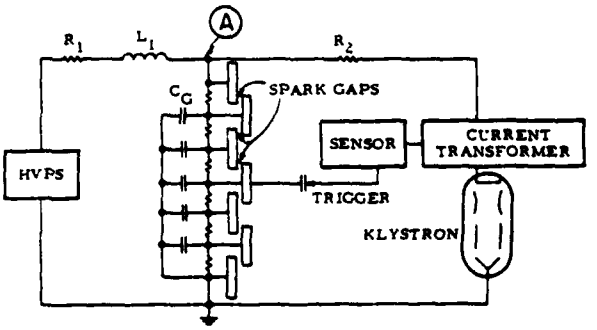

Figure 1 - Simplified Schematic

(Only six gaps are shown, although many more may be used in practice.) The inductance, L_1, is incorporated to limit fault current in the klystron at the moment of arcing[3,p7-88]. However, when an arc occurs in the klystron, the inductance causes the voltage at the top of the crowbar (point A) to fall almost to zero, thereby causing some, but not all, of the spark gaps to fire, the gap firing progressing sequentially from the top. If at least half of the gaps fire, the trigger will be essentially shorted to point A and may not be able to fire the remaining gaps. If the trigger does not fire the remaining gaps in the crowbar, the voltage at point A will start to rise as the current in L_1 increases. Eventually, the remaining gaps will self fire if the voltage at A becomes high enough. Often, however, this condition is not met and the HVPS discharges entirely through the klystron arc.

The reason that all the gaps do not fire can be explained as follows: Consider a 20-gap crowbar with 100 KV applied. Assume each gap will break down if the voltage across it

exceeds 9 KV. The resistive divider ensures equal division of the voltage, thus the differential voltage across any gap is 5KV. But note, however, the absolute voltage on the gap electrodes proceeds linearly from the bottom of the crowbar. Thus electrode one is at 0 volts, number 2 is at 5 KV, number 3 is at 10 KV, etc.

Now assume the klystron arcs. If the klystron had not been conducting at this instant, the inductance, L_1, causes the voltage at the top of the crowbar to drop to zero volts. The gaps sequentially break down (with each gap electrode falling to zero volts) until a gap with a differential voltage of less than 9 KV is reached. In this example, the top 18 gaps fire, but gaps one and two do not. Note that this essentially shorts out the trigger. As the current in the klystron arc increases, the voltage at the top of the crowbar increases because of the voltage drop across R_2. When the voltage at the top of the crowbar reaches 14 KV, gap two, and then gap one will self fire, but by this time, much of the power supply energy may have been dissipated in the klystron.

If the voltage at the time of the arc was less than 100 KV, self-firing of the crowbar may not occur at all, because the voltage at the top of the crowbar may never recover sufficiently to cause the remaining unfired gaps to be stressed more than 9 KV. For this example, if R_1 is three times R_2, self-firing will not occur for voltages less than 60 KV, and will be unreliable and relatively slow for voltages up to 80 KV.

The above explanation assumed no initial current in the klystron. Even if the klystron were drawing full load current at the time of the arc, however, the above explanation is valid. This is because the initial di/dt drop in L_1 is much greater than the voltage drop in R_2 due to the load current.

The Shunt Capacitor

Figure 2 shows the addition of a capacitor, C_s, shunting most of the gaps. Because of the symmetrical placing of this capacitor with respect to the triggering point, it does not affect triggering of the crowbar under static conditions. Under transient conditions, however, it ensures that a number of gaps near the bottom of the crowbar fire (in addition to the gaps at the top) thus ensuring rapid self-firing of the entire crowbar for voltages 20 percent or more of the voltage rating. For lower voltages, suitable trigger circuits can fire the crowbar[6], thus the device is now a full-range device under either static or transient conditions. C_s is about 10 times as large as C_g, but is small enough not to contribute significant extra energy to be dissipated.

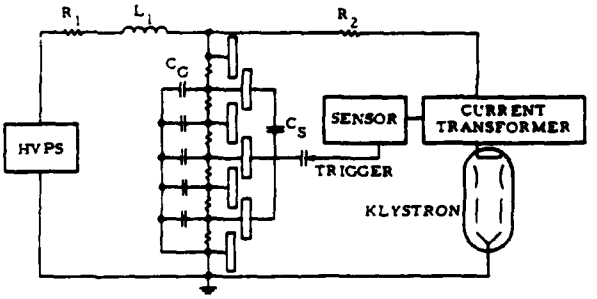

Figure 2 - Simplified Schematic With Improved Multigap Crowbar

To consider how this shunt capacitor aids operation, again consider a 20-gap crowbar with the shunt capacitor connected three gaps from the bottom and three gaps from the top of the crowbar. If the voltage on the crowbar is 100 KV, the voltage on the bottom of C_s is 15 KV, and on the top, 85 KV. Thus the voltage across C_s is 70 KV. When a load arc occurs, the voltage at the top of the crowbar drops to zero, and the gaps start to sequentially fire from the top as before. As soon as three gaps have fired, the top end of C_s drops to zero volts, driving the bottom end from 15 KV to 70 KV of the opposite polarity. This immediately causes a number of the bottom gaps of the crowbar to fire. When firing of the intermediate gaps has progressed to the fired bottom gaps, a short circuit is established and the HVPS can immediately discharge through the crowbar. Note that this complete self-firing now occurs in a fraction of a microsecond, whereas before, without C_s, the self-firing took (with typical circuit parameters) four to ten microseconds.

A 20-gap crowbar has been built employing the shunt capacitor. The shunt capacitor is connected 3 gaps from the top and bottom as described above. (These connecting points were empirically determined to be best from a number of tests made with different operating voltages on the crowbar.) This crowbar will withstand 200 KV and is reliably self-firing at all voltages above 40 KV. It can be reliably triggered under all static conditions, and also under transient conditions, if the HVPS voltage is too low to provide self-firing.

Acknowledgement

The author wishes to thank Thomas A.Weil, first, for suggesting the problem that led to the shunt capacitor, and, second, for directing the effort of developing and testing the finished hardware.

References

1. S. Schneider, M. H. Zinn, and A.J. Buffa, "A Versatile Electronic Crowbar System", Proc. Seventh Symp. Hydrogen Thyratrons and Modulators, pp 482-506, May 1962, AD296-002.

2. A. J. Buffa, S. Schneider, M. H. Zinn, U. S. Patent No. 2,260,895, "Electronic Circuit Protection Device Providing a Low Resistance Path Through A Series of Spark Gaps Connected Across Said Electronic Circuit", 12 July 1966.

3. T. A. Weil, "Transmitters", in Radar Handbook, M. I. Skolnik, Ed., New York: McGraw-Hill, 1970, pp 7-87 to 7-91.

4. W. W. Shrader, U. S. Patent 3,526,811, "Electronic Crowbar System", 1 Sept. 1970.

5. A. L. Gardner, D. H. Sloan, L.C. Marshall, W. J. McBride, Jr., "High-Power, Pulse-Line Switching Devices", Final Report, Microwave Laboratory Institute of Engineering Research, University of California, Berkeley, Calif., Apr. 1, 1952.

6. T. A. Weil, "Multigap Crowbar Triggering Study", Eleventh Modulator Symposium, Sept. 18-19, 1973.

MULTIGAP CROWBAR TRIGGERING STUDY

Thomas A. Weil
Raytheon Company
Wayland, Mass.

Summary

This paper reports the results of a study on triggering problems in the use of multigap crowbars. A trigger circuit was desired that could provide full crowbar firing even when a load arc causes partial but incomplete self-firing of the crowbar, leaving the trigger pulse shorted out by a direct path to ground or to the HVPS. Otherwise, this condition represents a "danger zone" in which crowbar protection is missing.

Sharpening gaps had previously been found to provide inconsistent benefits. This study found that a sharpening gap can sometimes permit completing the firing of a partially fired crowbar even when the trigger pulse is "shorted out", but that the sharpening gap itself may cause triggering misfires unless considerable overvoltage is used, or unless a radioactive source is used to provide pre-ionization.

The validity of various crowbar test methods was studied, and recommendations will be presented. The study also determined which stray inductances and capacitances in the crowbar and its triggering circuit have a significant effect on triggering performance.

"Bottom triggering" was studied as an alternative triggering method that provides firing under all conditions and requires no HVDC blocking capacitor.

A multigap crowbar using the results of this study will be described. The crowbar includes improvements in creepage paths and in the electrode capacitor design. The crowbar is corona-free at 180 kV and is reliably self-firing above 50 kV.

Triggering Study

Introduction

The paper by W. W. Shrader[1] describes how the USASRDL Electronic Crowbar[2] can be made reliably self-firing for load arcing at all voltages above about 1/3 of normal full operating voltage. Problems remaining to be resolved for completely reliable operation include:

1. How to ensure that the crowbar can be externally triggered at any operating voltage. The USASRDL crowbar design readily meets this requirement[2] unless a load arc has already caused partial but incomplete self firing, leaving the trigger pulse shorted out by a direct path to ground or to the HVPS. Although the addition of a "Shrader capacitor" confines this problem to the lower voltages, it may still represent a "danger zone" to the load if the HVPS capacitor bank energy is high enough.

2. How to reduce unintentional self-firing of the crowbar under certain normal and abnormal conditions under which crowbarring is not required but happens to occur.

Initial attempts to obtain test data on crowbar operation showed erratic results. Triggering reliability tended to vary from time to time and from one setup to another, leading to the conclusion that significant aspects of the circuit strays and the test conditions were not being recognized as significant and as a result were uncontrolled. Therefore, a study was undertaken to determine which factors were significant and how to obtain meaningful test results.

Basic Circuit Studied

Figure 1 shows the basic modulator circuit for which the crowbar study was undertaken; for a more detailed description, see reference 4. Figure 2 shows the schematic of a conventional multigap crowbar, from reference 2, and used in this triggering study; shown dotted is the "Shrader capacitor" described in reference 1. Both a 20-gap and a 30-gap crowbar were studied, with and without the Shrader capacitor. Fig. 3 shows the basic circuit of the trigger source used for most of these tests.

Spark Gap Breakdown Statistics

To determine why test results seemed to vary, the trigger circuit was set up alone with a single spark gap, consisting of two 1-inch diameter balls with adjustable spacing. It was soon evident that spark gap breakdown could only be described statistically, and that deviations from average values were greater than had first been expected. One reason found for these wide variations was that the commercial trigger transformer being used had inadequate primary (magnetizing) inductance, and the core was saturating, leading to a very short trigger pulse duration that tended to exaggerate the statistical breakdown problem. With an improved trigger transformer, the variations were reduced, and results were then reproducible, at least on a statistical basis. Figure 4 shows test data with a 1/2 inch gap spacing, using a 6:1 step-up ratio in the pulse transformer (T1 in Fig. 3). The resulting trigger pulse to the spark gap had a rise time less than 0.4 μsec and a decay time of 2 μsec to the 50% point. Although the gap would sometimes fire at a trigger HVPS voltage of 5.5 kV (charging voltage on C2 of Fig. 3), it would still misfire occasionally at 8.5 kV, as shown, based on a few hundred tries at 1 PPS at each point shown. Furthermore, it became very clear during these tests that the rate at which the tests were performed affected the results drastically. Tests at a faster rate than 1 PPS clearly showed a carry-over effect; i.e., if the gap had just fired, it was much more likely to fire the next time, presumably as a result of residual ionization and/or heat left from the previous breakdown. The carry-over time tended to be longer when more energy was discharged into the gap, and carry-over effects were noticeable even after 10 seconds during crowbar testing later with a large capacitor bank. In any case, the data shown in Fig. 4 were taken at 1 PPS in order to complete the testing in a reasonable time (several hours), and it is strongly suspected that the "tail" of the distribution curve would stretch even further out if the testing were done slowly enough to represent the real case where a crowbar must be fired reliably when it has not recently been fired. The fact that the data in Fig. 4 do not form a smooth curve, even with several hundred tests per point, is a further indication of the statistical nature of spark gap breakdown. Since there are conditions where crowbar protection is required to prevent loss of a klystron, and yet where

self-firing will not occur (excessive modulator pulse width, or loss of solenoid power, etc.), failure to trigger when required may have disastrous results. Figure 4 shows that an appreciable overvoltage factor is required to ensure that a spark gap will "always" break down when intended. It is also clear that dangerously optimistic "statistical" results can be obtained by testing at too rapid a rate.

Since residual ionization appeared to improve the chances that the spark gap would fire on the "next" pulse, the tests were repeated with the gap pre-ionized by placing 1 millicurie of radium inside one of the balls. This location was chosen to guarantee that the radium container could not be damaged by the arcing. The 1/8" copper wall of the ball would be expected to have little effect on the radiation intensity, since 0.55 inches of lead is required to reduce the strength of radium X-rays by 2:1. The results, as shown in Fig. 4, confirm what was expected; the presence of pre-ionization greatly reduces the statistical variations in spark gap breakdown. Ultraviolet radiation also helps to initiate breakdown, as noted in refs. 2 and 5, so the firing of subsequent spark gaps in a series of gaps in sight of each other should be reasonably consistent, too; the statistical problem applies primarily to the first gap to be fired.

Crowbar Firing Statistics

Crowbar self-firing tests are also subject to statistical variations and carry-over effects. Carry-over effects can be avoided by performing the testing at adequate intervals, and with a trigger of adequate duration it was then found possible to obtain consistent results in a given test setup. Self-firing tests were performed by substituting a "fault gap" in place of the klystron load and slowly raising the HVPS voltage until the fault gap fired. The fault gap was made from a pair of crossed multigap crowbar electrodes mounted in a frame, as shown in Fig. 5, and reasonably consistent DC breakdown was obtained.

It very quickly became clear that no special instrumentation was required to detect whether the crowbar diverted or not; since the fault gap was a single air gap, and since the crowbar was 20 or more air gaps, the noise was 20 times louder when the crowbar would self-fire than when it would misfire. Oscilloscope pictures of current waveforms, using Pearson current transformers properly loaded down externally so they would not saturate on the large I-T product, showed that there were no intermediate conditions; the crowbar would either divert promptly or not at all, and the waveforms were always the same in each of these cases, and were as would be expected from the high-power circuit constants (discussed more later).

By making enough tests, it was possible to draw a curve, such as that shown in Fig. 6, for any particular crowbar setup. Figure 6 shows the results for a 20-gap multigap crowbar without a Shrader capacitor, using a single triggering point in the middle of the crowbar. No sharpening gap (see later) was used. At 150 kV, a load arc causes the crowbar to self-fire consistently, as shown diagrammatically in Fig. 6 by the fact that the area marked "self-firing" fills the vertical probability scale at that voltage. With the trigger high-voltage supply turned off, the self-firing probability was measured to be as shown, falling off gradually to zero at about 50 kV. However, even with the trigger unit enabled, the crowbar failed to divert current from a load arc in the region shown as "no protection" in Fig. 6; in this region, the partial self-firing of the crowbar, caused by the load arc, shorts out the trigger source and prevents it from being able to complete the firing of the crowbar. The trigger circuit used in this case was capable of firing the crowbar, in the absence of a load arc, at any value of high voltage from 0 to above 180 kV, and it could do so consistently even when the HVPS in the trigger unit was reduced in half. Nevertheless, it can be seen that there was a large region where the crowbar would not fully self trigger and then could not be triggered by this trigger unit. A "danger zone" thus results in which the load is not protected. For example, at 100 kV, there is about a 40% chance that this crowbar will self-fire, but, if it does not, then there is very little chance that the trigger will be able to complete the firing of the crowbar.

Corresponding results are shown in Fig. 7 for the same crowbar with the Shrader capacitor added; it can be seen that the self-firing range is greatly improved. The dotted curve shows the performance initially obtained, with the Shrader capacitor connected 2 gaps in from each end of the 20-gap crowbar; the danger zone was greatly reduced and only extended from about 30 to 65 kV, as shown. The solid curve shows the further improved performance obtained later when the taps for the Shrader capacitor were optimized (at 3 gaps in from each end) by a subsequent series of tests; only a very small danger zone remains, between 30 and 45 kV. Depending on the chance of a load arc occurring at such a reduced voltage (and whether the load is worth protecting if it does so), and depending on whether an arc at reduced voltage may hurt the load or not, it may still be desirable to find methods of eliminating this danger zone. Further results obtained from this study show how this can be done, when desired.

Sharpening Gap Tests

A sharpening gap[6] is an additional spark gap placed in series with the trigger to the crowbar so that no trigger voltage reaches the crowbar until the sharpening gap fires; then, a very sharply rising trigger is applied to the crowbar. Sharpening gaps were studied as a means of improving trigger effectiveness in the hopes of eliminating the danger zone.

The characteristics of sharpening gaps were studied in the test setup previously described in connection with Fig. 4, by the addition of a second spark gap to the test setup, as shown in Fig. 8. In this setup, the top gap now represents a sharpening gap. A high-value resistor and small capacitor were placed across the bottom gap to cause the trigger voltage to appear across the top gap first. When the top gap fired, the bottom gap would also fire consistently if its spacing were such that the trigger voltage would have fired it by itself.

A shorting lead was then added across the bottom gap, to represent the case where a partially self-fired crowbar "shorts out" the trigger source through the load arc; such a "short" would contain several microhenries of inductance, and it was therefore of interest to see if the bottom gap could be fired when it was "shorted" by various values of inductance. It was found initially that the bottom gap would not fire consistently unless the "shorting" inductance was quite large. Further thought indicated that the time available for the "shorted" bottom gap to fire after the top gap fires depends on the ringing frequency of the stray capacity C4 and the shorting inductance L2. If C4 is 50 pf and L2 is 5 μH, the voltage will ring to zero in about 25 nanoseconds (1/4 cycle of the resonant frequency). Increasing C4 would extend this time, allowing the bottom gap more time to break down. A

low-inductance high-voltage capacitor of 1200 pF was added at C4, with very gratifying results. The bottom gap could then be fired consistently even when shorted out by a small clip lead of one microhenry inductance, as long as the top gap was at least as big as the bottom gap, and as long as the trigger was sufficient to fire the top gap. It can readily be seen from Fig. 8 that when the top gap fires, the voltage stored in C4 will divide according to the circuit inductances, and if the self-inductance of C4 plus its leads can be kept small compared to L2, then most of the voltage will appear across the bottom gap, for a time duration that depends on C4 and L2 as noted before. The effect of C4 on trigger circuit design is discussed later.

Based on the above tests, it was hoped that a trigger unit with a sharpening gap would eliminate the danger zone in multigap crowbar operation. However, when the trigger unit with a sharpening gap was first tried on a crowbar without a Shrader capacitor, the results were discouraging. The load arc (simulated by the fault gap previously described) would sometimes cause the sharpening gap to prefire, effectively removing the sharpening gap from the circuit before the trigger was applied; as a result, part of the danger zone remained. Therefore, other triggering techniques were investigated, as will be described below. With hindsight, however, it appears that the combination of the Shrader capacitor and a trigger unit with a sharpening gap should be able to eliminate the danger zone; if the Shrader capacitor connections are adjusted to provide reliable self-firing above 50 kV, as in the solid curve of Fig. 7, and if the sharpening gap is set not to fire at less than 50 kV, then the sharpening gap should never be prefired by a load arc unless the HVPS voltage is high enough to ensure that the crowbar will fully self-fire anyway. Although this combination was not demonstrated, it appears to be a reasonable basis for future designs.

Bottom Triggering

Since the sharpening gap was being prefired by a load arc when connected to the usual triggering point in the middle of the multigap crowbar, other arrangements were sought that would ensure that the sharpening gap would not be prefired. The only trigger connection point that would keep surge voltages away from the sharpening gap unless the whole crowbar self fired appeared to be the bottom of the crowbar.

Figure 9 shows the circuit used for testing "bottom triggering", as it was called, with the trigger pulse applied to the "grounded" electrode. Note also that no HVDC blocking capacitor is required in this arrangement (such as C3 in Fig. 3). The sharpening gap was put close to and in sight of the crowbar gaps to allow ultraviolet radiation from the sharpening gap to help speed firing of the crowbar gaps[2,5]. This arrangement worked surprisingly well, using the techniques previously described under sharpening gaps. It is only necessary that the lead inductance from the bottom crowbar electrode to ground be at least a couple of microhenries; in fact, typical high-power crowbars already have that much lead inductance in their return conductors to the capacitor bank. This value of inductance is not significantly harmful to energy diversion, since a multigap crowbar typically has 5 to 10 microhenries of inductance itself; it only increases very slightly the time it takes for the fault current to divert fully from the load arc to the crowbar after the crowbar fires.

Figure 10 shows the test results on "bottom triggering". Thanks to the Shrader capacitor, the multigap crowbar is reliably self-firing above about 50 kV. Prefiring of the sharpening gap did not occur. Thus, with bottom triggering, the crowbar can always be triggered when it does not fully self fire. It can also be triggered, of course, in the absence of a load arc. Testing to verify this latter condition emphasized the effectiveness of the sharpening gap technique; not only would the trigger fire the crowbar fully from the bottom up, but the "fault gap", if left connected, would also fire from the trigger pulse feeding through the crowbar, unless the gap were set to higher than 100 kV, which in this case was the trigger voltage being used. This led to some concern that too powerful a trigger might actually cause load arcs when the crowbar is test fired; this concern thus sets a limit on the maximum trigger voltage that should be used.

Required Trigger Voltage

The required value of trigger voltage for a given multigap crowbar design can be calculated as follows:

1. For safety against DC breakdown of the multigap crowbar, the total of the gap voltages should be twice the working voltage.

$$N \times E_g = 2 \times E_{dc}$$

2. To fire the gaps fast, the trigger voltage should be about 4 times the individual gap breakdown voltage.

$$E_t = 4 \times E_g$$

3. If a sharpening gap is used, the firing voltage of the sharpening gap determines the triggering voltage applied to the multigap crowbar. In turn, to ensure that the sharpening gap does not cause misfires, the trigger source must supply about twice that voltage (assuming the sharpening gap firing voltage is stabilized by radioactivity; otherwise a factor of three is recommended).

$$E_s = 2 \times E_{sg} = 2 \times E_t$$

Multiplying these factors together results in a recommended trigger source voltage of

$$E_s = 16 \times \frac{E_{dc}}{N} .$$

For a 20-gap crowbar for use at 150 kV DC, the recommended trigger voltage is 120 kV. This is sufficient for bottom triggering, assuming radioactivity is used to stabilize the firing of the sharpening gap; and this arrangement eliminates the danger zone. Without the sharpening gap, 60 kV is sufficient for conventional middle-triggering, but the danger zone is not eliminated entirely. The preferred choice of these alternatives for a particular system depends on many factors. For the intended system, it was decided that the crowbar self-firing range with the Shrader capacitor was sufficient to protect klystrons, so the conventional middle-triggering method was selected to avoid the nuisance of a radioactive source and the higher required trigger voltage.

The above trigger voltage calculation shows clearly how the trigger voltage requirement can be reduced by using more gaps in the multigap crowbar, at the expense of complexity. Nuisance firing (see below) may also limit the advantage that can be obtained by increasing the number of gaps. One further side effect of increasing the number of gaps is that the resulting higher drop across the crowbar slightly reduces its effectiveness in diverting current from a

load arc (see Diversion Effectiveness, below).

Trigger Circuit

As noted in connection with Fig. 8, added capacitance (C4) at the trigger source output makes it a more effective (stiffer) source for firing subsequent spark gaps following a sharpening gap. For similar reasons, a stiff source is desirable for firing the cascade of gaps in a multigap crowbar with conventional middle-triggering even when a sharpening gap is not used. Once the firing process begins, it goes so quickly (10 to 100 nanoseconds) that the trigger source effectively consists of only C4 during that time, and the trigger voltage must be maintained long enough to trigger all the way to both ends of the crowbar, even if the triggering goes slightly faster one way and "shorts out" the trigger to ground. As also noted, any inductance between C4 and the gaps it must fire reduces its effectiveness; similarly, any lead inductance preceding C4 is not harmful, in this sense, but simply affects how quickly C4 can be charged. The task of all the trigger circuitry preceding C4, then, as shown in Fig. 11, is merely to charge C4 as rapidly as possible to a suitable voltage so it can do its job of firing the gaps following it. Increasing C4, as suggested, will increase the energy that must be provided from C2 in Fig. 11 and will increase the time it takes to charge C4 when the thyratron is fired (or else the thyratron peak current and di/dt must increase), but this is the price one must pay to improve triggering effectiveness. It should be noted that triggering speed, usually considered one of the most significant characteristics of a crowbar trigger circuit, is not critical here, because a multigap crowbar with a Shrader capacitor is reliably self-firing under the conditions where firing speed is important (a load arc). Crowbar self-firing speed is hard to measure precisely, because of the high noise level present when the load arcs, but it is clearly of the order of 100 nanoseconds. For other conditions, a trigger reaction time of a few microseconds is certainly acceptable, and a 1200 pF capacitor at C4 can readily be charged to 100 kV in a few microseconds or less. The function of the trigger output transformer, T1 in Fig. 11, is simply to provide the needed voltage step-up with adequately low leakage inductance, for rapid charging of C4, together with sufficient magnetizing inductance to allow the output voltage to persist for a few microseconds. Choice of a large core for T1 makes it relatively easy to obtain suitable inductance values. Using a 39 pound core, a leakage inductance of 0.2 microhenries and a magnetizing inductance of 63 microhenries (both referred to the primary) was achieved. Used in the circuit of Fig. 11, the total primary circuit inductance, including the transformer leakage inductance, was 0.6 microhenries. The delay time from low-level trigger input to 100 kV output was only 1.4 microseconds total. To minimize lead inductances in the primary circuit, it was convenient to procure C2 and T1 in a single package (Axel Electronics, part no. SP689-1). A smaller transformer would suffice if slightly longer trigger delay time is acceptable, and the resulting higher circuit inductance would also reduce the peak current and di/dt stress on the thyratron.

Diversion Effectiveness

Photographs of current waveforms during crowbar testing showed several interesting points. Fig. 12 shows the simplified equivalent circuit of the HVPS, crowbar, and load, and Fig. 13 shows the waveforms observed. When the load arc occurs, the crowbar fires promptly. Since L1 limits the rate of rise of fault current to 500 A/μsec (at 60 kV), and since the crowbar fires in 100 nanoseconds, the initial spike seen on the load arc current was not expected. This spike turns out to be the result of finite crowbar inductance, which results in increased crowbar voltage drop $\left(L \frac{di}{dt}\right)$ during the rapid rise of current at the start of the discharge cycle. During the main portion of the discharge, the load current was observed to be nearly constant, as shown in Fig. 13, at about 80 amperes. This implies a nearly constant voltage drop across the 20-gap crowbar of 600 volts, or 30 volts per gap, over the range of several thousand amperes down to where it extinguishes. Note that the crowbar extinguishes before the load arc does; the tail end of the capacitor bank discharge is through the load arc only, since it is a single gap and has lower voltage drop than the crowbar. Nevertheless, 97% of the charge in the capacitor bank is diverted by the crowbar. It is also possible that a real arc in a vacuum tube (klystron, etc.) may extinguish itself sooner than occurred with the air gap used here to simulate load arcs. The slight rise in load arc current that occurs just before the crowbar extinguishes is caused by the well-known rise in arc drop[8] that occurs at low values of arc current.

Nuisance Firing

As shown in Figs. 1 and 12, an inductor is commonly used between the capacitor bank and the multigap crowbar to limit the rate-of-rise of current in a load arc and to ensure effective operation of the crowbar, as described in references 3, 4, and 7. Unfortunately, this inductor also causes the voltage appearing across the crowbar to fluctuate whenever the normal load starts or stops, as also described in the references noted. To prevent the crowbar from self-firing under normal pulse operation, it is customary to limit the rate of rise and rate of fall of the load current, as well as to "open up the top gap" of the crowbar to 1.5 to 2 times the spacing of the rest of the gaps in the multigap crowbar. Even then, nuisance (unnecessary) self-firing of the crowbar may still occur if the load current stops more quickly than usual, as may happen in a klystron when a mod-anode-to-cathode arc occurs. Such an occurrence does not require that the crowbar be fired, but self-firing is likely to occur because of the large voltage transient that occurs in this case because of the sudden interruption of the load current flowing through L1. Several possible solutions to this problem appear feasible, and, although they have not yet been evaluated directly, differences in performance observed on different modulators during mod-anode-to-cathode klystron arcing appear to be explainable on this basis. Proposed solutions include:

1. Open up the top gap even more. Eventually, this will spoil the self-firing ability of the multigap crowbar, and it may spoil the ability to trigger the crowbar at low values of HVPS voltage ("infinite range" firing, as described in reference 2).

2. Add capacitance from klystron cathode to ground. The amplitude of transients is reduced, but load arc energy and pulse ringing are both increased unless resistance is used in series with the added capacitance. A resistor in series with the modulator "OFF" dack, as suggested in ref. 7, helps but may not be sufficient for this purpose.

3. Add a damping resistor across L1. A value around 300 ohms added across L1 in Fig. 1 will greatly attenuate the voltage transient produced when load current is suddenly interrupted, and it will only raise the initial value of fault current into a load

arc by 500 amperes.

One or more of these techniques should reduce or eliminate nuisance firing without losing the important advantage of reliable self-firing when a load arc occurs.

Crowbar Construction

Figure 14 shows a multigap crowbar based on these principles and used in the circuit of Fig. 1. The crowbar electrodes are supported directly by ceramic high-voltage bushings, which eliminates the creepage-path problems of the conventional "trough" construction. The dividing resistors (see Fig. 2) are also supported by the ceramic bushings and are mounted behind the crowbar electrodes. A reliable construction was also worked out for the "ground capacitors", i.e., the capacitors from each crowbar electrode to ground (Cg in Fig. 2); since the ceramic bushings inherently had some capacity to ground (about 22 pF each), it was decided to add a simple sphere in the oil-filled columns behind the bushings to raise the capacitance to ground to the desired 45 pF, as shown in Fig. 15. The shield baffles shown in Fig. 15 not only help by increasing the capacitance from each sphere to ground, but they also prevent an increase in electrode-to-electrode capacitance, which would be undesirable (see ref. 2). The insulation resistance of conventional transformer oil (properly purified) is sufficiently high that it does not affect the voltage dividing action of the divider resistors. This approach allows conventional, conservative high-voltage design techniques to be used throughout the construction, leading to high reliability; the resulting crowbar is corona-free to 180 kV. It can be fired at any operating voltage, and it is reliably self-firing above 40 kV.

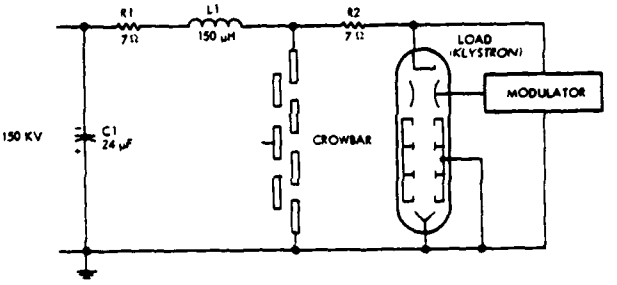

FIG. 1. MODULATOR CIRCUIT

References

1. W. W. Shrader, "Improved Multigap Electronic Crowbar". Proc. Eleventh Modulator Symposium, Sept. 1973.

2. S. Schneider, M. H. Zinn, and A. J. Buffa, "A Versatile Electronic Crowbar System", Proc. Seventh Symposium on Hydrogen Thyratrons and Modulators, pp. 482-506, May 1962, AD296002.

3. S. Schneider and G. W. Taylor, "Transients in High Power Modulators", IEEE Transactions on Electron Devices, Dec. 1966, pp. 977-984.

4. Radar Handbook, M. I. Skolnik, Ed., McGraw-Hill, New York, 1970. See Figure 7-44 and related text.

5. F. W. Peek, Jr., Dielectric Phenomena in High Voltage Engineering, McGraw-Hill, 1929, p-134. (University Microfilms.)

6. S. Schneider and A. J. Buffa, "The 'Hourglass' Energy Diverter", IEEE Transactions on Electron Devices, Aug. 1967, pp. 433-438.

7. J. H. Main, "Settling Time Considerations in Floating Deck Modulators", Proc. Ninth Modulator Symposium, May 1966, pp. 390-397.

8. E. E. Staff, MIT, Applied Electronics, Wiley and Sons, 1943, p. 151.

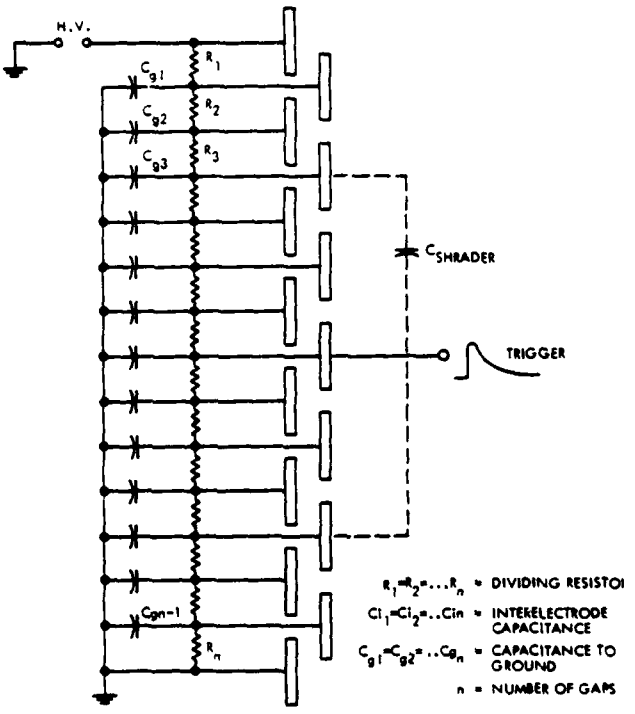

FIG. 2. MULTIGAP CROWBAR SCHEMATIC

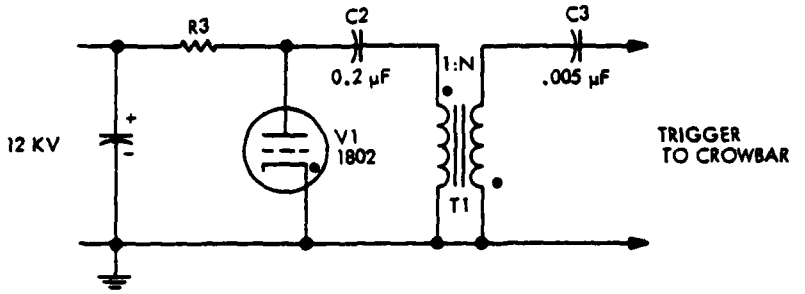

FIG. 3. BASIC TRIGGER CIRCUIT

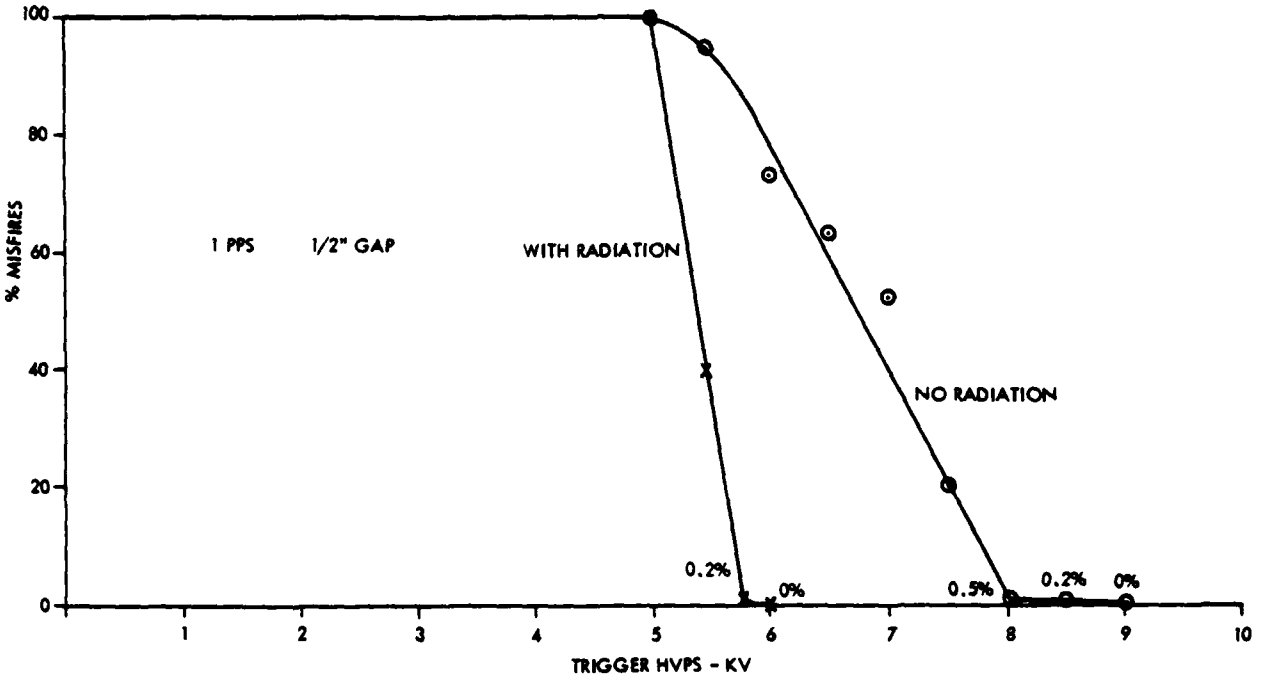

FIG. 4. SPARK GAP FIRING STATISTICS

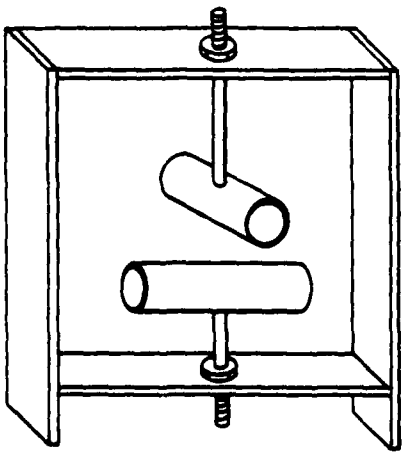

FIG. 5. FAULT GAP CONSTRUCTION

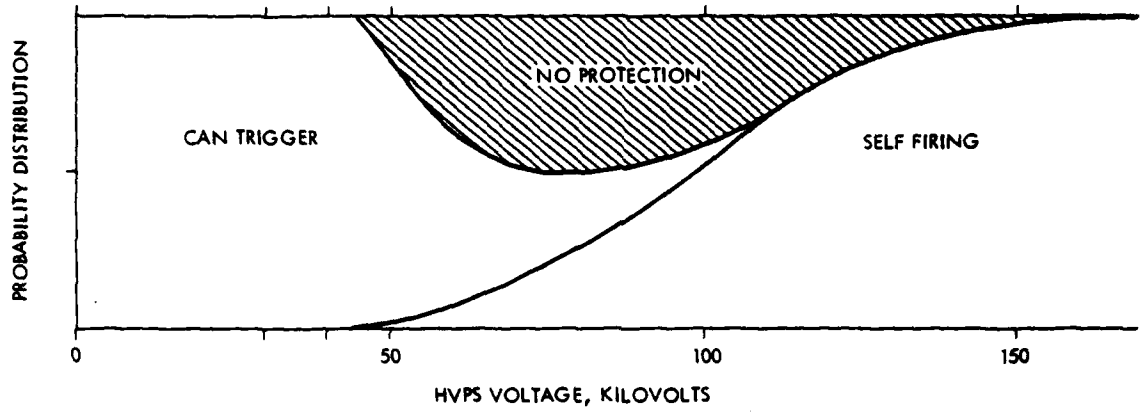

FIG. 6. PROBABILITY DISTRIBUTION. MIDDLE TRIGGER, NO SHRADER CAPACITOR

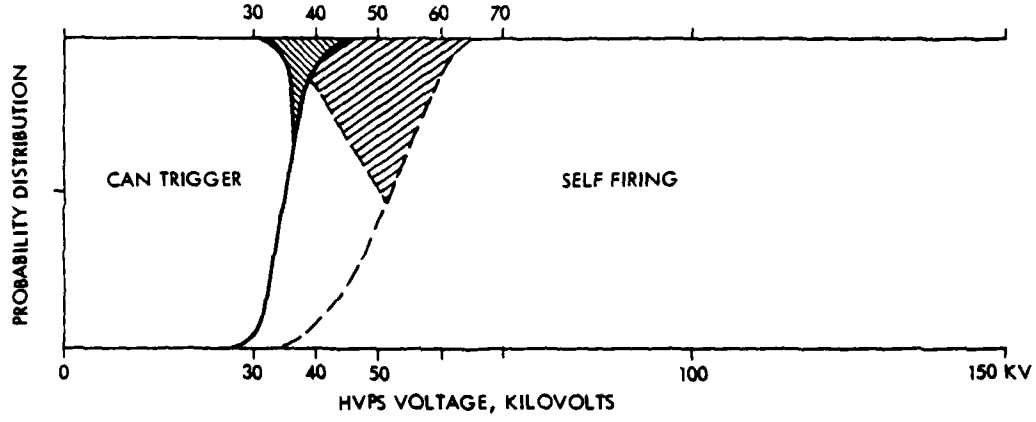

FIG. 7. PROBABILITY DISTRIBUTION. MIDDLE TRIGGER, WITH SHRADER CAPACITOR

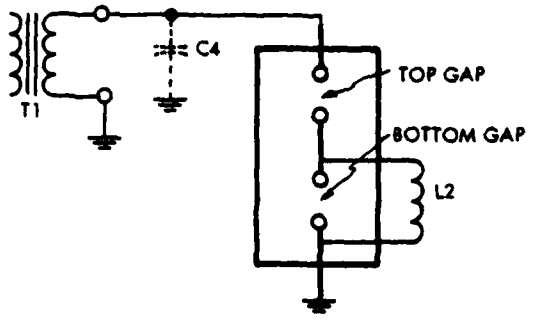

FIG. 8. SHARPENING GAP TESTS

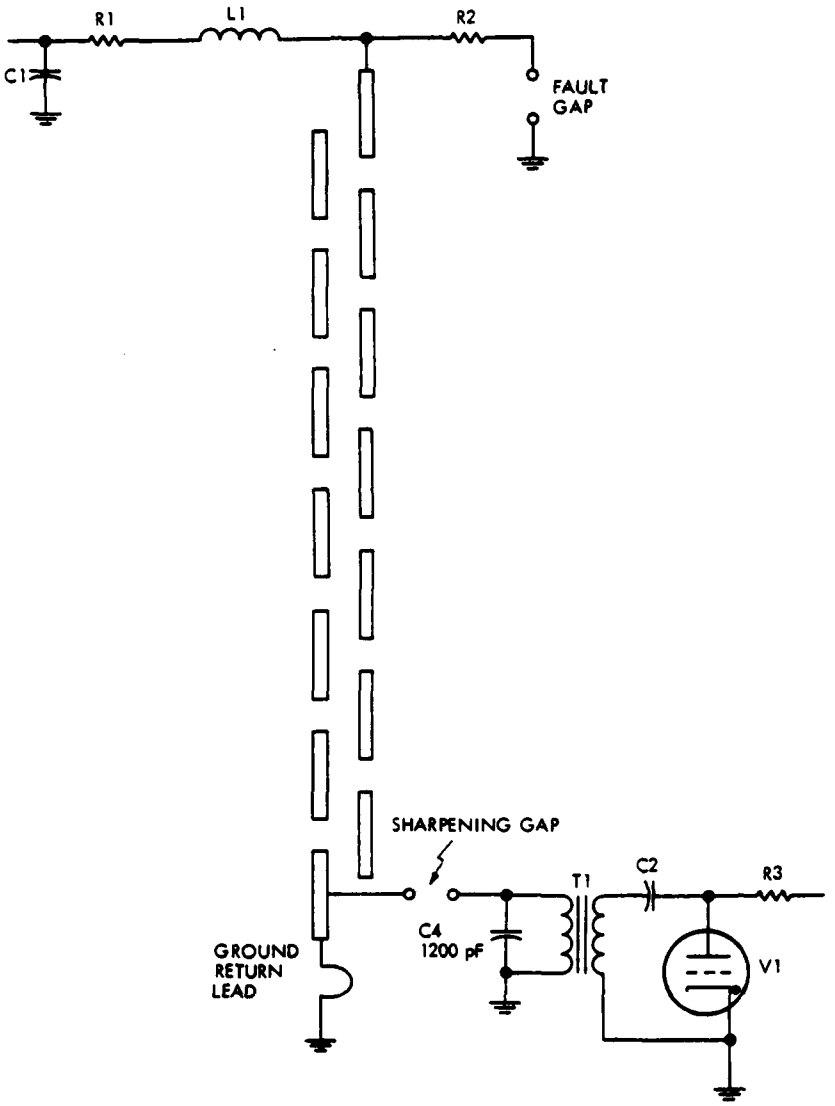

FIG. 9. BOTTOM TRIGGERING

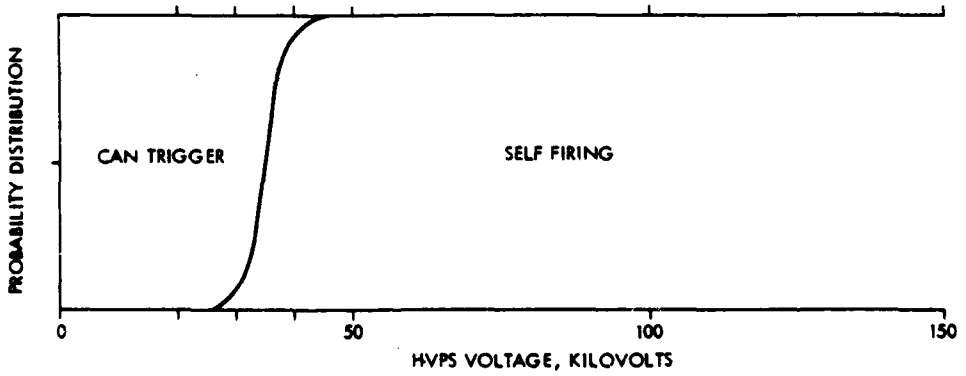

FIG. 10. PROBABILITY DISTRIBUTION. BOTTOM TRIGGER, WITH SHRADER CAPACITOR

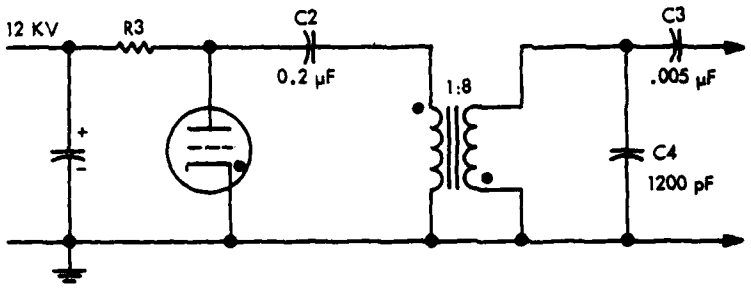

FIG. 11. TRIGGER CIRCUIT

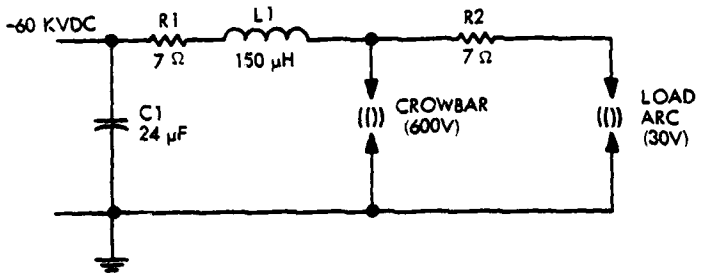

FIG. 12. SIMPLIFIED CROWBAR DISCHARGE EQUIVALENT CIRCUIT

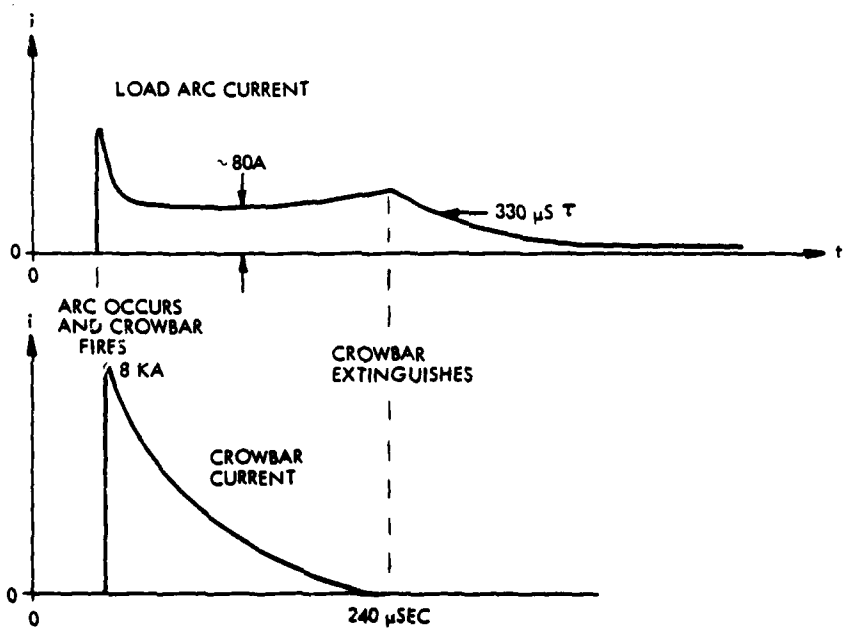

FIG. 13. CURRENT WAVEFORMS, CROWBAR DISCHARGE
(THIS TEST AT 60 KVDC WITH C_1 REDUCED TO 16 μF)

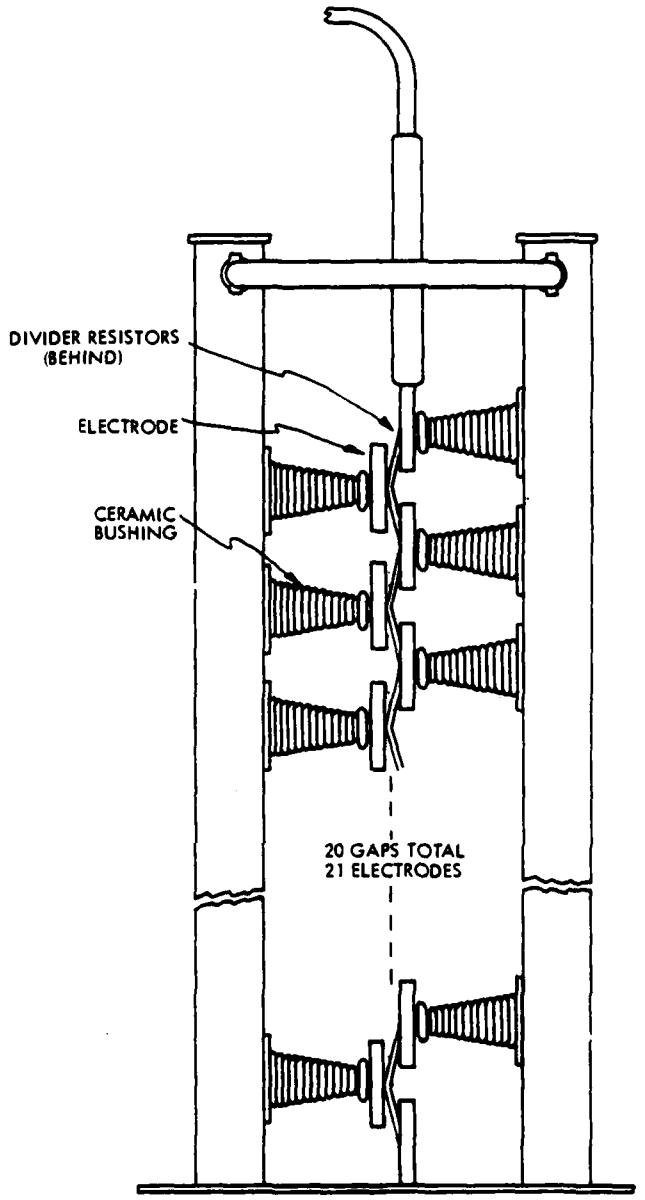

FIG. 14. CROWBAR CONSTRUCTION

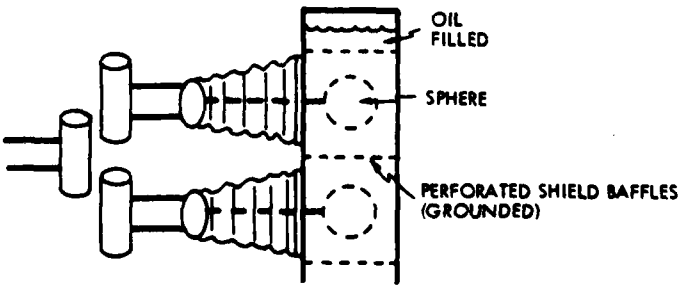

FIG. 15. CONSTRUCTION OF GROUND CAPACITORS

RAPID RECYCLE CROWBAR CIRCUITS

George R. Lyuta and Thomas A. Weil
Raytheon Company
Wayland, Mass.

Summary

Crowbar circuits are used across high voltage energy storage capacitors employed in the output stages of high power radar transmitters. Conventional high voltage power supply and crowbar systems require OFF-ON recycle times in the order of seconds. Circuits were studied which will allow the radar transmitter to be brought back into operation within a few hundred microseconds after a tube fault condition.

Two basic circuits were tested. In the first kind of circuit, the capacitor bank energy is dissipated, as in conventional crowbar circuits, and the bank is then quickly recharged from another capacitor. In the second kind of circuit, the energy in the capacitor bank is temporarily stored in reversed polarity on the same capacitor, and then returned to normal polarity to restore operation.

The tests showed that both kinds of circuits worked, with a preference for the second kind described above. Further work is needed on switching devices for this application, and it remains to be determined how fast voltage may actually be reapplied to an RF tube after an arc without causing it to arc again.

Program Objective

The program objective was to study the feasibility of reapplying power to a transmitter high-power RF amplifier stage within 500 microseconds of a crowbar action.

The term "crowbar" refers to a circuit configuration which isolates a faulted load from its power supply, and in particular from the power supply stored energies.[3] Figure 1 is a simplified diagram of a typical conventional crowbar circuit. The heart of the crowbar circuit is the crowbar switch. When a load fault occurs, the crowbar switch is activated and becomes a very low impedance compared to R1 and R2. The power supply stored energies are dissipated safely in R1, and the switch remains closed until the power supply is turned OFF.

Program Significance

High-power microwave tubes have a history of numerous arcs during their normal life. This situation impacts on system performance and has increased significance when an array of amplifier tubes are connected to a common power source.[4]

Crowbar circuits are used across high voltage energy storage capacitors employed in the output stages of high-power radar transmitters. Conventional high-voltage power supply (HVPS) and crowbar systems require OFF-ON recycle times in the order of seconds following a load fault. Circuits were studied which will allow the radar transmitter to be brought back into operation within a few hundred microseconds after a tube fault condition, assuming, of course, that the fault has cleared within the tube.

The concept of returning the faulted amplifier back to normal operation within microseconds time, or "rapid-recycle crowbarring" has been studied previously but without a reasonable or economical solution [1,4].

Approaches Studied

Various approaches were studied, resulting in the selection of four rapid-recycle circuits for breadboard testing to verify predicted performance. Figure 2 shows simplified diagrams of the four circuits.

The four circuits cover two basic approaches. One approach dissipates the stored energy and then rapidly recharges the storage bank following load fault recovery. This approach is used in circuits 2a, "series recharge", and 2b, "shunt recharge". The second basic approach does not dissipate the power supply stored energy following a load fault. Instead, it conserves the stored energy during the crowbar cycle and then returns the stored energy in such a manner as to restore normal operating conditions following load fault recovery. This approach is used in circuits 2c, "continuous (or prompt) energy cycling", and 2d "delayed energy cycling."

Critical Circuit Components

Examination of the four rapid-cycle crowbar circuits, shown in Figure 2, shows that they all use essentially the same components; resistors, capacitors, crowbar switches, solid-state diodes, and chokes. Of these components, the most critical are the crowbar switches and the solid state diodes.

Crowbar Switches

It was decided to perform breadboard tests at voltage levels up to 40 kilovolts dc. For such tests two types of crowbar switches were available, the General Electric triggered vacuum gaps (TVG) and the EGG triggered gas gaps.

An important requirement for a short-term device is short recovery time at zero or near-zero arc currents. Not much data is available on recovery time of either type of triggered gap. What information could be found indicated that the recovery time of a 24 kV EGG pressurized gas gap was around 100 μseconds[5]. Recovery time for the General Electric vacuum gaps was indicated as around 10 kV per μsecond[6,7]. As recovery time was expected to be one of the circuit problems, the vacuum gap was selected for use in the breadboard circuits. Further considerations in favor of the vacuum gaps over gas gaps were the general conceptions that the minimum holding (or arc sustaining) current was much higher for the vacuum gaps (ampere region), and that the vacuum gaps could be triggered with very low anode voltages (compared to maximum rated hold-off voltage).

Preliminary recovery time data was obtained on six G.E. vacuum gaps using the circuit shown in Figure 3. In this circuit, C1 discharges through R1 when the

TVG is fired. R2 establishes the minimum holding current, and C2 supports the supply voltage during the recovery period. R3 protects the power supply if the TVG doesn't recover.

The data listed in Table 1 show times in the range of 2 to 50 μseconds with one exception.

TABLE 1

TVG RECOVERY TIME DATA

Manufacturer:	General Electric
Anode Voltage:	3 kV
Holding Current:	~0.4 A at 3 kV
Peak Discharge Current:	~250 A

TYPE	TVG S/N	RECOVERY TIME
ZR7512	267	2 to 6 μsec
ZR7512	255	< 2 μsec
ZR7512	264	10 μsec
ZR7535	104	10 to 40 μsec
ZR7512	284A	20 to 500 μsec
ZR7519	103	10 to 30 μsec

It is realized that these results are by no means conclusive, but they did provide a starting point for initial breadboard tests. Accordingly, 50 μseconds recovery time was allowed for the first approach to be tested.

A TVG assembly is shown in Figure 4. The assembly includes the TVG and its trigger-electrode pulse transformer. The trigger electrode requires a pulse source having a minimum open-circuit pulse voltage of 5kV, and a minimum short-circuit pulse current of 40 amperes.

Fast Recovery Diodes.

The circuits shown in Figures 2c and 2d require high voltage diodes that can pass high peak currents (thousands of amperes) and withstand "instantaneous" application of reverse voltages immediately following their conduction periods. Also, it was decided to employ diode banks in series with each ZR7512 to ensure recovery under high di/dt rates (diodes not shown in Figure 2). Discussions with G.E. regarding expected gap current di/dt rates during the desired recovery periods indicated a strong possibility that the ZR7512 would not recover under certain of the expected test conditions (discussed further later). A survey of available fast-recovery diodes showed the G.E. A-97 to have suitable characteristics and that it was on the shelf[2]. The A-97 has an operating PIV of 1000 volts and a one-cycle peak current rating (half sine wave, 60 Hz of 3300 amperes). Recovery time following conduction of such peak currents was estimated at 1 to 2 microseconds. Forty-eight diodes were used in series to form a 40 kV PIV (operating) diode bank. Each such bank was made up of four assemblies of twelve diodes. Figure 5 shows a photograph of one of the twelve-diode assemblies. Each diode was shunted by an R-C suppression circuit (5 ohms in series with 0.2 μf), and a 100 kilohm resistor to maintain dc voltage balance.

Breadboard Tests

The required delivery time of the long-lead items created certain problems due to a relatively short program schedule (5 months). The most serious problem was the delivery of the power-supply isolating choke (L2 in Figure 2). The isolating choke is necessary to isolate the power supply from the energy-storage capacitor bank so that the power supply may remain active during a crowbar action. The choke is necessary to demonstrate that short-term crowbar circuits are compatible with conventional power supplies, i.e., the power supply remains on during the crowbar action. It was decided that a resistor could be used temporarily in place of the isolating choke, and the effects of the choke could be quickly evaluated as a last part of the program tests. The resistor value, R3 in Figure 6 (typical), was initially selected to allow a current through it approximately equal to the current that would exist through the isolating choke at the end of a 500 μsecond period. The use of a resistor is a worst-case condition except for the stored-energy effects of a choke. With a choke, the current builds up at an E/L rate. With a resistor, the final value of current exists throughout the entire crowbar cycle.

Series Recharge Circuit

The first circuit tested was the series recharge circuit, Figure 6. C1 represents the storage bank normally supplying pulse or dc currents to the load (microwave tube). C2 is the power supply recharge capacitor bank. R1 is the crowbar current-limiting resistor, R2 is the series recharge resistor, and R3 is the resistor simulating the isolating choke. The sequence of operation is as follows:

a) Load ("microwave tube") arcs, initiating a signal which triggers TVG1.

b) TVG1 shunts the faulted load with a low impedance, causing the energy in C1 to be dissipated in R1.

c) After discharging C1, in approximately 50 μseconds, TVG1 recovers. R3 isolates TVG1 from the voltage across C2.

d) After a preset delay time, TVG2 is fired, recharging C1 through R2 in approximately 100 μseconds.

The total time for a crowbar cycle (load fault to restoration of load operation) is the delay time between the firing of TVG1 and TVG2 plus the 100 μseconds time to recharge C1.

Evaluation of Circuit Performance. The circuit was sequenced at dc voltages up to 40 kV successfully, and with crowbar cycle times of approximately 200 to 500 μseconds. Photographs showing typical waveforms are in Figure 7. Figures 7a and 7b show the load voltage during a crowbar action with a power supply voltage of 40 kVdc, and with crowbar cycle times of 100 and 500 μseconds, respectively. The droop seen in Figure 7 is mostly due to the response of the capacitor voltage divider. (A suitable 40 kV compensated RC divider was not available during these tests.) The voltage to which C1 is recharged differs from its initial value essentially by the amount that the voltage across C2 drops as a result of charg-C1.

Proper performance of this circuit depends upon the recovery of TVG1 within a maximum period of 350 μseconds for a crowbar cycle time of 500 μseconds. The TVG used during these tests appeared to do this with some margin.

Recovery time of TVG2 is not a problem, as termination of its conduction period is followed by a steady-state condition of essentially zero voltage across its anode to cathode.

There were indications that TVG2 was being spuriously triggered upon firing TVG1. Sheilding of the trigger electrode and its triggering circuit appeared to be required. Subsequent testing of the shunt recharge circuit indicated that some of the failures of the circuit to cycle properly (such failure would cause power-supply shutdown) might have been due to non-recovery of TVG1. Further investigation of the recovery characteristics of the TVG is indicated to establish reliability of this circuit.

One limitation of this circuit is that the arced load must recover during the crowbar cycle and not suffer a second arc during the recharge of C1 (TVG2 conducting and voltage rising across the load); otherwise TVG2 will not be allowed to recover and the power supply will be shut down.

Shunt Recharge Circuit.

The shunt recharge circuit dissipates the stored energy during a crowbar cycle, as did the series recharge circuit, and then recharges the energy stored capacitor through a resonating choke. Referring to Figure 8, L1, TVG2, CR2, and C3 form the shunt recharge circuit. A separate power supply, E_{dc2}, feeds the recharge capacitor, C3. L1 is the resonant recharging choke, R1 is the crowbar current-limiting resistor, and R3 is the resistor simulating the isolating choke.

The sequence of operation is essentially the same as described for the series recharge circuit. The total time for a crowbar cycle (load fault to restoration of load operation) is the delay time between the firing of TVG1 and TVG2 plus the 50 μseconds time to recharge C1.

Evaluation of Circuit Performance. The shunt recharge circuit provided proper crowbar action at storage bank voltages up to 20 kVdc. Crowbar cycle times were approximately 500 μseconds. Above 20 kVdc, it was necessary to increase the value of the isolating resistor, R3, to maintain proper crowbar action. A value of approximately 200K was required for proper operation at 40 kVdc. The indications were that TVG1 was not recovering and/or was being spuriously triggered. It is not understood why these problems were not as severe during the series recharge circuit tests.

The shunt recharge circuit requires an additional capacitor bank, C3, and power supply, E_{dc2}, but it provides the capability of compensating for recharge circuit losses by appropriate adjustment of E_{dc2} and/or the value of C3. With circuit loss compensation, the load sees the same operating voltage immediately after a crowbar action as it saw at the time of the fault. This is shown in Figure 9a.

Recovery time of TVG2 is not a problem, as the charging diode, CR2, forces recovery by its reverse current blocking action.

A thorough investigation of the TVG recovery characteristics, for use in the TVG1 position, is required before the shunt (or series) recharge circuit should be considered as a reliable short-term crowbar circuit.

Alternate Shunt Recharge Circuit. Another possible circuit configuration would be to eliminate the recharge power supply, E_{dc2}, make C3 equal in value to C1, and connect C3 to the main power supply through an isolating choke. This configuration was simulated by making C3 = C1 and setting $E_{dc2} = E_{dc1}$ (an isolating resistor was used between C3 and E_{dc2}). Figure 9b shows the storage bank and recharge bank voltage waveforms during a crowbar cycle. At time t_1, the crowbar cycle is initiated and the storage bank is discharged. At time t_2, TVG2 is fired and charges the storage bank to essentially its original value, and the recharge bank is completely discharged. In this configuration compensation for circuit losses can be achieved by increasing the size of C3 such that it is a little larger than C1.

Continuous Energy Cycling Circuit.

The continuous energy cycling circuit differs from the series recharge circuit discussed above in that the stored energy is conserved rather than dissipated during a crowbar action. This eliminates the requirement for a secondary energy-storage bank (C2 of Figure 6, C3 of Figure 8) for recharging, and largely eliminates any surge power drain from the prime power lines during or following a crowbar cycle.

Referring to Figure 10, C1 represents the storage bank normally supplying pulse or dc currents to the load (microwave tube). C2 simulates a high-power dc supply, i.e., one which is capable of supplying high average currents. L1 is a choke which, with C1, determines the period of the crowbar cycle and the peak value of the current during the crowbar cycle. R3 is the isolating resistor (substitutes for the isolating choke.)

The sequence of operation is as follows:

a) Load (microwave tube) arcs, initiating a signal which triggers TVG1.

b) TVG1 and CR1 shunt the faulted load with a low impedance, causing the full voltage of C1 (essentially) to appear across L1.

c) L1 resonates with C1 such that the voltage across C1 swings from its initial negative value to an equal positive value (assuming zero losses). The circulating current passes through TVG1 and CR1.

d) The voltage across C1 continues its oscillatory cycle and swings back to its original polarity and value (assuming zero circuit losses). The reverse circulating current passes through CR2.

e) During the second half of the cycle, d) above, TVG1 recovers. CR1 ensures recovery of TVG1 by preventing any possible flow of reverse current through TVG1.

f) CR2 recovers as soon as the circuit has completed one full oscillatory cycle. At this instant the load voltage is reapplied at the pre-fault value (assuming zero losses).

It should be noted that during the entire crowbar cycle the load voltage is essentially zero. In other words, the crowbar circuit has completely reset itself before any voltage of any magnitude is reapplied to the load. This means that should the load suffer another arc when voltage is reapplied, the crowbar circuit is ready to perform another crowbar cycle.

Evaluation of Circuit Performance. The circuit was tested successfully at various voltage levels up to 40 kVdc. Waveforms of the load voltage, the voltage across C1 (storage bank), and the current through TVG1 are shown in Figure 11.

Maximum circulating currents were around 3000 amperes. At the end of one cycle the restored load voltage was aporoximately 90% of the original value. The cycle period was approximately 100 μseconds, which represents the recovery time allowed for a faulted load. The half-cycle period of 50 μseconds is the recovery time allowed TVG1.

Proper performance of this circuit depends upon recovery of TVG1 within a maximum period of 50 μseconds. The use of a reverse-current blocking diode (CR1) ensures recovery of TVG1. However, satisfactory operation was also achieved with CR1 shorted, which indicates the possibility of eliminating CR1.

With CR1 eliminated, this circuit differs from the standard crowbar circuit only by the addition of a diode bank, CR2, the resonating inductance, L1, and the isolating choke (R3 substitution). In some power supplies the isolating choke may already be there in the form of a filter choke. Of course, the specifications for the energy-storage bank capacitors, C1, would have to include the special requirement of withstanding full voltage reversal.

Instabilities noted during the tests all appeared to be caused by spurious triggering of the TVG's, indicating the necessity of shielding the trigger electrode and its trigger circuit.

A limitation of this circuit is the inability to vary the period of time allowed for load recovery without changing L1 or C1. For a pulse system the maximum value of L1 would be limited by the required rate of rise of normal load pulse currents. The minimum value of C1 would be limited by the allowable voltage droop during the pulse. A further restriction on L1 and C1 is the ratio $\sqrt{L1/C1}$, which determines the peak circulating current that the diodes and TVG have to handle.

Delayed Energy Cycling Circuit.

The delayed energy cycling circuit, Figure 12, was conceived to increase the recovery time allowed a a faulted load without increasing L1 or decreasing C1, and to provide adjustable control of the allowable recovery time. This is accomplished by including a second TVG in series with CR2 and programming its firing time relative to the firing of TVG1. CR2 is left in the circuit to ensure recovery of TVG2.

The sequency of operation is the same as for the continuous cycling circuit except:

a) After firing TVG1, the foltage across C1 reverses and TVG1 recovers. CR3 is used to isolate the faulted load from the reverse voltage.

b) The reverse voltage remains across C1 until TVG2 is fired, at which time the voltage across C1 again reverses (to its original polarity) and TVG2 recovers.

c) As TVG2 recovers, the load voltage is reapplied to the pre-fault value (assuming zero losses).

Evaluation of Circuit Performance. The circuit was tested successfully at various voltage levels up to 40 kVdc. Photographs showing typical waveforms are in Figure 13. Figure 13a shows the load voltage (e_1) dropping close to zero (TVG1 conducting) during the interval of time that the voltage across C1 is reversing, (leading edge of Figure 13b, note that the time base is shifted to the right in Figure 13b). The load voltage (e_1) then swings to the reverse value (approximately 40 kV), and remains there until TVG2 is fired (the droop is mainly due to the capacitor voltage divider). At the time TVG2 is fired, the voltage drops to near zero and remains there until the voltage across C1 again reverses.

At the end of the crowbar cycle, the restored load voltage was approximately 90% of the original value. The allowable load recovery time was demonstrated up to 500 μseconds. Operation in the region of the minimum available recovery time (approximately 100 μseconds) was demonstrated later. (Discussed later).

The necessity of CR1 is evident in Figure 13c. The voltage across CR1 is seen to rise to approximately 35 kV at the end of the first half of the crowbar cycle. This happens when TVG1 doesn't recover within a few microseconds. CR1 and CR2 had been added in anticipation of TVG recovery problems. It was noticed that the voltage impulse across CR1 did not always appear. Further investigation of TVG recovery time would be necessary to see if the diode could be eliminated. This might involve some TVG development effort, to insure consistently short recovery times.

This circuit offers the advantage of increasing the allowable load recovery time beyond the resonant period of L1 and C1 without changing the values of L1 and C1.

Restored load voltage at the end of a crowbar cycle was approximately 90% of the original value. An estimate of the circuit energy losses attributed 5% of the losses to the TVG, 23% to the diode banks, and 72% to the combination of the resonating choke (L1) and circuit leads. Reasonable caution was exercised, but no attempt was made to optimize L1 or the circuit leads from the loss standpoint. Restored load voltage of around 95% of original value could be expected in a real application by minimizing losses in L1 and circuit leads.

Isolating Choke Tests. The tests described above were performed with a resistor, R3, substituting for the isolating choke because of the unavailability of the choke. After receipt of the choke, time was available for tests in two of the four circuits, the shunt recharge circuit, Figure 8, and the delayed cycling circuit, Figure 12.

The inductance value selected for the choke (L2) was 6 henries. This would allow the current to build up to 2.67 amperes at the end of 400 microseconds with a driving voltage of 40 kV. The maximum voltage that the choke would see across its terminals

would be 80 kV. This occurs in the delayed cycling circuit following the reversal of voltage across C1 during the crowbar cycle.

A series combination of a diode and resistor were connected across the choke to dampen oscillations caused by the energy stored in the choke's magnetic field at the end of the crowbar cycle.

Shunt Recharge Circuit. The shunt recharge circuit sequenced satisfactorily at dc voltages up to 30 kV, with crowbar cycle times of 500 μseconds. Above 30 kVdc performance was unreliable due to pretirggering or non-recovery of TVG1 (as previously reported).

Other than the recovery problems, the circuit functioned satisfactorily. The load voltage waveform during a crowbar cycle looked exactly the same as in Figure 9a (R3 in place of L2).

The circuit was sequenced at 40 kVdc with eight satisfactory crowbar cycles out of twelve tries with a 500 μsecond cycle time (the failures were false TVG triggering or failure of a TVG to recover). There were four successful tries out of seven tries with a 250 μsecond cycle time. This performance was better than that obtained with the isolating resistor, indicating that the tests with the isolating resistor were conservative tests.

Delayed Energy Cycling Circuit. The delayed cycling circuit sequenced satisfactorily at dc voltages up to 40 kV and with crowbar cycle times of from 500 μseconds to 110 μseconds. No crowbar cycle failures were experienced.

The crowbar circuit performance was the same with the isolating choke as it was with the isolating resistor. The load voltage and storage bank voltages with crowbar cycle times of 500 μseconds and 110 μseconds are shown in Figure 14b, c, d, and e.

The voltages across CR1 and CR2 are shown in Figure 14a. The photograph shows that CR1 recovered before TVG1, but that TVG2 recovered before CR2 (as previously observed during tests with the isolating resistor, R3). This was not a consistent condition. Again, this verifies the present necessity of diodes and the possibility that some work on TVG recovery characteristics might permit the elimination of the diodes.

General Conclusions

1) All four short-term crowbar approaches studied appear to be feasible circuits for restarting a high-power rf amplifier stage within 500 μseconds of a crowbar action.

2) The circuit that provides the best operational flexibility and stability is the delayed energy cycling circuit.

3) The only critical components used in the circuits studied were the triggered vacuum gaps (TVG) and the blocking diodes. The triggered vacuum gaps are the same devices as are presently used in conventional crowbar circuits and are reliable. For the short-term crowbar application, however, the recovery time characteristics of the TVG's becomes important. This is an area requiring further study.

4) A comparison of some of the characteristics of the four approaches studied is made in Table 2. Selection of the optimum approach will ultimately depend upon the specific requirements of the application being considered.

CIRCUIT	SERIES RECHARGE	SHUNT RECHARGE	CONTINUOUS CYCLING	DELAYED CYCLING	STANDARD CROWBAR CIRCUIT
Observed Loss in Stored Energy	100%	100%	20%	20%	100%
Observed Restored Voltage Level (% of Original)	~50% Depends on size of recharge capacitor bank.) (1)	100% Adjustable	~90%	~90%	0%
Inductance Used in Pulse Path	None	None	200 uH	200 uH	None
Peak Crowbar Currents	4000 A (1)	4000 A (1)	3500 A (2)	3500 A (2)	TYP 2000 A
Number of Crowbar devices	2	2	1	2	1
Number of Diode Banks	None	1 (4)	2 (4)	2 (4)	0
Possible TVG Recovery Problems	Yes	Yes	No	No	No
Crowbar Recycle Time	100 to 500 usec.	100 to 500 usec.	100 usec.	100 to 500 usec.	Seconds

(1) With 10 ohms series resistance.
(2) With 200 uH series inductance.
(3) Restored voltage will be ~1% with a main capacitor bank ten times the size of the capacitor bank being recharged.
(4) Fewer diode banks may be permissible if TVG recovery time is improved.

TABLE 2. COMPARISON OF SHORT-TERM CROWBAR CIRCUITS

Areas For Further Investigation.

a) Further evaluation of recovery time of existing triggered vacuum gaps.

b) Development effort to obtain a triggered crowbar device which will recover without the use of reverse diodes.

c) Evaluation of the recovery time of high power vacuum devices (RF tubes) following normal arcing during their useful operating life, to determine how rapidly voltage may be reapplied without causing them to arc again.

Credits

The recharge circuits shown in Figures 6 and 8 are versions of an approach originated by J. C. Davis, and include contributions by J. H. Main.

The cycling circuits shown in Figures 10 and 12 are based on an approach originated by K. M. Smalley.

References

1. A. Michaelson and H. N. Price, "Triggered Vacuum Gaps as Energy Diverters in Electronic Equipment," Proceedings, 10th Modulator Symposium, May 1968.

2. General Electric A96/A97 Diode Data Sheet 145.55, December, 1967.

3. L. B. Woolaver, "The Use of Triggered Spark Gaps as Crowbars," Proceedings of Seventh Symposium on Hydrogen Thyatrons and Modulators, May, 1962.

4. ECOM Research and Development Report, ECOM-2897, November, 1971, "Energy Control for Microwave Amplifier Arrays."

5. EGG Data Sheet TSG-100.

6. General Electric Bulletin ETD-4397, "Triggered Vacuum Gaps."

7. J.M. Lafferty, "Triggered Vacuum Gaps," Proceedings of the IEEE, 1 January 1966.

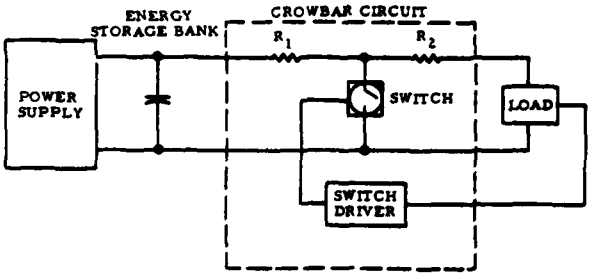

FIG. 1. SIMPLIFIED DIAGRAM OF A TYPICAL CROWBAR CIRCUIT

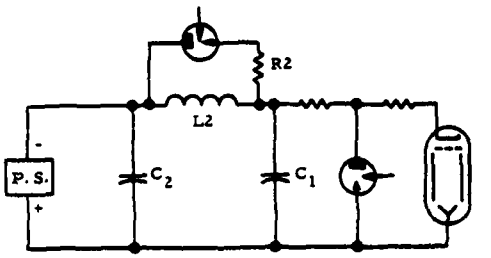

(a) SERIES RECHARGE

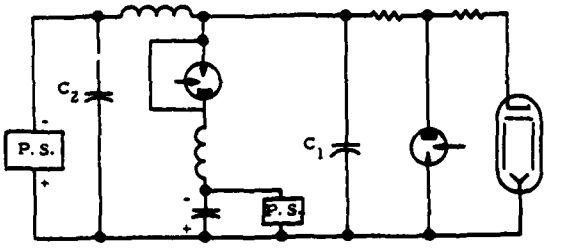

(b) SHUNT RECHARGE

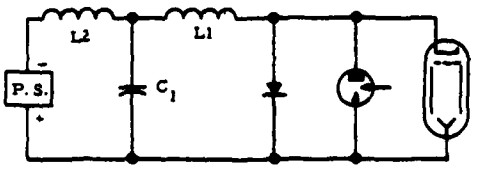

(c) CONTINUOUS (OR PROMPT) ENERGY CYCLING

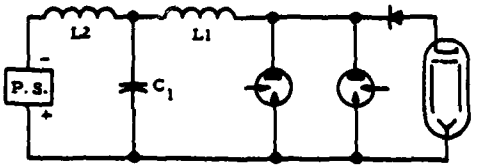

(d) DELAYED ENERGY CYCLING

FIG. 2. SHORT TERM CROWBAR APPROACHES

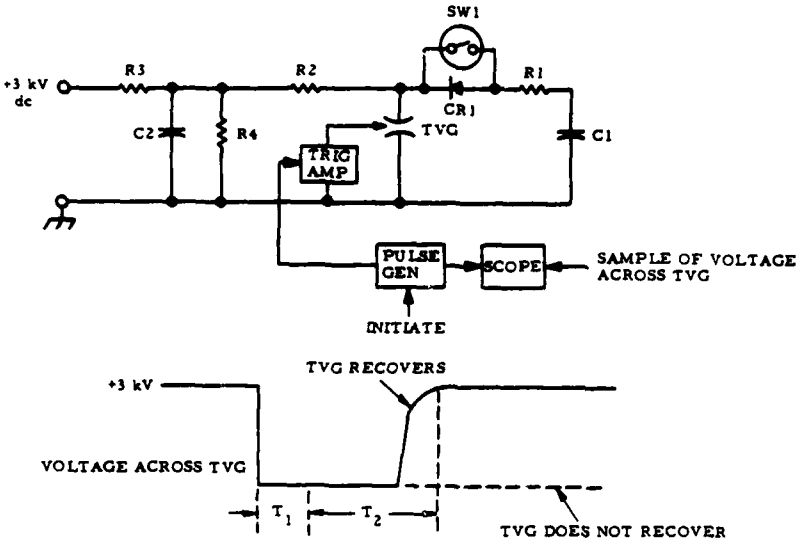

T_1	=	DISCHARGE TIME OF C1	R_3	=	100K
T_2	=	RECOVERY TIME OF TVG	R_4	=	5 MEG
R_1	=	12.5 OHMS	C_1	=	0.5 mfd
R_2	=	1K TO 8.5 K	C_2	=	1 mfd

FIG. 3. TRIGGERED VACUUM CAP RECOVERY TIME TEST CIRCUIT

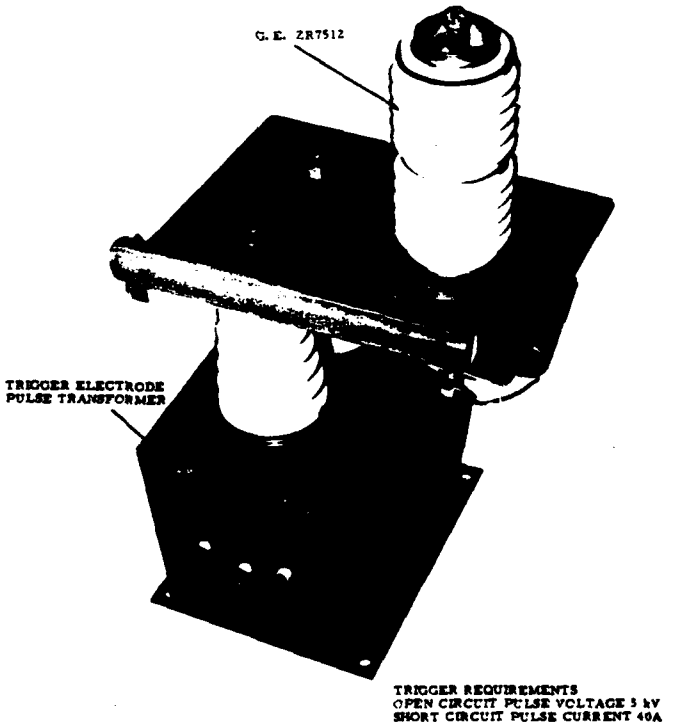

FIG. 4. TRIGGERED VACUUM GAP ASSEMLBY

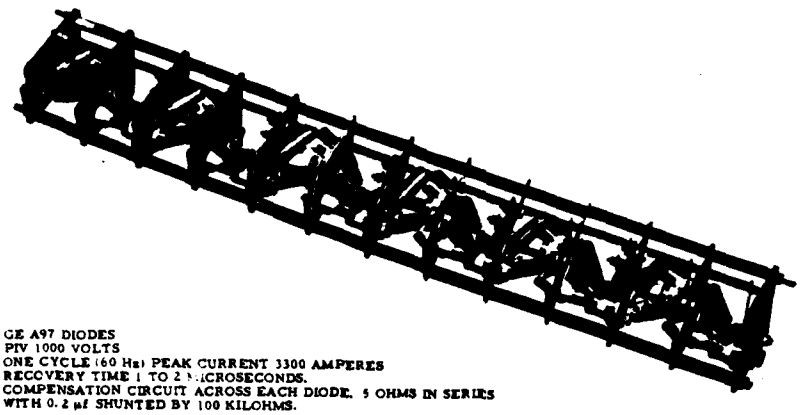

GE A97 DIODES
PIV 1000 VOLTS
ONE CYCLE (60 Hz) PEAK CURRENT 3300 AMPERES
RECOVERY TIME 1 TO 2 MICROSECONDS.
COMPENSATION CIRCUIT ACROSS EACH DIODE. 5 OHMS IN SERIES
WITH 0.2 μf SHUNTED BY 100 KILOHMS.

FIG. 5. 10 kV DIODE BANK ASSEMBLY

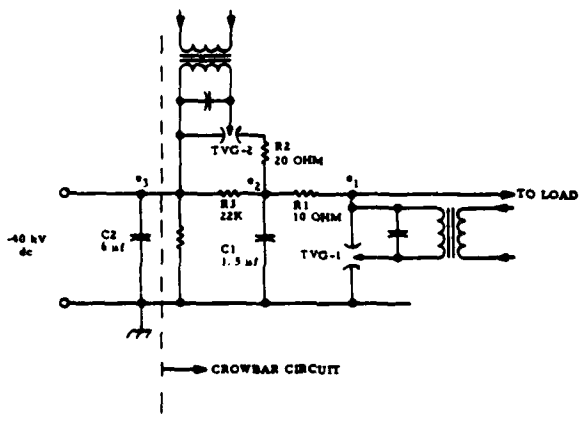

FIG. 6. SERIES RECHARGE CROWBAR CIRCUIT

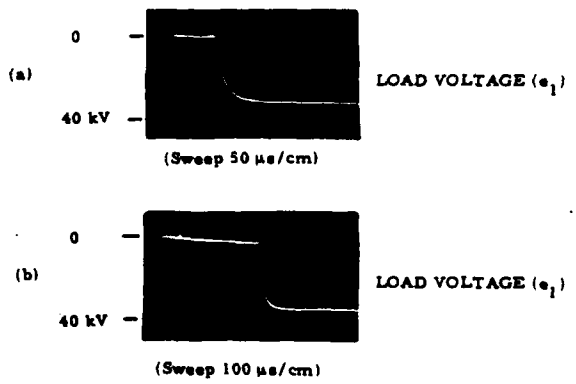

FIG. 7. SERIES RECHARGE CIRCUIT WAVEFORMS

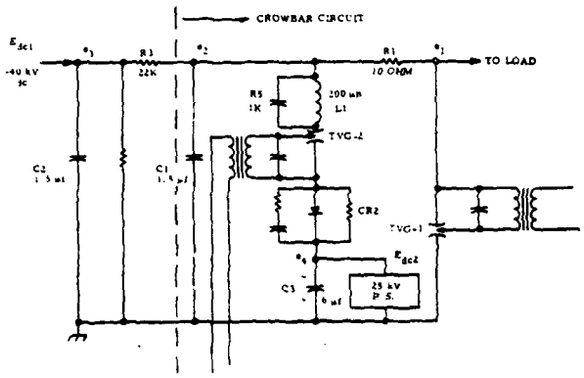

FIG. 8. SHUNT RECHARGE CROWBAR CIRCUIT

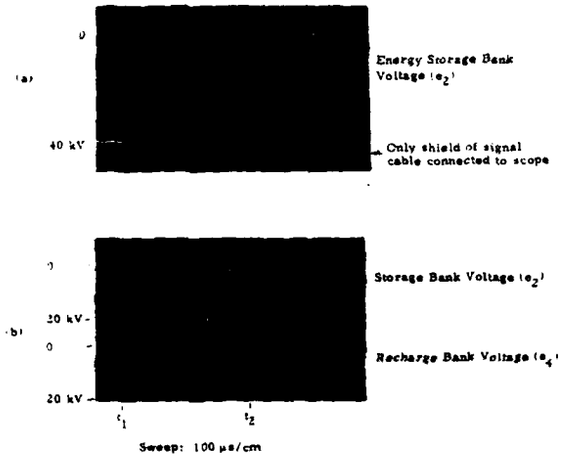

FIG. 9. SHUNT RECHARGE CIRCUIT WAVEFORMS

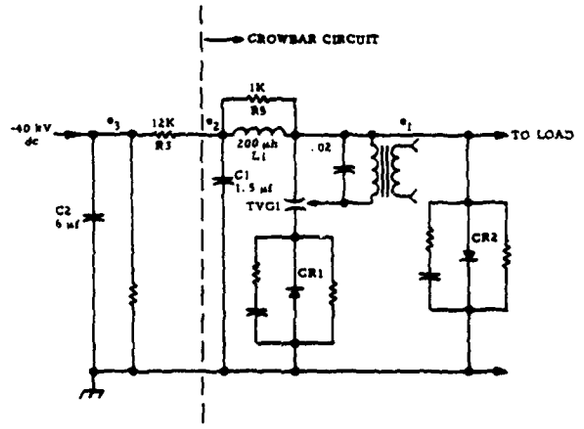

FIG. 10. CONTINUOUS ENERGY CYCLING CROWBAR CIRCUIT

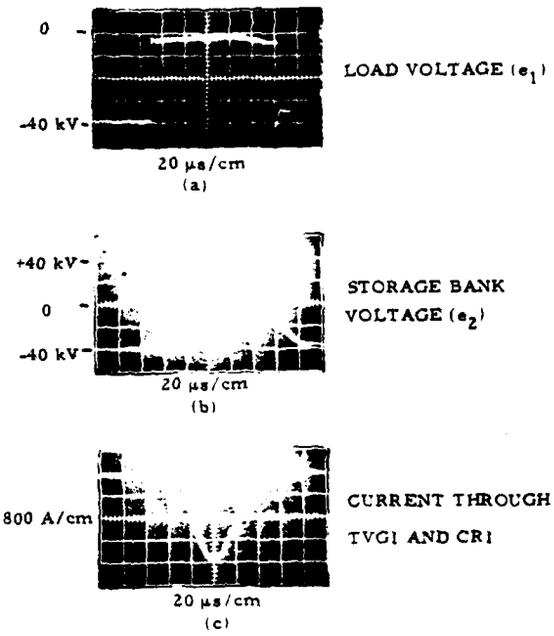

FIG. 11. CONTINUOUS ENERGY CYCLING CIRCUIT WAVEFORMS

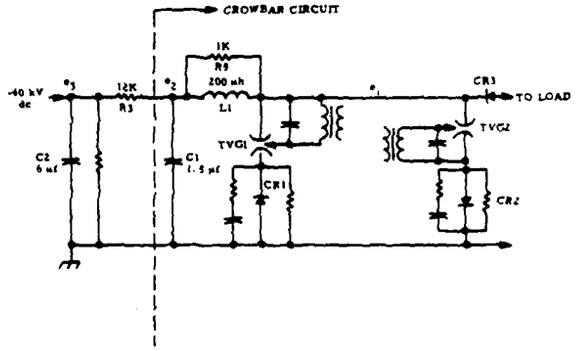

FIG. 12. DELAYED ENERGY CYCLING CROWBAR CIRCUIT

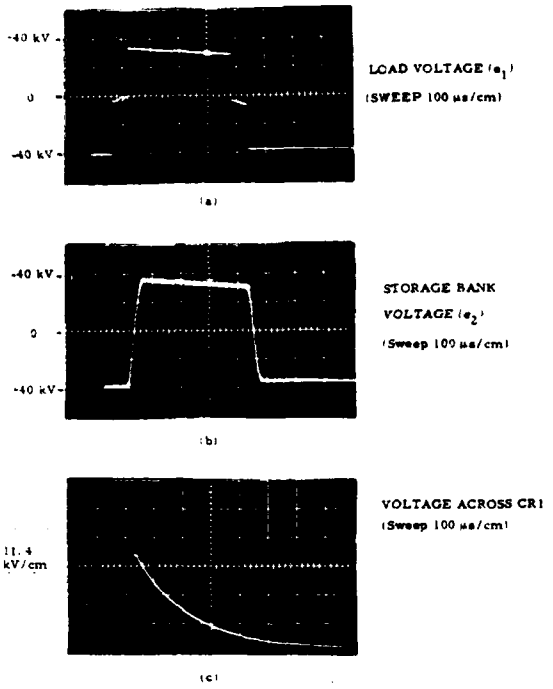

FIG. 13. DELAYED ENERGY CYCLING CIRCUIT WAVEFORMS

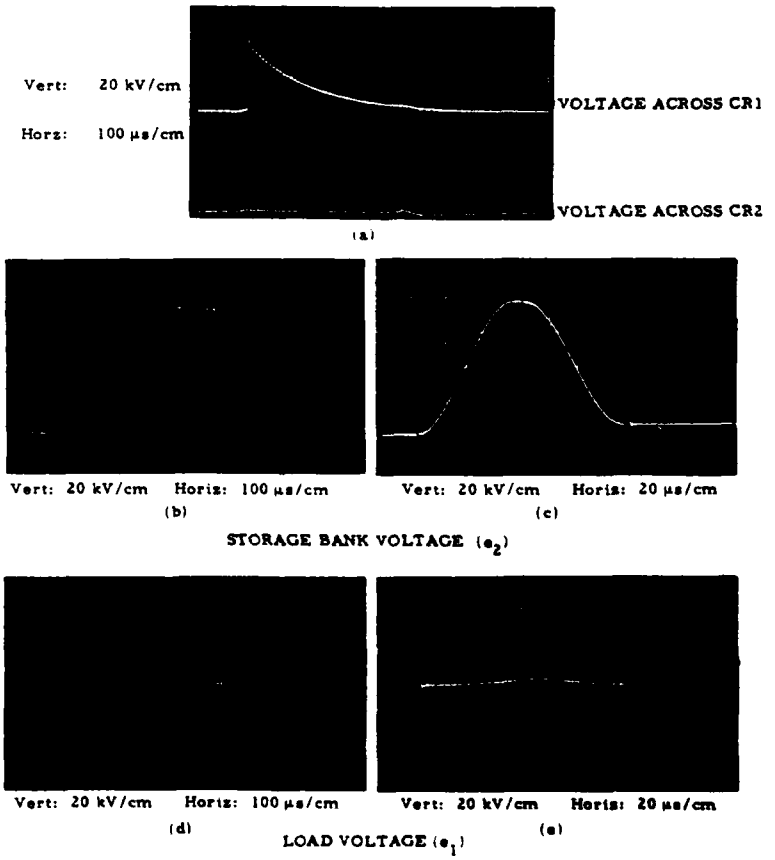

FIG. 14. DELAYED CYCLING CIRCUIT WAVEFORMS, WITH ISOLATING CHOKE

EVALUATION OF STATE-OF-THE-ART HYDROGEN THYRATRONS AT EXTENDED RATINGS

By Bobby R. Gray

Hqs Rome Air Development Center
Griffiss AFB, NY

Summary

Paper describes the background behind a comprehensive test on a group of selected off-the-shelf thyratrons. Specific objectives of the test were (1) determine the maximum operating anode voltage as a function of average current, (2) determine the maximum average current as a function of anode voltage, (3) determine short time on stability and (4) determine the above parameters with the tube operating in a vibration test stand. While the data is in the form of a preliminary report certain trends are evident. These are (1) the peak voltage which can be achieved is considerably above the rated value if average current is kept lower than rated value, (2) at rated voltage the average current is equal to or close to the rated value, and (3) average current can be raised above the rated value if anode voltage is lowered.

Introduction and Theory of Tests

The thyratron has been used extensively in pulser systems for accelerators and radar transmitters. In these systems continuous or long term operation is common. Designs tend to be very conservative. Some new pulser designs however are requiring that a very large number of thyratrons, all effectively in parallel, be operated simultaneously for short periods into a common load. In order to save system weight it is also desirable to extend the ratings of available tubes. Data available on data sheets often is limited so far as operation in the proposed designs is concerned. It is the intent of this program to evaluate five (5) different off-the-shelf tube types for the maximum voltage and currents that can be achieved. The common parameters by which thyratrons are rated include average current, anode voltage, peak current, and the anode heating or P_b factor. The maximum pulse width and pulse rate are often not specifically identified. In many cases the tubes have never been operated at pulse lengths greater than 5-6 microseconds.

Another factor about thyratrons worth considering is the stabilization time. In some of the newer high powered pulsers being built today, the total run time is 2-5 minutes maximum. Gradual run-up of voltage is often not provided for and in cases snap-on anode voltage at full value is required. In this test, we seek to determine stability for a short time period. The high average power system being planned or built today far exceeds the power capability of any single thyratron. This forces the designer to either attempt to stretch the published ratings of tubes in order to keep the system from getting extremely large or to play it safe and design around the published data. Either choice is subject to error since published data is taken under conditions which differ considerably from the proposed design. The objective of this test is to see how far the published ratings can be extended. We are not modifying the old tube or making new ones but merely filling in additional data points now missing from the data sheets. Consider the rated parameters presented graphically in Figure We want to see at what average current and maximum voltage the tube becomes unstable. At the high voltage limit, the inherent voltage limitations of the tube structure and spacings can be determined. In exercising the maximum current, the cathode emission and hydrogen pressure contact can be evaluated. It is doubtful if the anode heating factor will be of significance because the PRF is less than 1000.

This work sponsored by the Air Force Systems Command, Rome Air Development Center, Griffiss Air Force BAse, NY.

Organization

The tests have been organized to exercise the common thyratron parameters such as PFN voltage, average and peak currents, grid voltage variations, and reservoir voltage. Other observed indications, temperature, jitter, survival of conditioned state, and turn-on stability of tube performance and reliability, are also being evaluated.

Because of the interrelation of PFN and load impedance, pulse width and pulse rate on the average and peak currents, wide flexibility in a test circuit is necessary in order to evaluate the performance of a number of tubes. A fixed pulse width of 20 microseconds at pulse rates of 180 and 333 PPS are used for the test and serve as a baseline. With the fixed pulsed width, two pulse rates, a variable PFN and load impedance, and a variable voltage supply the tubes actual performance can be evaluated for average and peak current limits.

Test parameters selected for evaluation of the tubes is listed in the following table:

PARAMETER RANGES

Pulse Width	20 usec
PFN Z_o	1-64 ohms
PRF	180 - 333
Voltage (Rated)	35 - 80 KV
Current (Rated)	4 - 15 amps
Current (Peak Rated)	5 - 10K amps
Actual Maximums	?

Note the wide range of impedances listed. This impedance is the pulse forming Network Zo. The actual discharge circuit impedance is slightly less than twic the Zo with load impedance being lower than Zo.

Specific PFN impedances to be evaluated are 64, 45, 32, 22, 16, 11, 5, 8, 5.75, 4, 2 and 1 ohms. If each of these Zo values is examined at each PRF as many as 22 data points would be possible. It probably will not require this many points to determine the load rating curve.

Candidate Tubes

Tubes chosen for evaluation are listed below along with the ratings and shown in Figure 1.

Tubes	Voltage KV	Current Avg Amps
ITTKU275	50	8A
English Elec. CX1175	80	6A
M-O Value GHT-9	35	15A
EG-G HY-5	40	8A
Wagner Elec. CH1222	50	15

All of these except the HY-5 are provided with an auxiliary electrode for pretriggering the grid-cathode section of the tube. The GHT-9 and HY-5 are single gapped tubes while the other three tubes are double gapped.

Pulser Circuit

Conventional line modulator techniques have been used through the tests where possible in order to duplicate typical circuits. Using components from existing inventory or local design the circuit shown in Figures 2 & 3 was constructed. The most imaginative and challenging part of the circuit was to reconcile the demands for a constant pulse length at varying PFN impedances in a convenient manner. To change the impedance involves changes in both inductance and capacitance. Also the charging inductor size needs to change if approximate resonant charging conditions are maintained. Some leeway is possible on the latter requirement, however, either by using delayed resonant charging or by allowing a limited amount of anode voltage hold-off time.

Fortunately because of a ready supply of 0.25 microfarad pulse type capacitors, obtained from excess power supplies, a group of basic PFN's were designed. These basic PFNs have an impedance of either 16 or 11.3 ohms. Using the four inductors and capacitor groups in series combination allows the impedance to be raised above 16 ohms. Paralleling either unit PRN's or combinations of capacitors and inductors, allows the impedance range below 16 ohms to be reached. It has been found that the above procedure produces almost identical pulse shapes for any of the impedances. Since only 5 sections are used some loss of ripple control occurs however at 64 ohms. In general, the pulse ripple and droop can be held to a $\pm$ 5% with relatively little difficulty.

Grid Circuit

Because of the slightly different grid circuit requirements, adjustable unit type power supplies and an adjustable pulse trigger pulse generator are used. To simplify grid bias application, a pulse transformer is used to couple in the trigger pulse. Where a prefire electrode baffle, or grid No 1 discharge is required, a D.C. source is used rather than pulsed because of simplicity. In general the grid and prefire electrode voltages were set at the mid-point of the total range of each type tube unless some detrimental affect occurred.

Load

The load circuit also had to be versatile with quick change features and adequate power handling ability. An existing electrolytic or conductive liquid type load circuit was modified so that the very low impedance could be achieved without saturation of the electrolytic solutions or requiring extreme amounts of salt. Copper sulfate was used as an electrolyte because of the relative ease with which the solutions conductivity can be controlled. Fig re 3 shows the load in photograph. Figure 4 is a sketch of water flow path of the load. Adjustment of the load impedance is done by connecting the appropriate number of 6" diameter tubes and trimming with the 2" diameter tubes. In addition either fresh water or concentrated copper sulfate solution can be added to change the electrolyte conductivity. One common complaint of the electrolytic load is that it is unstable because of temperature changes. This is true if the primary cooling system is unable to absorb the heat from the load rapidly. No significant changes in the load impedance occurred in the test while running. Minor adjustments occurred if the outside ambient air varied considerably, however, load matching was always such that even at the lowest running temperature the load impedance was always less than the PFN impedance ensuring an inverse voltage on the thyratron. Thus if the temperature did change the inverse diode circuit would keep the amount of inverse voltage under control and prevent excessive voltage build-up on the PFN.

The following waveforms, Figure 5 and 6, are representative of the pulse obtained from the above circuit and the load.

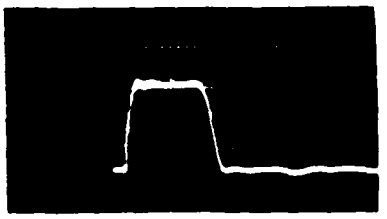

Figure 5. Anode Current Waveform

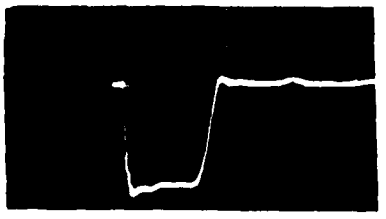

Figure 6. Load Voltage Waveform

Reservoir Voltage Adjustments

One of the most critical adjustments in a thyratron operation is the reservoir voltage. If the reservoir voltage or hydrogen pressure is too low, excessive tube dissipation results while too high a pressure will cause the tube to self-fire.

The ranging of the tube reservoir setting was done mostly in the usual manner. Usually the optimum reservoir voltage was equal to or less than the value stamped on each tube. As the average current increases at the lower load impedance, the reservoir voltages will have to be re-adjusted, however.

In addition to the usual ranging methods, some studies were made using the radio frequencies emitted from the tube during the grid-anode takeover time interval. Mr. R. Bradford[1] of SLAC has referred to this technique. We have found essentially the same resonant frequencies in ITT KU275 and the CH 1191 that he refers to. It has also been observed that under heavy loading conditions on the tube, there is an abrupt shift in the resonant frequencies just prior to a failure. Using a spectrum analyzer, as a receiver, we have observed that the spectral lines respond to changes in the reservoir voltage. It appears that certain discrete spectral lines show changes as the voltage varies. This phenomena may be a blessing in disguise. Further tests are required to establish the uniqueness of these rather sharp spectral lines with the most optimum reservoir voltage, but enough evidence points to this possibility. It may be possible to provide a curve with each tube as part of the test data sheet indicating the RF signal one should adjust the reservoir voltage for.

Delayed or Command Resonant Charge

Ideally one would want to have complete control of every process during any interval of time in a pulser system. For instance, by placing physical restraints, through careful selection of parts, on the rate of rise of PFN voltage we allow the thyratron to recover before the rising voltage causes conduction again. Also by operating at a slightly lower load impedance the tube is aided in its turn-off. With a charging diode the inductor can be made, within certain limits, smaller than necessary for exact resonant conditions. Unfortunately each of the techniques have certain penalties. Circuit component sizes become critical. The thyratron may either have to hold off voltage for a excessively long time, under certain conditions if the PRF is rated over a wide range. Inverse voltage for deionization control can cause anode heating and arc-back under extreme conditions particularly at high PRFs.

One way to improve on the above techniques is to supplement them with a delayed charging scheme. With electronic control of the start of the re-charge on the PFN, the load can either be equal to or greater than the PFN impedance if desired. An end of line clipper is still required, however, for load fault conditions. The interval of time in the charging process when no charging current flows and the PFN is not charging, normally occurring after the PFN is fully charged but before the thyratron is triggered, can be placed instead at the beginning of the charging cycle. With no positive rising anode voltage at the start, the tube is thus free to deionize. Without a standby voltage hold-off time at the end of the charge cycle, spurious breakdown is avoided.

The series of tests will investigate the effects, benefits and penalties of using both conventional charging schemes and the delayed charge technique. At present the conventional charging scheme is used.

Inverse Voltage Effects

One of the most critical periods in the pulsing operation of a thyratron is immediately after the pulse when the thyratron is attempting to deionize. This is when the ions are recombining and tube pressure is stabilizing before the next pulse. An inverse or negative voltage applied to the anode immediately after the pulse ceases can aid deionization. Too high an inverse voltage however causes excessive anode dissipation and arc-back. Insufficient inverse voltage however may prevent the tube from deionizing before the PFN charging voltage rises and causes continuous conduction through the thyratron.

We have observed failure due to excess inverse anode voltage in some of these tests while adjustments in the load were being made. The particular mode begins as a sudden chopping of the inverse voltage back to the base line or zero volts. This is most noticeable when no end of line clipper is used. Using an inverse diode circuit with an RC voltage integrating network tends to average out the inverse voltage and reduce the magnitude of the spikes.

Results

Data presented in this section is in the form of a preliminary report and covers the HY-5, CH1222, CX1175 and the GHT-9. To date the impedance range down to 16 ohms has been covered at the two selected pulse rates of 333 and 180 PPS. A data point is established when consecutive test runs agree. Also the tube must pulse for 5-10 minutes without failure in order to establish the point.

In general, all four of the tube types tested to date show some possible extension of the ratings. The curve sheets, Figure 7 through 10 shows the data points for the three impedance values of the two PRFs.

Note the rather close spacing of the data points particularly for the GHT-9, HY-5, and the CH1222. As the PFN impedance is changed the average current follows in the same ratio for the same pulse rate. Changing the pulse rate along with the widths keep approximately the same average currents. The voltage tends to reach a maximum limit at some point 20 or more KV above the rated value. It appears that the tube failures at the highest voltage mode is caused by field emission initiated breakdown. The GHT-9 in particular fails through anode ceramic flashover externally. Because of the almost vertical slope of the curve at the maximum voltage points, we can say that the tubes inherent voltage limitation, determined by the electrode spacing and geometry, has been reached.

The average and peak current limitations have not been reached as yet. The trend for all the tubes however, is to lower the anode voltage as the average current increases. It may be possible or even necessary to increase the filament voltage as higher than rated average current is attempted.

Reservoir voltage will also be re-adjusted upward. Some additional cooling may be also required.

CONCLUSIONS

To date we have shown that these tubes tested can operate at higher than rated voltage when the average current is less than rated value. Also it appears that at voltages less than rated value, the average currents can be raised above the data sheet value. At the rated voltage and current values the data sheet information appears to be accurate when the tube is operated under typical operating conditions. This report therefore shows that additional operating ranges are possible for off-the-shelf tubes.

References

1. Robert W. Bradford - SLDC, "Hydrogen Thyratron Performance in the SLAC Two-Mile Accelerator", Proc. Ninth Modulator Symposium, May 1966.

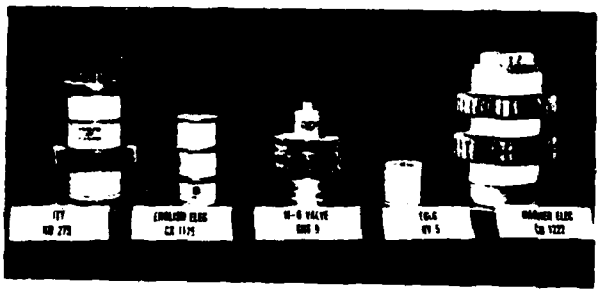

Figure 1. Candidate Tubes to be evaluated.

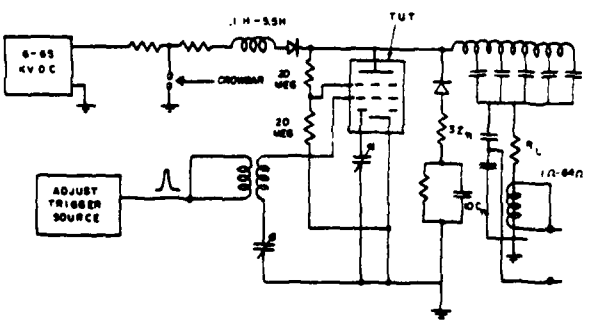

Figure 2. Simplified schematic of test circuit.

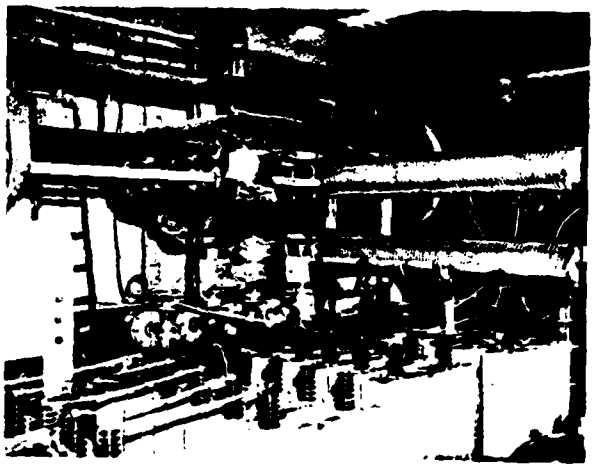

Figure 3. Photo of PFN and load circuit.

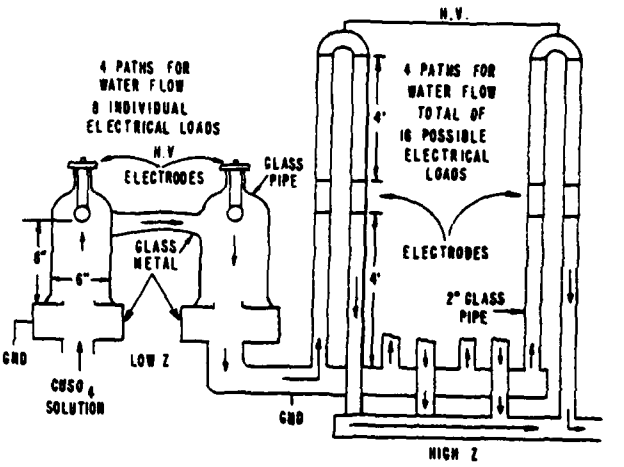

Figure 4. Liquid Load Circuits

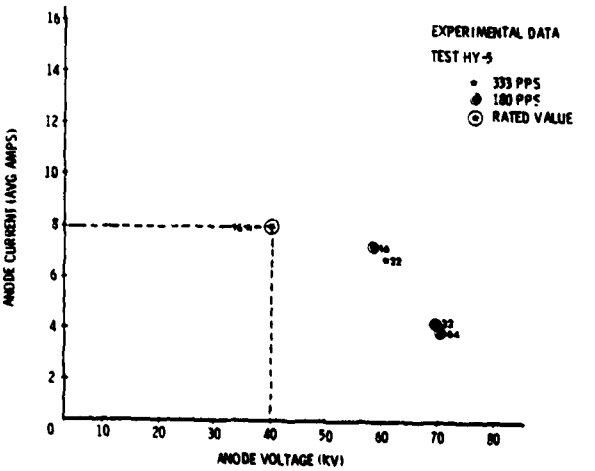

Figure 7. Experimental Data - HY-5

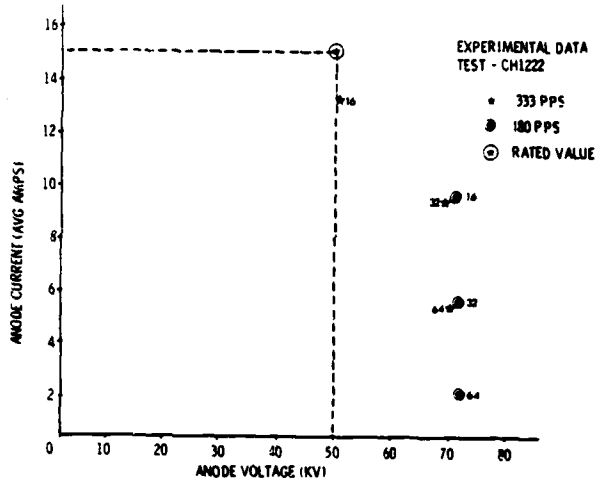

Figure 8. Experimental Data - CH1222

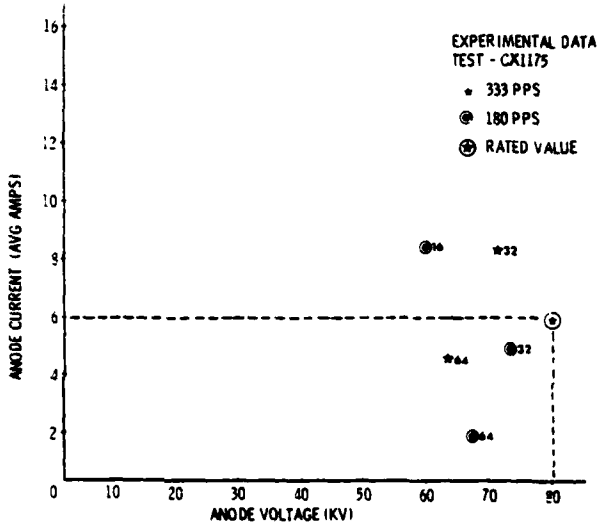

Figure 9. Experimental Data - CX1175

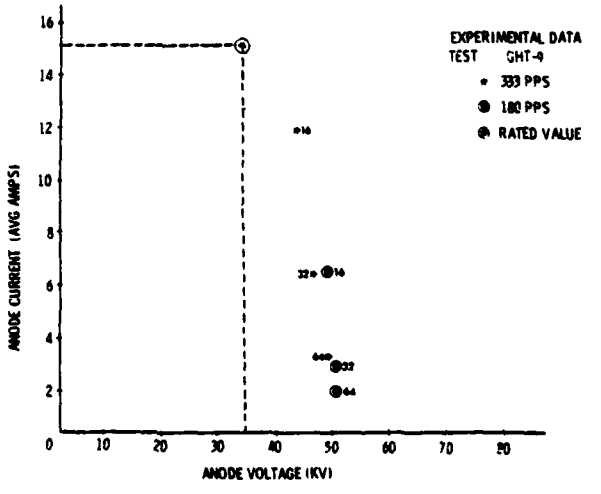

Figure 10. Experimental Data GHT-9

A MULTIGAP, DOUBLE-ENDED, HYDROGEN THYRATRON

H. Menown B. P. Newton
English Electric Valve Co. Ltd.
Chelmsford, Essex, U.K.

Summary

This paper discusses the limitations of conventional ceramic thyratrons with regard to inverse voltage and describes a double-ended, multigap thyratron capable of conduction in both directions. This new device behaves as a triggered, bidirectional switch and so improves commutation and simplifies circuit design. Methods of triggering, excitation and protection are described.

The ceramic hydrogen thyratron is now well established as a versatile, high-speed, high-current switch. Before triggering it can hold off up to about 40 kV per gap and when more than one gap is built into a single envelope the ability to hold off forward voltage increases in proportion to the number of gaps employed. A typical application for a hydrogen thyratron is to switch repeatedly pulse currents of several microseconds duration such as those required for powering magnetrons, klystrons or beam bending magnets in particle accelerators. The energy for producing such pulses is usually built up and stored over a period of several milliseconds, during which time a steadily increasing and then constant forward voltage is applied to the tube. If necessary the commencement of this energy storage can be slightly delayed by various triggered charging techniques so that no problems occur as a result of the recovery time of the thyratron.

The inverse voltage rating of a thyratron is generally the same as that for forward voltage, provided that the tube has not just ceased conduction. However, the problem frequently encountered with the design of modulator pulse circuitry is the limitation of the inverse voltage applied to the thyratron immediately following the cessation of the pulse current. At this time the active regions of the tube are full of a conducting plasma and if a negative voltage is applied to the anode the resulting ion bombardment may be heavy enough to produce secondary electrons and to start a destructive metallic arc with the anode acting as a cathode. The probability of a reverse arc being initiated depends upon the rate of arrival of positive ions at the anode and their energy at the moment of impact. Factors which encourage a large plasma density at the moment the current ceases are:-

i) A large peak pulse current amplitude and duration.

ii) A fast rate of fall of pulse current (so that the time for ion diffusion out of the plasma is a minimum).

iii) A high gas pressure.

Factors which encourage high power bombardment of the anode with positive ions are:-

i) A large inverse voltage.

ii) Too high a rate of rise of inverse voltage (so that the inverse voltage reaches a critical level before the ion density has fallen to safe levels owing to diffusion and recombination).

Due to the much faster recovery of hydrogen thyratrons in the anode region than elsewhere in the tube, the inverse voltage is developed between the anode and its adjacent electrode. This really becomes very important with multigap thyratrons since all the inverse voltage is initially developed across the gap at the anode end; such thyratrons are at this time no better at withstanding inverse voltage than single gap tubes. This can create quite a problem since the maximum achievable reverse voltage is a smaller percentage of the peak forward hold-off voltage and this may lead to tighter constraints on circuit design.

If the requirements of the pulse generator are such that the circuit design necessarily includes an inverse diode then a number of possibilities exist:-

a) The use of a conventional inverse diode, in series with a suitable load, across the thyratron. This has the disadvantage that some

inverse voltage is still applied across the thyratron and reverse arcing can still occur.

b) The use of a matched inverse diode system at the opposite end of the pulse forming network. This can be quite effective but does not protect the thyratron from inverse voltages produced by the load capacitance whose effective value can be quite large if the load is fed via a high-ratio pulse transformer.

c) The use of a diode reverse connected directly across the thyratron (with no inverse diode load). If the diode can switch-on sufficiently fast this will prevent any inverse voltage from appearing across the thyratron. It has the disadvantage that every time the current changes from reverse to forward the thyratron has to restrike from a partially recovered state and energy is dissipated in the form of a commutation spike so that the working life of the thyratron may be reduced.

d) The use of a bidirectional switch. Ideally such a switch, once triggered, conducts equally well in both directions and hence cannot be damaged by reverse arcing - it acts as its own inverse diode.

A bidirectional switch has certain advantages when compared with a thyratron plus a separate inverse diode system.

i) It is simpler (one device replaces two) and hence is likely to be more reliable.

ii) Commutation losses at the moments of current reversal are at a minimum since the same charge carriers conduct the current in both directions and do not have to be regenerated each time the current reverses direction.

When a requirement occurred at CERN for a 60 kV high current, bidirectional switch, work was started on the construction of a hydrogen thyratron capable of conducting equally well in both directions. The design was based on the CX1171 (a three-gap, tetrode thyratron) since this tube type had already been proved to give long and reliable service in modulators pulsing beam bending magnets. The anode of the CX1171 was replaced by a grid 2, grid 1, cathode and reservoir assembly so that the resulting tube was symmetrical across its centre plane. Figure 1 shows a photograph of this tube which was designated CX1171B together with a standard CX1171. When operated in a test modulator the tube behaved similarly to a CX1171 except that it went smoothly into reverse conduction, whereas in the case of the CX1171 the current either ceased or reverse arcing occurred if the circuit conditions were unfavourable.

With the CX1171B the mechanism of switching is similar to any other EEV multi-gap tube; each gap voltage collapses about twenty nanoseconds after the one below it from the triggered end and the plasma-filled intervening drift spaces act as virtual cathodes. The electron current is taken out at the top end of the tube by using the relevant grid 2 and cathode electrically connected together to form an anode. It is reasonable to assume that the grid 2 acts as the current pick-up electrode and so protects the cathode from the high energy spike at the moment of switching. At the end of the forward pulse the tube is full of ions and electrons so that the current can reverse very easily and is able to build up and flow normally in the reverse direction because of the presence of a cathode capable of supplying primary electrons at the top end of the tube. The reverse electron current is taken out at the bottom of the tube via the cathode structure at that end. Here grid 2 cannot carry any appreciable current because of the series impedance across which the trigger pulse is generated but as the electrons hitting the original cathode structure are unlikely to have much more than 100 eV of energy no damage is caused.

Fig. 2 shows an oscillogram of the current flowing through the thyratron in a deliberately mismatched modulator. It can be seen that the current reverses at the end of each half cycle with no break in continuity. Fig. 3 is an oscillogram of the voltage across the thyratron and this shows that, apart from the change in polarity of the arc-drop, very little disturbance occurs at the moments of current reversal.

Heating, priming and triggering of a double-ended tube follow normal practice except that the grid 2 is directly connected to the cathode at the top end of the tube (see Fig. 4). The reasons for this direct

connection are as follows:-

i) The grid 2 acts as the main current collector and protects the cathode at the top end of the tube.

ii) If grid 2 is used to carry any of the d.c.-priming current it tends to increase the dark current which flows through the top gap of the tube and upsets the voltage division across the tube gaps by causing unequal currents to flow in the divider resistors.

iii) If connected to the cathode via any resistive or inductive element, grid 2 is driven sharply negative relative to the cathode when the tube first starts to conduct. This voltage transient causes a risk of external spark-over and internal damage.

At both ends of the tube grid 1 is d.c.-primed. At the bottom end of the tube this is simpler than pre-pulsing and allows a d.c. current-operated interlock to be used; this allows a simple fail safe protective system to be incorporated. At the top end of the tube the d.c. priming current provides a plasma and hence a virtual cathode close to grid 2 so that the tube current can reverse without any interruption. Again, a simple HT interlock can be built using optical isolation to avoid the necessity for a high voltage stand-off relay.

It is essential that the two reservoirs (one at each end of the tube) are powered by similar rms voltages at all times, otherwise hydrogen will transfer from the hotter to the cooler reservoir and this may eventually upset the gas pressure stability in the tube.

Initial trials of the CX1171B have shown that it can conduct 4 kA pulses of duration up to 30 microseconds (see Fig. 2) and a larger tube to work at 10 kA for 25 microseconds is now being constructed.

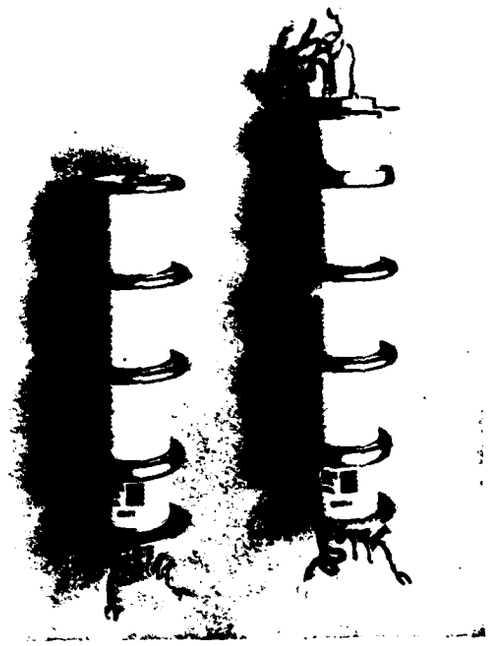

Figure 1

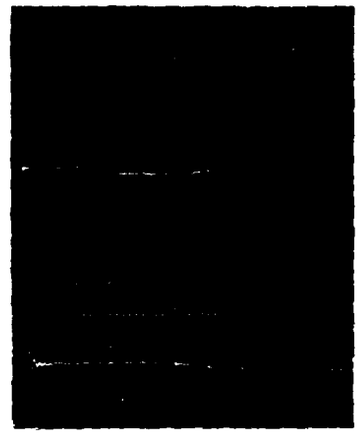

Figure 3

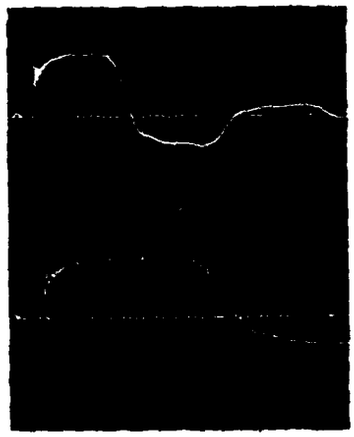

Figure 2

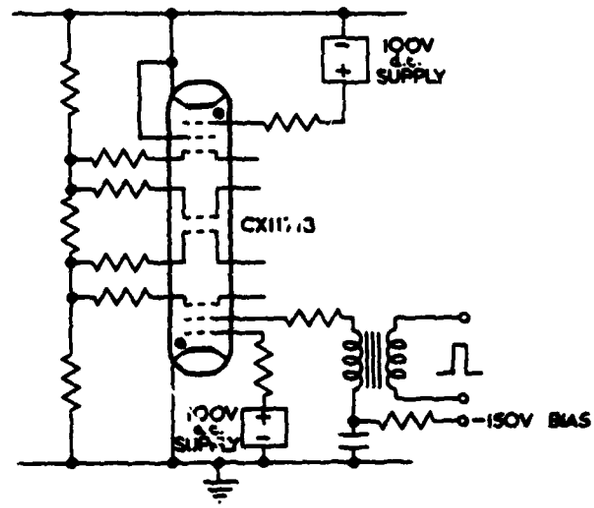

Figure 4

THE USE OF HYDROGEN THYRATRONS AS HIGH SPEED, HIGH VOLTAGE RECTIFIERS

H. Menown G. J. Scoles
English Electric Valve Co. Ltd.
Chelmsford, Essex, U.K.

Summary

The necessity for a high forward current, fast reverse recovery diode arose during the design of a thyratron test modulator. This paper describes how such a diode can be obtained by the use of hydrogen thyratrons in a parallel assembly.

Pulse generating circuits often incorporate diode rectifiers for charging and switching purposes but in certain cases it is found that a theoretically excellent arrangement cannot be made to work satisfactorily just because a diode able to switch rapidly enough or able to withstand suddenly applied inverse voltages cannot be found. The charging and inverse diode circuits of conventional pulse generators often make use of stacks of series-connected semiconductor diodes and in applications such as these where fast switching is not required from the diodes, satisfactory operation is normally achieved without much difficulty. It is essential to obtain correct voltage distribution between the various rectifiers of a series-connected stack when it is subjected to inverse voltage but so long as the maximum voltage, current and rate of rise of current ratings are not exceeded, such rectifiers will usually give reliable service. This applies particularly to low and medium voltage equipment, but as the working voltage increases the number of rectifiers required of necessity increases as well. Problems of screening and voltage distribution then become harder to solve due to the sheer bulk of the equipment which must be provided.

A further difficulty associated with semiconductor rectifiers is that they must at all times be able to withstand any voltage or current transients which may occur in service. There are many causes of such transients (apart from obvious overloads and short-circuits) and unless the designer is really expert he may well find that an apparently correctly rated rectifier stack suddenly fails for a reason which is not immediately obvious. Replacement then tends to be expensive and if many rectifiers are involved the storage of spares can also be a problem.

The normal alternatives to silicon or germanium semiconductor diodes are thermionic rectifiers and selenium rectifier assemblies: both have advantages and disadvantages in high power applications. Thermionic rectifiers are rugged and not readily damaged by overloads but they have the disadvantages of usually being suitable only for relatively small currents and of having a high internal impedance. This, in turn, results in the dissipation of a considerable amount of power if large currents have to be conducted. Selenium rectifiers, though less easily damaged than modern semiconductor rectifiers, are still liable to accidental damage or destruction if severely overloaded and they, too, have maximum current and thermal limitations to their use. Further, a certain amount of reverse current flow is unavoidable with such rectifiers and in some applications this may render them unsuitable.

A less well known solution is to make use of the rapid switching characteristics of hydrogen thyratrons by connecting the thyratrons as diodes. It is necessary to provide some means of ionising the gas between grids and cathodes and then a device exists which can conduct many thousands of amperes within tens of nanoseconds and which can also withstand up to about 30,000 volts inverse in many applications. Heater and grid excitation power is required continuously but the current and voltage ratings are such that the advantages gained far outweigh these where high energy switching is required. Large ceramic thyratrons are ideal where large currents have to be carried but they are liable to arc-back if sudden voltage reversal is applied immediately following such currents. A multiplicity of parallel-connected thyratrons, either glass or ceramic, gets over this problem. Since the peak current in each thyratron is inversely proportional to the number in parallel the chance of arc-back occurring is considerably reduced. Once the current requirements have been reduced in this way, it becomes preferable to use glass thyratrons as the individual diodes since this considerably reduces the cost of the assembly. A photograph (Fig. 1) of an assembly of eight CX1159 thyratrons

shows a typical set-up.

Thus where large currents and medium "switching off" speeds are required single large ceramic thyratrons can provide a satisfactory solution, whilst if the speed of voltage reversal is extra fast then an assembly of parallel-connected glass thyratrons should be used instead. Thus ceramic thyratrons have been used as charging diodes and inverse diodes in conventional high voltage pulse modulator circuits but where high currents and sudden reversal of voltage are involved simultaneously, a number of parallel-connected glass thyratrons have provided a solution to a problem which up to then was virtually insoluble.

Fig. 2 shows a circuit which was specially devised for testing thyratrons and in the low power version originally built no particular problems arose. The circuit is nominally loss-free, insofar as energy is stored in a network N alternately first at one polarity and then at the other, the thyratron under test V discharging N through D_3 to generate a current pulse whilst subsequently N reverses its polarity via L, D_1, and D_2 in series in readiness for the next pulse. Power supply unit A merely replaces any energy losses in the components whilst unit B provides the voltage datum necessary to establish the required working voltages for V. No load is present to dissipate the pulse energy, with the result that the saving in electrical power is considerable.

The original modulator of this type was designed for initially ageing ceramic thyratrons at voltages up to 30 kV and pulse currents of 3,000 amperes. It operated at the low p.r.f. of 5-7 pps in order to apply the hold off voltage to the thyratron for as long as possible and also to minimise the average current and hence the heating of the tube electrodes during ageing. Diodes D_1 and D_2 behaved similarly to the charging diodes of conventional modulators whereas diode D_3 had to carry the same current (3,000 amperes) as V and then almost instantaneously to withstand 15 kV inverse. CX1159 glass-envelope thyratrons were used as all three diodes and many thousands of hours of trouble-free service has been obtained in each of the three positions.

Following the successful use of thyratron diodes in several modulators of this general type, a very much larger version was built in order to test large thyratrons. A peak forward anode voltage of 40 kV was applied to the thyratrons under test and the peak and average currents were 6,000 amperes and 6 amperes respectively. This corresponds to a power supply of about 120 kW average and the cost of running the modulator worked out in the U.K. at the equivalent of 20 dollars per hour so that a life test for 1,000 hours would cost 20,000 dollars. In addition, the actual provision of a 120 kW supply of electrical power and of means of subsequently dissipating it would involve a considerable capital cost.

Using the "loss free" system the total power required at full load is about 6 kW and provision for cooling has not yet been necessary.

Diodes D_1 and D_2 each comprise two series-connected CX1154 ceramic thyratrons and these have operated satisfactorily since the equipment was built. To find a suitable diode for D_3, on the other hand, proved much more difficult. Although the actual inverse voltage across D_3 is only 20 kV, it is applied immediately after the diode has been conducting a current of 6,000 amperes. Various combinations of ceramic thyratrons proved unsatisfactory because of arc-back but finally a parallel assembly of eight CX1159 glass thyratrons was chosen. Evidence of unequal current sharing was at first apparent but this problem was solved by the inclusion of a few microhenrys in series with each individual "diode". The equipment has subsequently run for many hours and at currents up to about 9 amperes (average) and it is apparent that the assembly of glass thyratrons is quite capable of meeting the extremely severe voltage reversal requirements of this particular application.

This circuit is merely quoted as an example of one which imposes very severe requirements on rectifying devices but once a device has been found which can meet these conditions it is obvious that it is likely to be satisfactory for many other difficult rectifying and switching problems which can occur in practice.

The technique of using many of the EEV thyratrons as diodes is a relatively simple one. If a current of between 75 and 150 mA from a voltage source of between 75 and 150 V is drawn between the cathode and the control grid (or grids), this is sufficient to ionise the gas in the grid cathode region so that application of positive voltage to the anode immediately results in a flow of electron current to that electrode and the consequent ionisation of the gas in the grid-anode region will permit this current to flow with a very low anode-to-cathode voltage drop. No such mechanism exists

when the anode is made negative relative to the cathode and so a thyratron used in this manner can behave both as a carrier of very large currents and as a most effective rectifier. Current can build up within tens of nanoseconds of the application of forward voltage and once this has ceased to flow the ability of the thyratron to withstand inverse voltage will increase rapidly with time as a result of the very rapid decay of plasma in the anode region. The electron and ion clean up current in the grid-anode region at this time depends to a great extent on the size of the tube and thus several small tubes will have less plasma and also a faster decay exponential than one large tube.

Fig. 3 shows how the heater supply to the thyratron can be used also to provide excitation to the two grids of a tetrode thyratron, thereby converting the thyratron into an efficient rectifier. It is usual when using tetrode thyratrons as rectifiers to pass about 10 mA to the first grid and 100 mA to the second but in certain special applications these currents must be interchanged. For example, when inverse voltage is applied for a long period ion current flows between the anode and the electrode nearest to it and, clearly, the greater the volume of ionised gas adjacent to that electrode the greater the ion current that can flow and hence there is increased and undesirable dissipation. Thus in most applications for fast rectifier action it is found preferable to pass more current to the second grid (i.e. the one nearest to the anode) but where ion current flow is excessive there is a case for minimising the ionisation adjacent to the second grid at the expense of turn-on time.

Typically an ionising supply of about 100 volts is sufficient and the resistance values associated with the several grids are chosen to give the required currents.

Apart from the need to supply heater and grid excitation power, hydrogen thyratrons as diodes appear to have advantages over all existing types of diode rectifiers where high voltage, currents and switching speeds are involved. They are reliable and almost immune to damage from accidental overloading and they combine in a single item almost all the properties required from a rectifier for higher power applications.

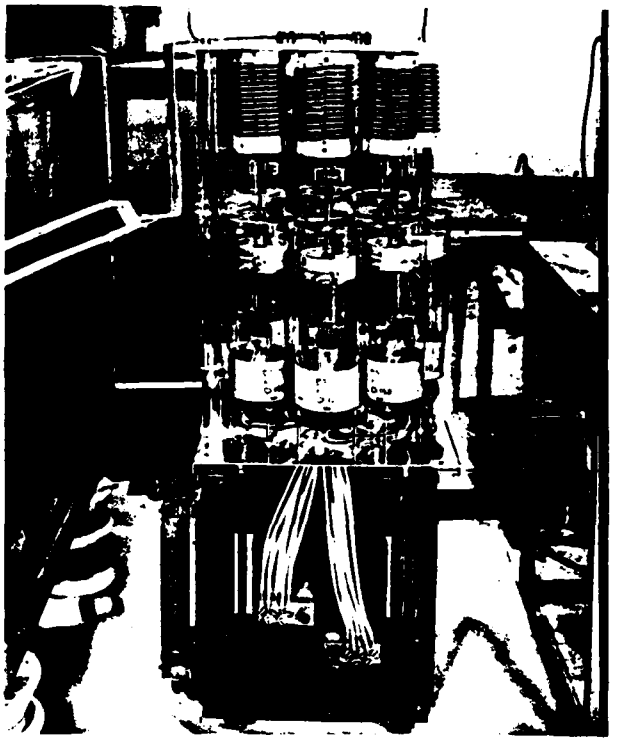

Figure 1

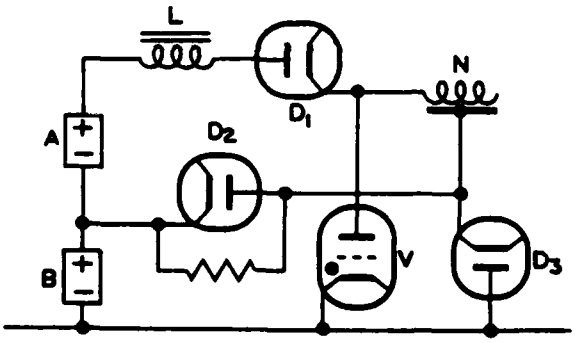

Figure 2

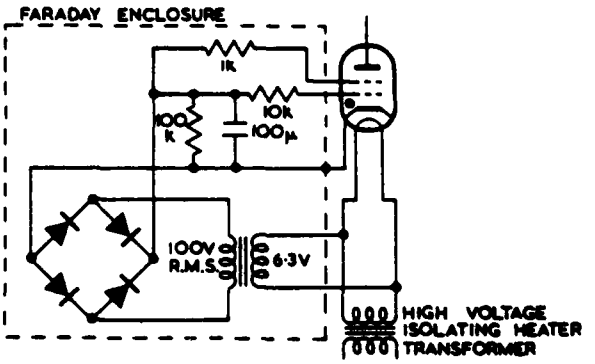

Figure 3

THE DEVELOPMENT OF DEUTERIUM THYRATRONS FOR OPERATION AT HIGH DUTY-RATIOS AND HIGH AVERAGE CURRENTS

by

R J Wheldon

MO Valve Company, Hammersmith, London, England

and

N S Nicholls

Royal Radar Establishment, Malvern, England

Summary

A circuit is described in which thyratrons have been operated at 50% duty-ratio with unusually high average current. Two valve types are described which have been developed to give long lives in this class of service. Good inverse-voltage performance and instant-start capability at full power were also necessary.

Introduction

The low power-loss and high switching speed of deuterium thyratrons, compared with alternative devices, suggested an examination of their suitability for use in audio frequency invertors required for induction heating equipment. Output powers up to a megawatt were involved.

The favourable experience which has been gained during this work may well be relevant to other fields of application of this type of tube.

The Invertor Circuit

One attraction of the deuterium thyratron for the above application was the potential availability of sufficiently high power devices to enable the simplest suitable circuit to be employed. This uses two valves (see Fig 1) in a parallel invertor, coupled to the load by a step-down transformer. The load consists of the heating coil connected in parallel with the capacitors required to correct its low power-factor. Together they comprise a resonant circuit whose resonant frequency is variable over the range from 2 to 5 KHz by capacitor switching. Each valve is extinguished by firing the other valve, the anodes of the two valves being coupled together by the load-circuit capacitance via the wide-band output transformer. Typical waveforms are shown in Fig 2. The current waveform in each valve is substantially a square-wave on account of the choke in series with the DC supply, which has a high impedance at and above the operating frequency.

At each commutation, the anode of the off-going valve is driven negative for a period which must be at least sufficient to permit recovery of the valve. This time must be kept short in order to keep the peak inverse voltage low and to obtain a high power factor at the audio frequency. The latter is necessary to give maximum power from the valves and good utilisation of the transformer.

The peak inverse voltage following commutation is increased by up to 40% by ringing in the stray reactances of the transformer, in spite of the damping circuits which are fitted (not shown in the diagram).

The problem of determining firing times for the valves which will ensure recovery without exceeding the inverse voltage ratings is handled by low power circuits which do not fall within the scope of this paper. In fact, a sufficient range of firing phase is found to exist between these two limits to enable the AF output voltage to be stabilised against all DC voltage variations arising from the electricity supply and from regulation of the transformer-rectifier combination. Variation of the phase-angle of firing alters the back EMF of the invertor for constant output voltage. Since the available range is restricted, a fairly low impedance rectifier system is indicated.

The Complete System

Taking advantage of the possibility of controlling the power flow by frequency and of stabilising the output voltage by varying the invertor phase angle, a simple silicon diode rectifier arrangement was used, and with on-off switching by means of a vacuum contactor in the AC supply lines (see Fig 3).

This has two consequences for the thyratrons. First, it requires that they be capable of direct-on starts at full power and maximum frequency, since this is required in the normal start-up of the equipment from cold. This led to some work on the thyratron which is described below.

Another problem was concerned with the rather high short-circuit current of the low-impedance DC supply. In the event of commutation failure, which may arise from incorrect use or equipment fault, this fault current flows through one or other of the thyratrons. When the existing thyratrons showed signs of damage under such conditions, a crowbar, in the form of a small ignitron, was introduced, connected across the DC supply. The fault current capability of the tubes is subjected to quality control, but little work was done to improve the thyratrons in this respect.

Valve Design

The limitation in peak or mean power handling capability of the hydrogen or deuterium[1,2] thyratron is largely set by its electrode temperatures, particularly of the grid where gas density reduction or grid emission must be avoided. This limit has been very significantly raised in very high power thyratrons by the use of metal or ceramic envelopes. In both types of tube better electrode cooling is achieved by bringing thermal conducting members from the active parts of the grids or anodes to or through the envelope, for external cooling.

In low duty ratio pulse applications of hydrogen thyratrons where peak currents may be many thousands of amperes, comparable electrode heating can occur

during the leading and trailing edges of each pulse as during the body of the pulse. In high duty ratio applications where pulses are much longer and the peak currents much lower, virtually all the dissipation occurs during the body of the pulse. Therefore the mean power handling capacity of a thyratron under high duty ratio conditions is significantly higher than under low duty ratio conditions.

Electrode Cooling

In the metal envelope tube, the cooling of the electrodes is separated from their insulation requirements. The active parts of the electrodes are joined directly to the metal envelope which provides a large surface for heat loss. Relatively short insulators are used, the anode insulator being behind the anode where it is unlikely to become coated by materials sputtered from the electrodes by the discharge. In early metal envelope tubes water cooling of the electrodes was used, this however proved to be expensive to produce and cumbersome in use.

Figure 4 shows the construction of a GHT12 metal envelope deuterium thyratron. It comprises a cathode C surrounded by a shield S at cathode potential; a baffle structure B which forms part of the envelope and shields the grid G from emissive material evaporated from the cathode and an anode A surrounded by a box at grid potential. The gas filling is deuterium, replenished by a titanium deuteride reservoir R controlled by a barretter. The grid and baffle are of copper and the short thermal paths to the envelope are of substantial cross section. With an average current of 60 amperes flowing through this tube at a high duty ratio a total grid dissipation of 1100 watts has been measured; for which the estimated maximum grid temperature is 150°C above that of the envelope. With the envelope finned, it may be cooled by forced air or by insulating liquid. The latter has been found very effective in compact high voltage installations, where an envelope temperature $\leq$100°C has been maintained. There is also a significant dissipation at the baffle, but again the cooling is good. In the GHT12 the anode ceramic has been shortened for use under insulating liquid and this has improved the heat conducting path from the anode.

The Cathode

The cathode used in this range of metal envelope thyratrons is of the barium aluminate impregnated tungsten type and has proved to give a good life at high average currents. The tungsten matrix of the cathode provides good thermal and electrical conductivity through the body of the cathode thereby reducing the likelihood of hot spot formation and damage to the coating due to back bombardment. The rate of loss of emissive material from the cathode is therefore more controlled than with the conventional oxide coated cathode. The cathode is compact and capable of providing the lower peak and high mean currents required for high power, high duty ratio operation. It is surrounded by an internally finned cylinder which by collecting positive ion currents makes a large contribution to the total cathode current when high peak currents are required.[3,4] This is called upon under fault current conditions even though a crowbar is used. Without a crowbar the fault current would be 4 or 5 times greater than that encountered in normal modulator service at maximum ratings.

The Gas Reservoir

Direct switching of a hydrogen thyratron at high average currents causes temporary gas clean up to take place. If the gas reservoir system does not compensate for this quickly enough there will be a transient fall in gas pressure in the tube. Current interruption can then take place at the grid aperture. The problem is made worse if the reservoir activity deteriorates during the life of the tube due to the slow evolution of poisoning gases from the electrodes. The use of a high and low temperature titanium deuteride reservoir, each with a good gas flow capability, has reduced the pressure 'dip' to a negligible value and eliminated 'poisoning' of the reservoir. Fig 5 compares pressure dips on the new and earlier reservoir systems during a full current direct on start.

Inverse Voltage Performance

In inverter service the tubes are subjected to a peak inverse voltage of up to 25kV within a few microseconds of the cessation of anode current. The metal envelope tubes have been shown to withstand this condition with a very low arcback rate for many thousands of hours.

Tube Ratings

Two metal envelope tube types are made for oil immersed inverter service, these are designated GHT11 and GHT12. Their principal ratings are as follows:-

	GHT11	GHT12
Peak anode voltage	35kV	35kV
Peak anode current	40A	120A
Surge current (20m.s)	200A	600A
Average anode current	20A	60A
Power output (2 tubes)	320kW	1000kW
Operating frequency (max)	6kHz	6kHz

Lives under these conditions are good, so far exceeding 6000h for the GHT11 and 3000h for the GHT12; based on some ten equipments in industrial service. These tubes were developed from pulse modulator tubes GHT8 and GHT9 which are designed for air cooling and have the following ratings:-

	GHT8	GHT9
Peak anode voltage	35kV	35kV
Peak anode current	2000A	7500A
Average anode current	5A	15A(at 7500A) 30A(at 300A)
Heating factor ($\times 10^9$)	40V.A.Hz	150V.A.Hz
Peak power	35MW	130MW

Good lives are also being achieved at these high peak and mean currents.

Conclusions

These tubes have been demonstrated to give reliable service in inverters at the elevated ratings described. Tube costs in inverter requirements are currently about 7 dollars/kW and 1.5 cents/kWh. The latter figure is expected to reduce with running experience. Costs in high duty ratio long pulse modulators would be about half the above. The tubes have shown themselves tolerant to faults in other parts of the equipment.

References

1. Cook K G, Isaacs G G Deuterium Filled Thyratrons Brit J App Phys 9 491 (1958)
2. Cook K G, Wheldon R J A Compact Metal-Ceramic Deuterium Thyratron Modulator Symposium 1962
3. Baker B O, Wheldon R J British Patent No 962681
4. Baker B O, Int Ini Electronics 25 (1968) 48-56

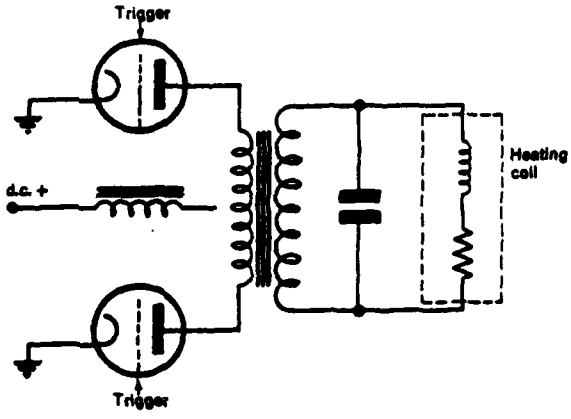

Fig 1. Inverter Circuit

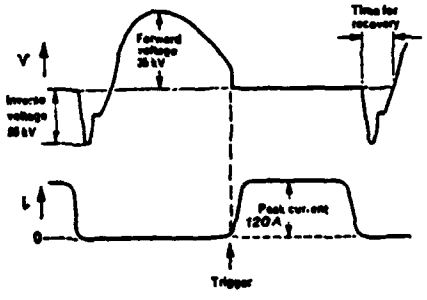

Fig 2. Anode Voltage and Current Waveforms

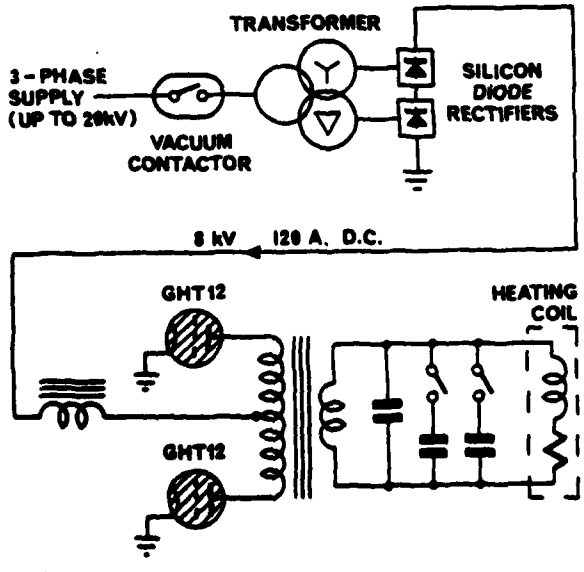

Fig 3. Induction Heating Inverter System

PHOTOGRAPH NOT AVAILABLE AT TIME OF PUBLICATION

Fig 4. Metal Envelope Deuterium Thyratron

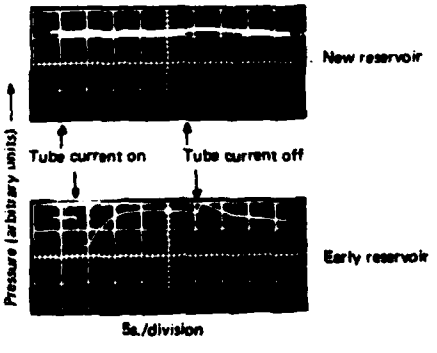

Fig 5. Reservoir Response Curves

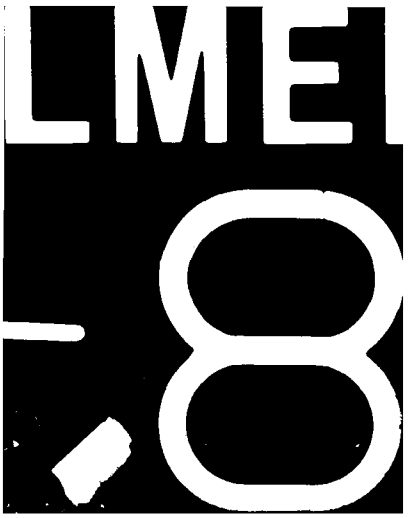
LME
8